

Reassessing early copper metallurgy: insights from the prehistoric site of Orti Bottagone, Tuscany

Alessandro Armigliato

Thesis submitted to
Newcastle University
for the degree of
Doctor of Philosophy (PhD)



School of History, Classics and Archaeology
Armstrong Building, Newcastle upon Tyne
NE1 7RU – United Kingdom

November 2023

Abstract

This research focuses on the study of the metallurgical assemblage discovered at the Final Neolithic (early 4th millennium BC) site of Orti Bottagone, Tuscany (Italy). It has two objectives: understanding the copper reduction technology employed at the site and exploring the feasibility of one-step sulphide ore reduction experimentally. The overarching goal is to comprehend how prehistoric smiths might successfully have smelted sulphide ores at a time when most were still engaged in the reduction of copper oxides and carbonates. The answer, although based on evidence from a single site, has important implications for our understanding of technological change in Western Europe.

Traditional belief has it that metal technology progressed from the working native copper in the Neolithic to the small-scale smelting of copper oxides and carbonates in the Chalcolithic and the large-scale reduction of copper sulphides in the Bronze Age. However, recent research has challenged this belief, highlighting that sulphide ores were already being reduced in the Chalcolithic, when most communities still relied on copper oxides and carbonates. Orti Bottagone can shed light on the transition from oxide/carbonate to sulphide smelting due to its early chronology and its location at the heart of a copper-rich ore district.

The research has employed a multi-analytical approach, combining materials science and experimental archaeology. Several samples of slags and a crucible fragment were analysed using Optical and Digital Microscopy (OM and DM), X-ray Powder Diffraction (XRD), X-Ray Fluorescence (pXRF) and Scanning Electron Microscopy coupled with Energy Dispersive Spectrometry (SEM-EDX).

Slag analysis has revealed that, at Orti Bottagone, copper was obtained from sulphide-rich charges through an immature slagging process. The experimental reconstruction of the process showed that sulphide ores were likely smelted through a one-step process without any roasting. These findings indicate that sulphide ores could be reduced at the initial stages of metallurgy under conditions that, although inefficient, secured the transformation of the ore into metal.

Acknowledgements

I want to extend my deepest gratitude to the individuals and institutions who played a crucial role in the completion of my long-dreamt doctoral thesis:

I am profoundly grateful to my first supervisor, Andrea Dolfini. He not only made this journey possible but also transformed it into a pleasant and enjoyable experience. Thank you for your unwavering support, guidance, and mentorship. Your expertise, encouragement, and constructive feedback have been invaluable in shaping the trajectory of my thesis.

Deep thanks to my second supervisor Alasdair Charles for what he has taught me over the years, and for what he has tried to teach me without success. Without your scientific insights, I might still be staring blankly at the machine.

A special thanks to the Northern Bridge Consortium for their financial support, not only for the PhD but also for enabling a transformative 6-month placement at the British Museum. This support allowed me to focus on both my research and personal growth, making a meaningful contribution to my career.

I extend my appreciation to the members of Newcastle University. The collaborative and intellectually stimulating environment within this community played a vital role in shaping the trajectory of my research. Heartfelt thanks to the PGR annex for their invaluable language advice, to whom I still owe many beers.

Thanks to my friend Marco R. P. for his extremely useful academic and non-academic advice. Also, a shoutout to the volunteers' community at the open-air museum at Jarrow Hall who made a significant contribution to the realisation of this thesis.

Sincere gratitude goes to the supervisors, mentors, colleagues, and friends Laura and Fred at the Scientific Research Department at the British Museum in London. Your warm welcome and insightful comments significantly enriched the quality of work during the placement.

I wish to express my deep gratitude to my parents, Mariella and Sergio, for their encouragement, interest and support throughout this arduous journey.

To my colleagues and friends in Newcastle, and particularly to Francesco, Gianluca, Filippo, Eleonora M. and Stefano, thank you for your constant support, shared ideas, laughter and comforting presence during the highs and lows of my PhD journey.

I want to acknowledge Sonali and Gareth for being amazing flatmates with whom I shared great moments. Your friendship has been a tremendous gift, providing solace during the challenges, especially when the weight of the pandemic bore down.

I want to extend a special and heartfelt acknowledgment to Eleonora N. for her invaluable support during the most personally challenging phase of my journey. Your assistance and understanding were crucial, providing much-needed comfort during a time when I needed it the most.

To the Italian squad - Marco, Andrea, Sebastiano, Emanuele e Alberto, Giacomo, Dave, Domenico, Fabrizio, Laura, Elena, Tullio, I want to express gratitude for the camaraderie and support you provided, even from afar. You made my Italian interludes extremely enjoyable.

Finally, to all who supported me, whether in significant or subtle ways, your contributions have not gone unnoticed and are deeply appreciated.

Table of contents

Abstract.....	iii
Aknowledgements	iv
Table of contents	vii
List of figures	xii
List of Tables.....	xxvii
Chapter 1. Introduction.....	32
1.1. Background and significance.....	32
1.2. Aims and research questions	34
1.3. Methodology and theoretical approaches in Archaeometallurgy	36
1.3.1. Theoretical frameworks in Archaeometallurgy	36
1.3.2. Methodological approach	38
1.3.3. Integration of Theory and Methodology	38
1.4. Thesis layout.....	39
PART I	43
Chapter 2. The study of pyrometallurgical by-products	44
2.1. Introduction	44
2.2. Historical overview of slag analysis.....	44
2.3. Mineralogy of slags	46
2.4. Weathering and ore formation.....	51
2.5. Early copper smelting technology: challenges and interpretations	54
2.5.1. Fluxes/non fluxes.....	59
Chapter 3. Early Smelting Technology in Europe.....	63
3.1. Introduction	63
3.2. Western Alpine region and Southern France.....	66
3.2.1. The Cabrières-Péret district	67

3.2.2. The Saint-Véran mining area	70
3.3. Central and Eastern Alpine region	72
3.4. Southeastern European region	83
3.5. The Iberian Peninsula.....	90
3.6. Northwestern European region	93
3.7. The site of Orti Bottagone, Tuscany	95
3.7.1. Archaeological context	99

Chapter 4. Analytical protocol for the analysis of slags..... 105

4.1. Introduction	105
4.2. Multi-analytical approach	105
4.2.1. Macroscopic investigation	105
4.2.2. Handheld X-ray fluorescence spectrometry (pXRF)	106
4.2.3. Microscopic investigation	107
4.2.4. Sample preparation for OM and SEM-EDX.....	108
4.2.5. Reflected Light Microscopy (RL-OM)	111
4.2.6. Scanning Electron Microscopy with Energy Dispersive spectroscopy (SEM-EDX)	114
4.2.7. Sample preparation for X-ray Powder Diffraction (XRD)	117
4.2.8. X-ray Powder Diffraction (XRD)	118
4.2.9. Limits of the slag analysis approach	119
4.2.10. Experimental archaeometallurgy	122

Chapter 5. Copper Smelting at Orti Bottagone: Insights from analytical chemistry 125

5.1. Introduction.....	125
5.2. The physical chemistry and mineralogy of the archaeological slags: analytical results	125
5.2.1. General observations.....	125
5.2.2. Density	129

5.2.3. Magnetism	131
5.2.4. Handheld X-ray fluorescence spectrometry (pXRF).....	132
5.2.5. Mineralogical phases	134
5.2.6. Inclusions and minor elements	141
5.2.7. SEM-EDX semi-quantitative analysis.....	143
5.2.8. Viscosity and Fe/SiO ₂ ratio	147
5.2.9. Copper bearing compounds	152
5.3. Characterisation of a crucible fragment from Orti Bottagone.....	158
5.3.1. The ceramic fabric	159
5.3.2. Bulk chemical changes	161
PART II.....	166
Chapter 6. Experimental archaeometallurgy I:	
Experiencing roasting and smelting.....	167
6.1. Introduction	167
6.2. Experimental archaeometallurgy: theoretical framework	167
6.3. Pilot experiments	171
6.3.1. Roasting	172
6.3.2. Experiments outline.....	175
6.3.3. Preliminary results and considerations	178
6.4. Smelting.....	181
6.4.1. Experiments outline, preliminary results, and considerations.	183
Chapter 7. Sulphide copper smelting experiments.....	193
7.1. Introduction	193
7.2. Brief overview of copper smelting experiments.....	193
7.3. Sulphide copper smelting experiments.....	195
7.4. Development of thesis experiments: sulphide ore smelting in Early Metallurgy.....	205

Chapter 8. Experimental archaeometallurgy II:	
Experimental copper smelting	209
8.1. Introduction	209
8.2. Experimental protocol.....	209
8.3. Ore collection and beneficiation	211
8.4. Fixed parameters	217
8.5. General observations.....	220
8.5.1. Phase I.....	220
8.5.2. Phase II.....	221
8.6. The physical chemistry and mineralogy of the experimental by-products: analytical results	222
8.6.1. Magnetism and density	223
8.6.2. Microscopy: inclusions and phases.....	226
8.6.3. Viscosity and Fe/SiO ₂ ratio.....	231
8.6.4. Copper bearing compounds	234
Chapter 9. Discussion.....	241
9.1. Introduction	241
9.2. The smelting process at the site of Orti Bottagone	242
9.3. Experimental vs Archaeological evidence	251
9.3.1. The similarities and their implications.....	251
9.3.2. The differences and their implications.....	254
9.3.3. Crucible reduction technology?	260
Chapter 10. Conclusions and avenues of future research.....	263
10.1. Introduction	263
10.2. Project results and reflections	263
10.3. Avenues for future research	269
10.4. Conclusion	271
References	274

Appendices 297

Appendix A 298

Appendix B 299

Appendix C 315

Appendix D 335

Appendix E 340

List of figures

Chapter 1

Fig. 1.1 Simplified *chaîne opératoire* showing the logical sequence of the steps necessary for the production of metal artifacts (from Georgakopoulou, 2016, pp. 47, 4.1) 37

Chapter 2

Fig. 2. 1 Chart illustrating a temperature profile chart. It provides a visual representation of the temperature changes that occur throughout the heating and cooling phases of slag formation processes. (Chart by the author). 48

Fig. 2. 2 Simplified model of ideal phase stratification in a crucible/reactor during the smelting process. In an ideal smelting process, in a fully liquid charge the higher density compounds settle at the bottom of the crucible (copper and copper oxides), while the less dense tend to move toward the surface (silica and gas bubbles). Cu = copper, FeOx = iron oxides, Fa = fayalite, Qz = quartz/silica. (Illustration by the author). 49

Fig. 2. 3 offers an ideal representation of the weathering processes affecting primary copper-bearing mineralisation (from Bastian Asmus, 2013). 52

Fig. 2. 4 (left) Smelting tray/reducing “crucible” - Approximately 50 cm in diameter. Unearthed at the site of La Ceñuela, in Murcia province (from Rovira 2007, p. 89, fig.3)..... 56

Fig. 2. 5 (right): Vase furnace from Almizaraque – Scaled to 5 cm, based on a drawing by Ruiz Taboada (Montero-Ruiz, 1993), (Bourgarit, 2007, p. 8, Fig. 4b)..... 56

Fig. 2. 6 depicts various potential furnace types, including the bowl furnace (left), domed furnace (centre), and shaft furnace (right). While the precise heights of these furnaces may require estimation, Rothenberg proposed different furnace types (1990). 56

Chapter 3

Fig. 3. 1. Map showing the main regions with the copper mining and smelting sites reviewed in this thesis..... 64

Fig. 3. 2. Map of the Western Alpine region and Southern France, indicating key sites categorized as mining and smelting locations.	66
Fig. 3. 3 (left) Cross section of a well preserved simple metallurgical structure at La Capitelle du Broum (Péret-Hérault),(Ambert et al., 2013: 63, 3).	69
Fig. 3. 4 (right) Back-scattered electron image (hereafter referred to as BSE) of a slag from La Capitelle du Broum (Péret-Hérault) showing metal droplets (3) embedded in the highly viscous silicate matrix (1) and unreacted silica (2) of the slag (from Ambert et al., 2013: 67, 6).....	69
Fig. 3. 5 provides a BSE micrograph revealing the microstructure of slag originating from the La Cabane des Clausis site. This slag sample exhibits four primary phases: a) fayalite (large grey needles), b) calcium-enriched clino-pyroxenes (dark grey chains inside the fayalite needles); c) magnetite (light grey polihedra); d) copper droplets (white), (from Bourgarit <i>et al.</i> , 2008, fig. 9a).	71
Fig. 3. 6 Map of the central and eastern Alpine region, showing relevant sites categorized as mining and smelting locations.....	73
Fig. 3. 7. BSE micrograph displaying a detailed area of a crucible fragment from Wetzikon. The copper prills (white) are located only in the inner part of the crucible, while copper-iron sulphides inclusions are only on its surfaces. From Rehren, 2009, fig. 8.	76
Fig. 3. 8 BSE micrograph showing a fragment of ore and gangue minerals decomposing and vitrifying inside the slag. The gangue exhibits a laminated texture with quartz (1) and decomposed phyllosilicates (2). The metalliferous phases (3) primarily consist of chalcopyrite together with lesser amounts of bornite, magnetite and pyrrhotite. Slag sample VB10, slide 2. (From Pearce et al. 2022, p. 12, fig. 5a).	81
Fig. 3. 9 Digital micrograph showing a chalcopyrite (Ccp) and pyrrhotite (Po) sulphide inclusion in quartz-rich gangue (Qz). Slag sample VB10-3. Scale bar 200 µm. (From Pearce et al. 2022, p. 13, fig. 6d).....	81
Fig. 3. 10 Map of the Southeastern European region, highlighting significant sites categorized into mining and smelting locations.....	84
Fig. 3. 11 shows two of the by-products collected from the site of Belovode (c. 5000-4600 BC): a) a typical green-stained slag measuring less than 1 cm in size and weighing only a few	

grams (sample 134); b) a slagged sherd 6 cm large heavily vitrified with small green stains on the upper surface. From Radivojević, 2013: 16, fig. 3b, c. 87

Fig. 3. 12 Map of the Iberian Peninsula, indicating key sites categorized as mining and smelting locations. While specific mining areas are not marked due to the vast number of deposits identified in the region, the main areas are described in the text. 90

Fig. 3. 13 Map of the Northwestern European region, showing relevant sites categorized into mining and smelting locations. 93

Fig. 3. 14 Three different types of furnaces unearthed at Ross Island mine, and an Early Medieval reproduction. From O'Brien, 2004, p. 466, fig. 217. 95

Fig. 3. 15 Location of the site of Orti Bottagone investigated in the current research. 96

Fig. 3. 16 Landscape characterised by alternating patterns of intertidal creeks and patches of shrubs. Photo taken from south-east by the author in the summer of 2022. 97

Fig. 3. 17 Distinct vessel forms aligned with Late Neolithic Ripoli Culture recovered at the site of Orti Bottagone. (From Fedeli 1999: a) p. 118, fig.3; b) p. 122, fig.6; c) p. 120, fig.4; d) p. 121, fig.5). 98

Fig. 3. 18 displays a) a simultaneous view of three different planes (XY, YZ, XZ), along with b) the use of a heatmap. This arrangement enables a comprehensive examination of the internal structure of the specimen. 99

Fig. 3. 19 The map highlights significant sites categorized as mining and smelting locations in the Western Italian peninsula, providing a comprehensive overview of the current body of knowledge regarding copper mining and smelting in this region. 100

Fig. 3. 20 Picture (a) and cross-section (b) of the fourth-millennium cal BC mineshaft (ML6 of Monte Loreto. After Maggi & Pearce 2005). 102

Chapter 4

Fig. 4. 1 Overview of the machines adopted for the sample preparation process: a) cutting machine, b) coarse grades rotary polishing machine (15µ, 30µ), c) Hot air-drying machine, d) fine grades rotary diamond polishing machine (6µ and 1µ). 109

Fig. 4. 2 Polished thick samples showcasing the flat and mirror-like surfaces ready for microscopic observations. 110

Fig. 4. 3 shows the Lighting Techniques adopted in this research. Left: Low-Angle Ring Lighting - Low-angle illumination with uniform and even lighting, providing contrasting illumination for specimen details. Right: Coaxial Lighting - Illuminates specimens from the same angle as the camera, brightening backgrounds and creating contrast with glossy objects (Sample ORTB 6). 113

Fig. 4. 4 illustrates an elemental compositional map that provides a visual representation of the elemental distribution in a specific area. This map reveals a Cu-Fe sulphide feature within an iron-silicate matrix. Additionally, it indicates the consistent presence of calcium (Ca) in the slag matrix, albeit in relatively low concentrations. For more detailed information on these findings, please refer to Chapter 5. 116

Fig. 4. 5 Overview of the tools and machine adopted for the sample preparation process: a) set of 6 agate grinding balls of varying sizes and grinding jar; b) a Planetary ball mill (PM100); c) approximately 7g of powdered sample ready to be loaded (sample ORTB 21). 118

Fig 4. 6 Ternary plot diagram showing the liquidus surfaces in the system $\text{FeO}_x\text{--Al}_2\text{O}_3\text{--SiO}_2$ (Kowalski *et al.*, 1995, fig. 3183). 123

Fig 4. 7 Ellingham diagram for several metals giving the free energy of formation of metal oxides and the corresponding partial pressure (pO_2) at equilibrium (Ellingham, 1944). 123

Chapter 5

Fig. 5. 1 Two views of sample ORTB 13 showing a concave indentation resembling a circular void within the bottom of the slag. 129

Fig. 5. 2 Box and whisker plot of the archaeological typologies of slags analysed from the site of Orti Bottagone. 130

Fig. 5. 3 Scatterplot illustrating specimen density categorised by slag type (shape) and magnetism (colour). 132

Fig. 5. 4 BSE micrographs showing the mineralogical phases of slag ORTB 5. a) five phases: a) fayalite (large grey needles), in a b) calcium-enriched clino-pyroxene matrix (dark grey); c) magnetite (grey polyhedra); d) copper droplets (grey) with e) an outer ring of covellite; b)

parallel fayalite chain olivines intermixed with silicatic glass and a Cu-Fe sulphide round feature..... 136

Fig. 5. 5 BSE micrographs showing the diverse range of olivine morphological crystallised features in the flat slags: a) euhedral grains (ORTB 20), b) hoppers (ORTB 16), c) small dendritic needles (ORTB 8), d) large chain structures (ORTB 16). 138

Fig. 5. 6 BSE micrographs showing the different morphologies of the iron-rich inclusions identified in sample ORTB 8: euhedral (cubic to prismatic) crystals, dendritic growths and round features in a fayalitic matrix. Their presence in such a reduced area indicates highly unstable reducing conditions during the smelting process. The light grey features in the image on the left are inclusions of metallic copper or copper-iron sulphides. 139

Fig. 5. 7 Series of micrographs showing the different iron-rich spinel morphologies/phases similar to those investigated here: a) BSE image showing wuestite dendrites in the fayalitic matrix from a sample from Montesei di Serso, Trentino - scale bar 200 μm (Artioli et al., 2015, Figure 4); b) the matrix, distributed among non-reacted silica grains, in a monticellite-like silicate. Magnetite is abundant (Müller et al., 2007, Figure 2). c) Reflected Light image (hereafter RL) showing magnetite in prismatic and round morphologies in a fayalitic matrix with metallic copper and newly formed Cu sulphides of digenite-chalcocite from Millan – image length 200 μm (Artioli et al., 2005). 140

Fig. 5. 8 Micrographs showing a) BSE image with relics of calcium carbonate as inclusions in a fayalitic glassy matrix (sample ORTB 13 flat); b) BSE image with relics of calcium carbonates found as inclusions in a fayalitic glassy matrix (sample ORTB 20 coarse); c) BSE image with quartz and Ca inclusions (sample ORTB 20 coarse); d) RL image with semi-reacted inclusion of a possible Ca carbonate. CaO is the main compound in the grey rim – scale bar 200 μm (ORTB 9). 142

Fig. 5. 9 RL (a) and BSE (b) micrographs of quartz inclusions in two coarse samples (respectively ORTB 6 and ORTB 5). Scale bar of a) 100 μm 143

Fig. 5. 10 ORTB 5. Three scanned 1mm²-areas were acquired for each slag. From left G21, I-H13-14, M4..... 145

Fig. 5. 11 Ternary plot diagram FeO–Al₂O₃–SiO₂ (wt%) of the bulk chemistry of the three areas analysed (I-H13-14, G21, M4) and mean of sample ORTB 5..... 145

Fig. 5. 12 Ternary plot diagram (FeO–Al₂O₃–SiO₂ (wt%) slag system) of the average composition of the three areas analysed. 146

Fig. 5. 13 Ternary plot diagram showing the average composition of archaeometallurgical slags from copper smelting (<i>medium-shaded area</i>) and iron smelting (<i>dark-shaded area</i>) shown in the ternary system FeO–Al ₂ O ₃ –SiO ₂ (wt%), (Hauptmann 2014:100, Fig. 5.6).	146
Fig. 5. 14 Ternary plot diagram (FeO–CaO–SiO ₂ (wt%) slag system) of the average composition of the three areas analysed.	146
Fig. 5. 15 Scatterplot showing a strong positive correlation (0.9) between the variables, indicating that as the Fe/SiO ₂ ratio systematically increases, there is a corresponding systematic increase in the viscosity index.	149
Fig. 5. 16 Binary diagram showing the liquidus effect of varying calcium oxide content and Fe/SiO ₂ ratio on CaO–FeO–Fe ₂ O ₃ –SiO ₂ slag system at pO ₂ of 10 ⁻⁸ atm (top right) and 10 ⁻⁵ atm (bottom right). From Kongoli & Yazawa, 2001, p. 585, figg. 4-5).	150
Fig. 5. 17 RL optical micrographs of the brown ore (sample ORTB 3) showing a) a semireacted fragment of pyrrhotite with an inner part of magnetite (scale bar 100 µm) and b) chalcopyrite (yellow) and pyrrhotite in a matrix of iron hydroxides (mid-grey) and quartz (dark grey), (scale bar 200 µm). c) Similar structures identified at the Chalcolithic site of Akladi Cheir (Rehren et al. 2020)	152
Fig. 5. 18 (Left) Ternary plot diagram (Cu–Fe–S (wt%) slag system) of the SEM-EDX analyses (orange= flat slags, red= coarse slags).	153
Fig. 5. 19 (Right) Ternary plot diagram (Cu–Fe–S (wt%) slag system) showing the vast range of chemical combinations along the sulphide axis chalcocite-bornite-chalcopyrite-pyrrhotite and the Cu–Fe axis of copper slags from data from Oman, Anatolia, Iran, Italy (Trentino), Grisons (Switzerland). (From Hauptmann, 2020, p. 277, fig. 5.55).	153
Fig. 5. 20 displays a selection of RL optical micrographs showcasing Cu–Fe sulphides and prills observed in the coarse slags. Starting from the top left: sample a) ORTB 6 (scale bar 100µm); b) ORTB 9 (scale bar 100µm); c) ORTB 20 (scale bar 100µm); d) ORTB 9 (scale bar 200µm); e) ORTB 5, prills in a fayalitic matrix surrounded by unreacted quartz inclusions (scale bar 500µm); f) ORTB 5, prill with a chalcocite extrusion (scale bar 100µm).	155
Fig. 5. 21 Optical micrographs of newly developed phases of copper hydroxides (e.g., Cu(OH) ₂ , and CuCl ₂ ·2H ₂ O) filling the empty spaces left in the slag; a) ORTB 6 (scale bar 250µm), ORTB 20 (scale bar 100µm).	155

Fig. 5. 22 displays a) a chalcopyrite dominant area (scale bar 100µm) characterised by b) the exsolution of bornite (pinkish brown) and partially oxidised bornite (sky blue), along with a covellite prill (light blue) observed in sample ORTB 19 (scale bar 50µm)..... 156

Fig. 5. 23 displays a selection of optical micrographs showcasing Cu-Fe sulphides and prills observed in the flat slags. Starting from the top left: a) round-shaped recrystallized compound characterised by covellite-like (blue) and chalcocite-like (greyish) compositions (ORTB 8 - scale bar 100µm); b) round-shaped Cu-Fe sulphide embedded in a fayalitic matrix (ORTB 16 - scale bar 100µm); c) round-shaped Cu-Fe sulphides high in copper (yellow) and high in sulphur (blue) (ORTB 13 - scale bar 200µm); d) ring-shaped formation of covellite-like composition (light blue) (ORTB 19 - scale bar 100µm); e) Cu-Fe sulphide within aggregates of magnetite (ORTB 19 - scale bar 100µm); f) round-shaped prill with a pure copper core (orange) surrounded by recrystallised digenite (bluish-grey) (ORTB 8 - scale bar 50µm)... 157

Fig. 5. 24 Cross-section of the crucible fragment ORTB 10 (digital micrograph) showing the bloated region (see Rademaker, 2015) and the possible location of the fragment. 159

Fig. 5. 25 Micrographs showing the elongated porosity/fractures in the ceramic zones on the outer side of the fragment (scale bar respectively 100µm and 250µm)..... 160

Fig. 5. 26 displays a) a RL optical micrograph (scale bar 100µm) and b) a BSE image showing different areas with several coarse rock inclusions in the crucible fragment ORTB 10..... 161

Fig. 5. 27 Composition of the ceramic and bloated areas in the a) SiO₂- Al₂O₃-FeO and b) SiO₂-Al₂O₃-CaO+MgO ternary diagrams. 163

Chapter 6

Fig. 6. 1 Chart summarizing the quantifiable (scientific) and non-quantifiable (experiential) data that can be obtained from a copper smelting experiment. From Heeb and Ottaway 2014, p.187, fig.8.34 169

Fig. 6. 2 Metallurgical structure interpreted as a possible roasting bed unearthed at the site of San Carlo Cave Solvay, Livorno (Italy). From Fedeli and Galiberti, 2016, p. 48, Fig. 32.... 175

Fig. 6. 3 Reconstruction of a roasting bed based on the archaeological evidence of San Carlo Cave Solvay (a), and the resulting melted charge from the experiment 2 - Roasting bed 2 conducted on June 16, 2021 (b). 177

Fig. 6. 4 illustrates the transformation of ore fragments before (a) and after (b) roasting, along with a cross-section of a roasted bornite (Cu_5FeS_4) sample, revealing surface oxidation limited to 1-2 mm and the unreacted inner portion (c). 178

Fig. 6. 5 displays a crucible filled with crushed malachite (a) and the preliminary warming process of the reactor (b). 185

Fig. 6. 6 depicts the crucible after the malachite smelting in Experiment 1 – Furnace 1. It includes a zenith view of the crucible (a) and provides detailed images of the vitrified rim after the experiment (b, c)..... 186

Fig. 6. 7 Exp 2_Furnace 2. Macroscopic view of the crystallised cross-section (a). RL optical micrographs of Cu-Fe sulphides (b-c) scattered over the surface of the specimen (scale bar $50\mu\text{m}$).. 188

Fig. 6. 8 a) Top view of the crucible from Pilot experiment JH2021_PE_Exp.3_F.2. Three different layers were identified: 1) an upper layer characterised by a greyish, porous, and slag-like appearance; 2) just beneath the top layer, there is a combination of greyish and reddish shining layers, giving off a shining quality; 3) the lowest layer exhibits a noticeable gleam and is rich in copper content. Within the crucible, marked by a red dotted circle, one can also identify an unreacted piece of bornite. b) the cross-sectional view A-B of the crucible reveals the products obtained during the experiment, which are scattered across the crucible's surface. 189

Fig. 6. 9 a) Melted product recovered from beneath the crucible leaked from a crack in the bottom, b) RL cross-sectional view and c) RL optical micrograph from the pilot experiment JH2021_PE_Exp.3-F.2 (scale bar $250\mu\text{m}$), d) Cu-Fe-S ternary diagram illustrating the composition of the product. The diagram visually represents the distribution of copper (Cu), iron (Fe), and sulphur (S) in the 5 analysed areas of the sample..... 191

Chapter 7

Fig. 7. 1 Flow-chart showing the process to obtain copper from sulphide ores. From Rostoker *et al.*, 1989, p. 70, fig. 1..... 196

Fig. 7. 2 In the sectioned crucible three distinct layers were identified: (A) slag mixed with the melted ceramic body and finely interspersed copper prill; (B) a grey-silvery shining layer of matte with lamellae of bornite and chalcocite; (C) globules and accumulation of metallic copper, partly mixed with slag (From Hanning *et al.*, 2010, p. 296, Pl. III. Experiment 14 (ore: Mercês I, P04c). Crucible width: 11 cm)..... 203

Fig. 7. 3 shows a diagrammatic section through ‘Ross Island-type’ furnace pit burning wood fuel. Subjected to the intense oxidizing environment of a substantial fire, succeeded by reducing conditions beneath a pile of embers, a notable portion of the copper within such ore may have undergone reduction, transforming into metallic form. (From Timberlake, 2007, p. 33, fig.7c. Drawing: S. Timberlake and B. Craddock). 204

Chapter 8

Fig. 8. 1 (above) illustrates the readjusted experimental plan, reducing the number of trials from 18 to 12 after realizing the unfeasibility of the initial arrangement. 211

Fig. 8. 2 (below) represents the original experimental plan..... 211

Fig. 8. 3 shows the mining areas explored where I collected the raw material for the experiments of this research: a) weathered material in an abandoned ancient tunnel of Lanzi mine, and b) an outcrop area of relatively high-grade leftovers of metallic ore bodies and c) the weathered growth in Temperino mine area (photos taken by the author)..... 213

Fig. 8. 4 a) Panoramic view of the landscape of Campiglia Marittima from the top of Monte Campiglia Vecchia, the highest point in the area; b) map showing the distance the mining areas of Temperino and Lanzi from the site of Orti Bottagone. 216

Fig. 8. 5 Selection of the different types of ore adopted for the experiments from the mines of Temperino and Lanzi. 217

Fig. 8. 6 Temperature gradients inside an experimental furnace. The further from the point where oxygen enters, the lower the temperature. After Tylecote and Boydell, 1978..... 219

Fig. 8. 7 Thermocouple trapped in the liquid slag (sample JH1B_T2-002). 219

Fig. 8. 8 displays two matte-like products recovered from trials JH1B_T2 (a) and JH2A_T3 (b). The pictures were generously provided by Sam, a volunteer at Jarrow Hall open-air museum in South Tyneside. 221

Fig. 8. 9 Box and whiskers plot of a) the experimental slags and b) the experimental matte fragments divided by phase and c) the archaeological typologies of slags analysed from the site of Orti Bottagone (see also 5.2.2)..... 225

Fig. 8. 10 Scatter plot of the archaeological typologies of slags analysed from the site of Orti Bottagone.....	226
Fig. 8. 11 RL optical images of a) the coarse slag ORTB 5, and b) the experimental sample JH1A_T2-002 showing a quartz core surrounded by a porous fayalite glassy matrix.....	227
Fig. 8. 12 RL Optical (a) and BSE (b) micrographs of quartz inclusions in two experimental samples (respectively JH1B_T1_001 and JH2A_T3_001).	227
Fig. 8. 13 BSE micrographs showing a) elongate hopppers and b) primary dendritic olivine in a fayalite matrix (sample JH2B_T1_002); c) Ca rich dendritic structure with magnetite euhedral crystals in a fayalite matrix (sample JH2B_T2_001); d) chain olivines and dendrites with a lot of tiny iron oxide phases (white), (sample JH2A_T1_001).	228
Fig. 8. 14 BSE micrographs showing a) the two main chemical compositions detected in the matte fragments: 1) Cu-Fe sulphide high in copper and iron (white) and 2) Cu-Fe sulphide high in sulphur (sample JH2A_T1_001); b) the inclusions identified in the matte (sample JH1B_T3_002); c) the copper prills (bright white) and cavities circular/elliptical vesicles entrapped in the matte (sample JH2A_T3_002).....	229
Fig. 8. 15 Ternary plot diagrams showing the average composition of the three areas analysed for each sample in the slag systems $\text{FeO-Al}_2\text{O}_3\text{-SiO}_2$ (wt%) and FeO-CaO-SiO_2 (wt%).....	230
Fig. 8. 16 Scatterplots of Viscosity (η) over Fe/SiO_2 ratio showing a) the experimental analyses plotted together with the archaeological analyses, b) the analyses of the experimental by-products categorised by phase, and c) the analyses of the experimental by-products categorised by type. The scatterplots show a positive correlation between the variables meaning that a systematic increase in the Fe/SiO_2 ratio correspond to a systematic increase in the viscosity index.	232
Fig. 8. 17 Binary diagrams showing the liquidus effect of varying calcia content and Fe/SiO_2 ratio on $\text{CaO-FeO-Fe}_2\text{O}_3\text{-SiO}_2$ slag system a) at $p\text{O}_2$ of 10^{-8} atm and b) at 10^{-5} atm for c) the experimental analyses plotted together with the archaeological analyses, d) the analyses of the experimental by-products categorised by phase, and e) the analyses of the experimental by-products categorised by type. The binary Flogen diagrams were taken from Kongoli and Yazawa, 2001, p. 585, figg. 4-5).	233
Fig. 8. 18 RL optical and BSE micrographs showing the Cu-Fe sulphides found in the experimental specimens. A diverse array of colours, shapes and chemical compositions were identified: a) partially reacted or unreacted chalcopyrite grains (sample JH1B_T1_001 – scale bar 200 μm), b) elongated and irregular morphologies (sample JH1B_T2_002 – scale bar	

100µm), and c-f) numerous prills with spherical shape with various diameters in the range of µm to mm size (respectively samples JH1A_T3_001 – scale bar 250µm, JH1A_T3_003, JH1A_T3_001 – scale bar 100µm, JH2B_T1_001), g) matte area distinctly separated from the slag matrix and mainly observed towards the outer sides of the slag (sample JH1A_T2_003 – scale bar 250µm). 236

Fig. 8. 19 illustrates a) the ternary plot diagram (Cu-Fe-S_(wt%) slag system) of the copper bearing compounds SEM-EDX analyses categorised according to their phases and types; b) the ternary plot diagram (Cu-Fe-S_(wt%) slag system) showing the vast range of chemical combinations along the sulphide axis chalcocite-bornite-chalcopyrite-pyrrhotite and the Cu-Fe axis of copper slags from data from Oman, Anatolia, Iran, Italy (Trentino), Grisons (Switzerland), adapted from Hauptmann, 2020, p. 277, fig. 5.55. See also Section 5.2.9. ... 236

Fig. 8. 20 illustrates the chemical compositions plotted in the ternary system Cu-Fe-S_(wt%) systematically compared across experiments and phases. 239

Chapter 9

Fig. 9. 1 displays two views of sample ORTB 13 showing a concave indentation resembling a circular void within the bottom of the slag (refer to section 5.2.1). 245

Fig. 9. 2 displays BSE micrographs illustrating the strikingly similar polyhedral features present (a) in a flat slag from Orti Bottagone (ORTB 20), and (b) in a slag from San Carlo Cava Solvay (sourced from Artioli et al. 2016, p. 77, fig.52d). 246

Fig. 9. 3 displays digital images of a) the coarse slag ORTB 5 and b) the experimental sample JH1A_T2-002 (scale bar 1000µm), showing a quartz core surrounded by a porous fayalite glassy matrix. 247

Fig. 9. 4 shows the proximity between the archaeological site of Orti Bottagone and its closest mining area in Campiglia Marittima, situated around 12 km north. 248

Fig. 9. 5 Optical micrographs showcasing round-shaped Cu-Fe sulphides high in copper (blue) and high in iron and sulphur (yellow) observed a) in the experimental slag JH1A_T3_003 (scale bar 100µm) and b) in the flat slag ORTB 13 (scale bar 200µm). 253

Fig. 9. 6 Optical micrographs showcasing a wedge-shaped feature observed (a) in the experimental slag JH1BT2_002 (scale bar 100µm) and (b) in the coarse slag ORTB 20 (scale bar 200µm). 254

Fig. 9. 7 BSE micrographs of (a) the experimental sample JH2B_T1_002, and (b) the flat slag ORTB 8 showing the almost perfect match of the morphologies.254

Fig. 9. 8 BSE micrograph of a region of the experimental slag JH2B_T1_002 highlighting abundant trapped Cu-bearing features (white).256

Fig. 9. 9 Visual representation of diverse features of copper at various stages of transformation (white), illustrating the step-by-step accumulation of copper during the experimental 30-minute smelting process. (a) sample JH2A_T3_001; b) sample JH2B_T2_001; c) and d) sample JH2B_T2_001).257

Fig. 9. 10 Comparison of BSE micrographs: (a) experimental sample JH2A_T3_001, and (b) an archaeological sample from Roussignole (Ambert et al., 2013, p. 67, 6), revealing analogous mineralogical phases. Both images depict metal droplets (3) embedded in a highly viscous silicate matrix (1) alongside unreacted silica (2) within the slag.257

Fig. 9. 11 Optical micrographs showing matte regions, distinctly separated from the slag matrix, predominantly positioned at the outer boundaries of the slag samples; a) sample JH1A_T2_003 (scale bar 250µm), b) sample JH2B_T2_001 (scale bar 250µm).259

Fig. 9. 12 illustrates a) a BSE and b) a SE micrograph of two samples from trial JH1B_T3 revealing the deceptive morphology, consisting of elongated fayalitic structures that can be misleadingly mistaken for flat slag inclusions.260

Appendix C

Fig. C. 1 depicts fayalitic crystallized polyhedral grains, featuring cubic to prismatic crystals. Notably, the grains exhibit larger dimensions in the core (d left) and smaller dimensions toward the surface (d right), suggesting variations in cooling rates. Samples: a) ORTB 12, b) ORTB 19, c-d) ORTB 20.315

Fig. C. 2 illustrates distinctive fayalitic crystallized structures featuring hoppers-like morphologies. Sample: ORTB 16.316

Fig. C. 3 illustrates distinctive fayalitic crystallized features, showcasing small elongated dendritic needles in a fayalitic matrix. Sample: ORTB 8.316

Fig. C. 4 highlights distinctive fayalitic crystallized features, presenting large chain structures. Samples: a) ORTB 16, b) ORTB 20, c) ORTB 5, d) ORTB 8.317

Fig. C. 5 showcases a series of BSE micrographs revealing diverse iron-rich spinel morphologies/phases identified in the slags. This includes euhedral crystals, ranging from cubic to prismatic (a), dendritic growths (c, d), and round features (b, d), all embedded in a fayalitic matrix. Samples: a) ORTB 8, b) ORTB 19, c) ORTB 8, d) ORTB 5..... 318

Fig. C. 6 Optical micrographs showing a range of compositions and morphologies found in the brown ore sample: semi reacted pyrrhotite (bright yellow) and chalcopyrite (gold yellow) in a matrix of iron hydroxides (mid-grey) and quartz (dark grey). Sample: ORTB 3..... 319

Fig. C. 7 Variations in copper-iron sulphide reactions depicted at different stages: remnants of chalcopyrite (yellow) displaying minimal bornite exsolutions (orange), intricately captured within a fayalitic matrix. Magnetite is also present as squared inclusions (a) and a continuous rim (b). Sample: ORTB 6..... 320

Fig. C. 8 round-shaped recrystallized compounds characterised by covellite-like (blue) and chalcocite-like (greyish) compositions. Sample: ORTB 8..... 320

Fig. C. 9 illustrates recrystallized compounds with covellite-like (blue) and chalcocite-like (greyish) compositions. Yellow compounds denote partially reacted chalcopyrite. Covellite, characterized by its deep blue to indigo colour, derives its hue from copper ions in its crystal structure. The colour may exhibit variations within the blue spectrum, influenced by factors such as specific mineral samples and impurities. Samples: a) ORTB 13, b) ORTB 16, c) ORTB 13, d) ORTB 20, e) ORTB 19, f) ORTB 13..... 321

Fig. C. 10 showcases unreacted chalcopyrite-pyrrhotite (yellow), partially reacted chalcopyrite (yellow orange), and distinct stripes of secondary sulphide exhibiting bornite-covellite composition (blue). Notably, a ring-shaped formation with a covellite-like composition (light blue) is highlighted in Fig. b). Samples: a) ORTB 19, b) ORTB 12..... 322

Fig. C. 11 presents a) a chalcopyrite-dominant area featuring b) the exsolution of bornite (pinkish brown) and partially oxidized bornite (sky blue), accompanied by a covellite prill (light blue). Sample: ORTB 19..... 322

Fig. C. 12 displays four optical micrographs illustrating four distinct stages of copper formation: a) a round-shaped prill with a small pure copper core (orange) surrounded by recrystallized digenite (bluish grey), b) a round-shaped prill with a larger pure copper core (orange) encircled by a ring of recrystallized digenite (bluish grey), c) a pure copper prill with recrystallized digenite or chalcocite extrusion, and d) pure copper prills. Samples: a-b) ORTB 8, c- d) ORTB 5..... 323

Fig. C. 13 presents optical micrographs capturing the evolution of copper phases through post-depositional growth. Newly developed phases of copper hydroxides (e.g., $\text{Cu}(\text{OH})_2$, and $\text{CuCl}_2 \cdot 2\text{H}_2\text{O}$) are observed filling the empty spaces left in the slag matrix.. Samples: a) ORTB 20, b) ORTB 6, c-d) ORTB 26. 324

Fig. C. 14 displays a series of Optical (a) and BSE (b-d) micrographs of quartz inclusions identified. Samples: a-b) ORTB 6, c-d) ORTB 5. 325

Fig. C. 15 displays a series of SEM (a-c) and optical (d) micrographs showing a) relics of calcium carbonate as inclusions in a fayalitic glassy matrix; b) relics of calcium carbonates found as inclusions in a fayalitic glassy matrix; c) quartz and Ca inclusions; d) semi-reacted inclusion of a possible Ca carbonate. CaO is the main compound in the grey rim. Samples: a) ORTB 13, b-c) ORTB 20, d) ORTB 9. 326

Fig. C. 16 presents a series of BSE micrographs depicting diverse morphologies observed in the experimental slags: a) elongated hoppers and b) primary dendritic olivine (light grey) in a fayalite matrix (grey); c-d) Ca-rich dendritic structure with magnetite euhedral crystals (light grey) in a fayalite matrix (grey). Copper at an intermediate stage of transformation is also shown (white); e-f) chain olivines and dendrites (dark grey) with a lot of tiny iron oxide phases (white) in a fayalitic matrix (grey). Samples: a-b) JH2B_T1_002, c-d) JH2B_T2_001, e) JH2B_T1_002, e-f) JH2A_T1_001. 327

Fig. C. 17 showcases a collection of optical micrographs highlighting diverse compositions and morphologies of copper-iron sulphides within the experimental samples. A spectrum of colors, shapes, and chemical compositions is evident: a-b) Partially reacted chalcopyrite (gold yellow) within a matrix of iron oxides (mid-grey) and quartz (dark grey). c) Wedge-shaped partially reacted Cu-Fe sulphide situated between two converging pyroxene dendritic structures, indicating an incomplete process that prevented Cu-Fe sulphides from migrating out of the slag. d) Irregularly shaped partially reacted Cu-Fe sulphide within a matrix of iron oxides. e-f) Elongated and round-shaped partially reacted Cu-Fe sulphide and recrystallized compounds with covellite-like (blueish) and chalcocite-like (greyish) compositions. g-h) Partially reacted copper sulphide, possibly carrollite, in a matte (g) and fayalitic matrix (h). i-l) Round and elongated pure copper prills. Samples: a-b) JH1B_T1_001, c-d) JH1B_T2_002, e-f) JH1A_T3_003, g-h) JH2B_T2_001, i) JH2A_T3_002, l) JH1A_T3_001. 329

Fig. C. 18 presents a sequence of BSE micrographs illustrating the step-by-step accumulation of copper throughout the experimental 30-minute smelting process. The images depict the diverse features that copper assumes at various stages of transformation, highlighting the continuous increase in copper accumulation (light grey and white). Samples: a) JH2A_T3_001, b) JH2B_T2_001, c-d) JH2B_T2_001, e) JH2B_T1_001, f) JH2B_T1_002. 330

Fig. C. 19 presents optical micrographs (a-c) and a BSE micrograph (d), illustrating the distinct separation of the matte area from the slag matrix, predominantly observed toward the outer edges of the slag. Samples: a) JH1A_T2_003, b) JH1B_T2_002; c) JH2A_T3_001, d) JH1B_T3_001. 331

Fig. C. 20 presents a series of BSE micrographs showing a) the two main chemical compositions detected in the matte fragments: 1) Cu-Fe sulphide high in copper and iron (white) and 2) Cu-Fe sulphide high in sulphur; b) the copper prills (bright white) and cavities circular/elliptical vesicles entrapped in the matte. Samples: a) JH2A_T1_001, b) JH2A_T3_002. 332

Fig. C. 21 presents optical micrographs capturing the emergence of newly developed phases, including copper hydroxides (e.g., $\text{Cu}(\text{OH})_2$) and $\text{CuCl}_2 \cdot 2\text{H}_2\text{O}$. Stalagmitic masses featuring copper carbonate radiating crystals are observed, having found space to grow within the cavities/voids of the matte fragment. The presence of water, whether due to humidity in storage or residual water from the sample preparation, facilitated chemical precipitation. Sample: a-b) JH1A_T1_001. 332

Fig. C. 22 illustrates a series of optical micrographs (a-c) and a BSE micrograph (d) displaying quartz inclusions in various phases of the experimental slags. Samples: a) JH1B_T1_001, b) JH1A_T3_003, c) JH1A_T2_001, d) JH2A_T3_001. 333

Fig. C. 23 illustrates a) a BSE and b) a SE micrograph of two samples from trial JH1B_T3, revealing elongated fayalitic structures that might be mistakenly interpreted as flat slag inclusions. Some of these inclusions may initially appear as remnants of flat slags. However, upon closer examination, they reveal themselves to be elongated structures with a composition resembling fayalitic minerals and quartz. This information holds significant value, potentially influencing the interpretation of archaeological findings and rectifying any potential misconceptions that could mislead scientists when analysing similar features in archaeological materials. Samples: a) JH1B_T3_001, b) JH1B_T3_002. 334

Fig. C. 24 illustrates two distinct occurrences of charcoal in the experimental fragments: a) depicts the typical structure of a charcoal fragment that remained entrapped on a matte fragment, while b) reveals negative traces in the form of voids left from the deterioration or burn of a charcoal fragment. Samples: a) JH2B_T2_001, b) JH2A_T1_001 334

List of Tables

Chapter 2

Table 2. 1 Main silicate and oxide compounds (simplified formulas) observed in early copper smelting slags. Adapted from Hauptmann 2020:257, Table 5.4.	50
Table 2. 2 List of the copper-bearing compounds known.	54

Chapter 3

Table 3. 1 Comparative chronological Tables showing the relative and absolute chronology of the Italian Peninsula, northern and southern France, Serbia, Bulgaria, Romania, the Iberian Peninsula, and the British Isles. Relative references are provided in the text.	65
--	----

Chapter 5

Table 5. 1 Overview of the samples analyzed in this thesis, including the macroscopic features observed and the corresponding analyses performed. Only the cross-sections of the samples that underwent full investigation are depicted.	126
Table 5. 2 Summary statistics for the density (ρ) values measured on the Orti Bottagone slag samples. Scale g cm^{-3} . Count = total number of slags for each group; SD = Standard Deviation; Min. = minimum; Max. = maximum; LQ = lower quartile; UQ = upper quartile; IQR = range interquartile.	131
Table 5. 3 Portable X-ray Fluorescence (pXRF) Analyses of Orti Bottagone Slags. The reported values represent the average of three analyses, with results presented in oxides (ox%). Elements marked as b.d.l. (below detection limits) were not detectable by the analytical method used.	133
Table 5. 4 XRD analytical results showing slags principal mineralogical phases, normalised, expressed in weight percentages ($\text{wt}\%$) and calculated with the Rietveld refinement method. Values reported as b.d.l. (Below Detection Limits) indicate that the concentration of the corresponding phase or compound was below the detection threshold of the analytical method. Phases: Qz = Quartz, Cr = Cristobalite (quartz polymorph), Ol = Olivine, Px = Pyroxene, Sp = Spinel, Cb = Carbonate	140

Table 5. 5 Average chemical composition of the Fe-silicate phases of the slag samples determined by SEM-EDS. The values reported are averages of 7 to 22 analyses of each sample. Large metallic and sulphide inclusions were excluded from the analyses. All elements are presented as oxides for comparison with the literature. 151

Table 5. 6 presents the key information of two potential crucible fragments identified through the non-invasive investigation of the assemblage. 158

Table 5. 7 Bulk chemical compositions and their averages of ceramic and bloated areas. Results are reported as oxides. 164

Chapter 6

Table 6. 1 Overview of the primary parameters utilized in the roasting experiments conducted in this thesis. 177

Chapter 7

Table 7. 1 details the parameters utilized by Bourgarit and Mille (1997, 2001) in both their laboratory and field experiments. 200

Chapter 8

Table 8. 1 Principal copper-bearing deposits of Central Italy (revised from Dolfini et al., 2020, p. 13, Table 3). 214

Table 8. 2 shows an overview of the amount of material collected before and after the beneficiation process from three different locations. I stopped the selection/beneficiation of the batch from Temperino (location 2) for its high amount of lead which would have not provided a useful comparison. This batch was not used for any of the following experiments (*). 217

Table 8. 3 Overview of weather conditions during the experiments. 219

Table 8. 4 Summary of the results of the trials divided by phase. 222

Table 8. 5 Summary statistics for the density (ρ) values measured on the experimental samples. Scale g cm^{-3} . Count = total number of slags for each group; SD = Standard Deviation; Min. = minimum; Max. = maximum; LQ = lower quartile; UQ = upper quartile; IQR = range interquartile.....	223
--	-----

Appendix A

Table A. 1 displays the results of the SEM-EDX area analysis (500X) conducted on a certified reference material (SGT11) to assess accuracy and precision. SGT11 is a green soda-lime-silica container glass provided by The Society of Glass Technology. Note: BaO (0.03 wt%) and Cr_2O_3 (0.2 wt%) were not measured. Oxide compositions are presented in wt%.	298
--	-----

Appendix B

Table B. 1 displays the SEM-EDX chemical compositional analyses of the archaeological slags from Orti Bottagone. Three random scans, each covering an area of approximately 1 mm^2 , were conducted for each slag. These analyses are graphically depicted in the FeO– Al_2O_3 – SiO_2 (wt%) and FeO–CaO– SiO_2 (wt%) ternary systems (see Fig. 5. 12 Ternary plot diagram (FeO– Al_2O_3 – SiO_2 (wt%) slag system) of the average composition of the three areas analysed.). It's important to note that for the sake of simplifying the analysis, all elements have been designated as oxides, although it is recognized that certain oxides, such as SO_3 , P_2O_5 , may not be present in the samples. For a more detailed discussion, please refer to Section 4.2.8. 'b.d.l.' has been used to indicate values that are below the detection limit of the instrument. This notation reflects instances where the concentration of the element was too low to be accurately quantified.....	299
--	-----

Table B. 2 displays the SEM-EDX chemical compositional analyses of both coarse and flat specimens, which have been graphically represented in the Cu-Fe-S ternary diagram (see Fig. 5. 18). The data are reported in weight percentage (wt%) rather than oxides (ox%), before being normalized to 100% for representation on the ternary diagram. 'b.d.l.' has been used to indicate values that are below the detection limit of the instrument. This notation reflects instances where the concentration of the element was too low to be accurately quantified. .	301
--	-----

Table B. 3 displays the SEM-EDX chemical compositional analyses of the experimental slags. Three random scans, each covering an area of approximately 1 mm^2 , were conducted for each slag. These analyses are graphically depicted in the FeO– Al_2O_3 – SiO_2 (wt%) and FeO–CaO– SiO_2 (wt%) ternary systems (see Fig. 8. 15). It's important to note that for the sake of simplifying the analysis, all elements have been designated as oxides, although it is recognized that certain oxides, such as SO_3 , P_2O_5 , may not be present in the samples. For a more detailed discussion, please refer to Section 4.2.8. 'b.d.l.' has been used to indicate values that are below the detection limit of the instrument. This notation reflects instances where the concentration of the element was too low to be accurately quantified.....	306
---	-----

Table B. 4 displays the SEM-EDX chemical compositional analyses of the experimental specimens, encompassing both slags and matte fragments. These analyses are graphically depicted in the Cu-Fe-S ternary diagram (see Fig. 8. 19). The data are reported in oxides (ox%) and were subsequently transformed to weight percentage (wt%) before being normalized to 100% for representation on the ternary diagram. 'b.d.l.' has been used to indicate values that are below the detection limit of the instrument. This notation reflects instances where the concentration of the element was too low to be accurately quantified.. 309

Appendix D

Table D. 1 In the following table a comprehensive and up-to-date overview of the techniques of slags investigation (both archaeological and experimental) employed over the past two decades. This includes both the well-established methods and those still in the nascent stages of development for this type of investigation. For description of the techniques refer to the references in the last three rows of the table. See the end of the table for explanations of techniques acronyms. 335

Chapter 1. Introduction

1.1. Background and significance

Copper has long been a central subject of early metallurgical studies due to its assumed pivotal role in shaping the development of élites in Old World prehistory (Kienlin et al., 2009; Stanley-Smith, 1975; Thornton & Roberts, 2009, Wertime, 1968, 1973). Previous research has predominantly concentrated on the study of copper objects, as they are relatively well-preserved and hold contemporary value associated with metals (Thornton & Roberts, 2009). However, these studies have largely focused on typological or archaeometric approaches, providing insights into only a limited part of the *chaîne opératoire*. While these approaches have yielded valuable information, particularly related to provenance (via isotopic fingerprinting) and elemental composition (alloying practice) (Roberts & Thornton, 2014 and references therein), they offer limited insights into the various stages of the technological process, which are influenced by different and complementary factors (Lemonnier 1986, 1993; Webley et al., 2020). Therefore, it is crucial to analyze and isolate each step of the technological process to gain a deeper understanding of copper production.

In recent years, metallurgical slags, which are residual materials generated during the smelting process, have emerged as valuable sources of technological information. Despite their initial disregard, in the last 20 years, slags have gained recognition as a significant focus of research (Bourgarit, 2019; Hauptmann, 2014, 2020; Martínón-Torres, 2018). Slags contain recorded information about the composition of the initial charge, presence of fluxing agents, temperatures and redox conditions within the smelting reactor, as well as metal yields. This data enables the reconstruction of specific processes carried out in a specific context, thereby providing insights into socio-cultural dynamics and knowledge transfer across regions.

Over the past two decades, the conventional linear evolution of prehistoric Old-World metallurgy has been challenged. Recent research has revealed a more intricate and multifaceted narrative. The traditional belief that copper technology progressed linearly, transitioning from working native copper in the Neolithic, to the small-scale smelting of copper oxide ores in the Chalcolithic, culminating in the large-scale reduction of copper sulphides during the Bronze Age, has undergone re-evaluation (Charles, 1980; Craddock, 2000; Hauptmann et al. 1993;

Muhly 1988; Wertime, 1973). While this sequence remains relevant in a broader historical perspective (Thornton, 2009, p. 303), recent research has helped to paint a richer and more diverse picture. Instances of sulphide ores found in Chalcolithic European sites such as Milland and Gaban in the Italian eastern Alps, Al Claus in the French south-western Alps, and La Cenuela in south-eastern Spain offset regions that still relied on oxides such as Los Millares, Almizaraque and Cabezo Juré in south-eastern Spain, or a combination of sulphide-oxide ores such as Dolnoslav in eastern Bulgaria, Brixlegg in the Italian eastern Alps and Cabrières in the French south-western Alps (Artioli et al., 2015; Bourgarit, 2007; Thornton, 2009). Nonetheless, even as a broad sequence emerges, the specific mechanism driving the transition from oxide to sulphide ore reduction remain elusive.

Amidst this intricate backdrop, the early 4th millennium BC metallurgical remains unearthed at the site of Orti Bottagone hold great significance in our quest to understand prehistoric metalworking practices and investigate this pivotal transition. The site occupies a unique position at the crossroads of oxide and sulphide technology, both chronologically and geographically. Chronologically, Orti Bottagone straddles key periods, with the 5th millennium BC in the Balkans primarily characterised by oxide technology (Radivojević & Roberts, 2021), while the late 4th and 3rd millennia BC in the rest of Europe witness the widespread adoption of sulphide technology (Ambert et al., 2013; Bourgarit, 2007; Höppner et al., 2005; La Duc et al., 2022). Regarding its geographical significance, the Italian peninsula stands out as a central driver of this technological shift (Dolfini, 2013, 2014). Recent findings suggest that substantial advancements in this transition did not occur in the Alps until the late 4th early 3rd millennium BC (Dolfini *et al.*, 2020). Consequently, Tuscany appears to have served as a stepping stone where this technological transmission was refined and likely diffused to northern and western regions (Dolfini, 2023). Situated precisely at this crucial juncture of transition, the site of Orti Bottagone offers an unparalleled opportunity to shed new light on this phenomenon like never before.

The results of this study revealed a rather intriguing aspect of copper production. It appears that, at the site of Orti Bottagone, copper was obtained from sulphide-rich charges. The experimental reconstruction of the smelting process carried out using local sulphide minerals, suggests that sulphide ores might have been smelted in a one-step process, bypassing the traditional need for roasting the ore before feeding it to the furnace. This insight demonstrates that copper sulphide smelting could have occurred at the initial stages of metallurgy under conditions that, while admittedly inefficient, successfully transformed the ore into metal.

To contextualise this discovery, similar smelting processes have been identified nearby. For instance, at the neighbouring site of San Carlo Cava Solvay, Artioli *et al.* (2016) documented a comparable method of copper production from sulphide-rich ores, albeit slightly later in date. This finding provides additional support for the feasibility of such practices during this period. It is also essential to acknowledge the groundwork that preceded this study. Preliminary results from samples collected at Orti Bottagone were initially explored by Artioli *et al.* (2009). These early findings hinted at the presence of sulphide smelting, sparking the curiosity that eventually led to this comprehensive investigation.

This disclosure not only highlights a partially uncharted technological approach but also underscores its potential significance in the transition from oxide/carbonate to sulphide smelting in prehistoric Europe. Despite relying on evidence from a single site, these thesis' results, along with the supporting evidence from San Carlo and the preliminary results by Artioli and colleagues, significantly contributes to a broader comprehension and potential reshaping of technological evolution in western Europe during the Final Neolithic period (3800-3600 BC).

1.2. Aims and research questions

This PhD thesis focuses on the study of residual products from smelting activities at the Final Neolithic site of Orti Bottagone, southern Tuscany (Italy), dating to the early 4th millennium BC. The overarching goal is to understand the smelting technology employed by prehistoric smiths during this period. Of particular interest is their ability to successfully smelt sulphide ores, a practice that was relatively uncommon at a time when most smiths were primarily engaged in the reduction of copper oxides and carbonates. This proposal is based on the examination of evidence from a single site, positioned at the initial phase of a significant regional sequence. The study combines experiments and analyses of archaeological and experimental data using archaeometric techniques to shed light on the early smelting sulphide technology.

This project aligns perfectly with the call made by Timberlake (2007, p. 35), and Dolfini (2014, p. 44), who claimed that more targeted projects on aspects of metal technology combining experimental archaeology and archaeometallurgy needs to be carried out in order to reach a more holistic understanding of the interaction between metals and societies.

Additionally, this thesis seeks to address a significant gap in current research by compiling a comprehensive catalogue of micrographs featuring both experimental and archaeological by-products from ancient smelting processes. This resource will offer scholars unrestricted access

to a valuable reference database, enhancing their understanding of ancient metallurgical by-products, smelting techniques, and contributing to broader knowledge in the field. Similar efforts were recently undertaken by Rademaker (2015) in the study of crucible technology, making it worthwhile to consider applying a similar approach to investigate smelting slags.

This thesis has two primary research objectives.

Objective 1: Characterise the copper reduction technology used at the Final Neolithic site of Orti Bottagone by addressing the following questions:

- Were sulphide ores employed in conjunction with oxides and carbonates, or was the ore usage primarily centred around sulphides?
- What are the types of slags produced? Can they be attributed to specific smelting stages within the overall metallurgical process?
- Is there evidence of intentionally added fluxes, or were self-fluxing ores smelted?
- What parameters (temperatures, reducing /oxidising conditions) were employed?
- Are there any traces of arsenic (As) and/or antimony (Sb) in the slags and in the crucible fragment?

Objective 2: Investigate the smelting of sulphide ores in the early stages of metallurgy, which has generated diverse opinions and conflicting theories within the field of archaeometallurgy (P. T. Craddock, 2000; Rostoker et al., 1989; Thornton & Roberts, 2009; Timberlake, 2007). To achieve this, experiments were conducted to reconstruct the smelting process carried out at Orti Bottagone, focusing on the feasibility of a one-step smelting process without intermediate roasting and without using a crucible to hold the charge. Two series of experiments one with partially roasted and the other with unroasted initial charge, were carried out aiming to answer the following questions:

- Is the local ore suitable for smelting without the addition of carbonates/oxides, or the deliberate addition of fluxes, utilising a one-step process (i.e., without roasting)?
- Can we ascertain whether the by-products of the smelting experiments resemble to the archaeological ones, and if such resemblance exists, which experiments and phases yield slag materials that exhibit a greater degree of similarity?

- Which smelting technique proposed in the literature, if any, best fits the experimental residues produced?

Furthermore, while not the central emphasis in this second part of the thesis, prior experiments supporting its viability, I explore smelting using local ore without the use of a crucible.

1.3. Methodology and theoretical approaches in Archaeometallurgy

In the field of archaeometallurgy, the integration of robust methodological approaches and theoretical frameworks is essential for reconstructing ancient metallurgical practices and understanding their broader social and technological implications. This section outlines the key methodology and theoretical perspectives that underpin the analysis of copper smelting technology at the Final Neolithic site of Orti Bottagone. By combining archaeometric analysis with experimental archaeology, this research not only seeks to identify the specific techniques employed by prehistoric metalworkers but also to situate these practices within a larger framework of technological evolution and craft production.

1.3.1. Theoretical frameworks in Archaeometallurgy

A central theoretical concept employed in this study is the *chaîne opératoire*. Originally articulated by Leroi-Gourhan (1943) and later expanded by Pfaffenberger (1992), consists of the logical sequence of stages in a technological process from raw material extraction to final product. This concept is pivotal for understanding how different stages of production—whether in the extraction of ores, smelting processes, or metalworking—are interconnected and influenced by social, economic, and environmental factors. In the context of metal production, the *chaîne opératoire* can be broadly divided into primary and secondary metallurgy. Primary metallurgy involves the extraction of raw materials and their subsequent refinement, resulting in the production of ingots or matte, while secondary metallurgy focuses on creating the final objects (Fig. 1.1). Some scholars, including Webley et al. (2020), propose additional stages to this framework. They identify a third stage that encompasses smithing and finishing processes, such as hot and cold working, which further shape and strengthen the metal and then a final stage is characterized by the use, reuse, and recycling of metal objects, including repairs and modifications over the course of their lifecycle. By examining these stages, we can discern the interplay between technology and society, illustrating how technological practices can both shape and be shaped by cultural dynamics. Lemmonier (1993b) emphasized that the *chaîne opératoire* not only involves technical procedures but is also dynamically influenced by the socio-cultural contexts in which these technologies are embedded. Moreover, it is essential to

recognize that techniques are social productions; while technical processes must operate within the physical constraints of matter, the knowledge surrounding these technologies encompasses a broader spectrum. This includes a mixture of ideas, beliefs, and symbolic systems that extend beyond mere material considerations and economic value. Such symbolic frameworks are crucial when addressing how technologies are conceived, developed, and produced in a specific context. The anthropological approach to technology plays a vital role in this discourse, as it sheds light on how societies adapt and innovate within their material environments.

In the context of Orti Bottagone, the application of the *chaîne opératoire* provides a systematic framework for analyzing the copper reduction technology, shedding light on the significance of each technological decision made by ancient smiths. This approach not only unveils the technical processes involved but also offers a window into the social contexts in which these technologies were developed (Miller, 2005; Hauptmann, 2020, Chapter 5). Through this dual lens of technical analysis and social understanding, the study of copper smelting at Orti Bottagone becomes a means of exploring both the material and cultural dimensions of early metallurgy.

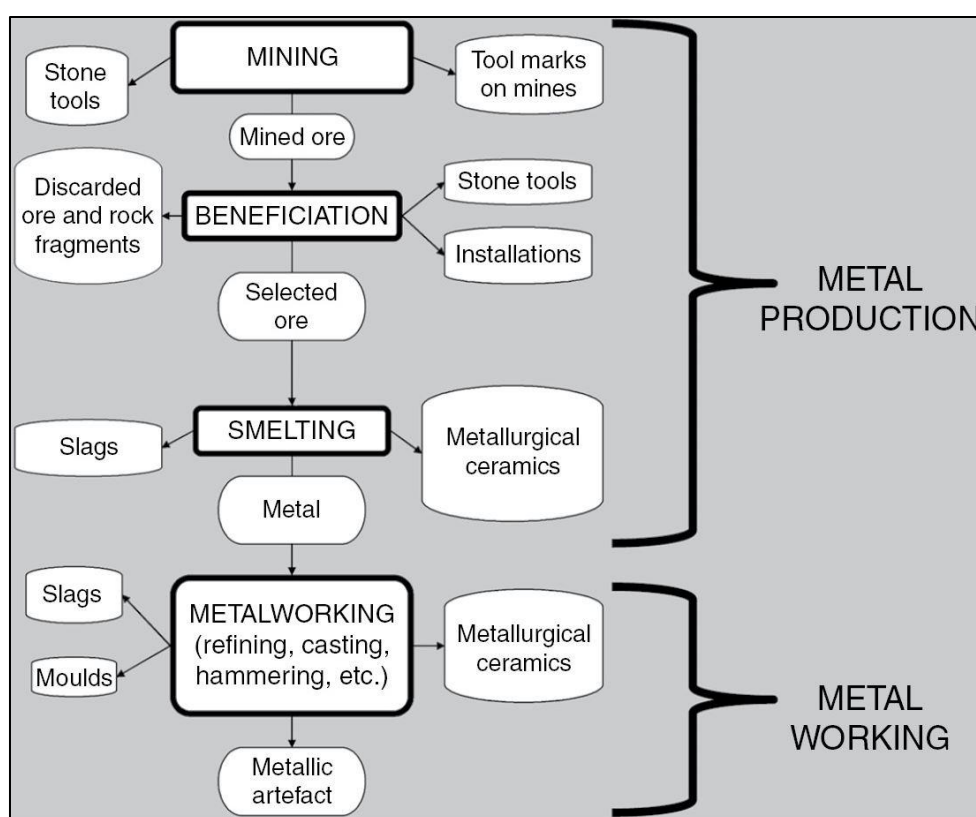


Fig. 1.1 Simplified *chaîne opératoire* showing the logical sequence of the steps necessary for the production of metal artifacts (from Georgakopoulou, 2016, pp. 47, 4.1)

1.3.2. Methodological approach

To address the research questions posed in this thesis, I have adopted a multi-analytical approach that combines materials science and experimental archaeology. I conducted analyses on various samples, which include both archaeological specimens (such as slags and a crucible fragment) and experimental specimens (comprising slags and matte fragments) using a combination of the most common techniques adopted in the field for slag and crucible characterization (see Appendix), namely:

- Optical and Digital Microscopy (OM and DM)
- X-ray Powder Diffraction (XRD)
- X-Ray Fluorescence (pXRF)
- Scanning Electron Microscopy coupled with Energy Dispersive X-Ray Spectrometry (SEM-EDX)

However, it is essential to emphasise that, as Pryce (2009) has pointed out, these archaeometric techniques alone have inherent limitations when it comes to offering a complete understanding of the prehistoric smelting process. To overcome these constraints, the second part of my research shift its focus to the experimental approach. Specifically, I concentrate on replicating the ore reduction technology employed at the early 4th millennium BC site of Orti Bottagone. Experimental archaeology, particularly within the field of archaeometallurgy, has been widely recognised as an essential tool for testing scholars' understanding of the technological aspects involved in ancient metallurgy. As a core component of this research, I conducted a series of targeted experiments involving the roasting and smelting of copper sulphide ores, which I personally gathered from the presumed local mining area. The aim of the experiments was to delve deeper into comprehending the technical choices and constraints faced by ancient smiths and to gain insight into the methods employed by local smiths in smelting their sulphide ores. It is important to clarify that the experimental approach I employed in this research serves as an analytical tool aimed at deducing specific pieces of information. It should not be seen solely as an experiential device for reproducing the entire process as a single event to test its feasibility or to determine copper production rates.

1.3.3. Integration of Theory and Methodology

The integration of these theoretical and methodological approaches provides a comprehensive framework for interpreting the copper smelting technology at Orti Bottagone. The experimental results not only offer practical insights into the feasibility of one-step smelting without roasting but also allow for a critical evaluation of existing theoretical models, such as those proposed by

Rostoker et al. (1989), Craddock (2000) and Bourgarit (2007). By comparing the experimental by-products with the archaeological specimens, this research identifies key similarities and differences that contribute to the ongoing debate about the technological transitions from oxide to sulphide smelting.

Furthermore, this study has broader implications for understanding the transmission of metallurgical knowledge across regions. The site of Orti Bottagone, positioned at a crossroads of technological change between the Balkans and the rest of Europe, offers a unique perspective on how copper technology evolved and spread. By situating the findings within the larger context of Old World metallurgy, this research sheds light on the mechanisms of technological diffusion and the role of southern Tuscany as a potential intermediary in the broader shift from copper oxide to copper sulphide smelting.

The combination of archaeometric techniques and experimental archaeology, framed within the theoretical constructs of the *chaîne opératoire* and craft production, provides a holistic approach to understanding the copper smelting technology at Orti Bottagone. This methodology not only allows for a detailed reconstruction of the technological processes involved but also situates these processes within the broader socio-cultural dynamics of the Final Neolithic.

1.4. Thesis layout

The thesis is divided into two parts, each dedicated to one of the previously mentioned objectives. The first part focuses on investigating the smelting technology developed at Orti Bottagone. The second part discusses the field experiments based on the analytical results obtained from the archaeological evidence. Overall, the thesis is organised as follows.

Part I. **Chapter 2** offers a concise historical overview of slag analysis, underscoring its significance in the field of archaeometallurgical research. This chapter equips the reader with essential knowledge to understand the nature of slag analysis and comprehend current approaches to research in this field. Subsequently, the focus shifts towards exploring the principal hypotheses concerning Chalcolithic copper smelting technology. **Chapter 3** is divided into two parts. The first part provides a thorough literature review of the existing evidence related to sulphide copper smelting in Europe. This review not only summarises the current knowledge but also identifies research gaps which the thesis aims to explore and address. The second part offers an in-depth overview of the early 4th millennium site of Orti Bottagone, including its geographical and archaeological context. It provides details of the discovery of the

metallurgical assemblage at the site and its significance in the study of early copper metallurgy. **Chapter 4** presents the comprehensive multi-analytical approach employed for this research, which combines materials science and experimental archaeology. It describes the key analytical techniques used, such as Optical and Digital Microscopy (OM and DM), X-ray Powder Diffraction (XRD), XRF (portable XRF), Scanning Electron Microscopy coupled with Energy Dispersive Spectrometry (SEM-EDX), and experimental archaeology. I provide a detailed account of each analytical technique, including its strengths, limitations, and intended applications. This includes an explanation of the sample selection, preparation, data collection process I opted for, as well as the associated analytical procedures. This ensures that the methods are clearly explained and reproducible, enhancing the reliability of the results obtained. The integration of these complementary analytical techniques ensures the acquisition of reliable and comprehensive data, facilitating a robust analysis of the research area. **Chapter 5** presents the results of the analysis of the metallurgical assemblage discovered at the site of Orti Bottagone. It provides insights into the metal technology employed at the site, including the process of obtaining copper from a sulphide charge through a slagging process.

Part II. **Chapter 6** provides an overview of experimental archaeometallurgy, distinguishing in general terms between pilot experiments and scientific experiments, and highlighting their respective importance in the field. Furthermore, the chapter reports the results of my pilot experiments and how they helped to design the experimental setup I used for the remainder of my research. **Chapter 7** comprises two sections. The first provides a comprehensive literature review of the sulphide copper smelting experiments carried out based on the archaeological evidence reviewed in Chapter 3. It outlines the current state of knowledge identifying gaps in the experimental archaeometallurgical field which the second part of this thesis aims to address. The second section critically discusses and provides the reasons of the research questions behind the scientific experiments. **Chapter 8** comprises three sections. The first describes the analytical protocol of the scientific experiments, combining the analytical results from Orti Bottagone's slags and the pilot experiments. The second focuses on the ore collection and beneficiation methods and parameters employed. The third presents the findings, analysis, and interpretation of the data collected from the experiments, addressing the second set of research questions. In the interest of enhancing the comparison, this concluding section adheres to the same structural framework as Chapter 5. **Chapter 9** discusses and contextualises the experimental results within the broader archaeological discourse and addresses any limitations of the research. Finally, **Chapter 10** summarizes the key findings of the research, highlights

their significance in the context of early copper metallurgy, and suggests potential avenues for future research in the study of early metal technology.

The thesis is complemented by four **Appendices**, each serving a distinct purpose. In **Appendix A**, I provide a certified reference material (SGT11) by SEM-EDS (area analysis at 500X) to assess accuracy and precision. In **Appendix B** I present the SEM-EDX analyses of both archaeological and experimental specimens, covering Cu-Fe sulphides and the average compositions of the slags. **Appendix C** features an extensive collection of detailed high-resolution micrographs showcasing mineralogical morphologies and features identified in the analysis of the archaeological and experimental by-products. Each micrograph relates to a description, serving as reference materials for future research. In **Appendix D**, I offer an overview of slag investigation techniques employed over the past two decades. This section encompasses well-established methods alongside those in the early stages of development for this specific type of inquiry. Lastly, in **Appendix E** I summarize the instruments and software employed throughout the thesis.

In the next chapter, I discuss the pivotal role of slag analysis within archaeometallurgical research, emphasizing its historical significance and relevance. Subsequently, the chapter explores prevalent mineralogical phases in copper smelting slags and their formation processes based on the ore deposits exploited. Then, the chapter addresses theories and hypotheses concerning early copper smelting practices, highlighting the challenges of interpreting ancient smelting technologies and the reliability of the archaeological record. The goal is to provide the reader with a foundation for grasping the significance of slag analysis and prepare them for the ongoing research journey that lies ahead.

PART I

Understanding Early Copper Smelting at Orti Bottagone

Chapter 2. The study of pyrometallurgical by-products

2.1. Introduction

This chapter serves as an introductory exploration of slag analysis within the context of archaeometallurgical research. It starts with a concise historical overview, underscoring the pivotal role of slag analysis within the field of archaeometallurgy. Subsequently, the chapter proceeds to elucidate the prevalent mineralogical phases commonly encountered in copper smelting slags, elucidating their formation processes. Following this, attention turns toward a comprehensive examination of the primary copper-bearing ore deposits that ancient smiths presumably used as their initial charges. This section seeks to distil the geological processes underlying the genesis of these ore deposits and meticulously elucidates the principal primary and secondary copper-bearing minerals exploited in the past. Consequently, the chapter explores the principal theories and hypotheses surrounding Chalcolithic copper smelting practices. It raises questions about the reliability of the archaeological record and the challenges of interpreting ancient smelting technologies given the constraints imposed by limited available evidence. The primary aim underscoring this chapter resides in equipping the reader with essential foundational knowledge, requisite for the comprehension of the nature of slag analysis, whilst concurrently setting the stage for the ongoing research.

2.2. Historical overview of slag analysis

Since the late 1960s, researchers have undertaken significant work on ancient metallurgical slags, recognising the hidden potential within these industrial remains. Notable early contributions include the pioneering research conducted by Wertime and his team, which included scientists such as Tylecote, Pleiner and Rothenberg. In 1966 and 1968, they embarked on surveys of early smelting sites in western and central Asia (Wertime, 1968, 1973), marking the initial efforts to create a large-scale map of ancient smelting sites. Their primary objective was to trace the origins of Old-World metallurgy, particularly in the ore-rich Taurus-Zagros highlands (Wertime, 1973).

During the same period, Rothenberg expanded this line of research by mapping and studying copper mines and smelting production sites in location such as Timna, the Sinai Peninsula, and the Iberian Peninsula. His multidisciplinary team included engineers, geoscientist, chemists and metallurgists (Rothenberg, 1972, 1973, 1990; Tylecote, 1992). Concurrently, Morton and Wingrove conducted mineralogical and chemical analysis on bloomery slags from Roman and Medieval periods in England (Morton & Wingrove, 1969a, 1969b, 1972). Similarly, Milton applied a similar analytical protocol to examine slags from Timna (Milton et al., 1976), while Koucky and Steinberg focused on copper slags from Cyprus (Koucky and Steinberg, 1982).

Although these studies provided valuable results, a significant turning point in the study of metallurgical slags occurred with the work of Bachmann, as evidenced in his notable publications (Bachmann, 1978, 198a, 1982b, 1982c; Bachmann & Rothenberg, 1980). Bachmann pioneered a systematic approach to the investigation of metallurgical slags, becoming the first researcher to define the fundamental principles and analytical methods required for identifying the working parameters and, consequently, the *chaîne opératoire* of ancient smelting processes. These methodologies, thoroughly detailed in his seminal work “*The Identification of Slags from Archaeological Sites*” (Bachmann, 1982c), encompass a combination of macroscopic observations and microscopic examination involving mineralogical and chemical-physical analyses.

The aforementioned scholars collectively contributed to the founding of archaeometallurgy as a sub-discipline of archaeology. A common thread among them was their ability to lead interdisciplinary teams, comprising archaeologists, chemical and mining engineers, geochemists, and geologists, and to define archaeometallurgy as an interdisciplinary science that seamlessly integrates analytical techniques with archaeological theory. Their foresight becomes all the more remarkable when considering the prevailing belief during the period (from the 1970s to the 1990s) that archaeologists and material scientists operated in separate fields, seemingly incapable of effective communication. (Jones, 2002, 2004; Knapp, 2000; Leavis, 1962; Martín-Torres & Killick, 2015; Olin, 1982; Snow, 1959).

In the 1980s, a surge of interest in the technological aspects of material culture emerged, driven by the radical perspective of material scientist C. Stanley-Smith. He contended that technologies were intricately entwined with and shaped by social and cultural choices rather than being solely driven by necessity or efficiency thereby shifting the focus towards the social dimensions of technology and the social roles of materiality in understanding ancient societies and behaviours (Stanley-Smith, 1970, 1975, 1981, 1988). Stanley-Smith’s approach,

corroborated by pioneering studies on ceramics (Vandiver et al., 1989), glass (Nicholson, 2007) and metals (Stech, 1990), led to a substantial increase in the application of material sciences techniques, making them indispensable to the study of technology and materiality (e.g., Childs, 1991; Childs & Killick, 1993; Herbert, 1993; Schmidt, 1997). Moreover, advancements in faster, more reliable, and less invasive analytical methods, facilitated by affordable analytical devices, have made collecting and comparing larger quantities of data more accessible, albeit occasionally at the expense of data quality (Killick, 2015).

The last few decades have witnessed an unprecedented proliferation of slag studies, with several researchers conducting significant projects on Chalcolithic and Bronze Age sites across Europe and the Levant/eastern Mediterranean, aiming to reconstruct the social and technological aspects of metallurgical processes. Notable among these is the comprehensive work on early copper metallurgy in the Faynan region southern Jordan by Hauptmann (2007). Suggested by Bachmann, this study was deemed crucial in unravelling the early copper production in the Southern Levant (Bachmann & Hauptmann, 1984). Hauptmann's extensive analysis spans the development of mining and smelting technologies from the 5th millennium BC to the Roman Byzantine period, employing a multidisciplinary approach that combines the most advanced research techniques. Complementary techniques have also been recently employed and are ongoing in the French western Alps (Ambert et al., 2013; Bourgarit et al., 2008; Burger et al., 2010), and in the eastern Alps, Trentino (Addis et al., 2016; Artioli et al., 2009, 2015; Cierny et al., 2004). For slag-specific studies, authors such as Hauptmann (Hauptmann, 2014, 2020, 2007) and Bourgarit (2007, 2019), have recently compiled handbooks and general guides/overview of the techniques and analytical protocols used in the field. For a comprehensive and up-to-date overview of the techniques utilized in the past two decades, encompassing both the well-established methods and those still in the nascent stages of development for this type of investigation, please refer to the Table in Appendix .

2.3. Mineralogy of slags

Slags are residual materials generated during pyrometallurgical activities (Artioli, 2010; Bourgarit, 2007, 2019; Hauptmann, 2014, 2020, 2007). Following Hauptmann's definition of slag as "any metal-containing material that has been fired or melted once" (2014, p. 92) any by-product originated from different stages of the metallurgical *chaîne-opératoire* such as smelting, melting, casting, and refining can be classified as slag. In this thesis, I will specifically refer to by-products generate during ore smelting activities.

Slags are typically formed within reactors, acting as invaluable records of past archaeometallurgical processes (Bachmann, 1982c, p. 3). They encapsulate “frozen” in them information about the original charge, including the type of ore used and the potential addition of fluxing agents, along with details about the technical procedures and working conditions (temperatures and redox conditions) applied in the smelting reactor, as well as metal yields. As extremely resistant to weathering, slags are among the most commonly encountered materials that may be found in proximity to metallurgical sites.

The composition of slags exhibits a wide spectrum, spanning from highly viscous, heterogeneous conglomerates containing unreacted and/or partially reacted materials embedded within a partially molten glassy matrix, commonly referred to as *coarse slags*, to homogeneous assemblages within a completely molten matrix, known as *flat slags* (Bourgarit, 2019, Figure 2). These slags originate from the non-metal-bearing and heat-resistant components of the ore, such as quartz, feldspar and baryte, and may also include substances deliberately added to the initial charge to enhance the outcomes of the extraction processes, such as fluxes.

The ideal slags should exhibit low viscosity and should not contain any metal-bearing phases such as copper, copper oxides, copper sulphides and copper-iron sulphides. This description aligns with the characteristics of modern slags obtained in blast furnaces. However, the reality within ancient smelting reactors is significantly more complex and depends on factors such as the nature of the initial charge, temperature levels, viscosity, and the duration of the process. Early smelting processes rarely achieved liquefaction of the charge. Consequently, a distinct separation of individual mineralogical phases was seldom achieved. This resulted in the retention of refractory phases with high melting points such as quartz (SiO_2 , with a melting point around 1600°C), remaining in the solid state within the slag. Moreover, the high viscosity of early slags prevented the complete settling of liquid phases, such as Cu-Fe sulphides, which have lower melting temperatures. Instead, these liquid phases often became entrapped within the slag.

From a mineralogical perspective, copper smelting slags are typically composed of a variety of minerals, primarily comprising silicate minerals composed of a combination of silica (SiO_2) and a vast array of oxides. Prominently featured among these oxides are FeO, CaO, MgO, Al_2O_3 , and MnO, collectively constituting approximately 80% by weight of the slag’s matrix chemistry (Bourgarit, 2019; Hauptmann, 2014, 2020). It is worth noting that these oxides, rather than being transformed into metal due to the high reducing conditions required, remain trapped within the slags.

Rapid cooling processes contribute to the formation of slags as aggregates of fine-grained mineralogical phases. The primary mineral phases found within slags belong to the silicate category, encompassing olivines, spinels, and pyroxenes, along with clinopyroxenes. In particular, iron-rich olivines such as fayalite (Fe_2SiO_4), spinels like magnetite ($\text{FeO} \cdot \text{Fe}_2\text{O}_3$), and pyroxenes such as hedenbergite ($\text{CaFeSi}_2\text{O}_6$) are commonly encountered. These mineral phases often exist as solid solutions with varying compositions (Table 2. 1). The specific is contingent on the mineral charge and the working conditions inside the system during the cooling process. The type of silicates formed vary influenced not only by the type of initial charge, but also by various factors, including the temperatures reached, the duration required to reach these temperatures, the overall processing time, and the subsequent cooling period. This variation in slag composition mirrors the temperature changes experienced when a substance is heated and subsequently cooled down over time. A simple graphical representation, as shown in Fig. 2. 1, illustrates these temperature fluctuations. On the graph, the x-axis denotes time, while the y-axis represents temperature. The curve initiates at the origin and steadily ascends, symbolizing the heating phase. Upon reaching a peak temperature, it levels off, indicating a period of constant temperature. Finally, the curve descends, marking the cooling phase.

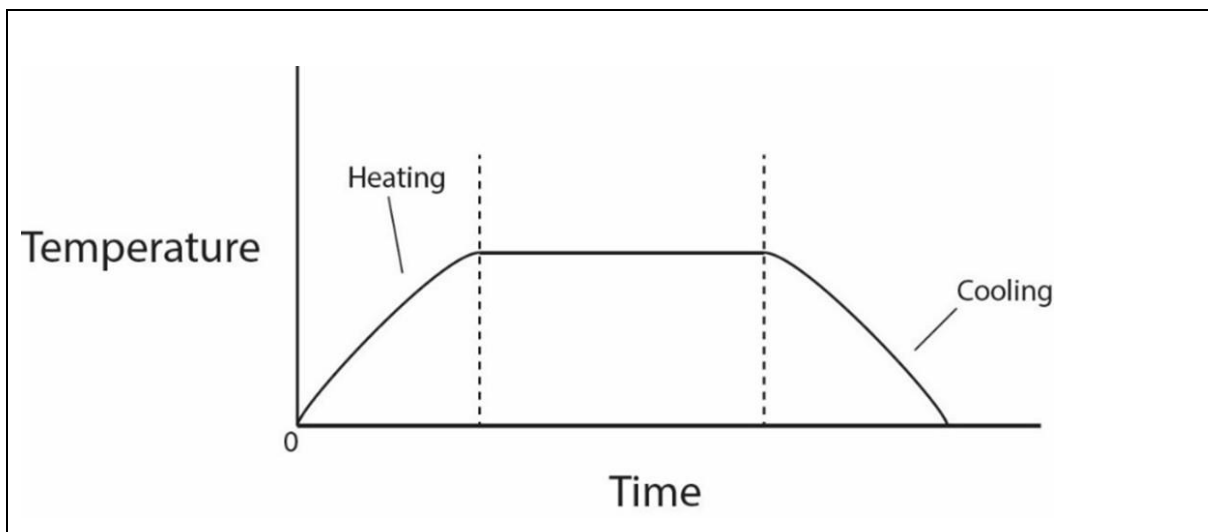


Fig. 2. 1 Chart illustrating a temperature profile chart. It provides a visual representation of the temperature changes that occur throughout the heating and cooling phases of slag formation processes. (Chart by the author).

When subjected to high temperatures, a remarkable separation phenomenon occurs between metal-bearing minerals and gangue. Gangue refers to the non-metallic minerals or materials that are present in the ore but are not of interest to the smelters. These materials are typically separated from the metal during smelting and ended up as part of the slag. Gangue minerals

might include quartz, feldspar, calcite, and other silicates or oxides that were naturally associated with the metal-bearing ore. This separation can be either complete or partial, resulting in the metal settling at the bottom of the crucible while the slags ascend to the surface. In the ideal smelting scenario, when the entire charge reaches a state of complete liquefaction, the force of gravity comes into play. In Fig. 2. 2 I depict the concept of ideal stratification during smelting. In a fully liquid charge, compounds with higher densities, such as copper and copper oxides (e.g., $\rho_{\text{Cu}} = 8.96 \text{ g cm}^{-3}$), are seen to settle at the crucible's bottom. Conversely, less dense components, like silica (SiO_2) and the presence of gas bubbles, have a propensity to move towards the surface. Noteworthy constituents within this smelting environment encompass iron oxides (FeOx), iron silicates (Fa) and quartz (Qz).

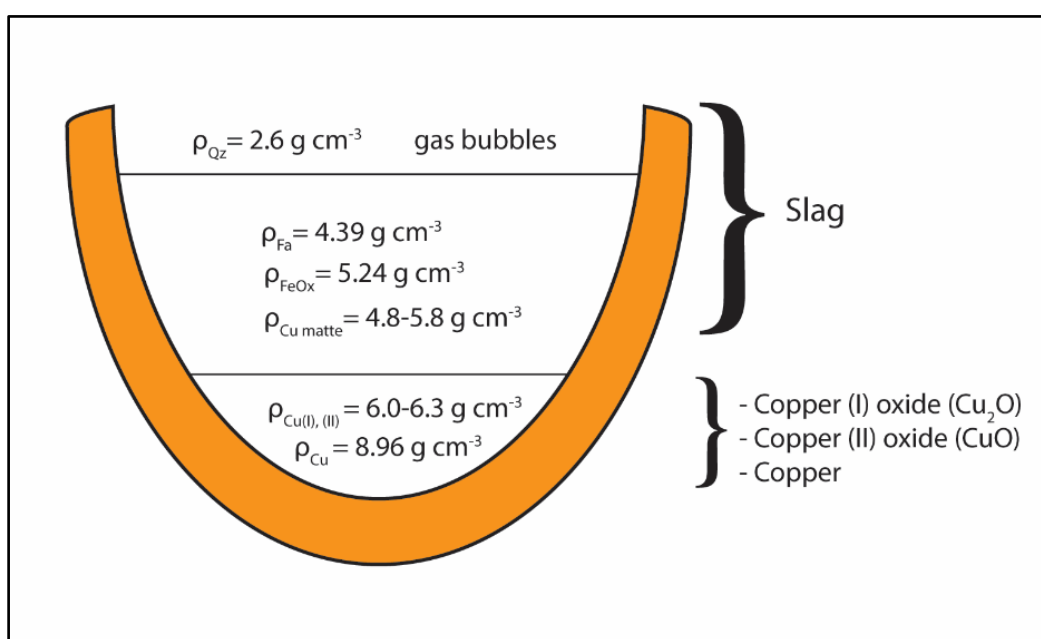


Fig. 2. 2 Simplified model of ideal phase stratification in a crucible/reactor during the smelting process. In an ideal smelting process, in a fully liquid charge the higher density compounds settle at the bottom of the crucible (copper and copper oxides), while the less dense tend to move toward the surface (silica and gas bubbles). Cu = copper, FeOx = iron oxides, Fa = fayalite, Qz = quartz/silica. (Illustration by the author).

In essence, the mineralogical composition of copper smelting slags is a complex interplay of silicate and various oxides, shaped by the unique thermal and chemical conditions of the smelting process. Understanding these mineralogical components is pivotal to unravelling the history and technological nuances of ancient metallurgical practices. To further our understanding of copper smelting processes and slag formation, the next section will concentrate on copper-bearing ore deposits, which ancient smiths likely used for their initial charges. It simplifies the geological processes that lead to the formation of these ore deposits and highlights the primary copper-bearing minerals exploited in the past.

Table 2. 1 Main silicate and oxide compounds (simplified formulas) observed in early copper smelting slags.
Adapted from Hauptmann 2020:257, Table 5.4.

Silicates	
<i>- Olivine</i>	
Fayalite	Fe_2SiO_4
Forsterite	Mg_2SiO_4
Kirschsteinite	$(\text{CaFe})_2\text{SiO}_4$
Knebelite	$(\text{MnFe})_2\text{SiO}_4$
Laihunite (Ferrifayalite)	$\text{Fe}^{2+}\text{Fe}^{3+}_2(\text{SiO}_4)_2$
Merwinite	$\text{Ca}_3\text{Mg}(\text{SiO}_4)_2$
Monticellite	CaMgSiO_4
Tephroite	Mn_2SiO_4
Willemite	Zn_2SiO_4
Iscoreite	$\text{Fe}^{2+}_5\text{Fe}^{3+}_2\text{SiO}_{10}$
<i>- Clinopyroxene</i>	
Augite	$(\text{Ca,Mg,Fe})_2\text{Si}_2\text{O}_6$
Diopside	$\text{CaMgSi}_2\text{O}_6$
Hedenbergite	$\text{CaFe}^{2+}\text{Si}_2\text{O}_6$
Melilite	$\text{Ca}_2(\text{Mg, Al})(\text{Al,Si})\text{SiO}_7$
Gehlenite	$\text{Ca}_2(\text{Al,Mg})(\text{Al,Si})\text{SiO}_7$
Åkermanite	$\text{Ca}_2\text{MgSi}_2\text{O}_7$
Melilite	$(\text{Ca,Na})_2(\text{Mg,Al})\text{Si}_2\text{O}_7$
Andremeyerite	$\text{BaFe}_2\text{Si}_2\text{O}_7$
<i>- Feldspar</i>	
Anorthite	$\text{CaAl}_2\text{Si}_2\text{O}_8$
Celsian	$\text{BaAl}_2\text{Si}_2\text{O}_8$
<i>- Feldsparoide</i>	
Leucite	KAlSi_2O_6
Kalsilite	KAlSiO_4
Wollastonite	CaSiO_3
Mullite	$\text{Al}_6\text{SiO}_2\text{O}_{13}$
Alite	Ca_3SiO_5
Oxides	
Cuprite	Cu_2O
Delafossite	CuFeO_2
Hematite	Fe_2O_3
Periclase	MgO
Cristobalite, Tridymite (quartz)	SiO_2
Magnetite (Spinel in the larger sense)	Fe_3O_4
Tenorite	Cu^{2+}O
Wuestite	FeO

2.4. Weathering and ore formation

Copper can be found in over 150 different mineral compounds. It is rarely discovered in its pure, native metal form but is more commonly bonded with other elements. Depending on its proximity to the Earth's surface, copper-containing minerals are typically found in primary hydrothermal sulphide deposits or in secondary mineralisation in the form of carbonates, hydroxides, and oxidised compounds. A mineral deposit can be schematically divided into two zones: an oxidising zone above the water table and a reducing enrichment zone below it. The upper zone is exposed to atmospheric agents and undergoes a series of processes collectively known as supergene enrichment. The percolation of water, which contains dissolved oxygen and carbon dioxide (CO₂), along with the influence of air, generates acidic solutions that oxidize and chemical weather the superficial primary sulphide deposits. The uppermost and most exposed part, known as gossan or “iron hat”, is characterised by the presence of iron hydroxides (limonite) and sulphuric acids. This zone results from copper iron sulphides leaching their copper metal content into liquid solution that move downward. The copper metal ions in these solutions react to form secondary minerals such as sulphates, hydroxides, and hydroxycarbonates (e.g., cuprite, malachite, azurite).

Once the water reaches the water table, conditions in the lower zone become more reducing. Below the water table, the precipitation of copper liquid solutions interacts with primary mineralisation, leading to the formation of high-grade copper secondary sulphides. This zone is characterised by sulphides such as chalcocite, covellite, bornite, and, in some cases, native copper. The main chemical transformation occurring in these zones are illustrated in Fig. 2. 3.

This scheme provides an idealised representation of the processes involved. However, the geology of metalliferous ore bodies is considerably more intricate, often featuring complex combinations of heterogeneous agglomerates of both primary and secondary mineralisation. For instance, sulphidic minerals can be encountered near the surface or intermingled with secondary mineralisation (Bastian Asmus, 2013; O'Brien, 2015).

Mineral deposits that yield metals for extraction, processing and delivering are termed “ores” (Guilbert & Park, 1986, p. 1). These ores comprise valuable metal-bearing minerals and non-metallic gangue minerals. The significance of a deposit and its classification as an “ore” is culturally determined and fluctuates over time, depending on technological advancements in smelting techniques and the value of the metal at a particular point in history and location (Martín-Torres, 2018). Nowadays, even a deposit with a mere 0.3_{wt}% copper concentration can be economically viable, whereas in the past, only deposits with substantially higher copper concentration rates were deemed worthy of mining. In prehistoric and protohistoric times,

copper mineral deposits with copper concentrations exceeding 20-30_{wt}% were the focus of exploitation, as indicated in Table 2. 2. These exploited ores belonged to various categories, spanning from secondary (hydroxides and carbonates) to primary copper minerals (sulphosalts and sulphides), each possessing distinct characteristics, constraints, and potentials. For instance, secondary minerals are relatively easier to transform, while primary minerals require greater investment and more advanced technological knowledge (Martín-Torres, 2018).

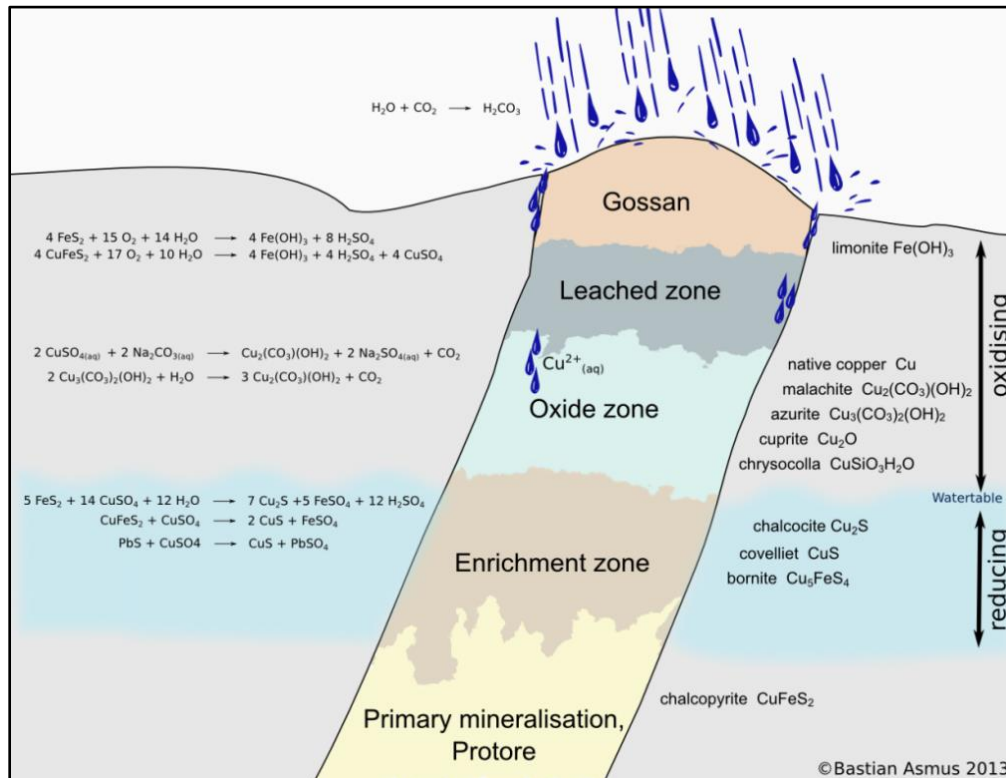


Fig. 2. 3 offers an ideal representation of the weathering processes affecting primary copper-bearing mineralisation (from Bastian Asmus, 2013).

Among the primary copper minerals, chalcopyrite stands out as one of the most prevalent worldwide. It is a copper iron sulphide with the ideal composition CuFeS₂. It has a brassy yellow colour, it contains approximately 34_{wt}% of copper and often occurs alongside pyrite and other sulphide minerals such as fahlore in polymetallic mineral mixtures (*ore-cocktail*). It forms in hydrothermal veins and is associated with porphyry copper deposits. Elements such as Ag, Au, Cd, Co, Ni, Pb, Sn, and Zn may be found in low amounts. Another noteworthy primary copper mineral is bornite (Cu₅FeS₄), often referred to as "peacock ore" due to its iridescent colors. It boasts a high copper content, typically around 63%, making it an important copper

ore. Bornite is often found in hydrothermal deposits and can exhibit vibrant shades of blue, purple, and bronze.

Covellite (CuS) is yet another primary copper mineral with dark blue to black appearance and relatively high copper content, around 66_{wt}%. It usually forms as an alteration product of other copper minerals within the oxidized zones of ore deposits. Its striking blue colour often appears in botryoidal or fine-grained masses. Another primary source of copper is a group of complex sulphosalt minerals, typically consisting of metal (Cu), semi-metal (As or Sb) and sulphur (S). They are known as fahlore or “fahlertz” in the Alpine region. The term was coined by Otto and Witter in the 1952, originally referring to “copper with a higher percentage of trace elements than raw copper (Otto & Witter, 1952). These minerals are distinguished by their elevated levels of arsenic and antimony and relatively low iron content. They are commonly found in association with other minerals containing copper, lead, zinc, and silver (Ixer and Patrick, 2003). The mineral group extends from tennantite - ideal formula $\text{Cu}_{12}\text{As}_4\text{S}_{13}$ - to tetrahedrite - ideal formula $\text{Cu}_{12}\text{Sb}_4\text{S}_{13}$, Tennantite consists of copper (Cu), iron (Fe), and arsenic (As) as its major constituents. It may also contain trace amounts of other elements, including antimony (Sb) and silver (Ag). Tetrahedrite often contains substantial copper content, typically ranging from 30% to 50%. It is frequently found in polymetallic ore deposits alongside other sulphide minerals, and it is valued for its copper, antimony, and sometimes silver content. Due to the variable substitution of copper by iron and zinc, formulas can also be expressed as $\text{Cu}_6[\text{Cu}_4(\text{Fe},\text{Zn})_2]\text{As}_4\text{S}_{13}$ and $\text{Cu}_6[\text{Cu}_4(\text{Fe},\text{Zn})_2]\text{Sb}_4\text{S}_{13}$. Shifting our focus to secondary copper minerals, malachite ($\text{Cu}_2\text{CO}_3(\text{OH})_2$) is one of the most prevalent. It forms as a result of the weathering and oxidation of primary copper sulphides. Malachite's characteristic green colour and distinctive botryoidal or fibrous masses make it a common find in the oxidized zones of copper deposits. Azurite ($\text{Cu}_3(\text{CO}_3)_2(\text{OH})_2$) is another secondary copper mineral with a deep blue colour. It frequently occurs alongside malachite in oxidized copper deposits and forms as a result of the alteration of primary copper minerals. Azurite crystals are well-known for their vibrant blue colour and distinctive crystal habits. Cuprite (Cu_2O) is a red secondary copper mineral that forms as a result of the oxidation of primary copper sulphides. It is composed of copper oxide and often occurs as fine-grained red or brownish-red masses. Cuprite is less common than malachite and azurite but is still an important secondary copper mineral.

Table 2. 2 List of the copper-bearing compounds known.

Mineral name	Chemical formula	Cu (wt%)
Native copper	Cu	99
<i>Hydroxides and Carbonates</i>		
Cuprite	Cu ₂ O	88
Tenorite	CuO	80
Atacamite	Cu ₂ (OH) ₃ Cl	59
Malachite	Cu ₂ (OH) ₂ CO ₃	57
Brochantite	Cu ₄ (OH) ₆ SO ₄	56
Azurite	Cu ₃ (OH) ₂ [CO ₃] ₂	55
Antlerite	Cu ₃ (OH) ₄ SO ₄	53
Chalkanthite	CuSO ₄ .5H ₂ O	25
Chrysocolla	CuSiO ₃ + aq.	30–36
<i>Sulphides and sulphosalts</i>		
Chalcocite	Cu ₂ S	79
Digenite	Cu ₉ S ₅	78
Covellite	CuS	66
Chalcopyrite	CuFeS ₂	34
Bornite	Cu ₅ FeS ₄	63
Cubanite	CuFe ₂ S ₃	23
Enargite	Cu ₃ AsS ₄	48
Tennantite	Cu ₁₂ As ₄ S ₁₃	42–52
Tetrahedrite	Cu ₁₂ Sb ₄ S ₁₃	30–45

2.5. Early copper smelting technology: challenges and interpretations

The presence and quantity of slags in archaeological contexts vary significantly depending on the period and on the context. In the early phases of metallurgy, such as the Final Neolithic and Chalcolithic periods, slags are relatively scarce. This scarcity aligns with the limited scale of metal production during these periods. As we move forward in time to what are considered more advanced “protoindustrial”, spanning from Late Bronze Age to the Late Medieval periods, slags become more abundant, sometimes accumulating in the hundreds of tons.

Impressive slag deposits have been discovered in various regions of Europe, providing invaluable insights into the evolution of metallurgical practices. For instance, in the southwestern Iberian Peninsula, at sites such Corta Lago/Rio Tinto (Blanco-Freijeiro & Rothenberg, 1981; Rothenberg et al., 1981) and on the island of Cyprus in the eastern Mediterranean (Constantinou, 1982, 2012) notable slag heaps have been excavated. Equally remarkable are the slag heaps found at the Late Bronze Age site of Passo del Redebus in the eastern Alps of Italy (Cierny, 2008; Cierny et al., 2004). These deposits, characterised by their substantial

volume, distinctive slag cake formations, and similar mineralogical compositions, have shed light on the entire *chaîne opératoire*, emphasising advanced extractive techniques, mass production, and the standardisation of smelting processes. In these advanced stages, smelting is associated with the reduction of sulphide minerals and the production of matte – an intermediate product, consisting of a mixture of Cu, Fe and S.

Conversely, despite significant advancements in the last two decades (Bourgarit, 2007; Hauptmann, 2020), our knowledge on the early stages of extractive metallurgy remains quite limited. Unlike the technologically efficient and mass-producing Late Bronze Age and subsequent periods, the early metallurgical phases present challenges. The scarcity of recovered slags, their small size, irregular shapes, and highly heterogeneity at both macroscopic and microscopic levels, coupled with the rarity of evidence for reactors/furnaces, has made it particularly challenging to reconstruct the various production steps involved in these early smelting processes (Bourgarit, 2007; Hauptmann, 2020).

Concrete evidence of early-stage copper smelting reactors and the associated clay remains exceedingly limited (Bourgarit, 2007; Martín-Torres, 2018; Martín-Torres & Rehren, 2014). The scarcity of well-preserved reactors can be attributed to both their age and their intrinsic nature as “disposable” apparatus. Given their primarily utilitarian purpose, it is conceivable that they were partially or entirely dismantled or abandoned after use. The high temperatures reached during smelting might also have caused deformation of the reactor walls, rendering them inoperable (Bourgarit, 2007). Some scholars have posited that for metal recovery, reactors had to be dismantled following each smelting operation (Hauptmann, 2014). Furthermore, the paucity of evidence could be attributed to the possibility that archaeologists have yet to locate the exact sites where smelting activities were conducted (O’Brien, 2015, pp. 53–54). Alternatively, it has been proposed that these reactors took the form of firepits dug into the ground, leaving only scant two-dimensional traces that are challenging to recognise in the field (Vidale, 1992). Consequently, the limited and sporadic traces that have survived are typically restricted to the foundational structures of reactors, sometimes dug into the ground to maintain concentrated heat over longer durations.

While the external appearance of later-period slags can offer insights into the type of reactor previously employed, the small and irregular shapes of slags from early extractive metallurgy fail to reveal the reactor’s design. Nonetheless, the few traces that have been unearthed, when combined with petrographic and chemical analysis of slags and smelting experiments, have provided an indirect means of reconstructing the early smelting reactor designs (Bourgarit,

2019; Hauptmann, 2014, 2007). This approach has also enabled researchers to ascertain the level of mastery ancient smelters achieved in the smelting processes.

The archaeological record, up to this point, has presented a range of reactor designs, including open configurations such as ground pits, small crucibles, and large ceramic vessels (Fig. 2. 4, Fig. 2. 5) to more closed shapes such as bowl- or dome-shaped reactors (Bourgarit, 2007; Hauptmann, 2020; Pleiner, 2000; Rothenberg, 1990; Tylecote & Tylecote, 1987) to larger heating structures as proper furnaces (Ambert et al., 2013; Nocete, 2004; Saez et al., 2003a), (see Fig. 2. 6).

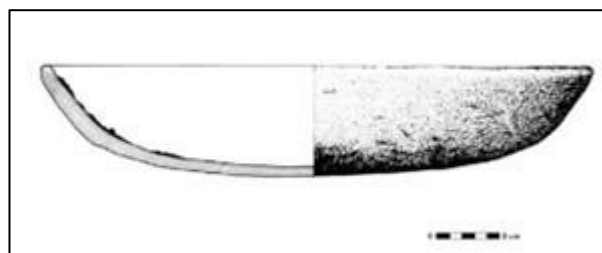
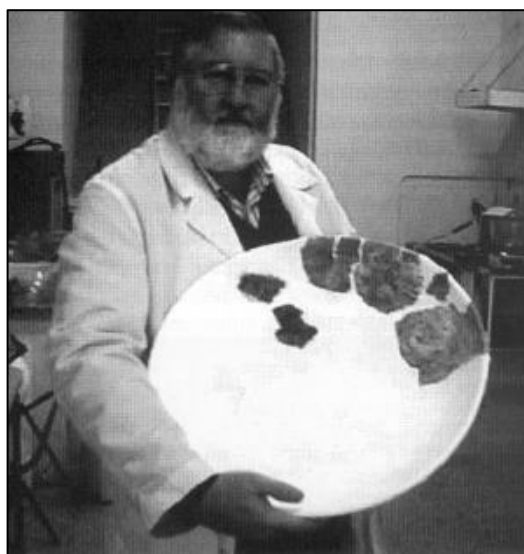


Fig. 2. 4 (left) Smelting tray/reducing “crucible” - Approximately 50 cm in diameter. Unearthed at the site of La Ceñuela, in Murcia province (from Rovira 2007, p. 89, fig.3).

Fig. 2. 5 (right): Vase furnace from Almizaraque – Scaled to 5 cm, based on a drawing by Ruiz Taboada (Montero-Ruiz, 1993), (Bourgarit, 2007, p. 8, Fig. 4b)

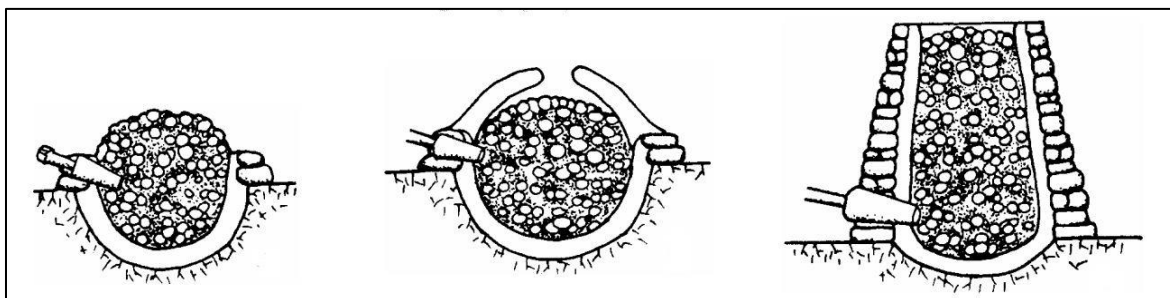


Fig. 2. 6 depicts various potential furnace types, including the bowl furnace (left), domed furnace (centre), and shaft furnace (right). While the precise heights of these furnaces may require estimation, Rothenberg proposed different furnace types (1990).

The almost total absence of slags in Final Neolithic, Chalcolithic and Early Bronze Age sites, has prompted numerous scholars to question representativeness of the recovered slags in reflecting early extractive processes. Various explanations have been put forth (Bourgarit, 2007, 2019; Pearce, 2015), with the most widely accepted notion until recently being that non-slagging processes prevailed in the early stages of metal production (Craddock, 1995). It was proposed

that the reduction of pure copper carbonates and oxides yielded such minimal slag amounts that they left few or no discernible traces on the ground (Craddock & Craddock, 1996; Craddock & Meeks, 1987; Mille & Carozza, 2009). These uncovered slags were often interpreted as outcomes of experimental or exploratory processes (“trial and error”), in which either low-grade or poorly sorted ores were subjected to smelting, or low-grade ores were intentionally smelted to assess the yield of new ore-mineral deposits (Bachmann, 1982c; Chapman & Chapman, 2013). However, the hypothesis of “slagless” metallurgy has been challenged in recent years, given conflicting archaeological evidence indicating Chalcolithic immature slagging practices. For instance, as reported in detail in the next chapter, examples of copper sulphide smelting have been unearthed at the c.5000 BC site of Belovode, in eastern Serbia, (Jovanović & Ottaway, 1976; Radivojević, 2013, 2021; Radivojević et al., 2010) as well as at Late Eneolithic sites like Milland (Artioli et al., 2005; Dal Ri & Tecchiati, 2005) and Riparo Gaban in eastern Alps, Italy (Anguilano et al., 2002; Cattoi et al., 2001; Perini, 1992).

Nonetheless, the absence of slags at the mining and smelting site of Ross Island remains unresolved (see next chapter). It has been proposed that smelting of exceptionally rich carbonate/oxide ores took place, resulting in the absence of any discard or slags (P. T. Craddock, 1995, 2000). While this process it is not infeasible in absolute terms, as demonstrated by experiments conducted by Hanning et al., (2010), this explanation is deemed unsatisfactory due to the assessment that the minerals exploited were complex polymetallic assemblages of sulphide and sulpharsenide ores along fahlertz group minerals rich in copper (40-45_{wt}%), arsenic, lead, zinc and low in iron content. The archaeological context, however, presents only a few traces of this specific type of mineralisation (O’Brien, 2015).

A diverse group of interpretative hypotheses has emerged concerning the distortion within the archaeological record. One line of thought posits that the smelting processes might have been occurred away from mining areas, on a small-scale mode, within domestic sites. As an everyday activity, slags may have either been intentionally transported for further processing, or regularly discarded outside the site. Examples of this model are found across Central and Southern Europe such as Al Claus (Carozza et al., 1997) and Los Millares (Hook et al., 1991; Keesmann & Onorato, 1999). Hauptmann (2020) has recently compiled numerous examples of this model, spanning from the Iranian Plateau (Arisman, Pernicka et al., 2011) to the Iberian Peninsula (Zambujal, Brandherm, 2016). Conversely, sites characterised by advanced extractive techniques and specialised production tend to yield higher quantities of slags, exemplified by locations like Cabezo Jurè (Nocete, 2006; Nocete et al., 1994).

Other scholars shift their focus to the working conditions, suggesting that short time-lasting processes, low temperatures, and limited reducing conditions compelled ancient metallurgists to recover metal inclusions in the shape of prills of various dimensions from the viscous slags. This technique involved systematic crushing and selection, possibly including washing and panning, of the slags to subsequently re-smelt the metal bearing inclusions. This process produced fine-grained sand-like pieces that might be challenging to recover during excavations (Bourgarit & Mille, 2005), a type of slag that Epstein termed “slag sand” (Epstein, 1993). While the washing residues near the furnace pits at Ross Island suggest this mechanical treatment, no slags or copper debris have ever been recovered (O’Brien, 2004, pp. 467–470).

Regarding the Alpine region, the rugged and uneven mountainous terrain might have made it difficult to identify slags. Another explanation suggests that the scarcity of slags could be attributed to the potential seasonality of the smelting sites (Bourgarit et al., 2008). Nevertheless, the increasing number of slag fragments recovered to date has demonstrated that slags were already produced during Chalcolithic times (Bourgarit, 2007).

The same author conducted an extensive investigation into copper smelting activities at 20 sites dating from the Late Neolithic to the Early Bronze Age, spanning from the Iberian Peninsula to the Iranian plateau. This research revealed a complex picture marked by copper production at both small-scale (e.g., Al Claus, Los Millares) and large-scale (Cabezo Jure’) sites, alongside varying working conditions, such as different reactor types with various air-supply systems and the usage of diverse copper ores. However, petrographical and physical-chemical analysis of slags enabled the identification of a set of common technical features. Slags from early copper smelting are **a)** heterogeneous and highly viscous, containing many unreacted or unmelted inclusions. Described by Bachmann as “furnace slags” (1980), they are characterised by high concentrations of copper-bearing compounds at different reaction stages and mineralogical phases. This “primitive” state of the slags indicates that ideal firing conditions were only partially achieved, and the smelting activities were carried out **b)** at relatively low temperatures and **c)** under poorly reducing conditions. The temperatures ranged between 1100 and 1350 °C (Bourgarit, 2019), sufficient to transform copper carbonates, oxides or ideal charge compositions, but not high enough to completely melt the far-from-ideal-eutectic charges recovered in early smelting sites. These chemical compositions, which deviated from the eutectic points, the substantial inconsistency in the bulk chemical compositions of the slags within each site (Bourgarit, 2007, Figure 3), and the aforementioned prevalence of unreacted copper-bearing fragments in the slags, led Bourgarit to assert that **d)** no fluxing agents were added to enhance the smelting processes (Bourgarit, 2007).

2.5.1. *Fluxes/non fluxes*

The topic of fluxes versus non fluxes in ancient smelting remains a subject of significant debate among scholars. A central challenge in the analysis of ancient slags lies in determining whether fluxes were intentionally introduced into the melt. In essence, this raises the question of whether ancient smelters possessed the knowledge to mix the perfect recipe for balancing the quantities of elements within the slag.

During the ore smelting process, fluxing involves the addition of exogenous materials (or chemical agents), known as “fluxes”, into the melt. This practice primarily serves to enhance the final yield and facilitate slag formation by promoting fluidity, reducing the melting temperature, and removing impurities from the melt. Distinguishing if the inclusions/chemical irregularities detected (e.g., quartz, feldspar) consist of unreacted remnants of the exploited mineralisation or are remnants of deliberately added fluxes to optimize the smelting process outcome is exceedingly challenging in heterogeneous slags. While some studies have provided evidence of deliberate flux use in the Early Bronze Age and later periods (e.g., Iron Age copper production at Timna, Israel, see Hauptmann, 2007), assessing this practice for earlier periods remains a formidable task, and a definitive answer remains elusive.

In the case of slags from Trentino, Italy, spanning from the Chalcolithic to the Early Bronze Age, researchers have put forth diverse interpretations. D’Amico et al. (1998a, p. 34) proposed that quartz found in the slag was added as a silica flux based on thermal alteration. Similarly, Cattoi et al. (2001, p. 152) posited that the abundance of quartz in the slag indicated its use as a flux and they further noted the likely addition of calcite, given its abundance, which is inconsistent with phyllitic chemical compositions. In contrast, Hauptmann and colleagues (Hauptmann, 2000, pp. 108–109, 2003, p. 205, 2020, pp. 240–243; Hauptmann et al., 1993) proposed an alternative perspective, suggesting that the un-melted remains of the original rock and quartz inclusions should be considered as residual components of a given charge. Additionally, Pearce *et al.* (2022) asserted that quartz was intentionally added to the smelt as a flux, often accompanied by the addition of small amounts of carbonatic flux. However, Angelini et al. (2013) provided a contrasting viewpoint, by summarising that slags from the Chalcolithic and Early Bronze Age failed to exhibit evidence of flux incorporation. In summary, the question of whether fluxes were deliberately incorporated into ancient smelting processes remains a complex and contentious issue, with varying perspectives and interpretations regarding the use of materials like quartz and calcium-bearing compounds.

Hauptmann (2020, p. 245) proposed a general rule that suggests if inclusions have microscopic dimensions, it is unlikely that fluxes were added. To illustrate this point, he referred to Metten's research on Early and Late Bronze Age slags in northern Italy (Metten, 2003). Clear evidence of flux addition should be critically examined with a good understanding of the mineralogy and chemical composition of the source material and substantiated by archaeological evidence (Hauptmann 2020, p. 258). Based on these criteria, it has been suggested that riebeckite was deliberately added as a fluxing agent at the Early Bronze Age site of Saint Véran in the French Alps. This mineral, characterised by its substantial silica content (chemical formula $\text{Na}_2\text{Fe}_3\text{Fe}_2(\text{Si}_8\text{O}_{22})(\text{OH})_2$), was hypothesized to have been intentionally transported to the site and used as a fluxing agent due to the significant amount found there, despite its distant location from the smelting site (Rostan & Malaterre, 1994).

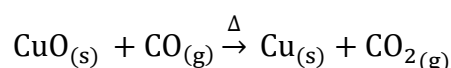
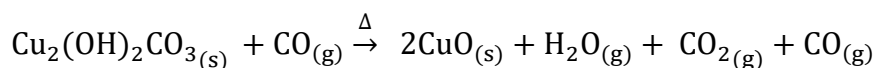
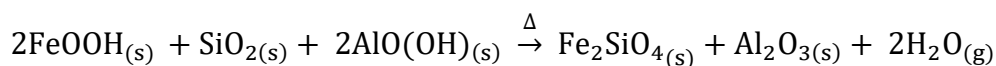
Supporters of the deliberate flux addition during the Chalcolithic period include Saez *et al.* (2003), who argued that the slag composition at Cabezo Juré does not match that of the processed ores. However, discrepancies in chemical compositions could be attributed to external factors such as fuel (charcoal, ash), materials used for building the reactor (clay, stones), and ceramic crucibles and tuyère res (Kronz, 1997). During the smelting process, elements such as potash (K) phosphorus (P), aluminium (Al), magnesium (Mg) and calcium (Ca) may chemically bond with the liquid compounds in the melt and subsequently “contaminate” the slags (Bourgarit, 2007). Potash (K) and phosphorus (P) are believed to originate from wood or charcoal ashes (Etiegni & Campbell, 1991; Kronz, 1997; Radivojević *et al.*, 2010).

Field experiments that replicated Chalcolithic slags from Roque Fenestre, in Southern France Alps (involving the co-smelting of sulphosalts (Cu-As-Ag-S) and malachite) demonstrated how dolomite reactor walls could impact the composition of partially fused slag. Dolomite, a carbonate rock rich in Ca and Mg (chemical formula $\text{CaMg}(\text{CO}_3)_2$), resulted in experimental slags with high Ca and Mg contents, approximately 20_{wt}% of the total slag weight, with an atomic Ca:Mg ratio matching with that of the dolomite (Bourgarit & Mille, 1997). This suggests that dolomite entered the melt, thereby excluding the deliberate addition of fluxes. However, contamination as an explanation for the slags from Cabezo Juré has been dismissed due to the proposed high flux content (50%) by Saez *et al.* (2003a) and the highly unreacted state of the slags, as noted by Hauptmann (2000).

In favour of deliberate fluxing, Shugar (2000) suggested that fragments of non-copper ore (iron oxides) found at the site might be parts of fluxes used. Nevertheless, this hypothesis raises

questions, as the low quantity of ore fragments recovered may not be representative and it is challenging to determine if they are raw material or debris (Bourgarit, 2007).

It has also been suggested that gangue and host rocks, typically associated with ores, might have functioned as natural fluxing agents (see Hauptmann 2020, p. 245). Among the most common materials found in the gossan part of mineral deposits are iron (hydro)oxides (e.g., limonite), quartz and clay minerals. An example is illustrated by the following chemical reactions:



In these reactions, non-copper bearing minerals (in the first line) and malachite (in the second line), if mixed in ideal proportions, could act as “self-fluxing” agents. This would facilitate the separation of copper from its chemical bonds and enhance the final yield. Herdits (1997:40-41) suggested the addition of old slags to expedite the smelting process. At the Brennerwald site in Mitterberg (Salzburg, Austria), semi-smelted plate slag in a slag cake has been interpreted as the recycling of slag to aid in the melting of silica-rich rock. The concept of using recycled slags as flux, as proposed by Pearce *et al.* (2022), could explain the absence of low occurrence of plate slags.

In summary, this chapter has laid the groundwork for a comprehensive understanding of slag analysis in the field of archaeometallurgy. It commenced with a brief look back at the history of slag analysis, emphasizing its crucial role in uncovering ancient metalworking techniques. Subsequently, the chapter proceeded to elucidate the compositions and typical mineralogical phases encountered in copper smelting slags, shedding light on the materials that offer insights into ancient metallurgical practices. Furthermore, it delved into the geological aspects associated with the formation processes of copper-bearing ore deposits. Moreover, the chapter undertook a detailed examination of Chalcolithic copper smelting technology, unveiling the

predominant theories and hypotheses related to this pivotal period. During the examination of the early phases of copper smelting technology, it emphasised the inherent challenges of interpreting the past, especially considering the constraints of archaeological evidence. This highlighted the need for thorough and careful analytical method. The overarching objective has been to endow the reader with the essential components required to grasp the intricacies intrinsic to slag analysis and to establish the bedrock for this ongoing research.

Armed with this understanding, the upcoming chapter will focus on two primary objectives:

1. To undertake an exhaustive and comprehensive review of the current state of knowledge regarding early sulphide copper smelting practices in Europe. The aim is to provide the reader with a thorough understanding of how sulphide copper smelting was carried out in Europe during the specified time period, including the techniques, technologies, geographical locations, and socio-cultural contexts.
2. To identify key gaps in the existing body of knowledge related to early sulphide copper smelting in Europe. By pinpointing these gaps, the chapter has set the stage for the subsequent sections of the thesis, outlining the specific areas and questions that the research aims to address and contribute to. This step is crucial for demonstrating the significance and originality of this thesis's research contributions.

Chapter 3. Early Smelting Technology in Europe

3.1. Introduction

In this chapter, I provide a comprehensive literature review on the earliest evidence of sulphide copper smelting in Europe. In the first part, I delve into the broader European context, whereas in the second part, I narrow the focus on the site of Orti Bottagone, which is the primary subject of this research, along with its archaeological context. This evidence dates to the Final Neolithic and Chalcolithic periods. It is essential to note the variability in period definitions, particularly in different regions, especially when considering areas on either side of the Alps. For a detailed overview, please refer to the chronological tables for Italian peninsula (Dolfini *et al.*, 2020), Northern France (Cottiaux *et al.*, 2006), Southern France (Carozza *et al.*, 2005), Serbia, Bulgaria, parts of Romania (Boyadziev, 1995, p. 2014; Schier, 1996, p. 2002; Whittle *et al.*, 2016), Iberian peninsula (Chapman, 2008), and British Isles (Needham, 2012). When necessary, I include in the text absolute chronology to prevent any misinterpretation (see Table 3. 1). This chapter serves a dual purpose: first, to provide an overview of the current state of knowledge, and second, to identify critical research gaps that this thesis aims to explore and address. Additionally, it sheds light on the various smelting techniques employed, which depend on the availability of local ore resources. By examining evidence from different geographical contexts, this section sheds light on potential connections between sites and regions, ultimately contributing to a broader understanding of the smelting practices during this period. To facilitate this analysis, Europe is divided into distinct macro-regions: western Alpine region (Southern France), central Alpine region (Switzerland and Austria), Eastern Alpine region (Italy), southeastern European region (Balkans), Iberian Peninsula, northwestern European region. (British Isles). The site of Orti Bottagone is treated separately.

In Fig. 3. 1 a map with the main regions with the copper mining and smelting sites reviewed in this thesis is provided.

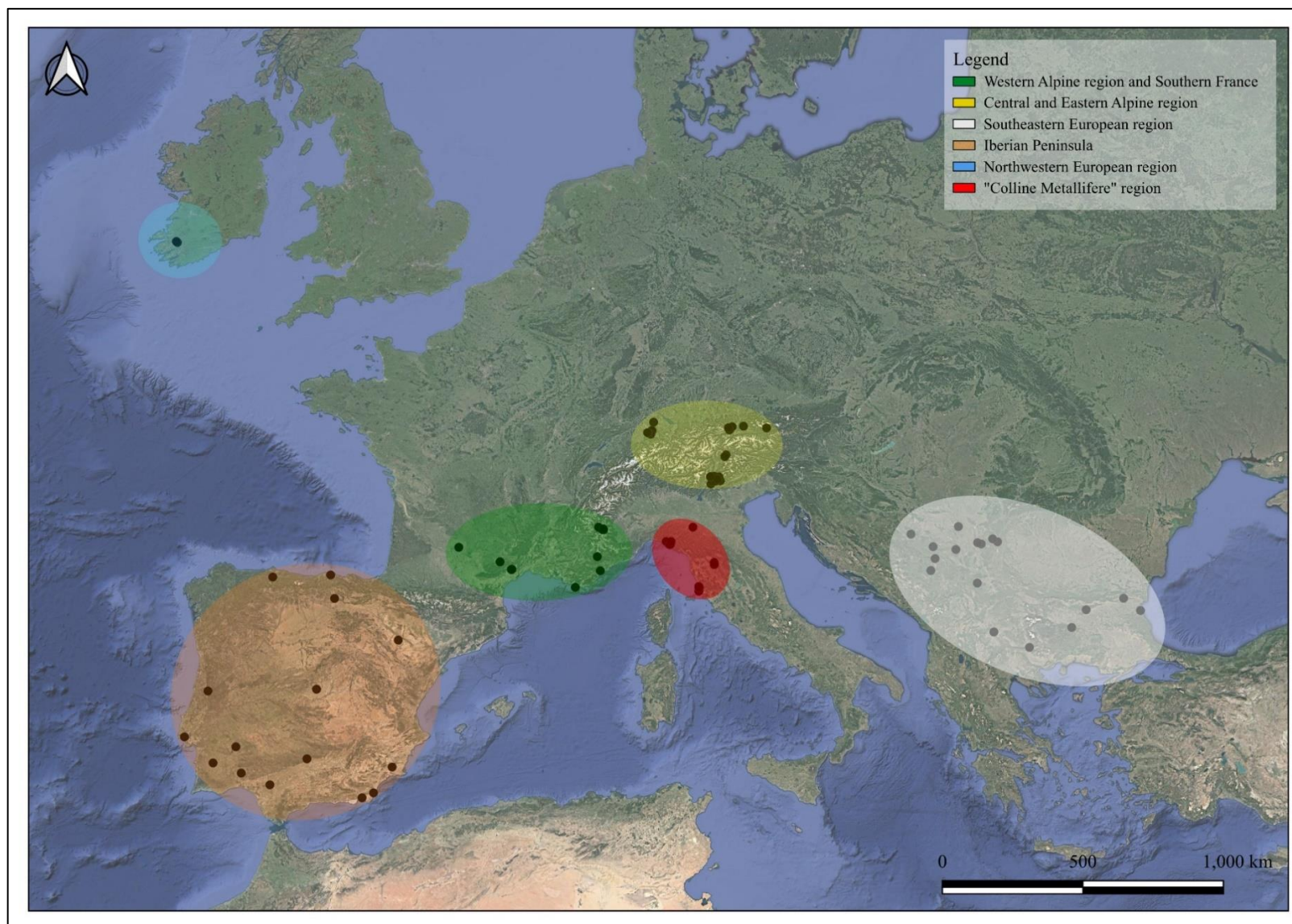


Fig. 3. 1. Map showing the main regions with the copper mining and smelting sites reviewed in this thesis.

Table 3. 1 Comparative chronological Tables showing the relative and absolute chronology of the Italian Peninsula, northern and southern France, Serbia, Bulgaria, Romania, the Iberian Peninsula, and the British Isles. Relative references are provided in the text.

Italian peninsula	
<i>Archaeological phase</i>	<i>Absolute chronology</i>
Late Neolithic	4500-3800 BC
Final Neolithic	3800-3600 BC
Early Copper Age	3600-3350 BC
Middle Copper Age	3350-2800 BC
Late Copper Age	2800-2200 BC
Early Bronze Age (phase I)	2200-1900 bc

Southern France	
<i>Archaeological phase</i>	<i>Absolute chronology</i>
Recent Neolithic	3500-3300 BC
Final Neolithic 1	3300-3000 BC
Final Neolithic 2	3000-2700 BC
Final Neolithic 3	2700-2500 BC
Final Neolithic (Bell Beaker)	2500-2200 BC
Early Bronze Age (phase I)	2200-1800 BC

Northern France	
<i>Archaeological phase</i>	<i>Absolute chronology</i>
Recent Neolithic	3500-2900 BC
Final Neolithic 1 (pre-Bell Beaker)	2900-2400 BC
Final Neolithic 2 (Bell Beaker)	2400-2100 BC
Early Bronze Age 1	2100-1800 BC

Serbia, Bulgaria, parts of Romania	
<i>Archaeological phase</i>	<i>Absolute chronology</i>
Early Neolithic	6200-5500 BC
Late Neolithic	5500-5000 BC
Early Chalcolithic	5000-4600 BC
Middle Chalcolithic	4600-4450 BC
Late Chalcolithic	4450-4100 BC
Final Chalcolithic	4100-3700 BC
Proto Bronze Age	3700-3200 BC

Southeast of Spain	
<i>Archaeological phase</i>	<i>Absolute chronology</i>
Early Neolithic	5600-4900 BC
Middle Neolithic	4900-4400 BC
Late Neolithic	4400-3800 BC
Final Neolithic	3800-3300 BC
Chalcolithic	3200/3100-2250 BC
Early Bronze Age (phase 1)	2250-2000 BC
Early Bronze Age (phase 2)	2000-1750 BC
Early Bronze Age (phase 3)	1750-1550 BC

British Isles	
<i>Archaeological phase</i>	<i>Absolute chronology</i>
Late Neolithic	Pre-2450/2400 BC
Earlier Chalcolithic	2450/2400-2300 BC
Later Chalcolithic	2300-2200
Chalcolithic/Early Bronze Age	2200-2150
Early Bronze Age	Post-2150

3.2. Western Alpine region and Southern France

The first area of focus in this thesis is the western Alpine region and the Southern France, which hold a crucial place in this thesis investigation (Fig. 3. 2). As the closest geographical area to the site of Orti Bottagone under examination, this region is of particular significance in understanding the early evidence of sulphide copper smelting and gain insights into the technical aspects of copper smelting that evolved within this distinctive Alpine environment.

The western Alpine region boasts several prehistoric mining districts and copper ore deposits that date back to the Chalcolithic period (3rd millennium BC). Notable locations include Saint-Véran, Clue de Roua, Maraval, Le Peirol, Cap Garonne, Cabrières and Bouco-Payrol (Craddock, 2011; O'Brien, 2015). Among these, two stand out for their significant contribution to our understanding of early copper smelting technology: the Cabrières-Péret district, in the department of Hérault and the Saint-Véran mining area, in Hautes Alpes.

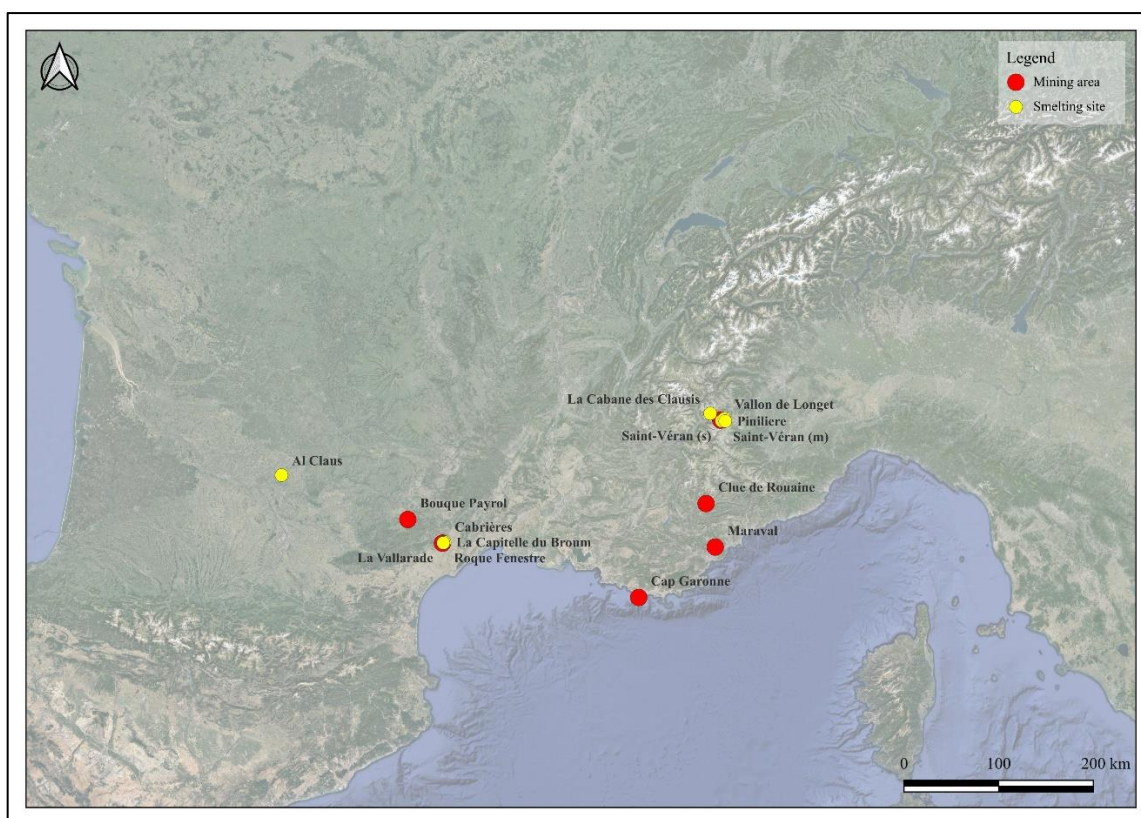


Fig. 3. 2. Map of the Western Alpine region and Southern France, indicating key sites categorized as mining and smelting locations.

3.2.1. *The Cabrières-Péret district*

The Cabrières region is renowned for its collection of mines and metallurgical sites. Radiocarbon dating (1σ) conducted at various sites within the mining district has revealed a continuous occupation spanning approximately one thousand years, commencing at the onset of the third millennium and culminating at the dawn of the Bronze Age (Carozza et al., 2005; Carozza & Mille, 2007; Mille & Carozza, 2009). The presence of pottery, which aligns with Final Neolithic groups in the Hérault valley, corroborates these findings (Mille & Carozza, 2009). Over the last three decades, three distinct mining areas have been identified: Pioch Farrus, La Roussignole, and Ballarade (Ambert, 1990, 1995, 1996; Ambert et al., 1996, 1984). The copper mineralisation primarily comprises fahlore and tetrahedrite, the latter being rich in copper, antimony, and silver, and relatively low in lead and arsenic. Occasionally, these ores are found alongside chalcopyrite or oxidized copper minerals like malachite and azurite (Prange, 2000; Prange & Ambert, 2005). The area's significance during the third millennium is evident, with over half of the metal objects discovered in the Languedoc region featuring antimonial copper corresponding to this mineralisation. Notably, copper ores with high lead content have been recently identified in this region as well (Ambert et al., 2009).

The earliest evidence of mine activities, dated to approximately 2400-2200 BC based on radiocarbon dating of Chalcolithic sherds, is linked to the Pioch Farrus area. It encompassed the working sites of Pioch Farrus I and IV, where compelling evidence of copper production have been uncovered. This evidence includes remnants of smelting slags, fragments of crucibles and small copper droplets. Furthermore, a potentially significant smelting crucible, initially overlooked, was discovered in the archaeological record (Rovira & Ambert, 2002). Dated approximately to 3100-2800 BC, the mine exhibited characteristics such as the presence of a tetrahedrite vein with traces of chalcopyrite (Espérou et al., 1994). Located just 200 meters away is the site of Roque Fenestre, which was closely connected to the Pioch Farrus mines and served as a hub for copper production from 2800-2000 BC (Ambert et al., 1996; Espérou, 1981). In the vicinity of La Roussignole, numerous stone hammers have been unearthed at both mining sites and metal production locations. At the heart of this district, a substantial presence of metallurgical activities has been discovered on the Vallarade plateau. Dating back to the third millennium are the mines of Les Neuf-Bouches (2900-2500 BC), which were also in operation during the Bronze Age (Ambert, 2002). Additionally, the area includes Petit-Bois and the permanent copper smelting settlement of La Capitelle du Broum, located less than a kilometre to the south (Ambert et al., 2013). Remarkably, the latter represents the earliest known evidence of a copper metalworking settlement in France. In an extraordinarily well-preserved state, it has

provided insights into copper mining and the smelting process in the western Alps, facilitating the identification of all stages of metal production, from ore beneficiation to smelting and casting (Bourgarit & Mille, 2005). The excavation of the specialised Area 1 documented the smelting process, revealing the presence of twenty standardised small-fire hearths (La Capitelle-type). Ten of these, exceptionally well-preserved, provided an opportunity to record their dimensions, construction, and operational techniques. These hearths take the form of oval basins, measuring 40 cm in length and 15-20 cm in depth, lined with a 2 to 5 cm thick layer of yellow clay. This find confirms that the smelting process was conducted in relatively simple shallow pit furnaces (see Fig. 3. 3). Ambert et al. (2013) compared these small fire structures to the furnace pits of Ross Island (O'Brien, 2004, pp. 223-266). According to Ambert et al. (2013) it is important to note that the process carried out at the latter site can only be hypothesised as a two-stage process, as no slags were discovered during excavations. Similar features, often associated with slags containing drops of copper and deposits of magnetite-rich sands have been recovered at contemporary sites such as Valat-Grand and Pioch Farrus A-448 (Ambert *et al.*, 2013).

The ores found at the site, present in small-size fragments, are characterised by partially weathered primary fahlores, primarily tetrahedrite, as well as malachite and azurite. These fragments exhibit a low concentration of chalcopyrite and a recurring presence of barite. They also contain high levels of antimony, silver, and, in smaller quantities, arsenic, zinc and lead. Chemical and isotopic analyses suggest that these minerals likely originate from the nearby mines of La Roussignole and La Vallarade (Prange & Ambert, 2005; Schifer, 2001). The slags recovered at the site, most of which were found in proximity to the pyrometallurgical structures, amount to approximately one kilogram in total. These slags are typically intentionally broken, with centimetre-sized or smaller dimensions (averaging around 0.5 cm³). They are characterized by a glassy matrix containing calcium and iron approximating a pyroxene composition, as well as significant quantities of copper, zinc and antimony. The high viscosity and the presence of unreacted silica within the slags prevented a clear separation of the metal from the gangue. Consequently, numerous metal droplet, ranging from a few microns to several millimetres in size are embedded within them (see Fig. 3. 4 and Section 9.3.2 for an interpretation of these features). Moreover, a substantial amount of copper sulphide is present, predominantly coating the metallic inclusions within the slags.



Fig. 3. 3 (left) Cross section of a well preserved simple metallurgical structure at La Capitelte du Broum (Péret-Hérault), (Ambert et al., 2013: 63, 3).

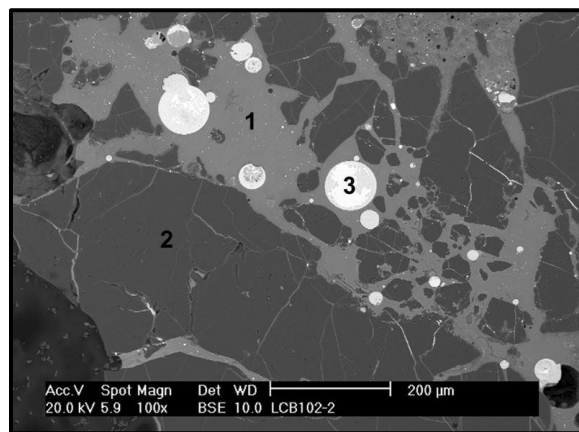


Fig. 3. 4 (right) Back-scattered electron image (hereafter referred to as BSE) of a slag from La Capitelte du Broum (Péret-Hérault) showing metal droplets (3) embedded in the highly viscous silicate matrix (1) and unreacted silica (2) of the slag (from Ambert et al., 2013: 67, 6).

The significant presence of silica, undecomposed inclusions such as quartz and potassium-rich clay, along with a notable quantity of copper sulphide droplets (also called “white metal”, Bourgarit et al., 2003), led Ambert et al. (2013) to deduce that the initial composition of the charge was not meticulously selected and that the necessary reducing conditions and temperatures were not entirely met. This suggests a lack of control by early metallurgists. The low reducing conditions are further substantiated by the frequent presence of magnetite, indicating an oxidising environment within the reactor (Ambert et al., 2009: 291).

The slags were likely produced through a process involving a highly oxygenated open fire, where partially weathered fahlores, primarily tetrahedrite, were smelted directly, mixed with some oxidized ore. The possibility of a one-stage co-smelting of oxides and sulphides has been experimentally demonstrated by Rostoker et al. (1989) and (Bourgarit et al., 2002). For details on the experiments see Chapter 7. The absence of roasting beds supports this position. On one hand, it has been suggested that the metal droplets were extracted after crushing the slag, as suggested by the typical nut-size slags. On the other hand, it has been proposed, albeit tentatively, that this might represent an intentional primitive smelting process aimed at producing matte, a semi-liquid copper-iron sulphide mass (Bourgarit & Mille, 1997; J. L. Espérou, 1993; Mille & Carozza, 2009). These slags have been compared to those from Roque-Fenestre based on size, microstructure, high quartz and copper content, and the relatively high oxidation levels of iron and copper (Bourgarit et al., 2003: 437-8). Similarities have also been identified with slags from Chalcolithic sites in the Near East including Abu Matar, Wadi Fidan 4, Shiqmim and Norsuntepe (see Hauptmann, 2000).

3.2.2. *The Saint-Véran mining area*

The Saint-Véran copper mining area lies in the upper Aigue Blanche valley, nestled between the borders of Switzerland and Italy (Bourgarit et al., 2008). Dating back to the end of the third millennium (Carozza et al., 1997), the site ranks among the earliest mining regions in the western Alps. Situated at an elevation of approximately 2400-2600 meters a.s.l., it holds the distinction of being the highest ancient smelting area in all of Europe. In contrast to other French Chalcolithic smelting sites like Al Claus, Roque-Fenestre, and La Capitel du Broum, which employed primitive smelting methods (Bourgarit et al., 2008), Saint-Véran boasts relatively advanced smelting technology and a remarkable scale production. Estimates suggest that 2000 tonnes of ore (extracted from 10000 m³ of rock) resulted in approximately 1400 tonnes of smelted copper (Rossi et al., 1997; Rostan et al., 1997, 2002).

The ancient mine at Saint-Véran is distinguished by a unique mineralisation, featuring copper, zinc and iron sulphides, primarily bornite (Cu₅FeS₄) with high copper content (approximately 63_{wt}%). It is often associated with chalcocite and iron oxides. Notably, no traces of copper oxides, carbonates, or silicates have been documented on exposed surfaces. The concentration of this copper-rich bornite sets it apart from other “Alpine-type” deposits in the region due to the ease of the beneficiation process (Bourgarit et al., 2008). 19th century literature, archival notes, and small native copper fragments discovered in ancient slag heaps provide indications that native copper may have been exploited in antiquity.

The contemporaneous smelting site, La Cabane des Clausis (Carozza et al., 1997) complements the mining operation. Situated at an altitude of 2250 meters, not far from the mine, this metallurgical workshop is supported by evidence of its activities. This includes numerous tuyères fragments, a stone crucible fragment (Barge, 1997), and approximately one hundred kilograms of slags. These findings have been found associated with burnt sediments and reddened surfaces, likely representing areas where ore was heated. Interestingly, the conical tuyères, featuring an aperture of 3-4 mm, show no signs of slagging, excluding their use in the smelting process. Although various hypotheses have been proposed, their exact function remains an open question (Carozza et al., 1997).

Upon close examination, Bourgarit et al. (2008) categorised the slags into two parts, characterised by a smooth and wrinkled top and a rougher, porous bottom. By analysing the side inclination of certain fragments, they inferred that the “slag cakes” had diameters ranging from 15 to 20 cm. The slags exhibit high density, fluidity, and homogeneity, with low porosity and few unreacted inclusions. The copper content ranges from 1% to 11% in the form of 10-

50µm-sized copper droplets. Notably, through mineralogical investigations on ten slags they identified four main phases suggesting that the smelting process was carried out under fluctuating reducing/oxidising conditions and temperatures (see Fig. 3. 5).

The authors also consider the possibility of a fluxing agent being used, as several fragments of riebeckite, a sodium-rich iron silicate ($\text{Na}_2\text{Fe}^{2+}_3\text{Fe}^{3+}_2(\text{Si}_8\text{O}_{22})(\text{OH})_2$), have been discovered on the site, far from their natural deposits (Rostan & Malaterre, 1994). On the other hand, the chance of an unintentional addition cannot be ruled out, as this mineral might naturally occur in the bornite ore (Bourgarit et al., 2008, p. 7).

The flat and thin shapes of these slags, have led researchers to draw comparisons with the *Plattenschlacke* from the Middle and Late Bronze Age (Anguilano et al., 2002; Artioli et al., 2009, p. 200; Martinek & Sydow, 2004; Metten, 2003). The smelting technology required for such slags is typically associated with later Bronze Age, making it notably advanced for the Alpine Chalcolithic-Early Bronze Age transition period. During this transitional era, smelting processes were still relatively primitive, resulting in coarse and porous slag production (Craddock, 1995). The consistent characteristics of the recovered slags have led Bourgarit et al. (2008, p. 8) to the proposal of a single-stage smelting process, which was experimentally confirmed as feasible during preliminary experiments conducted at Fiaavè.

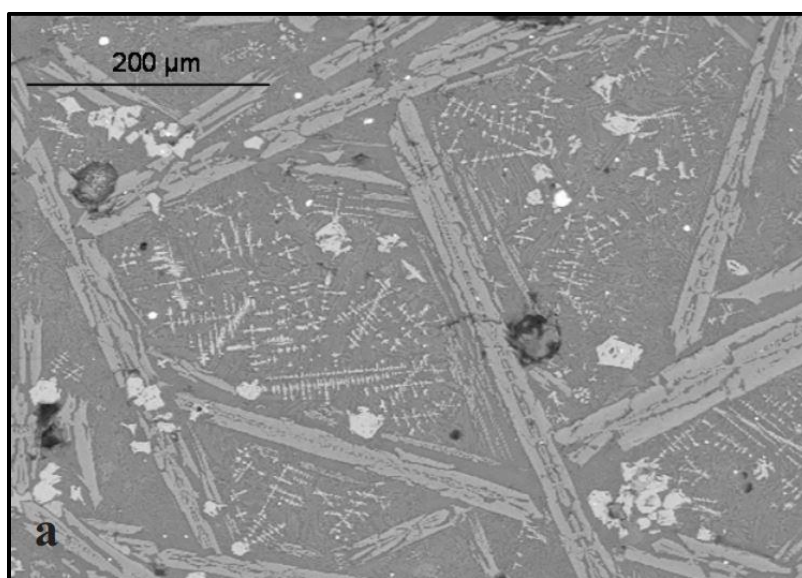


Fig. 3. 5 provides a BSE micrograph revealing the microstructure of slag originating from the La Cabane des Clausis site. This slag sample exhibits four primary phases: a) fayalite (large grey needles), b) calcium-enriched clino-pyroxenes (dark grey chains inside the fayalite needles); c) magnetite (light grey polyhedra); d) copper droplets (white), (from Bourgarit *et al.*, 2008, fig. 9a).

In the same region, smelting sites with similar slag have been identified, such as the rock shelter at Piniliere near the Trenchée des Ancients mine, dated to 2400-1900 BC (Rostan et al., 1994; Rostan & Malaterre, 1994), and at the Vallon du Longet, dated to 2210-2130 BC (Bourgarit et al., 2008). Notably, at the former site, an almost intact tuyère measuring 8,8 cm in length was found (Gattiglia & Rossi, 1995).

Dated to the second half of the third millennium (2400-2200 BC) is the multifunctional and specialized metallurgical domestic settlement of Al Claus, in the Aveyron Valley (Tarn-et-Garonne), (Bourgarit, 2007; Carozza et al., 1997; Mille and Carozza, 2009). Numerous combustion structures associated with domestic buildings have been uncovered, characterized by small stone-floor hearths and large circular pits filled with thermally altered limestone blocks (Mille & Carozza, 2009). Tuyères, slags, crucible fragments, a small mortar and several hammers have been recovered associated with these structures. The scarce number of slags recovered are primarily 2cm-sizes sulphide fragment, predominantly chalcopyrite. The mineral composition of the slags includes crystallised magnetite and fayalite with copper-iron sulphide inclusions embedded in a vitreous matrix (Bourgarit, 2007). These crystalline structures indicate that a smelting temperature of 1100°C was reached during the process (Mille & Carozza, 2009). Notably, among the crucibles, fragments of domestic vessels ranging from 5 to 30 cm² display traces of slagged layers on their inner surfaces. Approximately 1600 sherds with significantly thermally altered inside surfaces were discovered in the vicinity of three of the circular pits mentioned above. The smelting appears to have been conducted in ceramic vessels repurposed as small, rounded furnaces. The systematic fragmentation of these pots is attributed to the necessary procedure for recovering the smelting products. Experiments conducted by Bourgarit and Mille (2001) have confirm the feasibility of copper production using this technique, although the produced slags differ from those found at the site.

With regard to the rest of France, copper ore deposits have indeed been identified, including in Brittany, the Pyrenees, the Corbières, the periphery of the Massif Central, the Maures, and the Alps. However, it's worth noting that despite the presence of these deposits, there is a lack of evidence indicating smelting activities in these areas.

3.3. Central and Eastern Alpine region

Shifting eastward, the focus of this section is first on the Central Alpine region and then on the eastern Alpine region (Fig. 3. 6). In recent years, there has been a substantial increase in the discovery of evidence related to mining and smelting activities. Neverthelss, despite this

growing body of evidence, comprehension of early metallurgy in this region remains limited (Bartelheim, 2013). The majority of our knowledge in this region largely stems from the analysis of metal objects. The impurity patterns observed in these artefacts have led scholars to posit that early metallurgy in the north Alpine revolved around the exploitation of grey copper/fahlores (O'Brien, 2015 and references therein). Remarkably, the period spanning from the Late Neolithic through the entire fourth millennium has left no discernible traces of mining operations in this area (Goldenberg, 1998).

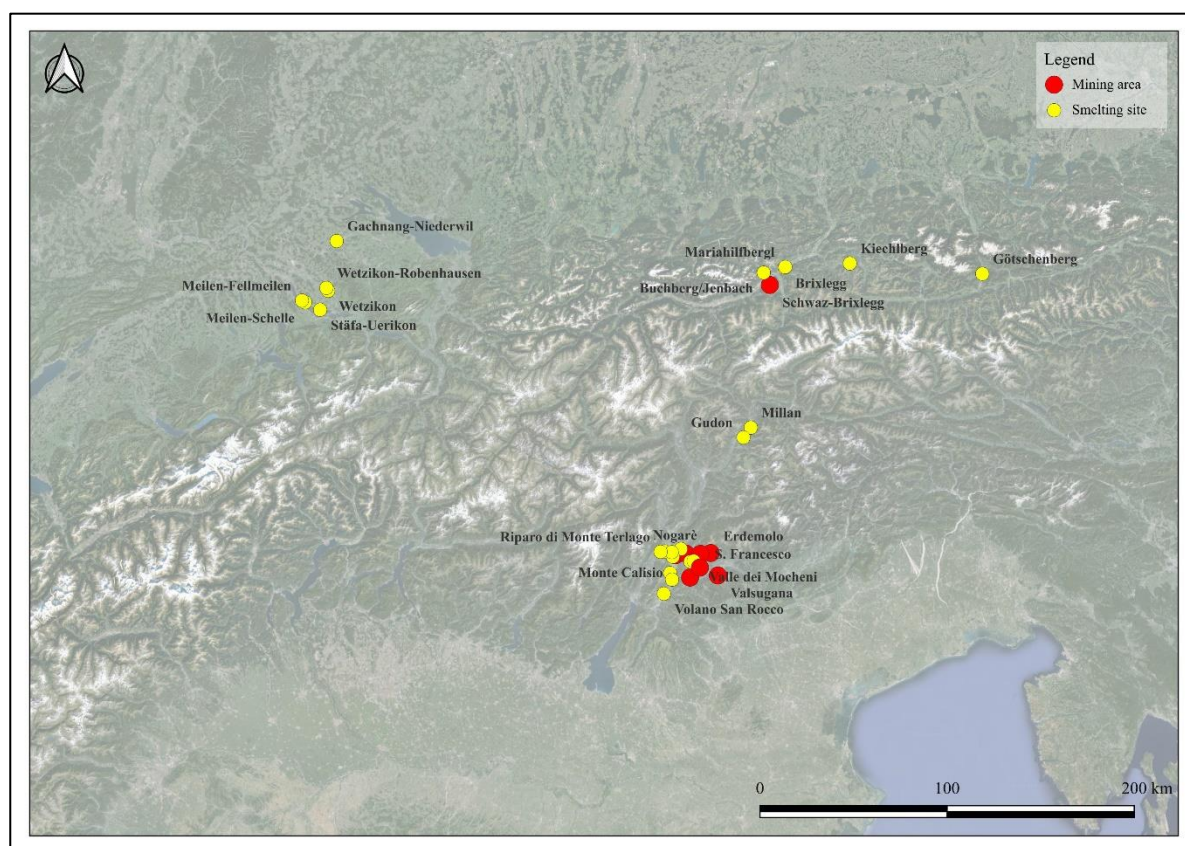


Fig. 3. 6 Map of the central and eastern Alpine region, showing relevant sites categorized as mining and smelting locations.

The earliest recorded smelting activity in this region is associated the Mariahilfbergl settlement, located not far from Brixlegg in the Inn Valley of North Tyrol, Austria. Initially dated to the second half of the fifth millennium BC, approximately 4500-3900 cal BC (Höppner et al., 2005), it was attributed to the south German Munchslofen culture. However, recent research suggests that it may belong to the subsequent Pfyn, Altheim and Mondsee cultural horizon, ranging from 3900 to 3600 BC. Fragments of copper slags, weighing 250 grams and measuring between 0.5 to 2cm in size, along with two clay nozzles and two copper objects, were

discovered associated with a fireplace (Bartelheim et al., 2002, 2003). These slags are derived from local carbonate-hosted fahlore deposits, primarily characterised by tetrahedrite, which is widespread in the Brixlegg area. They exhibit high porosity and unreacted mineral inclusions. Due to their distinctive characteristics, they have been compared to those found at La Capitellet du Broum (Bartelheim et al., 2002). Analysis of the objects revealed that they were crafted from low-impurity copper, and that their chemical signatures can be traced back to an ore deposit from the Majdanpek mine in Serbia (Pernicka et al., 1997). The site is thought to represent a smelting trial conducted by local groups attempting to replicate the copper metalworking techniques of the Balkans (Höppner et al., 2005; Pernicka et al., 1997). The long-distance connection between the north Alpine region and the southeastern Europe is further supported by similarities in the pottery assemblages between the Mondsee culture and the Hungarian Balaton 2/3 and Boleráz groups (Ruttkey, 1981, pp. 282–284; Matuschik, 1998, pp. 241–242).

Following this early evidence, copper exploitation expanded further in the Alpine region during the fourth millennium BC. As an illustration of this copper metallurgy, traces of smelting of oxide ores, crucibles and few copper objects were discovered at the Götschenberg settlement, in the Mühlbach valley, Salzburg. Dated to the first half of the fourth millennium BC, this settlement is associated with the Mondsee culture, which was a significant group known for their use of copper. Unfortunately, despite the unearthing of numerous artefacts, including tools, weapons and ornaments (Bartelheim et al., 2002, Fig. 20), direct evidence of copper mining in the region has yet to be identified (Goldenberg, 1998; Goldenberg, Breitenlechner, et al., 2011).

Recent archaeological investigations (2007-8, as part of the HiMAT project) have unveiled a multiphases settlement in the Kiechlberg area, located a few kilometres northeast of Innsbruck in the Tyrolean Inn Valley (Krismer et al., 2013). Due to its excellent preservation, researchers have been able to establish its occupation span from the fifth to the second millennium BC.

The site has yielded a variety of metallurgical findings, including raw copper ore, slags, technical ceramics and finished objects. The majority of the slags and copper-rich semi- and by-products come from Chalcolithic and Early Bronze Age layers. These slags are associated with a sulphide-rich mineralisation, specifically Fe-Zn tetrahedrite-tennantite (fahlore), which was likely imported from the Schwaz-Brixlegg deposits located approximately 30-50 km away. The slags exhibit low density and a vesicular appearance. Apart from some slags that display a thin and flat shape, most are irregular in form. They are heterogeneous, with unreacted quartz inclusions visible to the naked eye, variable amounts of sulphide inclusions ranging in size from less than 1 µm to over 100 µm, and metal droplets surrounded by sulphide rims of variable thickness embedded in a silicate glass matrix. The estimated firing temperatures for these

smelting activities are a minimum of approximately 1100°C. Because of their chemical characteristics and the relatively low copper concentration, ranging from 3.28_{wt}% to 5.54_{wt}%, these slags have been compared to Early Bronze Age slags found at the Buchberg/Jenbach and Mariahilfberg sites in the Lower Inn Valley (Bartelheim et al., 2002; Martinek, 1996; Martinek & Sydow, 2004). Additionally, a crucible fragment characterised by thermal alteration and a slagged surface has been unearthed (Töchterle et al., 2011; Trauner, 2010).

The scarcity of recovered slags, their distinctive mineralogical characteristics and the presence of a slagged ceramic vase have led Krismer et al. (2013) to propose that a primitive copper smelting technology was conducted in small-scale workshops at this site. This hypothesis suggests that the metallurgical activities were relatively rudimentary, in contrast to more advanced smelting methods seen in later periods.

Evidence of potential sulphide copper smelting has been discovered in north-west Switzerland (Schlichtherle & Rottländer, 1982; Fasnacht, 1991; Rehren, 2009). Notably, several crucible fragments dating back to the Neolithic period have been unearthed, associated with the Pfyn and Horgen cultures (c. 3800-3300 BC). Fasnacht (1991) initially proposed that these fragments might have served as casting crucibles (referred to as “*Gusslöffel*”). However, Maggetti et al. (1991) challenged this hypothesis after conducting mineralogical investigations, which included XRF and XRD analyses. Their research revealed the presence of copper-iron sulphides inside the crucibles, leading to an alternative interpretation as smelting vessels (Maggetti, 2010; Maggetti et al., 1991).

Crucible fragments from the same region, specifically from the locations of Wetzikon, Wetzikon-Robenhausen, Stäfa-Uerikon, Meilen-Schelle, Meilen-Fellmeilen and Gachnang-Niederwil, originally examined by Baumgartner (1982), and partially reported by Maggetti et al. (1991), have recently been the subject of analysis by Rehren (2009). This analysis identified copper-iron sulphide inclusions, primarily composed of chalcopyrite but also including chalcocine and pyrite. These inclusions, due to their distinct stratigraphic separation from the prills and their texture, could not be attributed to the smelting process (see Fig. 3. 7). Rehren suggested that these sulphide inclusions may have formed later, as a result of deposition in a highly oxygenated, low temperature aquatic environment.

Both interpretations of the crucibles as casting or smelting devices rise unresolved questions. In the case of casting, the origin of the raw material must be explained, as it can only be found outside the cultural context without native copper. Conversely, the smelting interpretation fails to clarify why the smelting technique vanished after hundreds of years of use (Rehren, 2009).

Remaining in the Swiss context, the last two decades have witnessed a significant surge of interest in the South-eastern Alps, particularly the Oberhalbstein valley in the modern canton of Grisons. While the region has yielded substantial discoveries of prehistoric copper mining and production sites since the 1970s (Wyss, 1977, 1982), alongside numerous research projects (Della Casa *et al.*, 2016), revealing significant evidence of metalworking activities, the comprehensive understanding of the various stages of Chalcolithic copper production remains largely elusive. This knowledge gap sets the Alpine region, especially the Swiss area, apart from Austria and the northern Italian Alps, where the historical trajectory of copper production is better documented.

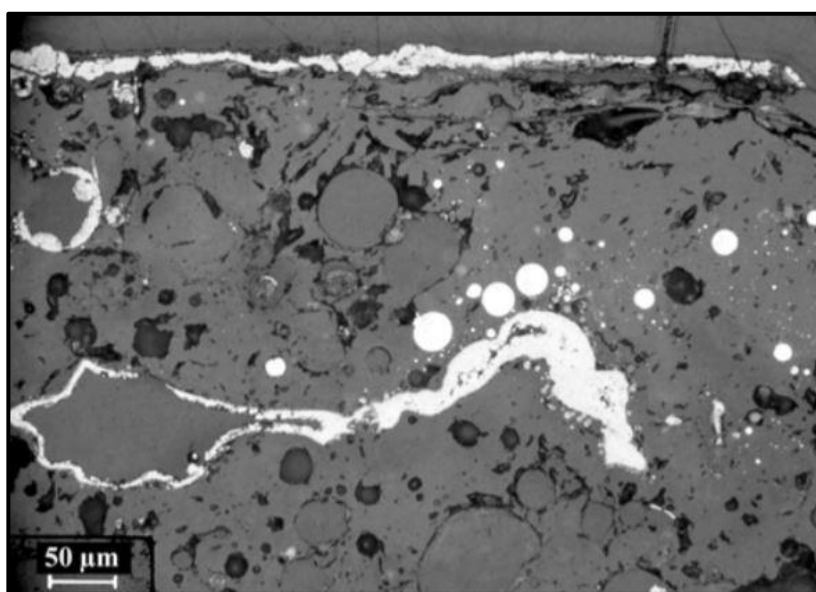


Fig. 3. 7. BSE micrograph displaying a detailed area of a crucible fragment from Wetzikon. The copper prills (white) are located only in the inner part of the crucible, while copper-iron sulphides inclusions are only on its surfaces. From Rehren, 2009, fig. 8.

Turning to the eastern Alpine region, the area of Trentino and Alto Adige/South Tyrol stands out as an area with numerous mining and copper smelting sites. This territory has been the subject of systematic surveys over the years, spanning from the 1960s (Preuschen, 1962; 1965; 1968a, 1973), the 1970s and 80s (Šebesta, 2000), to the 1990s (Perini, 1992), with ongoing investigations by the Archaeological Heritage Office of Trento and the Deutsches Bergbau-Museum, Bochum (Germany) from 1981 (Cierny *et al.*, 1998; Cierny, 2008).

The region boasts a wealth of copper ore exploitation and metalworking occurrences, with over 200 sites documented (Silvestri *et al.*, 2019). However, in many instances, medieval and modern activities have concealed the traces of ancient exploitation, and to date, no data on prehistoric copper mines have surfaced. Among these sites, only a few have been dated to the

Chalcolithic period (11 in total as of 2019, according to Silvestri *et al.*, 2019). Others, determined through pottery typology and radiocarbon dating (Acqua Fredda, Malga Pontara, Cambroncoi, Brombisc, Malga Stramaiolo, Bedelar, Prati di Montagna, Malga Trenca, Val Morta, Luserna Platz or Pletz von Mozze, Segonzano Peciapian, Transacqua, Valcava, Sant’Orsola, Terrebis) or by examining slag morphology (specifically, flat and homogeneous “*Plattenschlacken*”) have been dated to the Late and Final Bronze Age.

The ore deposits are primarily situated to the east of Trento, along the ENE-WSW Valsugana tectonic line (“Linea della Valsugana”), to the east of Monte Calisio, and along the north-northeast of the Mocheni Valley. These deposits feature a combination of sulphidic, carbonatic and oxidic ores. The principal minerals include chalcopryrite (abundant at Nogarè, Erdemolo, S. Francesco and Cinque Valli according to Preuschen (1973, pp. 122–129) and Cierny (2008), pyrite, arsenopyrite and galena.

The earliest copper smelting sites, dating back to approximately 3300-2900 BC, are often situated near rock shelters or conoids along the Adige valley floor (e.g., Riparo Marchi, Romagnano Loc III-IV, Romagnano Tof de la Val and Maso Monache, La Vela di Valbusa, Riparo Gaban, Volano San Rocco) and in open areas (Montesei di Serso, Croz del Cius above Pergine Valsugana), (Silvestri *et al.*, 2014). These sites offer insights into the initial phases of metallurgy’s development and dissemination throughout the region. They are all located at low altitudes, close to the river at the bottom of the valley. Smelting was commonly conducted in shallow pits lined with clay and possessing an oval shape or in furnaces with an open front.

For instance, the rock shelter of Riparo Marchi, located at 380m a.s.l. and 5 km from the city of Trento, on the left side of Adige valley, has revealed seven smelting furnaces through recent excavations carried out 2008-2009 (Mottes *et al.*, 2014). These furnaces were associated with slag heaps, ash, and wooden charcoal, distributed across various chronological phases. These furnaces all have one open side and range from 40 to 100 cm in length and a maximum depth of 20 cm. Within the central area of the shelter, traces of hole-in-the-ground smelting pits have also been discovered, with one of them lined with clay. Additionally, fragments of tuyères, including one entirely preserved, have been recorded (Mottes *et al.*, 2014). Preliminary analyses of five distinct flat and slim slags have been carried out, revealing mainly fayalite with magnetite inclusions. The presence of copper and iron sulphides in the magnetite suggests the use of copper sulphides in the charge.

In proximity to this site, at Gardolo di Mezzo, several coarse slags and grinding stones have been found. These artifacts are distributed across the entire lifespan of the settlement, from from the end of the Chalcolithic period to the Late Bronze Age, indicating intensive copper smelting

activities throughout its. The evidence from this site holds particular significance, as it may help bridge the chronological and geographical gaps in Trentino's archaeological record of Bronze Age copper smelting activities existence (Mottes *et al.*, 2012; Angelini *et al.*, 2013; Silvestri *et al.*, 2014).

In addition to these sites, evidence of smelting activities has been uncovered at Romagnano Tof de la Val, Trento. At this site, a thin ellipsoidal basin-like hearth was discovered characterised by a well-preserved base with a flat and smooth thermally altered “concolato” layer, measuring approximately 4.5 cm in thickness. This structure was built on top of a slag bed, and a well-preserved tuyere was found in a shallow pit near the hearth. Fragments of tuyeres were collected in the surroundings and scattered slags were detected across the site. These slags and tuyeres exhibit similarities to those found at Romagnano Loc IV and La Vela di Valbusa, which are associated with the Polada A culture (c.2300-1900 BC, Perini, 1973). Analyses of three slags (Cattoi *et al.*, 2000) at this site revealed their heterogeneity, featuring voids, unreacted chalcopyrite ore, and abundant calcium and silica embedded in a fayalitic glassy matrix. The matrix mainly consists of newly formed fayalite with skeletal or needle-like structures and micro-spinifex growths. Small amounts of magnetite are also present.

Further evidence of smelting activities has been recovered at the sites of Riparo Gaban, Acquaviva di Besenello and Romagnano Loc, Trento (D'Amico *et al.*, 1998; Cattoi *et al.*, 2000; Cattoi *et al.*, 2001; Pedrotti, 2002; Metten, 2003; Artioli *et al.*, 2009). In the first site, slag were discovered under a layer radiocarbon dated between 2600-2400 (Artioli *et al.*, 2009). In the latter location, a crucible fragment dated to the end of the fourth millennium (layer Q) was discovered (Perini, 1971, 1989; Cattoi *et al.*, 2000; Cattoi *et al.*, 2001; Metten, 2003; Artioli *et al.*, 2009). The analysis of the slags, including 12 from Riparo Gaban, 10 from Acquaviva, and 3 from Romagnano revealed their predominantly heterogeneous nature. They contain a notable amount of unreacted silica embedded in a glassy matrix, along with partially transformed sulphides and secondary sulphide segregations and copper droplets. They are primarily composed by fayalitic olivines and by pyroxenes and spinels (Artioli *et al.*, 2009; Cattoi *et al.*, 2001). The fayalitic olivines display variable quantities of zinc and calcium, often with a skeletal texture. The high presence of calcium, exceeding what can be attributed to the original charge (4.41% in the Romagnano Loc slag, 2.33% and 3.26% in those from Tof de la Val), along with the high presence of quartz, has led the authors to suggest that carbonate ores, such as calcite (CaCO_3), were intentionally added as fluxing agents to the smelting charge (Cattoi *et al.*, 2000; 2001).

Differences in the petrographic characteristics and compositions of the slags indicate that the ore, primarily chalcopyrite with small amounts of sphalerite, pyrite and covellite, likely originated from various deposits. These deposits were most probably situated at Calceranica, Vetriolo, at east of Riparo Gaban and Acquaviva in the Valsugana valley, or Val Felsina. Recent LIA analyses support this provenience (Artioli et al., 2015, p. 81). The abundance of iron olivines and the use of quartz as flux led Cattoi et al. (2001) to suggest that a single-stage process (i.e., excluding the roasting stage) was employed. According to them, if subjected to oxidation on a roasting bed, the fayalitic olivines would have transformed into hematite (Fe_2O_3) or magnetite (Fe_3O_4), making their re-reduction to iron olivines very difficult.

Moreover, slags, fragments of tuyères and potential roasting floors have been found at La Vela di Valbusa (Artioli et al., 2009; Fasani, 1990; Metten, 2003; Pearce et al., 2022; Perini, 1989a; Storti, 1991). Bulk quantitative analyses of 4 slags were performed by Storti (1991), who proposed that three of the slags are associated with the matte smelting process, while one, due to its higher concentrations of iron oxides and zinc oxide, is related to matte conversion (i.e., transformation of matte to metallic copper) (Storti, 1991, Table 1). Storti assumed that chalcopyrite was used.

A recent study carried out by Pearce et al. (2022) investigated 11 slags from La Vela di Valbusa and thirteen from Riparo di Monte Terlago. Overall, the authors proposed that the slag cakes from the first site had an original diameter of 12–14 cm and a weight of approximately 436 g. Most of the slag fragments exhibited relatively flat faces, bubbles and protuberances and are characterised by visible bits of quartz and chalcopyrite to the naked eye. A large area of matte was detected in the sample VB6. The slags from the latter site differ from those from La Vela only in being more fragmentary with fewer and smaller inclusions. All the slags are visually and morphologically similar, and they all appear to contain the same constituents. According to Pearce et al. (2022) they belong to a relatively standardised technological process.

After a macroscopic investigation, Pearce et al. (2022) selected two slags from La Vela di Valbusa and five from Riparo di Monte Terlago for an in-depth analysis using a combination of XRD, ICP-MS, and SEM-EDS. The primary aim was to gain insights into the smelting process that took place during the third millennium in Trentino. They identify substantial quantities of heavily thermally altered rock inclusions, primarily associated with chalcopyrite and pyrrhotite. These inclusions exhibited either foliated textures, as observed with quartz, phyllosilicates, and ore minerals, or they appeared as fine-grained ($<100\text{ }\mu\text{m}$) uniform clusters of ferromagnesian aluminosilicates with compositions resembling iron-rich chlorite. Often the voids are filled with chalcopyrite and pyrrhotite (Fig. 3. 8). The composition of the rock

inclusions closely mirrored that of other prehistoric slags discovered in the Trentino-Alto Adige/Sudtirol region (Pearce et al., 2022, p. 10). The predominant mineralogical compositions consisted of olivines, spinels from the hercynite-magnetite series, and high temperature silica phases such as tridymite and cristobalite. The olivines are primarily characterised by fayalitic cores (Fe-rich) with occasional detection of forsteritic cores (Mg-rich). By considering the temperatures at which olivine crystals took shape, with the formation temperature being 1320°C for the magnesium-rich core and 1220-1240°C for the iron-rich core, a temperature range spanning 80-100°C was identified between the commencement and culmination of olivine crystallization. It is important to note that the presence of inclusions and other components within the original charge that interacted with the olivine crystals had the effect of reducing the overall system temperatures. From a morphological perspective olivines presented a range of characteristics. These included hoppers, typically measuring less than 100µm, which varied from well-defined euhedral features to hollow elongated structures featuring distinct edge growth. In contrast, when it comes to spinels, aluminum oxide-rich spinels were evenly distributed throughout the slag. On the other hand, iron oxide-rich spinels were less prevalent and often clustered together. These could be interpreted as either residues from the initial charge or as products resulting from the oxidation of matte on the slag's surface. The presence of magnetite was also observed, both on the surface and within the slags. It appeared in the form of rims or bands within small clusters or oxidized layers. These iron-rich features displayed variations in size, ranging from 0.5 to 3 mm, as well as differing shapes and compositions. They were typically found in association with Cu-Fe sulphides and copper prills. The analysis additionally unveiled the existence of Cu-Fe sulphides at various stages of transformation in all the slags. Pearce and colleagues identified three primary categories: Cu-Fe sulphides trapped in gangue, primarily as undecomposed pyrrhotite and chalcopyrite (Fig. 3. 8 Fig. 3. 9); those confined within the slag, often exhibiting a round shape and occasionally linked with bubbles, characterized by a wide spectrum of Cu:Fe ratio compositions; and intermittent matte sulphides arranged in layers measuring 100µm to 1mm.

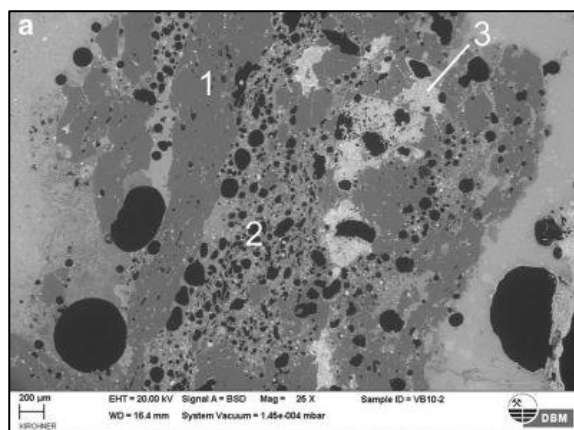


Fig. 3. 8 BSE micrograph showing a fragment of ore and gangue minerals decomposing and vitrifying inside the slag. The gangue exhibits a laminated texture with quartz (1) and decomposed phyllosilicates (2). The metalliferous phases (3) primarily consist of chalcopyrite together with lesser amounts of bornite, magnetite and pyrrhotite. Slag sample VB10, slide 2. (From Pearce et al. 2022, p. 12, fig. 5a).

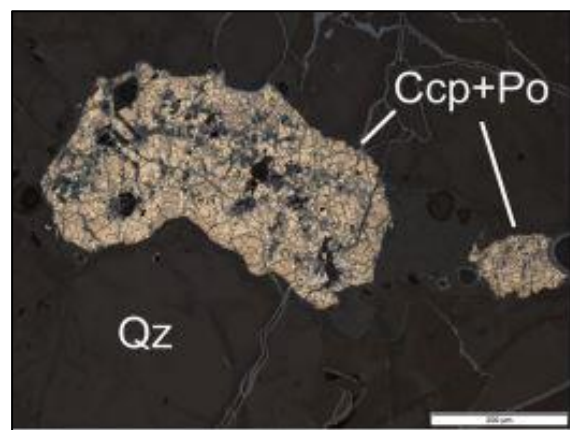


Fig. 3. 9 Digital micrograph showing a chalcopyrite (Ccp) and pyrrhotite (Po) sulphide inclusion in quartz-rich gangue (Qz). Slag sample VB10-3. Scale bar 200 µm. (From Pearce et al. 2022, p. 13, fig. 6d).

Another site with evidence of smelting activities is Montesei di Serso, situated in the upper Valsugana Valley, not far from the city of Pergine (Artioli et al., 2009; Marzatico, 1997; Metten, 2003; Perini, 1989a). A hearth with a series of smelting slags has been unearthed. Among these slags, a few exhibited a flat shape, a characteristic commonly associated with Late and Final Bronze Age sites. Interestingly, an investigation of the flat samples (Artioli *et al.*, 2009) revealed a high density and a substantial fayalite content. These samples also displayed a notable quantity of wuestite (FeO), indicating that the smelting process was carried out under highly reducing conditions. Similar characteristics have been found in some of the flat samples from Romagnano Loc. The primary copper ore use was chalcopyrite, although it was regionally associated with tennantite-tetrahedrite minerals. The minerals smelted at the site were likely sourced from mines located in Mocheni valley (Addis et al., 2017; Angelini et al., 2013; Artioli et al., 2014, 2015; Silvestri et al., 2014).

In close proximity to Montesei, the site of Croz del Cius has also revealed evidence of basin-like structures and square-shaped hearths associated with smelting activities. Nevertheless, determining the exact chronological context of these findings remains challenging, as radiocarbon dating results are currently lacking (Silvestri *et al.*, 2019).

Moving further north in the Isarco valley, traces of copper smelting have been found at the sites of Millan and Gudon. A substantial amount of slags, totaling around 1 tons was discovered at Millan, near Bressanone, in the Isarco Valley (Dal Ri *et al.*, 2005; Colpani *et al.*, 2009;

Tecchiati, 2009; Angelini *et al.*, 2013). These slags were found within the filling of an elliptical basin-like structure measuring 16 meters in length and 6-8 m in width. The filling also contained a thick charcoal, fragments of thermally altered clay, various-sized gravel, and numerous ceramic sherds. Notably, four fragments of tuyères for bellows were collected in the vicinity. The site has been interpreted as a ritual backfilling (Dal Ri *et al.*, 2005), and its dating has been established between 2800 and 2500 BC based on Bell Beaker-type pottery and a radiocarbon date. The slags themselves exhibit a wide range of dimensions, varying from a few millimetres to a maximum length of 20 centimeters and minimal thickness. These slags have been categorised into two groups. The first group includes heterogeneous and coarse slags characterised by a significant presence of gas bubble and vesicles, along with unreacted or partially reacted chalcopryrite (CuFeS_2) and quartz (SiO_2). The second group comprises homogeneous and dense slags, where very few bubbles and unreacted silica have been identified.

A similar and complementary situation was discovered at Gudon, a site situated on a gentle slope at an altitude of 600 meters a.s.l. near Chiusa in the Isarco Valley. The site features the remains of two circular stone structures that are open on one side and show traces of fire-related activities. Unfortunately, the poor state of preservation of these structures has made it challenging to directly associate them with metalworking activities. However, the suggestion of such activities is supported by the discovery of few kilograms of smelting slags, crucibles, and two tuyeres' fragments found in their vicinity. A radiocarbon dating of a charcoal sample from a layer above the structures yielded a date between 2504-2295 BC (Colpani *et al.*, 2009). The slags recovered from this site, which can reach a maximum length of 7 cm have been categorised into coarse, dense (lobate) and flat ("*plattehschlaken*") types. According to the authors, the presence of flat slags at this early period is particularly rare and unusual, as they are more commonly found in later periods.

The analyses of the slags from both Millan and Gudon indicate that they originated from sulphide-rich ores, primarily based on chalcopryrite minerals, with varying amounts of sphalerite ($(\text{Zn}, \text{Fe})\text{S}$) and galena (PbS). Their chemical signatures suggest that the ores came from different deposits. One of the significant sources is in Monte Fondoli/Pfundererberg near Chiusa/Klausen. The coarse slags are characterised by a high content of unreacted silica (80-90 wt%) and fayalite-rich olivines with variable percentages of magnesium and zinc. It remains uncertain whether the quartz was originally part of the charge or was deliberately added as a fluxing agent. The presence of residual quartz in the slags suggests that they never reached a fully liquid state and did not reach the eutectic melting point. The hopper and polyedrical

morphologies of the fayalitic olivines indicate slow cooling rates ($CR < 50^{\circ}\text{C/h}$) of the slags (Donaldson, 1976; Anguilano et al., 2002; Artioli, 2010). In the less reacted slags, newly formed copper sulphides in the form of digenite are present, while in the more reacted ones, covellite and chalcocite are detected. Although rare, the presence of zinc-rich sulphides (spahlerite) within the unreacted silica compounds in the Millan slags may indicate the deliberate addition of the same gangue as a fluxing agent. Very few copper droplets have been found in these slags (Artioli et al., 2005; Cremante & Storti, 2005). The coarse copper slags from Millan exhibit a mineralogical and textural composition similar to those found at Riparo Gaban, Acquaviva di Besenello, and La Vela di Valbusa (Artioli et al., 2009). Based on the slags advance stage, Artioli et al. (2009) proposed that ancient smelters did not need to undertake additional work to extract matte prills since the necessary matte had already been efficiently removed during the smelting process.

The flat slags, found exclusively at Gudon, are primarily characterised by a fayalitic glassy matrix (comprising 50-80 wt%), sometimes containing magnetite (Fe_3O_4) and wustite (FeO), and exhibit a limited presence or absence of unreacted quartz. These slags display a variety of olivine textures, ranging from chain-like to feather-like morphologies, indicating rapid cooling rates (hundreds $^{\circ}\text{C/h}$), in contrast to the coarse slags (Donaldson, 1976; Anguilano et al., 2002; Artioli, 2010). Within the magnetite-rich matrix, dispersed metallic copper droplets coated with a thin layer of chalcocite (Cu_2S) have been discovered. The variation in chemical composition, the occurrence of high temperature mineral phases, the olivine morphologies, and the presence of magnetite in certain samples collectively suggest that a non-standardized and poorly controlled process was carried out. This process was characterised by different time/temperature ratios in the charges and varying oxidising and reducing conditions in the reactors, aligning with the criteria of an inefficient copper extraction process typical of the Chalcolithic period (Bourgarit, 2007; Craddock, 2000).

3.4. Southeastern European region

Heading further east, this section focuses on the southeastern European region, commonly referred to as the "Balkans." This region encompasses the lands situated between the eastern shores of the Adriatic Sea, the southern borders extending to the Ionian and Aegean Seas, and the eastern boundaries reaching out to the Black Sea. It holds particular significance as it hosts the oldest evidence of copper minerals exploitation on the European continent (Fig. 3. 10).

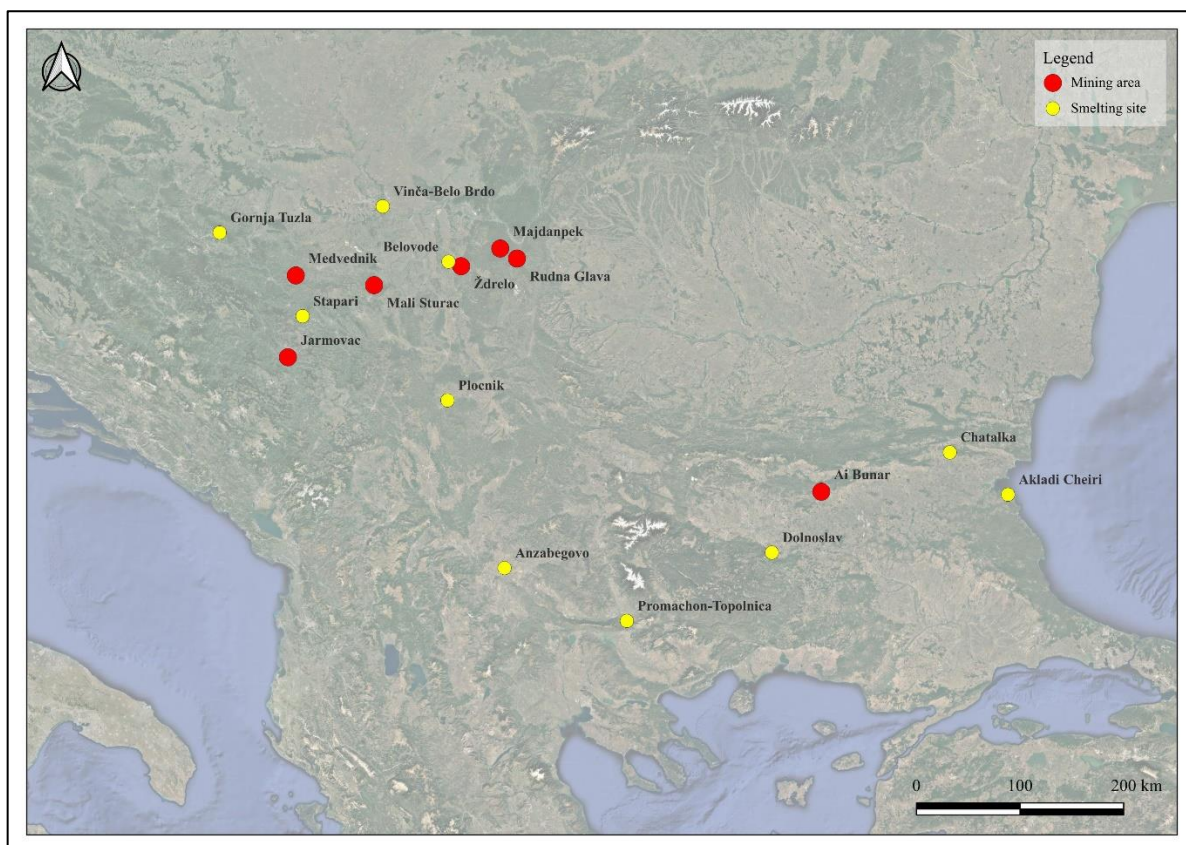


Fig. 3. 10 Map of the Southeastern European region, highlighting significant sites categorized into mining and smelting locations.

The first traces of copper metallurgy in the region date back to the transition from the Late Mesolithic to the Early Neolithic (c. 6200-5500 BC). This early copper mineral exploitation was likely initiated by hunter-fisher-gatherer communities coming from Anatolia (Radivojević & Roberts, 2021, p. 14). They left behind artifacts such as awls, fishhooks and rolled wire beads crafted from native copper and carbonates like malachite and azurite. These items have been unearthed in both settlement and funerary contexts associated with the agricultural cultures of the Balkan and Carpathian Basin (Kienlin, 2012; Radivojević & Roberts, 2021, p. 15).

With regards to mining activities all the following mines are situated within the copper bearing belt that stretches across the modern Bulgaria and Serbia (Chapman, 1981; Krajnović & Janković, 1995). The oldest mining evidence has been found at Rudna Glava in eastern Serbia (Borić, 2009; Jovanović, 1971; O'Brien, 2015), and at Ai Bunar, in central Bulgaria (Chernykh, 1978; Jovanović, 1976; Pernicka et al., 1997). It is worth noting that while other evidence exists, these are the only two mines securely dated to the fifth millennium BC.

The Rudna Glava mine, radiocarbon dated to approximately 5400-4650 BC (O'Brien, 2015, p. 161; Pernicka et al., 1993; Radivojević & Kuzmanović-Cvetković, 2014) is composed by

deposits rich in iron, primarily consisting of magnetite and pyrrhotite, with small veins of chalcopyrite, and by a zone under a gossan cover particularly rich of secondary copper minerals, mainly malachite, azurite and cuprite. The mining area features eight groups of mine shafts with access platforms, with thirty-two locations situated only in the northern side. Excavations in these shafts have revealed pottery associated with the Vinča culture, dating to the Gradac phase of the early and mid-fifth millennium BC, as well as stone mallets and tools made from deer antlers. The exploitation of the mining area gradually increased, reaching its peak around 5000 BC. However, surveys conducted by Radivojević and Roberts (2021, p. 18), led them to conclude that the mining area did not possess significant amounts of malachite. Unfortunately, no evidence of smelting or metalworking activities has been found in the proximity of the mine.

Another copper mine, where copper ores were extensively exploited, as evidenced by artifact provenance analysis (Pernicka et al., 1993, 1997), has been discovered in Majdanpek, situated only 12 km away from Rudna Glava (Krajnović & Janković, 1995). Unfortunately, any prehistoric evidence at this site has been obliterated due to modern mining operations. Copper mines associated with the Vinča culture have also been identified at various locations, including Ždrelo in eastern Serbia near Belovode, Mali Sturac in the Rudnik mountains in central Serbia, Medvednik in western Serbia, and Jarmovac in southwest Serbia along the homonymous river valley (Derikonjić et al., 2011; Jovanović, 1971, 1983; Pecikoza, 2011; Radivojević et al., 2010). The Mali Sturac mine, likely exploited by the Vinča groups based on similarities in the groove stone mallets recovered (Bogosavljević, 1995; Jovanović, 1983) and other materials dated to the mid to late fifth millennium (Antonović et al., 2014; Antonović & Vukadinović, 2012), is characterized by copper ores rich in lead and zinc, along with secondary copper minerals under a thick gossan cap.

The mine of Ai Bunar, near Stara Zagora, in central Bulgaria, was active during the period of approximately 4600-4100 BC, based on the materials associated with the Kodzadermen-Gulmenita-Karanovo (KGK) VI culture (Chernykh, 1992). This mine is primarily characterized by secondary copper minerals such as malachite and azurite, along with a small amount of low-grade copper sulphides (Pernicka et al., 1997). Eleven working locations were discovered, indicating an intense exploitation estimated to have extracted around 2000 to 3000 tonnes (500 tons of copper) of malachite (Chernykh, 1982; Chernykh, 1998) allowing for comparison with the Rudna Glava mine (O'Brien, 2015, p. 161). Despite the presence of copper minerals in the vicinity of the mining area and at several settlements associated with Gumelnita (Karanovo VI) and Maritza cultures pottery, no traces of smelting activities have been found.

Lead isotope analyses suggest that other mines were also exploited in that period, including the mine of Prochorovo, located 70 km east of Ai Bunar during the Karanovo V-VI period (Chernykh, 1978: 216), as well as mines around Burgas, Mednui Rud and Rosen in southeast Bulgaria during the Late Copper Age (Pernicka et al., 1997; Gale et al., 2003).

Smelting activities from the Early Chalcolithic are quite scarce in the central Balkans and are primarily associated with the Vinča culture. The oldest evidence of smelting, dating to approximately 5000-4600 BC, specifically during the Early Vinča period (Vinča B2) at the outset of the Gradac Phase, has been discovered at the site of Belovode. Belovode is located about 50 km from the mining site near the town of Petrovac na Mlavi in eastern Serbia, and it is the world's earliest known evidence of copper production (Radivojević, 2021; Radivojević et al., 2010, 2013). All the findings related to metal production, spanning the entire life of the site until around 4650 BC, comes from domestic contexts (Šljivar *et al.*, 2006). These findings include a range of thermally altered copper-bearing minerals, slags and slagged ceramic sherds fused with charcoal and ash and groove stoned mallets. Two small shallow pits, outlined by ceramic sherds along their edges, have been identified (Trenches 10 and 13) and interpreted by Radivojević (2021, p. 53) as furnaces, given their resemblance to small hearths previously discovered in the region (Dimitrov, 2002; Šljivar et al., 2006, p. 253). Compositional analysis conducted on the copper-rich ores reveal the presence of both copper oxides (carbonate) and sulphides. Notably, these minerals all share a common black and green colour. The black colour is attributed to the manganese content, while the green colour is due to the malachite content. Given the vast geological variability in the region (Janković, 1997), this colour consistency led Radivojević (2013; Radivojević & Rehren, 2016) to speculate that it might represent a deliberate choice by the metalworkers who deliberately limited their selection to these kind of minerals. The eight slag pieces uncovered in Trench 3 display strong magnetism, green-staining, highly viscosity and an abundance of copper droplets. These pieces measure approximately 1 cm in size and weigh only a few grams (Fig. 3. 11a). Although their small dimensions, no traces of breakage have been found on them. Major phases identified in these slaga include copper oxides (such as cuprite, Cu_2O), spinels, delafossite and metal prills entrapped in the glassy matrix. Furthermore, four slagged sherds found in two spits in trench 3 were heavily vitrified, exhibiting small green stains on the upper surface (Fig. 3. 11b), (Radivojević, 2013; Radivojević & Rehren, 2016). Analysis confirmed the presence of manganese (MnO) and copper oxides affirming their use in metallurgical activities. Embedded in the glassy matrix, multiple phases have been recorded, primarily copper-oxide-based

(ranging from cuprite to newly formed tenorite), delafossite, iron-rich spinels, leucite (KAlSi_2O_6) and pyroxenes (hedenbergite, $\text{CaFeSi}_2\text{O}_6$).

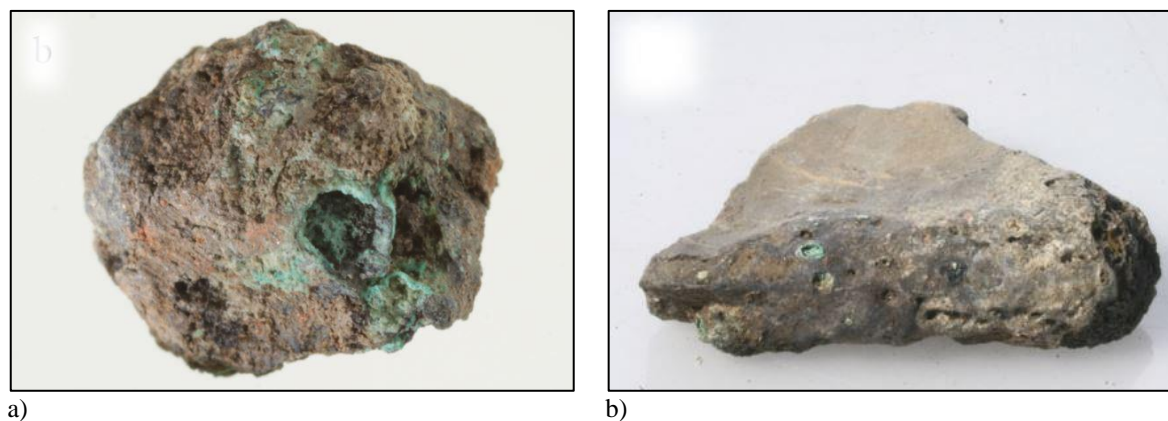


Fig. 3. 11 shows two of the by-products collected from the site of Belovode (c. 5000-4600 BC): a) a typical green-stained slag measuring less than 1 cm in size and weighing only a few grams (sample 134); b) a slagged sherd 6 cm large heavily vitrified with small green stains on the upper surface. From Radivojević, 2013: 16, fig. 3b, c.

Similar results have been obtained from the analysis of the free slags, which revealed a diverse composition of copper-rich phases (tenorite and cuprite), iron spinels, leucite and fayalite crystals, all intricately merged and distributed within the glassy matrix. Sulphur was detected in sample Belovode 131, and in the copper droplet M6, metallic iron prills and sulphur-rich phases were identified. These findings led Radivojević (2013) to propose the utilization of a combination of primary copper ore and carbonates (or oxides) in the smelting process at the site.

Traces of smelting activities have also been identified in other settlements in the region (Radivojević, 2013; Radivojević et al., 2010). In close proximity to the modern village of Vinča, at the site of Vinča-Belo Brdo, located 16 km south-east of Belgrade, evidence of smelting dated to the latest phase of occupation, between c. 4770 BC and c. 4600 BC (Vinča D) has been uncovered. These materials were discovered in domestic contexts. Four samples were studied, comprising one copper mineral (Vinča 99) and three copper slags (Vinča 79 e 91), with one of them (Vinča 79) found in close proximity to a heated surface (Radivojević, 2013; Radivojević et al., 2010).

Around the same period, a copper metal workshop has been dated to the site of Plocnik, situated approximately 20 km from Prokuplje in southern Serbia (Šljivar & Kuzmanović-Cvetković, 2009; Radivojević & Kuzmanović-Cvetković, 2014). Various artifacts were unearthed at this site, including pieces of copper minerals and lumps, a copper metal droplet and remains of a possible smelting oven. Notably, no traces of slag were found at the site, and these findings

span the entire period of the site's existence until its abandonment around 4650 BC (Radivojević & Kuzmanović-Cvetković, 2014; Sljivar, 2006).

In summary, the copper slags from the previously described sites exhibit a consistent series of characteristics in the assemblage over a 600-year period. The analyses carried out consistently revealed several key features: high iron, manganese, zinc and cobalt, arsenic, tin, and antimony content, the occurrence of various phases (heterogeneity), trace elements within the slag composition, the existence of fayalite crystallisations and metallic iron within the copper phases, the co-occurrence of cuprite and iron spinels and residual remnants of chalcocite (Radivojević, 2013). With the exception of the presence of delafossite (CuFeO_2), which merely indicated that the process occurred under moderately reducing conditions, all of these characteristics confirmed the occurrence of smelting activities (Radivojević, 2013).

Furthermore, the presence of copper sulphides in small quantities, often only as traces, in all of the examined assemblages suggests that their presence in the charge is related to the systematic heterogeneity of the ore bodies, which are typically characterised by both secondary (weathered) and primary minerals. This presence is not a deliberate choice made by ancient smiths. As previously noted by Rostoker et al. (1989), it is likely that the easily reducible carbonates and oxides exploited in the earliest stages of metallurgy incorporated bits of sulphide minerals. The deeper the ancient metallurgists mined, the higher the probability of encountering sulphide minerals (see the ideal representation described in Section 2.4).

The structures in which the smelting processes appeared to have been carried out were typically 'hole-in-the-ground' installations lined with ceramic sherds. These installations likely received their air-supply through the use of blowpipes or bellows. It is estimated that they reached a similar temperature, just slightly over 1083°C , under moderately reducing or partially oxidising conditions. This is suggested by the slagged sherds from Bolovode (Fig. 3. 11b) and a small ceramic sherd, measuring 5 mm in width, with green-stained droplets embedded in a grey mass found at the slightly later dated site (c.4400 BC) in Gornja Tuzla, located near the modern city of Tuzla in Bosnia and Herzegovina. The second artefact has not been interpreted as a crucible fragment, as the thermal alteration of an old fracture seems to indicate the potential adaptation of the piece to line a smelting pit for use after the break (Radivojević & Rehren, 2016).

These striking similarities in the materials, both at macroscopic and microscopic scales, suggest that the ancient metalworkers possessed comparable technological expertise and smelting principles. They also appeared to exploit similar ores, having a common understanding of the suitability for smelting distinctively coloured mixed minerals (Radivojević & Roberts, 2021, p. 17).

Some other evidence has emerged in the region, such as at the site of Anzabegovo in the eastern part of northern Macedonia (c. 5200 BC, Ferguson *et al.*, 1976), the site of Promachon-Topolnica on the Greek-Bulgarian border (Koukouli-Chrysanthaki, 2007, Fig. 7.4), and at the site of Stapari, in the southwest of Serbia (Jurišić, 1959). Unfortunately, no analyses have been carried out at these sites, making it challenging to provide characterisation of their smelting activities.

Moving to the Mid- Late Chalcolithic (c. 4600-4100 BC) there is a higher number of smelting-related evidence compared to the previous period. In Bulgaria, the oldest crucibles in the Balkans have been found at sites such as Dolnoslav, Chataalka, Akladi Cheiri (Ryndina *et al.*, 1999; Rehren *et al.*, 2016; Rehren *et al.*, 2020). Unfortunately, the crucible fragment from Chataalka has not been preserved. At Dolnoslav the crucible has an oval plan, a round base and walls that are 10-25 mm thick. Remarkably, analyses revealed that smelting activities involved polymetallic ores, including malachite and primary copper ores rich in zinc and lead oxides. The low traces of copper, along with the substantial presence of zinc and lead in the slag matrix, led Radivojević (2015, p. 332) to suggest that a more efficient smelting technology was adopted at this site compared to the process(es) conducted at Vinča. Differently, the crucible found at Akladi Cheiri does not exhibit other evidence than copper oxide on the inner walls, indicating its use for (re)melting purposes than smelting (Rehren *et al.*, 2020). Alongside this crucible, around 300 slagged ceramic sherds were discovered, similar to the slagged fragments found at Belovode and Gornja Tuzla above mentioned. Analyses of these materials showed the presence of fayalite, magnetite associated with matte and copper, copper sulphides and olivine crystals. These findings suggest unstable reducing conditions during the smelting process and the use of polymetallic ores.

Given their close proximity to metalworking tools and by-products, several potential other instances of smelting evidence from the Late Chalcolithic period have been discovered at various locations. These include Kmpije in Bor in eastern Serbia (notable for slagged sherds), Tibava and Tiszaplgár-Hajdúnánás in eastern Slovakia (where crucibles were found), Poduri-Dealul Ghindaru in Romania (also featuring a crucible), Sitagroi in northern Greece (with slagged sherds as well). Unfortunately, no archaeometallurgical analyses have been carried out on these findings, making it impossible to confirm their role in the copper production *chaîne opératoire* (Radivojević & Roberts, 2021, p. 21). It is worth noting that the mining area surrounding Bor is characterised by the presence of copper sulphides (covellite), pyrite and quartz, suggesting the potential exploitation of primary ores.

3.5. The Iberian Peninsula

A distinct narrative emerges when examining the archaeometallurgical landscape of the Iberian Peninsula (Fig. 3. 12). This region is one of the most mineralized areas in Europe (O’Brien, 2015, p. 77). In particular, the southwestern region stands out, featuring the highest amount of prehistoric copper mines. These mines are predominantly located in Huelva province and in the neighboring provinces of Badajoz, Cordoba, and Sevilla forming a significant part of the Iberian Pyrite Belt, a globally renowned mining area (Sáez *et al.*, 1996; Almodóvar *et al.*, 1997). Impressively, approximately 75 major ore deposits have been identified within a vast 250 km stretch westward from Sevilla through Huelva province into southern Portugal (Blanco-Freijeiro & Rothenberg, 1981; Hunt Ortiz, 2003). Pyrite Belt ores have systematically been mined from the 3rd millennium BC onwards. Additionally, the Galician and Cantabrian mountains in northern Spain, for instance, boasted a diverse array of mineral resources, including copper, lead, tin, silver, and gold mineralisations (O’Brien, 2015).

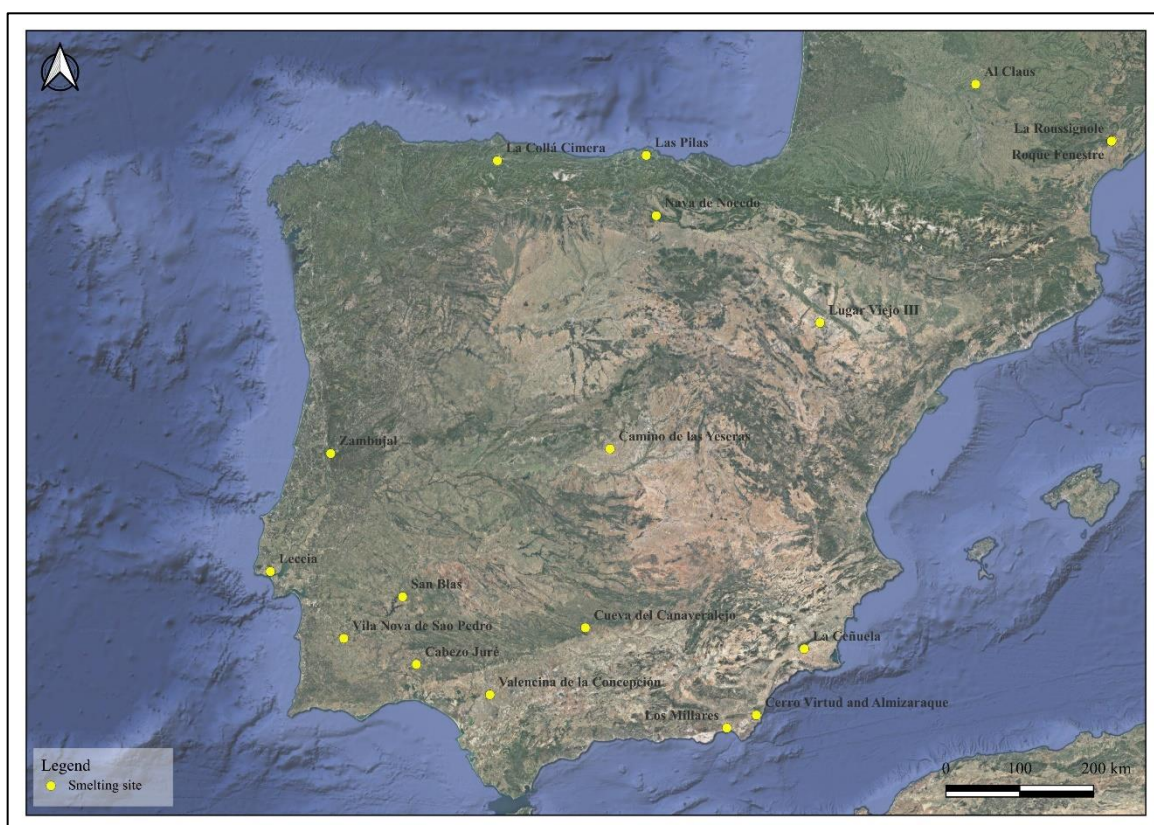


Fig. 3. 12 Map of the Iberian Peninsula, indicating key sites categorized as mining and smelting locations. While specific mining areas are not marked due to the vast number of deposits identified in the region, the main areas are described in the text.

In this mineral-rich landscape, copper resources were widespread, albeit often on a relatively modest scale, primarily manifesting as copper oxides and carbonates, particularly malachite (O'Brien 2014). As a result, the earliest evidence of copper smelting activities predominantly consists of slags and other by-products stemming from the exploitation of copper oxide and carbonate ores (R. Chapman, 2008). Remarkably, the earliest traces date back to the early 5th millennium BC and were unearthed in the settlement of Cerro Virtud in Almeria, south-eastern Spain. At this site, a fragment of a crucible used for smelting oxidized copper ores was found (Montero-Ruiz & Ruiz-Taboada, 1996; Ruiz-Taboada & Montero-Ruiz, 1999). However, this finding has raised some skepticism as it would predate the established origin of metallurgy in the Peninsula by a thousand years (Roberts, 2008, 2009; Roberts et al., 2009). Despite these doubts, copper minerals, primarily carbonate ores have also been found at the Neolithic sites of Nava de Nacedo in Burgos (Murillo-Barroso & Montero-Ruiz, 2012) and La Collá Cimera in Quirós, Asturias (de Blas, 1996), reinforcing the hypothesis of early copper production in the region.

Nevertheless, traces of sulphide exploitation have been sporadically identified at sites like La Ceñuela, in Murcia province (Rovira & Ambert, 2002, p. 91), and Lugar Viejo III, in Zaragoza province (Le Duc *et al.*, 2022).

At La Ceñuela, several slagged fragments of a 50cm-diameter reducing crucible were found (Rovira, 2007, pp. 88–89). The analyses of a few of these displayed fayalitic structures, as opposed to the slags from Almizaraque. The absence of slags at the site led the authors to think that the fayalite was the result of the smelting of a specific charge rather than the product of an intended slagging method. A series of pure copper sulphide idiomorphic crystals were identified, which the author interpreted as the exploitation of sulphide ores probably naturally mixed with other polymetallic ores containing arsenic, antimony, lead and bismuth (Rovira, 2007, Fig. 6). The site of Lugar Viejo III, dated to Chalcolithic based on its ceramic assemblage aligning with the Bell Beaker culture (2650-2100 BC, Harrison 1988, provided several slagged crucible fragments. Recent investigations conducted by Le Duc *et al.* (2022) focused on the analysis of two of these fragments. In one of the samples, the research team discovered a white prill of chalcocite, although only a limited number of sulphides and sulphates were detected in the entire sample set. According to them, the presence of these compounds may also be attributed to post-depositional weathering processes. The low sulfur content in the samples implies a prevalent utilization of oxide and carbonate ores.

While sulphides in the region have typically been considered as contaminants from oxidic ores (Müller *et al.*, 2004; Müller *et al.*, 2006, p. 51), rather than remnants of intentional sulphide

utilisation, as observed in other regions like the southwestern French Alps (see Section 3.2) and the Italian peninsula (see Section 3.8), recent findings in Cueva del Canaveralejo, Córdoba, Andalucía (La Duc *et al.*, 2022) offer evidence suggesting a tradition of sulphide smelting. Two slag cakes dating to the third quarter of the third millennium BC, were found and investigated (Jabalquinto Expósito, 2022). These slags differ from other evidence in the Peninsula in several aspects. They are notably larger, weighing 127g and 124g, measuring 6.3x7.8cm and 5.6x6.5cm respectively, whereas slags from Las Pilas weigh a total of 377g with an average weight of 4g per slag (Murrillo-Barroso *et al.* 2017, 1541 and 1552-3) and slags from Zambujal a total of 30g (Gauß, 2013, p. 213). Exceptions are Cabezo Juré cakes up to 1 kg (Saez *et al.*, 2003a), and Valencina de la Concepción where approximately 16 kg of slag were found (Nocete *et al.*, 2008, p. 725). Large slags suggest the performance of a slagging process.

Furthermore, their fayalitic composition with iron oxide content at 66.6% and 69.0%, and silica content at 23.7% and 24.3% respectively is unexpectedly high. They also contain a lower copper content, indicating higher smelting efficiency compared to other evidence in the Peninsula. Moreover, the presence of sulphides has led the authors to suggest co-smelting of oxides and sulphides. In support of this hypothesis is the high copper production rate, which might have been achieved through the co-smelting of oxides and sulphides, as experimentally demonstrated by Rostoker *et al.* (1989). However, whether the addition was intentional or simply the result of using mixed ores remains uncertain.

As recently emphasised by Le Duc *et al.* (2022), previous research in the Iberian Peninsula has primarily focused on the south-west, encompassing Southern Portugal, southwestern Spain, and the south-east. The former has seen extensive research conducted at notable sites such as Zambujal (Müller *et al.*, 2007), Vila Nova de Sao ~ Pedro (Müller & Soares, 2008), Cabezo Juré (Saez *et al.*, 2003), Valencina de la Concepcion (Nocete *et al.*, 2008), and San Blas (Hunt Ortiz *et al.* 2009). Meanwhile, the latter region includes sites like Almizaraque (Müller *et al.*, 2004; Murrillo-Barroso *et al.*, 2020), Los Millares (Hook *et al.*, 1991), and Las Pilas (Murrillo-Barroso *et al.*, 2017), all located in the province of Almería. It is crucial to note that this limited scope of investigation overlooks potentially valuable sources of evidence, notably the resource-rich central Sierra Morena and Catalonia, both renowned for their substantial copper-bearing ore deposits (La Duc *et al.*, 2022). Such a concentrated research focus might unintentionally result in a biased understanding of the broader context.

3.6. Northwestern European region

Although far from the chronological focus of this work, I reported the evidence collected from the north-west of Europe, as it gave interesting insights, and it has been helpful providing valuable examples of the smelting techniques developed enhancing the overall context of the research.



Fig. 3. 13 Map of the Northwestern European region, showing relevant sites categorized into mining and smelting locations.

The current state of the research in north-west Europe reveals a significant disparity in knowledge between mining and smelting technology. While ample evidence exists for mining activities, our understanding of the smelting processes remains quite limited.

The bulk of available information has been collected from investigations carried out at the Ross Island mine in Ireland (O'Brien, 2004), and, to a certain extent, from scientific analyses of metal artefacts (Needham, 1996; Needham et al., 1989). The latter approach has played a pivotal role in unravelling the technological intricacies of metalworking during the Beaker period (and the Bronze Age) in this region. Ross Island, located in County Kerry in the south-west of Ireland,

stands as a pioneering copper source that was exploited around 2400 BC (O'Brien, 2004). The mine boasts distinctive cave-shaped entrances leading to tunnels descending to depths of 10-12m. Adjacent to this site, evidence of metal production activities has been uncovered within a working camp. Excavations at the site, exposing an exceptionally productive mine, have successfully linked mine workings and high-grade tennantite ore deposits (residues of the early ore washing operations) to a Beaker/Final Neolithic working camp (2400-1900 BC). This intersection of mine operations and ore deposits facilitated the early processing of low-arsenic copper-bearing ores by ancient metalworkers. It is noteworthy that within a fully Neolithic context on the island, there has been no indication of heat treatment applied to native metals or oxide ores (O'Brien, 2004; O'Brien & Comber, 2008).

The minerals extracted from Ross Island comprised complex polymetallic combinations of sulphide and sulpharsenide ores, along with fahlertz group minerals rich in copper (40-45%), arsenic, lead, zinc and low iron content (<5%). O'Brien (2004, p. 235) classified the samples from the Beaker/Early Bronze Age period into three primary categories: a) "*fine-grained, banded, massive sulphides, mostly banded chalcopyrite-pyrite ores with tennantite and minor galena and sphalerite*", from the Blue Hole mine, period 2A (2400-2200 BC); b) "*coarse-grained, non-banded sulphides*" and c) "*cross-cutting veinlets of chalcopyrite-tennantite ore*" from western mine area (2200-1900 BC). According to him, the composition of this ore, characterised by its low iron content, the presence of volatile arsenic (20%) and sulphur impurities within tennantite mineralisation, may elucidate the absence of slags. Various experiments using ores from the western mine (roasted tennantite-rich copper ore) have demonstrated the feasibility of a two-steps, non-slagging smelting process (O'Brien, 2004). This primitive, low temperature smelting process (Craddock, 1995) was conducted under suboptimal reducing conditions in a rudimentary pit furnace operated with manual bellows for ventilation.

Evidence of smelting activities during the Beaker period at Ross Island is substantiated by the discovery of a stratigraphic sequence (period 2A) containing several furnace pits and stone-chambered hearths. The dimensions of the furnace pit C.1034 measure 1.07 meters in diameter from east to west, 0.70 meters from north to south, and has a depth ranging from 0.25 to 0.35 meters (Fig. 3. 14). The surroundings are characterised by reddened soil, scatter deposits of crushed copper ore, residues of fuel ash-charcoal, quartz sand flux deposits, and a small droplet of copper containing 0.01% of iron and 7% of arsenic. These findings suggest that copper ore was likely subjected to roasting and/or smelting processes (O'Brien, 2004).

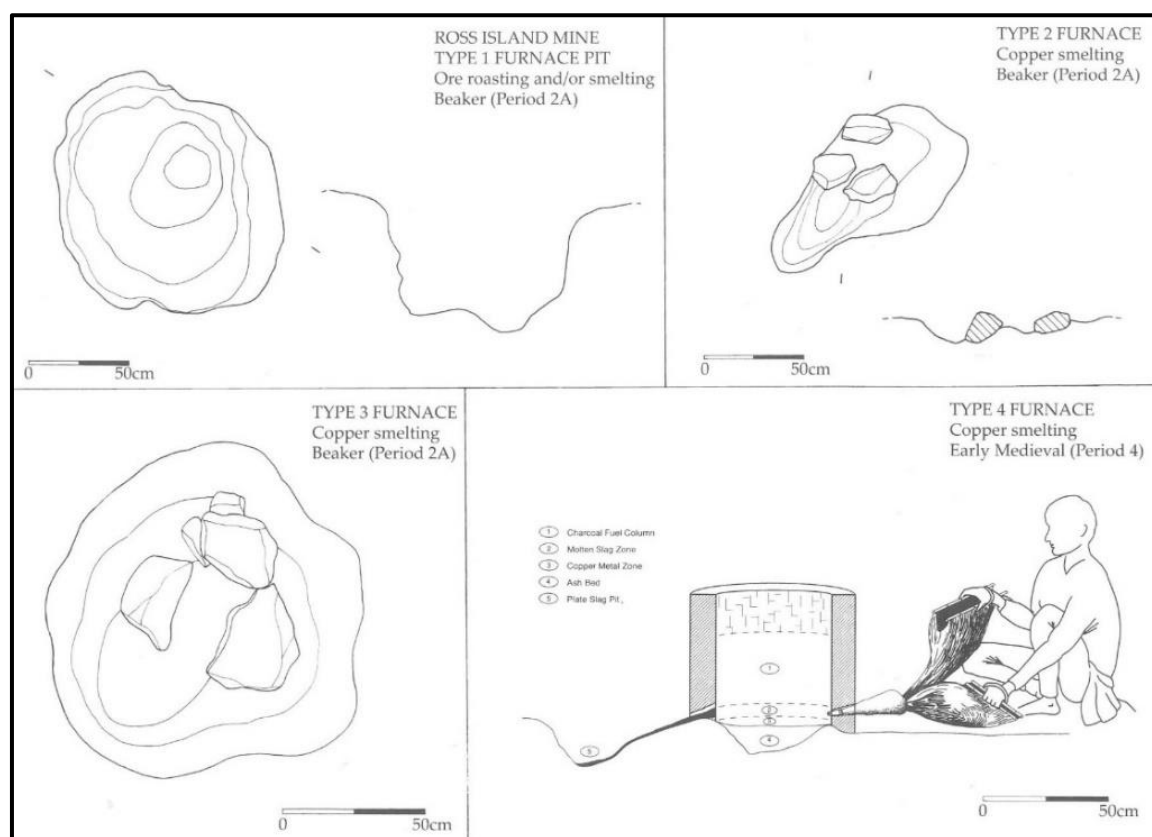


Fig. 3. 14 Three different types of furnaces unearthed at Ross Island mine, and an Early Medieval reproduction. From O'Brien, 2004, p. 466, fig. 217.

3.7. The site of Orti Bottagone, Tuscany

In the subsequent section, the main focus pivots towards the primary research site, Orti Bottagone, and a comprehensive overview of the current body of knowledge regarding copper mining and smelting in the designated region is presented (Fig. 3. 19).

The site is located within the municipality of Piombino, Italy, in a level coastal region situated 2 kilometers inland from the coastline (Fig. 3. 15). It holds a significant position where the maritime brackish marsh of the Orti intersects with the freshwater swamp of the Bottagone. This confluence creates the protected natural oasis known as Padule Orti-Bottagone, which has been a part of the WWF since 1991. The oasis serves as a valuable testament to the once-extensive marshlands of the lower Val di Cornia, which were lost due to reclamation efforts.

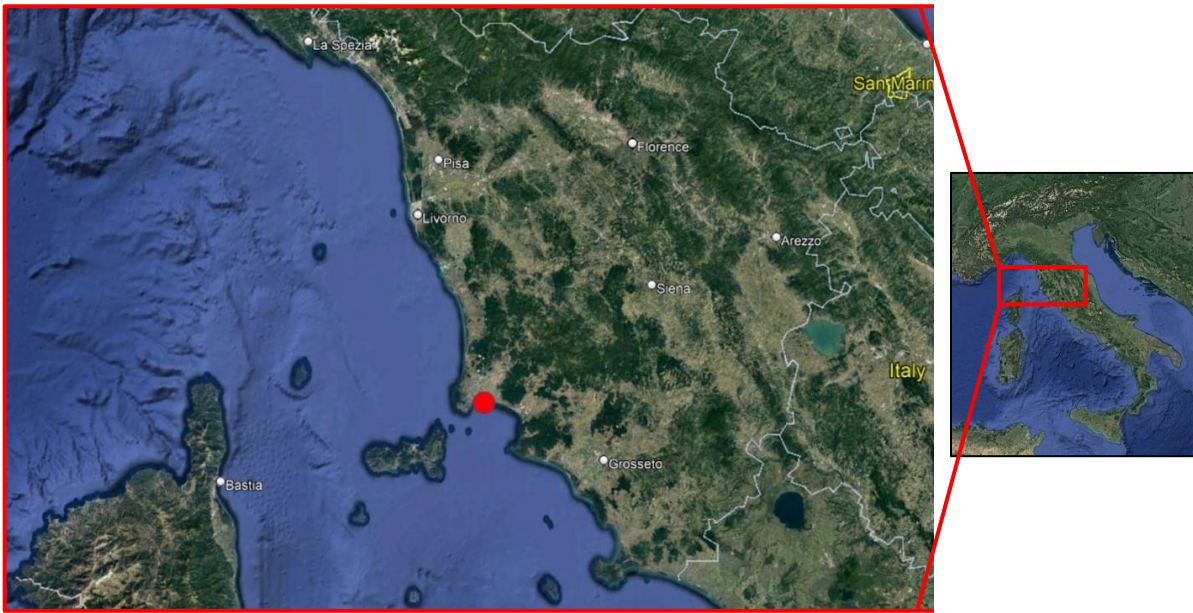


Fig. 3. 15 Location of the site of Orti Bottagone investigated in the current research.

The site was initially unearthed by the archaeologist Fabio Fedeli in 1997 during extension work on the Orti Bottagone wildlife oasis, as noted in his work (Fedeli, 1999). Unfortunately, shortly after its discovery the site was submerged by floodwaters, effectively hindering any further excavation efforts. In July 2022, I personally visited the site's location with the primary aim of conducting an assessment to determine the feasibility of starting an excavation. The area exhibited a distinctive landscape characterised by the alternating patterns of intertidal creeks and patches of shrubs. During my visit, I had the opportunity to converse with the local oasis manager, who provided valuable insights. I learned that the site remains predominantly submerged under a mixture of water and mud throughout the year, influenced by both freshwater and saltwater due to the ebb and flow of tides (Fig. 3. 16). The sole exception to this inundation occurs during a brief period at the end of August, following the summer draught.

However, prior to the flooding incident, a series of surveys were conducted at the site, leading to the identification of various areas containing dispersed materials and the collection of stray artifacts, including several slags. Despite the absence of a stratigraphic context, the ceramic assemblage recovered reveals distinct vessel forms that align with the Late Neolithic Ripoli culture. Notably, the presence of a series of tubular handles equipped with horn-shapes appendages (see Fig. 3. 17 a, b), as well as truncated-conical bowls with walls featuring either a convex or straight profile (see Fig. 3. 17c), provides the most discernible diagnostic evidence.

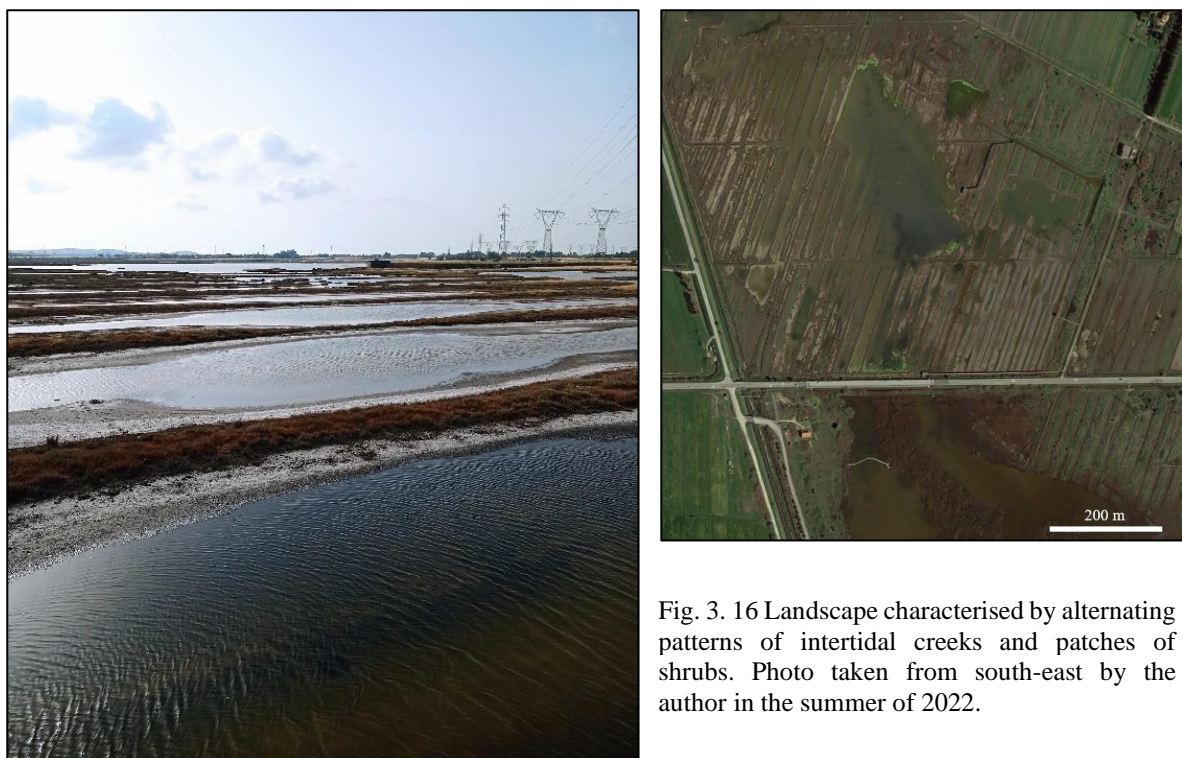


Fig. 3. 16 Landscape characterised by alternating patterns of intertidal creeks and patches of shrubs. Photo taken from south-east by the author in the summer of 2022.

Furthermore, charcoal samples obtained from one of the slag specimens underwent recent analysis (AMS) by Artioli, resulting in a calibrated radiocarbon date pointing to the second half of the 4th millennium. Regrettably, this date remains unpublished and has only been mentioned *en passant* in Fedeli and Galiberti's work (2016, p. 147). If confirmed, this dating would place it contemporaneously with the Monte Loreto mine (Beta-203528: 5010±40 BP, calibrated 2σ range: 3940-3700 BC), making it one of the most ancient pieces of evidence for copper smelting in Europe (see Maggi & Pearce, 2013, Table II). Moreover, similar archaeometallurgical evidence have been uncovered at the nearly contemporaneous, neighboring site of San Carlo Cava Solvay (Artioli et al., 2016) as mentioned previously. However, it is worth noting that Pearce (2015, p. 51) has cautioned against drawing conclusions, as Bronze Age materials were also found at the site as reported by Fedeli (1999).

Given the paucity of detailed archaeological information, this study focuses more on the technical aspects of the evidence, allowing for a deeper understanding of the metallurgical processes involved.

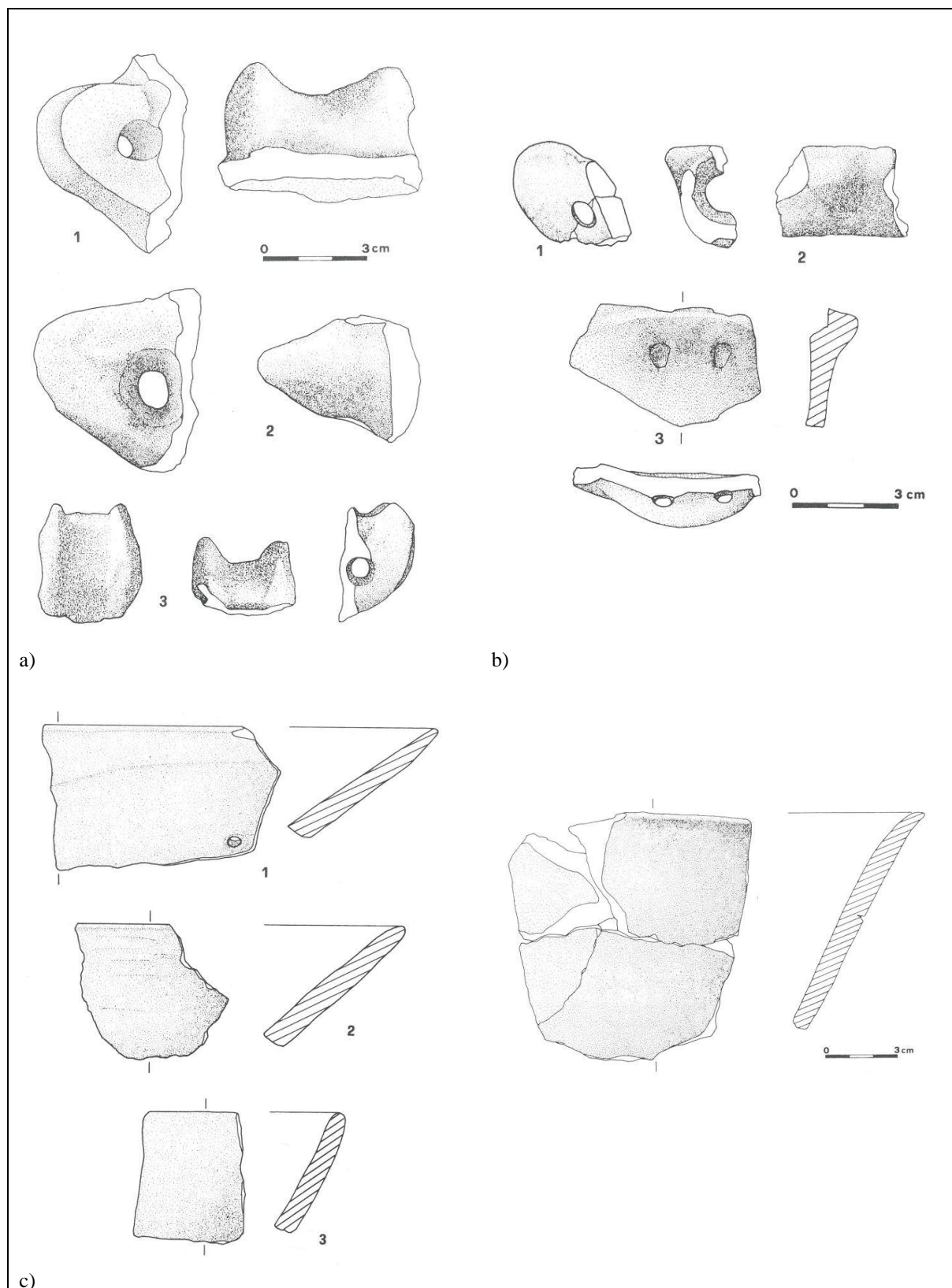


Fig. 3. 17 Distinct vessel forms aligned with Late Neolithic Ripoli Culture recovered at the site of Orti Bottagone. (From Fedeli 1999: a) p. 118, fig.3; b) p. 122, fig.6; c) p. 120, fig.4; d) p. 121, fig.5).

In an innovative approach to sample investigation, an X-ray computed tomography (CT) scanner was employed with the intention of identifying charcoal samples in the slags. This

technique, which had not been previously applied for slags investigation, offered a fresh perspective on the matter. The primary objective was to explore the inner composition of the slag without the necessity of physical sectioning, with the aim of identifying any remaining charcoal fragments and determining the most suitable locations for their extraction. Three coarse samples underwent virtual dissection, combining simultaneous views from three different planes (XY, YZ, XZ) and heat-maps to better highlight the internal features. As shown in Fig. 3. 18 this allowed for the assessment of various compositional features and voids within the specimen. However, despite the meticulous efforts, the investigation of the three samples did not yield any charcoal samples. The potential advantages and implications of this innovative technique for slag analysis will be further develop in the concluding remarks of this thesis.

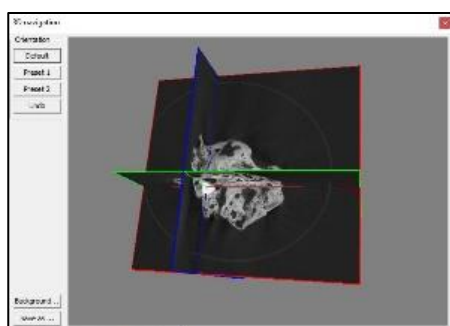
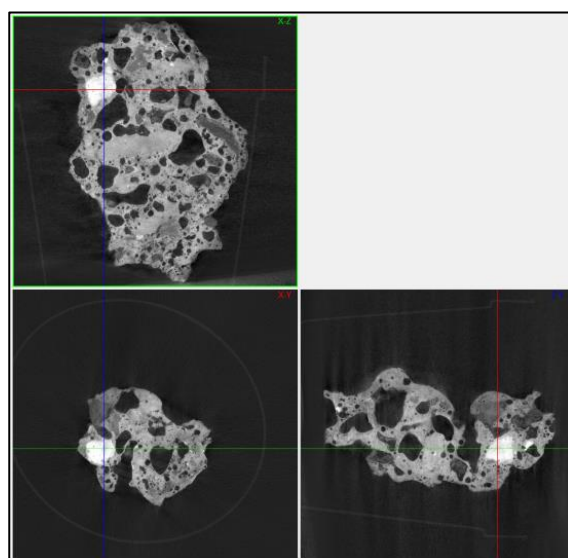
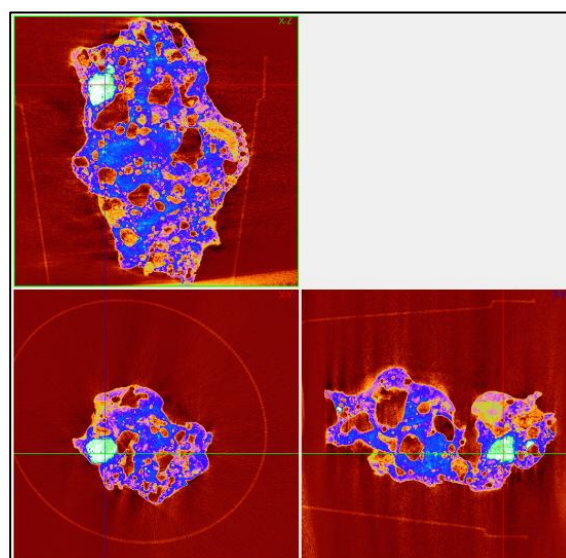


Fig. 3. 18 displays a) a simultaneous view of three different planes (XY, YZ, XZ), along with b) the use of a heatmap. This arrangement enables a comprehensive examination of the internal structure of the specimen.



a)



b)

3.7.1. Archaeological context

To date, the earliest evidence of copper metallurgy discovered in the Italian peninsula date back to the Late and Final Neolithic (4500-3600 BC), (Dolfini, 2014). Notably, the north-west region of the Italian peninsula, particularly eastern Liguria, stands as a significant area with the earliest

traces of copper mining and metalworking discovered to date (Campana et al., 1996, 1997). Discovered by the geologist Arturo Issel during mineral exploration, the earliest evidence of copper mining can be traced to the Libiola and Loreto mines, situated in the area of Sestri Levante, within the Genoa province. These mines respectively date back to the end of the 4th millennium and the period between approximately 3500-2500 BC (Maggi & Pearce, 2005; Pearce, 2007).

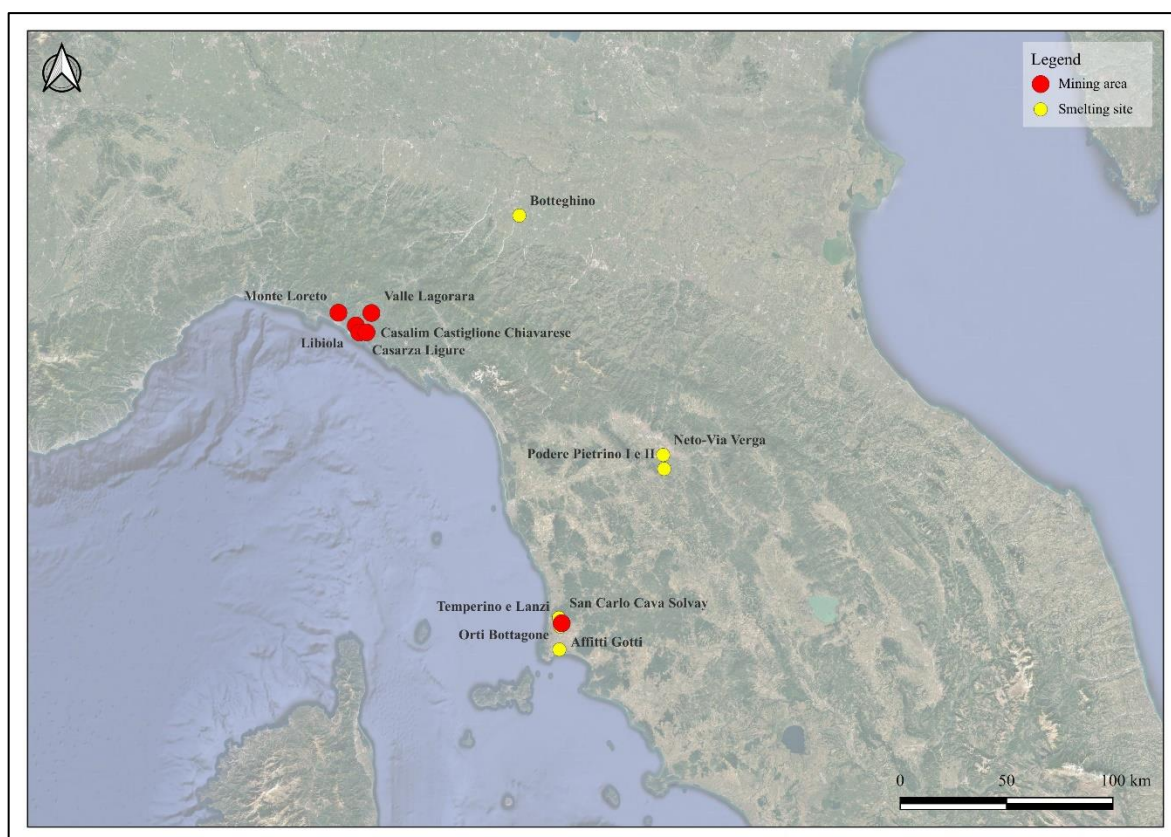


Fig. 3. 19 The map highlights significant sites categorized as mining and smelting locations in the Western Italian peninsula, providing a comprehensive overview of the current body of knowledge regarding copper mining and smelting in this region.

The Libiola mine, located 8 kilometers northeast of Sestri Levante in the eastern side of Gromolo valley, is characterised by extensive deposits of pyrite and chalcopyrite-rich mineralisation (25-35_{wt}% sulphides). Despite the destruction of most ancient mining evidence during early modern activities, a number of mine working tools were uncovered, including stone hammers, wooden wedges, a shovel and an oak pick-handle (Issel, 1879, 1892: 4-6). Radiocarbon dating of the latter artifact has placed the site in the timeframe of 3490-3120 BC (Campana et al., 1996, pp. 16–22; Maggi & Del Lucchese, 1989, pp. 336–338).

Not far from Libiola mine, just a few kilometres inland, lies the mining area of Monte Loreto. This region primarily contains chalcopyrite distributed within a number of copper veins embedded in a basalt geological context (Pearce, 2007). O'Brien's research (2015) suggests that weathered secondary copper minerals, such as malachite, associated with the exposed part of the mineralisation, were the primary targets of mining activities at Monte Loreto. Several traces of mine workings and evidence of ore-dressing facilities (Maggi & Pearce, 2005) have been recorded on the slopes of the mountain. These features include vertical trenches, some of which appear to have been backfilled once fully exploited, steeply inclined pits, shallow mine working areas, graded deposits of gangue and "country rock" (the rock surrounding the ore, Maggi & Pearce, 2005, p. 69). Additionally, compacted ore surfaces have been interpreted as temporary working floors for activities like grinding, sieving or roasting (Fig. 3. 20). However, it's essential to highlight that none of the metal objects analyzed and reported in the existing literature exhibit the isotopic signature associated with the ophiolitic mines of eastern Liguria (Dolfini *et al.*, 2020).

Apart from the Libiola and Loreto mines, geologist Issel's explorations in the Ligurian Alps led to the discovery of additional mining sites, including Val di Spine, Bargone in Casarza Ligure, Casali in Castiglione Chiavarese, and Monte Bardeneto in Statale (Issel, 1879, 1892). Unfortunately, no further investigations have been carried out at these locations. During his extensive explorations, in close proximity to a copper mineralisation site, Issel also came across copper smelting slags dating from approximately 3365-3045 BC at Valle Lagorara in Maissana (Cortesogno & Gaggera, 2002; Maggi *et al.*, 1995). Subsequently, a sample of these slags was subject to analysis by Artioli *et al.* (2009), who concluded that, despite the presence of glassy and crystalline phases, such as olivine, pyroxenes, and spinel, which is indicative of high temperatures processes, the absence of copper-bearing phases suggests that these slags are not the by-products of copper smelting processes.

Within this region, one of the most extensively investigated and published sites, albeit now destroyed, is the site of San Carlo - Cava Solvay, dating to the late fourth millennium BC (Fedeli & Galiberti, 2016). The site, along with the one currently under study, stands as one of the earliest sites in Western Europe revealing traces of copper smelting technology. Situated near the small town of San Carlo in the municipality of San Vincenzo, Tuscany, it resides within the Colline Metallifere (Ore Mountains) region.

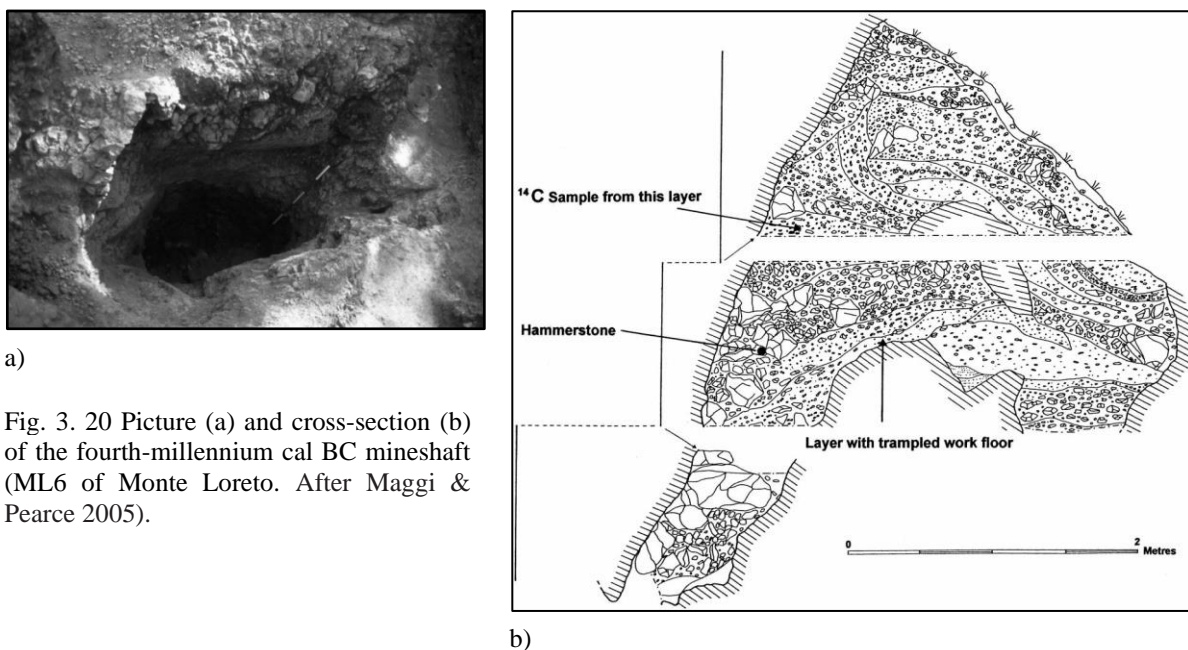


Fig. 3. 20 Picture (a) and cross-section (b) of the fourth-millennium cal BC mineshaft (ML6 of Monte Loreto. After Maggi & Pearce 2005).

The Temperino and Lanzi mines are located just 3 km away, with the Cornia river flowing 6 km to the South and the coastline of San Vincenzo lying 5 km to the west (see Section 8.3). The discovery of this settlement can be traced back to the 1970s during quarry expansion works. During these operations, slags and pottery fragments were collected, underscoring the great importance of the site. It wasn't until 1991, due to the advancement of quarry works, that a rescue archaeological excavation was initiated, overseen by Dr. Romualdi, at the time a local official of the Archaeological Superintendence of Tuscany, and led by Dr. Fedeli, in collaboration with the Piombinese Archaeological association (Fedeli & Galiberti, 2016). The excavation uncovered several fired-clay platforms partly surrounded by curvilinear limestone walls (refer to Section 6.3), as well as various slag remnants. The analysis of these slags revealed that copper was extracted from sulphides and sulphosalts ore. Remarkably, the analyses showed mature silica slags devoid of unreacted ore, Cu-Fe sulphides or prills embedded within them. This composition contrasts with the typical findings observed in Chalcolithic metallurgical residues (Bourgarit, 2007). These results prompted Dolfini et al. (2020) to suggest the use of an advanced smelting technology, involving the crucible co-smelting of mixed charges consisting of copper sulphides and oxides. This thesis challenges the idea of crucible co-smelting and puts forward an alternative smelting process, which has been tested and evaluated (see PART II).

As evidence of the region's significance during the Final Neolithic and subsequent periods, copper smelting evidence has been discovered in multiple locations. Unfortunately, none of the

smelting by-products has undergone analysis. Several slags have been unearthed at the nearby contemporary site of Affitti Gotti (Fedeli, 2000). At the site of Neto-Via Verga in Sesto Fiorentino, an awl, a crucible, multiple slags, alongside metalworking hearths (horizon 5) were uncovered, dating to 3710-3370 cal BC (Sarti & Volante, 2002, pp. 441, 444; Volante, 2003, p. 378, 487, 499; Sarti *et al.*, 2005). Near to this site are the sites of Podere Pietrino I e II (PO73 e PO74). Both of these sites have yielded a series of slags, crucibles, and a tuyere (Sarti *et al.*, 1999, p. 37; Sarti *et al.*, 2005; Perazzi and Poggesi, 2011). At the site of Botteghino, in Parma province, located in the northwest of Italy, a fragment of a crucible has been discovered in a Chassey-Lagozza culture context, dating to around 4300 cal BC (Pearce, 2015). This finding has been considered as indicative of smelting activities conducted at the site (Mazzieri & Dal Santo, 2007). However, it is essential to exercise caution, as initial macroscopic investigations carried out by the writer did not provide the necessary information to identify the artifact as a smelting crucible. Microscopic and chemical investigations are required to substantiate these claims. Copper slags were also identified at the Final Neolithic site of Santa Maria in Selva, located in east-central Italy (Silvestrini *et al.*, 2002, p. 458).

It is worth underscoring that a portion of these by-products should have been incorporated into the current research. Unfortunately, the COVID-19 pandemic hindered the possibility to proceed with the analysis.

The literature review has provided valuable insights into the earliest evidence of sulphide copper smelting in the European context, challenging the conventional assumption that copper production during the early stages of metallurgy primarily involved reducing carbonate and/or oxide ores with sulphide ore smelting emerging later. This growing body of evidence suggests that the simple metallurgy of sulphide ores may have been more widespread during this time than previously believed, portraying a more complex and varied scenario. To summarise, copper sulphide smelting has been discovered at Chalcolithic European sites, such as Millan and Gaban in the Italian eastern Alps, Al Claus in the south-western French Alps, and La Cenuela in south-Eastern Spain. Conversely, sites like Los Millares, Almizaraque, and Cabezo Juré in south-eastern Spain continued to rely on oxides, while others like Dolnoslav in eastern Bulgaria, Brixlegg in the Italian eastern Alps, and Cabrières in the south-western French Alps

used a combination of sulphide-oxide ores. Despite the emergence of a broad chronological sequence, the specific factors driving the transition from oxide to sulphide ore reduction remain enigmatic.

The smelting by-products uncovered at the Orti Bottagone site, dating back to the early 4th millennium BC, are of immense significance due to their unique position at the intersection of oxide and sulphide technology, both in terms of chronology and geography. Chronologically, Orti Bottagone bridges pivotal periods, with the fifth millennium BC in the Balkans primarily characterized by oxide technology (Radivojević & Roberts, 2021), while the late 4th and 3rd millennia BC in the rest of Europe saw the widespread adoption of sulphide technology (Ambert *et al.*, 2013; Bourgarit, 2007; Höppner *et al.*, 2005; La Duc *et al.*, 2022). In terms of its geographical importance, the Italian peninsula stands out as a central driver of this technological shift (Dolfini 2013; 2014). Recent findings suggest that significant advancements in this transition did not occur in the Alps until the late 4th to early 3rd millennium BC (Dolfini *et al.* 2020). As a result, Tuscany appears to have served as a crucial intermediary, refining and likely disseminating this technological shift to northern and western regions (Dolfini, 2023). Positioned precisely at this critical juncture of transition, the Orti Bottagone site offers an unparalleled opportunity to provide fresh insights into this phenomenon.

In the following chapter, I will delve into the methodological framework employed in this research to address the identified research questions and provide a comprehensive analysis of our findings.

Chapter 4. Analytical protocol for the analysis of slags

4.1. Introduction

In this chapter, I provide a detailed description of the analytical methodology I employed in this thesis. Following the latest research in the field (Artioli, 2010; Bourgarit, 2019; R. C. Doonan & Dungworth, 2013; Hauptmann, 2014, 2020), the approach adopted here combines materials science with experimental archaeology. The samples I selected for the present study underwent a comprehensive analysis, involving macro-analysis, bulk chemical analysis (pXRF, XRD, SEM-EDX), micro-structural analysis (reflected light microscopy and electron microscopy), and compositional phase analysis (XRD, SEM-EDX). This multifaceted approach was crucial in building a comprehensive understanding of the slags. In the initial part of this chapter, I outline the mineralogical and chemical analysis carried out, starting with the selection and macroscopic investigation of the slags. I then offer a detailed account of the sample preparation, describing all the steps, from cutting, to cold mounting, hand-grinding and polishing. Subsequently, I delve into the specifics of each analytical technique, outlining their functioning and highlighting the respective purposes within the context of this study.

In the second part of the chapter, I discuss the limitations inherent in the slag analysis approach. By recognising these constraints and the potential challenges I encountered during the analysis, my research maintains transparency and a balanced perspective. This acknowledgement is essential for interpreting the results and drawing meaningful conclusions based on the data obtained through my multi-analytical approach.

4.2. Multi-analytical approach

4.2.1. Macroscopic investigation

Analysing slags involves a multi-stage process, encompassing both macroscopic and microscopic investigations. In the initial stage the goal is to visually identify the slags among various residues resulting from the smelting process, such as rocks, vitrified clay, and thermally altered ceramic fragments. This step relies on the naked eye's observation and focuses on discerning slags based on their observable characteristics, including morphology, size, shape, colour, porosity, and texture. As emphasised by Bachmann in his introductory work on slags

analysis “*The identification of slags from archaeological sites*” (1982c), a macroscopic description is fundamental, often providing essential information and preliminary interpretations of slag formation. This can prevent unnecessary and time-consuming laboratory analysis. In some instances, macroscopic investigation may even reveal the orientation of specific mineralogical phases¹ or other structural constituents such as gas bubbles, along with their distribution (Hauptmann 2014; 2020).

It is essential to gather as much information as possible in this stage since the subsequent microscopic analysis techniques, as described below, are invasive and require a polished surface or a thin section of the sample.

The first step was to catalogue the slags in a dedicated dataset (Excel), creating specific forms. Each sample was meticulously documented with photographic evidence using a portable LED-illuminated photographic studio and metric reference. The images were edited in Adobe Photoshop CC (2014) where a black background and a colour balance metric reference were added. Subsequently, the specimens were spread over a table and sorted into categories: ore, coarse and flat slags, and crucibles. Following this, a representative sample of each category was selected for further scrutiny. A total of 21 specimens were selected. The slags were weighed using a common scale, and their densities were measured, with density ($\rho=m/V$) expressed in grams per cubic centimetre (g/cm^3). Density provides a quick and preliminary check on the sample classification as it is related to the mineralogical and chemical composition of the slags. Moreover, a basic magnet was employed to assess the presence of iron-bearing compounds within the slags and to speculate about their orientation. Out of 21 slags chosen, 9 have been selected for further analysis.

4.2.2. Handheld X-ray fluorescence spectrometry (pXRF)

Following the macroscopic investigation, X-ray fluorescence spectrometry was carried out by means of a portable device. A Bruker Tracer III-SD Spectrometer was used, in combination with the S1PXRF© software and ARTAX software. The spectrometer was mounted on a manufacturer-designed test stand and powered with a hard-wired power source. The test stand provided optimum beam-sample-detector geometry and a relatively clean analytical environment as opposed to a hand-held, open environment (Knight et al., 2021:2). The instrument is equipped with a Rhodium anode (target X-Ray tube) with a maximum voltage of 40 kV and a silicon drift detector (SDD) with a resolution of 145 eV. The instrument’s analytical

¹ A mineralogical phase is a physically homogenous state of matter with a given chemical composition and structure (Hauptmann, 2014). As newly formed anthropic minerals the different compounds in slags are referred to as phases, differentiating from naturally occurring minerals.

window (spotsize) is 10 mm in diameter with an X-ray beam of 5×7 mm. The machine was warmed up for 1 hour with the voltage set at 40 kV, 13 μ A. Data were acquired in a vacuum atmosphere and each scan lasted 120 seconds. The Bruker's yellow filter used for metal analysis was used. Although this filter has little sensitivity to elements below Ca, it increases the sensitivity of heavy elements like copper, arsenic and lead. It also limits the Rh and Pd L-lines from the spectra, which unfortunately are always present in this instrument as it uses Rh X-ray source and Pd slits. These peaks can obscure the presence of elements such as Cl and S. While pXRF is a valuable tool for non-destructive analysis, it has certain limitations. The technique is surface-sensitive, analyzing only the outer layer of the material, which may be affected by surface contamination or alterations. It also has reduced precision compared to laboratory-based XRF, especially for lighter elements such as sodium, magnesium, and aluminum. Matrix effects can further influence results, requiring careful calibration or post-analysis corrections. Additionally, pXRF has limited depth penetration and cannot detect elements with atomic numbers below 11 (e.g., hydrogen, carbon, oxygen). Despite these limitations, the technique was effective for the purposes of this study. Following the initial data acquisition, a post-data correction was performed, utilizing Bayesian deconvolution to enhance the accuracy and quality of the acquired data. The main reason of the adoption of this analytical technique was to assess the presence of arsenic (As) and antimony (Sb) in the slags. The analysis was performed in triplicate for each sampled location to ascertain the central tendency (mean) of the elemental concentration detected. The values reported in Table 5. 3 are the average of the three analyses. I used Certified Reference Standards (CRS) of copper alloys (MBH-32X SN6 B and MBH-32X SN7 B) to monitor and verify the stability and accuracy of the portable XRF measurements, ensuring minimal drift during analysis. The aim was to identify the presence of copper, arsenic, and antimony in the slags, rather than to quantify their concentrations.

4.2.3. Microscopic investigation

The primary goal of microscopic analysis is to investigate the structure and texture of the slags. This exploration aids in understanding the composition of these phases and the features that can provide insights into the technological processes that led to their formation, such as the initial charge, temperatures reached, and whether reducing or oxidising conditions prevailed. It is through scientific analyses, both mineralogical and chemical, that it is possible to unlock valuable information to decipher the history of a slag.

In this project I utilised two common analytical techniques employed in the scientific examination of slags: Reflected Light Microscopy (OM) and Scanning Electron Microscopy with Energy Dispersive Spectroscopy (SEM-EDX). However, it is important to note that these techniques are invasive, as they require either a polished surface or a thin section of the sample (refer to Artioli, 2010). This means that a portion of the artifact must be cut or cross-sectioned. The microscopic investigations were conducted on thick samples that were mounted and polished (Ineson, 2014; Leng, 2009).

4.2.4. *Sample preparation for OM and SEM-EDX*

Once selected the most representative and informative slag samples, the first crucial step is their proper preparation. This preparation process consists of four key stages: **a)** cutting; **b)** cold mounting; **c)** hand-grinding; **d)** polishing (Leng, 2009).

a) Cutting. First, the specimen was cut to create a cross section. A precision abrasive cutting machine with thin-bladed wheel's edge coated with a tiny layer of diamond paste was used for this purpose (Fig. 4. 1a). To prevent heating of the specimen and improve the quality of the cutting while also removing dust and fragmented particles, a mixture of water and a small amount of lubricant (common hand soap) was added. In some cases, circular weights were placed on top of denser specimens to maintain a consistent downward force during sectioning. The choice of where to make the cut was made based on maximising the information to be obtained and staying within the constraints of a maximum 32 mm diameter of the cylindric moulds. It is worth noting that there are no universal guidelines for sample selection and sectioning, as each batch has its own peculiarities. In situations where the section to be analysed exceeded the mould size, a custom-made (by the author) plastic mould was used.

b) Cold mounting. After cutting, the specimens were embedded in mounting materials to give them a regular shape for further processing. Cold mounting at ambient temperature was preferred to avoid altering the microstructure of the slags due to high temperatures. First, the moulds were lubricated with silicon grease to facilitate the removal of the specimen once it was ready. A label with the sample ID was attached to the mould's wall. The slag was then placed face-down in the mould, and the cold mounting medium was poured into it. The medium was a 4:1 mixture of two components: a fluid epoxy resin (11 10 61) and a hardener (11 10 62). These mounting materials were chosen for their hardness compatibility with the specimens. After letting the specimen harden at ambient temperature for at least 24 hours, it could be removed from the greased mould.

c) **Hand-grinding.** The next step was to flatten the faced-down surface and remove any damage caused during sectioning. The specimen's surface was ground by hand, pressed onto a rotating machine using abrasive papers. Initially, coarse-grained papers graded with a 500 grit (15μ) were employed, followed by a progression to finer-grained papers with a 1200 grit (30μ), (Fig. 4. 1b, d).



a)



b)



c)



d)

Fig. 4. 1 Overview of the machines adopted for the sample preparation process: a) cutting machine, b) coarse grades rotary polishing machine (15μ , 30μ), c) Hot air-drying machine, d) fine grades rotary diamond polishing machine (6μ and 1μ).

Before shifting to finer abrasive paper, the specimen's surface was carefully cleaned with water to remove any debris. The decision to switch to a finer graded abrasive paper was made after a

quick examination under an optical microscope confirmed that the marks and scratches from the previous grade had been effectively removed. It is worth mentioning that the time required for this step can vary significantly, depending on the material and structure of the sample, as well as the aims of the analysis. The duration may range from just a few minutes to hours. During this transition to a finer grit, the specimen was rotated by 90 degrees from its previous orientation. This rotation ensured the removal of any grinding damage, such as marks and scratches, that had been generated by the coarser grit. This process guarantees that the final specimen surface is smooth and free of imperfections.

d) Polishing. The final step was polishing to achieve a smooth, marks-free, mirror-like surface. Two different rotating wheels with diamond paste cloths as abrasives were used: one with a grit size of 6μ and the other with 1μ (Fig. 4. 1d). During the switch from a coarser to a finer polishing stage, an ultrasonic cleaning of the specimen was performed. This process involved immersing the specimen in methylated spirit in an ultrasonic cleaner for 2-3 minutes. Hot air drying was applied before proceeding with further polishing (Fig. 4. 1c). Once the specimen achieved the desired level of polish (Fig. 4. 2), meaning that nearly all the surface scratches and marks from previous steps had been eliminated, it was observed under a stereoscope (Sz-Pt Olympus). Images were acquired using a related camera and software (LissView7).

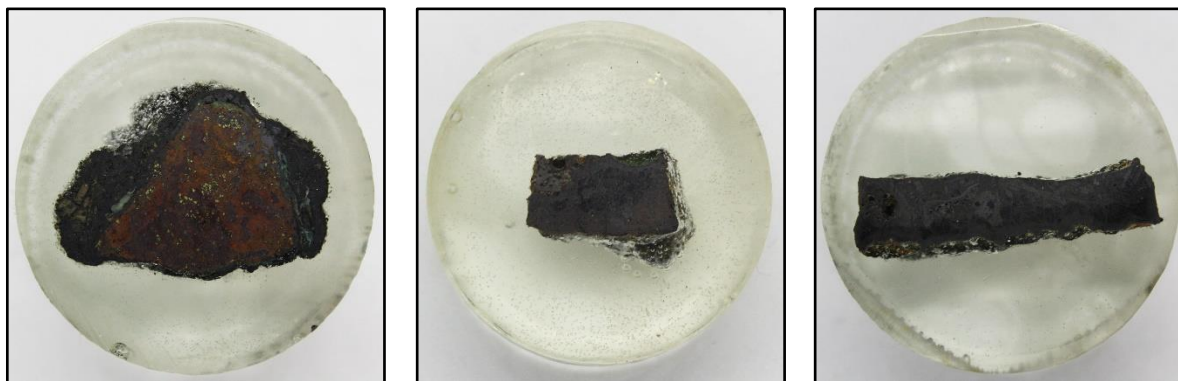


Fig. 4. 2 Polished thick samples showcasing the flat and mirror-like surfaces ready for microscopic observations.

Typically, 2 to 4 images of each sample were taken and then overlaid and merged. This operation allowed the creation of a low-magnified image of the specimen. Some images were altered and adjusted using Adobe Photoshop CC (2014) to highlight specific features and structures within the specimens. A 1cm grid overlay was added to the image to facilitate feature recognition at different magnifications. The image was then printed out and used as a map and note-taking paper during the OM and SEM investigations.

4.2.5. *Reflected Light Microscopy (RL-OM)*

Reflected light microscopy is one of the methods of light (or optical) microscopy. It is often referred to as epi-illumination. This technique is specifically designed for imaging specimens that maintain their opacity. It is one of the oldest but still widely established technique to examine the microstructure of materials. While it can be applied to the investigation of almost all solid materials, the most common historically related applications are in the study of metals – known as metallography (Scott, 1991; Chen et al., 2009; Yahalom-Mack et al., 2014) – and in the investigation of the mineralogy and petrography of minerals and rocks (Artioli, 2010; Ineson, 2014). Among the most prominent in developing ore microscopy at the dawn of the 20th century were the American scholars (e.g., Campbell and Knight, 1906; Murdoch, 1916) and the German school of Paul Ramdohr (1890–1985). RL-OM is also applied to the study of slags, which, due to their composition and opacity, share similarities with geological samples, such as ores. However, it is important to note that the mineralogical composition in slags, shaped by human activity, differs significantly from naturally occurring geological samples (F. Rademakers, 2015). The basic principle behind this technique involves plane-polarized light directed at an opaque, polished specimen. This specimen absorbs some of the light and reflects the rest. The reflected light re-enters the objective and is then directed to the ocular and/or the camera. Based on the visible wavelength of light (λ) between 0.4 to 0.7 μ , this technique allows to investigate portions of the sample only to a certain magnification. Given the fact that the resolution of the light microscope cannot be smaller than the half of the wavelength of the visible light, the diffraction resolution limit is about 0.2 μ . Although this limit is considerably lower than the magnification achievable with other techniques such as Scanning Electron Microscopy (as discussed below), RL-OM remains an indispensable method for slag analysis. Bachmann (1982c) provides a comprehensive example of how to systematically apply Optical Microscopy to the study of slags.

Optical Microscopy observations serves as a valuable tool for determining the mineralogical phases present in the slags and their mutual relationship, texture, morphology and size. Mineral compounds are primarily distinguished by factors such as crystal form, colour, light etching and brightness. As emphasised by Hauptmann (2020, p. 273), the colours and textures of inclusions observed under light-optical microscopy on polished thick sections offer an approximate assessment of the Cu:Fe ratio and enable the identification of the compounds and composition of the sample. While dedicated atlases containing reference materials for archaeometallurgical waste are not yet prevalent in archaeological science, as already noted by

Bachmann back in the 80's (1982c) in his first attempt in building a guide, identification of anthropogenic phases - those produced during metallurgical processes - has been achieved through the use of standard mineralogy textbooks. A notable resource in this regard is the optical guide by Pracejus (2015), which includes images of polished sections of minerals observed under reflected light. Furthermore, practical identification of ore minerals has greatly benefited from the work of Paul Ramdohr (2013) and remains an indispensable resource. Additionally, similar to ore microscopy (Killick, 2014), information about mineral compounds in ores and slags can be inferred from the shape and dimension of scratches on the specimen's surface, which may indicate the relative hardness of the minerals. Detailed colour optical microphotographs found in atlases (Ixer, 1990; Ixer & Duller, 1998) are crucial to identify mineral compounds in ores and slags. Coloured images are particularly helpful to recognise metal inclusions and the primary mineralogical phases, such as fayalite, magnetite, wuestite and pyroxenes. For other phases, identification may require additional techniques like XRD and SEM-EDX (Hauptmann, 2014, 2020).

At the time of writing, only a limited number of occasional papers (Bourgarit, 2019; Hauptmann, 2014, 2020) and case-study (Hauptmann, 2007) addressing specific and contextual assemblages have been published. To bridge this knowledge gap, a comprehensive catalog of micrographs showcasing both experimental and archaeological by-products from ancient smelting processes has been compiled. The list of phases is continuously evolving and expanding as the research advances and as more comparative analyses are conducted.

Once the specimens were prepared, I conducted the observations using two distinct microscopes: an inverted reflected light microscope (Leica DFC295) equipped with a Leica DFC295 digital microscope colour camera, and the Digital Microscope (Keyence VHX7000). Unlike the conventional reflected light microscope, the inverted microscope is designed with a stand/stage on which the specimen is placed facing downward, as the name suggests. This configuration allows for investigation of samples too large to fit within the confines of the upright microscope and streamlines the sample preparation process, as only the side facing the objectives needs to be perfectly flat.

The Keyence VHX-7000 Optical Microscope delivered high-resolution images with the flexibility of both light and dark field viewing modes. To enhance contrast in the images, acquisitions were performed under full coaxial lighting, ring lighting, or a combination of both. Coaxial lighting, which irradiates the specimen from the same angle as the camera, brightens the background while darkening the figures on the specimen.

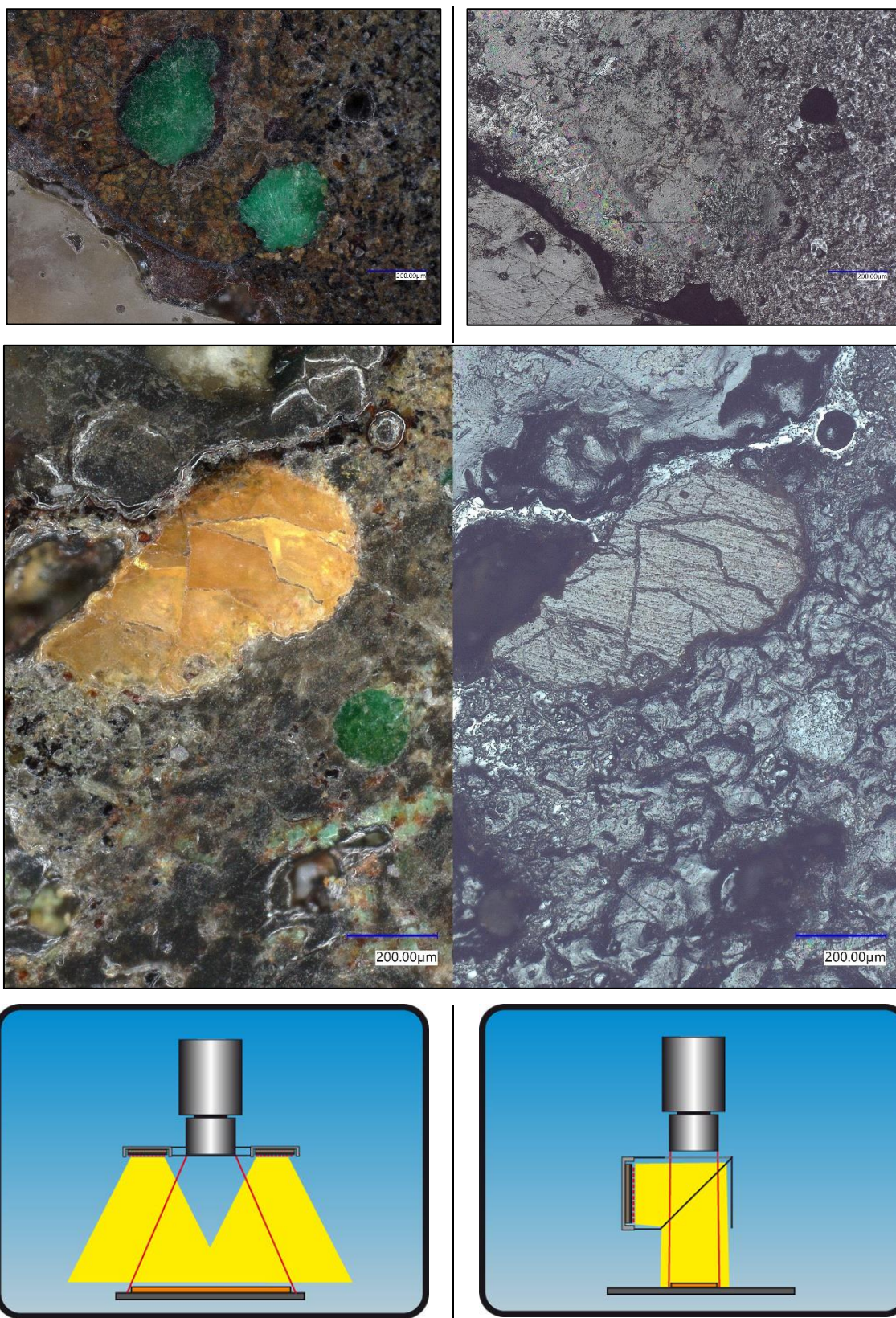


Fig. 4. 3 shows the Lighting Techniques adopted in this research. Left: Low-Angle Ring Lighting - Low-angle illumination with uniform and even lighting, providing contrasting illumination for specimen details. Right: Coaxial Lighting - Illuminates specimens from the same angle as the camera, brightening backgrounds and creating contrast with glossy objects (Sample ORTB 6).

This technique is employed for illuminating reflective surfaces by diverting light from a side-mounted source almost parallel to the camera's optical axis using a beam splitter or semi-transparent mirror. It primarily allows reflection from the flat surface into the camera, enhancing contrast for glossy objects (Fig. 4. 3 shows the Lighting Techniques adopted in this research. Left: Low-Angle Ring Lighting - Low-angle illumination with uniform and even lighting, providing contrasting illumination for specimen details. Right: Coaxial Lighting - Illuminates specimens from the same angle as the camera, brightening backgrounds and creating contrast with glossy objects (Sample ORTB 6).

On the other hand, ring lighting is used to irradiate specimens from a low angle, with the object positioned in the middle of the light. This produces the opposite effect of coaxial light, making the background darker while brightening the figures on the specimen. Low-angle ring lights offer uniform and even illumination Fig. 4. 3 shows the Lighting Techniques adopted in this research. Left: Low-Angle Ring Lighting - Low-angle illumination with uniform and even lighting, providing contrasting illumination for specimen details. Right: Coaxial Lighting - Illuminates specimens from the same angle as the camera, brightening backgrounds and creating contrast with glossy objects (Sample ORTB 6).

The microscopy examination was carried out in a systematic manner. I initially conducted a visual inspection of each specimen's entire surface at low magnifications (x5, x10) to gain a general overview of the sample's various mineralogical phases, their locations, and distributions. If required, I proceeded to higher magnifications (x20, and x50) for the identification of specific phases. Notably, I selected the most representative and interesting areas with distinct phases and features, aided by computer monitoring. I systematically acquired images using the associated LAS V4.7 software. In some cases, adjustments in colour and exposure were applied to enhance the identification and visualization of phases, structures, and inclusions. To facilitate relocation during SEM examination, the acquired features' locations were marked on grid maps.

4.2.6. *Scanning Electron Microscopy with Energy Dispersive spectroscopy (SEM-EDX)*

Electron microscopy offers high-magnification imaging, with the ability to reveal microscale details of a specimen, such as size, shape, composition and crystallography (Goldstein et al., 2018). Unlike Optical Microscopy, it employs a beam of electrons for imaging (in the range of 10^2 - 10^4 eV). The electrons' wavelengths which are in the order of 0.123-0.012 nm do not have

the diffraction limit of the visible light, allowing for significantly higher resolutions and magnification, as well as greater depth of field. (Artioli, 2010; Goldstein et al., 2018).

In SEM, a focused electron beam, generated from an electron source, is directed onto a specimen placed on a stage within a high vacuum environment (pressure $<10^{-4}$ Pa). These conditions are required to prevent the interference of atmospheric gas atoms that could distort imaging outcomes. The interaction between the electron beam and the specimen generates multiple signals containing valuable sample information.

These signals are detected and scanned into a raster (x-y) pattern producing two main electron products: **backscattered electrons** (BSE) and **secondary electrons** (SE) images. The first are images characterised by high-energy electrons that provide mainly information about the composition of the sample, its topography, mass thickness and crystallography. They are especially valuable for highlighting compositional differences in multi-phases samples. Heavier elements (high atomic number, Z) appear brighter in the imaging process than lighter elements (low Z), (Heinrich, 1966; Goldstein et al., 2018). In contrast the second, characterised by lower energy electrons (<50 eV) offer insights into the surface structure of the specimen. When SEM is equipped with an Energy Dispersive X-ray (EDX) spectrometer, it can provide enhanced characterization of the sample's elemental and chemical compositions through qualitative and quantitative analyses, elemental mapping, and elemental variation assessment across the specimen surface (Frahm, 2014, p. 6489).

Over the past two decades, SEM has become an integral part of the commonly adopted analytical protocol in slag studies. Its higher magnification and resolution capabilities have not only facilitated the identification of mineral phase but have also allowed for the detection of chemical compositions in amorphous phases and the localisation of chemical segregations like “zoning” (Hauptmann, 2014; Bourgarit, 2019). Through the EDX analysis method involving qualitative and quantitative spot- and elemental map- analysis, SEM-EDX proves effective in overcoming the limitations of analysing heterogeneous powdered slag samples, where bulk chemical analysis interpretation could be distorted by various inclusions and/or undecomposed constituents (Frahm, 2014; Hauptmann, 2014, p. 97). It is important to note that a deep and thorough understanding of mineralogy is essential when using this technique.

The samples prepared for the OM analysis are also suitable for SEM-EDX analysis. The sites of interest individuated through OM were re-observed under this microscope and EDX analyses were performed to identify/confirm the different compounds. The analyses were carried out using a Jeol JSM-5600LV Scanning electron microscope, working in high vacuum mode. The machine was equipped with an Oxford INCAx-act energy-dispersive spectrometer (EDX) and

the INCA software was used for data-processing. The EDX system is calibrated yearly and regular checks are performed using a pure nickel standard (flat polished sample).

The samples were analysed under high vacuum conditions with an energy of 20 keV and a working distance of 20 mm. Both BSE and SE images were acquired and EDX analyses were carried out in different acquisition modes such as spot-analysis, line analysis, area-analysis, and elemental map analysis. Spot analyses were performed to qualitatively interpret specific features observed on the slag surface, providing valuable insights into the sample's composition. Line analyses were used to detect possible zoning areas and other distinct features within the samples. Notably, area-analyses were preferred due to the potential volume measurement inaccuracies associated with point impact areas (Hodoroaba, 2020). In addition, elemental compositional maps were generated to pinpoint regions where elements were present at concentrations exceeding 1% by weight (Fig. 4. 4), further enhancing the understanding of the samples chemical compositions (see also Wenk et al., 2019).

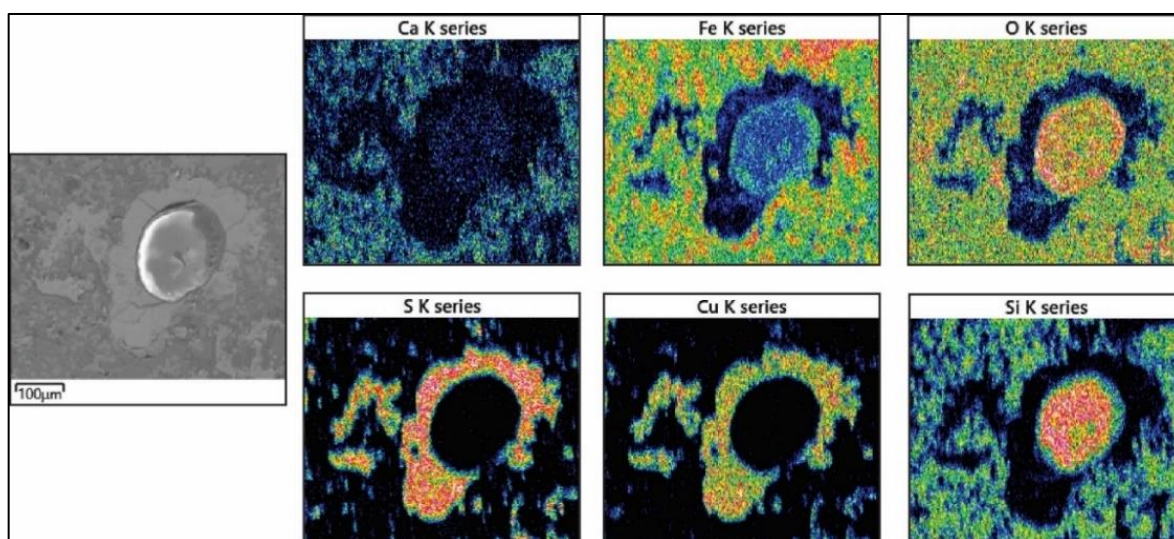


Fig. 4. 4 illustrates an elemental compositional map that provides a visual representation of the elemental distribution in a specific area. This map reveals a Cu-Fe sulphide feature within an iron-silicate matrix. Additionally, it indicates the consistent presence of calcium (Ca) in the slag matrix, albeit in relatively low concentrations. For more detailed information on these findings, please refer to Chapter 5.

However, it's essential to acknowledge the limitations of SEM-EDX. This technique is known to face challenges when detecting elements at low concentrations due to high background noise levels which can obscure less intense energy peaks in spectra. While literature often mentions the possibility of detecting elements down to 0.1%, a more realistic limit for many elements is about 0.5% (Williams, 2014). It is worth adding that the accuracy of any data depends on the

surface roughness of the samples and what elements are present. Therefore, for the detection of trace elements, particularly elements like As and Sb, which might suggest ancient sulphosalts exploitation, alternative methods such as portable X-ray fluorescence (pXRF), Electron Microprobe Analysis (EMPA), Atomic Absorption Spectroscopy (AAS), and Laser Ablation-Inductively Coupled Plasma-Mass Spectrometry (LA-ICP-MS) are considered more effective (Artioli, 2010; Bourgarit 2019, Hauptmann, 2020).

4.2.7. Sample preparation for X-ray Powder Diffraction (XRD)

Sample preparation for X-ray Powder diffraction (XRD) is a critical step to obtain accurate diffraction patterns. It involves two main stages: **a)** grinding/milling and **b)** preparing the medal/coin. While only 3 grams of material are required, collecting around 5-6 grams of material per sample accounts for potential losses during preparation (Buhrke et al., 1998).

a) Grinding. The sample underwent a two-stage grinding process: - *hand-grinding*. Initially, it is manually ground into a coarse powder, creating millimeter-sized grains, and protected from material dispersion by hammering within a plastic bag; - *mechanical grinding*. Subsequently, it is transferred into an agate grinding jar and ground for 5 minutes at a speed of 450rpm, using a set of 6 agate grinding balls of varying sizes in a Planetary ball mill (PM100), as shown in Fig. 4. 5a-b. The desired particle and crystallite size should ideally fall within the range of 1-5 μ . To prevent cross-contamination between samples, the grinding jar was meticulously cleaned by grinding a few grams of sand for 2 minutes at 450rpm, followed by washing and drying.

b) Medal/coin preparation. The powdered samples (Fig. 4. 5c) were then loaded into 23mm diameter circular low-background sample holders. Due to limited material, sample ORTB 8 was loaded into a 13 mm holder.



a)



b)

c)

Fig. 4. 5 Overview of the tools and machine adopted for the sample preparation process: a) set of 6 agate grinding balls of varying sizes and grinding jar; b) a Planetary ball mill (PM100); c) approximately 7g of powdered sample ready to be loaded (sample ORTB 21).

4.2.8. X-ray Powder Diffraction (XRD)

The X-ray powder diffraction (XRD) method is a valuable analytical technique for identifying crystalline materials like minerals and inorganic compounds, as well as for quantifying phase abundance in polycrystalline mixtures (powders). It is widely used in archaeology to determine the mineralogical composition of various material such as ores, crucibles, slags, and ceramics. A typical X-ray diffractometer comprises three main components: an X-ray tube, a sample holder, and an X-ray detector. The X-ray tube produces electrons which, through the application of a voltage, accelerate and bombard the targeted sample. If the energy of the irradiated X-ray electrons is higher than the binding energy of the electron, inner shell electron(s) are displaced from their atomic orbital positions and expelled from the atom, leaving a void in a shell, and making the atom unstable/excited. To restore the original configuration and replace the vacancy, electrons from outer shells are transferred to the inner shells. As the electrons in the outer shells have higher energy than those in the inner shells, during the transition that surplus of energy is released as X-ray photons (characteristic radiation). Since each atom has its own

energy levels the emitted radiation is indicative of the atom. Moving in a synchronize motion with the X-ray tube, the X-ray detector detects this excess of energy (scattered intensity) and converts the signal to graphs (characteristic X-ray spectra) where peaks related to the atomic structure of the sample are observed. Mineralogical phases are identified by comparing unknown sample spectra to those in a reference database (Ermrich & Opper, 2013). To delve into the intricacies of the X-ray diffraction technique, refer to the following sources: Artioli, 2010; Klein and Philpotts, 2013; Monaco et al., 2002)

This technique offers rapid results (typically less than 20minutes per sample) and is relatively easy to interpret, making it accessible to archaeologists without extensive material science backgrounds (it is necessary to have access to a standard reference file of inorganic compounds – d-spacings, hkl's). However, it has its limitations, including sample invasiveness, the need for a minimum of 3 grams of pressed-powder, and restrictions related to sample size and preservation. Furthermore, poorly crystallized (cryptocrystalline) minerals as iron hydroxides and chrysocolla, usually found in the weathered oxidised zone of copper-bearing ore deposits, are not detected (Killick, 2014).

I conducted mineralogical semi-quantitative phase analyses using a Bragg–Brentano θ – 2θ diffractometer (PANalytical X'Pert PRO). To ensure accurate results, I configured the following parameters: I employed CuK α _{1,2} radiations with a wavelength of 0.0217329 nm, utilised parallel beam optics, and employed an energy-dispersive counter. The detector and beam optic were theta/theta coupled, with standard operating conditions set at 40 kV and 15 mA. I recorded diffraction patterns via continuous scanning within the 5° to 80° θ range. For phase identification and semi-quantitative phase analysis, I utilised the X'Pert HighScore Plus version 3.0a software package and the Rietveld refinement method. This technique employs a least-squares approach to refine a theoretical line profile until it aligns with the measured profile. It is worth noting that the reference values for agreement indices were not provided, as they heavily depend by data collection conditions. Generally, a visual assessment is preferred over relying solely on agreement indices for assessing the quality of the fit.

4.2.9. Limits of the slag analysis approach

The reconstruction of ancient copper smelting pyrotechnological processes is mainly based on the understanding of the operating temperatures and atmospheres/partial pressure(s) inside the reactor (Bachmann, 1982c; Tylecote & Tylecote, 1987, p. 295). However, although copper is produced only within certain conditions – temperatures around 1150-1250°C and partial

pressures of oxygen (p_{O_2}) between 1×10^{-5} and 1×10^{-9} –, the limitations of this common analytical method are widely known. As clearly argued by Pryce (2009) the investigation of slags and metallurgical by-products are heavily built on their *liquidus* determinations, meaning that are ground on a series of “indirect imperfect estimations based on a large number of assumptions and simplifications” (Pryce, 2009, p. 113). In other words, their calculations alone would not provide enough data to determine and characterize different operational chains and technological choices (Pryce, 2009, p. 112).

Usually, the *liquidus* determinations are defined by plotting bulk chemical compositional data in ternary phase diagrams. A ternary diagram, or triangular graph, is designed specifically for the purpose of displaying three-category data sets expressed as percentages. It can only be used for three variables (or groups of them) where their total equals one hundred percent of the data (“reduced analysis”, Hauptmann, 2014; 2020). Ternary plot diagrams work well for systems with three dominant chemical components. In the diagram a series of contours and boundary curves called **isotherms** represent lines of constant temperature. They are used to show exactly what phases will coexist (at equilibrium) for each bulk composition at the temperature selected (Campbell, 2012). An example is provided in Fig 4. 6. However, this *modus operandi*, although increases the readability of the data, it comes at the expense of their accuracy:

- the selection of three components and their normalisation to one hundred do not consider minor elements, trace components and impurities present in the slag which might have lower the melting points in the system (melting point depression process²), affecting the solidification behaviour and alter the thermodynamics of the system.
- the bulk chemistry of a sample refers to its mean composition, assuming homogeneity, ignoring the “phasescape” (Pryce, 2009) and the stratigraphy/topography of the slag. Early slags did not solidify homogeneously but are characterized by different areas with multiple micro-equilibria and thermal gradients.
- the temperatures and cooling rates are estimated based on reference thermodynamic models mainly derived from modern industrial activities (Davenport et al., 2002, p. 62) and/or lab experiments carried out within pure systems (Pryce, 2009, p. 114).

² From a chemical perspective, most solids form as crystalline lattices of repeating clusters of ions or molecules. This lattice is held together by intermolecular forces that create a strong structure. The presence of impurities reduces the strength with which the substance is held together the lattice, making it less stable. As a result, the compound melts at a lower temperature (see Klein & Philpotts, 2017).

- the temperatures estimated are specific only of the area where the slag formed without giving any additional information on the temperature gradients inside the reactor.
- the temperatures are determined by calculations of assumed fully melted and homogeneous slags where oxygen partial pressure is in equilibrium with air for the entire length of the process (Artioli & Angelini, 2010; Bourgarit, 2007; Burger et al., 2007; Hauptmann, 2020). Since we are dealing with open reactors where the air is pumped through bellows/blowpipes/wind, the oxygen partial pressure conditions (p_{pO_2}) underwent constant fluctuations hardly reaching the thermodynamic equilibrium.
- to reconstruct the reducing/oxidising conditions in the reactor, the bulk chemical composition figures are transposed to an Ellingham diagram – a graph showing the temperature dependence of the stability of compounds - (Fig 4. 7). However, given that one is contingent upon the other, deducing the reducing/oxidising conditions from temperatures estimates might lead to systematically imprecise outcomes (circular reasoning), (Kongoli & Yazawa, 2001, p. 583; Pryce, 2009, p. 114).

Another limitation, related less to the method *per se*, and more to the displaying of the data is that chemical analyses for silicate minerals are usually reported (for historical reasons³) in weight percentages (wt%) of the oxides of the elements determined. Although many of the elements will be oxidised during heating, some either have very reactive oxides (melting temperatures of potassium oxide, $\text{K}_2\text{O} = 740^\circ\text{C}$; phosphorus pentoxide, $\text{P}_2\text{O}_5 = 360^\circ\text{C}$; sodium oxide, $\text{Na}_2\text{O} = 1132^\circ\text{C}$) and/or form other compounds with other elements in the melt. Some oxides are more stable than others so during heating many elements/compounds unbound or react further. Therefore, the composition expressed using oxides is just a representative way to show the result and it does not mean that all elements are associated to oxygen.

While this analytical approach can be applied with a low margin of error to the homogeneous proto-industrial slags from Late Bronze Age (1350-1150 BC) onwards, it becomes more critical the more we go back in time, especially when dealing with non-ferrous archaeometallurgy. The slags considered in this thesis are by-products of copper-smelting activities dating to the 4th millennium BC (Fedeli & Galiberti, 2016). They are among the first evidence of copper smelting in the Italian peninsula, when the process was at its early stages. The slags reveal highly heterogeneous compositions showing a vast range of mineralogical phases. However,

³ Although it might be easier to recognise the compounds present in the slag if expressed in atomic percentages, weight percentages are reported as the first chemists performed their analyses using gravimetric techniques. (See https://serc.carleton.edu/research_education/equilibria/mineralformulaerecalculation.html).

being aware of these limitations, this is still the best method widely known applied to the investigation of archaeological slags (Hauptmann, 2020). To overcome these limitations and include in my research the variability/complexity of the technological processes ancient smelters faced, I integrated this analytical method with a more qualitative approach:

- First, to better assess the heterogeneity of the slags, I meticulously observed each slag in all its extension and all the mineralogical phases and inclusions were carefully recorded and, where possible, localised on a map of the slag. This approach is rather new as only Pearce et al. (2022) have recently performed analyses of complete profiles (thin sections) of Chalcolithic (CA; 3500-2200 BC) and Early Bronze Age (EBA; 2200-1650 BC) slags arguing that more accurate analyses of few pieces can be more informative than few analyses of a larger number of slags. This part will be discussed in the following sections of this chapter.
- Second, once the complex “history” of the slags with the “phasescape” and the related temperatures of formation were defined, I carried out a series of targeted experiments to try to go a little further in our understanding of the technical choices and limitations ancient smelters went through. This part will be discussed in second part of the thesis.

4.2.10. *Experimental archaeometallurgy*

An integral component of this research involved conducting archaeometallurgical experiments, encompassing roasting and copper smelting processes. The comprehensive examination of this aspect can be found in Chapter 6, 7, and 8, with in-depth discussions presented in Chapter 9.

To analyse the data collected through each of the techniques described in this chapter, I utilized R version 4.0.3 (R Core Team, 2020). To create all the ternary plot diagrams, I relied on the Ternary package (Smith, 2017) and *ggtern package* (Hamilton & Ferry, 2018)

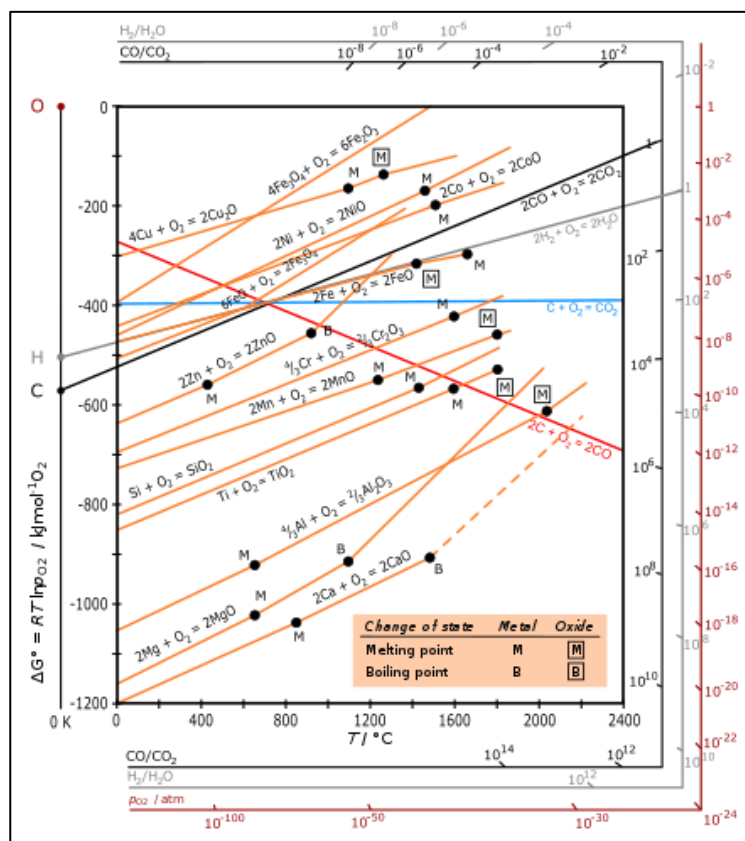
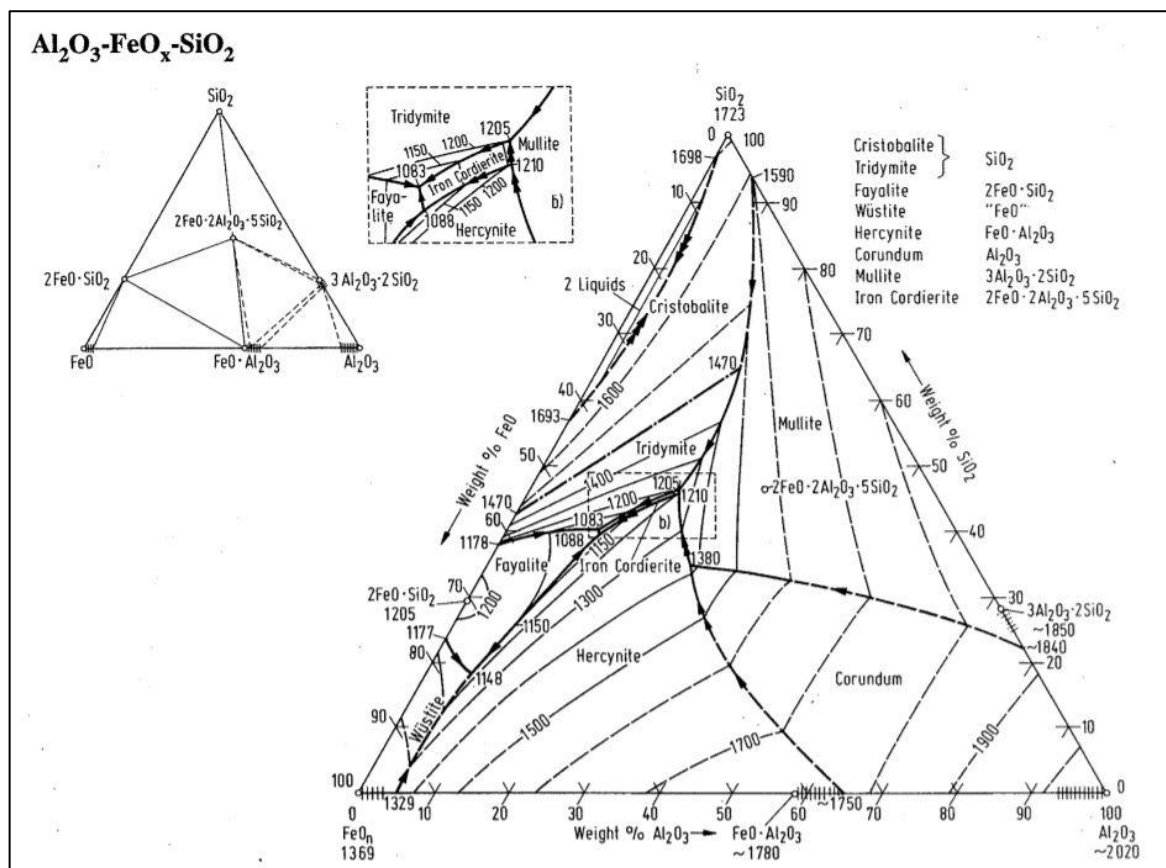


Fig 4. 6 Ternary plot diagram showing the liquidus surfaces in the system FeO_x-Al₂O₃-SiO₂ (Kowalski *et al.*, 1995, fig. 3183).

Fig 4. 7 Ellingham diagram for several metals giving the free energy of formation of metal oxides and the corresponding partial pressure (p_{O_2}) at equilibrium (Ellingham, 1944).

By integrating these complementary analytical techniques, the study aims to attain a thorough analysis of the samples. This approach enables the acquisition of reliable and detailed data concerning the mineralogical, chemical, and elemental compositions of the materials being examined. The utilization of this multi-analytical approach is a potent tool as it enriches the robustness of the research analysis and facilitates a comprehensive exploration of the research questions.

In the upcoming chapter, I critically showcase the results obtained through the various techniques describe above. These results, alongside the experimental results in chapter 7 and 8 provide the groundwork for the subsequent discussion and conclusions.

Chapter 5. Copper Smelting at Orti Bottagone: Insights from analytical chemistry

5.1. Introduction

In this chapter, I will present the results of the analyses carried out as part of my doctoral research on the Orti Bottagone slag assemblage. The samples were characterised using a combination of analytical techniques: handheld X-ray fluorescence spectrometry (XRF) was adopted with the aim of detecting the trace elements in the slags; Reflected-Light Optical (RL-OM) and Digital Microscopy (DM) and X-ray Powder Diffraction (XRPD) were adopted to understand slag mineralogy and petrography; and Scanning Electron Microscopy with Energy Dispersive Spectrometry (SEM-EDX) was adopted for chemical and elemental mapping. For machines details and setting parameters see Chapter 4. In the first part of the chapter, I will report the physical chemistry and mineralogy of the slags identified through the analysis of their chemistry and physical properties and their microscopic inclusions and mineralogical phases. In the second part, I will employ SEM-EDX semi-quantitative analyses and viscosity and Fe/SiO₂ ratio indexes as indicators to delve deeper into the bulk chemical composition and properties of the samples. In the last section, I will present the analytical results obtained from a crucible fragment.





5.2. The physical chemistry and mineralogy of the archaeological slags: analytical results








5.2.1. General observations

Among the slags collected on the field by the excavators (Fedeli & Galiberti, 2016), I sampled for further observation 20 specimens: 18 slags, 1 ore fragment, 1 crucible fragment. Based on the observable properties I sorted the slags into two groups, coarse (8 slags), and flat (10). Due to the deteriorated state of conservation, identifying specific inclusions with the naked eye posed considerable challenges. The surfaces were highly weathered and covered with newly-formed mineralogical phases such as copper hydroxides (e.g., Cu(OH)₂) and calcium carbonate thin layers. The entirety of the assemblage is characterised by fragmentary shapeless

Table 5. 1 Overview of the samples analyzed in this thesis, including the macroscopic features observed and the corresponding analyses performed. Only the crossss-sections of the samples that underwent full investigation are depicted.

* Magnetic values were categorized using a three-point scale to denote magnetic intensity: 1 (grey) – no magnetism; 2 (yellow) – low magnetism; 3 (blue) – high magnetism (see section 5.2.3)

Rep	Slag type	Picture	Area	Weight (g)	Volume (cm ³)	Density (g cm ⁻³)	Magnetism (1,2,3) *	Analysis				
								pXRF	OM	SEM-EDX	XRD	MicroCT
ORT B. 3	Ore		Zona T	21.6	7	3.09	2	X	X	X	X	
ORT B. 5	Coarse		Zona T	29.4	17	1.73	3	X	X	X	X	
ORT B. 6	Coarse		Zona T	36.5	15	2.43	1	X	X (3D)		X	
ORT B. 9	Coarse		Zona T	108	60	1.80	2	X	X	X	X	X

ORT B. 20	Coarse		Sporadi ci Lato N	29.8	15	1.99	3	X	X	X	X	
ORT B. 8	Flat		Zona T	5.3	5	1.06	3	X	X	X	X	
ORT B. 12	Flat		Punto S	38.3	10	3.83	3	X	X	X	X	
ORT B. 13	Flat		Punto S	13.9	5	2.78	3	X	X	X	X	
ORT B. 19	Flat		Sporadi ci Lato N	73	20	3.65	3	X	X	X	X	
ORT B. 16	Flat		Zona T	16.5	5	3.30	3	X	X	X	X	
ORT B. 10	Crucible		Sporadi ci Lato N	9.7	6	1.62	/	X	X		X	
ORT B. 1	Coarse		Estremi ta' NE	32.7	16	2.04	1	X			X	
ORT B. 4	Coarse		Zona T	33.4	12	2.78	1	X			X	

ORT B. 7	Coarse		Zona T	166.2	80	2.08	1	X			X	X
ORT B. 21	Coarse		Sporadi ci Lato N	52	24	2.17	1	X			X	
ORT B. 2	Flat		Zona T	15.8	6	2.63	1	X			X	
ORT B. 14	Flat		Zona T	12.8	4	3.20	2	X			X	
ORT B. 15	Flat		Zona T	10.2	3	3.40	2	X			X	
ORT B. 18	Flat		Sporadi ci Lato N	21.6	6	3.60	2	X			X	

fragments rendering the reconstruction of the original slag shape produced in the reactor arduous. The coarse samples show rather rough surfaces with bubbles and protuberances, whereas the flat samples present smooth and platy-like surfaces. Of particular interest is the flat sample ORTB 13 which displays a uniform concave indentation resembling a circular void within the bottom of the slag (Fig. 5. 1). The edges of the indentation are smooth and well-defined, possibly produced by a round tool rather than being a random occurrence. The contact surface do not differ in colour and texture from the surrounding area and the rest of the slag. This indentation is similar to those identified on some Chalcolithic and EBA slags (VB1, VB2, VB5) recovered from la Vela di Valbusa (Pearce et al., 2022, Figure 8). Sample ORTB 19 exhibited a distinct curvilinear side. An attempt to identify the dimension of the original slag cake formed inside the reactor was made.

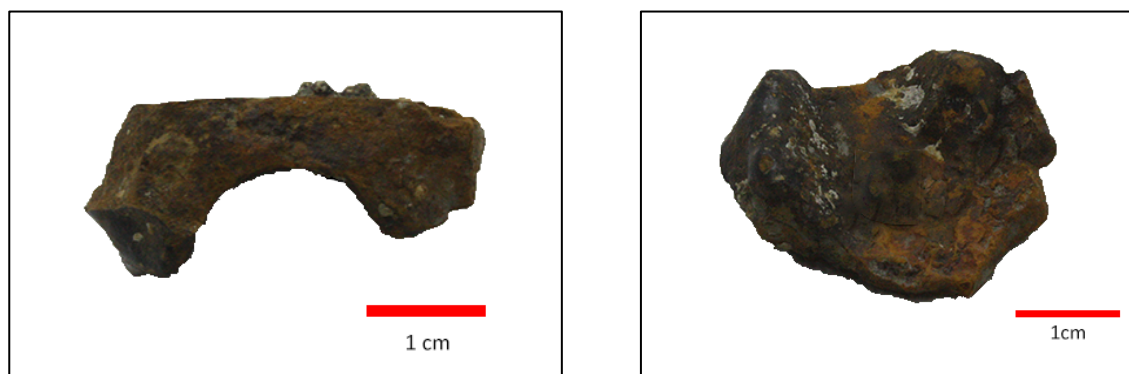


Fig. 5. 1 Two views of sample ORTB 13 showing a concave indentation resembling a circular void within the bottom of the slag.

5.2.2. Density

I weighted the slags using a digital balace and the volume was measured by immersion in water at room temperature ($\sim 25^{\circ}\text{C}$). Density ($\rho = m/V \text{ g cm}^{-3}$) and the related distribution information are helpful parameters for reconstructing the smelting process operations. They provide a preliminary assessment of the sample classification as they are connected to the chemical and mineralogical composition of the slags. A comprehensive summary of the whole dataset was provided by the measure of the central tendency of the values (mean and median), the spread of the data about the mean (Standard Deviation) and the dispersions of the data (minimum, maximum, range, lower quartile, upper quartile, interquartile Range). I analysed the data using R version 4.0.3 (R Core Team, 2020) and the *ggplot2* package (Wickham, 2016). The density measurements are summed up in Table 5. 2 and graphically described in the box and whisker plot (Fig. 5. 2). The ensuing observations were made. The coarse slags show a mean value of

2.13 g cm⁻³ and density range of 1.05 g cm⁻³ with a minimum value of 1.73 g cm⁻³ and a maximum value of 2.78 g cm⁻³. The flat slags show a higher mean value of 3.05 g cm⁻³ and a higher dispersion of the values (density range of 2.77 g cm⁻³) from a minimum value of 1.06 g cm⁻³ and a maximum value of 3.83 g cm⁻³. The density measurements of the coarse slags are lower than the average density of many coarse Chalcolithic slags, which, according to Artioli et al. (2010:338), falls in the range of 2.6–3.0 g cm⁻³ (close to the theoretical density of pure quartz, $\rho_{Qz}=2.66$ g cm⁻³). The flat slags also differ from the Late Bronze Age *plattenschlake* ranging from an average density of 3.8 to 4.4 g cm⁻³ (close to the theoretical density of pure fayalite, $\rho_{Fa}=4.39$ g cm⁻³), (Addis et al., 2016). Within the coarse slags the divergence of the density measurements and the expected values might be explained by the high porosity of the samples. The heterogeneous compositions of both coarse and flat slags, characterised by a vast range of chemical compounds, might also lead to an underestimation of the density values (Addis et al., 2017).

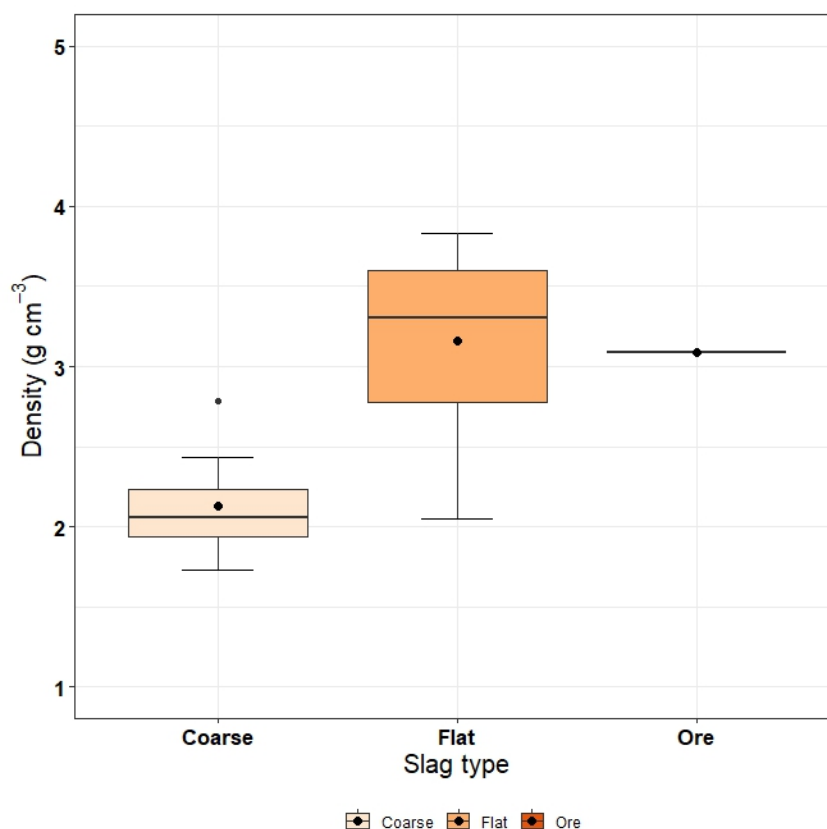


Fig. 5. 2 Box and whisker plot of the archaeological typologies of slags analysed from the site of Orti Bottagone.

Table 5. 2 Summary statistics for the density (ρ) values measured on the Orti Bottagone slag samples. Scale g cm^{-3} . Count = total number of slags for each group; SD = Standard Deviation; Min. = minimum; Max. = maximum; LQ = lower quartile; UQ = upper quartile; IQR = range interquartile.

Slag Type	ρ measured (g cm^{-3})									
	Count	Mean	Median	SD	Min	Max	Range	LQ	UQ	IQR
Ore	1	3.09								
Coarse	8	2.13	2.06	0.34	1.73	2.78	1.05	1.94	2.24	0.30
Flat	10	3.05	3.30	0.84	1.06	3.83	2.77	2.78	3.60	0.82
Total	19									

Nevertheless, it should be noted that internal pores were not detected, and the range of sample dimensions will influence the apparent density values observed for these closed-pored specimens. Consequently, the error in density measurement increases as the sample volume increases.

5.2.3. Magnetism

Using a permanent magnet, I assessed the magnetism of the 8 coarse slags, 10 flat slags and the ore fragment. A categorical scale was used to identify and record the magnetic intensity: 1 (grey) – no magnetism; 2 (yellow) – low magnetism; 3 (blue) – high magnetism (fig 6.3). Magnetism helped to assess first the presence of iron-bearing compounds in the slags and to hypothesize slag orientation (top and bottom). Since the compounds with higher densities tend to sink and the less dense tend to move toward the surface, the orientation might help to recognise the compounds present in the slag.

Among the coarse slags only three specimens out of 8 showed magnetism. Only in two of these was possible to determine any orientation (ORTB 5, ORTB 9), whereas the third (ORTB 20) showed magnetism on both sides. Unexpectedly, the magnetic samples are those characterised by the lowest densities.

Differently, the flat slags, except for one case (ORTB 2) all showed a magnetic signal. Three specimens showed low magnetism on both sides (ORTB 14, ORTB 15 and ORTB 18), while two cases (ORTB 8, ORTB 12) were not thick enough to determine the magnetic side. The orientation was determined only for 3 specimens. The ore fragment (ORTB 3) showed a low magnetic signal.

Looking at the scatterplot in Fig. 5. 3, all the samples with density higher than 3.0 g cm^{-3} (flat slags and the ore fragment) show magnetism suggesting the presence of magnetic iron

compounds. However, it is not possible to rule out the presence of magnetic iron compounds from coarse samples with density lower than 2.0 g cm^{-3} .

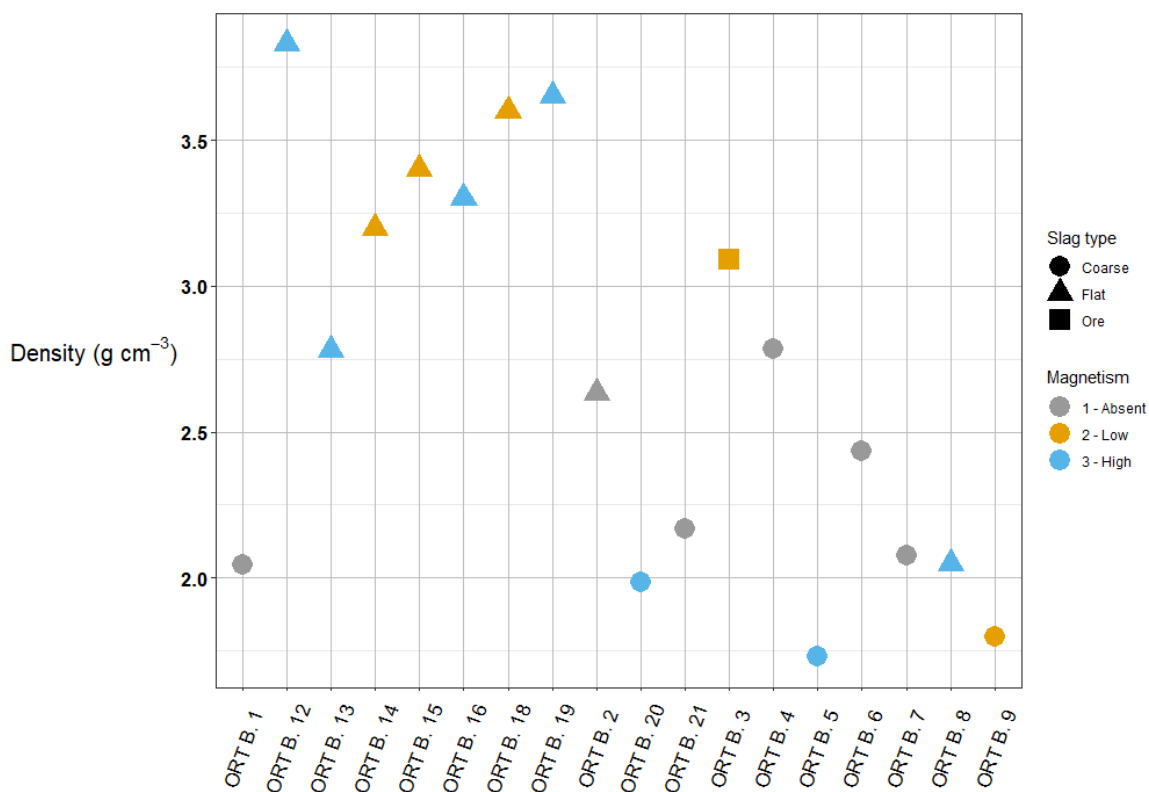


Fig. 5. 3 Scatterplot illustrating specimen density categorised by slag type (shape) and magnetism (colour).

5.2.4. Handheld X-ray fluorescence spectrometry (pXRF)

I analysed a total of 20 samples: 8 coarse slags, 9 flat slags, 1 ore fragment and 2 crucible fragments, which are dealt with in another section. The surface of each specimen was analysed. The machine settings, procedure and reference materials used are detailed in the corresponding section (4.2.2) in Chapter 4. Although it has rarely been considered a suitable technique for this type of material, mainly because of their compositional heterogeneity and their mineralogical composition, XRF analysis is a suitable technique to qualitatively assess the presence/absence of Cu, As and Sb and, if present, compare the relative amounts. The following observations were made. As expected, given that slags are commonly iron based by products, iron is the main element found in the samples. Fe is found in many chemical bonds associated with silicates, sulphur and oxygen with different valency states such as Fe, FeO, Fe₂O₃ and Fe₃O₄. I reported the analyses as oxides (Table 5. 3) to provide a clearer representation of the iron's chemical environment and its interactions within the slag matrix. Reporting as oxides

simplifies the interpretation of the slag composition and aligns with standard practices in slags characterization. In general, copper is present in variable amounts in all the analysed materials. As expected, the highest percentages of Cu are in the ore fragment (ORTB 3) and in the coarse slags. The coarse slags have a relative average of 10_{ox}% Cu with a minimum value of 4.6_{ox}% (ORTB 21) and a maximum value of 17.1_{ox}% (ORTB 5). Conversely, lower Cu percentages were detected in the flat samples with a relative average of 3.1_{wt}%, with a minimum value of 1.7_{ox}% (ORTB 12) and a maximum value of 6.9_{ox}% (ORTB 8). If we assume that the coarse samples belong to the first smelting activities, the higher amount of copper might be explained by the fact that the slags need to be re-smelted in order to gradually recover the copper still trapped in them in the form of prills, Cu-Fe sulphides or unreacted copper-bearing compounds. Extremely informative is the presence of significant traces of arsenic in all the samples. The ore fragment exhibits the highest value at 1.2_{ox}%, while the rest of the assemblage ranges from below detection limits (b.d.l.) to 0.5_{ox}%. Similarly, significant traces of As were detected by Artioli et al. (2016) in several slags from San Carlo Cava Solvay, a nearby late 4th millennium copper smelting site, leading them to infer an ancient exploitation of sulphosalts. Zinc was also found in all the samples in variable amounts between 0.5_{ox}% in the ore fragment to 12.3_{ox}% in a flat sample (ORTB 18). However, no trends were identified. Unexpectedly, traces of lead were detected only in the ore fragment and in the coarse slags. The highest value is in the ore fragment with 0.4_{ox}%. As Pb is a chalcophile elements, its absence in the flat samples might be explained by its migration out of the slag in the copper bearing compounds.

Table 5. 3 Portable X-ray Fluorescence (pXRF) Analyses of Orti Bottagone Slags. The reported values represent the average of three analyses, with results presented in oxides (ox%). Elements marked as b.d.l. (below detection limits) were not detectable by the analytical method used.

Object	Type	FeO	CuO	ZnO	PbO	As ₂ O ₃
ORTB 3	Ore	83.2	14.8	0.6	0.4	1.2
ORTB 20	Coarse	92.2	5.3	1.9	0.1	0.5
ORTB 21		91.6	4.6	3.6	b.d.l.	0.2
ORTB 1		82.7	13.6	3.2	b.d.l.	0.5
ORTB 4		83.9	6.8	8.8	0.1	0.4
ORTB 5		78.2	17.1	4.4	0.2	0.1
ORTB 6		77.8	11.8	9.7	0.3	0.4
ORTB 7		89.5	6.2	4.0	0.1	0.3
ORTB 9		78.9	14.6	5.8	0.3	0.4
ORTB 2	Flat	93.2	4.2	2.4	b.d.l.	0.2
ORTB 8		85.4	6.9	7.6	b.d.l.	0.1
ORTB 12		93.5	0.9	5.1	b.d.l.	0.5
ORTB 13		95.7	1.7	2.3	b.d.l.	0.3
ORTB 14		90.9	2.5	6.6	b.d.l.	b.d.l.

ORTB 15		91.8	3.7	4.3	b.d.l.	0.2
ORTB 16		95.5	2.1	2.0	b.d.l.	0.3
ORTB 18		85.6	2.0	12.3	b.d.l.	0.1
ORTB_19		93.2	2.7	3.9	b.d.l.	0.2

5.2.5. Mineralogical phases

The entire assemblage (20 samples) was investigated by means of XRD with the aim to characterise their mineralogical phases (Table 5. 4). A semi-quantitative phase evaluation using the Rietveld refinement method was performed. For machine details and setting parameters refer to Chapter 3. Among the 20 slags selected, 9 were selected for further analysis as they were determined to be representative of the entire assemblage. This selection was based on the results of previous macroscopic, pXRF, and XRD analyses, which identified these samples as encompassing the key variations in composition and structure observed across the full dataset. By focusing on these representative samples, the study ensures that the analysis is both comprehensive and efficient, capturing the essential characteristics of the broader collection. Optical observations were carried out by mean of a RL-OM, while micro-structural and element compositional characterisations of the slags were carried out by means of SEM-EDX analyses. Data were acquired in weight percentages (wt%) of the oxides of the elements determined for the sake of comparability with other studies (Addis et al., 2017; Pearce et al., 2022; Radivojević et al., 2021). With regards to SEM-EDX analyses, a total of 419 analyses between spot-, line-, area- and element compositional map analyses were acquired. Spot- and line- analyses aimed at a qualitative interpretation of specific features detected on the slag surface, while area-analysis were carried out to pursue a semi-quantitative evaluation of slags' composition (see below). Element compositional maps aimed at displaying the spatial distribution of elements in a sample in concentrations greater than 1_{wt}%. Qualitative interpretations of spectra and semi-quantitative analyses were performed by means of the SEM Aztec and INCA software. I analysed the data using R version 4.0.3 (R Core Team, 2020) and the *Ternary* (Smith, 2017) and *ggtern* (Hamilton & Ferry, 2018) packages to produce the ternary plot diagrams. Before starting the statistical analysis on semi-quantitative data, chemical data were checked for anomalies and outliers, which might indicate the presence of an unusual material and impair the final analytical results.

The coarse slags are mainly composed of fayalite (30%) and pyroxenes (42%). Quartz is found in the average amount of 14% with a range from 5 to 41%. In four samples, spinels (14%) are also observed. The principal spinels recognised are magnetite (FeO·Fe₂O₃) and magnesioferrite

($\text{Mg}(\text{Fe}^{3+})_2\text{O}_4$). A relative considerable amount of cristobalite (quartz polymorph with a melting point at 1713°C) has been detected in three samples. Sample ORTB 20 shows a high carbonate content identified as calcite ($\text{Ca}(\text{CO}_3)$). In two samples ORTB 9 and ORTB 20 no olivine structures were detected, instead they showed a very high percentage of pyroxene (74%) and quartz + cristobalite (33%), respectively (refer to Table 5. 4). Observation under optical, digital and electron microscopes revealed chain olivines and needle-like crystals chains and laths only in the coarse sample ORTB 5 (Fig. 5. 4a, b).

Fayalite (Fe_2SiO_4) is the Fe-rich endmember of the olivine solid solution series. Its presence indicates that the temperatures reached in the reactor during the smelting process were sufficiently high to allow the iron minerals to bond with silica (Artioli, 2010; Bachmann, 1982c; Donaldson, 1976; Hauptmann, 2020). Based on the quantity of iron and impurities, temperatures ranged between 1000 to 1300°C . However, the exact compositions of the olivines series are difficult to define as both Ca and Fe can be substituted in their structures for other elements (e.g., zinc) and therefore many different compounds/variables are possible (Dević & Marčeta, 2007). Ca enrichment was observed in most of the olivine structures, likely caused by the overall composition of the slag melts and the oxygen partial pressure of the gas atmosphere ($p\text{O}_2$) in the reaction vessel (Snyder & Carmichael, 1992).

The different morphologies of the crystals in the olivines are particularly informative as they make it possible to roughly assess the thermal path and the cooling rates of the liquid slags (Donaldson, 1976). It is not unlikely that more morphologies coexist and change very fast within the same slag (Hauptmann 2020, p. 258). Different habits within the same slag indicate extremely variable cooling conditions. The formation rates of crystals and therefore their shapes are directly related to the time necessary for the melt to solidify. According to Donaldson (1976), ten types of olivine morphologies exist. Hopper and polyhedral crystal textures indicate cooling rate $<7^\circ\text{C}/\text{h}$, while skeletal crystal textures, acicular (slender, needle-like crystals) chains and laths indicate cooling rates in the range of $40\text{--}80^\circ\text{C}/\text{h}$. Instead, chain olivines crystallizing out of the quartz grains, and feathered spinifex-type and branching olivines had respectively rapid cooling rates in the range of $50\text{--}200^\circ\text{C}/\text{h}$ (tapping process or rapid quenching) and fast cooling rates of more than $500^\circ\text{C}/\text{h}$ (see also Artioli, 2010). Another experimental study carried out by Faure et al. (Faure et al., 2003), however, showed that the morphological features of olivines have a more rapid progression: hopper-type crystals form at cooling rates in the range of low hundreds $^\circ\text{C}/\text{h}$, while laths and rods at high hundreds $^\circ\text{C}/\text{h}$. However, the extended laboratory cooling experiments carried out by Donaldson were mainly built on natural volcanic basaltic melts (forsterite-rich olivines). Therefore, the identified cooling rates do not

apply to the fayalite-rich olivines usually detected in archaeological slags (Ettler *et al.*, 2009). In addition, Ettler *et al.* claim that the cooling rates of human-made (anthropic) olivine are likely to be faster than lava flows, based on the amount of slags produced (Ettler *et al.*, 2009). It must be said that both the experiments were carried out in controlled environments not simulating the real condition of an open prehistoric furnace.

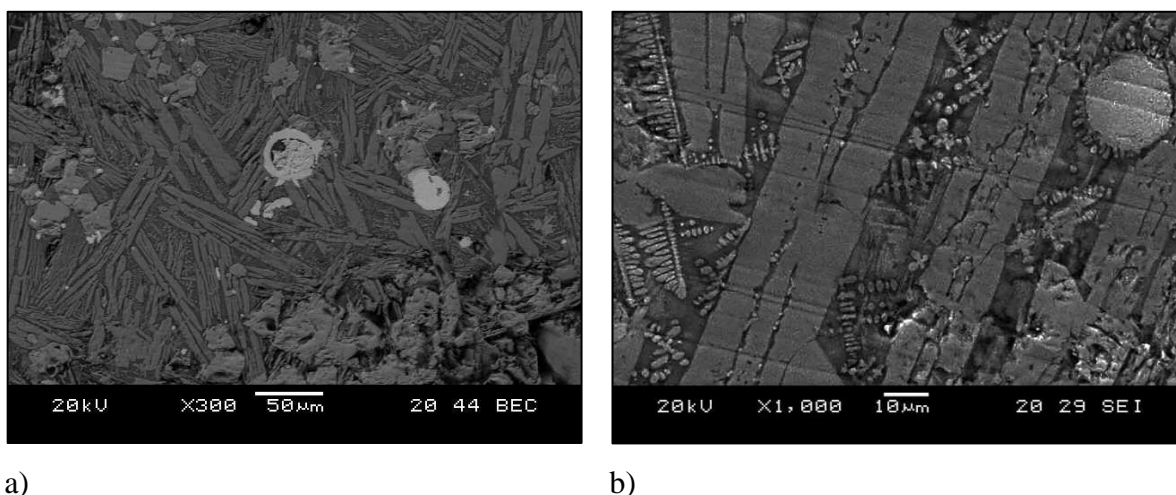


Fig. 5. 4 BSE micrographs showing the mineralogical phases of slag ORTB 5. a) five phases: a) fayalite (large grey needles), in a b) calcium-enriched clino-pyroxene matrix (dark grey); c) magnetite (grey polyhedra); d) copper droplets (grey) with e) an outer ring of covellite; b) parallel fayalite chain olivines intermixed with silicatic glass and a Cu-Fe sulphide round feature.

The highest percentage of pyroxenes in the coarse samples is unexpected as they are usually in lower concentrations than olivines in earlier copper slags. A possible explanation might be the high Ca content in the initial charge. The principal pyroxenes identified are diopside ($\text{CaMgSi}_2\text{O}_6$), hedenbergite ($\text{CaFeSi}_2\text{O}_6$), ferrohedenbergite ($\text{CaFe}^{2+}\text{Si}_2\text{O}_6$), johannsenite ($\text{CaMn}^{2+}\text{Si}_2\text{O}_6$) and petedunnite ($\text{Ca}(\text{Zn}, \text{Mn}^{2+}, \text{Mg}, \text{Fe}^{2+})\text{Si}_2\text{O}_6$). Similarly to the olivines, Ca is accumulated in pyroxenes which can be enriched in Zn replacing Fe in their structure (Ettler *et al.*, 2009). According to Hauptmann's reports on prehistoric and protohistoric slags from Oman, Timna region, Anatolia and Iran, the most common clinopyroxene composition found in ancient copper smelting slags is close to hedenbergite ($\text{CaFeSi}_2\text{O}_6$) and ferrohedenbergite ($\text{CaFe}^{2+}\text{Si}_2\text{O}_6$), (Hauptmann, 2020, p. 264). The same mineralogical compounds were also identified by Manasse *et al.* (2001) in a number of Etruscan slags (VIII century BC) from the Capattoli valley (Campiglia Marittima, Italy), which is located in the same area as Orti Bottagone.

The ore sample shows a mineralogical composition characterised by a high iron oxide content (39%), a similar amount of carbonate (32%) and the same content of quartz and olivine (15%). Two alternative interpretations can be proposed. First, the quartz and the high carbonate content might suggest that poorly beneficiated charge might have been used. Alternatively, the piece might represent a low copper-bearing fragment that was discarded from the charge. Unfortunately, the only fragment recovered meant that it was not possible to further understand the type of ore exploited.

The flat slags are characterised by a higher amount of fayalite (61%) and spinels (39%), and a lower content of pyroxenes (10%) compared to the coarse slags. Pyroxenes were detected only in 3 samples out of 9. Only one sample (ORTB 2) showed a relatively low quartz content and another (ORTB 12) low carbonate content (refer to Table 5. 4). A vast range of olivine morphologies depending on their positions in the samples was observed by means of optical and electron microscopy. Chain olivines and elongated crystals were detected mainly on the surfaces, whereas cubic and polyhedral habits, hoppers and elongated hoppers were found in the inner part of the slag (Fig. 5. 5). Identical cubic and polyhedral morphologies were observed in the almost contemporary site of San Carlo Cave Solvay, located few kilometers north (Artioli et al., 2016, Figure 52d). Even if the cooling rates are still not clearly defined, these morphologies indicate different cooling gradients. As expected, the inner part of the specimens shows lower cooling rates than the surface, suggesting that the slags were left to cool within the reactor (see Addis et al., 2016, p. 990). None of the prismatic features revealed Mg core enrichment (zoning). The low amount of Mg (average 4.6%) in the olivine structures, according to the forsterite-fayalite phase diagram (Bowen & Schairer, 1935), places their crystallisation temperatures on the fayalitic side of the diagram at around 1200°C. In reality, in the assemblage under study, the presence of minor constituents in the charge such as Ca, K, As, and Zn interacting with the olivine crystallisations, certainly modifies the crystallisation temperatures, lowering them by around 100-150°C depending on the relative compositions (Hauptmann, 2020, p. 180). At the same time, the amount of impurities vary, based on the temperatures reached during the smelting process (Misra et al., 1993). It must be pointed out that the values reported in binary and ternary diagrams are just estimates of the temperatures in the system and should be used just as reference. They reflect the equilibrium conditions in the system, which are not met during the smelting (Freestone, 1988; Kresten, 1986).

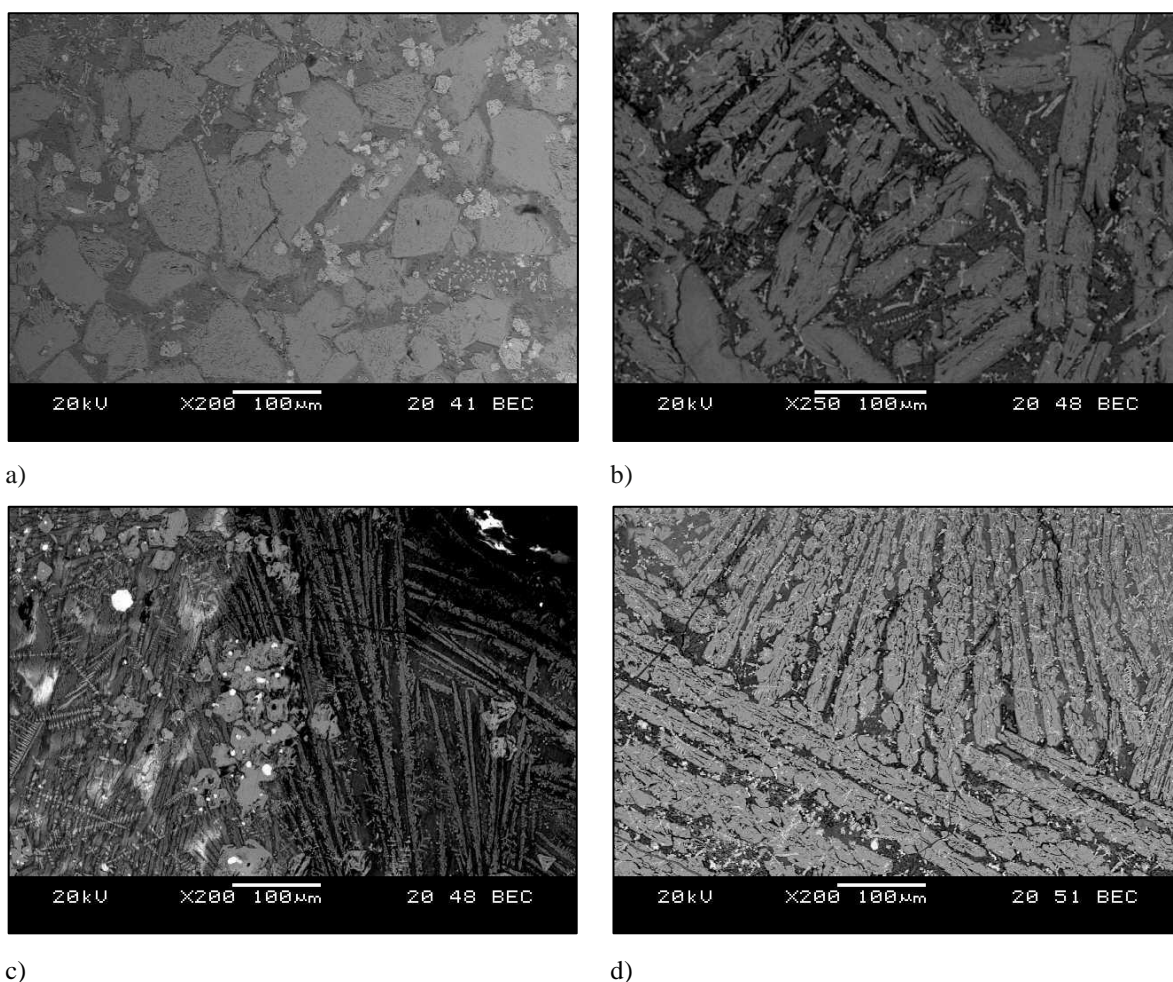


Fig. 5. 5 BSE micrographs showing the diverse range of olivine morphological crystallised features in the flat slags: a) euhedral grains (ORTB 20), b) hopper structures (ORTB 16), c) small dendritic needles (ORTB 8), d) large chain structures (ORTB 16).

Among the spinels, magnetite, wuestite and magnesioferrite were identified. They have diverse morphologies ranging from euhedral crystals (rare) to dendritic elongated herringbone-like structures and round morphologies (common), (Fig. 5. 6). As expected, a higher amount of magnetite appears due to the unfavourable reducing conditions in early smelting reactors.

Magnetite contains both Fe^{2+} (ferrous) and Fe^{3+} (ferric) oxidation states, which suggest crystallization in an environment with lower oxygen levels than the atmosphere (Hauptmann 2020). Due to its higher melting point compared to other mineralogical phases, magnetite crystallises first, without competition, forming large euhedral (cubic and prismatic) crystals. Except for isolated features, the general absence of this morphological feature points toward a rapid cooling process of the slag. Wuestite occurs in lower amount as it requires high reducing conditions (low oxygen fugacity) rarely met in the reactor. Nevertheless, it appears in the form of dendritic aggregates or spheres sometimes mixed with magnetite. Similar morphologies have been found in a number of Chalcolithic sites such as Montesei di Serso (Artioli et al., 2009) and

Millan (Artioli et al., 2005) in Italy, and El Picacho (Müller et al., 2007), in Spain (Fig. 5. 7a-c). The blunted edges are the results of fast cooling that did not allow the grains to develop crystal faces.

Continuous rims of pyrrhotite-magnetite were also identified in sample ORTB 6. Due to the high amount of oxygen (low reducing conditions) in the reactor, and because of the high chemical propension (or affinity) of Fe to bond with O (higher compared with Cu), it is common to find Fe sulphides (e.g., pyrrhotite) associated with Fe oxide (e.g., magnetite). Similar structures were detected by Hauptmann (1985) who placed their crystallisation temperatures between 1030-1050°C.

The phase association of fayalite plus magnetite (the latter mainly embedded in the first) identified in the majority of the samples investigated is typical of earlier copper smelting slags (Artioli, 2010, p. 334; Hauptmann, 2020, p. 180).

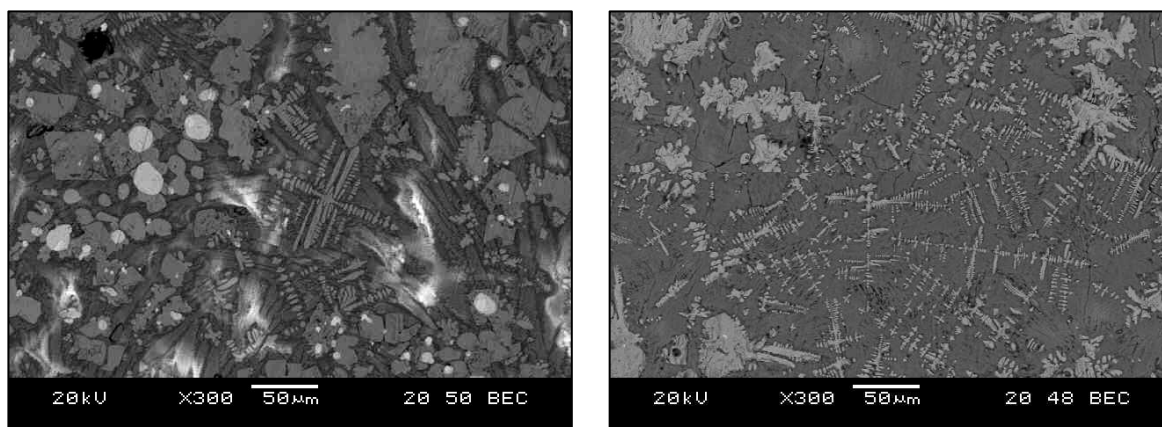
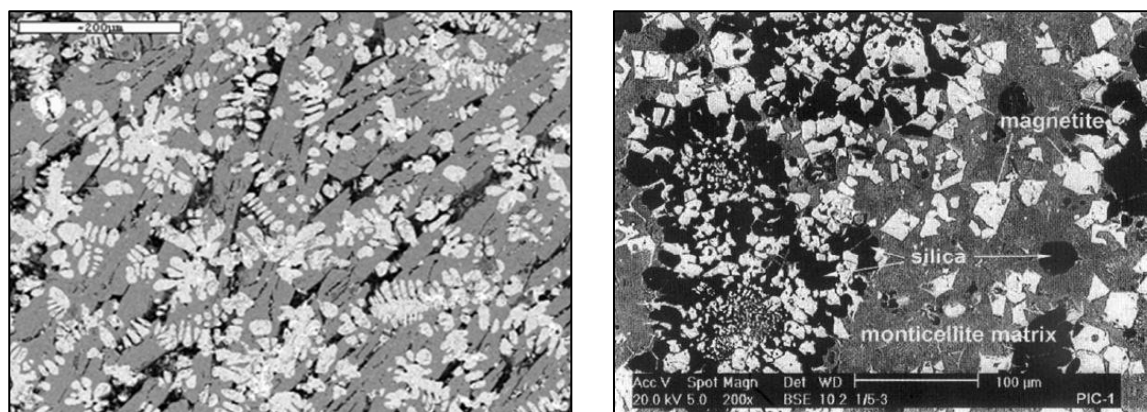


Fig. 5. 6 BSE micrographs showing the different morphologies of the iron-rich inclusions identified in sample ORTB 8: euhedral (cubic to prismatic) crystals, dendritic growths and round features in a fayalitic matrix. Their presence in such a reduced area indicates highly unstable reducing conditions during the smelting process. The light grey features in the image on the left are inclusions of metallic copper or copper-iron sulphides.



a)

b)

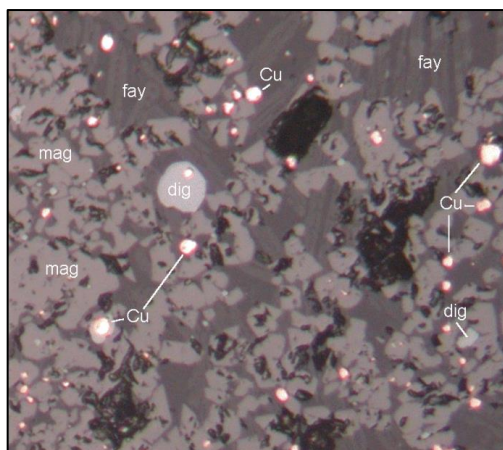


Fig. 5. 7 Series of micrographs showing the different iron-rich spinel morphologies/phases similar to those investigated here: a) BSE image showing wuestite dendrites in the fayalitic matrix from a sample from Montesei di Serso, Trentino - scale bar 200 μm (Artioli et al., 2015, Figure 4); b) the matrix, distributed among non-reacted silica grains, in a monticellite-like silicate. Magnetite is abundant (Müller et al., 2007, Figure 2). c) Reflected Light image (hereafter RL) showing magnetite in prismatic and round morphologies in a fayalitic matrix with metallic copper and newly formed Cu sulphides of digenite-chalcocite from Millan – image length 200 μm (Artioli et al., 2005).

c)

Table 5. 4 XRD analytical results showing slags principal mineralogical phases, normalised, expressed in weight percentages ($\text{wt}\%$) and calculated with the Rietveld refinement method. Values reported as b.d.l. (Below Detection Limits) indicate that the concentration of the corresponding phase or compound was below the detection threshold of the analytical method. Phases: Qz = Quartz, Cr = Cristobalite (quartz polymorph), Ol = Olivine, Px = Pyroxene, Sp = Spinel, Cb = Carbonate

Rep	Slag type	Qz	Cr	Ol	Px	Sp	Cb
ORT B. 3	Ore	15	b.d.l.	15	b.d.l.	39	32
ORT B. 1	Coarse	7	b.d.l.	56	26	11	b.d.l.
ORT B. 4		10	b.d.l.	44	46	b.d.l.	b.d.l.
ORT B. 5		41	7	34	b.d.l.	19	b.d.l.
ORT B. 6		11	b.d.l.	23	51	15	b.d.l.
ORT B. 7		12	b.d.l.	36	53	b.d.l.	b.d.l.
ORT B. 9		7	9	b.d.l.	74	10	b.d.l.
ORT B. 20		21	12	b.d.l.	37	b.d.l.	30
ORT B. 21		5	b.d.l.	48	47	b.d.l.	b.d.l.
Mean		14	9	30	42	14	30
St. Dev		11.8	2.6	20.9	21.7	4.1	
ORT B. 2	Flat	16	b.d.l.	b.d.l.	52	32	b.d.l.
ORT B. 8		b.d.l.	b.d.l.	b.d.l.	21	79	b.d.l.
ORT B. 12		b.d.l.	b.d.l.	65	b.d.l.	20	15
ORT B. 14		b.d.l.	b.d.l.	54	b.d.l.	46	b.d.l.
ORT B. 15		b.d.l.	b.d.l.	59	b.d.l.	41	b.d.l.
ORT B. 18		b.d.l.	b.d.l.	79	b.d.l.	21	b.d.l.
ORT B. 19		b.d.l.	b.d.l.	66	b.d.l.	34	b.d.l.
ORT B. 13		b.d.l.	3	49	18	30	b.d.l.
ORT B. 16		b.d.l.	b.d.l.	56	b.d.l.	44	b.d.l.
Mean		15	3	61	10	39	15
St. Dev		b.d.l.	b.d.l.	9.9	17.9	17.8	

5.2.6. Inclusions and minor elements

The slags investigated showed two different types of rock inclusions: calcium-based compounds and quartz. They are distributed unevenly across the assemblage with a higher presence in the coarse samples.

So far in literature, the presence of Ca has been ascribed to three main reasons:

- contamination of charcoal/ash (Tylecote *et al.*, 1977, pp. 310–311; Bourgarit, 2007), which chemically bond with the liquid compounds in the melt; sometimes it is associated with the presence of potash (K) and phosphorus (P);
- natural association with the ore as calcium compounds. The most common calcium compound on Earth is calcium carbonate (limestone) with the formula CaCO_3 ; this indicates that the presence of Ca in the ore belongs to the country rock and results from poor beneficiation.
- addition as fluxing agent.

Although Ca contamination can be due to the wood/charcoal ash used as fuel (Tylecote *et al.*, 1977, pp. 310–311; Bourgarit, 2007), the relatively high Ca contents in the form of oxides, carbonates (e.g., FeCO_3 , CaCO_3) and iron oxide-rich melts suggest two possible scenarios: 1) the initial charge, along with the sulphides, was characterised by Ca-based compounds; 2) Ca-based compounds were added as fluxing agents at some point during the smelting process. The addition of carbonatic flux (limestone, CaCO_3) has been suggested for CA/EBA sites of Riparo Gaban and La Vela di Valbusa in Trentino/Alto Adige (D'Amico *et al.*, 1998b); and Romagnano Loch and Romagnano Tof de la Val (Cattoi *et al.*, 2000). Despite the relics of Ca oxides and iron oxides rich in calcium detected in some of the slags (Fig. 5. 8a-c) might make this last hypothesis plausible, its constant presence in the matrix, in the ore fragment (ORTB 3), and in a number of semi-reacted inclusions' rims (Fig. 5. 8d) seem to support the first scenario, i.e., that the initial load, together with the sulphides, exhibited a presence of Ca-based compounds. Additionally, although there is not absolute certainty of the provenance of the ore adopted, the geology of the closest mining area seems to match the composition of the slags.

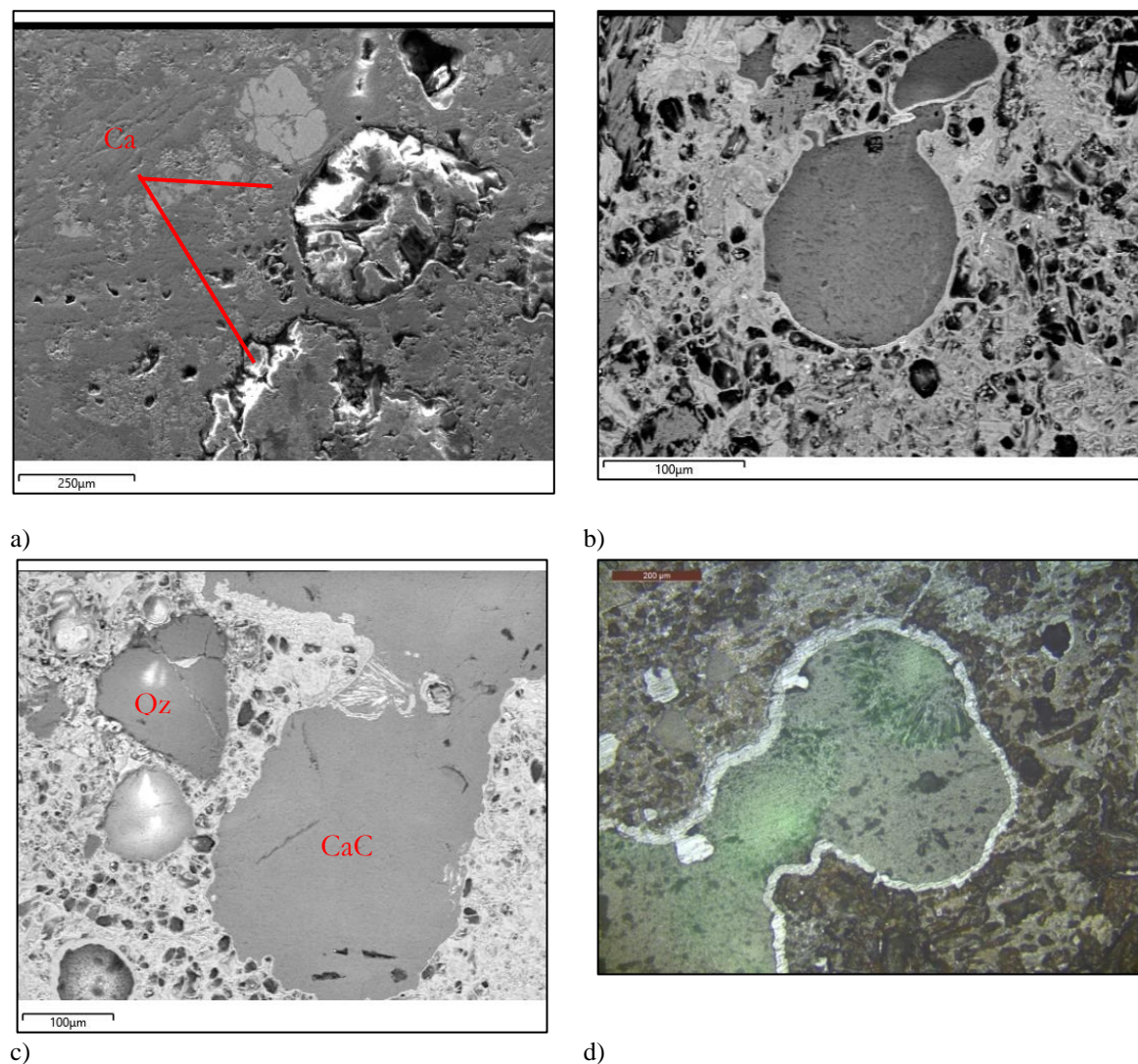


Fig. 5. 8 Micrographs showing a) BSE image with relics of calcium carbonate as inclusions in a fayalitic glassy matrix (sample ORTB 13 flat); b) BSE image with relics of calcium carbonates found as inclusions in a fayalitic glassy matrix (sample ORTB 20 coarse); c) BSE image with quartz and Ca inclusions (sample ORTB 20 coarse); d) RL image with semi-reacted inclusion of a possible Ca carbonate. CaO is the main compound in the grey rim – scale bar 200 µm (ORTB 9).

Quartz inclusions were identified in variable amounts in the ore fragment and in the coarse slags (Fig. 5. 9). In sample ORTB 5 the quartz inclusions were all concentrated in the centre of the slag. Although it is largely agreed upon, even if with exceptions (Pearce et al., 2022; Saez et al., 2003a), that fluxing agents were normally not added to improve the smelting processes at the early stages of copper smelting metallurgy (Bourgarit, 2007), it has not been possible to establish if the inclusions detected consisted of unreacted bits of the mineralisation exploited or are remnants of fluxes deliberately added to optimize the outcome of the smelting process (see Hauptmann, 2020, pp. 240–243). However, whatever the provenance (ore/deliberate addition), unreacted or partially melted quartz fragments are informative on two technological aspects of the smelting process: a) they indicate that the temperatures in the furnace were not

high enough to melt the SiO_2 based compounds (Ettler et al., 2000; Saez et al., 2003a) and/or that the process did not last long enough to allow the charge to entirely melt (Ettler et al. 2009); b) they show an excessive high contents of SiO_2 , far from the desired eutectic composition for slagging. Slagging is the process in which impurities and waste materials are separated and removed from a metal during its refining or smelting. It helps purify the metal by forming a separate layer of unwanted materials that can be easily removed.

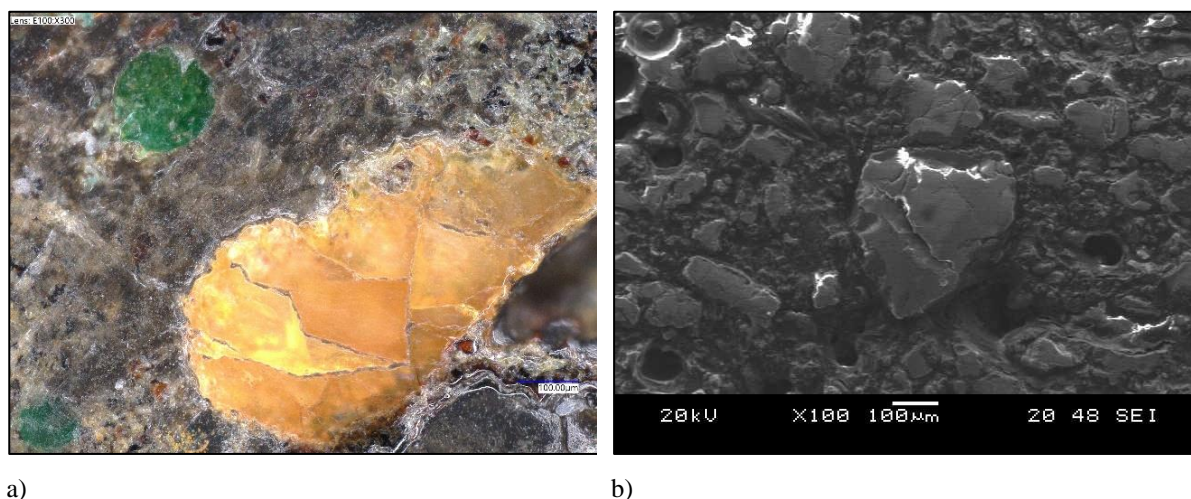


Fig. 5.9 RL (a) and BSE (b) micrographs of quartz inclusions in two coarse samples (respectively ORTB 6 and ORTB 5). Scale bar of a) 100 μm

SEM-EDX analyses identified zinc occurring in minor but relatively constant amounts across the assemblage. The average is 1.21_{ox}% (coarse slags 0.82_{ox}%, flat slags 1.91_{ox}%). It was mainly detected in the olivines and spinels. Zinc enrichment in fayalitic olivine is a common phenomenon as it replaces Fe in the octahedral position of their crystal structure (Ettler *et al.*, 2009). According to Shannon (Shannon, 1976) the ionic radii have the same length (0.74 Å for Zn and 0.76 Å for Fe). A little higher percentage of zinc has been reported in the olivine structures of the slags from Capattoli (Campiglia Marittima, Italy) by Manasse et al. (2001). It has been associated with the abundance of sphalerite in the ore deposits closeby.

5.2.7. SEM-EDX semi-quantitative analysis

A semi-quantitative evaluation of the elemental composition of the slags was carried out by means of SEM-EDX. Data are reported in Appendix B. Three random scans, each covering an area of approximately 1 mm², were conducted for each slag (Fig. 5.10). Prills, copper-iron sulphide compounds and residual minerals were avoided and are discussed separately. I used the term semi-quantitative as only an estimation of their approximate concentrations could be

done with this analytical technique, first because only three small areas of the entire surface were considered for each specimen and second because the electrons penetrate a depth of 0.02–1.0 μm into the sample, thus returning a 2D bulk chemical analysis of the cross-section's surface. Considering the average composition of ancient archaeometallurgical slags (Hauptmann, 2020, p. 99) ternary systems within the materials tetrahedron of $\text{CaO-SiO}_2\text{-FeO-Al}_2\text{O}_3$ were adopted. Each scan was plotted in the ternary diagrams displaying the $\text{FeO-Al}_2\text{O}_3\text{-SiO}_2$ (wt%) and FeO-CaO-SiO_2 (wt%) systems.

It must be kept in mind that, when dealing with heterogeneous slags, the mean compositional values do not always mirror the real composition of the slags. As already noted by Humphris et al. (2009), if the sample is not representative of the whole, it might lead to skewed mean compositional data. As an example, the bulk chemistry of sample ORTB 5 reported in Fig. 5. 11 shows that the three areas analysed completely differ microstructurally and chemically from one another and therefore their compositional mean does not reflect its high heterogeneity. As illustrated in the plot in Fig. 5. 11 the mean value evenly distributes the M4 and I-H13-14 readings. Therefore, in order to avoid biased interpretations and have a general trend of the matrices' compositions, all the three readings for each sample were plotted.

The ternary plot diagram $\text{FeO-Al}_2\text{O}_3\text{-SiO}_2$ (wt%), shows all the readings categorised according to their typology (Fig. 5. 12). All the readings cluster along the FeO-SiO_2 compositional area reflecting the nature of the raw material, high in iron and silica (Hauptmann, 2014, p. 100). The ore fragment shows a composition particularly high in iron in one area and rich in silica with ca. 20_{wt%} of Al_2O_3 in the other two. A clear difference between coarse and flat slag composition is illustrated. Significantly, all the readings of the chemical compositions of flat slags cluster in the area of average composition of archaeometallurgical slags from copper smelting identified by Hauptmann (2020, 2007), mainly matching the eutectic area of the fayalite region (*fa*) in the system (Fig. 5. 13). The flat slags cluster towards the FeO corner. Overall, their mean compositions do not differ much from the areas analysed.

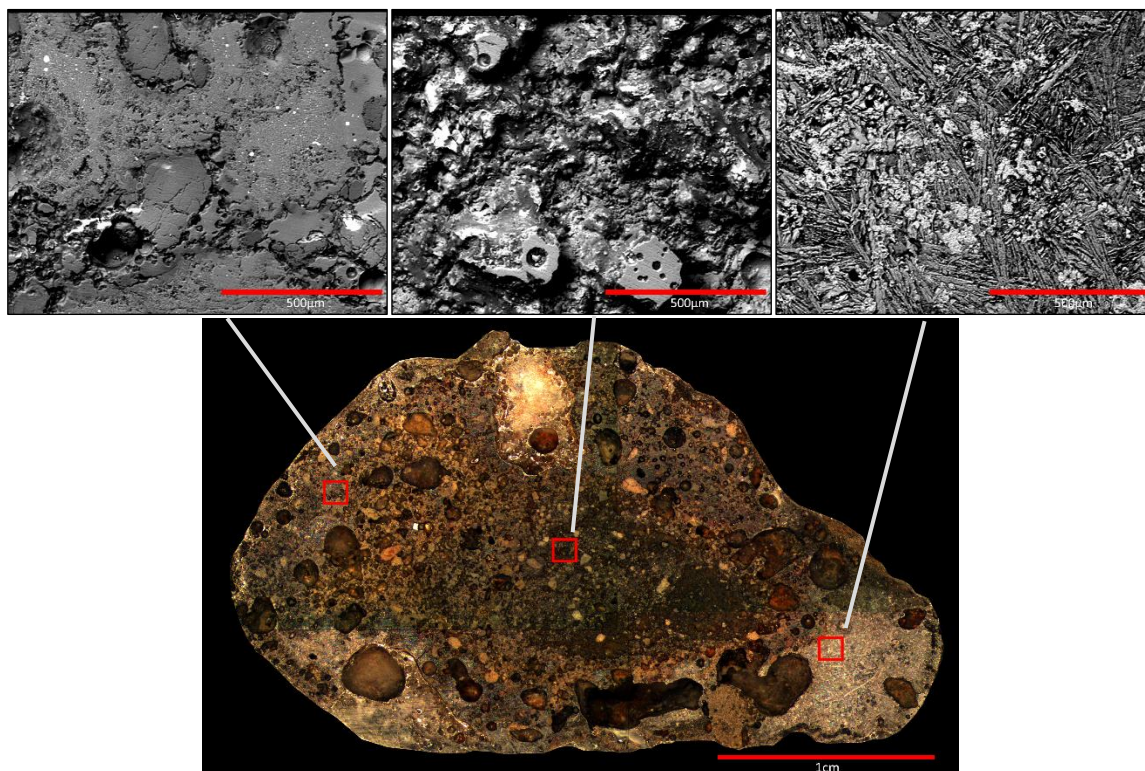


Fig. 5. 10 ORTB 5. Three scanned 1mm²-areas were acquired for each slag. From left G21, I-H13-14, M4

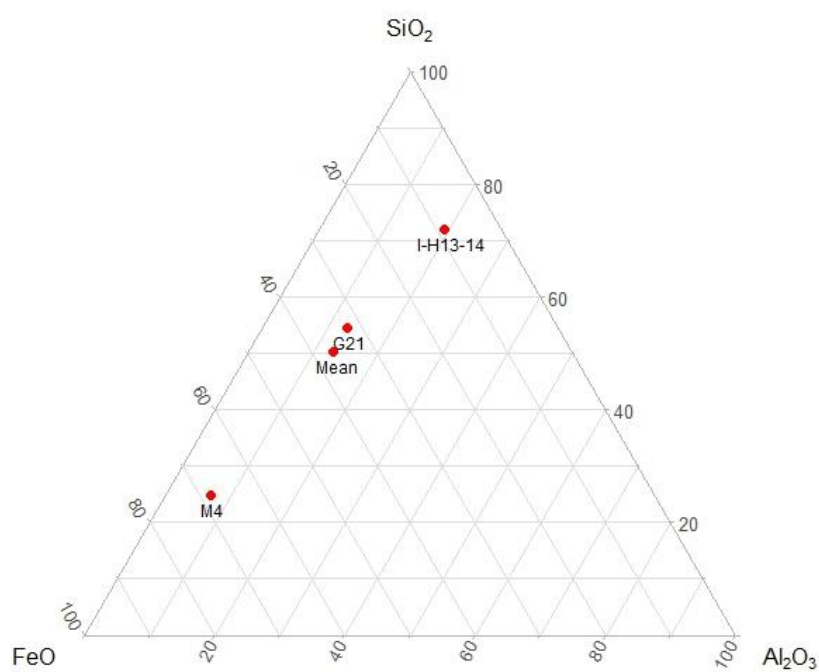


Fig. 5. 11 Ternary plot diagram FeO–Al₂O₃–SiO₂ (wt%) of the bulk chemistry of the three areas analysed (I-H13-14, G21, M4) and mean of sample ORTB 5.

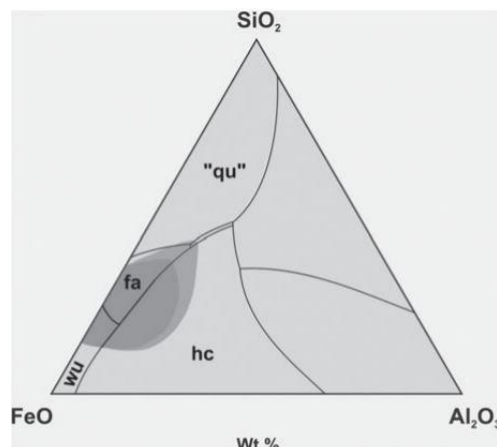
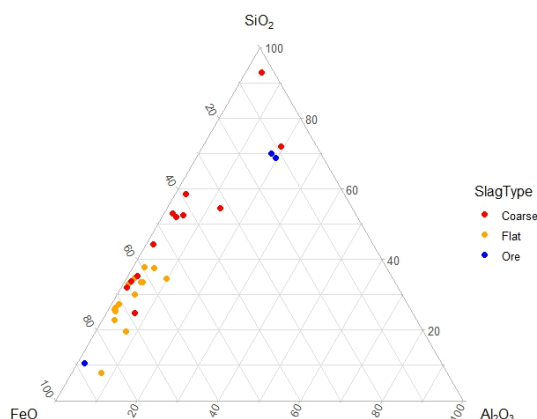


Fig. 5. 12 Ternary plot diagram (FeO–Al₂O₃–SiO₂ (wt%) slag system) of the average composition of the three areas analysed.

Fig. 5. 13 Ternary plot diagram showing the average composition of archaeometallurgical slags from copper smelting (*medium-shaded area*) and iron smelting (*dark-shaded area*) shown in the ternary system FeO–Al₂O₃–SiO₂ (wt%), (Hauptmann 2014:100, Fig. 5.6).

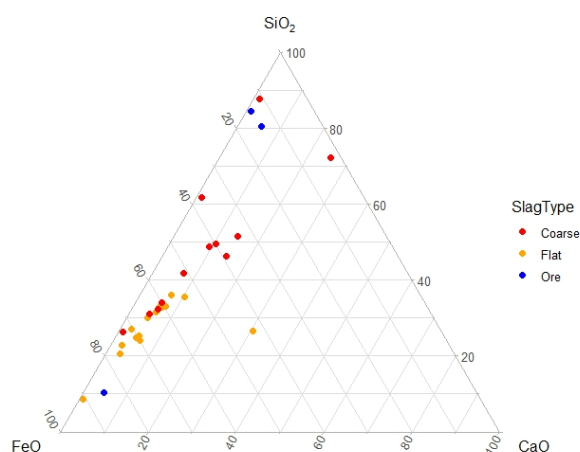


Fig. 5. 14 Ternary plot diagram (FeO–CaO–SiO₂ (wt%) slag system) of the average composition of the three areas analysed.

On the contrary, the coarse slags' readings partly distribute far from the average composition of copper smelting slags, i.e., far from the low-melting region of the system (Fig. 5. 12). Conversely, the coarse slags are more dispersed along the FeO–SiO₂ compositional area, showing a higher degree of intra-sample variability. This variability shows that a vast range of mineralogical phases, given by fluctuating temperatures and unstable reducing/oxidising conditions, existed during the slag formation process. The readings plotted on the FeO–CaO–SiO₂ (wt%) ternary system follow a similar chemical patterning (Fig. 5. 14). Except for an outlier, all the flat slags cluster in the fayalite rich area. In comparison, the coarse slags show a higher variability along the FeO–SiO₂ axis.

5.2.8. Viscosity and Fe/SiO₂ ratio

To gain a deeper insight into the formation processes of slags, two key parameters, viscosity index and the Fe/SiO₂ ratio were determined through SEM-EDX analyses of the matrices. Viscosity measures a fluid's resistance to flow and is directly influenced by reactor temperatures (higher viscosity corresponds to lower temperatures). Bachmann (1982c, p. 19) and Lutz. et al. (1988) developed a method for its measurement, which allows for a rough estimation of the temperature ranges within the reactor. This method involves calculating a “viscosity index” (K) by comparing the weight percentages of “basic” oxides (CaO, MgO, FeO, MnO, K₂O) to “acid” oxides (SiO₂, Al₂O₃). A lower viscosity index (K) indicates a melt viscosity (see also Manasse & Mellini, 2002). Bachmann's formula, simplified by Addis et al. (2016, pp. 107, 217) is expressed as:

$$K = \frac{(\text{CaO} + \text{MgO} + \text{FeO} + \text{MnO} + \text{K}_2\text{O} + \text{Na}_2\text{O})}{(\text{SiO}_2 + \text{Al}_2\text{O}_3)}$$

Ideally, slags should exhibit low viscosity, and they should not contain metal-bearing phases such as copper, copper oxides, copper sulphides, copper-iron sulphides. However, this description applies only to modern slags obtained in blast furnaces. In reality, reactions and transformations inside ancient reactors are considerably more complex and depend on various factors, including the nature of the initial charge, temperature(s), reducing conditions, and process duration. Early smelting processes often failed to reach the temperatures required for complete charge liquefaction, resulting in a lack of distinct separation of individual mineralogical phases. Consequently, refractory phases with high melting temperatures, such as quartz (SiO₂, melting temperature = ~ 1600°C), remained in the solid state alongside metal-bearing phases at intermediate reaction states.

The Fe/SiO₂ ratio was also determined. Iron exists in slags in various chemical compounds associated with silicates, sulphur and oxygen exhibiting different valency states (Fe, FeO, Fe₂O₃, FeO·Fe₂O₃, FeS). Since SEM-EDX and most analytical techniques used for slag analysis cannot differentiate these valency states, the Fe/SiO₂ ratio, which assumes the conversion of all Fe oxides into metallic iron, offers a meaningful indication of the slag's core composition (Pryce et al., 2010, p. 118). The following formula was employed:

$$x = \frac{\left(\frac{56 * \text{FeO}}{72}\right)}{\text{SiO}_2}$$

Here, 56 represents the atomic weight of Fe and 72 is the sum of the atomic weights of Fe and O. Given the heterogeneity observed in the slags under study, the Fe/SiO₂ ratio was calculated for each analysis conducted to provide a more comprehensive overview of the slag composition. The values reported and plotted represent the averages of these individual analysis (refer to Table 5. 5).

The coarse slags exhibited a viscosity index value of 1.2, while the flat slags displayed a higher value of 2.4. As anticipated, the coarse samples exhibited higher viscosity values (a lower value signifies higher viscosity), indicating that the liquid phases, such as Cu-Fe sulphides with lower melting temperatures, did not fully settle at the bottom of the reactor/crucible. Instead, they remained entrapped within the slag. Conversely, the flat slags' better fluidity favoured their separation.

It is crucial to emphasise that these values provide only a rough estimate of the actual slag viscosity. While this study can be effectively conducted for Late Bronze Age relatively homogeneous proto-industrial slags, the high heterogeneity of the early smelting slags under investigation prevents the evaluation of copper prill separation rates through the slag and the rough estimation of smelting step velocity and duration (see Addis, 2013; Addis et al., 2016). However, intriguing insights can be gleaned when K indexes are plotted against Fe/SiO₂ ratio values (Fig. 5. 15 Scatterplot showing a strong positive correlation (0.9) between the variables, indicating that as the Fe/SiO₂ ratio systematically increases, there is a corresponding systematic increase in the viscosity index.). Outliers, consisting of six observations significantly differing from the others, were excluded from the plot. The plot reveals a strong positive correlation between the variables, indicating that a systematic increase in the Fe/SiO₂ ratio corresponds to a systematic increase in the viscosity index. The correlation coefficient is 0.9, signifying an almost perfect association between the two variables. Pearson's correlation method was adopted as more appropriate with a linear, more or less continuous distribution of points (VanPool & Leonard, 2011). Most of the values cluster in the region between 2.5 k value and 2 Fe/SiO₂ ratio values, with the coarse samples generally exhibiting lower values than the flat ones. The analysis of flat samples displays slightly greater dispersion compared to the coarse samples, indicating a higher intra-variability in the mineralogical composition.

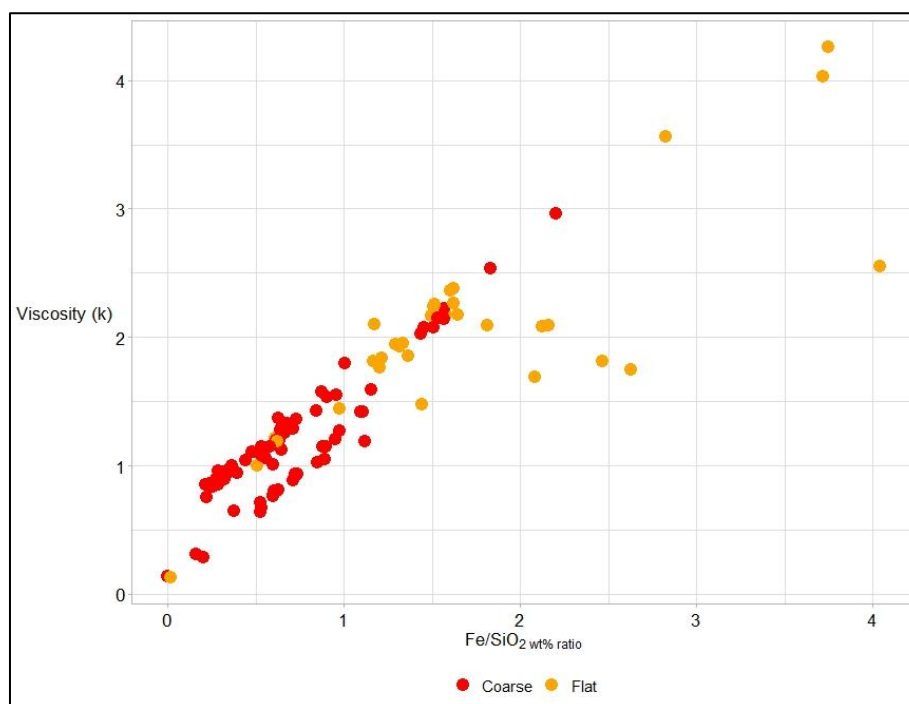


Fig. 5. 15 Scatterplot showing a strong positive correlation (0.9) between the variables, indicating that as the Fe/SiO₂ ratio systematically increases, there is a corresponding systematic increase in the viscosity index.

Fe/SiO₂ ratio values were also plotted against CaO on two binary Flogén diagrams (see Fig. 5. 16). These diagrams are deemed more suitable for non-ferrous archaeometallurgical data because they offer advantages over ternary diagrams and the Ellingham diagram in estimating redox conditions more precisely and calculating crystallisation temperatures within the system (refer to Kongoli & Yazawa, 2001, p. 583; Pryce, 2009, p. 114 for detailed thermodynamic explanations). These diagrams take into account the relatively high calcium content in the slags and the presence of minor oxides, which act as fluxing agents, reducing the melting temperatures of the charge. Unfortunately, binary Flogén diagrams are not available for Fe/SiO₂ ratio values exceeding 2.5. However, most of the values fall within the diagram's defined range. Given the impossibility of determining intermediate partial pressures in ancient reactors, the data were plotted in two different Flogén diagrams at pO₂ level of 1x10⁻⁵ and 1x10⁻⁸ atm.

The plot in Fig. 5. 16 illustrates a curvilinear relationship between the CaO content and the Fe/SiO₂ ratio values. As expected, the analyses of coarse slags are distributed along the CaO vertical axis, indicating a lower Fe/SiO₂ ratio compared to the analyses of the flat slags, which are spread along the horizontal axis representing the Fe/SiO₂ ratio, primarily falling within the range of 1 to 4. The latter group generally exhibits higher Fe/SiO₂ ratio values and clusters in the region near silica saturation, where crystallisation temperatures are estimated to be between 1175 °C and 1250 °C.

Three distinct clusters were identified. The first comprises several coarse slags analyses, clustering in the low CaO content silica saturation zone. The second, characterised by coarse slag analyses, is observed in the CaO-rich area (15 to 20_{wt%}) and exhibits Fe/SiO₂ ratios between 0 and 1. These analyses fall in the transition zone between silica saturation and calcium silicates, suggesting potential crystallisation temperatures between 1150°C and 1225°C at pO₂ of 1x10⁻⁸, or between 1225°C and 1300°C at pO₂ of 1x10⁻⁵. The third group of analyses included both types of slags, with the majority belonging to the flat type. They cluster in the so-called fayalitic zone ("F"), indicating crystallisation temperatures in the range of 1150°C and 1250°C at pO₂ of 1x10⁻⁸, which roughly corresponds to the olivine formation temperatures proposed earlier in the mineralogical phases section. According to Kongoli and Yazawa (2001) olivines should not form under intermediate partial pressures implying variable redox conditions in the system (Kongoli & Yazawa, 2001, p. 585).

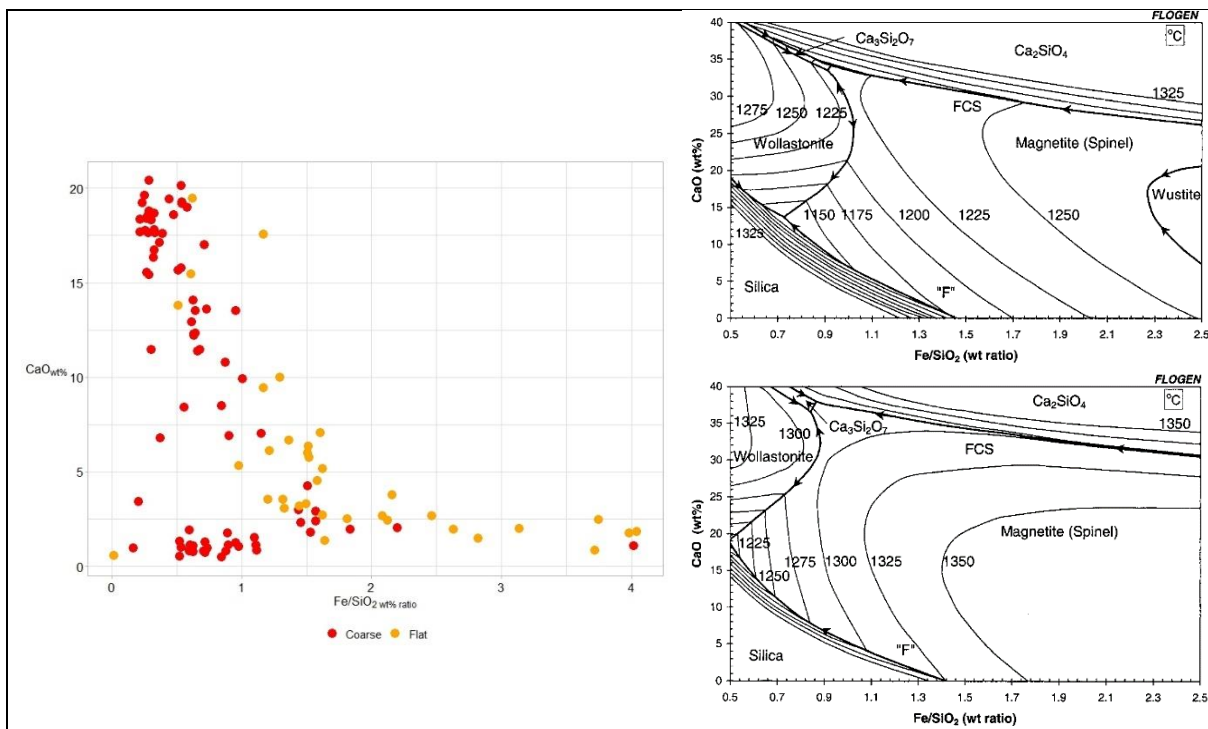


Fig. 5.16 Binary diagram showing the liquidus effect of varying calcium oxide content and Fe/SiO₂ ratio on CaO-FeO-Fe₂O₃-SiO₂ slag system at pO₂ of 10⁻⁸ atm (top right) and 10⁻⁵ atm (bottom right). From Kongoli & Yazawa, 2001, p. 585, figg. 4-5).

Table 5. 5 Average chemical composition of the Fe-silicate phases of the slag samples determined by SEM-EDS. The values reported are averages of 7 to 22 analyses of each sample. Large metallic and sulphide inclusions were excluded from the analyses. All elements are presented as oxides for comparison with the literature.

Rep		Count	Na ₂ O	MgO	Al ₂ O ₃	SiO ₂	SO ₃	P ₂ O ₅	K ₂ O	CaO	TiO ₂	MnO	FeO	CuO	ZnO	Density (g cm ⁻³)	Fe/SiO ₂ ratio	Viscosity (k)	
ORT B. 5	Coarse	22	2.1	1.7	8.3	44.5	0.8	0.7	1.7	1.0	0.5	1.4	39.7	1.9	0.7	1.73	0.7	0.9	1.2
σ			1.8	1.9	3.3	7.6	0.3	0.1	0.9	0.3	0.1	0.5	8.5	4.3	0.1		0.3		
ORT B. 9		22	0.5	8.3	1.2	48.6	b.d.l.	0.9	b.d.l.	16.0	b.d.l.	1.3	24.0	2.3	1.0	1.80	0.3	0.9	
σ			0.2	2.4	0.4	10.7	b.d.l.	b.d.l.	b.d.l.	4.0	b.d.l.	0.3	14.5	2.8	0.3		0.1		
ORT B. 20		18	1.3	1.0	2.2	33.6	0.8	b.d.l.	b.d.l.	9.8	b.d.l.	1.4	51.0	1.6	1.3	2.78	2.0	1.7	
σ			b.d.l.	0.6	0.7	11.0	0.1	b.d.l.	b.d.l.	8.7	b.d.l.	0.6	18.2	1.9	0.2		2.7		
ORT B. 6		21	1.5	4.5	4.0	41.6	1.9	1.0	0.7	12.5	0.5	1.3	32.5	3.3	1.9	2.43	0.6	1.2	
σ			b.d.l.	1.8	4.8	6.0	1.2	b.d.l.	0.5	4.3	b.d.l.	0.3	8.4	3.1	0.4		0.2		
ORT B. 8	Flat	10	3.5	2.3	10.4	23.9	0.7	1.9	2.4	3.1	0.6	1.3	54.1	4.2	2.5	1.06	2.0	3	2.4
σ			b.d.l.	1.7	6.5	19.2	b.d.l.	0.5	0.7	3.9	b.d.l.	0.7	24.9	2.0	1.3		1.4		
ORT B. 12		10	b.d.l.	2.0	2.2	28.6	3.8	1.0	b.d.l.	4.8	b.d.l.	1.4	58.1	1.5	3.1	3.83	1.7	2.1	
σ			b.d.l.	0.9	1.2	4.8	4.4	0.2	b.d.l.	2.5	b.d.l.	0.4	5.8	1.5	1.2		0.3		
ORT B. 13		7	b.d.l.	2.5	9.3	18.0	0.5	1.5	b.d.l.	6.6	b.d.l.	2.6	58.3	3.9	1.7	1.99	3.9	2.5	
σ			b.d.l.	2.0	18.3	12.6	b.d.l.	0.4	b.d.l.	7.1	b.d.l.	3.5	21.2	1.7	1.2		2.1		
ORT B. 19		10	b.d.l.	1.2	0.8	29.2	0.7	b.d.l.	b.d.l.	6.1	b.d.l.	1.6	59.5	1.4	2.2	3.65	1.4	2.0	
σ			b.d.l.	0.3	0.2	9.5	0.1	b.d.l.	b.d.l.	4.8	b.d.l.	0.3	13.2	b.d.l.	0.5		0.2		

5.2.9. Copper bearing compounds

Copper bearing compounds were observed using optical and electron microscopes. A total of 191 spot analyses were conducted using an energy-dispersive X-ray spectrometer. The analyses are reported in Appendix A. In all specimens, the presence of Cu-Fe sulphides was evident, either trapped within the gangue or embedded in the slag matrix, appearing in the form of matte (a copper-iron-sulphide compound) and copper prills. A wide array of Cu-Fe-S mineralogical phases was identified, spanning from unreacted or semi-reacted minerals to intermediate solid solutions, depending on their transformation stage.

Within the ore fragments, the Cu-Fe sulphides consisted of inclusions of chalcopyrite (CuFeS_2) and pyrrhotite ($\text{Fe}_{(1-x)}\text{S}$), primarily embedded in the gangue rock. Chalcopyrite, characterized by a higher copper content (approximately 30_{wt}%), displayed a darker and more vibrant yellow hue. In contrast, pyrrhotite, with its iron content ranging from 60-64_{wt}% and copper content below 4.5_{wt}%, exhibited colours ranging from bright, light yellow to pale brownish pink and bronze (Fig. 5. 17a, b). Similar structures of sulphide raw materials were identified by Rehren et al. (2020) at the Chalcolithic site of Akladi Chir (Fig. 5. 17c)

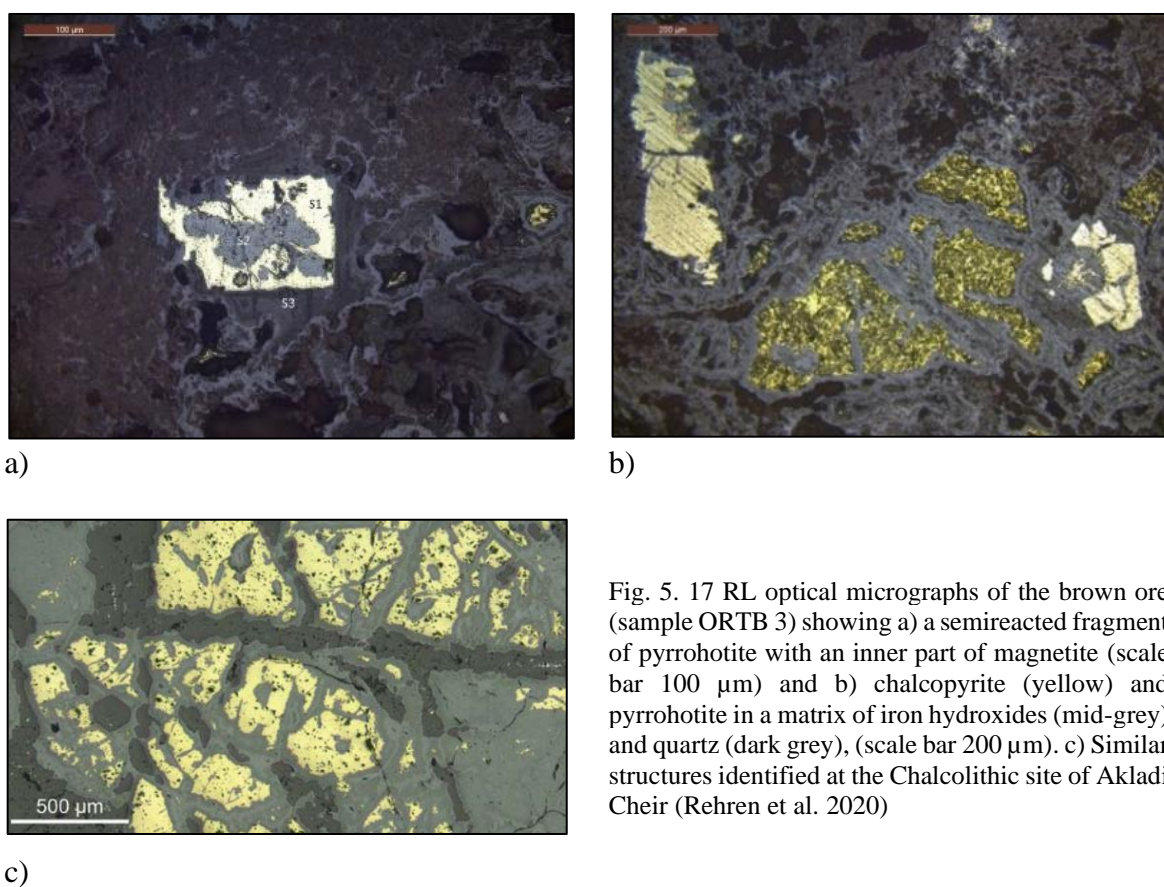


Fig. 5. 17 RL optical micrographs of the brown ore (sample ORTB 3) showing a) a semireacted fragment of pyrrhotite with an inner part of magnetite (scale bar 100 µm) and b) chalcopyrite (yellow) and pyrrhotite in a matrix of iron hydroxides (mid-grey) and quartz (dark grey), (scale bar 200 µm). c) Similar structures identified at the Chalcolithic site of Akladi Chir (Rehren et al. 2020)

To simplify the interpretation of the compositional variability in Cu-Fe sulphides between and within samples, the mean chemical compositions of both coarse and flat specimens were plotted in the Cu-Fe-S ternary diagram (Fig. 5. 18). The analyses of ore sulphides (in blue) were also included on the same plot. The ternary diagram Cu-Fe-S (wt%), categorises all mean chemical compositions based on their typology, leading to the following observations:

- Overall, the readings reveal a wide spectrum of phases with varying Cu/S ratios, primarily clustering along the sulphide axis, including chalcocite (Cu_2S) – bornite (Cu_5FeS_4) – chalcopyrite (CuFeS_2) – pyrrhotite (FeS).
- A lower quantity of copper-bearing features was detected in the coarse slag (53 features) compared to the flat slags (105 features).
- Nearly all the readings collected from the flat slags concentrate along the Cu-S side, with an average content of 46.36_{wt%} Cu and 39.22_{wt%} S.
- The coarse slags exhibit a notable discrepancy in Cu-Fe-S compositions, while the flat slags demonstrate greater compositiona consistency and uniformity.
- These readings align with Cu-Fe-S inclusions previously reported by Hauptmann in ancient copper smelting slags from various regions, including Oman, Anatolia, Iran, Italy and Grisons (Switzerland) (Fig. 5. 19).

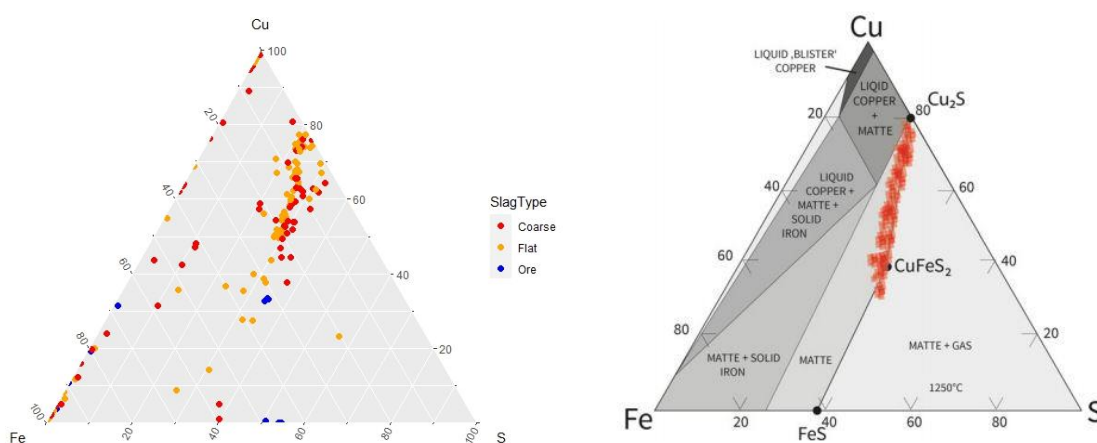
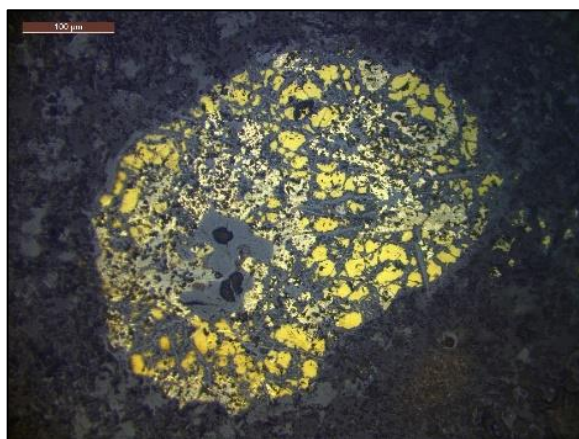


Fig. 5. 18 (Left) Ternary plot diagram (Cu-Fe-S (wt%) slag system) of the SEM-EDX analyses (orange= flat slags, red= coarse slags).

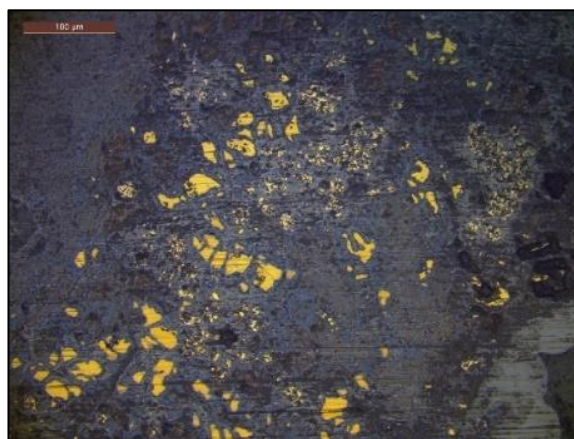
Fig. 5. 19 (Right) Ternary plot diagram (Cu-Fe-S (wt%) slag system) showing the vast range of chemical combinations along the sulphide axis chalcocite-bornite-chalcopyrite-pyrrhotite and the Cu-Fe axis of copper

slags from data from Oman, Anatolia, Iran, Italy (Trentino), Grisons (Switzerland). (From Hauptmann, 2020, p. 277, fig. 5.55).

In the coarse slags, the observed copper-bearing compounds consist of partially reacted chalcopyrite grains with diameters ranging from 50 to 250 μm . Additionally, there are grains of semi-reacted Cu-Fe sulphides displaying a wide variety of shapes and chemical compositions. Spheroidal segregations were also identified (Fig. 5. 20d). Interestingly, pure copper prills were unexpectedly found only in the sample ORTB 5. Notably, these prills exhibit the most advanced stage, boasting a mean copper content of 96.5 wt%. They fall within a diameter range of 50-100 μm , with some of them surrounded by a ring-shaped layer resembling covellite-like composition (Fig. 5. 20f). These findings have been interpreted as representing an intermediate transition state from the original sulphide charge to matte and metallic copper (Fig. 5. 20). Except for sample ORTB 5, the coarse slags (ORTB 6, ORTB 9 and ORTB 20) showed the presence of green features, which have been interpreted as weathering products. Newly formed phases of copper hydroxides (e.g., $\text{Cu}(\text{OH})_2$ and $\text{CuCl}_2 \cdot 2\text{H}_2\text{O}$) have either replaced the rounded copper metal prills or filled the cracks in the matrix (Fig. 5. 21). Similar features were detected in two free slag pieces from Belovode (Radivojević & Rehren, 2021, p. 141, fig. 15a). It is worth noting that in sample ORTB 20, Cu-Fe sulphides are present only in a small area, while in all the other samples they are dispersed across the entire sample surface.



a)



b)

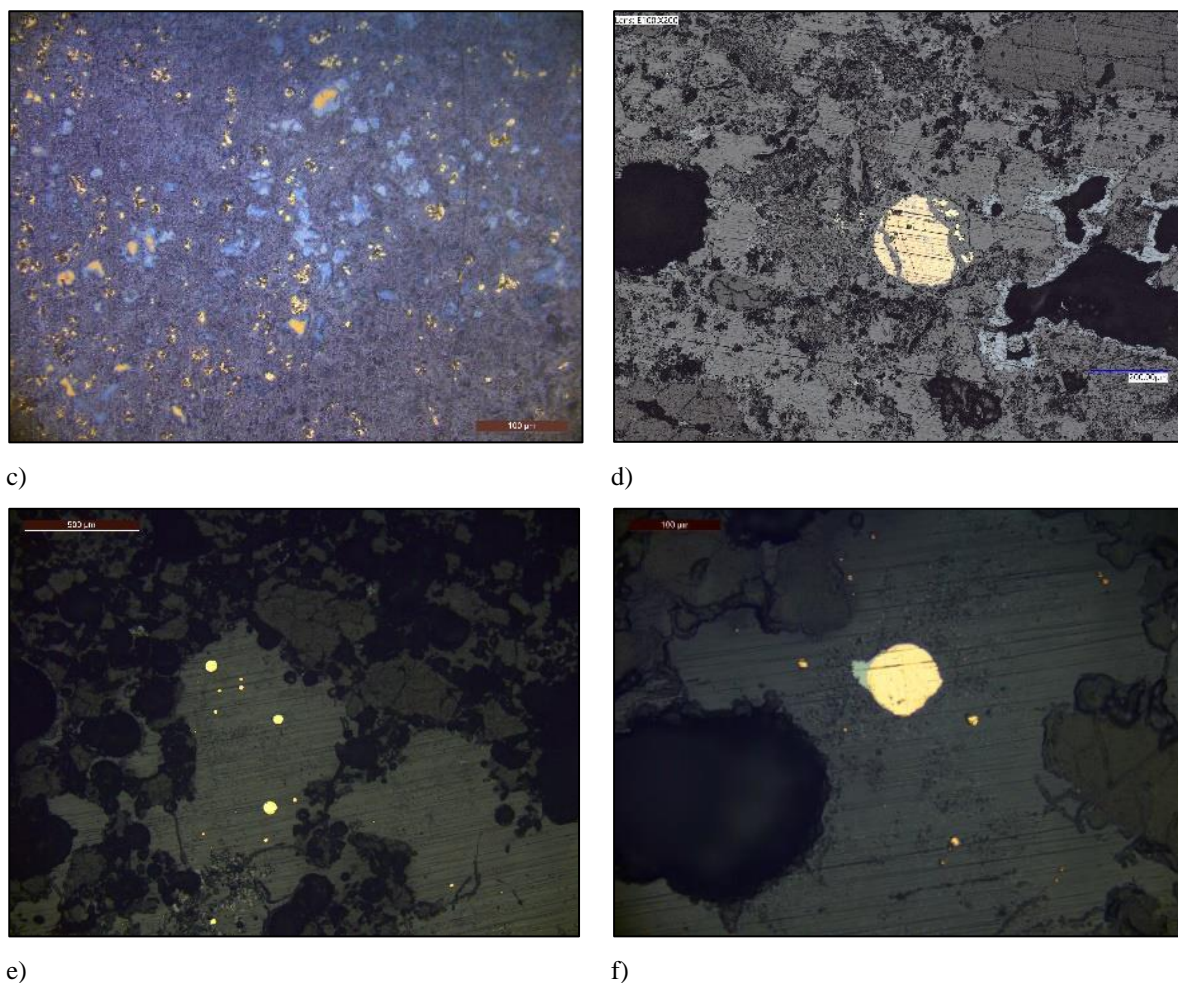


Fig. 5. 20 displays a selection of RL optical micrographs showcasing Cu-Fe sulphides and prills observed in the coarse slags. Starting from the top left: sample a) ORTB 6 (scale bar 100 μ m); b) ORTB 9 (scale bar 100 μ m); c) ORTB 20 (scale bar 100 μ m); d) ORTB 9 (scale bar 200 μ m); e) ORTB 5, prills in a fayalitic matrix surrounded by unreacted quartz inclusions (scale bar 500 μ m); f) ORTB 5, prill with a chalcocite extrusion (scale bar 100 μ m).

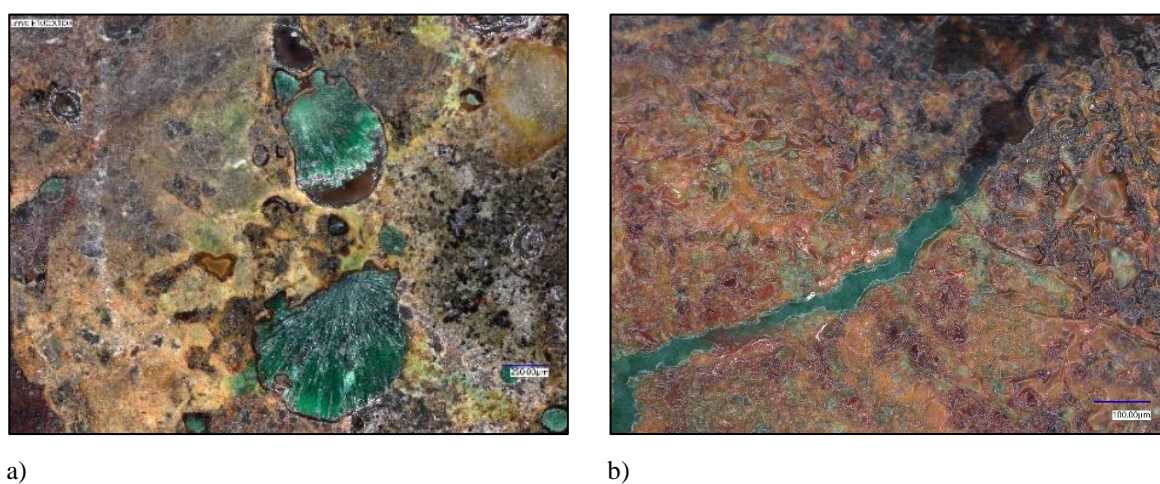
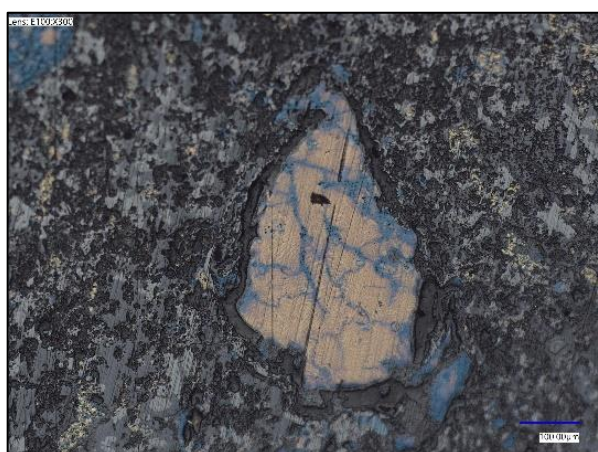


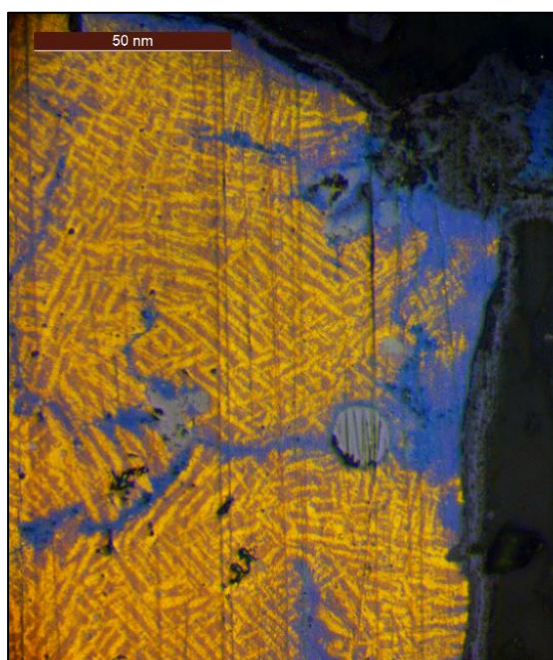
Fig. 5. 21 Optical micrographs of newly developed phases of copper hydroxides (e.g., $\text{Cu}(\text{OH})_2$, and $\text{CuCl}_2 \cdot 2\text{H}_2\text{O}$) filling the empty spaces left in the slag; a) ORTB 6 (scale bar 250 μ m), ORTB 20 (scale bar 100 μ m).

The flat samples exhibited a similar range of Cu-Fe sulphides at varying stages of Cu enrichment and desulphurisation. Within these samples, dominant areas resembling chalcopyrite-like compositions were prevalent, characterised by intermediate bornite-chalcopyrite and chalcopyrite-pyrrhotite compositions (Fig. 5. 22a-b). As per Barton and Skinner (1967) solid miscibility between bornite-chalcopyrite and chalcopyrite-pyrrhotite can occur in sulphides, even at relatively low temperatures, leading to complex intergrowths (see also Addis, 2013). The sulphides in the flat samples exhibited spheroidal shapes ranging from microns to millimetres in diameter (Fig. 5. 23a-d, f). Additionally, intermediate sickle- or ring-shaped formations were observed surrounding pure copper or copper oxide prills, which were dispersed and embedded within the fayalitic and clinopyroxenic matrix (Fig. 5. 23d, f) or present within aggregates of magnetite (Fig. 5. 23e). Moreover, small droplets of recrystallized compounds with compositions akin to digenite (Cu_9S_5) (Fig. 5. 23f), covellite (CuS) (Fig. 5. 23b), chalcocite (Cu_2S) (Fig. 5. 23a, c) were also identified.



a)

Fig. 5. 22 displays a) a chalcopyrite dominant area (scale bar 100µm) characterised by b) the exsolution of bornite (pinkish brown) and partially oxidised bornite (sky blue), along with a covellite prill (light blue) observed in sample ORTB 19 (scale bar 50µm).



b)

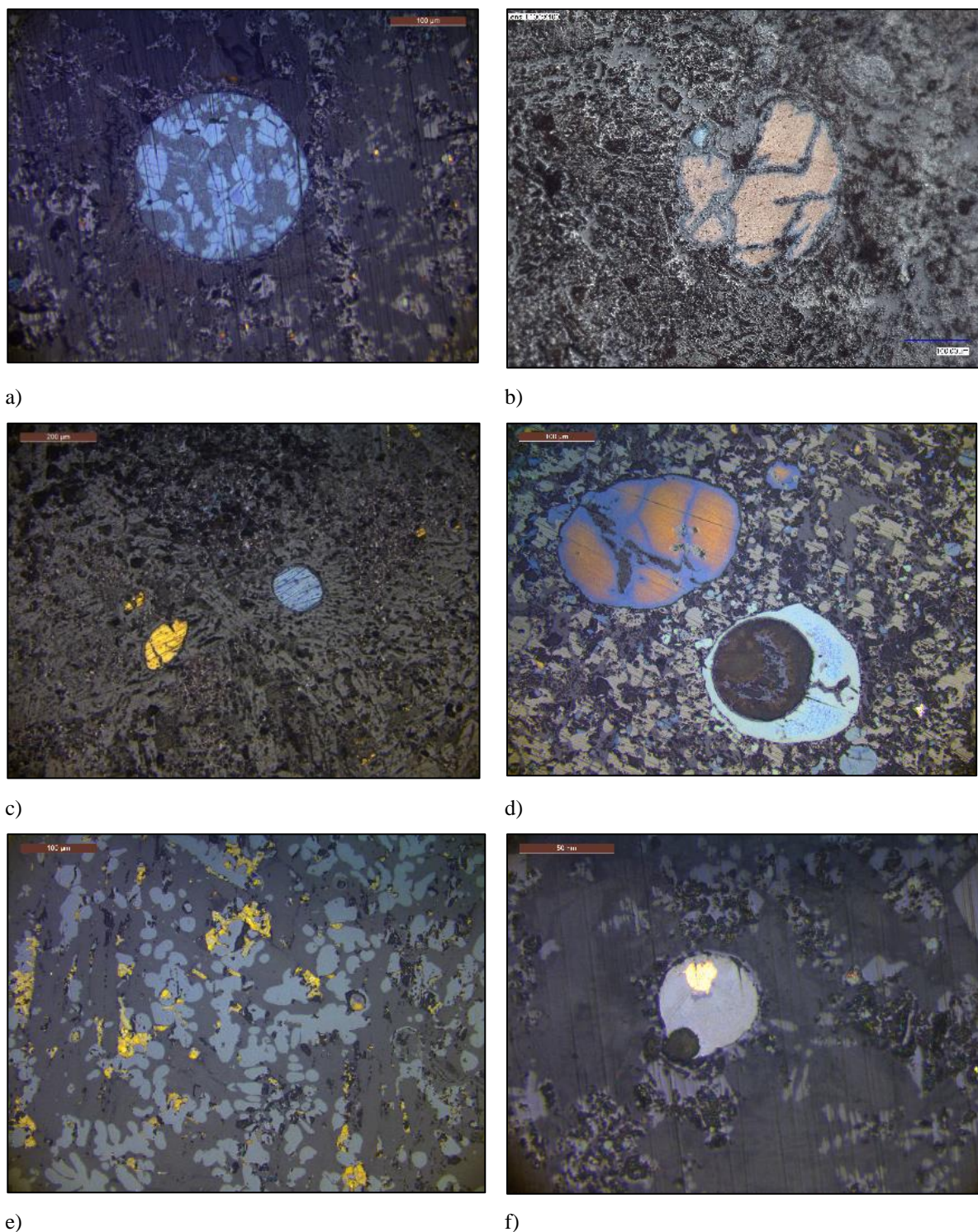


Fig. 5. 23 displays a selection of optical micrographs showcasing Cu-Fe sulphides and prills observed in the flat slags. Starting from the top left: a) round-shaped recrystallized compound characterised by covellite-like (blue) and chalcocite-like (greyish) compositions (ORTB 8 - scale bar 100µm); b) round-shaped Cu-Fe sulphide embedded in a fayalitic matrix (ORTB 16 - scale bar 100µm); c) round-shaped Cu-Fe sulphides high in copper (yellow) and high in sulphur (blue) (ORTB 13 - scale bar 200µm); d) ring-shaped formation of covellite-like composition (light blue) (ORTB 19 - scale bar 100µm); e) Cu-Fe sulphide within aggregates of magnetite (ORTB 19 - scale bar 100µm); f) round-shaped prill with a pure copper core (orange) surrounded by recrystallised digenite (bluish-grey) (ORTB 8 - scale bar 50µm).

5.3. Characterisation of a crucible fragment from Orti Bottagone.

In this section, I provide an overview of the analyses carried out on the crucible fragment in the Orti Bottagone assemblage, first focusing on the ceramic fabric and then on the bulk chemical changes.

The study of crucibles places itself between ceramic and slag analysis (F. Rademakers, 2015). In the last three decades, several analytical studies have been carried out on this type of archaeological material (Artioli, 2010, p. 338; Martínón-Torres & Rehren, 2014). Their aim was to identify the chemical and mineralogical composition (phases) to acquire information on the following:

- temperature gradients and redox conditions,
- location and extent of the heating source,
- nature of the charge,
- and type of processes carried out, including smelting, melting, refining, and alloying.

In this study, among the samples selected, two possible crucible fragments were identified by inspecting the assemblage (Table 5. 6). The samples (ORTB 10 and ORTB 11), whose densities were lower than those of the rest of the assemblage (1.62 and 1.04 g cm⁻³ respectively) and of the average of chalcolithic slags (Artioli, 2010, p. 338), were at first visually inspected and described. To the naked eye, fragment ORTB 10 had the shape, the coppery colour and the slight thermal alteration of the surface that are reminiscent of the upper part of the rim of a crucible (Fig. 5. 24). Unfortunately, the small dimension of the fragment did not provide information to reconstruct the real dimension and shape of the crucible.

Table 5. 6 presents the key information of two potential crucible fragments identified through the non-invasive investigation of the assemblage.

Find n.	Findspot	Weight (g)	Volume (cm ³)	Density (g/cm ³)	Magnetism
ORT B. 10	Sporadici Lato N	9.7	6	1.62	/
ORT B. 11	Sporadici Lato N	10.4	10	1.04	/

Before engaging in destructive and time-consuming sample preparation, I performed qualitative analyses using a pXRF on the samples' surface. Although this technique only provides surface analysis and does not produce reliable quantitative data, the main goal was to assess if they had

contained metal, or if the altered surface was just a thermal alteration produced by prolonged exposure to high temperatures (Fig. 5. 24).

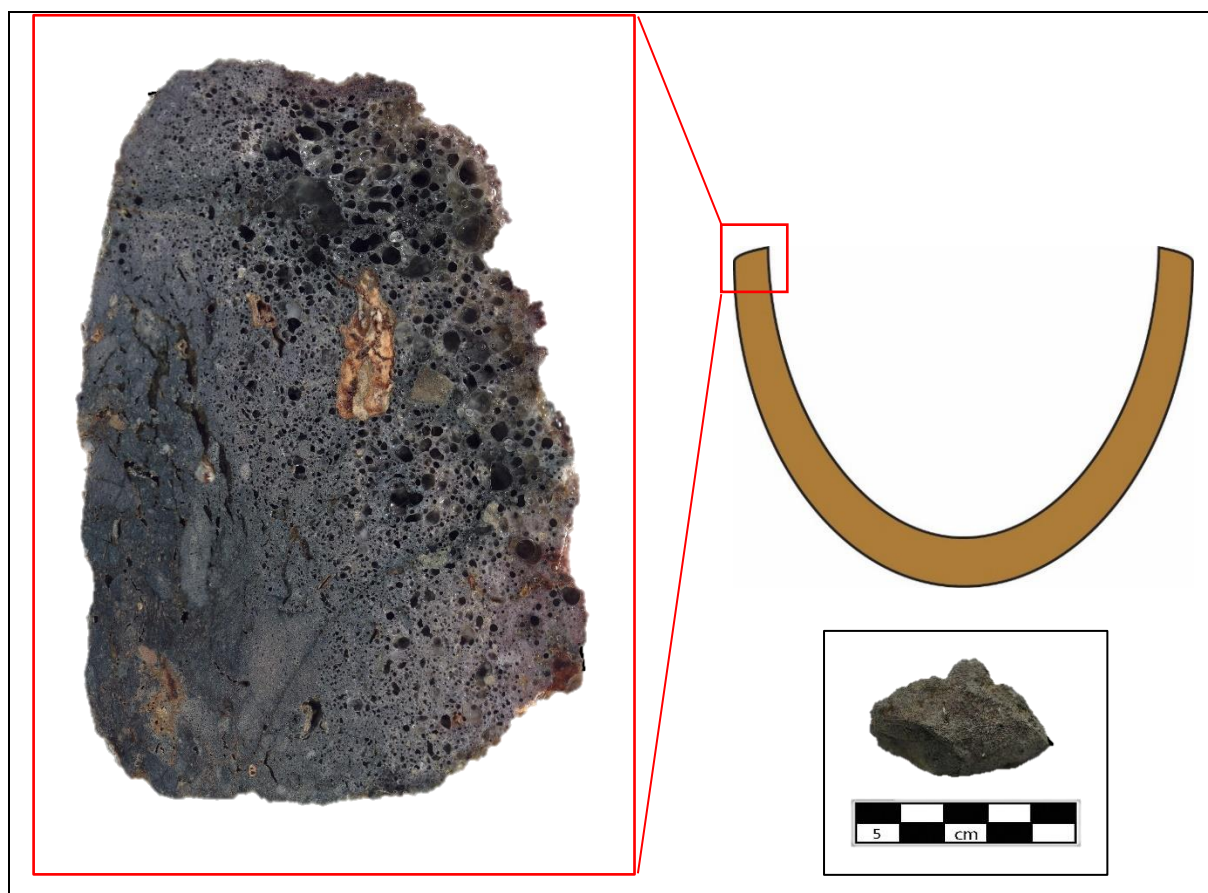


Fig. 5. 24 Cross-section of the crucible fragment ORTB 10 (digital micrograph) showing the bloated region (see Rademaker, 2015) and the possible location of the fragment.

Traces of copper and arsenic were detected only in fragment ORTB 10. Thus, I built a polished mounted thick sample for further analyses. This method was preferred to the preparation of polished thin section as the latter is more time-consuming and does not dramatically increase the information that can be obtained (F. Rademakers, 2015; Thornton & Rehren, 2009). I adopted Scanning Electron Microscopy with Energy Dispersive Spectrometry for chemical and elemental mapping (see Artioli, 2010; Martín-Torres and Rehren, 2014).

5.3.1. The ceramic fabric

In the outer area of the crucible fragment, elongated fractures were observed which might equally have been produced either by the burnt-out organic temper, or by the expansion and shrinkage of the clay minerals ((Rademakers *et al.*, 2018), (Fig. 5. 25a-b). The ceramic part is made of fine clay with coarse angular quartz fragments and Ca-rich rock inclusions of variable

dimensions. SEM-EDX analyses allowed the identification of quartz and plagioclase (approximate anorthite composition). However, it is impossible to say whether these inclusions were deliberately added to the clay as temper, or if they were naturally present in the clay as residual fragments, (Fig. 5. 26a-b).

The crucible was likely heated from above, perhaps under a charcoal cover, as can be deduced from the thermal alteration in the inner wall profile. The internal heating has caused the ceramic to gradually transform and become more porous and partly vitrify towards the inner side of the fragment.

Among the three parts usually detected in a crucible wall, an external fired ceramic zone, a central bloated zone and an internal slag zone (Rademakers *et al.*, 2018), only the first and the second are present. Unfortunately, no slagged surface lining or green corrosion products were detected. The absence of metallic phases or copper-bearing by-products made it impossible to identify the nature of the charge smelted and to clearly assess the redox condition in the crucible. The lack of this evidence might be explained by the fact that usually the charge and then the molten metal accumulate, lay, and chemically interact with the bottom of the crucible. It is likely that the top rim is thermally altered because it was close to the point where the air was pumped into the reactor.

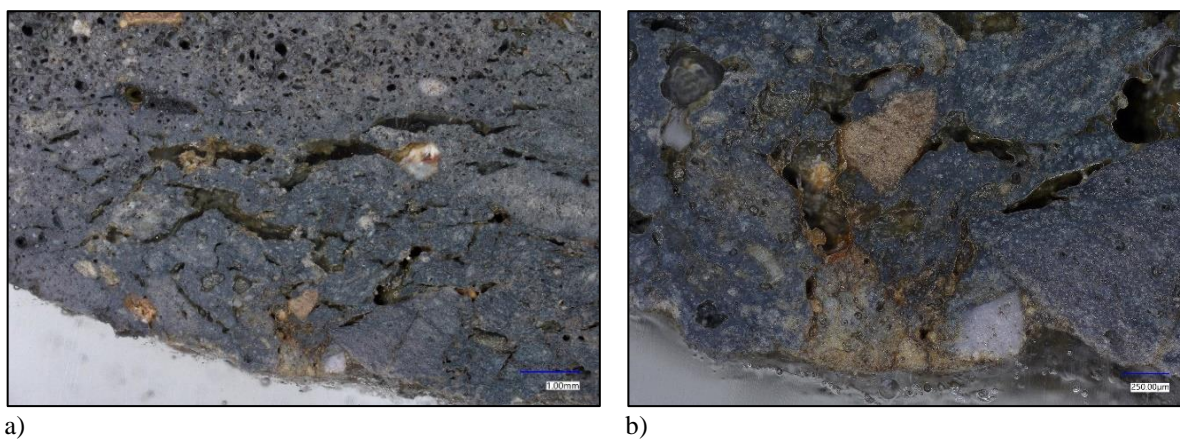


Fig. 5. 25 Micrographs showing the elongated porosity/fractures in the ceramic zones on the outer side of the fragment (scale bar respectively 100µm and 250µm).

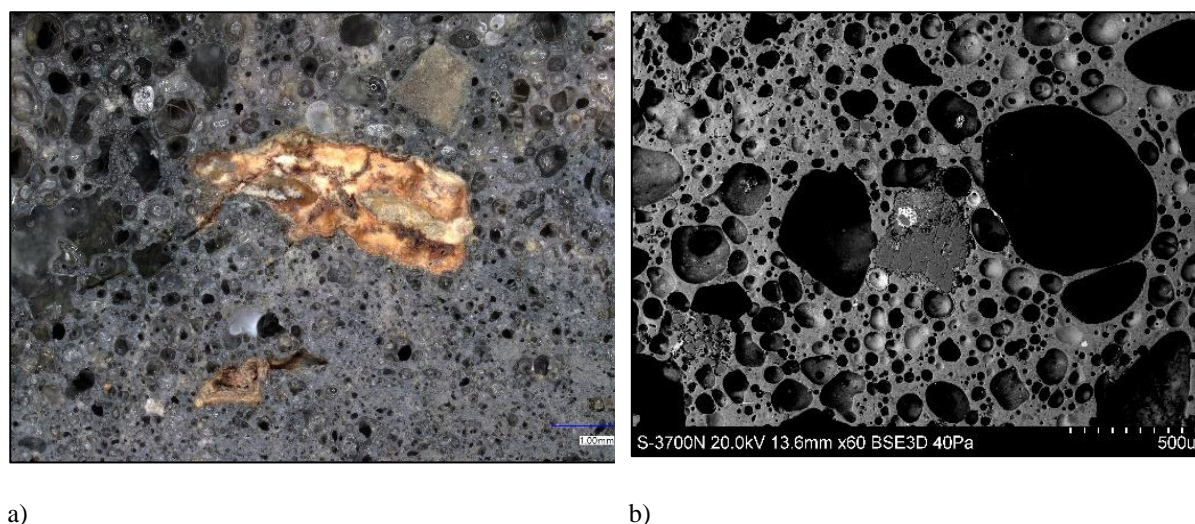


Fig. 5. 26 displays a) a RL optical micrograph (scale bar 100µm) and b) a BSE image showing different areas with several coarse rock inclusions in the crucible fragment ORTB 10.

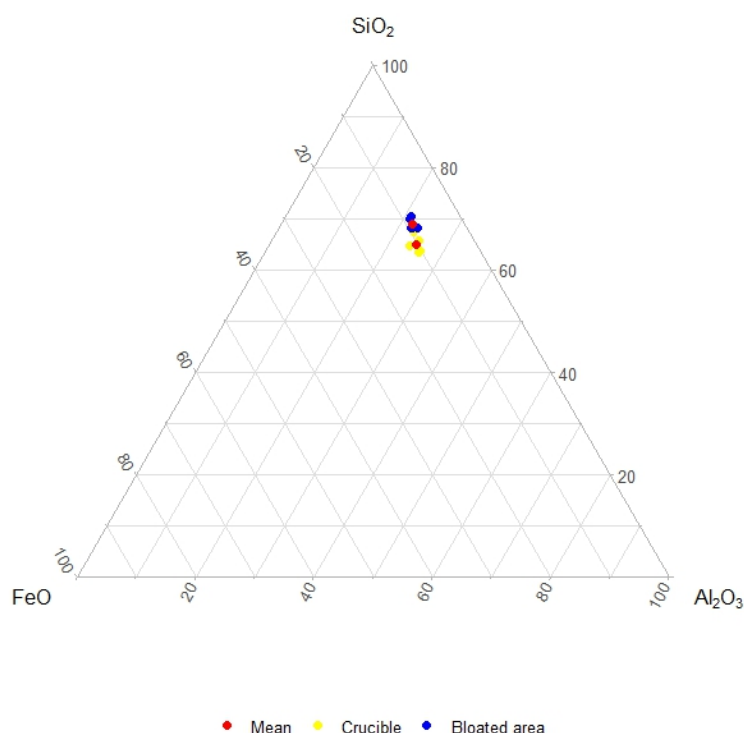
5.3.2. Bulk chemical changes

Following the methodology developed by Rademaker (2015; see also Freestone and Tite, 1986), the outer ceramic and the inner bloated zones were compared. The analyses were carried out at the British Museum laboratory, using a Hitachi S-3700 Scanning Electron Microscope equipped with an Oxford Inst. EDX. The analyses were acquired with the Aztec 5.1 software. An accelerating voltage of 20 kV was used, with a working distance of 10 mm and a live time of 90 seconds. To optimise quantitative analyses a cobalt standard was used. The methodology consists in the analysis of 5 different areas for each part. The area analysed is the visible area at 100x magnification ($\pm 1\text{mm}^2$). The “Analyzer” tool in the software allows to calculate the average composition of the viewed area. Given the absence of slagged zones or metallic phases in the sample, the usual comparison between the ceramic and the slag could not be undertaken, therefore the ceramic zones were compared to the bloated ones. Since only one sample is considered, the coarse angular inclusions were avoided as their inclusion would have biased the comparison of the matrices. The entire surface of the fragment was also observed at high magnification using the SEM-EDX to allow a better understanding of the inclusions and chemical structures and phases.

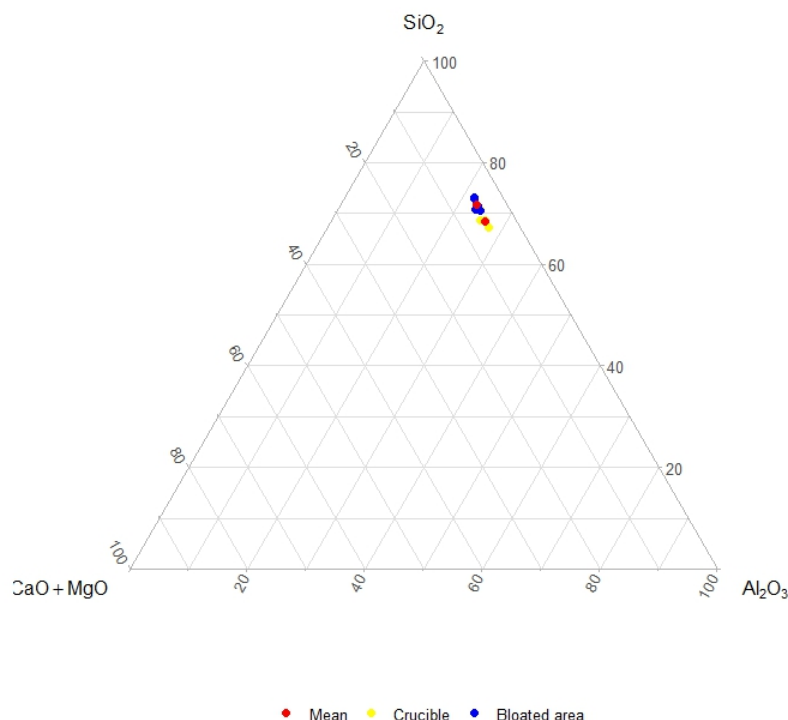
As sometimes the software recognises elements not actually present in the area analysed, while other times it fails to identify existing elements, I carefully inspected each spectrum and, where necessary, I manually added or removed the elements. The elemental measurements were processed by stoichiometry and reported as oxides. This means that instead of measuring the actual amount of oxygen present in the analysis, the software bonds the oxygen to the other elements according to a fixed oxidation state (ex. Si as SiO_2 , or Fe as FeO and not Fe_2O_3). The

following elements were considered: Na_2O , MgO , Al_2O_3 , SiO_2 , P_2O_5 , K_2O , SO_3 , CaO , TiO_2 , MnO , FeO , and CuO (Table 5. 7), although it is acknowledged that some of these oxides are not stable in solids at room temperature (refer to Section 4.2.9).

The main elements detected are respectively SiO_2 , Al_2O_3 , FeO and MgO . The average of the bulk composition counts for a total of ca. 94% for the ceramic and ca. 92% for the bloated parts. These elements were plotted in ternary diagrams (Fig. 5. 27 Composition of the ceramic and bloated areas in the a) SiO_2 - Al_2O_3 - FeO and b) SiO_2 - Al_2O_3 - CaO + MgO ternary diagrams.a-b). In each plot, the 3 elements considered were normalised to 100%, ignoring the other elements detected in the analysis. In the second plot, CaO was added to the MgO as chemically similar. In both the SiO_2 - Al_2O_3 - FeO and SiO_2 - Al_2O_3 - CaO + MgO ternary diagrams, the measurements cluster together showing uniformity both in the ceramic and in the bloated compositions. All the measurements cluster on the SiO_2 - Al_2O_3 axis showing only a slight variability between their contents. The main difference is the appearance of copper contents in the bloated areas. The arsenic detected with the pXRF was not found using the SEM (see Section 4.2.6 on detection limits of the SEM).



a)



b)

Fig. 5. 27 Composition of the ceramic and bloated areas in the a) SiO_2 - Al_2O_3 -FeO and b) SiO_2 - Al_2O_3 -CaO+MgO ternary diagrams.

The relative changes in ratio of oxides to Al_2O_3 (in wt%) in the bloated areas with respect to the ceramic are measured following the formula outlined by Rademaker (2015, p. 75) and Freestone and Tite (1986):

$$\frac{\Delta \text{MeO}}{\text{Al}_2\text{O}_3} = \frac{\frac{\text{MeO}_{\text{bloated}}}{\text{Al}_2\text{O}_3_{\text{bloated}}} - \frac{\text{MeO}_{\text{ceramic}}}{\text{Al}_2\text{O}_3_{\text{ceramic}}}}{\frac{\text{MeO}_{\text{ceramic}}}{\text{Al}_2\text{O}_3_{\text{ceramic}}}}$$

Alumina is not usually part of the smelting charge in the crucible, therefore normalising each metal oxide to Al_2O_3 allows avoiding distortion from the presence of metals and inclusions when considered. The comparison of the ceramic and bloated areas shows significant increases of sodium (160% $\Delta \text{Na}_2\text{O}/\text{Al}_2\text{O}_3$) and potash (52% $\Delta \text{K}_2\text{O}/\text{Al}_2\text{O}_3$) and a slight increase in lime (27% $\Delta \text{CaO}/\text{Al}_2\text{O}_3$), (Table 5. 7). As already largely stated by a number of authors (Evans and Tylecote, 1967; Tylecote, 1982; Misra *et al.*, 1993; Rovira, 2007; Wood, 2009), these changes in ratios are due to the chemical interaction of the ceramic body with the fuel/ash added to the

charge. Although these differences cannot provide information about the type of fuel adopted (Rademakers *et al.*, 2018, p. 1657), they strengthen the interpretation proposed above of a crucible heated from above under a charcoal cover.

Table 5. 7 Bulk chemical compositions and their averages of ceramic and bloated areas. Results are reported as oxides.

Area analysed		Na ₂ O	MgO	Al ₂ O ₃	SiO ₂	P ₂ O ₅	SO ₃	K ₂ O	CaO	TiO ₂	MnO	FeO	CuO	Total
Crucible	1	0.7	3.3	20.8	60.6	0.2	0.1	3.6	1.0	0.9	0.3	8.4		99.9
	2	0.6	3.4	22.5	59.1	0.3	0.1	3.2	1.1	0.8	0.3	8.5		99.8
	3	0.6	3.7	23.5	57.5	0.2	0.1	3.0	0.8	1.0	0.1	9.5		99.9
	4	0.5	3.3	23.4	57.1	0.3	0.2	2.7	1.2	1.0	1.0	9.2		99.9
	5	0.3	4.2	21.5	58.5	0.2	0.3	2.2	1.0	1.1	0.2	10.4		99.7
Max		0.7	4.2	23.5	60.6	0.3	0.3	3.6	1.2	1.1	1.0	10.4		
Min		0.3	3.3	20.8	57.1	0.2	0.1	2.2	0.8	0.8	0.1	8.4		
Mean		0.5	3.6	22.3	58.6	0.2	0.2	2.9	1.0	1.0	0.4	9.2		99.83
σ		0.2	0.4	1.2	1.4	0.1	0.1	0.6	0.2	0.1	0.4	0.8		
Bloated areas	1	1.2	3.3	20.7	60.1	0.2	0.1	4.3	1.1	0.9	0.4	7.5	0.1	99.9
	2	1.2	3.1	18.9	62.8	0.0	0.1	3.6	1.1	0.9	0.3	7.4	0.3	99.7
	3	1.3	3.4	19.8	60.1	0.2	0.2	3.7	1.5	0.8	0.3	8.1	0.4	99.8
	4	1.0	3.3	19.8	60.5	0.1	0.2	4.0	1.0	0.9	0.3	8.5	0.5	99.9
	5	1.2	3.3	18.9	62.2	0.2	0.2	3.9	0.9	0.9	0.1	7.9	0.5	99.9
Max		1.3	3.4	20.7	62.8	0.2	0.2	4.3	1.5	0.9	0.4	8.5	0.5	
Min		1.0	3.1	18.9	60.1	0.0	0.1	3.6	0.9	0.8	0.1	7.4	0.1	
Mean		1.1	3.3	19.6	61.1	0.2	0.2	3.9	1.1	0.9	0.3	7.9	0.4	99.9
σ		0.1	0.1	0.8	1.3	0.1	0.1	0.3	0.3	0.0	0.1	0.5	0.1	

In this chapter, I have presented a comprehensive overview of the analytical findings obtained from the by-products of Orti Bottagone. With this chapter, the first part of the thesis draws to a close. These findings will be discussed in Chapter 9 in conjunction with the experimental analytical results from the second part of the thesis.

The following chapter will introduce the experimental work undertaken as the second objective of the thesis. The primary aim is to familiarize the reader with the concepts of experimental archaeometallurgy, distinguishing between pilot experiments and scientific experiments while elucidating their distinct yet complementary roles in the field. I will provide a detailed outline

of the pilot experiments and how they contributed to the organization of the scientific experiments in this thesis.

PART II

Experimental Insights and Smelting Process Reconstruction

Chapter 6. Experimental archaeometallurgy I: Experiencing roasting and smelting.

6.1. Introduction

This chapter introduces the second part of the thesis dedicated to the experimental work. It is divided into two distinct sections. The first section provides a general overview of what experimental archaeometallurgy is, encompassing a differentiation between pilot experiments and scientific experiments, elucidating their distinctive but complementary roles in the field. The second section of the chapter delves into the roasting and smelting pilot experiments I conducted. These experiments are meticulously outlined to allow their reproducibility. An introduction to the concepts of roasting and smelting is provided at the outset of the respective sections. Following this detailed outline, the results of the experiments are presented, and subsequently, the key findings are critically appraised.

6.2. Experimental archaeometallurgy: theoretical framework

Experimental archaeometallurgy is a sub-field of experimental archaeology. It is concerned with the reproduction of the *chaîne opératoire* of metal making through experiments replicating ancient mining, ore processing, roasting and smelting, as well as object casting, alloying and patinating.

Experimental archaeology is a widely accepted and integrated method in archaeological science (Schöbel, 2019) that uses experimental simulation and reproduction of archaeological processes in order to test hypotheses that have been developed from the clues that are left in the archaeological record (artefacts, by-products, hearths, furnaces/reactors). It employs a number of different methods, techniques, analyses, and approaches cutting across, often in original ways, the natural and social sciences and humanities (Mathieu, 2002).

The fundamental aspect of experimental archaeology is the need to collect systematic and detailed data aimed at answering specific archaeological questions (Busuttill, 2013). It is crucial that the experiment is well planned, reproducible and well documented but also as realistic as possible to the conditions that would have existed in the archaeological record (Lammers-

Keijzers, 2005; Outram, 2008). This aspect differentiates experimental archaeology by reenactment, living history, and recreational activities, whose aims are instead more oriented towards emotional and educational experience, as well as entertainment (Outram, 2008; Reynolds, 1999; Schindler, 2018).

Following these premises, experimental archaeology can be an invaluable research method to investigate archaeometallurgical questions. Most of the time, metallurgical installations are poorly preserved in the archaeological record. Interpreting and reconstructing the entire *chaîne opératoire* from the few pieces available may therefore be an extremely challenging endeavour. The sparse evidence does not always allow researchers to completely rebuild the ancient installations. This might be due to their antiquity, which did not allow for an integral preservation (the upper part, e.g., the chimney, is nearly always missing), but also to their intrinsic nature of “disposable” devices. Because of their mainly practical aim, they might have been partly or completely dismantled or abandoned after use. The high temperatures reached might have deformed the walls of the reactor making it further inoperable (Bourgarit, 2007).

The aim of metallurgical experiments is to gain a better understanding of ancient technologies and of the craftspeople behind the objects (Heeb & Ottaway, 2014). Furthermore, experimental archaeology is a predictive tool that might help to reduce ambiguities in our analogies, enhance hypotheses and understand what to look for in the field (Timberlake, 2007, p. 28). With regard to archaeometallurgy, in the analysis of primary production processes, the focus of the experiments are mainly not products or something tangible, but are instead invisible data gathered from a combination of verbal-theoretical data and hands-on experiences (Paardekooper, 2015). Specifically referring to smelting processes, the ability of the experimenter/archaeologist/archaeometallurgist is to infer the invisible (non-quantifiable) data (blue circle quarters) from those which can be scientifically collected, as clearly sum up by Heeb and Ottaway (2014a), (Fig. 6. 1).

Scientific experiments are part of a ‘hypothetic-deductive’ process through which formulated hypotheses are either verified and regarded as valid or falsified and discarded in favour of a new hypothesis to be tested (Outram, 2008). However, if it is possible to prove an impossibility, in case it is verified, the experiment only shows one of the possibilities that ancient craftspeople might have performed (Popper, 1959:57-73). Archaeological experiments were already undertaken in the second half of the XIX century (Andraschko & Schmidt, 1991; Schöbel, 2019). However, the lack of a scientific approach and of analytical protocols to collect data, in

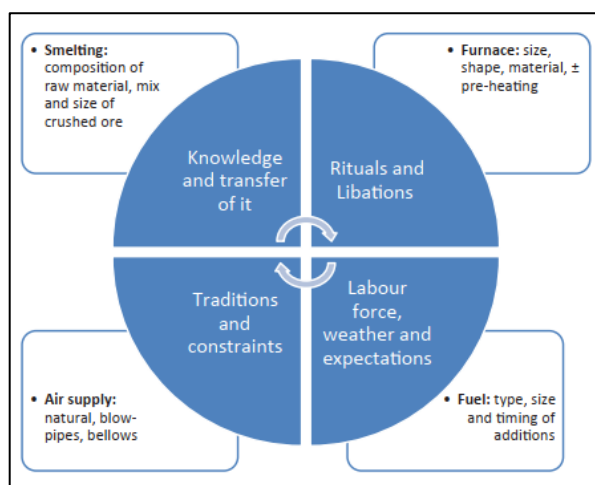


Fig. 6. 1 Chart summarizing the quantifiable (scientific) and non-quantifiable (experiential) data that can be obtained from a copper smelting experiment. From Heeb and Ottaway 2014, p.187, fig.8.34

hindsight, make them more like experiential activities than proper scientific experiments (Ascher, 1961; Schöbel, 2019). For example, in 1894 Cushing carried out trial roasting and smelting tests but instead of focusing on a careful collection of experiment data, which would have allowed him (or other researchers) to repeat the experiment(s), he focused more on the archaeological context and ethnographic similarities (Cushing, 1894). The same problems with data collection are seen in co-smelting trials carried out by Gowland in 1912 (Gowland, 1912a, 1912b). The first to focus on the technological aspects of smelting was Coghlan, who, after a number of smelting experiments with malachite suggested that the first metallurgists used a ceramic kiln as an open fire would not have led to the smelt of copper (Coghlan, 1939). The origin of experimental archaeology as a proper scientific discipline can be traced back to the work of John Coles in the 1970s (Coles, 1973, 1979). He was the first to stress that strict guidelines need to be followed and data must be thoroughly collected if archaeologists are to increase their understanding of the technologies under study.

Key aspect of a successful experiment is the preparation before it. Before starting the real experiment, it is crucial to carry out a series of experiential tests. They are also known as “pre- or pilot experiments” (Cunningham *et al.*, 2008, p. v), “hypothesis-forming” experiments (Richter, 1992), or “soft” experiments (Kucera, 2004). Already at the beginning of the 1960s, Ascher made the theoretical distinction between scientific and imitative experiments (Ascher, 1961).

Since there is always an element of experience in an experiment (Cunningham *et al.*, 2008), I believe that experiential tests form an integral part of the experimental process. Scholars usually do not report their pilot experiments in the publications, neither because they did not run pilot

experiments before the “real” ones, nor because they did not consider them significant enough to the end of the experiment. However, as already stated by Cunningham et al. (2008), even if they cannot be considered scientifically driven experiments, they are equally important to the end of developing a proper scientific experiment.

Many different activities fall under the definition of experiential tests, from re-enactment, to living history, to educational demonstrations, and leisurely experiences. Some authors consider impossible to bridge the gap between the experiential and the experimental world (Cunningham et al., 2008; Dungworth, 2013; Outram, 2008; Reynolds, 1999), as they consider the first hierarchically inferior to the second. The main concern is that all the experiential activities have demonstrative, educative or just fun purposes, locating them in the trivial and unscientific world so deep far away from the realm of academic research (Millson, 2011; Reynolds, 1999).

However, I think that, if put in the right perspective and carried out with awareness, all the “experiences” perform the valuable and essential task of guiding the experimenter through the trial and error process and through the not linguistically encoded bodily actions (Doonan, 1994; cf. Keller & Keller, 1996). Indeed, the only way to learn a craft is through experiencing. Often a technique can be easy to learn, but much more complicated to master sufficiently, as it is for copper smelting. Among the main reasons at the base of an experiment failure (e.g. insufficient metal yielded) stays the fact that the experimenter(s) are not fully skilled craft metalworkers (Paardekooper, 2008; Shimada, 2005).

Therefore, the principal aims of these experiential tests are not to answer straightaway specific scientific research questions, but instead: 1) to acquire the practical skills (expertise) and gain a degree of personal competence of the techniques supposedly used in the past (experience). The process requires all our senses and needs agility. It leads to an understanding of space, form, technique and material (Kucera, 2004); 2) to lower the chances of unexpected incidents that might arise during the execution of the experiments; 3) to enter the mindset of the ancient smelters to grasp the practical solutions adopted (Timberlake, 2007, p. 28), and how they might have engaged with the environment (Cunningham *et al.*, 2008); 4) narrow the focus of the research and clarify the research questions (hypothesis forming) avoiding the lack of aims (Outram, 2008; Richter, 1992). In some cases an issue encountered during an “experience” can lead to completely new research avenues (Cunningham *et al.*, 2008); 5) determine the static (no changes made in the test) or dynamic (result oriented) structure of the test (Lammers-Keijsers, 2005, p. 22); 6) establish a functioning ad hoc experimental analytical protocol, (i.e., find the correct data collection method).

There is no rule of thumb indicating a minimum number of trials to undertake to develop the real research questions. It depends on the discipline you want to explore and from the individual experience of the techniques.

Once the confidence and the correct technological skills have been acquired, the “hard” experiments (Kucera, 2004) can be carried out. The steps to “transform” a pilot/experiential experiment into a meaningful (scientific) experiment can be summarized as follows (adapted from (Lammers-Keijzers, 2005, p. 22):

1. define archaeological problem.
2. design of an experimental setup (hypothesis testing).
3. Test the hypothesis through scientific and methodologically designed studies (variables like persons, tools, materials, techniques, and environment have to be carefully controlled).
4. Reproduction of it at least 3 times.
5. Compare the experimental data with the archaeological ones.

6.3. Pilot experiments

In this section, I will discuss the pilot ore roasting and copper smelting experiments I have conducted as part of my doctoral research. Part of the experiments were carried out during a copper smelting workshop (“The Jarrow Hall Teaching Experience”) held for students by Newcastle University in the late spring of 2021 and in two other occasions (summer 2021) with the help of the volunteers at Jarrow Hall open-air museum, South Tyneside. The workshop had the double role of bringing students toward the field of experimental archaeology and acquiring the theoretical and practical skills to run the scientific experiments needed for my research. The experiments consisted in the roasting and smelting of sulphide ores. I carried out the experiments using bornite, a common copper-iron sulphide ore bearing high percentages of copper (up to 63%). I did not use the original sulphide ore from the supposed location exploited in the past (see chapter 8) mainly because no chemical analyses of the slags were available at the time when the pilot experiments were undertaken and because of the ready availability and cheaper price bornite compared to other sulphide ores. However, it is worth noting that bornite (Cu_5FeS_4) and chalcopyrite (CuFeS_2) are similar in their chemical components and behaves similarly whilst roasting and smelting. Although I knew that, given the higher copper percentage present in the compound, it might be easier to obtain some copper, the aims of these

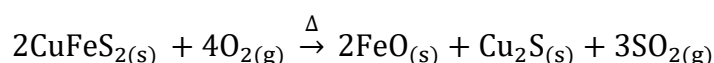
experiments are to focus on the formation of by-products and what remains in the field after the experiment.

The pilot experiments were conducted following an initial investigation involving optical microscopy (OM) and scanning electron microscopy with energy-dispersive X-ray (SEM-EDX) analysis of a random sample of slags from the site of Orti Bottagone. These preliminary investigations provided essential “pilot data” that guided the design of the subsequent experiments (see Chapter 8). Two distinct sets of considerations were taken into account. The first set revolved around theoretical and practical reflections that aided in defining the experiment’s objectives and framing specific research questions (refer to points from 1 to 4). The second set pertained to the logistical aspects, including the digital tools and devices required to optimise data collection methodology and minimise variables (refers to point 5).

6.3.1. Roasting

To effectively reduce sulphide minerals, an additional step known as roasting is assumed to have been performed. The primary objective of the roasting process was to oxidise the ore, removing water, sulphur, other gases and impurities, while increasing its porosity and brittleness (Davenport et al., 2002). Roasting involved heating the ore on an open fire, or roasting bed, at temperatures typically ranging from 600 °C to 900 °C (Rose *et al.*, 2020).

From a chemical perspective, the roasting of copper-iron sulphides follows the ideal simplified formula:



The example provided uses chalcopyrite, whose chemical formula is CuFeS_2 .

Roasting is primarily a surface reaction, where the outer layer of the ore oxidises, remaining porous and allowing the oxygen to penetrate the unreacted inner sulphide portion of the ore.

Upon oxygen reacting with sulphur, sulphur dioxide (SO_2) is released in a solid-state reaction in the form of gas and produces a mixture of iron oxide and copper sulphide compounds (Shamsuddin, 2020, p. 40). More complex chemical transformations might also take place, potentially producing sulphates (SO_4^{2-}) alongside ongoing oxidation. The roasted product from chalcopyrite could encompass several ternary phases and solid solutions of iron (ex. FeS) and copper (ex. Cu_2S) sulphides (Shamsuddin, 2020, p. 47).

Despite roasting being widely assumed as a critical practice for dealing with sulphide ores (Doonan, 1994; Rose et al., 2020), scant archaeological evidence has been discovered to date. Until recently, the almost complete absence of these features in the archaeological record led

many authors to doubts about their existence (R. Doonan et al., 1996; Metten, 2003). Evidence of potential roasting beds (fire-hardened clay areas) have been found at the Early Bronze Age sites of La Vela di Valbusa, Romagnano Tof de la Val, Acquaviva di Besenello and Montesei di Serso (Storti, 1991, p. 354). The two areas unearthed at the rock shelter of La Vela di Valbusa, in the Adige/Etsch valley just north of Trento are among the oldest evidence interpreted as roasting beds. They are made of baked clay with a roughly oval bowl shape. They are 4 m far from each other and one is at the centre of a spread of some hundreds of slag pieces and associated with three tuyères (Fasani, 1990, pp. 165–175; Perini, 1989b, Figure 11). Their interpretation remains controversial. However, recent interpretations suggest that these structures could have been used for roasting matte (Pearce et al., 2022).

Better-preserved examples include elongated burnt clay structures with an elongated shape of roughly 1x4 m found at Fennhals-Kurtatsch, located on a slope at 1160 m a.s.l. above the Etschtal valley, in South Tyrol (Anguilano et al., 2006), as well as those identified in the Mitterberg area (Hanning, 2012; Hanning & Pils, 2011; Goldenberg et al., 2011; (Stöllner et al., 2011). Some potential roasting beds have also been uncovered at other sites (Cierny et al., 2004; Goldenberg, 2004; Weisgerber, 2004). Nevertheless, most recorded evidence dates from the Middle and Late Bronze Age onwards, leaving their existence in earlier periods, i.e., when the smelting processes were still at early stages, a topic of debate. The lack of comprehensive documentation regarding this step can likely be attributed to a combination of factors. Firstly, there has been a lack of extensive excavations that would have increased the likelihood of discovering areas where roasting took place. Most of the areas investigated so far focused on a small fraction of the actual settlement size. Additionally, the roasting process might have occurred near the mining zones, which could be distant from the smelting sites. Lastly, the method used for roasting possibly involved simple, temporary structures such as de-turfed zones with compacted earth surfaces. These ephemeral structures may have left minimal traces on the ground, making them susceptible to being erased by natural processes over time.

Relatively little experimental work has been done to investigate the pre-treatment of copper sulphide ore. Many experiments have primarily focused on the later stages of copper production, often overlooking the supposed crucial steps of beneficiation (crushing and hand sorting) and roasting (Radivojević, 2013; Renzi et al., 2018; Verly, 2017). Nonetheless, a handful of authors have undertaken significant studies exploring the effects of pre-treatment on ores. Among the pioneers in investigating ore preparation techniques was Merkel, who discovered the substantial impact of pre-treatment – specifically beneficiation and roasting – on the concentrations and inclusions of trace elements, in both copper ores and the resulting

smelted metal (Merkel, 1985). This realisation bears particular significance for archaeologists who categorise artifacts based on trace elements, as the outcomes are heavily contingent on these pre-treatment methods. In 1994, Doonan (1994) conducted experimental studies on beneficiation and roasting techniques, drawing from evidence found at the Bronze Age site of Ramsau S1, in the eastern Austrian Alps (Doonan et al., 1996b; Klemm, 1992, 1993, 1994, 1995). The initial phase of Doonan's experiments delved into detailing the various physical techniques employed to achieve a high-grade charge. He placed a strong emphasis on the beneficiation of 150kg of sulphidic ore, encompassing chalcopyrite associated with digenite, malachite and azurite. This ore was sourced from an old mine within the Erzberg mining district in Eisenerz Austria. Subsequent stages of the experiments involved a series of roasting trials conducted in a rectangular pit measuring 2 meters in length, 0.9 meters in width and 0.2 meters in depth. The pit's bottom was compacted to minimise the ore waste and facilitate post-roasting ore collection. Notably, elements present in the archaeological evidence, such as flagstones and clay lining, were deemed unnecessary for the culmination of the roasting process. Soft pinewood served as the chosen fuel. The experiments were split into two campaigns: Campaign RI aimed to understand the behaviour of the burning fuel stack, while Campaign RII sought to examine the correlation between the results of Campaign R and the chemistry of the beneficiated mineral. A pivotal variable under scrutiny was the positioning of the mineral within the roasting fire. The outcomes of these experiments validated Merkel's findings (1985), reinforcing the notion that choices made during beneficiation and roasting significantly influence the chemical composition of the smelting charge. Moreover, Doonan concluded that producing copper from sulphides within a bonfire might have been more feasible than from oxides (Doonan, 1994, p. 95).

I conducted four roasting tests based on archaeological evidence from San Carlo - Cava Solvay (referred to as San Carlo hereafter), a late 4th millennium metallurgical site located in Tuscany (Fedeli & Galiberti, 2016). For a comprehensive introduction to the site, please refer to Section 3.8 of this thesis.

During the excavations carried out between 1991 and 1992, three sub-circular plano-convex platforms made of "concolato" (baked clay) were uncovered (Fedeli & Galiberti, 2016). However, the absence of further microstratigraphic and micro-chemical analysis has fueled ongoing debates regarding a definitive interpretation of these structures. Nonetheless, drawing upon coeval comparisons in central Italy (Le Coste, L'Aquila, Radi and Danese, 2003) and the Italian Alps (Tof de la Val-Romagnano, Trento, Perini, 1973) where similar features were identified, the excavators similarly proposed a potential association of these archaeological

features with metallurgical activities (Fedeli & Galiberti, 2016, p. 51). However, the exact nature of these metallurgical activities remains unspecified. Although one of the platforms, contains embedded a smelting slag, their plano-convex shape (see Fig. 6. 2) seems unsuitable for creating the reducing conditions required for ore smelting. The shallow and flat shape does not facilitate heat concentration, as observed in bowl-like reactors (Ambert et al., 2013). Conversely, using an open fire on the same platform would likely lead to highly oxidising conditions, a crucial requirement for liberating minerals from their sulphur contents. Beyond the broader goals outlined for the pilot experiments, the focus extended to evaluating the functionality of San Carlo's structures as roasting beds. This encompassed the monitoring of their thermal behaviour and the assessment of the final de-sulphurisation of sulphidic ores. Furthermore, a pivotal aspect of the investigation involved a thorough exploration of the most suitable fuel type for the roasting process, thereby comparing the efficacy of softwood versus charcoal.



Fig. 6. 2 Metallurgical structure interpreted as a possible roasting bed unearthed at the site of San Carlo Cave Solvay, Livorno (Italy). From Fedeli and Galiberti, 2016, p. 48, Fig. 32.

6.3.2. Experiments outline

I built the roasting platforms as follows. Initially, the clay was collected, and beneficiated, involving the removal of stones and other major impurities. The clay was then mixed with weighty wooden chunks to ensure homogeneity and prevent breakage during drying. Concurrently, two areas of approximately 1.5m² were de-turfed and the soil compacted.

Subsequently, the clay was molded into circular plano-convex platforms as previously described. Platform 1 measured 1.10 x 1.12 m and 5-7cm of thickness, while platform 2 measured 0.95 x 1.01 m in diameter and 6-8 cm in thickness. Fires were ignited at the rim of the platforms and gradually moved toward the centre to ensure uniform drying of the platform surface. Following this, any cracks on the plasters were filled to prevent material loss and facilitate the removal of roasted ore. After repairs, a final fire was kindled on top of the plaster for complete drying (Fig. 6. 3).

For each experiment, I weighed 1 kg of bornite, crushed it to nut-shell size, and then hand sorted to remove nodules with gangue. Detailed data were recorded using specific tables and a dairy (Fig. 6. 1). To determine the optimal recording device, temperatures for Experiment 2 were recorded using both a thermocouple (Mineral Insulated Thermocouple with miniature flat pin plug Type N – Microbell D Sheath – 1250°C) and an infrared thermometer with laser pointer.

Experiment 1 - Roasting bed 1 (16 June 2021): Experiment 1 utilised softwood fuel. The weather was sunny with some occasional clouds, humidity was at 58-60% and the average temperature was 23°C. The platform was preheated for approximately 40 minutes. Subsequently, 1 kg of bornite was placed at the centre of the heated platform, covered with fire, and roasted for 2 hours. The wood was piled up on the top of the charge. The experiment lasted 2.40h. To facilitate the progress of the experiment, a mean of the weight of 10 wood logs was calculated and the number of logs added to the fire was calculated. Overall, a total amount of 7.8 kg of wood was used (35 logs, mean 0.223 g/log). Temperatures were acquired every 10 minutes resulting in an average temperature of 714°C with a peak of 797°C. It was possible to maintain a constant temperature without the aid of man-powered bellows. The roasted ore, totalling 0.776 kg, displayed reddish-black outer layers indicating iron and copper oxide presence (see Fig. 6. 4b). The difference from the starting amount is ascribed both to material and sulphur losses.

Experiment 2 - Roasting bed 2 (16 June 2021): Experiment 2 employed charcoal as fuel, conducted simultaneously with Experiment 1. After preheating the platform for 50 minutes using wood, 1 kg of bornite was placed at the centre, covered with 1.2kg of charcoal. The roasting lasted 2.10h, using a total of 4 kg of charcoal. The experiment reached a maximum temperature of 1036°C. Unlike Experiment 1, two man-powered bellows were used for 1h to sustain charcoal combustion and maintain adequate temperature levels. Temperatures were recorded using the infrared thermometer every 10 minutes near the mouth of the bellows. After 40 minutes, bluish and green flames appeared, accompanied by an acrid sulphur odor. The charge was collected 50 minutes after the bellows activity ceased. Most of the ore pieces had

fused together, forming a slaggy vitreous material (Fig. 6. 3b). Unfortunately, due to melting and adherence to the platform, the final weight could not be determined, necessitating the removal of part of the platform.

Experiment 3 - Roasting bed 1 (17 June 2021): For Experiment 3, the same parameters as Experiment 1 were applied. On a cloudy day, with humidity at 65% and an average temperature of 18°C, the platform underwent a warming phase of approximately 40 minutes. The experiment lasted 3.40h and a total of 7.5 kg of wood was consumed (32 logs, mean 0.223 g/log). In contrast to Experiment 1, temperature measurements were acquired every 5 minutes. This resulted in an average temperature of 711°C, with a maximum temperature reaching 842°C. Notably, no bellows were employed during this experiment. Similar to the previous trials, a comparable weight loss was observed, leading to a final yield of 0.882 kg.

Table 6. 1 Overview of the primary parameters utilized in the roasting experiments conducted in this thesis.

	Roasting Bed	Date	Fuel (Type and kg)	T. °C		Hours	Weather			
				Av.	Max		T.°C	Humidity	Rain	Wind
Exp. 1	1	16/06/2021	Softwood 7.8	714	797	2.40	24	~60%	N	N
Exp. 2	2	16/06/2021	Charcoal 4	776	1036	2.10	26	~58%	N	N
Exp. 3	1	17/06/2021	Softwood 7.5	711	842	3.40	18	~65%	N	N



a)



b)

Fig. 6. 3 Reconstruction of a roasting bed based on the archaeological evidence of San Carlo Cave Solvay (a), and the resulting melted charge from the experiment 2 - Roasting bed 2 conducted on June 16, 2021 (b).

6.3.3. Preliminary results and considerations

One of the central inquiries was aimed at understanding the type of fuel used by ancient smelters for ore roasting – wood or charcoal. A comparison of the outcomes from the two conducted experiments yielded the following insights: in the wood roasting experiment (Experiment 1) a consistent temperature of 700-800°C was maintained by adding logs to the fire as needed. However, in the charcoal roasting experiment (Experiment. 2) temperatures varied significantly across the platform. They ranged from 1000°C near the air outflow from the bellows to approximately 300-350°C at the edges of the charcoal cover. Additionally, it proved challenging to sustain a consistent average temperature throughout Experiment 2, which utilised charcoal and bellows. Notably, the higher temperatures reached in the charcoal experiment resulted in a more substantial release of sulphur – evident through the green flames and characteristic odor. While this may seem advantageous for copper production, a drawback emerged as the initial charge reached a liquid state and adhered to the clay plaster surface. The melting of the charge led to the entrapment of excess sulphur in the form of copper sulphides. This outcome is contrary to the desired oxidation during solid-state reactions to prevent a reduction in particle surface area and gas-oxidising contact (Shamsuddin, 2020, p. 40).

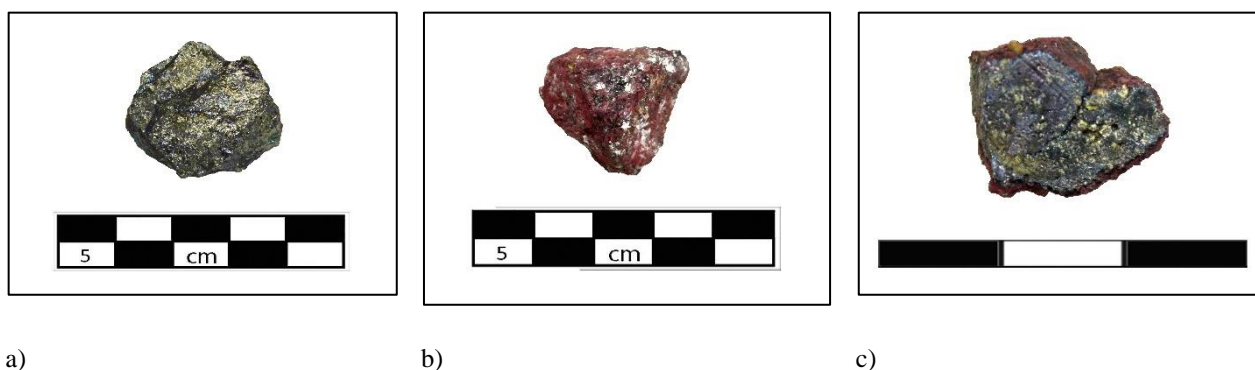
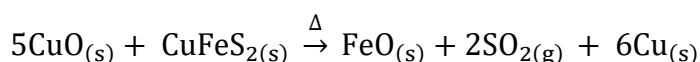


Fig. 6. 4 illustrates the transformation of ore fragments before (a) and after (b) roasting, along with a cross-section of a roasted bornite (Cu_5FeS_4) sample, revealing surface oxidation limited to 1-2 mm and the unreacted inner portion (c).

The initial trial resulted in a partially roasted ore, distinguished by a core made of copper and iron sulphides, surrounded by an outer layer made up of iron oxides and copper sulphides. These chemical reactions primarily stems from the greater affinity of sulphur to copper and iron's affinity to oxygen (Burger et al., 2011). While the ore's external appearance indicated successful roasting (Fig. 6. 4b), closer inspection revealed that only around 1-1.2 mm of the surface had oxidised, leaving the inner portion of the ore unchanged (Fig. 6. 4c).

The importance of the roasting process has been comprehensively established. Undoubtedly, roasting the ore prior to smelting stands as the most efficient method to attain high-quality copper from a chemical and thermodynamic standpoint (Shamsuddin, 2020). However, the origins and development of roasting technology remain subjects of ongoing debate. Notably, certain scenarios exist where sulphide minerals may not necessitate roasting. For instance, Rostoker et al. (Rostoker *et al.*, 1989), demonstrated through laboratory experiments that the co-smelting sulphides and oxides could potentially supplant the roasting process. This can be illustrated with the simplified chemical reaction:



In this reaction, when copper oxide combines with iron-copper sulphide (chalcopyrite in the formula), sulphur dioxide (SO₂) is released in a solid-state reaction in the form of gas and produces iron oxide and copper. Considering the morphology of naturally occurring ore bodies, characterised by regions containing both oxidic and sulphidic ores (primarily chalcopyrite), Rostoker et al. (1989) argued that ancient smelters likely utilised mixed batches of these ores. A similar concept, albeit applied to the Early Bronze Age (EBA), has been employed for reducing fahlore. Martinek (2011) proposed that the more complex two-step roasting process required for ores consisting of complex sulfosalts would be considerably more challenging compared to the simpler and more effective approach of co-smelting combined ores. Conversely, Moesta (Moesta, 1986), held an opposite view, suggesting that sulphidic ore bodies were initially considered unprofitable resources during the early stages of smelting technology and were discarded as non-copper-bearing ores.

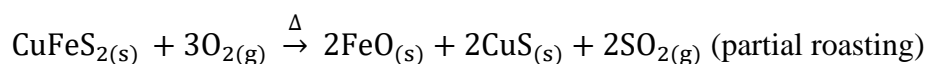
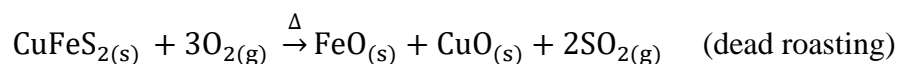
In addition to the hypothesis presented by Rostoker et al. (1989) and Martinek (2011), several lines of evidence and reasoning have led me to question the presumed central role of roasting when dealing with sulphidic ores:

- a) Limited and often disputed traces of roasting beds have been discovered for the relevant period, except for the potentially functional roasting platforms found at San Carlo.
- b) the roasting experiments conducted in this study released a relatively small amount of sulphur (Fig. 6. 4), yet the subsequent smelting experiment successfully yielded copper (as shown in the copper smelting pilot experiment 1).
- c) Notably, archaeological slags from Orti Bottagone consistently contained sulphur bound in various compounds, along with a substantial quantity of unreacted Cu-Fe bearing sulphides. Most of these iron-bearing sulphides, such as chalcopyrite (CuFeS₂) or pyrrhotite (Fe_(1-x) S), were not accompanied by iron oxides, indicating their iron-rich

nature. Had roasting been carried out, these iron-rich sulphides would have oxidised, potentially serving as fluxing agents to reduce silicates, and thereby affecting melting conditions/temperatures (see Pearce et al., 2022).

- d) Under the conditions of prehistoric metallurgy, achieving complete sulphur removal from the charge, a process known as dead-roasting (formula), seems to have been virtually unattainable. This challenge stems from the frequent stagnation of the oxidation process, which hinders the infiltration of oxygen into the inner regions of the ore, as highlighted by Burger et al. (2011). As a result, a significant amount of sulphur remained within the ore. This notion finds support in an experiment carried out by Doonan (1994) involving the roasting of 100g of chalcopyrite within a muffle furnace set at 700°C. In this experiment, a continuous flow of air targeted to the ore nodules, establishing the indispensable oxidising conditions for roasting. Surprisingly, despite extending the experiment to 48 hours, the extent of oxidation remained limited. Only a thin, 4mm layer on the surface exhibited signs of oxidation (Doonan, 1994, p. 95). This observation underscores the ongoing challenge of achieving significant oxidation throughout the ore volume, even with prolonged exposure to meticulously optimised roasting conditions.

Within the context of the Bronze Age Alpine tradition, the prevailing hypothesis suggests a preference for partial roasting (formula), rather than the complete dead roasting approach (Doonan et al., 1996; Sperl, 1980). This choice was likely influenced by the potential formation of iron metal from iron oxides upon complete sulphur elimination, yielding a largely unusable Cu-Fe alloy. Maintaining some sulphur in the ore would have been advantageous, potentially serving as a fuel during the smelting process (Bachmann, 1993; Czedik-Eysenberg, 1958).



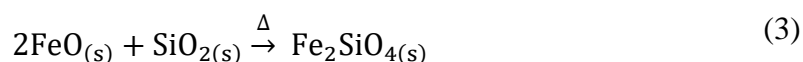
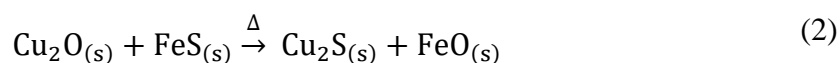
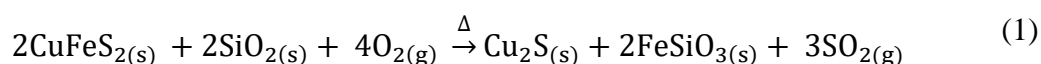
These chemical reactions are expressed through the equations depicting dead roasting and partial roasting. Handling substantial amounts of sulphidic ore, however, could lead to sulphur remaining trapped within the semi-liquid charge within the reactor, obstructing both the smelting process and the extraction of pure copper (Rose et al., 2020).

- e) Ethnographic evidence from copper smelting practices in the Himalayas (Sikkim and Nepal), as reported by Anfinset (2001), suggests that preliminary roasting might not be a necessary step (Pearce et al., 2022).
- f) If ore pre-treatment was not conducted, an alternative approach to accelerate the smelting process might have involved incorporating aged slags into the charge (Pearce et al., 2022). This procedure has been assessed both from an ethnographic standpoint (Anfinset, 2001, pp. 50–57) and through archaeological investigations (Herdits, 1997). In archaeological context, evidence emerged at the Brennerwald smelting site within the Mitterberg district (Salzburg, Austria), where an incomplete smelted platy slag was discovered within a slag cake. This find was interpreted as the intentional use of recycled slag to enhance the reduction of silica-rich rock (Herdits, 1997, pp. 40–41). Another potential strategy involved the cyclic addition of fresh iron-rich sulphidic ore to the charge. This practice would have introduced the necessary amount of FeO, thereby contributing to an advantageous fluxing of the system. This approach could have facilitated the smelting process effectively.

6.4. Smelting

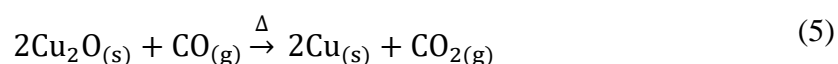
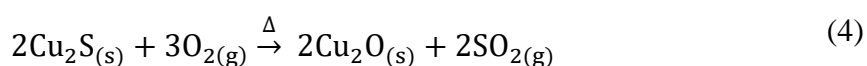
Smelting is the process through which a metal is extracted from its mineral deposits. It consists of a series of chemical reactions (redox reactions) which separates metals from their original chemical bonds. During the smelting process the initial charge is subjected to a change in temperature, pressure and reducing conditions. One or more mineralogical phases of the original composition might be rendered unstable and recrystallise to more stable compounds. Focusing on copper-bearing ore smelting, based on the initial charge different chemical reactions can take place in the reactor. In a very ideal and simplified form, it is possible to summarize them as follow.

If the initial charge is composed of copper sulphide (i.e., chalcopyrite) and quartz, the overall equations is



In the (1) reaction, chalcopryrite (CuFeS_2) associated with quartz - SiO_2 , either naturally occurring in the ore or consciously added (see paragraph on fluxing agents), is reduced to copper(I)sulphide (Cu_2S). The iron in the chalcopryrite is transformed into an iron(II)silicate (FeSiO_3) and the sulphur is released as sulphur dioxide gas (SO_2). More generally iron oxides react with silica-rich material producing slags. Copper has a higher affinity for sulphur than it does for oxygen and therefore any copper(I)oxide present will be converted into copper(I)sulphide during the smelting process. Conversely iron bonds better with oxygen forming iron(I)oxides (FeO) and iron silicates (Fe_2SiO_4) (2), (3). They are the main impurities recovered in the reactor charge and they usually float on the surface because less dense and heavy than the metal itself.

Once the iron is removed the copper(I)sulphide yields to the formation of copper(I)oxide (Cu_2O) again releasing sulphur dioxide as gas (4). Copper(I)oxide is then reduced to copper with the aid of carbon monoxide (CO) and carbon dioxide (CO_2) is released as gas (5).



In archaeological literature, three distinct smelting models, each offering unique insights into the ancient metallurgical practices, have been identified:

1) The ‘Timna model’ is primarily rooted in the evidence for the Late Bronze Age (LBA) and Early Iron Age (EIA) smelting activities in the Negev region, which hosted predominantly oxidised sedimentary copper ore deposits. These ores differed significantly from the complex copper sulphides found in European settings (Craddock, 2009, pp. 3–4).

2) Eibner’s (1982) model draws inspiration from the sixteenth-century AD account of Georgius Agricola (1912 [1556]). This model involves a two-step process where the ore is initially roasted and then subjected to smelting. The resulting matte is subsequently roasted again before the final smelting to yield metallic copper (known as matte conversion).

3) The Chalcolithic copper smelting model reflects the earliest small-scale smelting methods. In these processes, copper rich ores, mainly oxide or mixed oxide-sulphide ores were employed. No flux was added during the smelting, with the process being inherently

self-fluxing. This approach yielded small, nut-sized slags that remained partially liquefied, not optimised from a modern perspective.

4) A fourth model, known as the “Himalaya model” has been recently proposed by Pearce et al. (2022). This model is based on the ethnographic observation of the smelting practices conducted in Sikkim and Nepal regions. In this model, the ore is initially reduced to cm-sized pieces and subjected to matte smelting, with platy slags introduced as a fluxing agent. Wooden tools are employed to remove the non-liquid slags, creating space in the smelting reactor for the addition of fresh ore. This approach enhances the process efficiency. Subsequently, the resulting material undergoes roasting and is re-smelted to yield copper. This controlled process, as interpreted by Pearce et al. (2022) also found application in the Trentino-Alto Adige/South Tyrol during the Chalcolithic (CA) and Early Bronze Age (EBA).

These various smelting models provide valuable insights into the diverse techniques and technologies employed by ancient metallurgists across different regions and time periods.

6.4.1. Experiments outline, preliminary results, and considerations.

In this section, smelting pilot experiments explanation and ensuing preliminary considerations and results are combined and described in a temporal order as I slightly changed and adapted each experiment based on the observation of the previous. As for the roasting experiments, useful “pilot” data were collected during the smelting trials.

The pilot experiments were based on contemporary archaeological contexts and on preliminary chemical and physical analysis carried out on slags collected from the site of Orti Bottagone. Three experiments were carried out. I dedicated the first one to the smelting of a copper carbonate (malachite, $\text{Cu}_2(\text{CO}_3)(\text{OH})_2$). The other two focused on the smelting of sulphide minerals (bornite). The aim was to assess a series of parameters like the shape of the reactor, the position of the tuyeres, the depth of the furnace, the location of the crucible and to get used to the alternate motion of the bellows. The air was supplied using arm-powered bellows instead of human-blowing blowpipes. Although it is commonly assumed that blowpipes were the earliest technique used in antiquity to supply oxygen, when looking at the archaeological copper smelting evidence, it is often impossible to determine if bellows were used instead of blowpipes (Rehder, 1994; Weisgerber, 2004). Since the techniques adopted to supply oxygen in the reactor were not among the targets of the research, I decided to adopt bellows to decrease the physical effort necessary to reach the right temperature to smelt copper and to limit the fluctuation in the temperatures over the experimental trial. The use of blowpipes by untrained people would have

caused abrupt drops and peaks of temperatures. Furthermore, as I carried out the experiments in 2020 during the global pandemic of Covid-19, bellows were my preferred option to reduce to a minimum the number of people involved in the experiments (1-2 people instead of 4-6).

The construction of the reactors took 2 days. The first day (14/06/2021) with the help of students under the supervision of the EXARN team⁴, was dedicated to the collection of the clay and the preparation of the reactors. Once dug, the clay was crushed with wooden clubs to get rid of all the large clumps and pebbles were removed. Water was then added to make a smooth mixture to line the reactors. Two areas of around 1 m² were de-turfed and a pit of ca. 15 cm of depth and a 30 cm diameter was dug at the centre of each area. The clay was then manually applied to coat the pits and to fasten the tuyeres in the right position. In the meanwhile, a group of students crushed the malachite using pestles and mortars into tiny pieces in the range of few mm to cm-size (Fig. 6. 5a). The day after the reactors were dried out and the cracks opened filled using the same procedure applied for the roasting platforms. For all the experiments thermocouples reaching a max of 1250°C were used (Type N Thermocouple - Nicrotherm D™ Sheath, 1250 °C).

The first experiment (Exp.1 – Furnace 2) was carried out during the workshop (17/06/2021).

The weather was mainly cloudy with humidity at 58-60% and temperature of 17-18°C.

For the first hour, students just pumped air through the bellows into a wood fire in the hole to get the furnace up to temperature (Fig. 6. 5b). After 1 hour, a circular crucible of 12 cm of diameter and 8 cm of depth containing 0.6 kg of malachite was placed on top of the remains of the wood fire, and then charcoal was added on top to produce a reducing environment necessary to smelt the malachite. The experiment lasted 1.10h. To maintain a constant air supply (and thus temperature), students regularly alternate at the bellows. Regular temperature checks were done every 10 minutes. In order to have an idea of the different temperatures inside the reactor, I decided to place a thermocouple under the crucible, and another one at the top of it. The first recorded an average temperature of 420°C, while the second of 817°C. Overall, around 5 kg of charcoal was used. 1 kg was added every 20 minutes.

⁴ EXARN, Experimental Archaeology Newcastle. A Postgraduate Researchers-led Experimental Archaeology research group within the Archaeology Department at Newcastle University established in 2018. EXARN, affiliated with the Cluster for Interdisciplinary Artefact Studies (CIAS), promotes the study of material culture, archaeo-materials and ancient technologies through experimental archaeology.

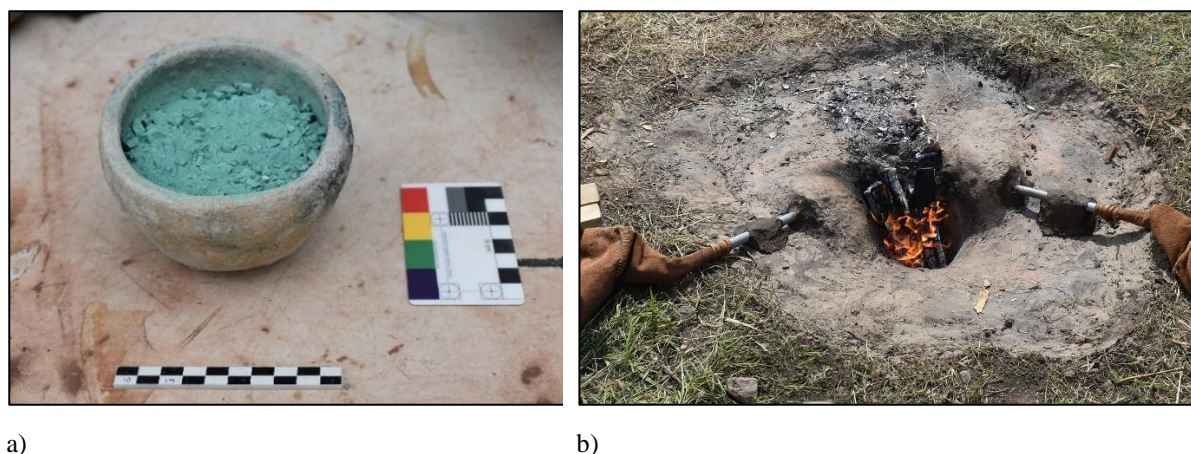


Fig. 6. 5 displays a crucible filled with crushed malachite (a) and the preliminary warming process of the reactor (b).

The experiment (Exp.1 – Furnace 1) successfully produced small solid chunks of dark copper oxides with hints of red. When basic copper (II) carbonate (malachite) is heated to high temperatures (above 400°C), it decomposes according to the following equation



Malachite turns into black solid copper oxide and carbon dioxide and water are released in the form of gases. However, the solid chunks were recovered only from the top of the crucible, while the rest of the charge turned black but remained mostly unreacted. A number of factors might have contributed to the incomplete reduction of the charge. First, the discontinuous airflow, i.e., students did not properly alternate at pumping the bellows and/or they did not change rapidly enough, led to periods of air inactivity and thus temperature drops. Second, the crucible depth did not allow the heat to reach the bottom of the crucible, impeding the ore to melt. Third, the environment was not reducing enough. Four, the crucible was misplaced inside the reactor, or the tuyeres did not point exactly to the centre of the crucible. The latter is confirmed by the deep vitrification and collapse of part of the rim (Fig. 6. 6a-c). Its position close to the air flow inside the reactor hindered the temperature to rise properly inside the crucible, and as a consequence led to an incomplete smelting. This also explain why the temperature inside the crucible started rising steadily but slowly only after 30 minutes of pumping air.

The rest of the crucible had no discernible traces of thermal alteration. From an archaeological perspective, this indicates that crucible sherds might not show any indication of metallurgical activity and then being easily dismissed as common ceramic sherds. Most of the time only the bottom and the parts of the rim close to the air flow show thermal and chemical alteration, while

the rest of the crucible does not show any traces of metallurgical activities as slagged surfaces or vitrified and bloated rims.

The second experiment (Exp. 2 – Furnace 2) was carried out at the beginning of July (03/07/21) in a cloudy weather with a little wind and humidity at 67-69%. The average temperature was 18°C. Two volunteers helped. The reactor was warmed up for ca. 90 minutes. In the meanwhile, I selected and ground to powder 0.400 kg of bornite from the roasting experiment 1 – roasting bed 1. Once the reactor reached the temperature, I placed the crucible in it with the charge mixed with powdered charcoal. The experiment lasted 1.30h. I placed only one thermocouple inside the crucible. The starting temperature was 648°C. The temperature to start the reaction was reached after 20 minutes ($> 950^{\circ}\text{C}$). After 30 minutes, the temperature dropped for about 2 minutes due to a sudden shower and strong gusts of wind. Unfortunately, the average temperature was impossible to determine as the thermocouple stopped working after 40 minutes when by mistake the temperature overtook the detectable limit of 1250°C peaking at 1334°C . Overall, I used 9 kg of charcoal. I added 1 kg every 10 minutes.

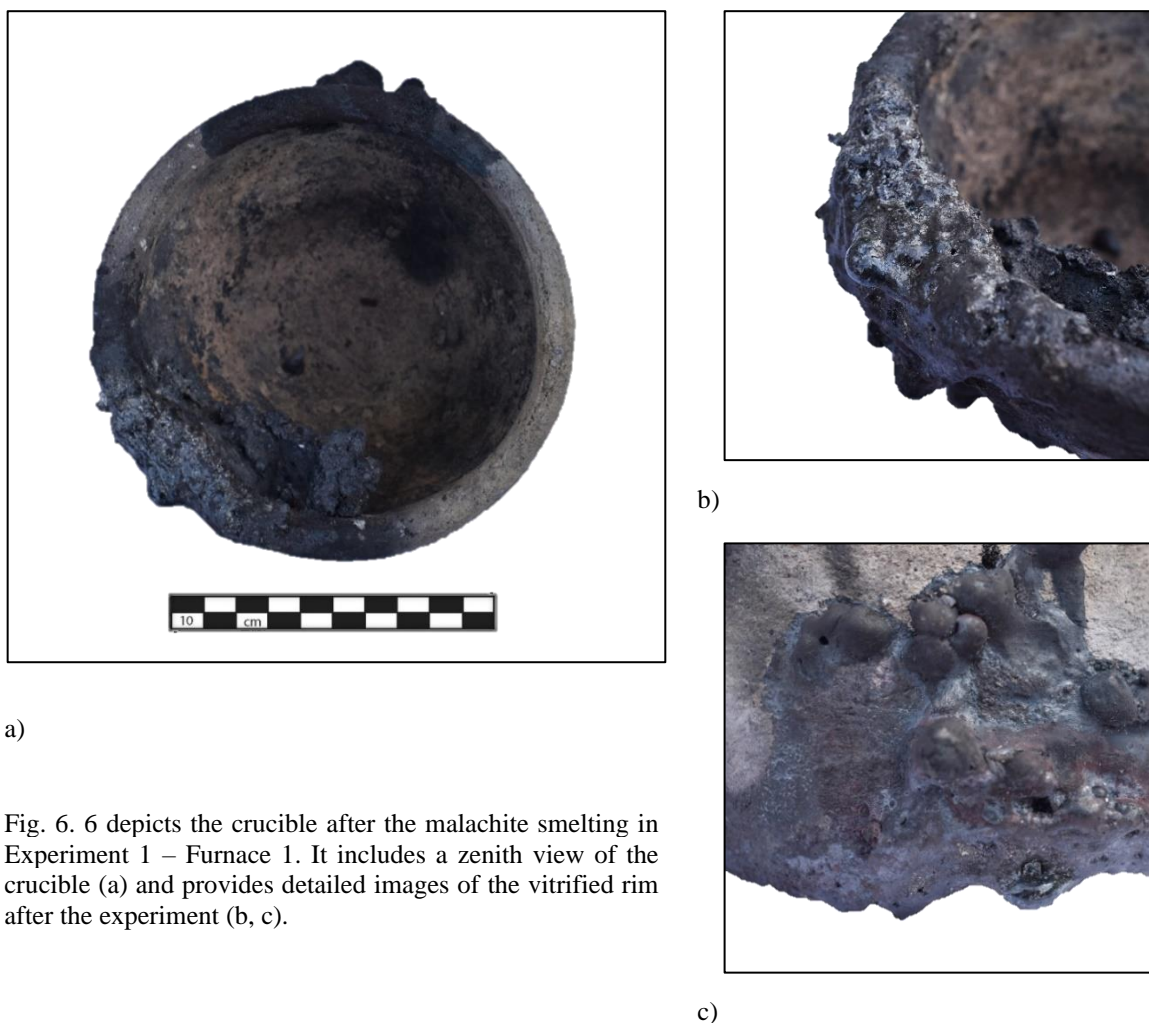


Fig. 6. 6 depicts the crucible after the malachite smelting in Experiment 1 – Furnace 1. It includes a zenith view of the crucible (a) and provides detailed images of the vitrified rim after the experiment (b, c).

To avoid the same outcome of the previous experiment, instead of a deep-bottom crucible, I used a shallow dish-shaped crucible with slightly elevated rim (diam. c. 17 cm, depth 3 cm). I also relocated the tuyeres, this time oriented towards the middle of the furnace instead of the bottom. However, the outcome of the experiment (Exp.2 – Furnace 2) had not been successful from a copper production perspective, as most of the charge remained mostly unreacted. Again, the more likely reason is the position of the crucible too far from the air supply, which did not allow the heat to reach the bottom of the crucible. In favour of this hypothesis, two considerations can be made: 1) the only slag recovered was on the top of the crucible, the closest part to the air supply, presumably in the area where the temperature and the reducing conditions to start the smelting were reached; 2) the crucible walls did not show any trace of thermal alteration. Another potential reason that might have contributed is that the powdered bornite mixed with powdered charcoal might not have allowed the air to be conveyed to the crucible and start the reaction.

The slag (JH2020_PE_Smelting1_YF_S1) was investigated following the same analytical protocol used for the archaeological specimens. The slag is 4 cm long and 2.5 cm wide (Fig. 6. 7a). Macroscopically, it is homogeneous and presents a grey/greenish colour probably derived from the mixing of the melted charge with ash and charcoal. It is very light, characterised by high porosity spread all over the surface. A fragment of charcoal embedded into the slag. No magnetism was detected. To have a first assessment of the chemical composition of the slag, I analysed the surface using a pXRF device. Results showed that the main constituent was Fe with 95%, then Cu at 3% and the rest 2% divided between Mn, Pb, and Zn. OM investigation made possible to detect Cu-Fe sulphides at an early reaction stage and prills scattered over all the surface investigated (Fig. 6. 7b-c).

I carried out the third experiment (JH2021_PE_Exp.3-F.2) the week after (09/07/21) in a cloudy but mainly warm and steady weather. Average temperature 22°C, humidity 57-59%. One volunteer helped.

The reactor remained uncovered and exposed to rain and humidity for the entire week. I removed the charcoal left in it and lit a fire at its bottom using dry wood and charcoal. I warmed it up for 90 minutes, the first hour with a simple fire, while the rest half an hour with the aid of bellows to increase the temperature inside the reactor more rapidly. Upon considerations, in order to avoid the same outcome

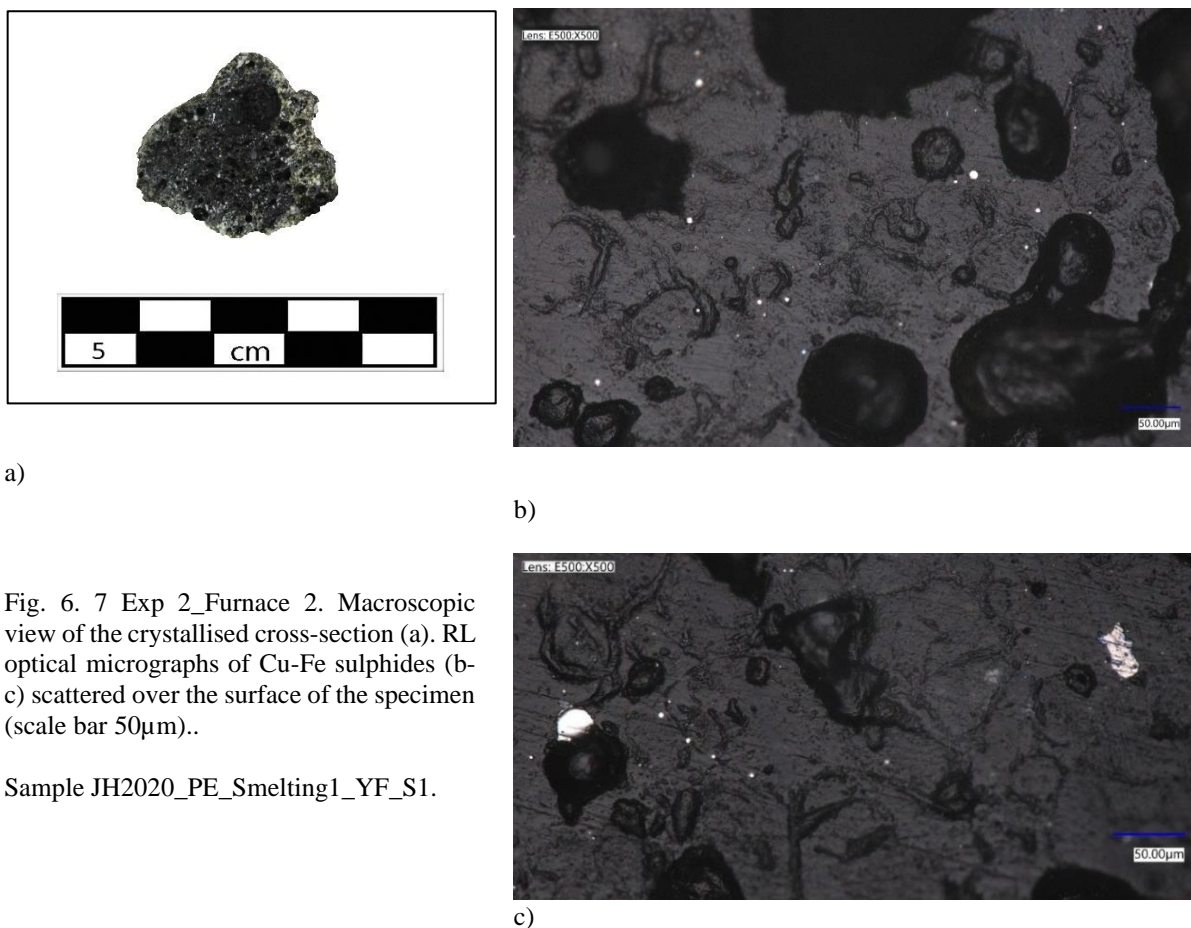


Fig. 6. 7 Exp 2_Furnace 2. Macroscopic view of the crystallised cross-section (a). RL optical micrographs of Cu-Fe sulphides (b-c) scattered over the surface of the specimen (scale bar 50µm)..

Sample JH2020_PE_Smelting1_YF_S1.

of the previous experiment (Exp. 2 – Furnace 2), the following adjustments were made:

- I crushed the ore to nut-sized fragments, and I did not add powdered charcoal to the initial charge.
- While pumping air in the reactor, I pay heed to not overtake the thermocouple limit temperature of 1250°C.
- To have an idea of the temperature fluctuations in the reactor, I recorded the temperature every 5 minutes instead of every 10. I place the thermocouple again inside the crucible.

When reached the temperature, I placed in the reactor the shallow dish-shaped crucible with 0.400 kg of the slightly roasted bornite from experiment 1 – roasting bed 1. The experiment lasted 60 minutes. An average of ca. 1 kg every 10 minutes for a total of 5 kg of charcoal. The average temperature was 1105 °C, with a peak at 1194°C after 40 minutes. Five minutes after placing the crucible in the reactor, green flames and a strong smell of sulphur started. The sulphur release lasted for around 6 minutes.

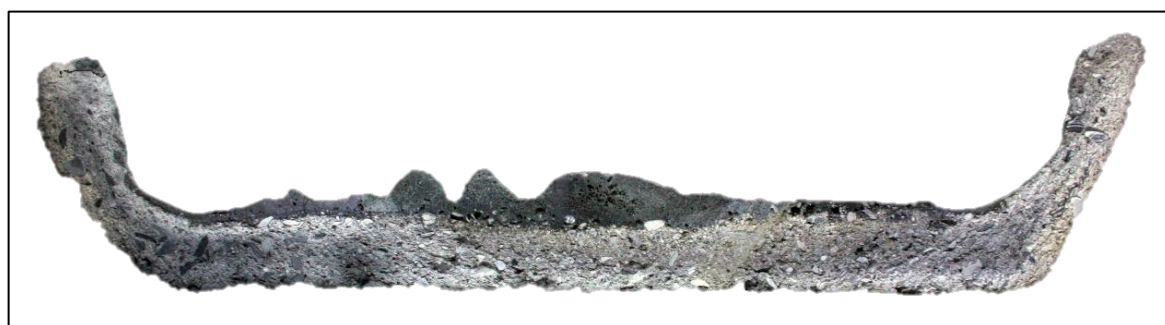
The experiment was successful on several respects. First, some matte was produced. Even if I used an open vessel, the heat did not dissipate and did not hinder the smelting process. Mostly

the entire surface of the crucible was covered with molten material. Inside the crucible, I identified three different layers: a) a greyish slag layer on the top, b) a reddish shining layer, c) a shining copper bearing layer, likely matte. I also recognised an unreacted fragment of the initial charge glued to the crucible rim (Fig. 6. 8a). Even if close to the point where the air reached the crucible, as confirmed by the almost vitrified and crumbled rim, this bornite bit did not melt. The only way to recover the materials produced was to chisel out the melted charge or to break the crucible and collect the copper-bearing bits (Fig. 6. 8b). Therefore, the crucible was unusable for a second run.



Fig. 6. 8 a) Top view of the crucible from Pilot experiment JH2021_PE_Exp.3_F.2. Three different layers were identified: 1) an upper layer characterised by a greyish, porous, and slag-like appearance; 2) just beneath the top layer, there is a combination of greyish and reddish shining layers, giving off a shining quality; 3) the lowest layer exhibits a noticeable gleam and is rich in copper content. Within the crucible, marked by a red dotted circle, one can also identify an unreacted piece of bornite. b) the cross-sectional view A-B of the crucible reveals the products obtained during the experiment, which are scattered across the crucible's surface.

a)



b)

While cleaning the reactor, I observed a striking array of colours on the reactor's inner walls. Starting from a yellowish-brown hue at the rim, the colours progressively darkened as they descended towards the bottom. Near the highly vitrified region near the tuyères, shades of grey green became evident. The charcoal within the reactor displayed a similar diversity of colours based on its placement. The layer underneath the crucible appeared deep black, seemingly untouched, and perfectly preserved. This might be attributed to the absence of oxygen, which impeded the combustion process, or to the lower temperatures beneath the crucible. At the top of the crucible, where the chemical reactions took place, the charcoal assumed a grey and white appearance, indicating the highest temperature reached in this area. Remarkably, on the uppermost part of the reactor, the charcoal exhibited a yellowish tinge, likely linked to the sulphur emanating from the bornite. The intricate layering observed within the crucible and the varying shades of the charcoal throughout the reactor underscore the presence of temperature gradients not only within the reactor as a whole but also within the crucible itself.

Beneath the crucible's charcoal layer, I uncovered a melted by-product that had seeped through a crack in the bottom (from the same experiment JH2021_PE_Exp.3-F.2). This specimen solidified, encapsulating multiple fragments of charcoal (Fig. 6. 9a). Upon removing the charcoal, it was apparent that the specimen contained numerous voids and was notably fragile. To gain insights into its nature and composition I conducted OM and SEM-EDX analyses. Five distinct analyses were performed in various region of the specimen. The chemical composition consistently revealed an average of 54.8 wt% of copper, 23.2 wt% of sulphur and 22 wt% of iron Fig. 6. 9d. These values align with the typical composition of the intermediate smelting product in the smelting process, often referred to as "matte" or "black copper". The fragment also displayed a series of round features composed of iron and sulphur, which are likely to be remnants of the initial charge (Fig. 6. 9b-c), along with voids.

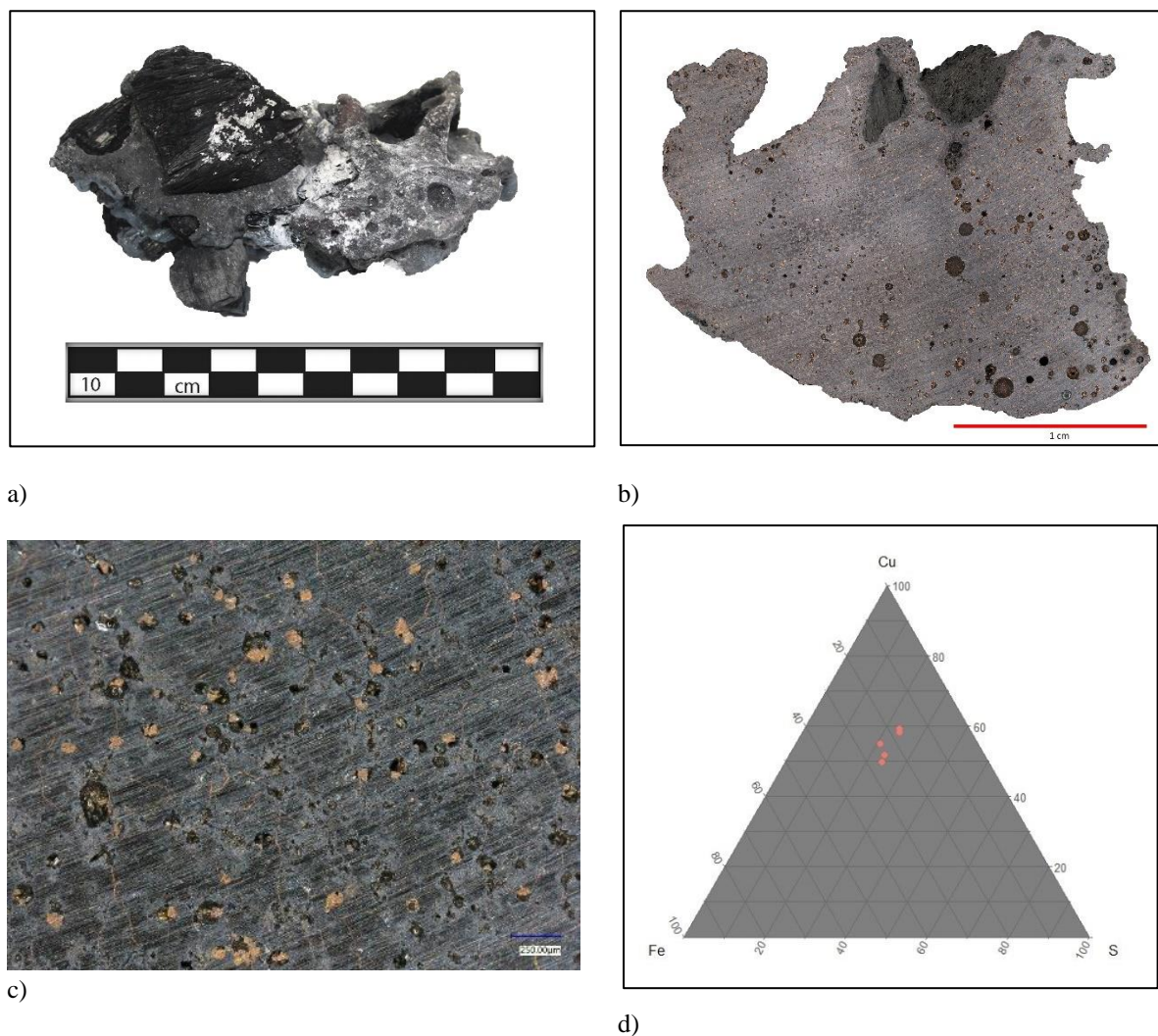


Fig. 6. 9 a) Melted product recovered from beneath the crucible leaked from a crack in the bottom, b) RL cross-sectional view and c) RL optical micrograph from the pilot experiment JH2021_PE_Exp.3-F.2 (scale bar 250µm), d) Cu-Fe-S ternary diagram illustrating the composition of the product. The diagram visually represents the distribution of copper (Cu), iron (Fe), and sulphur (S) in the 5 analysed areas of the sample.

In this chapter, I have delved into the crucial role played by pilot experiments in shaping the trajectory of the experimental part in this research endeavour. These preliminary trials laid the foundation for better defining the archaeological problems and clarifying the research questions. Specifically, the pilot experiments focused on roasting have yielded valuable insights into how roasting might have been conducted in the past, or perhaps not at all. These findings have compelled me to question long-standing assumptions regarding the role of roasting in ancient smelting practices and consider alternative approaches to smelting. Notably, I have begun to contemplate the feasibility of bypassing the intermediate roasting step altogether.

These pilot experiments have not only enriched my understanding but also guided me in the design of the experimental setup. They influenced the development of a robust analytical protocol, encompassing both fixed and variable parameters, which will be elaborated in detail in Chapter 8.

Furthermore, the pilot experiments illuminated several technical and logistical aspects that are vital to the success of the scientific experiments. Firstly, maintaining precise temperature control throughout the process proved to be of paramount importance. I discovered that temperature fluctuations beyond 1250°C could significantly compromise the reliability of the measurements. Secondly, to gain a more comprehensive understanding of temperature trends and fluctuations, I made the crucial decision to reduce the recording interval from 10 to 5 minutes. This adjustment ensured that I obtained higher-resolution temperature data, a key factor in the experimental setup (refer to Section 8.4 for detailed information). Thirdly, the experiments were crucial to acquire the practical skills (expertise) and gain a degree of personal competence of the techniques supposedly used in the past (experience).

Moreover, through these initial experiments I also came to recognise the critical role of the crucible's placement within the reactor and the positioning of the tuyeres. Proper orientation of the tuyeres, directing them towards the charge rather than the rim of the crucible, as emerged as a vital factor for the success of the smelting process.

In summary, the importance of pilot experiments cannot be overstated. They are not “mere and fun preludes” but serve as integral components of any archaeometallurgical research. Their meticulous execution and comprehensive reporting are indispensable. In the next chapter I will delve into a comprehensive overview of sulphide copper smelting experiments conducted to date. This will equip the reader with the analytical protocol developed by other researchers and prepare them to navigate the parameters and analytical results discussed in Chapter 8.

Chapter 7. Sulphide copper smelting experiments

7.1. Introduction

This chapter is divided into two sections. The first section presents a comprehensive literature review of smelting experiments involving copper sulphide ores, conducted in alignment with the archaeological evidence discussed in Chapter 3. It provides an overview of the current state of knowledge and identifies the gaps within the specific domain of experimental sulphide copper smelting. These gaps serve as the focus for the second part of this thesis.

The second section outlines the second objective of the thesis, involving a critical discussion and the presentation of the research questions that form the foundation for the subsequent scientific experiments in Chapter 8.

7.2. Brief overview of copper smelting experiments

After the post-processual challenge to science and methods (Clarke, 1973; Feyerabend, 1975; Outram, 2008) which showed a decline in the number of archaeological experiments undertaken, experimental attempts on one or more of the different stages of copper metalworking has risen up and steadily increased over the last decades (Hauptmann, 2020; Heeb & Ottaway, 2014). Experimental archaeology has been widely considered the primary tool to investigate hypotheses on metal technology and fill the gap given by the paucity of metalworking technologies related archaeological data. Each stage of the *chaîne opératoire* of copper making has been investigated and a remarkable body of literature produced. Considerable attention has been given to Bronze Age smelting (Bunk et al., 2002; Cadet et al., 2021; Della Casa et al., 2016; Doonan, 1994; Dungworth & Doonan, 2013; Fasnacht, 2009; Girbal, 2013, 2013; Goldenberg, Anfinset, et al., 2011; Hanning, 2012; Hanning et al., 2010a; Merkel, 1990; Phelps, 2013; Reitmaier-Naef et al., 2019; Rose et al., 2019, 2020; Tylecote & Merkel, 1985), casting, refining and polishing artefacts (Ottaway and Wang, 2004; Kearns *et al.*, 2010; Barbieri and Cavazzuti, 2014; Barbieri *et al.*, 2015) and to artefact testing (Dolfini & Crellin, 2016; Gentile & van Gijn, 2019; Hermann *et al.*, 2020; Molloy, 2011). Instead, experiments regarding ore mining and roasting (Merkel, 1985; Doonan, 1994; Timberlake,

2007; Silvestri *et al.*, 2014; Rose *et al.*, 2020) have rarely been undertaken. This may be due to the unavailability of suitable geological resources already widely exploited in the past (Doonan & Dungworth, 2013).

Nevertheless, little has been done on the earliest phases of copper production (Bourgarit, 2019). The following section aims to critically review and discuss the most relevant early copper smelting experiments carried out to date. Both laboratory and field experiments are considered. It must be acknowledged that the research aims of these approaches, largely differ from one another. Lab experiments are carried out in settings specifically designed for it, where most variables under study are carefully controlled. Their aim is to build up a specific knowledge of the scientific principles under investigation, such as chemical reactions and working conditions (Outram, 2008, p. 2). Conversely, a field experiment, or “actualistic” (Outram, 2008, p. 2), with its natural setting and less control upon the environment, simulates real-world occurrences where unpredictable phenomena might occur. Examples are the high variability in temperatures and reducing conditions and the fluctuating thermodynamic transformations that might occur in an open reactor. The main aims are observing, analysing, and describing what exists and reproducing the process under study as credible as and as closely as possible. It must be highlighted that these two approaches are not mutually exclusive, but instead are essential and complementary to each other (Hermann *et al.*, 2020; Outram, 2008).

When experimental archaeometallurgy emerged as a separate archaeological field in the 1970s, started by Breno Rothenberg after the excavations at Timna (Bachmann & Rothenberg, 1980; Merkel, 1990; Tylecote & Boydell, 1978), many researchers developed and carried out mainly laboratory-based experiments. The natural development of scientific research explains the prevailing of lab experiments (of course with some exceptions). At the beginning of the archaeometallurgical discipline, the phenomena under study were still largely unknown and a first basic knowledge was required to generate analytical research protocols and accurate research questions. Therefore, archaeometallurgists carried out the first experiments in the close and controlled environment of the laboratory. Once they acquired a preliminary scientific knowledge, they designed and developed field experiments with new added variables like human factors (individual skills and mistakes) and external environment (Outram, 2008). The experiments reviewed focus primarily on the smelting of copper sulphides, and co-smelting of copper carbonates/oxides and sulphides in the same reactor in a one-step process. I will also discuss other experiments concerning specific steps and parameters of technological processes I considered important to the end of this thesis.

7.3. Sulphide copper smelting experiments

In this section I present an overview of the most significant experiments conducted on sulphide copper smelting up to the present day.

The first scientifically relevant sulphide ore smelting experiment was undertaken by Böhne in 1968 (Böhne, 1968). He carried out an initial smelting in a shaft furnace, which gave an iron-sulphidic metallic copper known as matte. Subsequently, this matter was subjected to crushing, sorting, re-roasting and re-smelting in a clay-lined, bowl-shaped furnace. Importantly, Böhne, for the first time, meticulously recorded the experiments' details, including the dimensions and construction materials of the furnaces. He also conducted an in-depth analyses of the resulting products, scrutinising their sulphur and chemical compositions (Tylecote & Merkel, 1985, p. 5). Unfortunately, the scarcity of recorded details limits the ability to replicate the experiment. Pioneering experiments, which continue to hold significance and are frequently referenced, were carried out by Rostoker et al. (Rostoker, 1975; Rostoker and Sadowski, 1980; Rostoker *et al.*, 1989). These experiments were grounded in the premise that the earliest smelting technology likely employed a simple and straightforward approach. In his 1975 research, Rostoker argued that the matte smelting process involved too many steps to be the initial sulphide ore smelting technique employed by ancient metallurgists. His objective was to uncover a simpler method that might have been adopted in the early stages of metallurgy. Rostoker roasted powdered chalcopyrite with a copper content of 20% for 8 hours at low temperatures (400-500°C). Subsequently, he heated the material in a gas-fired pit furnace using a clay crucible, conducting multiple attempts at different temperature settings. The experiments revealed a significant reduction in metallic copper production rates as temperatures decreased, dropping from a 90% recovery at 1300°C to a mere 15% at 1100°C. Rostoker dismissed the highest temperature as being too impractical for ancient smelting. According to him, the issue lays in the increasing viscosity of the slag as temperatures decreased. However, he postulated that even at lower temperatures, and with reduced production rates, metallic copper could be recovered by crushing the slags and manually sorting the visible prills. The results of these experiments allowed Rostoker to propose a two-stage process that might have been employed in sulphide ore smelting. Once again, no specific details were provided to allow the reproducibility of the experiments.

Probably the most cited work in the field among the experiments carried out in a laboratory, is the work by Rostoker et al. (1989). The premises of their study were the following: 1) copper production was carried out either by reducing carbonate and/or oxide ores, or by smelting sulphide ores (Caley and Easby, 1959; Forbes, 1971; Koucky and Steinberg, 1982); 2) the

process to smelt sulphide ores is complex and characterised by several stages (Fig. 7. 1), therefore, the transition towards it must have come with the “conscious” adoption of a new smelting technology; 3) the world’s ore bodies are characterised by heterogeneous deposits of secondary (weathered) and primary minerals (see Section 2.4) which would have made likely that part of the carbonates and oxides exploited at the earliest stages of metallurgy incorporate cores of sulphide minerals. In addition, the deeper ancient metallurgists mined, the higher was the probability to collect sulphide minerals associated with oxide and carbonate ores.

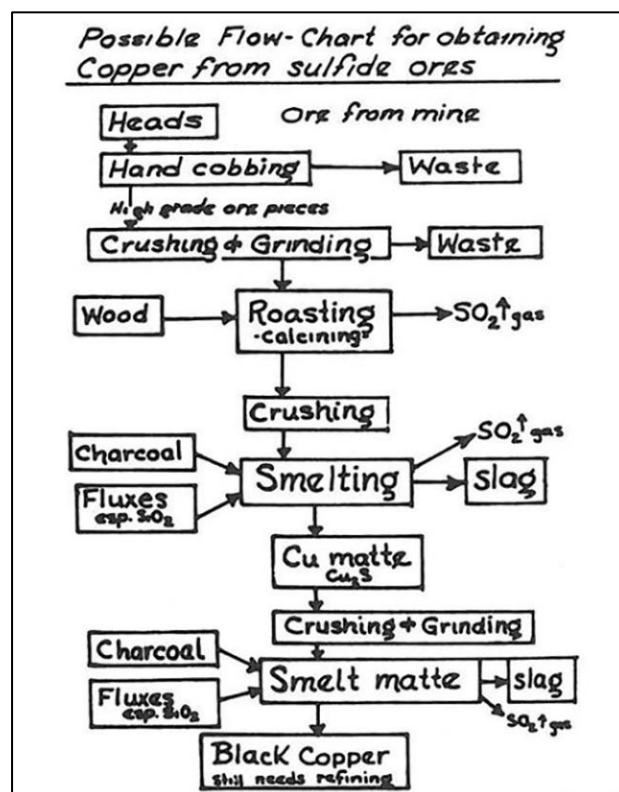


Fig. 7. 1 Flow-chart showing the process to obtain copper from sulphide ores. From Rostoker *et al.*, 1989, p. 70, fig. 1.

Based on these points, the purpose of their study was to test if copper-iron sulphides could be directly reduced to metallic copper in a single stage when combined with copper oxide minerals. To this end they carried out a series of copper smelting experiments mixing together different amounts of malachite ($\text{Cu}_2(\text{CO}_3)(\text{OH})_2$), chalcopyrite (CuFeS_2) and pyrrhotite/troilite (FeS). To increase the reactions' efficiency the charge was covered with crushed slags from previous experiments (Stanley-Smith & Walruff, 1974). The experiments were carried out in a gas-fired pot furnace at a temperature of about 1250°C . The charge was placed in an open crucible placed in turn in a covered bigger one to hinder the combustion gases to react/interact with the charge.

Two types of crucibles were adopted: 1) a fireclay composition with a softening temperature⁵ of 1300° C and 2) a fire composite of graphite and fireclay (plumbago type). Metallic copper was obtained in all the experiments assuming different forms (wires in the matte, copper lumps surrounded by matte at the bottom of the crucible, prills embedded in the slags) according to the length of time the copper was left in the furnace and the temperature reached. Although carried out in a lab environment, these results are extremely important as they empirically proved that co-smelting of oxides/carbonates and sulphides is a viable route to produce metallic copper. The co-smelting carried out **a)** is a one-stage process where the intermediate roasting stage is not required; **b)** there is no need for specific ratios of oxide to sulphide compounds in the initial charge; **c)** - there is no need for a reducing atmosphere (no charcoal required) only wood. **d)** it could be carried out at small scale; **e)** it does not produce slags; and **f)** the only essential condition required was the high temperature. These results allowed the authors to suggest that the transition towards sulphide smelting technologies developed gradually, making unnecessary to hypothesise a “conscious” leap (a “discovery”) towards the sulphide smelting technology.

The question of employing the simplest technology to smelt sulphide-based copper ore at the early stages of metallurgy was also raised and experimented upon by French scholars in the first half of the 2000s. The inquiry was prompted by the discovery of Chalcolithic smelting evidence at Al Claus, in southern France (Tarn-et-Garonne) (Bourgarit et al., 2002), and Cabrières (Hérault), (Bourgarit et al., 2003). At Al Claus, dating back to 2400-2200 BC, researchers found a series of ceramic potsherds with slagged material lining the internal surface. Bourgarit et al. (2002) sought to test whether a one-step extraction process could be used for smelting sulphide ores. Their research involved systematic experimental surveys focusing on temperature, atmosphere, and ore composition, including both field and laboratory copper smelting experiments. This work is significant not only as one of the few experimental studies investigating the earliest phase of copper production in the Chalcolithic/Early Bronze Age, but also as one of the first works comparing field and laboratory experiments.

In their experiments, the researchers fixed certain parameters: **a)** a ceramic pot as reactor; **b)** heat source from above; **c)** sulphide and oxide ore in different combinations as the charge; and **d)** a single-step extraction process. However, other parameters varied between the field and laboratory experiments, with details provided in the table below. The field experiments produced three different products from five configurations tested: 1) “sulphidic slag” or matte, 2) “metallic slag” as a multiphase product of copper sulphide, siliceous glass and metallic

⁵ The softening point is the temperature at which a material softens beyond some arbitrary softness

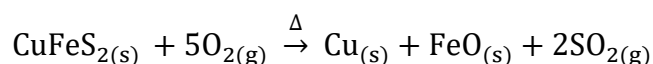
copper, and 3) “oxidic slag” characterised by highly oxidised compounds like delafossite and cuprite.

The results allowed the authors to identify the following points:

- The “metallic slag” (2) closely resembled the archaeological evidence, supporting the feasibility of a one-step extraction process for producing metallic copper.
- The type and amount of product obtained depended on the oxygen introduced into the system, either as “solid oxygen” (O/S ratio – malachite/chalcopryrite – in the initial charge), or as gas (stirring/no stirring).

The laboratory experiments, which focused on temperature and oxygen’s influence, produced similar results to the field experiments. They tested a series of temperatures, ranging from those insufficient to melt the charge (1000 and 1050°C) to temperatures between 1100°C and 1300°C, which yielded similar products. Temperatures exceeding 1250°C, while capable of producing metallic copper, generated products different from the archaeological samples. Regarding oxygen’s impact, the results confirmed that oxygen control was crucial for achieving metallic slag in a one-step process.

The successful production of copper and the presence of slag comparable to the archaeological findings in both field and laboratory experiments, allowed Bourgarit et al. (2002) to validate the efficiency of co-smelting, consistent with the findings of Rostoker et al. (1989). Furthermore, the authors demonstrated that sulphide copper ores (chalcopryrite), within a narrow range of O:S ratios, could be reduced in a one-step process without the need for copper oxide. According to the following formula,



it does not matter if the oxygen comes as solid oxygen or as gas. The critical factor is that oxygen enters the system. Additionally, the researchers showed that charcoal is unnecessary as a reducing agent (CO/CO₂) in the reduction process (see [Hauptmann, 2020, p. 190](#) for a clear explanation of the carbon chemical reactions in the furnace). These results have two significant implications: first, the process could have been conducted in domestic vases (i.e., in an open reactor), and second, a technologically simple one-step process, without the addition of carbonates/oxides, could have been adopted for reducing sulphide minerals. This simplicity, coupled with the relatively low production rates, aligns with the evidence from Chalcolithic sites.

The experimental work by Bourgarit and Mille (1997, 2001) based on the evidence from Cabrières consisted in laboratory and field experiments. The specific aim of the experiments was to try to reproduce the sulphide smelting technology adopted through the comparison of the slags found at the site with those produced experimentally. A summary of the parameters adopted in the experiments is provided in Table 7. 1. A two-stage process was adopted for the field experiment. 2 kg of a ground to ~1 mm-size mixture of chalcopyrite, tetrahedrite, malachite and quartz collected in the area were used as charge. No fluxes were added. They roasted the ore on an open fire for 2 hours. Differently from Al Claus, the smelting reactor was assumed to be a bowl-furnace surrounded by four 30 cm-dolomitic blocks. The smelting process was carried out for 4 hours with the air supplied by a hand-powered bellows. The products were left to cool in the furnace. A series of similarities among the slags were identified. Both batches showed a) μm to mm size prills and Cu-Fe sulphides indicating high viscosity; b) high amount of Ca, which the authors attributed to the dolomitic blocks of the reactor although no archaeological evidence of this type of furnace was found in the area; c) the same oxidation states for copper and iron, probably indicating the same reducing conditions. The main difference was in the crystallisation of the silicates, due to their faster cooling rates, which might have been given by a better thermal insulation in the reactor.

Once tested the feasibility of this method, the authors tried a single-step process. Considering the ores in the Cabrières district, they focused on the co-smelting of sulphides and oxides. They carried out the experiments in the lab in an electric furnace. The changing variables were the charge, i.e., the proportion of solid oxygen in the system (oxides/sulphides, O:S) and the atmosphere, i.e., the oxygen partial pressure ($p\text{O}_{2\text{ext}}$) in the system. As per the charge three different mixtures of 5 g of quartz, dolomite ($\text{CaMg}(\text{CO}_3)_2$), chalcopyrite and malachite were attempted. As per the atmosphere, two different $p\text{O}_{2\text{ext}}$ were tested: 0.21 atm (air stream), and 10^{-3} - 10^{-2} atm. They introduced the charge at 800°C reaching the temperature between 1000-1300°C, at 8°C/min. Each experiment lasted 30 minutes. Three types of products were obtained: Type O – highly oxidised products, mainly cuprite and delafossite with a good amount of metallic copper dispersed in a glassy matrix rich in Ca, Mg and Fe; Type I- intermediate reduced products, mainly iron and calcium rich pyroxenes and spinels with nodules of metallic copper and copper sulphides (Cu_2S); Type R – highly reduced products, mainly matte with fine structures rich in Ca and S, grains of pyrrhothite (FeS) and nodules of metallic copper. Although all the products carried metallic copper, only the Type I showed similarities with the archaeological evidence. These “Intermediate” products were carried out under O/S=1 at 10^{-3} - 10^{-2} atm, and O/S=0 at 0.21 atm. The results allow the authors to assess the feasibility of copper

production with a one-step process through co-smelting. Most importantly, they also observed the analogous roles of gaseous oxygen and solid oxygen on the type of products obtained. However, the experiments did not provide them with information to define the ranges of variation of these two parameters and determine what role exactly each of these two have.

Table 7. 1 details the parameters utilized by Bourgarit and Mille (1997, 2001) in both their laboratory and field experiments.

Parameter	Field experiments	Lab experiments
Reactor	pit in the ground	tubular electrical furnace (temperature and gas measured)
Crucible	refractory feldspar-rich clay ceramic U-shaped domestic pot ($\varnothing_{int}=H_{int}=30\text{cm}$)	U-shaped hand-made kaolinite pot ($\varnothing_{int}=H_{int}=1.5$)
Charge	500g of copper ore and quartz in the amount to balance stoichiometrically the reaction to produce fayalite (Fe_2SiO_4). Chalcopyrite (O/S =0) Chalcopyrite and malachite (O/S =1) Malachite (O/S =0)	similar charges
	Chalcopyrite and malachite: particles from 0.5 to 2 mm in size Quartz: particles less than 0.5 in size	Particles range from 63 to 500 μm
Fuel	Charcoal added to the pot (1 kg – cm-size)	no charcoal added
Temperatures	around 1250°C up to 1300°C (Pt/Pt-Rh thermocouple)	Numerous experiments at 1250°C, range investigated 1000-1300°C
Air supply	human-powered single bellow and a clay tuyère.	
$p\text{O}_2$	Not measured	0.21 atm (air stream) 0.03 atm (mixture air-nitrogen stream) 6.10^{-5} atm (nitrogen stream) ~ 0.1 atm (no gas stream, only gas from the system – SO_2)
Duration	1 hr pre-heating 1 hr experiment	30 minutes in an already hot furnace

This significant technological aspect was discussed almost a decade later by Burger et al. (2010) who proposed a model to estimate the amount of oxidic vs. sulphidic copper in the initial charge. They focused on the provenance of oxygen during the smelting process, which either is provided in its gaseous form by natural or artificial draught ($p\text{O}_2$), or in its solid form by the initial amount of copper oxides in the charge (O:S ratio). They run 50 experiments in a laboratory tubular electronic furnace where they investigated the oxidation state and the

microstructural distribution of iron using a combination of analytical techniques as Mossbauer spectrometry, XANES spectroscopy and electronic microprobe. The initial charge consisted of a total of 3g for each experiment in a combination of powdered chalcopryrite (CuFeS_2), malachite ($\text{Cu}(\text{CO}_3)\text{Cu}(\text{OH})_2$) and quartz (SiO_2). The changing variables were the oxygen partial pressure ($p\text{O}_2$) and the oxygen/sulphur ratio (O:S), i.e., different amounts of powdered materials, from $63\mu\text{m}$ to $500\mu\text{m}$, in the system. From a mineralogical perspective they identified three types of slags: -micrometric droplets of quartz and crystallized zones of fayalite (Type A – high reducing conditions); - Type A microstructures plus polyhedral crystals of magnetite (Type B – intermediate reducing condition); - crystals of copper oxides such as delafossite with addition of cuprite (Type C – most oxidising conditions). They then tested the methodology on archaeological slags. The majority of the slags from the Chalcolithic site of La Capitelle du Broum (Hérault, France) presents, in the melted phases, similar compositions and microstructures to the Type B slags with the only difference of augite-like silicates instead of fayalite. The rest belong to the Type C. Differently, slags from the chalcolithic site of Riparo Gaban correspond to the Type A, whereas the more advance slags from the Early Bronze Age site of Saint-Véran (Hautes Alpes, France) show similarities with the Type B. The authors tried also to investigate the overall distribution of Fe^{2+} and Fe^{3+} according to $p\text{O}_2$ and O:S. However, the application of this method alone to the archaeological slags, given the small amount of data available, can be misleading and, considering all the approximations, provide inaccurate approximate figures of the partial oxygen pressure during the smelting processes. Overall, the study showed how the oxygen in the system, both as solid oxygen (O:S), proven to be the principal source of oxygen, and as gas ($p\text{O}_2$), is fundamental to reconstruct the processes and can be useful to distinguish and compare the production modes of ancient smelting processes.

Moving to the eastern side of the Alps, Martinek (2011) carried out a series of co-smelting experiments based on the findings from the Early Bronze Age site of Buchberg, near Wiesing in the Inn Valley. The aim was to test the feasibility of the co-smelting using local ore. He mixed in different ratios malachite and fahlore ground to $<1\text{mm}$ -size, the latter from Schwaz-Brixlegg, one of the primary sources of carbonate-hosted fahlores in the Inn Valley, Austria. He run the experiments in clay crucibles reaching a temperature up to 1200°C . The outcome was copper metal, copper sulphides, and cuprite (Cu_2O) in different amounts according to the ratios of the raw materials. The ease to produce copper allowed the author to propose this one-step process as the one likely adopted at the beginning of fahlore metallurgy in the Inn Valley. Moreover, he proved that the amount of copper oxides in the initial charge largely affects the amount of fahlore impurities (i.e., As and Sb) in the final metal.

Based on the findings at the Chalcolithic site of Zambujal, in southern Portugal, Hanning et al. (2010) carried out a series of copper smelting experiments exploring the ways in which the smelting of local ores could have been carried out. They conducted a series of trials in which they used high-grade copper ores from five different mining sites in Portugal. They never mixed the ores in the initial charge as the focus of the research was to understand which smelted ore produced the closer match to the archaeological slags. The trials were carried out in open stone-lined structures, whose shape and design were re-thought as the experiments proceeded with the aim of reaching a better copper production rate. The first reactor was a shallow pit slightly dug in the ground with an internal diameter of 70cm. Given the high heat loss, the authors decided to reduce gradually their dimensions reaching at the last experiment a reactor of 25x25cm made of a flat stone at the bottom, 17 cm high stones on three sides, and a 6cm high stone on the fourth side. The ore was crushed to a 5 mm-size and the gangue was removed. No fluxes were added to the charge. The roasting, when necessary, was carried out in a crucible on a wood fire with no forced air draft for a variable time from 20 to 76 minutes. Before each experiment, the reactors were preheated for an hour. The experiments were carried out in flat open shaped clay crucibles similar to the archaeological ones found at a number of sites in south-west of the Iberian Peninsula (Hunt Ortiz, 2003; Nocete, 2004; Sangmeister & Schubart, 1981). The charge was heated from above using bamboo clay-tipped blowpipes powered by human lungs and hand pump. The experiments lasted a variable amount of time between 30 to 120 minutes.

It is beyond of the scope of this study to report the details of each experiment carried out. Overall, all the experiments gave highly heterogeneous and poorly smelted slags matching the archaeological ones on several aspects. The slags were characterised by many unreacted bits, quartz, olivines, pyroxenes, and iron and copper in their oxide phases (e.g., magnetite, hematite, cuprite, delafossite) embedded in a silicate glassy matrix. Pure copper with variable amount of trace elements such as As and Fe was found either in the form of prills in the slags, or at the bottom of the crucible. These results indicated that the process was carried out under similar conditions such as uncontrolled/fluctuating temperatures and poor reducing conditions. Even if all the experiments produced copper and showed a series of features commonly found in the archaeological slags, the ores primarily composed of carbonates and oxides produced higher amount of copper and evidence more similar to the archaeological ones, indicating a more likely source exploited in the past.

To the end of this work, one of the experiments is particularly interesting as it focused on the co-smelting of oxide and sulphide charge collected from Mercês I (P04c). In experiment 14 the

authors identified three layers inside the crucible: - A) slag mixed with the melted ceramic body and finely interspersed copper prills; - B) a grey-silvery shining layer of matte with lamellae of bornite and chalcocite; - C) globules and accumulation of metallic copper, partly mixed with slag (Hanning et al., 2010a, p. 296), (

Fig. 7. 2). The results showed the feasibility of the process. However, it did not show similarities with the chalcolithic samples from the Estremadurian settlements and in other sites of southern Iberia, ruling out the local smelting of this sulphide ore in the past.

While this study is among the few that describes carefully all the steps undertaken from the collection of the ore to the final outcomes, the main limitation is that the authors fail to keep consistent standardised variables through the entire set of experiments (varying amount of initial charge in the crucible, from 100 to 250g, different reactors' shapes, different roasting times, from 20 to 76 minutes and different lengths of the experiments, from 30 to 120 minutes), which hinder their reproducibility.



Fig. 7. 2 In the sectioned crucible three distinct layers were identified: (A) slag mixed with the melted ceramic body and finely interspersed copper prill; (B) a grey-silvery shining layer of matte with lamellae of bornite and chalcocite; (C) globules and accumulation of metallic copper, partly mixed with slag (From Hanning et al., 2010, p. 296, Pl. III. Experiment 14 (ore: Mercês I, P04c). Crucible width: 11 cm).

A series of sulphide ore smelting experiments have been performed based on evidence showing that sulphide ore was already mined during the Beaker/Early Bronze Age periods in a number of locations around the British Isles. Particularly interesting is the experiment carried out by O'Brien and colleagues who managed to successfully smelt tennantite in a one-step process in a Ross Island-type reactor (reported in Timberlake, 2007). The process consisted in the charge being roasted when poured on the top of an oxidising wood fire and then getting reduced when

at the bottom of the reactor covered by embers (Fig. 7. 3). Unfortunately, the details of the experiment are not reported.

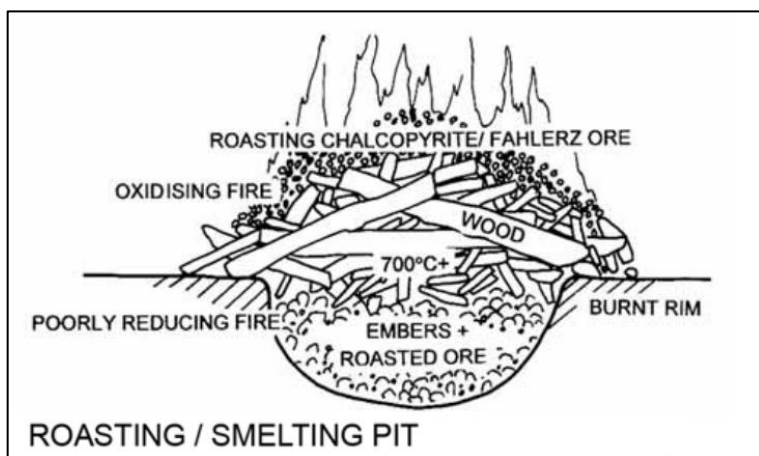


Fig. 7. 3 shows a diagrammatic section through 'Ross Island-type' furnace pit burning wood fuel. Subjected to the intense oxidizing environment of a substantial fire, succeeded by reducing conditions beneath a pile of embers, a notable portion of the copper within such ore may have undergone reduction, transforming into metallic form. (From Timberlake, 2007, p. 33, fig.7c. Drawing: S. Timberlake and B. Craddock).

A chalcopyrite smelting experiment in an open reactor dug into the ground and partially covered with turf was set up by Timberlake at Roewen, North Wales (Timberlake, 2007). Roasting and crucible smelting were carried out. The author produced copper sulphide/copper-iron sulphide matte showing small growths of copper metal. This outcome led Timberlake to suggest that the process of extracting copper from the ore(s) was extremely slow as the copper metal had to be gradually recovered through crushing and selecting (washing and panning) the semi-smelted ore. He argued that the washing residues close to the furnace pits at Ross Island (O'Brien, 2004, pp. 467–470), seem to suggest this recovery stage. However, no slag or copper debris were recovered at the site.

O'Brien performed another smelting experiment with the aim of reproducing the chalcopyrite smelting process of Ross Island using a "Type 1" furnace pit (O'Brien, 2004, p. 467). The experiment, carried out at the Butser Iron Age Farm, consisted in a two-steps process where he roasted gangue-free copper-rich ore using charcoal for a total of 4.30 hours at 750°C, and then smelted it for 2.15 hrs under a thick layer of charcoal. He reached temperatures above 1300°C with an average of 1180°C using hand powered bag bellows. Only a few grams out of the starting 430 g were collected from the bottom of the reactor, mostly in the form of matte with tiny copper cones ("moss copper") grown within the matte gas voids. This low production rate led the author to suggest the gradual recovery of prills after repeated smelts as a potential method to produce metal.

In summary, when examining the technological aspects presented in the literature, it becomes evident that the reduction of sulphide ores, more complex given their polymetallic nature, at the early stages of metallurgy was carried out either through a multi-step process, i.e., considering the intermediate roasting step, or through a one-step process. While the multi-step processes, more efficient from a production standpoint, are well-documented in the archaeological record, especially in the European region from the Middle Bronze Age onward, there remains a significant gap in our understanding regarding the smelting processes employed during the earliest stages of metallurgy. It is commonly agreed among scholars that during these early stages of metallurgy, the processes employed must have been as simple as possible. Consequently, there is a quest for a technologically straightforward extraction method that relies on a single step and demands minimal energy, considering that the oxidation of copper and iron is exothermic in nature.

7.4. Development of thesis experiments: sulphide ore smelting in Early Metallurgy

The site of Orti Bottagone stands as one of the oldest pieces of evidence for copper smelting activities in Europe and is among the few known examples in Italy. Notably, it provides evidence of smelting of sulphide ores and of an advanced (good production rates) although still immature slagging process characterised by fluctuating temperatures and unstable redox conditions. The increased evidence of Chalcolithic sites in Europe and Middle East (Artioli *et al.*, 2015; Thornton, 2009) with sulphide ore exploitation (see Chapter 3) led to question the linear evolution of prehistoric metallurgy. It was long believed that metal technology would have developed from working native copper in the Neolithic, followed by the small-scale smelting of copper oxide ores in the Chalcolithic and the large-scale reduction of copper sulphides in the Bronze Age (P. T. Craddock, 2000). This new batch of evidence has raised one of the largely discussed topic among archaeometallurgists: how was the smelting of sulphide ores carried out at the early stages of metallurgy? Among scholars, two techniques are agreed upon to have been used for smelting sulphides: a one-step process involving the co-smelting of carbonates/oxides and sulphides and a multi-step process involving the intermediate roasting step.

Concerning co-smelting many authors believe that it was the most likely one-step technology first deployed to reduce sulphides in prehistoric Europe (Rostoker *et al.*, 1989; Bourgarit, 2007; Hanning *et al.*, 2010; Killick, 2014; Dolfini *et al.*, 2020). Firstly because, from a chemical perspective, co-smelting of sulphides and oxides could replace the intermediate second-step

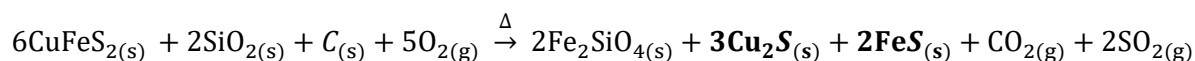
roasting process. Secondly because, from a geological perspective, the world's ore bodies are characterised by a systematic heterogeneity of secondary (weathered) and primary minerals (see Section 2.4) which would have made likely that part of the secondary minerals exploited at the earliest stages of metallurgy incorporate cores of sulphide minerals. The deeper ancient craftpeople mined, the higher was the probability to collect sulphide minerals and then mix them in the charge. However, according to Rostoker et al. (1989), co-smelting does not produce coarse and flat types of slags, which instead have been identified in the current research. These particular slags are often associated with more advanced smelting technologies that involve two separate steps: slagging and matting. Conversely, Piel et al. and Mettel argue that both type of slags could be the results of one single smelting process and be found together in the reactor (Metten, 2003; Piel et al., 1992).

Regarding the second technique, several important considerations need to be kept in mind:

- a) It is essential to note that the site under study is one of the oldest in Europe exhibiting evidence of sulphide ore smelting. This advanced technology does not align with the assumed one-step process associated with the early stages of smelting technology. Scholars, as mentioned in the literature reviews (see Chapter 3 and Chapter 7), argue that metallurgical practices in the early stages of metallurgy must have been as simple as possible.
- b) The scarcity of roasting beds from this particular period suggests the possibility of a one-step process being employed.
- c) It is worth noting that the local ore likely used in the smelting process contains relatively high amounts of calcium and silica gangue. These components could have acted as self-fluxing agents, thereby facilitating the smelting process in a single step.
- d) Experimental evidence, provided by Bourgarit et al. (2002), demonstrates the effective reduction of sulphide ore in a one-step process without the presence of copper oxide.

From these premises, the experiments consist in the reconstruction of the smelting process carried out at Orti Bottagone. The primary hypothesis under investigation is whether the local ore is suitable for the smelting of sulphide ore without the addition of carbonates/oxides, or the deliberate addition of fluxes in a one-step process, eliminating the need for the intermediate roasting process. Two series of experiments have been performed, one with a partially roasted initial charge and another with an unroasted initial charge. The aim is to determine which experimental series yields slags that closely resemble the archaeological samples.

The tested process follows the simplified formula:



During the reaction, the sulphide ore (CuFeS_2) combines with silica (SiO_2), charcoal (C) and oxygen (O_2). The heat and chemical reactions involved in the smelting process led to the formation of iron silicate (Fe_2SiO_4), copper sulphide (Cu_2S), iron silphide (FeS) as solid products, and release as gases carbon dioxide (CO_2) and sulphur dioxide (SO_2).

It is important to note that this description is based on the simplified formula provided, and the actual reaction in a real smelting process may involve additional complexities and variations depending on the specific conditions and compositions of the ore being smelted. The experiments conducted do not aim to determine the copper production rate but rather to test the feasibility of the one step-process hypothesis.

In addition, the pilot experiments led to the identification of an additional research question. What I wanted to address was if the experiments could be carried out without the aid of a crucible. Instead, to prevent any loss of copper sinking, the bottom of the reactor was covered with a layer of fine-grained charcoal. The hypothesis of a non-crucible smelting process is supported by the scarce evidence of crucibles in the archaeological record, matter of ongoing discussion among scholars, the results of the pilot experiment (see Chapter 6), and by a series of experimental works (Fasnacht, 1999; Hanning *et al.*, 2010b; Timberlake, 2018). Moreover, evidence of this method is provided by the ethnographic report of the so-called “Himalayan model” carried out at Sikkim, in Okharbot, western Nepal, where the use of a crucible was replaced by the covering of the bottom of the furnace with a bed of thoroughly crushed charcoal (Anfinset, 2001; Blanford, 1861; Pearce et al., 2022).

In the next chapter, my primary focus will be on establishing the analytical protocol for the experiments. I will provide a detailed account of the analytical protocol, materials, and procedures to ensure that future researchers can faithfully replicate my experiments.

Following this I will critically present the results derived from the analyses of the experimental by-products. These results, in conjunction with the archaeological results discussed in Chapter 5, will form the basis of the subsequent discussion and conclusions.

Chapter 8. Experimental archaeometallurgy II: Experimental copper smelting

8.1. Introduction

In the first part of the chapter, I define the experimental approach and analytical protocol that I have deployed to my copper smelting tests. I discuss, in particular, the fixed and changing parameters that I have applied to the tests, drawing upon archaeological, experimental, and ethnographic evidence. I present analytical protocol, materials, and procedures in detail to enable future researchers to fully reproduce my experiments. The second part of the chapter offers a detailed overview of the results. By utilising the same analytical protocol employed for the analysis of the slags from Orti Bottagone, I present the findings following the same structure as Chapter 5.

8.2. Experimental protocol

I designed two sets of experiments as in Fig. 8. 1. Experiment #1 (Phase 1A and 2A) involved using unroasted charge, while experiment 2 (1B and 2B) involved the use of charge previously roasted on an open fire for about 8 hours at an average temperature of c. 600°C. Each experiment is divided into two distinct phases, and within each phase, there are three individual trials (T1, T2, T3). With the term “trial” I denote the repetition of the same experiment.

I carried out each trial using 0.5 kg of nutshell-size sulphide ore. I roasted the charge following the same protocol adopted for the first pilot experiment (see Section 6.3.2). 1.5kg of nutshell-size pieces of ore was placed on the roasting bed (the same used for the pilot experiments). The circular roasting bed was warmed up for half an hour and the roasting lasted 8 hours at an average temperature of c. 700°C. Many pieces of the ore broke into mm-size fragments making the collection time-consuming. It took 3 hours to collect all the visible fragments, while many sand-size fragments were left behind. However, a total of 0.9 kg of roasted ore was collected and most of the pieces showed a good roasted colour (see section on pilot experiment). The charge was a mixture of a selection of the most copper bearing fragments from the mines of Temperino and Lanzi (see next section). In each trial the charge was poured on the top of the charcoal.

The experiment's initial plan, as depicted in Fig. 8. 2, aimed to include 18 trials. However, after conducting the first two trials, I realized that the planned series was unfeasible due to insufficient material outcome from each trial. As a result, I made the necessary adjustment to the original plan reducing the number of trials from 18 to 12. I made this decision in response to the practical constraint of limited material outcome from each trial. By reducing the number of trials, I ensured that enough material for the subsequent Phase 2 trials, allowing for effective experimentation.

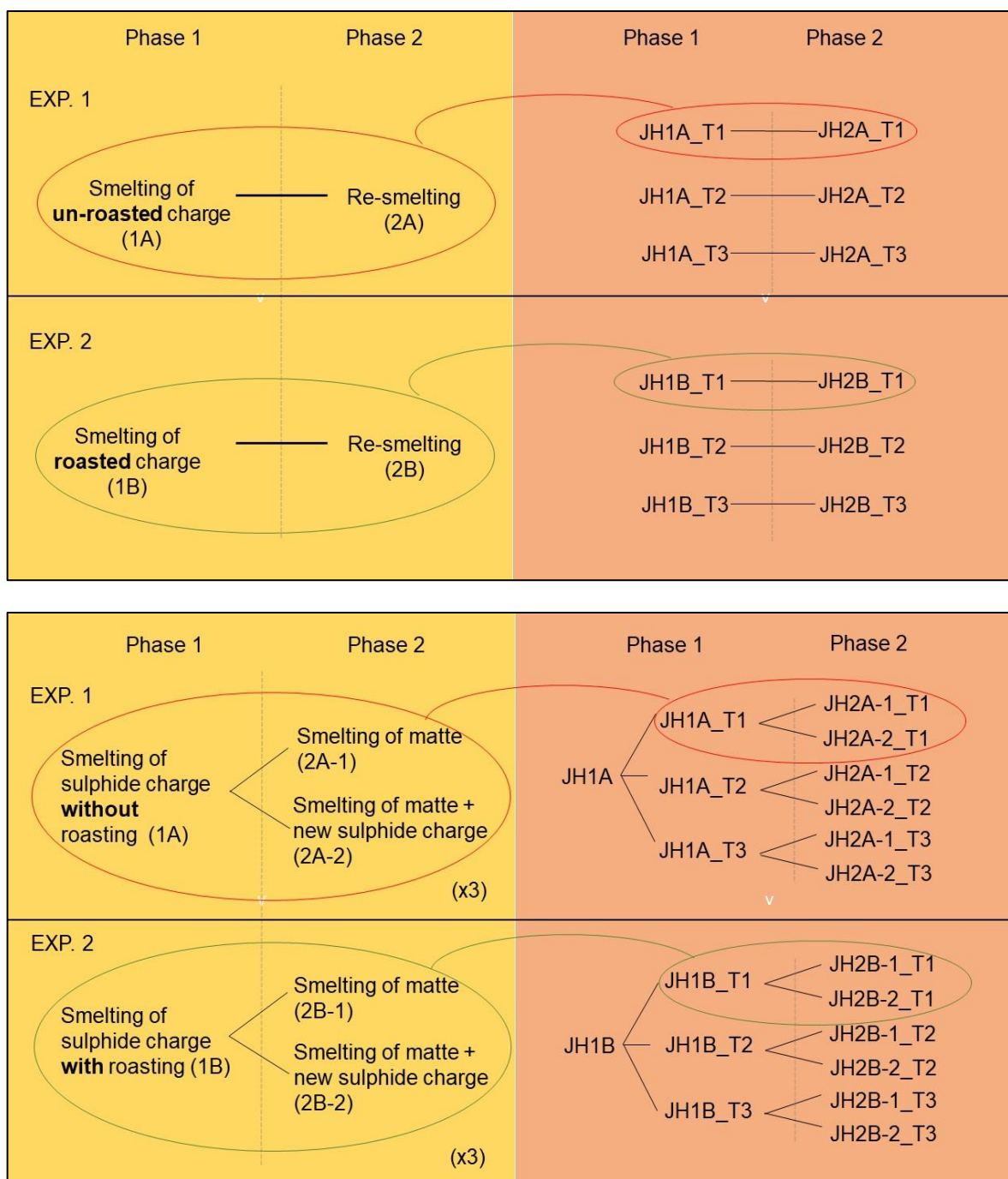


Fig. 8. 1 (above) illustrates the readjusted experimental plan, reducing the number of trials from 18 to 12 after realizing the unfeasibility of the initial arrangement.

Fig. 8. 2 (below) represents the original experimental plan.

JH stands for Jarrow Hall, which is the location where all the experiments took place (see chapter 7 for details). The letter A refers to the trials of experiment 1, while the letter B refers to the trials of experiment 2. “T” stands for “Trial” denoting the repetition of the same experiment).

With “Phase” (e.g., 1A) I mean the sum of the 3 trials (T1, T2, T3)

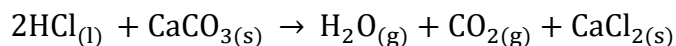
8.3. Ore collection and beneficiation

In June 2022, I personally collected the raw minerals for the experiments from the mining area of Campiglia Marittima. As discussed in the previous chapter, based on the mineralogical composition of the slags and its vicinity to the site, I assumed to be the most likely mining area exploited by Orti Bottagone smelters. Unfortunately, no evidence of prehistoric mining has been found in the area, primarily due to ongoing mining activities. The mine of Temperino, the last metallic mine, closed in 1976. Currently, the area is just exploited for carbonatic rocks. However, Manasse et al. (2001), whose research provided evidence of extensive mining activities in the Colline Metallifere district dating back to the 8th century BC primarily related to the significant concentration of Cu-Ag-Pb sulphides, suggested that even older dates cannot be ruled out for lower levels.

I spent three days surveying the Archaeological-Mineral Park of San Silvestro looking for the right ore. I gathered the material from the mining areas of Temperino and Lanzi⁶. I explored abandoned mining chambers’ walls and ancient tunnels, as well as outcrop areas of high-grade metallic ore bodies (Fig. 8. 3 shows the mining areas explored where I collected the raw material for the experiments of this research: a) weathered material in an abandoned ancient tunnel of Lanzi mine, and b) an outcrop area of relatively high-grade leftovers of metallic ore bodies and c) the weathered growth in Temperino mine area (photos taken by the author).). I carried out the selection of the mineral based on my ability to recognise the copper-bearing compounds, i.e., mainly by colour and crystal shapes. When necessary, I run tests with hydrochloric acid (HCl) to determine whether the gangue contained calcium carbonate and/or silica⁷. The aim was to select primarily ore with quartz inclusions as the bulk chemical analyses carried out on the Orti Bottagone slags showed a high presence of quartz in the coarse slags (see Section 5.2.7). I poured few drops of a dilute solution of HCl (5% concentration) with water on a small area of the unknown sample ore. Hydrochloric acid

⁶ Special thanks go to Thomas Rosi without whom I would have never been able to find the right spots from which to collect the ore.

reacts with carbonates (here calcium carbonate, CaCO_3) to produce carbon dioxide (CO_2) gas, calcium chloride (CaCl_2) and water (H_2O) according to the following balanced formula:



If the compound contains calcium carbonate an effervescent reaction, with the formation of gas bubbles will be observed. If, instead, the compound contains silica, there will be no significant observable reactions with HCl. Silica is resistant to acid attack and remains unaffected by HCl.

The west-central Italian peninsula is renowned for its diverse range of ore deposits, spanning from eastern Liguria and the Appennines in the north to Upper Latium in the south, and extending eastwards to the hinterland of Arezzo (Table 8. 1 Principal copper-bearing deposits of Central Italy (revised from Dolfini et al., 2020, p. 13, Table 3).). Among these deposits, the Campiglia Marittima area stands out as one of Central Italy's principal copper-bearing regions and is considered one of the most important mining district on the Italian peninsula (Lazzarotto et al., 2003). Located in the southern region of Tuscany, Campiglia Marittima hosts abundant mineral deposits rich in chalcopyrite, bornite, chalcocite and tennantite, alongside various other copper-bearing compounds (Tanelli, 1983; Dini et al., 2013; Dini & Boschi, 2017; Tanelli & Lattanzi, 1986).

The area is primarily characterised by skarn deposits which are deposits composed of calc-silicate minerals rich in calcium, magnesium, iron, manganese, aluminium and quartz geologically formed through the metasomatic interaction between hydrothermal fluids and carbonate-rich rocks (Manasse *et al.*, 2001; Meinert *et al.*, 2005). These deposits exhibit diverse polymetallic sulphides (Cu-Pb-Zn-Ag±Au) encompassing a wide range of primary ores, predominantly chalcopyrite, magnetite, sphalerite, pyrrhotite and silver-bearing galena. Chalcopyrite is usually associated with hedenbergite gangue ($\text{CaFe}^{+2}\text{Si}_2\text{O}_6$), (Capitani & Mellini, 2000), while galena and sphalerite minerals are associated with johannesite gangue ($\text{CaMn}^{+2}\text{Si}_2\text{O}_6$) (Manasse *et al.*, 2001). This mineral association facilitates the segregation of the sulphides from each other.

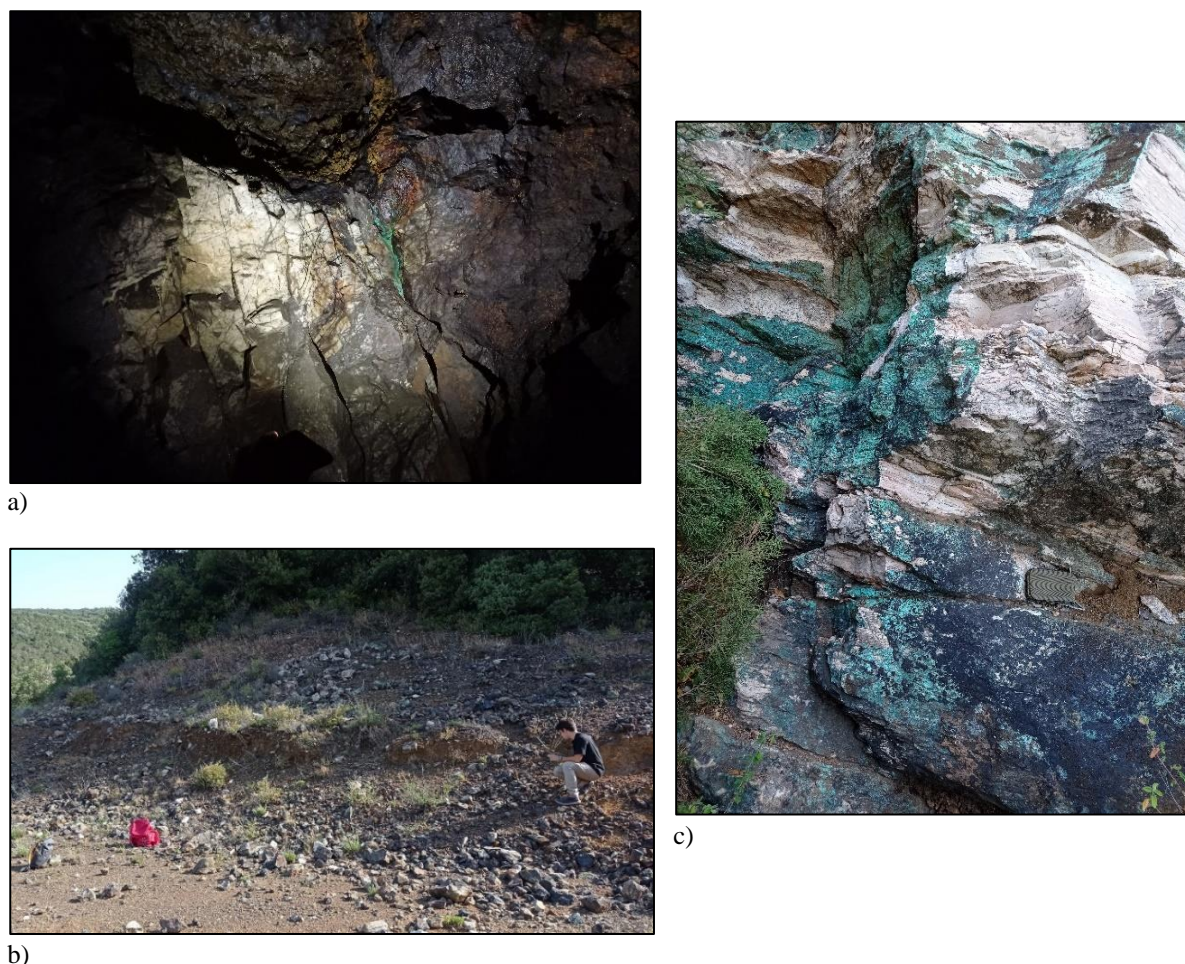


Fig. 8. 3 shows the mining areas explored where I collected the raw material for the experiments of this research: a) weathered material in an abandoned ancient tunnel of Lanzi mine, and b) an outcrop area of relatively high-grade leftovers of metallic ore bodies and c) the weathered growth in Temperino mine area (photos taken by the author).

Additionally, there are smaller quantities of pyrite, hematite and other trace amounts of sulphide minerals as documented by Tanelli & Benvenuti (1998) and Dini *et al.* (2013). Furthermore, the area contains enriched copper-bearing secondary minerals such as cuprite, malachite, azurite, aurichalcite, brochantite, antlerite, chalcantite, chrysocolla, alongside documented occurrences of native copper (Tanelli & Benvenuti, 1998). More specifically, between Temperino valley and Ortaccio valley, the predominant mineralisations consist of Cu-Fe (Pb-Zn-Ag), whereas in the valleys of Lanzi and Manienti, the mineralisations are primarily characterised by Pb and Zn, and the Lanzi mine exhibits skarn formations of hedenbergite with sulphurs of Pb and Zn (galena and sphalerite), (Da Mommio *et al.*, 2010; Dini *et al.*, 2013). The primary mineralisation has undergone considerable alteration due to the interaction of meteoric water with sulphides and silicates. The skarns and the carbonatic rocks are crossed by deep vertical fractures which allowed the secondary transformation/alteration of substantial portions of surface mining bodies. Supergene enrichment of skarn bodies with hedenbergite-ilvaite and

sulphides has occurred particularly in outcropping areas with high metal contents, on the walls of ancient mineshafts or in fractured areas between mineral bodies. Meteoric water played a crucial role in triggering supergene enrichment in the Temperino-Lanzi orebodies, further shaping the mineralisation in the Campiglia Marittima area.

Table 8. 1 Principal copper-bearing deposits of Central Italy (revised from Dolfini et al., 2020, p. 13, Table 3).

Geological formation	Area	Main mines/ore bodies	Ore group
Inner Ligurides (Jurassic ophiolites embedded in Jurassic-Cretaceous sediments)	Ligurian Apennines	Libiola, Monte Loreto, Reppia	Ligurian Apennines
Outer Ligurides (Jurassic ophiolites embedded in Cretaceous turbidites)	Tusco-Emilian Apennines	Corchia, Boccassuolo, Val di Secchia, Vigonzano, Impruneta	Ligurian Apennines
Inner Ligurides–Tuscanian Units (Jurassic ophiolites embedded in Jurassic-Cretaceous sediments)	Ophiolites of the Tuscanian Units	Montecatini-Val di Cecina, Impruneta	Ligurian Apennines
Outer Ligurides–Umbro-Marches Units (Jurassic ophiolites embedded in the sediments and carbonates of the Adriatic margin)	Ophiolites of the Umbro-Marches Units	Monti Rognosi, Arezzo, Anghiari	Ligurian Apennines
Apuanian metamorphic unit (Triassic orogeny overprinted by Apennine orogeny with peak metamorphism 15–20 My ago)	Apuanian Alps (northwest Tuscany)	Bottino, Pollone, Monte Arsiccio	Apuanian Alps
Tuscanian Domain (Ophiolitic s in Mid-Tertiary Tuscan Nappe)	Colline Metallifere, Campigliese, Grossetano (central-southern Tuscany)	Boccheggiano, Campiano, Campiglia Marittima, Temperino, Lanzi	Southern Tuscany
Tuscanian Domain (Ophiolitic s in Mid-Tertiary Tuscan Nappe)	Elba Island	Vallone, Capo Calamita, Santa Lucia, Sant’Andrea	Southern Tuscany
Tuscanian Domain–Tertiary magmatism (Magmatism and metamorphism of Eocene sediments related to the plutonic complex)	Massetano (southern Tuscany)	La Pesta, Fenice Capanne	Southern Tuscany

To carry out the experiments, I collected: 5.11 kg of ore from the Temperino mine. The batch was mainly characterised by chalcopyrite with traces of copper carbonates and chrysocolla; other 10 kg of material from the same mine, but from a different vein. However, I soon realised that this vein was mainly composed of galena (PbS) with tiny inclusions of copper bearing compounds (mainly chalcopyrite). Considering the very small percentage of lead found in the slags, I decided to stop the selection/beneficiation of this batch (Temperino (location 2) as it would have not provided a useful comparison (Ambert et al., 2013). The material from this batch was discarded and not used for any of the following experiments. I also collected 6.70 kg of ore from the Lanzi mine. Compared to the previous batch it is characterised by a higher

presence of gangue mainly in the form of quartz (see Table 8. 2 for an overview of the amount of material collected and beneficiated).

After the collection, I ascended to the top of Monte Campiglia Vecchia, the highest point in the area, to conduct a comprehensive survey of the landscape and gain a better understanding of the surrounding territory. In the accompanying Fig. 8. 4a, a panoramic 180° view of the territory taken from the top of Monte Campiglia Vecchia is presented. Within the image, the blue arrow indicates the location of the nearest mines in the Campiglia Marittima area where the ore for the experiments was collected. As for the red arrow, it points to the coastal site of Orti Bottagone. Notably, the distance between these two locations measures approximately 14-15 km, which would necessitate approximately 3 hours of slow walking to traverse (Fig. 8. 4b). One of the questions that emerged during the survey was to comprehend the reason(s) behind conducting smelting operations not in the mining area. A number of factors need to be considered.

Among the technological factors, the most likely explanation is that the coastal area had access to suitable sources of water necessary for cooling the smelting process and to prevent the risk of accidental fire. Regarding social reasons, since metallurgy was in its early stages, metal goods might have been considered valuable and required a safe environment to produce such precious items, hidden from potential competitors or adversaries. Furthermore, it is important to note that metalworking was a specialized skill, and individuals skilled in smelting may not have been the same ones engaged in mining activities. This division of labor could have contributed to the establishment of dedicated smelting sites in coastal areas. Another possible social reason for choosing a coastal site is its accessibility to trade routes. Being located on coast might have facilitated the distribution and exchange of metal goods with other communities, fostering trade networks and economic development.

Unfortunately, due to the limited knowledge of the prehistory of the territory, definitive reasons for this choice remain challenging to ascertain.



a)

Fig. 8. 4 a) Panoramic view of the landscape of Campiglia Marittima from the top of Monte Campiglia Vecchia, the highest point in the area; b) map showing the distance the mining areas of Temperino and Lanzi from the site of Orti Bottagone.



b)

The beneficiation procedure involved meticulous hand-crushing and hand-sorting. To initiate the ore beneficiation process, I transported the three distinct batches back to my home understanding it would be a slow and time-consuming operation. The labor-intensive process required the collaborative efforts of two individuals over a span of six hours, ultimately yielding a total of 4.61 kg of raw charge. The crushing was carried out on a steel flat plaster, initially using a river cobblestone and then, as the task became strenuous, a modern hammer. Considering the bulk chemistry of the slags (see Section 5.2.5) the gangue was only partly removed. Fragments of gangue were left in the selected charge as it was impossible to fully remove it. An overview of the types of ore adopted for the experiments is provided in Fig. 8. 5. Subsequently, I brought the beneficiated raw charge from Italy to the Jarrow Hall open-air museum, South Tyneside, UK, where I conducted the proper experiments for my thesis.

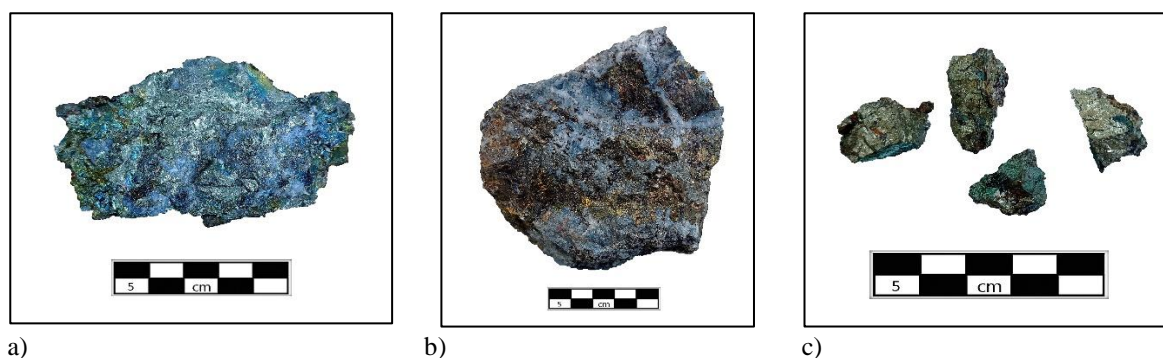


Fig. 8. 5 Selection of the different types of ore adopted for the experiments from the mines of Temperino and Lanzi.

Table 8. 2 shows an overview of the amount of material collected before and after the beneficiation process from three different locations. I stopped the selection/beneficiation of the batch from Temperino (location 2) for its high amount of lead which would have not provided a useful comparison. This batch was not used for any of the following experiments (*).

Mine	Date	Weight before beneficiation (kg)	Weight after beneficiation (kg)
Temperino (location 1)	20/06/2022	5.11	2.33
Lanzi		6.70	1.48
Temperino (location 2)		10	0.80*

8.4. Fixed parameters

Since the experiments were carried out in the field, in an open system, to reduce to a minimum the variability in the experiments, the following parameters were kept fixed for each trial:

Reactor. Although Bourgarit (2007) claimed that the reactor design may not be a “crucial parameter”, as the slags displayed similar characteristics regardless of the reactor shapes they were obtained from, it is worth noting that all the experiments in this study were conducted using the same reactor. Due to the lack of excavations at the site, the specific designs of the reactors at Orti Bottagone remains unknown. To address this gap, I decided to rely on evidence from a well-known Chalcolithic smelting site, La Capitelle du Broum (Ambert et al., 2013), which provided valuable data for my reconstruction. At La Capitelle, the smelting reactors were shallow oval cuvettes (or basins) measuring approximately 40 cm in length and 15-20 cm in depth, covered with a layer of yellow clay, whose thickness was between 2 and 5 cm (see chapter 2 for more context). Based on this evidence, I built an open, oval-shape structure with the exact same dimensions: 40 cm of length, 15-20 cm of depth and 4-5 cm of clay lining thickness. I built the reactor 2 days before running the first experiment and the day before I dried it out for few hours. Cracks were filled minutes before starting the experiment.

Air supply. Hand-powered bellows with a bag dimension of 50x50 cm were adopted. Hand-powered bellows were also used at Cabrieres (Bourgarit & Mille, 1997, 2001). The air was conveyed in the reactor from above. Bamboo reeds were attached to the bellows, and ceramic tips were placed at the reeds' end close to the reactor to protect them against heat. Unlike the pilot experiments described in Section 6.4, I placed the pipes channelling the air in the reactor close to each other instead of on opposite sides. Since I carried out the experiments during the global outbreak of Covid-19 (2020-2022), I wanted to reduce to a minimum the number of people involved in the experiments. Therefore, only one person at a time activated the bellows. A different person for each trial (30 minutes long) was considered. It is worth saying that these persons had been trained in how to alternatively run the bellows (to keep constant the air flow in the reactor) during the pilot experiments' week.

Fuel. I used charcoal in cm-size pieces as fuel. The dimension of the pieces was to fill the voids inside the reactor in order to create a sufficient reducing environment. I carefully reported the amount of charcoal used and the moment in which I added it to the reactor. Unfortunately, very few studies have been carried out on the subject. It is assumed that charcoal was used in the past rather than wood (Timberlake, 2007), although previous experiments (Bourgarit et al., 2003; Fasnacht, 2009; Hanning, 2012; Rostoker et al., 1989) and historical records (Morgan, 1867) show that dried wood could have also been used as fuel in the smelting process (see also Hauptmann, 2020, pp. 190–192, for an explanation of the carbon (C) chemical reactions in the furnace).

Temperature. I kept the temperature in the range of 1000-1200°C (see Hauptmann 2020 and earlier references therein). I placed a thermocouple in the reactor close to the heat source and I recorded the temperatures every 2 minutes. It is worth pointing out that the recorded temperatures are only indicative of the real temperatures developed in the reactor: first because only one thermocouple was placed recording only a specific area of the reactor, when instead different temperature gradients are present (Fig. 8. 6); second because during the trials the thermocouple moved and had to be relocated a number of times as they showed very low temperatures probably when close to a still unburned charcoal piece (see temperature section below); third, because the liquid charge can embed the thermocouple and hinders the recordings (Fig. 8. 7). Nevertheless, I recorded the temperatures to maintain coherence and consistency across the trials, as this would help to eliminate temperature variability as a potential reason for unsuccessful smelting.

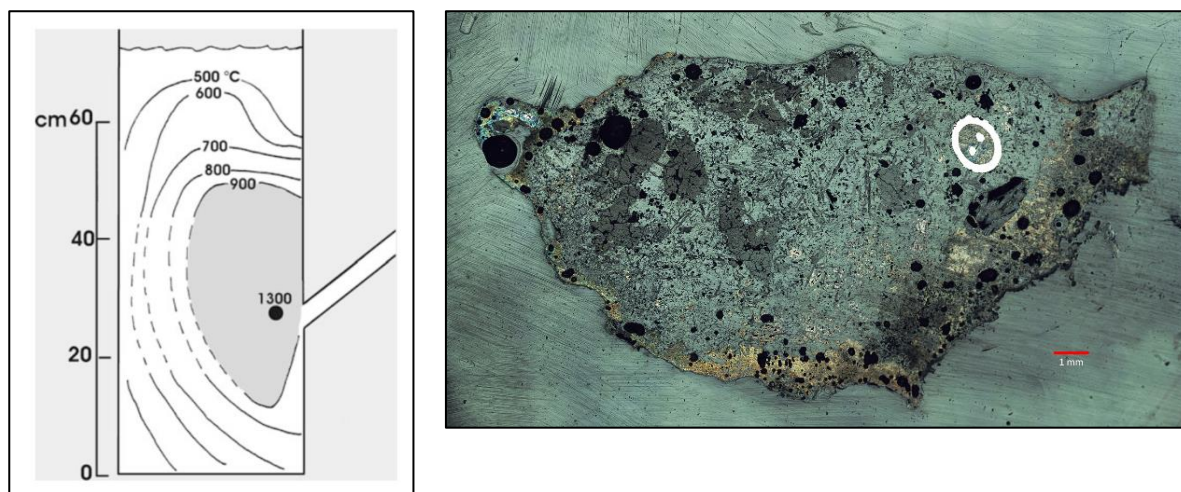


Fig. 8. 6 Temperature gradients inside an experimental furnace. The further from the point where oxygen enters, the lower the temperature. After Tylecote and Boydell, 1978.

Fig. 8. 7 Thermocouple trapped in the liquid slag (sample JH1B_T2-002).

Reactor warm-up and experiment duration. The reactor was warmed up at the beginning of each experimental phase for 40-50 minutes with an open fire with the aid of bellows. Pilot experiments showed that after the reactor is warmed up for the best part of an hour, 30 minutes are more than enough to smelt small amount of charge (0.5 kg). Each experiment lasted 30 minutes.

Slag recovery. Given that the morphology of some slags' mineralogical compounds is determined by the cooling rates, the slags and by-products were collected after 5 to 7 minutes at the end of each experiment.

The first 2 experimental series (1 series = 3 trials) were carried out in similar atmospheric conditions, whereas in the last two the weather was colder a little more humid and windier than previously (Table 8. 3). Nevertheless, the necessary temperature was easily reached, and the trials carried out.

Table 8. 3 Overview of weather conditions during the experiments.

Experiment series	Date	Temp. °C	Humidity	Rain	Wind
JH1A	11/07/2022	24	~58-60%	N	N
JH1B	18/07/2022	26	~57-59%	N	N
JH2A	24/07/2022	23	~65-67%	N	Y
JH2B	06/08/2022	17	~68-70%	N	Y

8.5. General observations

I decided to report the analytical results by phase and not by Experiment for a better comparison and comprehension. A summary of the trials' results divided by phase is provided in Table 8. 4 below.

8.5.1. Phase I

- Experiment#1. JH1A (T1, T2, T3) – unroasted charge.

The first series of experiments (1A) aimed at smelting an un-roasted sulphide charge. The JH1A trials gave respectively a total weight of 0.152 kg (JH1A_T1), 0.120 kg (JH1A_T2) and 0.297 kg (JH1A_T3). Except for few pieces probably fallen in the back of the reactor far from the heat source, the charge of each trial reacted. Common to the three trials was a strong smell of sulphur, noticed for the entire duration of the trials, and the yellow tinge of parts of the charcoal, likely given by the release of sulphur. The reactor's wall showed an increasing thermal alteration close to the air supply. The bed of ground charcoal at the bottom of the reactor where the charge solidified remained unreacted for all the trials. Green flames were only observed in T2, mainly during the first part of the trial. In T1 and T2, part of the charge was found liquified at the bottom of the reactor above the layer of ground charcoal, while another part had to be removed from the reactor's wall between the tuyeres. In T3, to prevent the material loss on the reactor's wall during T1 and T2, more ground charcoal was placed at the bottom of the reactor and the charge was poured into the fire further away from the reactor's wall. These solutions allowed to recover almost 60% of the initial charge. Differently from T1 and T2, less charcoal was used as the furnace was already warm from the previous trials.

- Experiment#2. JH1B (T1, T2, T3) – partially roasted charge.

The second experimental series (1B) aimed at smelting a roasted sulphide charge. The JH1B trials gave respectively a total weight of 0.122 kg (JH1B_T1), 0.230 kg (JH1B_T2) and 0.160 kg (JH1B_T3). The charge reacted in all trials. Both the smell of sulphur and green flames were still present although in lower amounts. The charcoal did not assume a yellow tinge. The ground charcoal at the bottom remained unreacted for the entire experimental series. An example of the products recovered during this phase (trial JH1B_T2) is provided in Fig. 8. 8a. The fragments exhibit matte-like appearance accompanied by a shiny metallic glare. Their shape is the result of solidification upon contact with the ground charcoal at the bottom of the reactor. Except for the trial JH1A_T3 which returned 59.4% of the initial charge the quantity of metal produced within these incomplete smelting trials was only ca. 1/5 of an initial charge of 0.5 kg.

8.5.2. Phase II

- Experiment#1. JH2A – re-smelting of unroasted charge.

The third experimental series (2A) consisted in the re-smelting of the un-roasted sulphide charge obtain from the first series (1A). The JH2A trials gave respectively a total weight of 0.184kg (JH2A_T1), 0.130 kg (JH2A_T2) and 0.183 kg (JH2A_T3). The charge in all trials reacted. Despite in lower amount, the smell of sulphur and green flames was still present. The charcoal remained devoid of any yellow tinge. The ground charcoal layer at the bottom of the reactor remained unaltered. Matte-like products with non-reflective surface similar in shape and composition to those collected from phase 1 trials were recovered (Fig. 8. 8 displays two matte-like products recovered from trials JH1B_T2 (a) and JH2A_T3 (b). The pictures were generously provided by Sam, a volunteer at Jarrow Hall open-air museum in South Tyneside.

- Experiment#2. JH2B – re-smelting of partially roasted charge.

The fourth experimental series (2B) consisted in the re-smelting of the roasted sulphide charge obtain from the second series (2B). The JH2B trials gave respectively a total weight of 0.130 kg (JH2B_T1), 0.128 kg (JH2B_T2) and 0.105 kg (JH2B_T3). For this final experimental series, I re-built and dried the reactor a few hours prior to conducting the trials. Despite the temperature being adequately high, only a portion of the charge underwent transformation, likely attributed to the tuyères being improperly positioned. No green flames, smell of sulphur or traces of yellow tinge on the charcoal were observed.

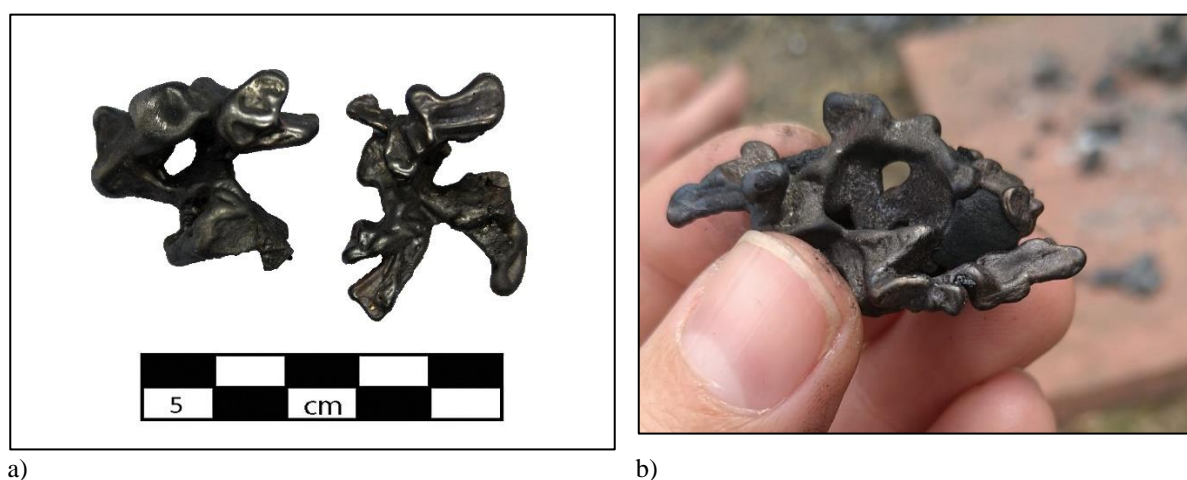


Fig. 8. 8 displays two matte-like products recovered from trials JH1B_T2 (a) and JH2A_T3 (b). The pictures were generously provided by Sam, a volunteer at Jarrow Hall open-air museum in South Tyneside.

Table 8. 4 Summary of the results of the trials divided by phase.

Initial charge (kg)	Trial	Final charge (kg)*	%	Av. Temp (°C)	Initial charge (kg)	Trial	Final charge (kg)	Av. Temp (°C)	%
Phase 1**					Phase 2				
0.5	JH1A_T1	0.152	30.4	1007	0.272	JH2A_T1	0.184	1086	67.6
0.5	JH1A_T2	0.120	24	1020					
0.5	JH1A_T3	0.297	59.4	1024	0.297	JH2A_T2	0.130***	1038	43.8
/	JH1A_T1-T2-T3 (reactor's wall)	0.207 (after removing the reactor wall)		/	0.207	JH2A_T3	0.183	1034	88.4
0.5	JH1B_T1	0.122	24.4	1044	0.167	JH2B_T1	0.130****	1001	77.8
0.5	JH1B_T2	0.230	46	1059	0.230	JH2B_T2	0.128	1006	55.6
0.5	JH1B_T3	0.160	32	1050	0.205	JH2B_T3	0.105****	998	51.2
/	JH1B_T1-T2-T3 (reactor's wall)	0.90 (after removing the reactor wall)		/					

8.6. The physical chemistry and mineralogy of the experimental by-products: analytical results

Based on the observable properties two types of by-products were identified: slags and matte. Among them, I collected 22 samples for further investigations: 13 slag and 9 matte fragments. Matte is a dense and dark-coloured substance, also named black copper (Valciukas, 1984), that is usually composed of copper-iron sulphide phases in any metal proportion from chalcopyrite (CuFeS_2), covellite (CuS), digenite (Cu_9S_5) to chalcocite (Cu_2S), (Rostoker et al., 1989). It is distinct from the slags, and it requires further refining to extract the desired metals.

Due to their small dimensions the slags could not be sorted by naked eye in the commonly adopted coarse and flat categories. However, under the optical and electron microscopes it was possible to identify mineralogical features and morphologies characteristic of one type or the other. For details of the methods adopted for each of the following section refer to the relative sections in Chapter 5.

* Collected including charcoal embedded in the samples and unreacted bits.

** Around 10 grams must be taken off when considering the measurement of the outcome from Phase 1 to Phase 2 as few fragments were selected and mounted for physical and chemical analysis.

*** JH1A_T1 and JH1A_T2 were mixed to obtain a good amount of material to smelt.

**** The remains glued to reactor walls (*JH1B_T1-T2-T3 (reactor walls)*) were equally divided (0.45 g) between trial JH2B_T1 and trial JH2B_T3.

8.6.1. Magnetism and density

To ensure comparable results, the same analytical protocol used for the archaeological slags was adopted (see Chapter 5 for details). The density measurements are summed up in Table 8. 5 and graphically described in the box and whiskers plot in Fig. 8. 9 Box and whiskers plot of a) the experimental slags and b) the experimental matte fragments divided by phase and c) the archaeological typologies of slags analysed from the site of Orti Bottagone (see also 5.2.2).a-b. It was possible to make the following observations. The slags show a mean value of 2.85 g cm^{-3} and density range of 3.54 g cm^{-3} with a minimum value of 1.43 g cm^{-3} and a maximum value of 4.97 g cm^{-3} . The density measurements of the slags are consistent with the average density of Chalcolithic coarse slags in the range of $2.6\text{--}3.0 \text{ g cm}^{-3}$, close to the theoretical density of pure quartz, $\rho_{\text{Qz}}=2,66 \text{ g cm}^{-3}$ (Artioli, 2010, p. 338). None of the slags, except for a case (JH1AT2_002), shows similar values to the average density of the flat slags ranging from 3.8 to 4.4 g cm^{-3} , close to the theoretical density of pure fayalite, $\rho_{\text{Fa}}=4.39 \text{ g cm}^{-3}$ (Addis et al., 2016).

The matte fragments show a mean value of 2.89 g cm^{-3} and a lower dispersion of the values (density range of 1.37 g cm^{-3}) from a minimum value of 2.23 g cm^{-3} and a maximum value of 3.60 g cm^{-3} . Unfortunately, matte fragments are extremely rare in the archaeological record for this period, so a density average has not been calculated yet. The chronologically closest average matte density is dated to the Late Bronze Age and fall in the range of $4.8\text{--}5.8 \text{ g cm}^{-3}$ (Artioli, 2010, p. 338).

Table 8. 5 Summary statistics for the density (ρ) values measured on the experimental samples. Scale g cm^{-3} . Count = total number of slags for each group; SD = Standard Deviation; Min. = minimum; Max. = maximum; LQ = lower quartile; UQ = upper quartile; IQR = range interquartile.

	Type	ρ measured (g cm^{-3})									
		Count	Mean	Median	SD	Min	Max	Range	LQ	UQ	IQR
1A	Slag	4	3.01	2.43	1.32	2.20	4.97	2.77	2.24	3.19	0.96
	Matte	4	2.91	2.91	0.58	2.23	3.60	1.37	2.62	3.21	0.59
1B	Slag	2	3.05	3.05	0.48	2.71	3.39	0.67	2.88	3.22	0.34
	Matte	4	2.95	2.93	0.20	2.73	3.20	0.47	2.82	3.05	0.23
2A	Slag	3	2.81	3.26	1.22	1.43	3.73	2.30	2.34	3.50	1.15
	Matte	1	2.57	/	/	/	/	/	/	/	/
2B	Slag	4	2.61	2.67	0.48	2.00	3.13	1.13	2.38	2.91	0.53
	Matte	0	/	/	/	/	/	/	/	/	/
Total	Slag	13	2.85	2.71	0.89	1.43	4.97	3.54	2.25	3.26	1.01

	Matte	9	2.89	2.86	0.39	2.23	3.60	1.37	2.72	3.08	0.36
		22									

As shown in Fig. 8. 9 a) and b) there is not a significant difference between slags and matte density measurements. Except for the PE which was carried out using a different charge, all the results of slags and matte for each phase overlap. This might suggest that they are still by-products at a very early stage of reduction which need to undergo other re(s)melting processes to obtain some copper. The coarse archaeological slags have a lower density than the experimental ones, which might indicate that either a) the charge adopted by ancient smelters had more impurities or b) the trials did not last long enough to allow more quartz to migrate from the charge. As expected, the experimental slags' samples show higher ranges compare to the matte samples. The pilot experiment's matte samples show the highest density values. It must be kept in mind though that the pilot experiment was carried out using almost pure bornite (Cu_5FeS_4), which is a high-grade copper bearing compound (11.13% Fe, 63.31% Cu, 25.56 % S), and none or very low amount of silica was present in the initial charge. However, it must be stressed that the information provided in this section is only a preliminary assessment of the samples' characteristics. The high heterogeneity and porosity might lead to an underestimation of the density values (Addis et al., 2017).

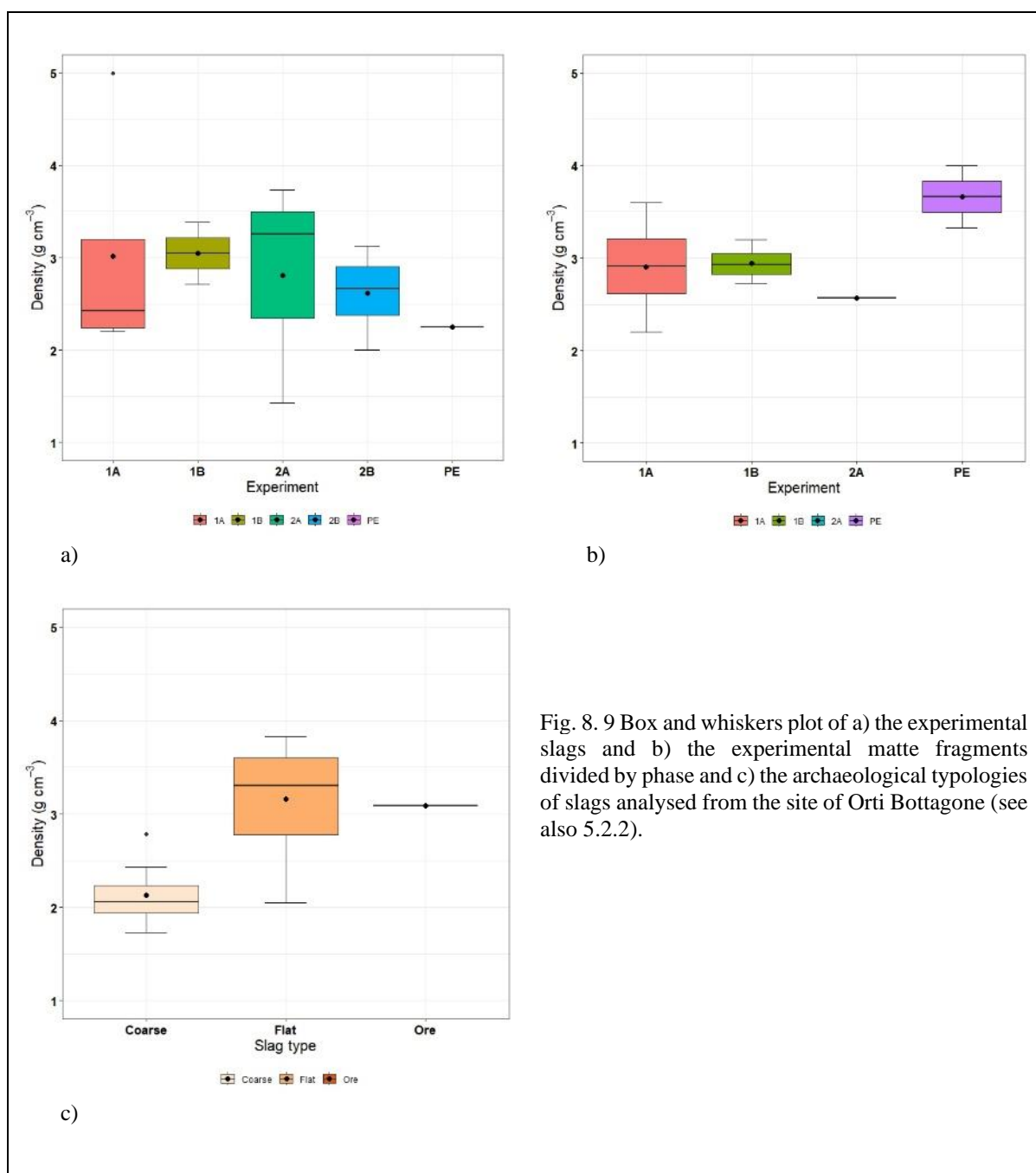


Fig. 8.9 Box and whiskers plot of a) the experimental slags and b) the experimental matte fragments divided by phase and c) the archaeological typologies of slags analysed from the site of Orti Bottagone (see also 5.2.2).

I assessed the magnetism of the 22 samples. The same categorical scale adopted for the archaeological specimens was used to identify and record the magnetic intensity: 1 (grey) – no magnetism; 2 (yellow) – low magnetism; 3 (blue) – high magnetism (Fig. 8.10 Scatter plot of the archaeological typologies of slags analysed from the site of Orti Bottagone.). Only 6 pieces show magnetism. Except for one sample of matte (JH1BT3_001) the magnetic pieces identified are all slags. Given the small dimensions of the pieces it was not possible to determine the orientation. The highest magnetism belongs to two slags from the 2B phase. Interestingly, all the magnetic samples belong to the re-smelting phase trials (2A-2B), indicating an increase in the magnetic power of the slags.

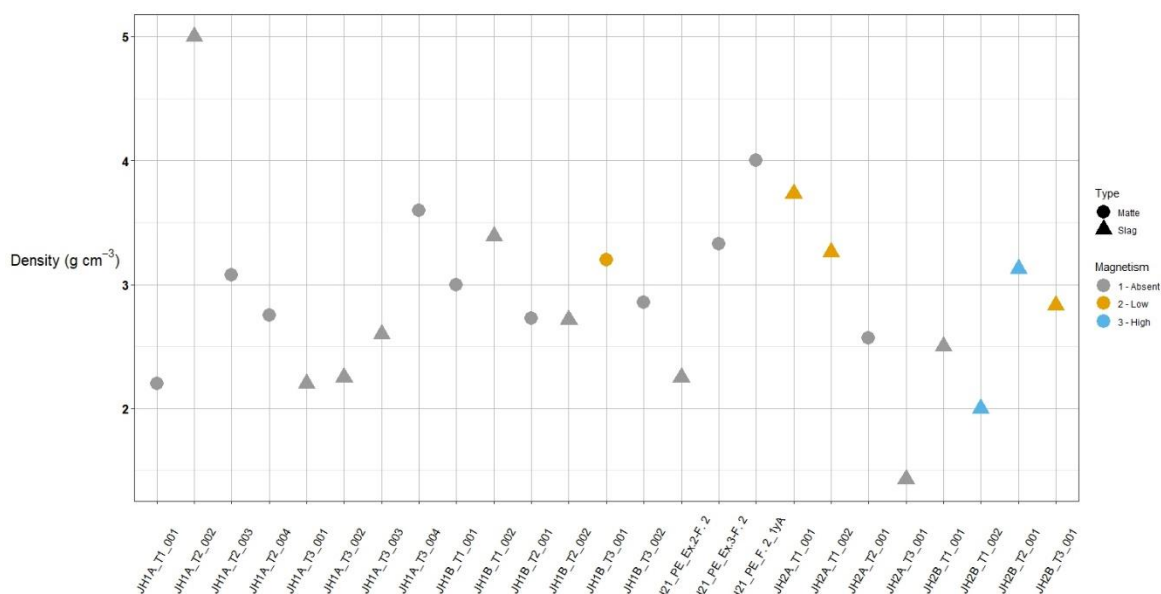


Fig. 8. 10 Scatter plot of the archaeological typologies of slags analysed from the site of Orti Bottagone.

8.6.2. Microscopy: inclusions and phases

The entire assemblage underwent meticulous investigation by means of OM and SEM-EDX. The 13 slags revealed a wide range of mineralogical characteristics and morphologies. Frequent particles of quartz were consistently observed as unreacted residues throughout the entire assemblage, although in lower amounts in the slags from phases 2A and 2B. The morphologies of the sample JH1A_T2-002 exhibits striking similarities with the coarse slag ORTB 5, as both display a quartz core surrounded by a porous fayalite glassy matrix (Fig. 8. 11). Abundant Ca with an average of 21_{ox}%, primarily detected in olivine and pyroxene structures, was observed throughout the assemblage, their distribution varying depending on their positions in the samples. These shared characteristics have led to the development of interesting considerations, which will be discussed in the next chapter.

While quartz and calcium-rich residues are present throughout the entire assemblage (Fig. 8. 12), distinct olivine morphologies have been observed only in the slags from phases 2A and 2B. Elongate hoppers, similar to those observed in ORTB 16 were observed (Fig. 8. 13a). Herring-like dendrites with round ends (Fig. 8. 13b, c) and chain olivines and dendritic structures with a lot of tiny iron oxide phases (Fig. 8. 13d) were also identified. These observations confirm the fast-cooling rate of the surface of the archaeological slags.

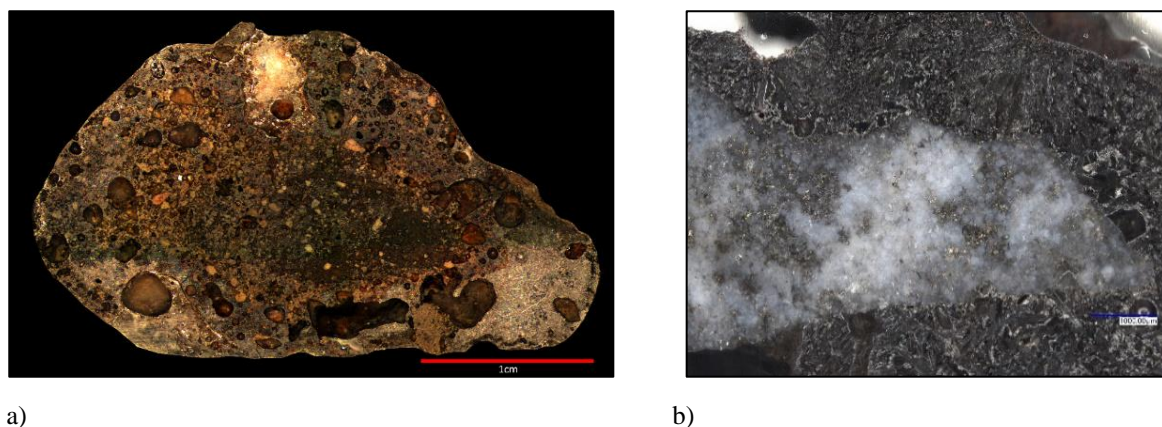


Fig. 8. 11 RL optical images of a) the coarse slag ORTB 5, and b) the experimental sample JH1A_T2-002 showing a quartz core surrounded by a porous fayalite glassy matrix.

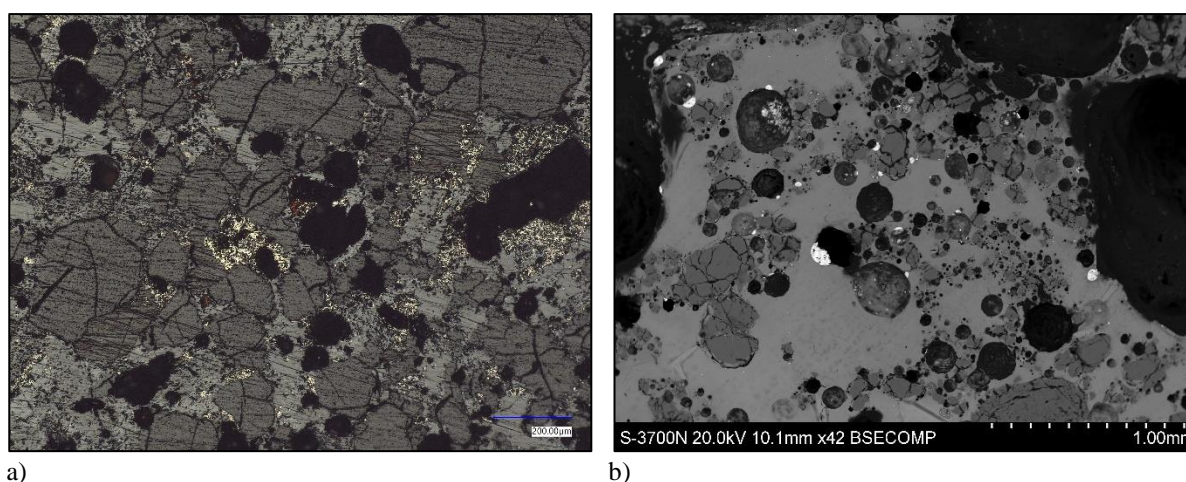


Fig. 8. 12 RL Optical (a) and BSE (b) micrographs of quartz inclusions in two experimental samples (respectively JH1B_T1_001 and JH2A_T3_001).

It is noteworthy that these features exhibit smaller scales compared to their archaeological counterparts. In the slags from Phase 2, the absence of cubic and polyhedral features indicates rapid cooling rates during the formation of the slags which is in line with the prompt recovery after the completion of the process (5-7 minutes). Conversely, the archaeological slags investigated (e.g., ORTB 20), along with numerous chalcolithic slags in literature (e.g., Cave Solvay, Artioli et al., 2016, p. 77, Fig. 52d; and Akladi Cheiri, Rehren et al., 2016, p. 149, Fig. 12) exhibit these large fayalite crystals, indicating that these slags were allowed to cool inside the reactor rather than being promptly removed from the reactor at the end of the process, suggesting a longer cooling period. Magnetite mainly occurs in the 2A and 2B phases. It appears as minute iron oxide phases and small euhedral crystals. Notably, newly formed magnetite clusters have been identified. Striking similarities both in morphologies, dimensions and distribution have been observed in sample ORTB 8 and JH2B_T1_002 (see Fig. 9. 7 BSE

micrographs of (a) the experimental sample JH2B_T1_002, and (b) the flat slag ORTB 8 showing the almost perfect match of the morphologies.in the following discussion chapter). The small dimensions of these features indicate a rapid cooling formation process of the slag.

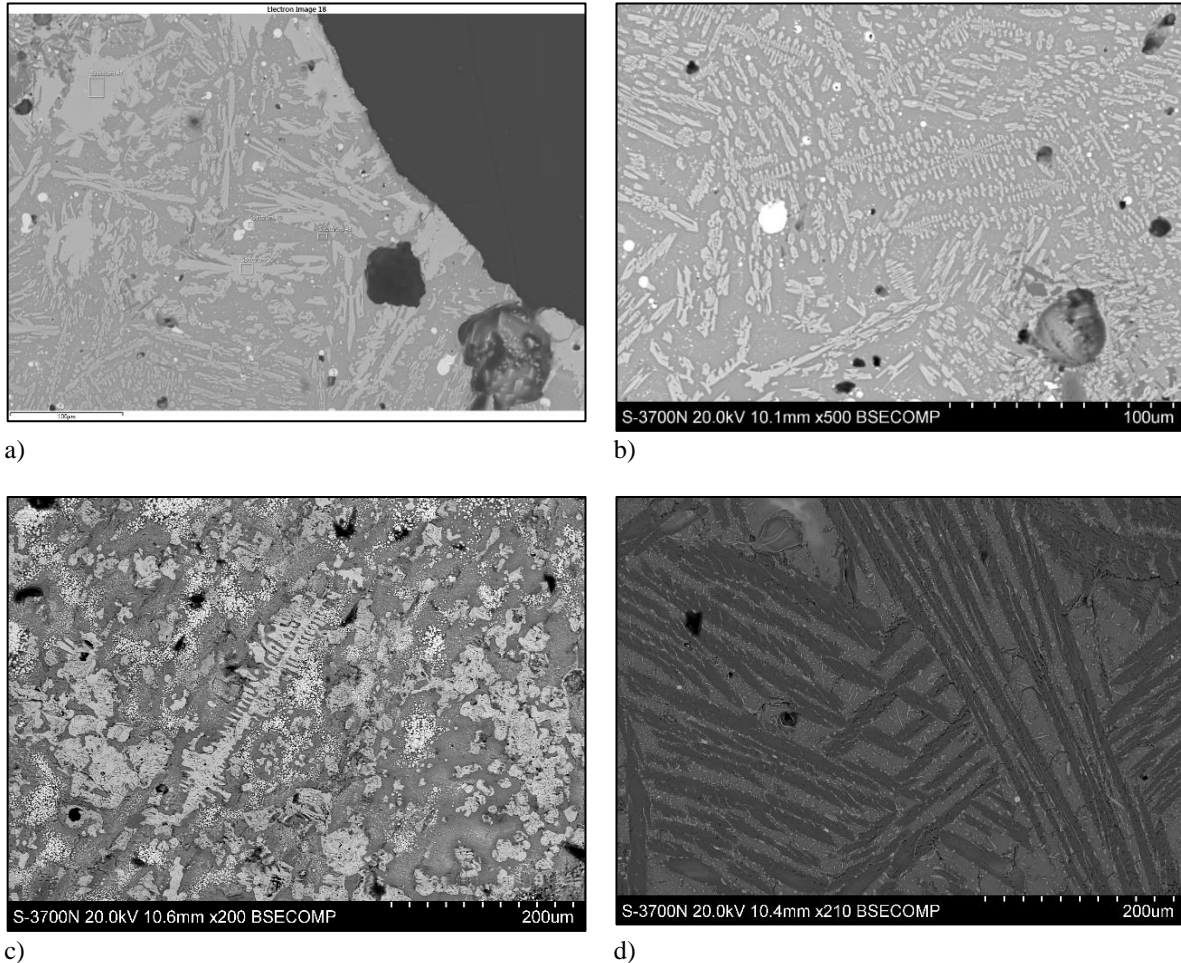


Fig. 8. 13 BSE micrographs showing a) elongate hopper and b) primary dendritic olivine in a fayalite matrix (sample JH2B_T1_002); c) Ca rich dendritic structure with magnetite euhedral crystals in a fayalite matrix (sample JH2B_T2_001); d) chain olivines and dendrites with a lot of tiny iron oxide phases (white), (sample JH2A_T1_001).

The 9 fragments of matte display remarkably consistent characteristics with no discernible differences identified between phase 1 and phase 2. All the samples exhibit the typical blackish grey colour, high porosity with features going from minute cavities to large circular/elliptical vesicles (Fig. 8. 14c). Two main chemical compositions were detected: a Cu-Fe-sulphide high in copper and iron (white) and Cu-Fe-sulphide high in sulphur (grey), (Fig. 8. 14a). Their round morphologies indicate that the substance reached the liquid state and solidified under suitable conditions. Many inclusions were also identified in the matte (Fig. 8. 14b) mainly interpreted as slag remnants. Rare copper prills were observed (Fig. 8. 14c).

A series of chemical elements occurring in minor but relatively constant amounts across the slag and matte assemblages were also identified. Zinc occurs in the slags with an average of 1.33_{ox}% (max value 4.78_{ox}%), whereas a higher average of 2.30_{ox}% (max value 17.04_{ox}%) was detected in the matte samples. Like in the archaeological samples it was mainly detected in the olivines and spinels. Traces of arsenic and antimony were observed primarily in the slags with an average of 0.13_{ox}% (max value 2.94_{ox}%). It is noteworthy the high presence of antimony in the average of 1.13_{ox}% (max value 3.75_{ox}%). Lead was detected in both assemblages with an average of 0.59_{ox}% in the matte (max value 2.52_{ox}%), and an average of 0.14_{ox}% in the slag (max value 1.44_{ox}%). The higher amount detected in the matte might be explained by the higher affinity of lead to sulphur than to the slag. Since lead is not chemically attracted to the slags in the same way as it is to sulphur, it does not tend to be incorporated onto the slag phase during the copper smelting.

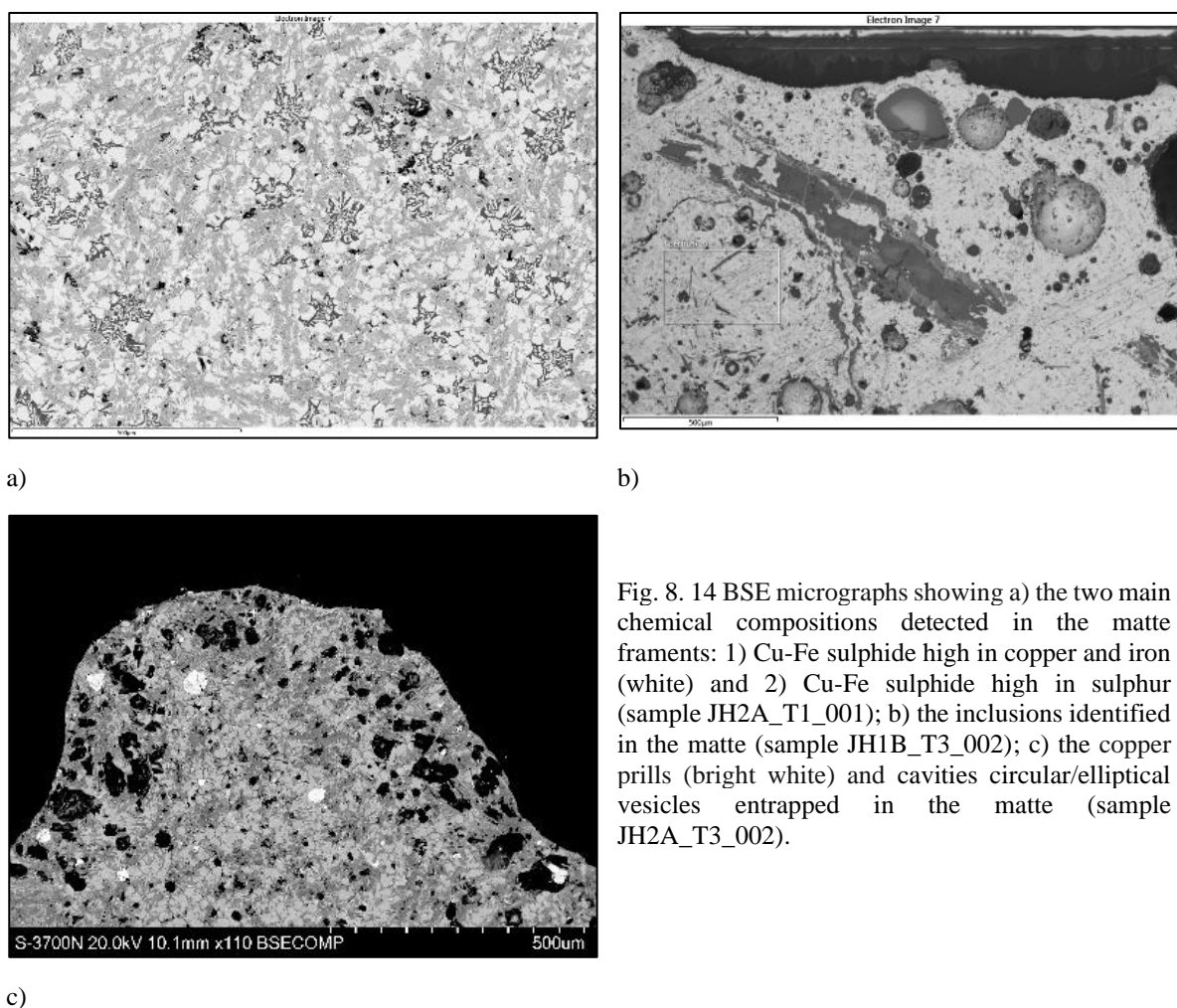


Fig. 8.14 BSE micrographs showing a) the two main chemical compositions detected in the matte fragments: 1) Cu-Fe sulphide high in copper and iron (white) and 2) Cu-Fe sulphide high in sulphur (sample JH2A_T1_001); b) the inclusions identified in the matte (sample JH1B_T3_002); c) the copper prills (bright white) and cavities circular/elliptical vesicles entrapped in the matte (sample JH2A_T3_002).

A semi-quantitative evaluation of the elemental composition of the slags was carried out by means of SEM-EDX. The analyses are reported in Appendix A. The readings (three for each slag) were plotted into the FeO–Al₂O₃–SiO₂ (wt%) and FeO–CaO–SiO₂ (wt%) ternary systems categorised by phase (Fig. 8. 15). I colour coded the phases for the entire section, therefore from now on I will refer to the readings just with the name of the relative phase. In the plot Fig. 8. 15a), as expected, all the readings were distributed within the FeO–SiO₂ compositional area, identifying the two main mineralogical compounds of the smelting slags. Specifically, PE, 1A, and 2A clustered toward the SiO₂ vertex, away from the low-melting region of the system (see Fig. 5. 13). This clustering indicates a significant concentration of silica-based mineralogical compounds in the slags, with silica content ranging from 60wt% to almost 100wt%. However, few readings from phase 1A displayed higher level of FeO, resulting in increased variability along the FeO–SiO₂ axis. In contrast, 1B and 2B cluster midway on the FeO–SiO₂ axis. Although not in the eutectic area, 2B exhibited higher FeO content compared to the other phases, highlighting a distinct difference between them. This increased iron content in the slag might be produced by the re-smelting of the iron-rich copper sulphides. 1B illustrates reduced intra-phase variability, with all the readings tightly clustering along the FeO–SiO₂ axis within the 40 wt% to 50 wt% silica range. In the FeO–CaO–SiO₂ (wt%) ternary system (Fig. 8. 15b), an unexpected observation was the presence of high CaO content in all the readings, reaching up to 40_{wt%}. This finding indicates a higher concentration of CaO than expected.

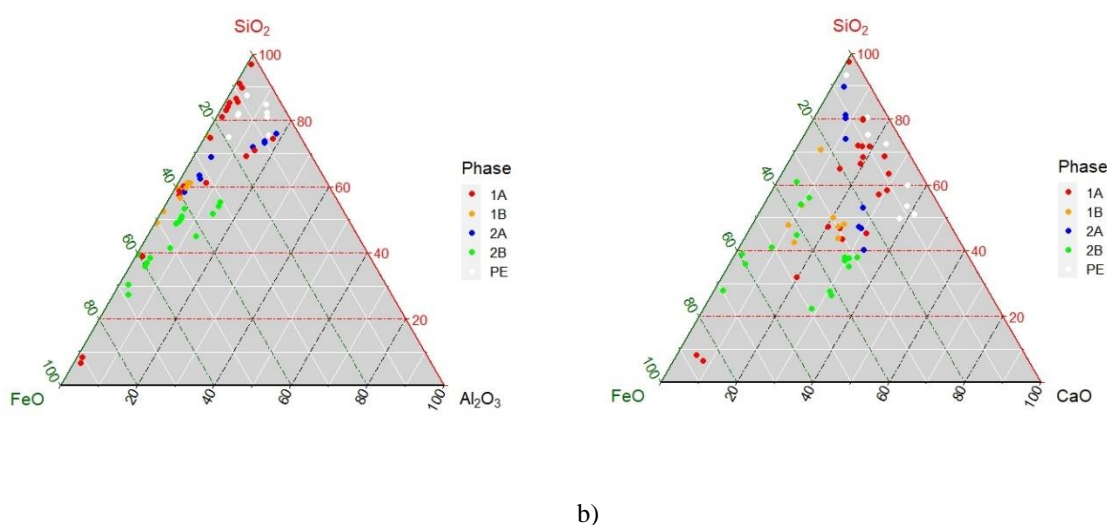


Fig. 8. 15 Ternary plot diagrams showing the average composition of the three areas analysed for each sample in the slag systems FeO–Al₂O₃–SiO₂ (wt%) and FeO–CaO–SiO₂ (wt%).

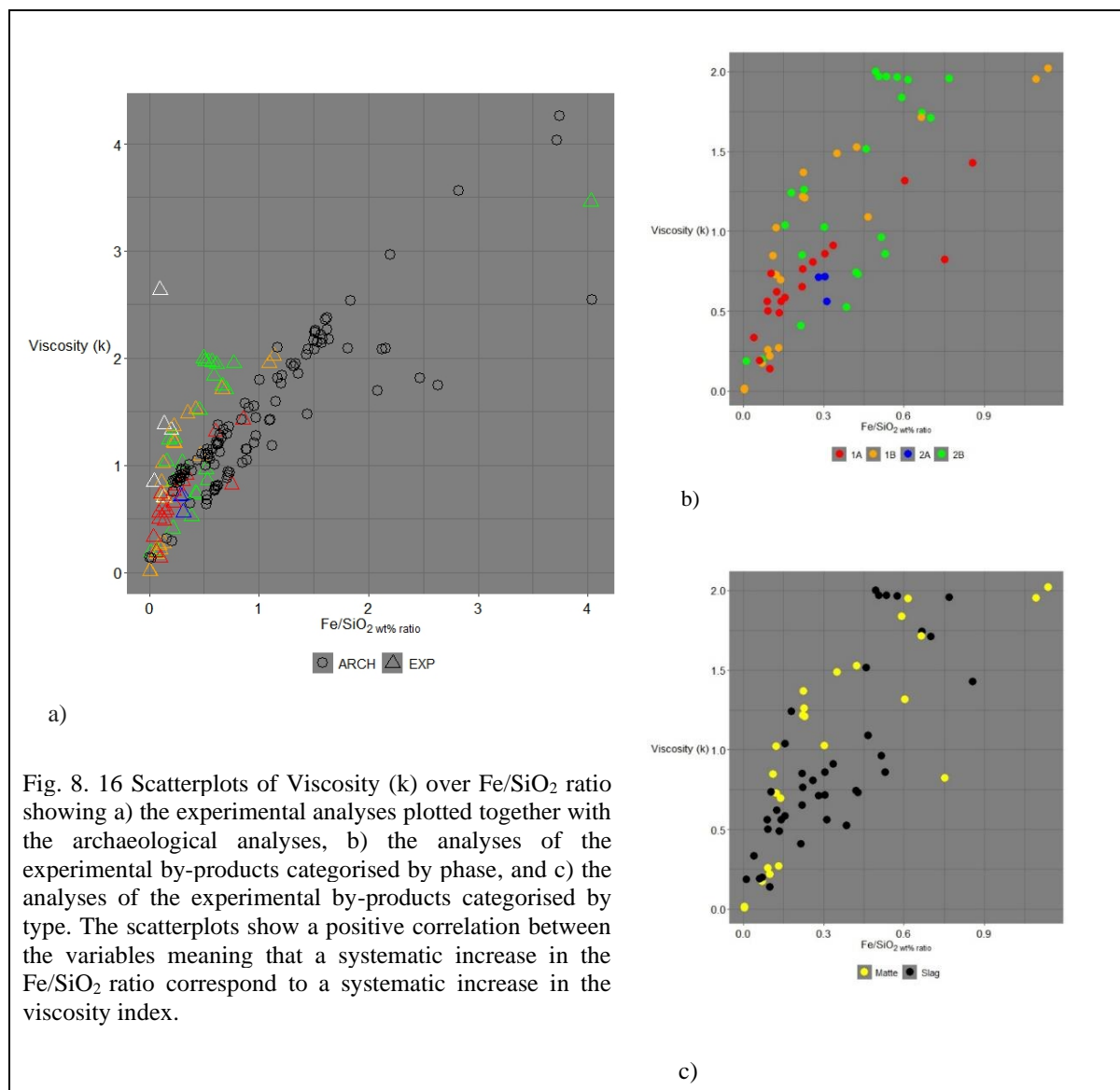
8.6.3. Viscosity and Fe/SiO₂ ratio

Viscosity and Fe/SiO₂ ratio values were calculated by means of the SEM-EDX analyses of the matrices. Unexpectedly, the slags and matte showed the same average viscosity value of 1.25. This value is close to that of the Orti Bottagone coarse slags calculated at 1.20.

The viscosity K indexes were plotted against the Fe/SiO₂ ratio values. In order to have a useful comparison, the experimental analyses were plotted together with archaeological analyses (black) and categorised by type (Fig. 8. 16 Scatterplots of Viscosity (k) over Fe/SiO₂ ratio showing a) the experimental analyses plotted together with the archaeological analyses, b) the analyses of the experimental by-products categorised by phase, and c) the analyses of the experimental by-products categorised by type. The scatterplots show a positive correlation between the variables meaning that a systematic increase in the Fe/SiO₂ ratio correspond to a systematic increase in the viscosity index.a). Four analyses with significantly differing values were removed as outliers. Looking at the plot, it is apparent that the experimental analyses cluster in a lower range of values compared to the archaeological data. Specifically, they fall in the area between the max viscosity value of ~2 and the max Fe/SiO₂ ratio value of ~1.2. They show lower amounts of iron phases in the slag and in turn higher amounts of quartz. Interestingly, except for one case, they all cluster in the same area of the coarse slags (see Fig. 5. 15 Scatterplot showing a strong positive correlation (0.9) between the variables, indicating that as the Fe/SiO₂ ratio systematically increases, there is a corresponding systematic increase in the viscosity index.), showing only a slightly higher viscosity index.

The experimental data shows a strong positive correlation (correlation coefficient of 0.8) between viscosity and Fe/SiO₂ ratio. A similar correlation coefficient (0.9) was calculated for the slags of Orti Bottagone. The PE values were not considered in the experimental plots because of the different initial charge which might have introduced biases in the results.

Looking at the data categorised by phase (Fig. 8. 16b) values are equally dispersed. Specifically, the slags' viscosity values fall between 0.1 and 2, and Fe/SiO₂ ratio values fall between 0.1 and 0.9, whereas the matte's viscosity values fall between 0.1 and 2 and the Fe/SiO₂ ratio values fall between 0.1 and 1.1. The majority of slag's values roughly concentrates in the area between 0.5 and 1 k value and 0.1 and 0.5 Fe/SiO₂ ratio values. Similarly, the plot categorised by type (bottom right) depicts an equal dispersion for each phase (Fig. 8. 16c).



The Fe/SiO₂ ratio values were also plotted against CaO on two binary Flogen diagrams (Fig. 8. 17a, b). Unfortunately, the horizontal axis in the diagrams begins at 0.5 leaving out the analyses with a balanced ratio between Fe and SiO₂. The data were plotted regardless as the aim was to identify a rough estimation of the crystallisation temperatures undergone in the reactor.

Differently from the archaeological samples the experimental values are scattered along the vertical axis showing a larger variation in the amount of CaO and a lower variation in the Fe/SiO₂ ratios. Only a small number of analyses falls in the low CaO content silica saturation zone, whereas the rest fall above the silica saturation zone up to a max of ca. 40 wt% of CaO, possibly indicating a crystallisation temperature between 1150°C and 1275°C at pO₂ at 1x10⁻⁸, or between 1225°C and 1325°C at pO₂ at 1x10⁻⁵. As shown in the plot in figure Fig. 8. 17c only a tiny amount of the analyses overlaps with the coarse slags' values. No values were identified in the transition zone between silica saturation zone and calcium silicates. Interestingly, none of the analyses overlap with the flat slags' values, neither is found in the "F" area. Looking at

the data categorised by phase (Fig. 8. 17d) values are equally dispersed. The same pattern is shown when data are categorised by type (Fig. 8. 17e).

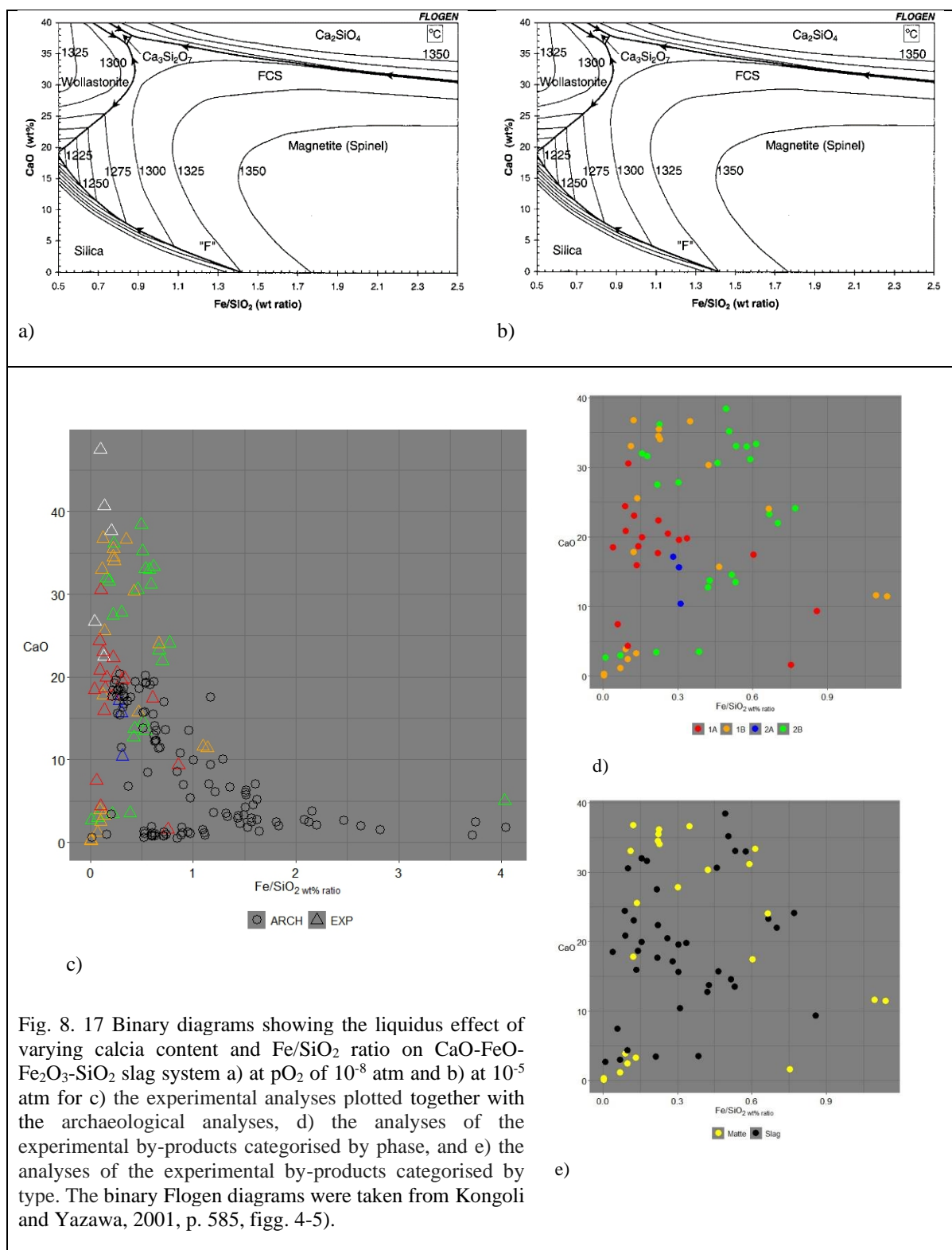


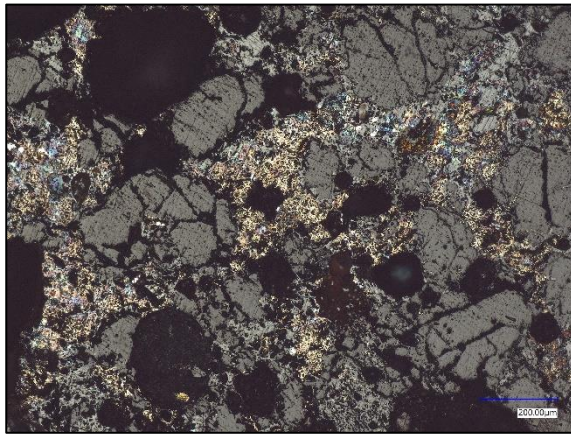
Fig. 8. 17 Binary diagrams showing the liquidus effect of varying calcia content and Fe/SiO₂ ratio on CaO-FeO-Fe₂O₃-SiO₂ slag system a) at pO₂ of 10⁻⁸ atm and b) at 10⁻⁵ atm for c) the experimental analyses plotted together with the archaeological analyses, d) the analyses of the experimental by-products categorised by phase, and e) the analyses of the experimental by-products categorised by type. The binary Floger diagrams were taken from Kongoli and Yazawa, 2001, p. 585, figg. 4-5).

In summary, the comparison between experimental and archaeological slags reveals the following: firstly, the experimental slags exhibit lower variability in viscosity and Fe/SiO₂ ratio when compared to the archaeological slags. Secondly, the balanced ratio between Fe and SiO₂ in the experimental slags indicates a reduced presence of iron phases and a higher concentration of quartz. Furthermore, all the values from the experimental slags show high percentages of CaO, up to 40_{wt}%. This suggests that the initial charge selection was conducted with greater care, intentionally avoiding the use of gangue materials and favouring copper-rich compounds. Additionally, the low viscosity k indexes observed in all the values indicate a high viscosity of the melt. It is challenging to determine whether this viscosity is a result of low temperatures in the reactor, an incorrect recipe in the initial charge, or a combination of both factors. With the exception of one case, all the experimental slag values fall within the range predominantly associated with coarse slags, as reported in Chapter 6 (refer to Section 5.2.8). Lastly, both matte and slag values display similar dispersion, indicating similar properties and ratios between the two. Considering all these points, it can be inferred that the experimental slags are still in the early stages of the smelting process (see Discussion in Chapter 9).

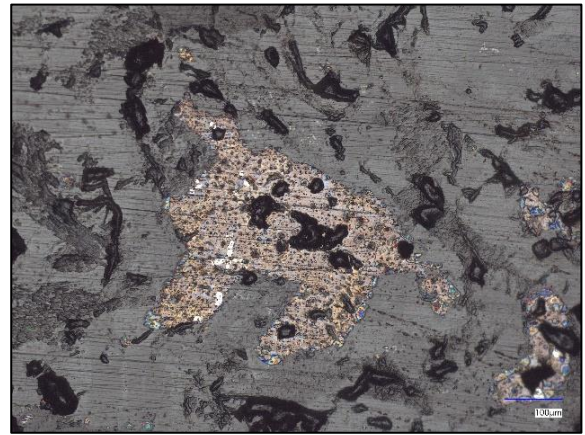
8.6.4. Copper bearing compounds

The 22 samples were first carefully investigated under optical and electron microscopes and then analysed by means of EDX. A total of 231 Cu-Fe sulphide analyses were acquired. These compounds were found to be evenly distributed throughout the entire assemblage showing diverse array of colours, shapes and chemical compositions that point towards various stages of transformation. Among the observed forms were partially reacted or unreacted chalcopyrite grains (Fig. 8. 18a), as well as elongated and irregular morphologies (Fig. 8. 18b) and numerous prills with spherical shape with various diameters in the range of μm to mm size (Fig. 8. 18c-f). A remarkably similar wedge-shaped feature was observed in the experimental slag JH1B_T2_002 and in the archaeological slag ORTB 20. Within it, the Cu-Fe sulphide compounds were found to be trapped between two converging pyroxene dendritic structures, indicating that the process did not last enough to allow the Cu-Fe sulphides to migrate out of the slag (see fig. 9). In many specimens circumscribed matte areas were identified. These parts were distinctly separated from the slag matrix and were mainly observed towards the outer sides of the slag (Fig. 8. 18g). Overall, the slags from phase 1 show many unreacted parts of the initial charge compared to phase 2 where instead all the copper bearing bits were detected as copper-iron sulphide prills or matte. Interestingly, within a span of less than a year (the experiments were carried out in July 2022 and the analyses from 6 to 8 months later) newly developed phases of copper hydroxides (e.g., Cu(OH)₂ and CuCl₂·2H₂O) were observed to occupy the pores

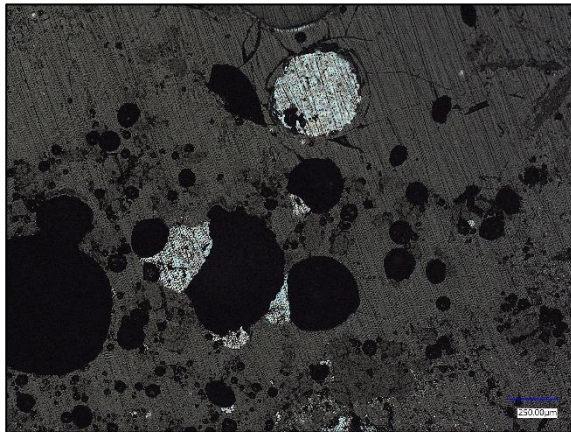
within the matrix. This occurrence is likely associated with the fact that the specimens were stored while still wet.



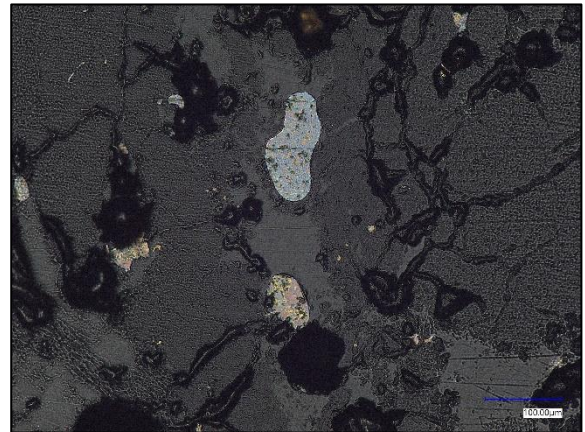
a)



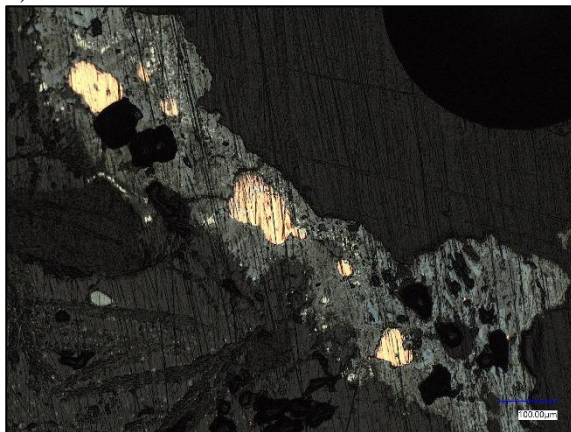
b)



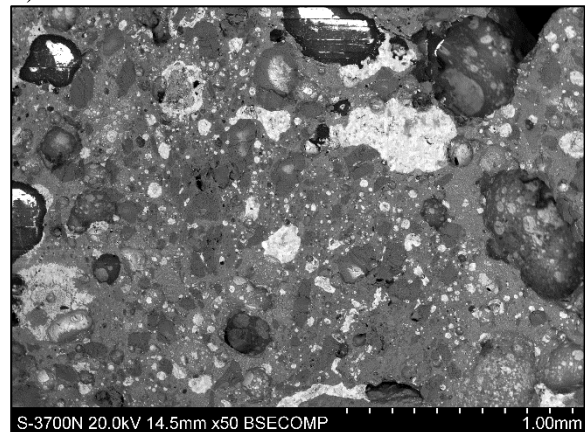
c)



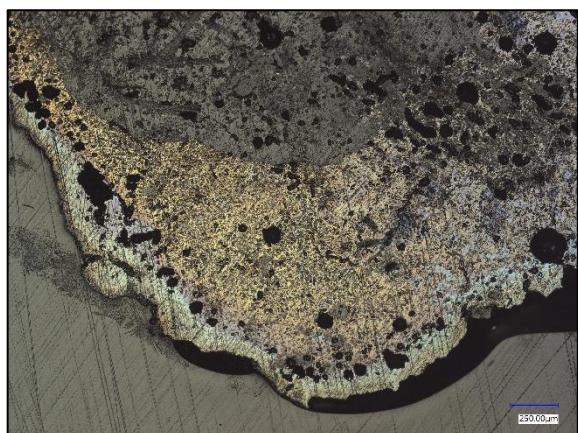
d)



e)



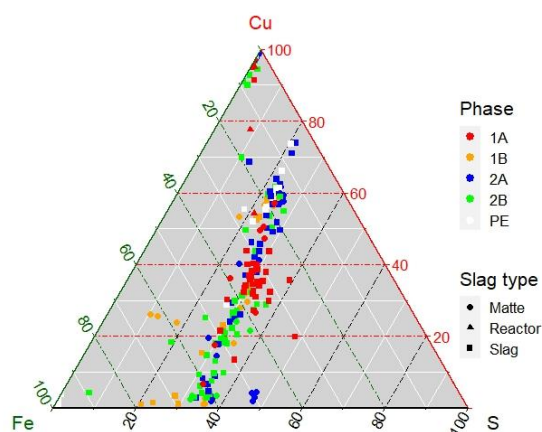
f)



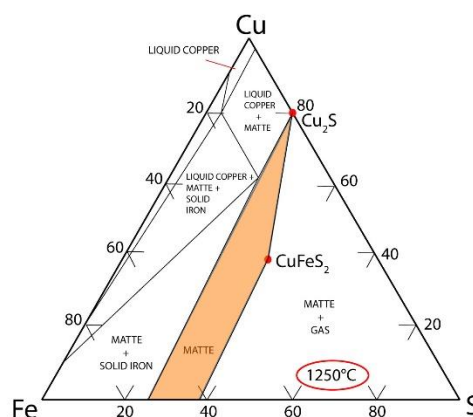
g)

Fig. 8. 18 RL optical and BSE micrographs showing the Cu-Fe sulphides found in the experimental specimens. A diverse array of colours, shapes and chemical compositions were identified: a) partially reacted or unreacted chalcopryite grains (sample JH1B_T1_001 – scale bar 200μm), b) elongated and irregular morphologies (sample JH1B_T2_002 – scale bar 100μm), and c-f) numerous prills with spherical shape with various diameters in the range of μm to mm size (respectively samples JH1A_T3_001 – scale bar 250μm, JH1A_T3_003, JH1A_T3_001 – scale bar 100μm, JH2B_T1_001), g) matte area distinctly separated from the slag matrix and mainly observed towards the outer sides of the slag (sample JH1A_T2_003 – scale bar 250μm).

The chemical compositions were plotted in the ternary system Cu-Fe-S (wt%) and categorised according to their phase (Fig. 8. 19a). The analyses are reported in Appendix A **Error! Reference source not found.** It is important to note that the PE analyses are shown in the plots but are not considered in the average calculations. This is because for the pilot experiment I utilized bornite (Cu_5FeS_4), a high-grade copper bearing compound with specific composition (11.1 wt% Fe, 63.3 wt% Cu, 25.6 wt% S). The readings reveal a wide range of phases with varying Cu/S ratios, dispersed along the sulphide axis from chalcocite (Cu_2S) to bornite (Cu_5FeS_4), chalcopryite (CuFeS_2) and pyrrhotite (FeS) within the matte zone (as indicated by the orange area in Fig. 8. 19b). Differently, the archaeological specimens exhibit a significant level of compositional consistency/uniformity.



a)



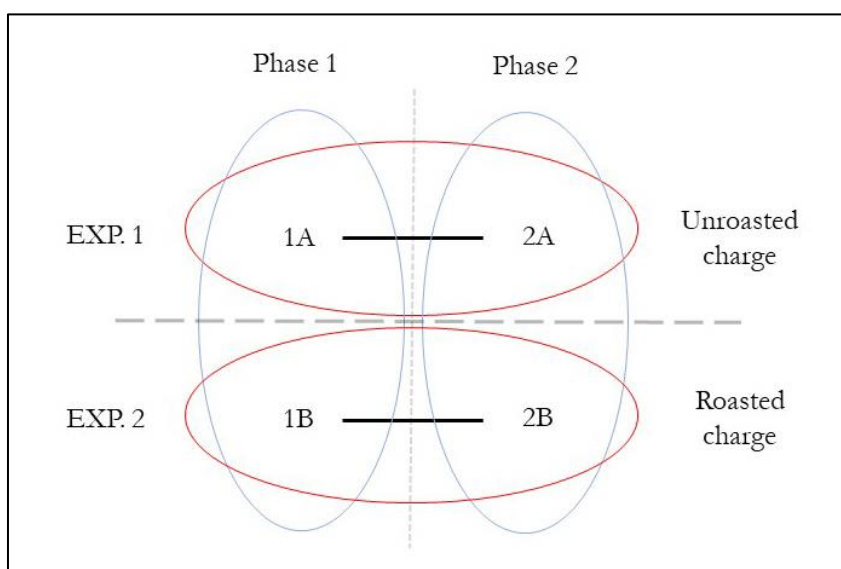
b)

Fig. 8. 19 illustrates a) the ternary plot diagram (Cu-Fe-S (wt%) slag system) of the copper bearing compounds SEM-EDX analyses categorised according to their phases and types; b) the ternary plot diagram (Cu-Fe-S (wt%) slag

system) showing the vast range of chemical combinations along the sulphide axis chalcocite-bornite-chalcopyrite-pyrrhotite and the Cu-Fe axis of copper slags from data from Oman, Anatolia, Iran, Italy (Trentino), Grisons (Switzerland), adapted from Hauptmann, 2020, p. 277, fig. 5.55. See also Section 5.2.9.

All the analyses in the archaeological samples fall within a specific matte area between the Cu_2S - CuFeS_2 axis (refer to Fig. 5. 18 (Left) Ternary plot diagram (Cu-Fe-S_(wt%) slag system) of the SEM-EDX analyses (orange= flat slags, red= coarse slags).

To investigate and enhance possible trends and differences, the data were systematically compared across experiments and phases in the same ternary system Cu-Fe-S_(wt%), according to the subsequent scheme:



Experiment #1 – unroasted charge (Phases 1A, 2A), (Fig. 8.20a). In Phase 1A (red) the readings primarily cluster around the compositional area of chalcopyrite. This clustering indicates consistency in elemental compositions. Interestingly, despite the presence of a strong smell during the experiments, the readings suggest that the compounds did not release a significant amount of sulphur when melted. Notably, a few readings in Phase 1A indicate an almost pure copper content, which is an intriguing observation within this phase. Moving to Phase 2A (blue), the readings reveal higher variability and a broader distribution within the matte zone along the sulphide axis. The compositions range from chalcocite-like (Cu_2S) to pyrrhotite-like (FeS). The majority of the analyses in Phase 2A are located in the upper part of the triangle, displaying a shift in composition. This shift is characterised by a decrease in sulphur and iron contents and an enrichment in copper content. Additionally, several readings exhibit a composition similar to pyrrhotite.

Experiment #2 – partially roasted charge (Phases 1B, 2B), (Fig. 8.20b). In phase 1B (orange) the readings are dispersed within the matte zone along the sulphide axis ranging from bornite-like (Cu_5FeS_4), to chalcopyrite-like (CuFeS_2) to pyrrhotite-like (FeS) like compositions. Notably, this phase lacks pure or nearly pure copper prills. Instead, compositions with the lowest amount of sulfur among all the phases are observed. Moving to Phase 2B, the readings are also dispersed within the matte zone. The majority of the readings are concentrated in the lower part of the matte zone, spanning from chalcopyrite-like (CuFeS_2) to pyrrhotite-like (FeS) like compositions. These readings show a low amount of copper in the range of approximately 40wt% to 0. Furthermore, the readings in Phase 2B display an increase in copper-rich Cu-Fe sulphides.

Phase 1 - unroasted (1A) and partially roasted (1B) charge, (Fig. 8.20c). The readings from both phases exhibit distinct compositions, with only a few overlapping readings in the chalcopyrite-like compositional area. However, the readings from the partially roasted charge (1B, orange) demonstrate a higher degree of compositional variability compared to the unroasted charge (1A). This higher variability is expected, considering the partial roasting process that was carried out. Specifically, within the partially roasted charge (1B), some readings display a higher amount of copper in the range of 50-60 wt%, which aligns with the anticipated outcome of the partial roasting. These readings might indicate a better successful copper extraction rate from the charge during the process. Conversely, other readings from the partially roasted charge (1B) show lower copper and sulfur contents, and they are located towards the iron (Fe) vertex. Unexpectedly, no readings close to the copper (Cu) vertex have been observed in this particular phase (1B), which differs from all the other experimental trials. This finding raises questions about the effectiveness of the partial roasting process in concentrating copper towards the Cu vertex in this specific case.

Phase 2 - unroasted (2A) and partially roasted (2B) charge, (Fig. 8.20d). The readings from both phases exhibit distinct compositions, with only a few instances of overlap. Starting with the unroasted charge (2A, blue), the majority of the readings demonstrate a compositional range from chalcocite-like (Cu_2S) to pyrrhotite-like (FeS). These compositions align with the average composition of the Cu-Fe sulphides identified by Hauptmann in various regions such as Oman, Anatolia, Iran, Italy (Trentino), Grisons (Switzerland), (Hauptmann, 2020, p. 277, fig. 5.55; and fig. Fig. 5. 19 in this thesis). On the other hand, in Phase 2B, the readings from the partially roasted charge are dispersed in the lower part of the matte zone, ranging from chalcopyrite-like (CuFeS_2) to pyrrhotite-like (FeS) compositions. Unexpectedly, these readings do not align with the average composition of the Cu-Fe sulphides identified by Hauptmann. This discrepancy

raises questions about the factors influencing the composition during the partial roasting process. It is noteworthy that both phases exhibit copper-rich Cu-Fe sulphides in their respective compositions.

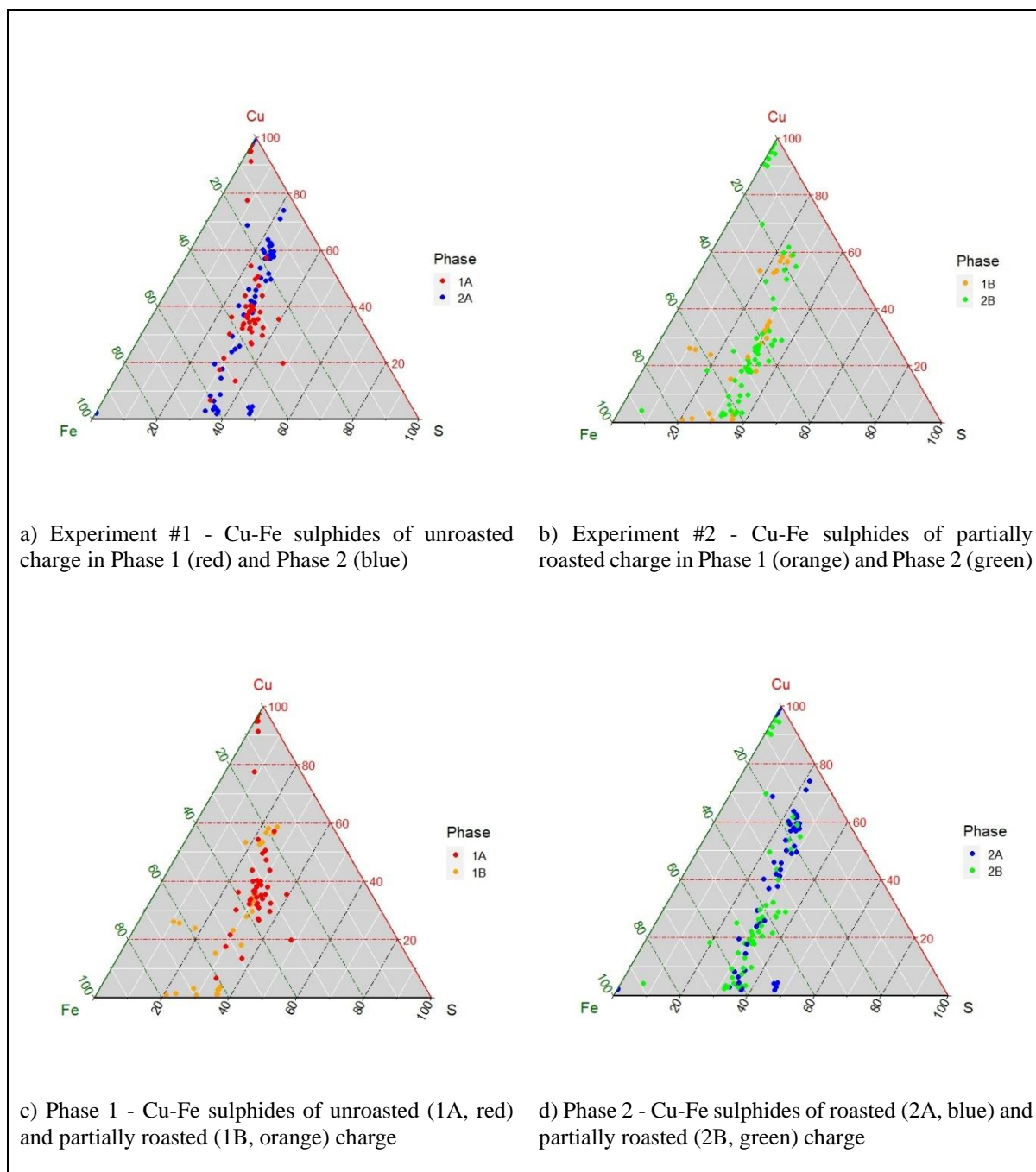


Fig. 8. 20 illustrates the chemical compositions plotted in the ternary system Cu-Fe-S_(wt%) systematically compared across experiments and phases.

In this chapter, I've provided a comprehensive overview of the experiments conducted in this thesis, covering the experimental protocol, experiment descriptions, and the analysis of key findings from the experimental by-products. These findings will be further discussed in the following chapter, alongside the analytical results obtained from the by-products of Orti Bottagone analyzed in Chapter 5. The primary goals are to reconstruct the copper smelting technology employed at Orti Bottagone during the early 4th millennium BC, using insights gained from experimental research, and to illuminate the smelting technology in use during the early stages of metallurgy in central Italy.

Chapter 9. Discussion

9.1. Introduction

In this chapter, I undertake a critical analysis of the research findings, with the aim of reconstructing the copper smelting technology employed at the site of Orti Bottagone during the early 4th millennium BC. The chapter is divided into two parts, each serving a distinct purpose. In the first part of the chapter, I provide a comprehensive characterisation of the copper reduction technology used at the site. To achieve this, I address the initial research questions that were introduced in Chapter 1, and, for clarity, I restate them here:

- Were copper sulphide ores employed in conjunction with oxides and carbonates, or did the ore solely, or primarily, consist of copper sulphides?
- What types of slags were produced? Can they be attributed to specific smelting stages within the overall metallurgical process?
- Is there evidence of intentionally added fluxes, or were self-fluxing ores smelted instead?
- What parameters (e.g., temperatures, reducing /oxidising conditions) were employed during ore smelting?
- Are there any traces of arsenic (As) and/or antimony (Sb) in the slags and in the crucible fragment analysed as part of this research?

In the second part of this chapter, the focus shifts to the experiments detailed in the previous chapter, specifically concentrating on replicating the smelting process carried out at Orti Bottagone. The research questions guiding this section are as follows:

- Is the local ore suitable for smelting without the addition of copper carbonates/oxides, or the deliberate addition of fluxes, utilising a one-step process (i.e., without roasting)?
- Can we ascertain whether the by-products of the smelting experiments resemble the archaeological ones, and if such resemblance exists, which experiments and phases yield slag materials that exhibit a greater degree of similarity?

- Which smelting technique proposed in the literature, if any, best fits the experimental residues produced?

Furthermore, while not the central emphasis in this second part of the thesis, prior experiments supporting its viability, I explore smelting using local ore without the use of a crucible.

This part of the chapter aims to assess the feasibility of a one-step smelting process, eliminating the need for intermediate roasting and the use of a crucible to contain the charge. The experimental data are then meticulously compared and critically evaluated in conjunction with the archaeological evidence. The results of these experiments shed light on previously unclear technological aspects of early copper reduction, contributing a comprehensive understanding of the smelting processes carried out at Orti Bottagone.

In the following sections, I will endeavour to reconstruct the smelting process as observed at Orti Bottagone, leveraging insights gained from experimental research. This reconstruction not only sheds new light on the smelting technology employed during the nascent stages of metallurgy in central Italy but also deepens our understanding of this process compared to what is discussed in the literature.

9.2. The smelting process at the site of Orti Bottagone

The site of Orti Bottagone provides compelling evidence of the reduction of copper from a sulphide ore. Analyses conducted on 1 ore fragment and 18 slag fragments, and 1 crucible fragment (as reported in Chapter 5 and Appendix) reveal that copper was obtained from a sulphide-rich source. The ore fragment exhibited significant heterogeneity in its composition. A substantial portion of the fragment consisted of gangue rock with small amounts of ore minerals, suggesting a coarse beneficiation process. Furthermore, the fragment's size suggests that the ore was crushed to centimetre-scale. However, interpreting this fragment presents two distinct and contrasting possibilities. On one hand, the presence of quartz and high carbonate content suggests the utilisation of a poorly beneficiated charge. This interpretation implies that the ore used in the smelting process may not have undergone extensive processing to eliminate impurities. On the other hand, an alternative explanation posits that the fragment might represent a discarded piece with low copper content. Unfortunately, since this is the only ore fragment recovered from the site, further insights on the type of ore exploited at Orti Bottagone remains unattainable at this stage.

Type of slags. Two types of slags were identified. The first type, referred to as coarse slags, comprises highly viscous conglomerates characterised by a heterogeneous composition. These slags contain both unreacted and partially reacted materials embedded in a partly fayalitic glassy matrix. In contrast, the second type, known as flat slags, also exhibits heterogeneity but differs from the coarse slags as it is less viscous and contains fewer unreacted inclusions. These characteristics set this group apart as technologically more advanced than the most typical Chalcolithic slags, which are highly porous, heterogeneous, and containing unreacted or semi-reacted inclusions (Bourgarit, 2007). It is worth noting that the only nearly contemporary site exhibiting flat slags is the nearby site of San Carly Cava Solvay, dating to the late 4th millennium BC (Fedeli, 1999; Fedeli & Galiberti, 2016). Evidence of this type of slag becomes widespread in Europe in the late 3rd and early 2nd millennia BC, for example at Saint Veran in the western Alps or the eastern Alpine smelting sites of Trentino and Alto Adige/South Tyrol regions (Bourgarit et al. 2008).

These sites primarily produced coarse slags, with flat slags reported in small numbers at locations such as Millan (Artioli et al., 2015), Gudon, Montesei di Serso, Riparo Marchi, Romagnano Loch, Romagnano Angeli, and La Vela di Valbusa (Pearce et al., 2022); in the western Alps at Saint Veran; and in south-eastern Spain at El Picacho (Müller et al., 2007). Traditionally, coarse and flat slags have been interpreted as by-products of distinct stages in multiple-step copper smelting processes, specifically, slagging (coarse) and matting (flat) stages (Addis et al., 2016). However, it is important to note that these types of slags have primarily been found at sites dating to the Late Bronze Age onwards and these definitions have predominantly been applied to relatively advanced smelting processes. Considering the very early chronology of the site under study, I propose an alternative interpretation. I argue that, as already proposed by Piel et al. and Metten (Piel *et al.*, 1992; Metten, 2003), both type of slags could result from a one-step smelting process and coexist in the same reactor. If this is true, the conventional classification of slags into distinct smelting stages does not apply to the early stages of metallurgy. The difference between the two types of slag may result from reprocessing the same charge multiple times, gradually skimming out more slagged by-products from the surface of molten copper at each reprocessing step and by the fluctuating reducing/oxidising conditions and temperatures inside the reactor. In the second part of this chapter, I will justify this point. The labels “coarse” and “flat” are retained in the remainder of this chapter solely for the purpose of maintaining coherence when referring to the main mineralogical compositions of the slags, without any reference to multi-stage smelting technology.

The fragmentary condition of the entire assemblage implies that the slags were intentionally broken in antiquity, most likely to recover the copper prills contained within. This evidence aligns with the technique proposed by a number of authors for the Chalcolithic smelting processes wherein immature slagging processes generated highly viscous and heterogeneous slags characterised by partially melted materials and unreacted inclusions (Bourgarit, 2007; Bourgarit & Mille, 2005; Ottaway, 2001). To recover the metal inclusions trapped in the slags, prehistoric metalworkers needed to crush, collect and re(s)melt them. The systematic process of crushing, selecting, and subsequently remelting the slags has been suggested by authors who focused on the challenging working conditions of that time, such as short-duration processes, low temperatures, low reducing conditions, and potentially poor metal-bearing ores. It is worth noting, however, that some authors argue that, during the early stages of metal production, prospectors and smelters might have primarily targeted high-grade mineralisations, which may present a counterpoint to the notion of 'poor metal-bearing ores' in this context.

Of particular interest is the concave indentation observed on slag fragment ORTB 13 (Fig. 9.1), which bears resemblance to similar markings identified on Chalcolithic and Early Bronze Age artefacts recovered from la Vela di Valbusa, Trentino (Pearce et al., 2022, p. 16, fig. 8). Expanding on this similarity, it is reasonable to adopt Pearce et al. (2022) interpretation, which suggests that the concave indentation represents the impression left by a stick, roughly the width of a finger, measuring approximately 1.5 cm in the case of sample ORTB 13, likely made of wood. This interpretation aligns with Pierce et al.'s findings and reinforces the hypothesis that the stick was employed for poking, stirring, or lifting the slag out of the reactor. Pearce et al. refer to ethnographic comparisons described by Anfinset (2001, p. 53) in Nepal, and Blandford (1861, p. 390) in Sikkim, India. They suggest that due to the rudimentary working conditions of early smelting technologies, it was unlikely that one could produce fully liquid slags during the initial smelting stage. Instead, the objective was to melt the gangue in a single piece for removal from the liquid matte, likely with the assistance of wooden tongs or sticks. Confirming the use of such a tool for extracting by-products from the reactor implies the potential for repeated operations within a short timeframe, potentially increasing production efficiency.

However, an alternative explanation for the concave indentation may exist. While the stick interpretation appears consistent with the available evidence, an interpretation less influenced by ethnographic comparisons could be that the concave indentation was formed as a result of slag cooling on a partially burnt, rounded piece of charcoal.

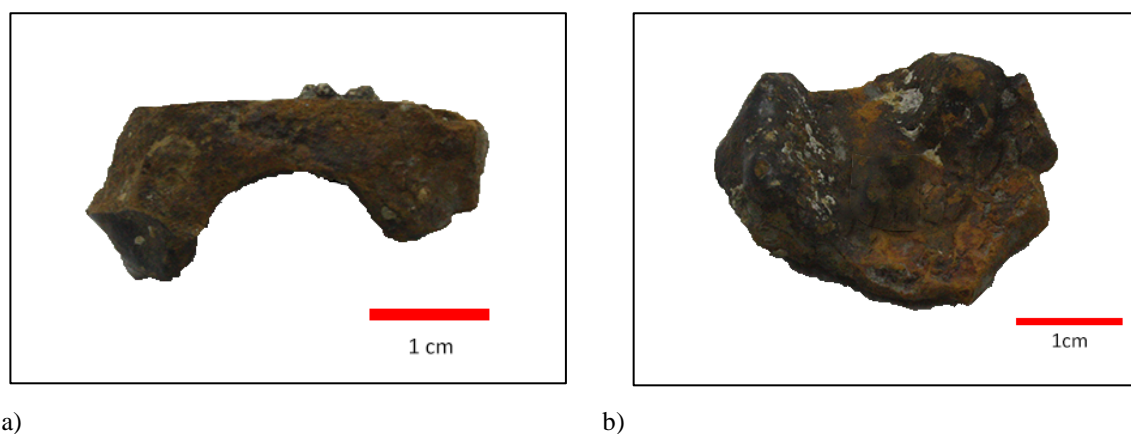


Fig. 9. 1 displays two views of sample ORTB 13 showing a concave indentation resembling a circular void within the bottom of the slag (refer to section 5.2.1).

Redox conditions and temperatures. Despite the well-reacted slags and the high copper production rates observed in the overall slag sample, approximately 4_{wt}% of CuO with a minimum of 1_{wt}% and a maximum of 11_{wt}%), the extensive variety of mineralogical phases and morphologies within the samples strongly indicate a state of highly unstable reducing conditions (alternating episodes of oxidising and reducing atmospheres influenced by the rhythm of the air-supply pumped into the reactor) and fluctuating temperatures within the reactor, alongside a lack of standardised ratio between mineral and fuel charge. The observed heterogeneity in the slags can also be plausibly attributed to the presence of remains from multiple separate smelting events, each utilising slightly different charges and smelting conditions. Moreover, the prevalence of fayalite matrices with high magnetite contents indicates that the slags likely formed during the progressive oxidising conditions within the smelting system.

Based on Donaldson's research (1976), the presence of chain olivine fayalitic-rich structures within the slags suggests rapid cooling rates, ranging from 50-200°C/h (tapping process) to over 500°C/h (fast cooling). However, applying these findings to archaeological slags is challenging because Donaldson focused on natural volcanic basaltic melts, which differ from the fayalite-rich olivines typically found in archaeological contexts. Furthermore, Ettler et al. argue that human-made olivine likely cools faster than lava flows, based on slag production rates (Ettler *et al.*, 2009). Both studies conducted experiments in controlled laboratory environments, which may not fully replicate the conditions of open prehistoric furnaces. Therefore, given the current state of knowledge, the presence of fayalitic olivine structures can only suggest that the smelting process in the reactor achieved sufficiently high temperatures for iron minerals to bond with silica, with estimated temperatures ranging from 1000°C to 1300°C.

The presence of polyhedral features in the slag core (Fig. 9. 2a) indicates that the slags underwent cooling while still inside the reactor prior to being recovered. While it remains difficult to precisely determine the cooling rates (Donaldson suggested slow cooling rates of $<7^{\circ}\text{C/h}$), it is possible to conclude that the slags experienced in-reactor cooling followed by recovery. This interpretation aligns with the findings of Artioli et al. (2016), who observed identical morphologies at nearby San Carlo-Cava Solvay (see Fig. 9. 2b).

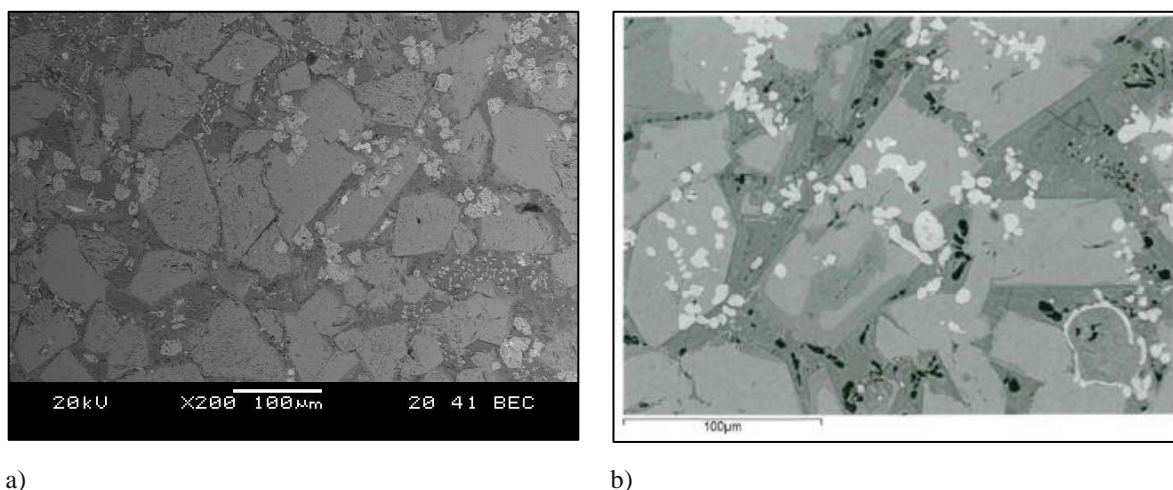


Fig. 9. 2 displays BSE micrographs illustrating the strikingly similar polyhedral features present (a) in a flat slag from Orti Bottagone (ORTB 20), and (b) in a slag from San Carlo Cava Solvay (sourced from Artioli et al. 2016, p. 77, fig.52d).

Fuel. The precise type of fuel used, whether charcoal or wood, has not been determined with certainty. While previous research has demonstrated that charcoal is unnecessary as a reducing agent (CO/CO_2) in the reduction process (Bourgarit *et al.*, 2002; Rostoker *et al.*, 1989; also refer to Hauptmann, 2020, pp. 193–4 for a clear explanation of carbon chemical reactions inside the reactor), it is my contention, consistent with Timberlake’s assertion (Timberlake, 2007), that wood is ill-suited as a fuel for copper smelting. This is primarily due to its lower energy content in comparison to charcoal. Furthermore, the substantial size of wood logs presents an incompatibility with the reactor’s interior voids, which are essential for creating an efficient reducing environment. If the logs were resized to dimensions typical of charcoal, typically a few centimetres in size, they would burn rapidly. This would necessitate a continuous supply of fuel and result in a considerable consumption of both wood resources and labour in preparing the logs to the required dimensions.

Fluxes/no fluxes. While there is general consensus among scholars, with some exceptions (Pearce et al., 2022; Saez et al., 2003a), that fluxing agents were not employed in the

Chalcolithic to enhance copper smelting processes (Bourgarit, 2007; Hauptmann, 2020), the nature of the inclusions detected remains uncertain. It remains unclear whether these inclusions represent unreacted fragments of the exploited ore or remnants of intentionally added fluxes aimed at optimizing the smelting process (see Hauptmann, 2020, pp. 240–243).

Initially, the discovery of a quartz core in the coarse sample ORTB 5 led to considering that quartz might deliberately have been added to the charge as a fluxing agent. However, the presence of an almost identical quartz core surrounded by a porous fayalite glassy matrix in an experimental slag (JH1A_T2-002) demonstrates that quartz separation within the slag could occur naturally Fig. 9. 3).

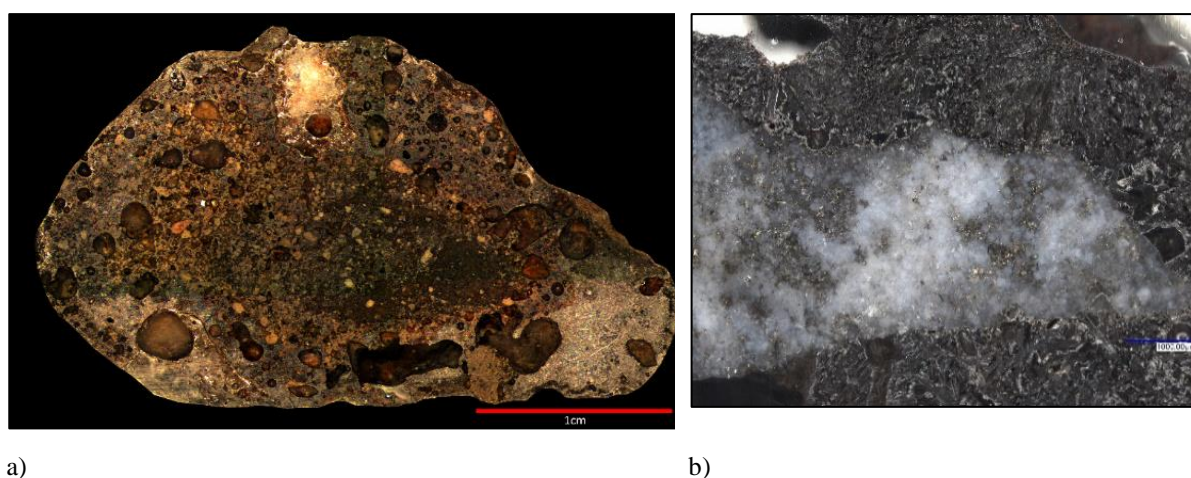


Fig. 9. 3 displays digital images of a) the coarse slag ORTB 5 and b) the experimental sample JH1A_T2-002 (scale bar 1000µm), showing a quartz core surrounded by a porous fayalite glassy matrix.

Despite the potential for calcium (Ca) contamination from wood or charcoal ash used as fuel (Tylecote *et al.*, 1977, pp. 310–1; Bourgarit, 2007), the relatively high presence of Ca in the form of oxides, carbonates and iron oxide-rich melts (e.g., FeCO_3 , CaCO_3) suggests two potential scenarios. Firstly, the initial charge, along with the sulphides, may have naturally contained Ca-based compounds. Alternatively, Ca-based compounds could have been intentionally added as fluxing agents during the smelting process. The use of carbonatic flux, such as limestone (CaCO_3), has been proposed for Chalcolithic and Early Bronze Age sites such as Riparo Gaban, La Vela di Valbusa, Romagnano Loch, and Romagnano Tof de la Val in Trentino Alto Adige/South Tyrol (Cattoi *et al.*, 2000). While the presence of Ca oxides and calcium-rich iron oxides detected in some of the slags (Fig. 5. 8) might support the possibility of deliberate flux addition, its consistent occurrence in the matrix (Fig. 5. 5), ore fragment (ORTB 3), and several partially reacted inclusion rims (Fig. 5. 8d) appears to align more closely

with the first scenario, where the initial charge, along with the sulphides, may have naturally contained Ca-based compounds. Additionally, the investigated slags primarily consist of quartz, hedenbergite ($\text{CaFeSi}_2\text{O}_6$), ilvaite ($\text{CaFe}_3\text{Si}_2\text{O}_8(\text{OH})$), and johannesite ($\text{CaMnSi}_2\text{O}_6$). These minerals closely resemble the composition of the local ore found at the Temperino and Lanzi mines in Campiglia Marittima, which lay approximately 12 km from the site and might thus have been the source of the copper ore used at 4th millennium BC Orti Bottagone (Fig. 9. 4, refer to Section 8.3 for details). A study conducted by Manasse et al. (2001) identified similar chemical compositions in several slags dating back to the 8th century BC, tracing the ore's origin to the Campiglia Marittima area. Although the exact source of the adopted ore cannot be definitively pinpointed, the geological characteristics of the nearest mining area appear to closely align with the slags' composition. These findings, coupled with Campiglia Marittima's proximity as the nearest mining area to the archaeological site, strongly suggest that the prehistoric smiths of Orti Bottagone processed local sulphide ores. Unfortunately, no evidence of prehistoric mining has been found in the area, perhaps due to historic mining activities that might have obliterated the prehistoric workings.

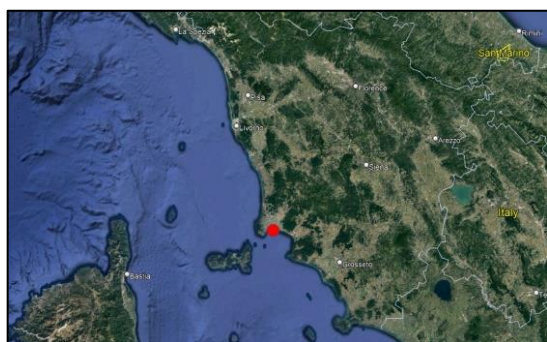


Fig. 9. 4 shows the proximity between the archaeological site of Orti Bottagone and its closest mining area in Campiglia Marittima, situated around 12 km north.



Additionally, the presence of flat slags at the site allows to rule out that they were repurposed or recycled as flux during the ore smelting stage, as has been suggested for other sites (see Pearce et al., 2022). It is therefore plausible that the gangue and host rocks typically associated with the ores unintentionally acted as natural fluxing agents (see Hauptmann, 2020, p. 245). This fits well with an archaic smelting technology where the desired eutectic composition was still unknown. Additionally, the consistent presence of significant amounts of calcium (Ca) and

silica in the slags, with the latter deviating from the desired eutectic compositions for slagging, may have functioned as self-fluxing agents, potentially aiding the smelting process. This could have favoured relatively efficient copper production, representing a form of “serendipitous co-smelting,” as suggested by Pryce et al. (2010, p. 253) and Rostoker et al. (1989).

Arsenic. The examination of the entire assemblage characterised by ore, slags and crucible samples has yielded a significant discovery – the presence of traces of arsenic. Arsenic is a crucial element in understanding the smelting process and charge used at Orti Bottagone. This finding has far-reaching implications for comprehending metal production during this early time – the Final Neolithic period in the central Italian sequence (c.3800-3600 BC). According to Rehren et al. (2012 and references therein), three potential methods existed for the production of arsenical copper in antiquity: a) exploitation of ores characterized by the presence of both sulphides and arsenides such as arsenopyrite (FeAsS), cobaltite (CoAsS), and nickel arsenide (NiAs) minerals, known as sulphosalts; b) the co-smelting of native copper and copper-arsenide minerals; and c) the deliberate addition of an arsenic-rich mineral, such as realgar, orpiment, arsenopyrite, or löllingite, to copper metal or the copper ore. Alternatively, d) arsenic could stem from the presence of arsenates such as olivenite ($\text{Cu}_2\text{AsO}_4(\text{OH})$), clinoclase ($\text{Cu}_3\text{AsO}_4(\text{OH})_3$) and scorodite ($\text{FeAsO}_4 \cdot 2\text{H}_2\text{O}$) within the smelting charge (Killick, 2014). The latter are minerals that contain the arsenate ion (AsO_4^{3-}) and are commonly found in the weathered supergene zone of copper deposits (“supragossans”; Ixer, 1999; see also chapter 2.4 and references therein), resulting from the oxidation of primary copper-arsenic sulphide minerals above the hypogene fahlore deposits (Ixer & Patrick, 2003). Arsenates contain arsenic, oxygen, and other elements like copper or iron. It is interesting to note that Killick (2014, p. 41) proposed that the blue-green colour of these minerals might have misled ancient smelters into believing that they were copper carbonate, inadvertently leading to their exploitation.

The detection of arsenic in the slag samples serves as compelling evidence for the potential occurrence of arsenical copper production at the site. The production of arsenical copper is a remarkable testament to the high level of expertise achieved by the metalworkers in central Italy during the Final Neolithic period (c.3800–3600 BC) and would be one of the earliest instances of arsenical copper production in western Europe.

Yet, uncertainty persists regarding how arsenic was introduced into the slag samples and its specific source. While the possibility that prehistoric metalworkers exploited arsenates cannot

be dismissed outright, pinpointing the exact technique employed for arsenical copper production at the site remains challenging. Nonetheless, several factors lean towards the likelihood of sulphosalts exploitation at Orti Bottagone: the absence or the low quantities of arsenates in local geological reports (as detailed in the section on ore collection in Chapter 8); the evidence of sulphosalts exploitation at the nearby site of San Carlo (as reported by Artioli *et al.*, 2016); and the prevalence of sulphur in almost every copper-bearing compound investigated, along with the consistent presence of zinc in the samples, which can be linked to sphalerite (ZnS), a sulphide mineral that is abundant in nearby ore deposits (Manasse *et al.*, 2001). Nevertheless, further targeted research is needed to determine the precise technique and sources involved.

In the broader western European context, sulphosalts mining deposits have been identified in districts in the Inn Valley in Austria (Weber *et al.*, 1997) and in the mineral ores from Cabrieres, in the Massif Centrale, south-west France (Ambert, 1995, 1996). However, slags from sulphosalts deposits remain relatively rare in early Europe compared to those from copper-iron sulphide deposits. Notably, third millennium Alpine smelting sites predominantly utilised chalcopyrite or other copper sulphides (Addis *et al.*, 2017; Artioli *et al.*, 2016), while research on Early Bronze Age Saint Veran revealed the exploitation of bornite, another Cu-Fe sulphide (Bourgarit *et al.*, 2008). However, it must be noted that the absence of arsenic and antimony in the slags may be attributed to the volatile nature of arsenic, which tends to evaporate at high temperatures, resulting in very low concentrations or even becoming undetectable. Remarkably, if confirmed by further research, this discovery establishes the site of Orti Bottagone as one of the oldest pieces of evidence of sulphosalts smelting, dating back to the Final Neolithic period. Similar results were previously uncovered in slags from the nearby site of San Carlo, which belongs to the early Copper Age, slightly later in chronology (Artioli *et al.*, 2016). While only these two sites have been investigated from an archaeometallurgical perspective in the region thus far, the exploitation of sulphosalts at both sites suggests that this region might have played an important role in the smelting of sulphosalts and producing arsenical copper during the early stages of Italian metallurgy.

Upon reviewing the literature, it becomes apparent that almost all the Chalcolithic daggers/halberds from Italy are made of Cu-As or Cu-As-Sb compositions, whereas axes primarily consist of pure copper (Dolfini, 2014). It is important to highlight that the pure copper and copper-arsenic compositions found in these items aligns with the chemical compositions of the metal droplets analysed at the 4th millennium BC smelting site of San Carlo (Artioli *et al.*, 2016). The earliest securely dated daggers and halberds date back to 3650 BC, and although no

arsenical objects are known from 3800-3600 BC, it is important to acknowledge that the chronology of the earliest metal objects it is not always entirely reliable (Iaia & Dolfini, 2021 and references therein). Variations and uncertainties may exist in accurately dating these objects. Although it has been proven that some of the copper circulating in Italy in the Late/Final Neolithic was imported by the Balkans based on Lead Isotope Analysis (Artioli et al., 2020; Höppner et al., 2005) and object morphology (Iaia & Dolfini, 2021), this discovery suggests that arsenic-bearing sulphosalts might have been exploited in west-central Italy from the Final Neolithic.

9.3. Experimental vs Archaeological evidence

In the previous chapter, I detailed the results of the experiments aimed at replicating the smelting process carried out at Orti Bottagone. The primary focus was to assess the feasibility of a one-step smelting procedure, which entailed bypassing the traditional intermediate roasting stage and forgoing the use of a crucible to contain the charge. I conducted two sets of experiments: one with partially roasted initial charges and the other with unroasted ones. For a comprehensive overview of the parameters employed in the experiments, please refer to Chapter 9. The objective was to compare the smelting of unroasted charges (1A and 2A) with the smelting of roasted charges (1B and 2B). It is important to acknowledge that the number of trials conducted does not replicate all the potential working conditions employed by ancient smiths, including variables like charge composition, temperature, reducing/oxidising conditions, and timing. Nevertheless, this limited set of trials has yielded valuable results. The comparison of the slags recovered from Orti Bottagone with the by-products obtained from the designed experiments has produced compelling and numerous resemblances across various key aspects of the smelting processes, while also highlighting some differences.

9.3.1. *The similarities and their implications.*

No significant differences were observed between the experiments that employed unroasted and partially roasted charges. While it is worth noting that these experiments might have been inconclusive, as both unroasted and partially roasted ores produced identical signatures in the resulting slag, the absence of substantial distinctions between the experiments suggests that smelting the ore without prior roasting and without the deliberate addition of copper carbonates/oxides or fluxes could have been the actual process. This consideration arises from the understanding that roasting would have been more time and fuel consuming, yet it would

have yielded the exact same outcome, i.e., effectively initiating the conversion of the ore into metal.

Features resembling those found in archaeological specimens were detected in both sets of experiments, irrespective of the charge type or roasting stage. These features exhibit similarities in terms of mineralogical compositions and morphologies. One of the most notable parallels can be observed in the round-shaped Cu-Fe sulphides present in both experimental slags (roasted and non-roasted), as well as flat slags. An illustrative example showcasing this similarity between the experimental slag JH1A_T3_003 and the flat slag ORTB 13 is presented in figure Fig. 9. 5. These formations are characterized by their high copper content (in blue) and significant iron and sulfur content (in yellow). The former is a by-product produced during the initial set of experiments, while the latter is a flat slag traditionally interpreted as a by-product of the advanced matting stage. This observation lends support to the hypothesis that both types of slags could result from a one-step smelting process and coexist in the same reactor, as proposed by Piel et al. and Metten (Piel *et al.*, 1992; Metten, 2003). As such, this coexistence challenges the conventional classification of slags into distinct smelting stages, particularly during the early stages of metallurgy. The distinctions between these slags may arise from variations in the charge type and/or from multiple reprocessing cycles of the same charge, progressively removing more slagged by-products with each reprocessing step. Importantly, these variations are influenced by the fluctuating temperatures and shifting reducing/oxidising conditions inside the reactor. Another significant similarity emerges in wedge-shaped features containing a Cu-Fe sulphide compound, which were observed trapped between converging pyroxene dendritic structures. These features can be found in the experimental slag JH1B_T2_002 and in the coarse slag ORTB 20 (Fig. 9. 6). In yet another notable discovery, similarities were observed between experimental slag JH2B_T1_002 (phase 2B) and flat slag ORTB 8 (Fig. 9. 7). In both cases, these specimens exhibited magnetite in prismatic and round morphologies, along with elongated pyroxenes within a fayalitic matrix. These shared morphologies within a relatively confined area suggest highly unstable and variable thermodynamics, accompanied by fluctuating reducing/oxidizing conditions during the smelting process, as highlighted by Bourgarit (2019).

Adding to these observations, it is important to mention that there is a remarkable consistency in viscosity and density among the by-products studied. Both experimental by-products, which include slags and matte fragments, demonstrated an average viscosity value of $k=1.25$, closely mirroring the previously calculated viscosity of 1.2 for the coarse slags discovered at Orti Bottagone. However, the matte fragments, despite showcasing the anticipated glossy and shiny surface, deviated from the expected elevated specific density due to their high porosity. This

deviation suggests that these matte fragments are indicative of early-stage by-products, suggesting an extended production timeline that may involve the crush-select-resmelt technique proposed in Section 2.5.

Overall, these remarkable similarities in experimental and archaeological slags compellingly support the notion that the one-step smelting process carried out in the experimental sets may indeed have replicated the approach adopted in the past.

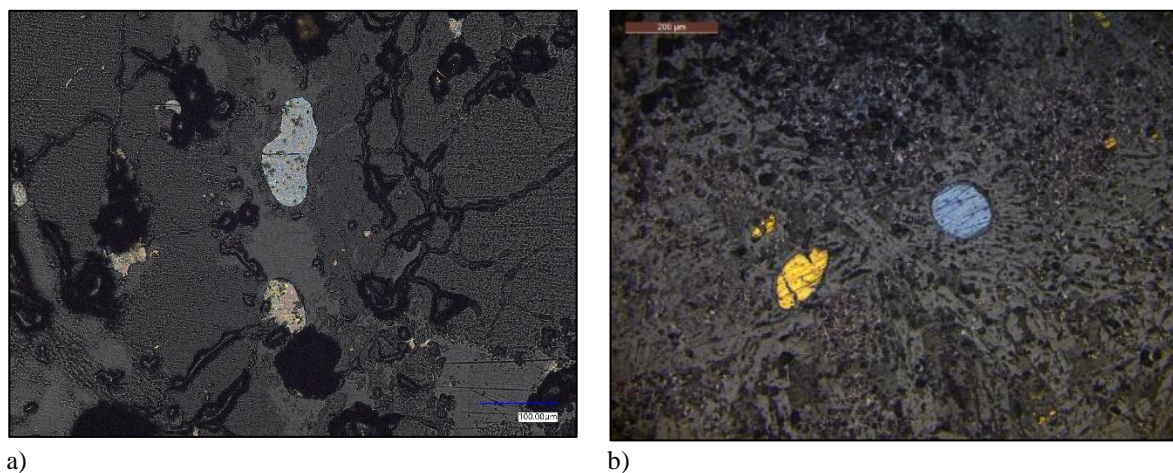


Fig. 9. 5 Optical micrographs showcasing round-shaped Cu-Fe sulphides high in copper (blue) and high in iron and sulphur (yellow) observed a) in the experimental slag JH1A_T3_003 (scale bar 100µm) and b) in the flat slag ORTB 13 (scale bar 200µm).

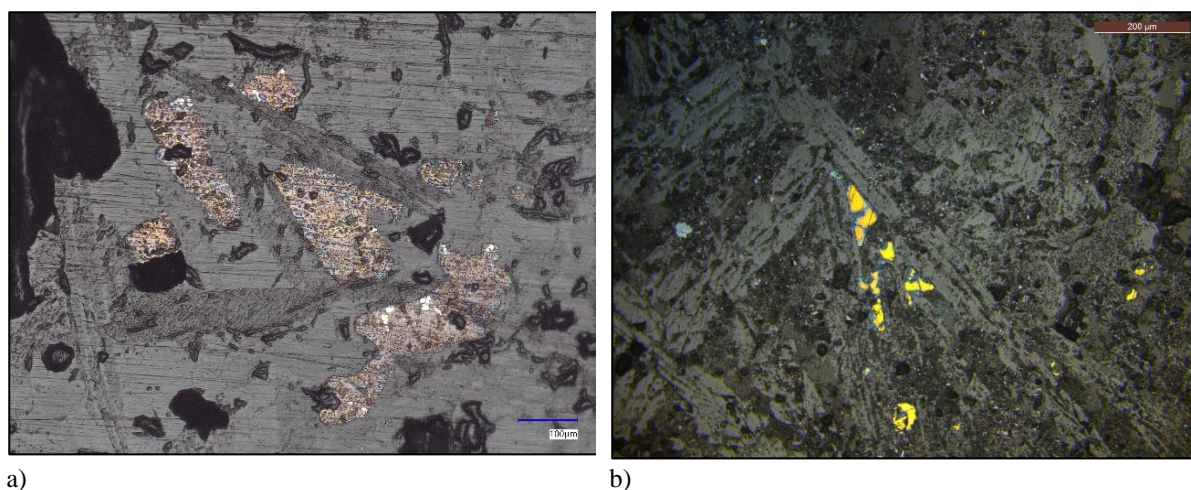


Fig. 9. 6 Optical micrographs showcasing a wedge-shaped feature observed (a) in the experimental slag JH1BT2_002 (scale bar 100µm) and (b) in the coarse slag ORTB 20 (scale bar 200µm).

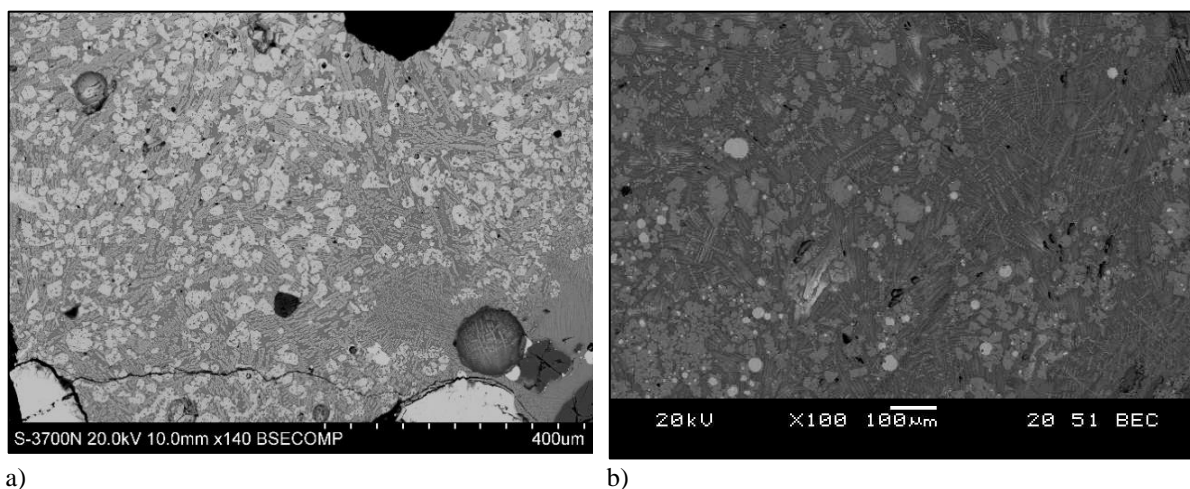


Fig. 9. 7 BSE micrographs of (a) the experimental sample JH2B_T1_002, and (b) the flat slag ORTB 8 showing the almost perfect match of the morphologies.

9.3.2. The differences and their implications

Despite the presence of similarities between the experimental and archaeological assemblages, it is crucial to address significant differences that have also come to light. The first notable discrepancy concerns, the quantity of by-products produced in all experiments. The experiments showed that, despite selecting ore containing a high amount of calcium in various forms and quartz, only a small quantity of slags was produced. Apart from trial JH1A_T3, which yielded a return of 59.4% of the initial charge, the incomplete smelting trials produced only approximately one fifth of an initial charge (0.5 kg) in the form of slags and variable matte compositions. Similar results were achieved in the experiment conducted by Timberlake in 2004 at Butser Iron Age Farm where only a few grams were obtained overall out of 430 g using sulphide ore, in a reconstruction of one of the Ross Island type 1 furnace pits (Timberlake, 2007) (see Chapter 7 for a detailed experiment outline). This observation raises two possible interpretive hypotheses, which are not mutually exclusive. First, the larger volume of archaeological slags may be attributed to the use of a higher amount of charge in the reactor during ancient smelting practices, exceeding the 0.5 kg utilized in the experiments. Second, it is plausible that ancient smelters used initial materials without meticulous beneficiation, opting for copper-bearing ore rich in gangue. Nevertheless, a closer examination of the SEM semi-quantitative analyses between the two assemblages reveals higher silica and calcium contents in the experimental slags. Given that no dolomitic rocks, which could have significantly contributed to calcium content in the slags (Bourgarit, 2007), were used to build the reactor,

nor was an excessive amount of calcium deliberately introduced into the system, this finding lends support to the hypothesis that a more meticulous beneficiation process was carried out in ancient times, ensuring the selection of only high-grade copper ore.

An intriguing difference that has been identified lies in the absence of euhedral features in the experimental slags. Conversely, the archaeological slags from Orti Bottagone (Fig. 9. 2a), as well as numerous Chalcolithic slags documented in the literature (e.g., San Carlo, Artioli et al., 2016, p. 77, fig. 52d; and Akladi Cheiri, Rehren et al., 2016, p. 149, fig. 12) display relatively large polyhedral fayalitic features within the slag core. The experimental slags were removed from the reactor shortly after the process (typically within 5-7 minutes). The presence of these features proves that these slags cooled inside the reactor rather than being promptly extracted at the end of the process, suggesting a more extended cooling period inside the reactor.

Unlike the archaeological specimens, the experimental slags from both sets showed a notably higher number of trapped copper-bearing compounds (as seen in Fig. 9. 8). These compounds were dispersed across the specimen surfaces as either lumps of matte or copper droplets, often in agglomerated forms, with isolated occurrences in smaller quantities. Notably, several of these features, intriguingly absent in typical archaeological specimens, showcased copper at various stages of transformation. As depicted in Fig. 9. 9, four distinct stages illustrate how copper progressively clustered over the 30-minute smelting process. These findings imply that the duration of the experimental trials proved insufficient for copper to effectively separate from the charge and accumulate in a single piece. Furthermore, given the absence of these intermediate features in archaeological specimens, it suggests that the smelting process carried out in antiquity likely extended over a time longer than 30 minutes.

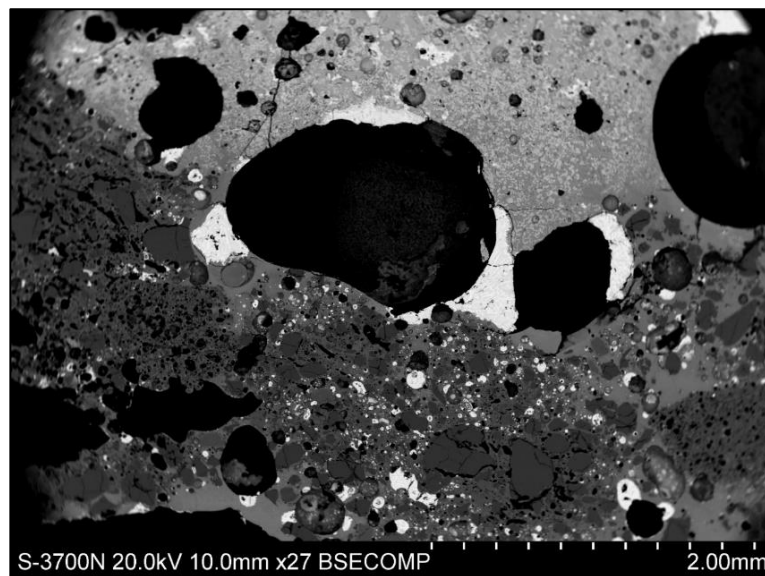
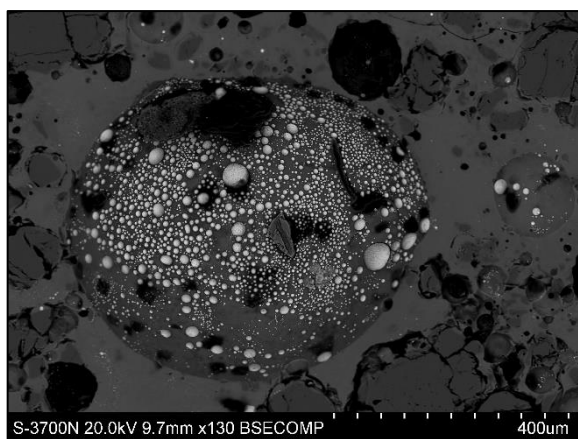
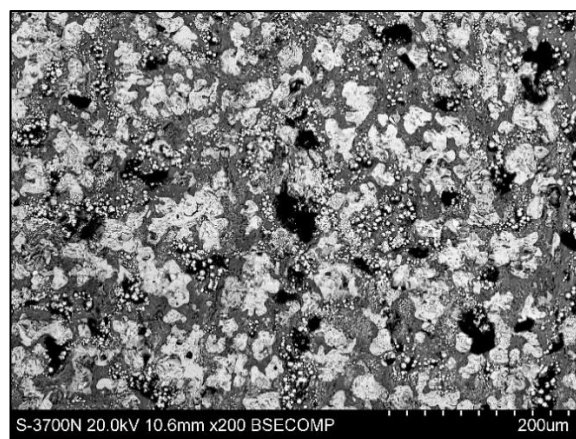


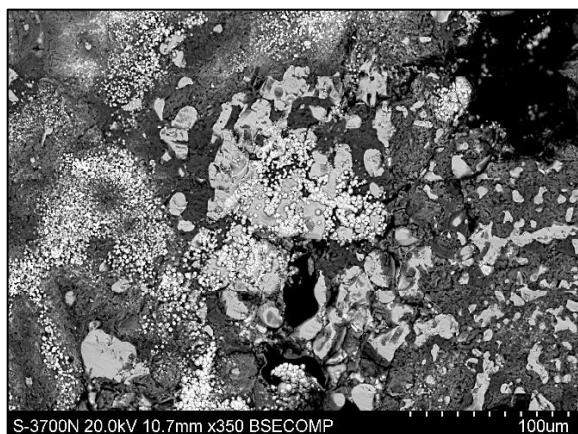
Fig. 9. 8 BSE micrograph of a region of the experimental slag JH2B_T1_002 highlighting abundant trapped Cu-bearing features (white).



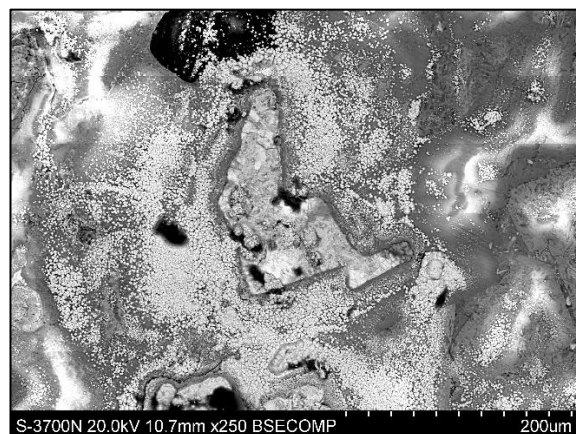
a)



b)



c)



d)

Fig. 9. 9 Visual representation of diverse features of copper at various stages of transformation (white), illustrating the step-by-step accumulation of copper during the experimental 30-minute smelting process. (a) sample JH2A_T3_001; b) sample JH2B_T2_001; c) and d) sample JH2B_T2_001).

A distinctive feature consistently observed in all the experimental slags is the presence of Cu-Fe sulphide droplet "belts", a term I have coined for this phenomenon. The term refers to a cluster of Cu-Fe sulphides, predominantly exhibiting a rounded morphology, densely concentrated, and arranged in a straight line within a vitreous matrix, interposed between partially unaltered or partially reacted components, primarily composed of quartz (see Fig. 9. 10a). Remarkably, these features bear a striking resemblance to Chalcolithic slags discovered at various sites across Europe. As illustrated in figure Fig. 9. 10a, the experimental sample JH2A_T3_001 displayed Cu-Fe sulphide droplets embedded within a highly viscous silicate matrix, alongside unreacted silica. This closely mirrors the mineralogical phases of slag discovered at Final Neolithic/Chalcolithic sites like La Roussignole and La Vallarade in the south-west French Alps during previous studies (Ambert et al., 2013, p. 67), as shown in Fig. 9. 10b (refer to Section 3.2 for details). These "belt" features can be attributed to the elevated viscosity of the slag, which may have arisen from several factors, including suboptimal temperatures in the reactor, an imbalanced initial charge composition (possibly characterized by an excessive amount of silica), or a combination of these factors. Unfortunately, pinpointing the exact cause of the feature remains elusive. Nonetheless, this heightened viscosity posed a significant obstacle to the effective separation of metal from the slag. Consequently, numerous metal droplets at various stages of transformation, ranging from a few microns to several millimetres in size, are dispersed and embedded within the experimental slags.

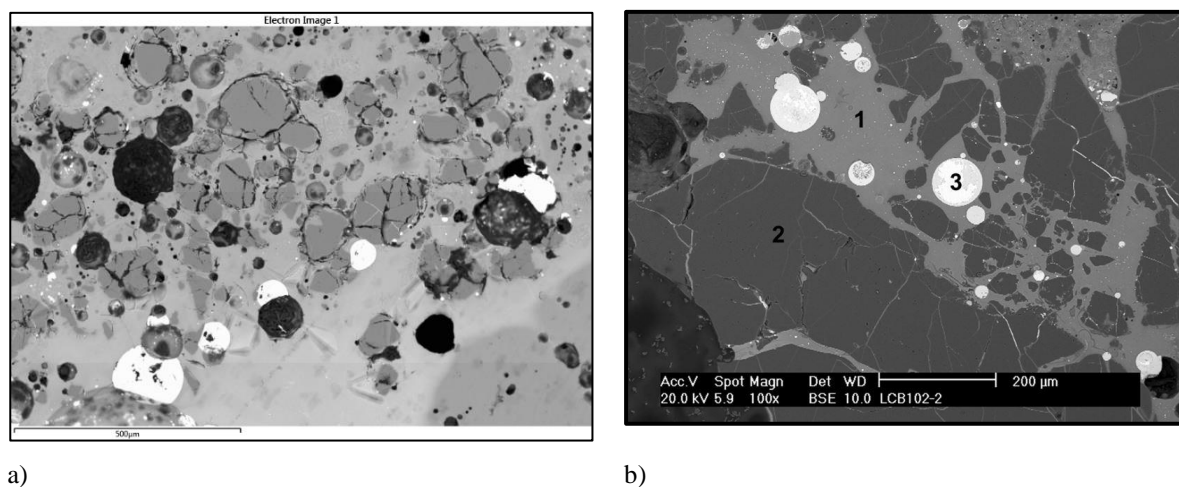


Fig. 9. 10 Comparison of BSE micrographs: (a) experimental sample JH2A_T3_001, and (b) an archaeological sample from Roussignole (Ambert et al., 2013, p. 67, 6), revealing analogous mineralogical phases. Both images

depict metal droplets (3) embedded in a highly viscous silicate matrix (1) alongside unreacted silica (2) within the slag.

The substantial quantity of these “belt” features, combined with their diverse transformation stages, suggests that they represent early-stage products, lending strong support to the hypothesis of a slow and gradual metal recovery process. Furthermore, the outcome of re-smelting the same charge in the trials of Experiment #2 (2B) reinforces the idea that the smelting process likely entailed repetitive cycles. This re-smelting resulted in an augmented presence of metallic copper and matte toward the outer areas of the slags. This repetition seems to have been designed for the gradual recovery of matte and/or metallic copper from these early-stage products. However, none of these “belts” features have been found in the archaeological specimens examined in the current research (refer to Section 5.2.9). Their absence can be interpreted in two distinct yet not necessarily conflicting ways. Firstly, it may suggest that the slags resulted from a subsequent cycle of processing. Alternatively, it hints at a higher level of operational efficiency in the original smelting process. Both interpretations contribute to a more significant accumulation of copper-bearing compounds at the base of the reactor, effectively separating them from the original charge.

A type of product consistently observed throughout the experimental assemblage was matte. Notably, no fragments of matte were detected within the Orti Bottagone assemblage, and such fragments are typically exceedingly rare in the archaeological record. This scarcity may be attributed to its recognised high value as an intermediate copper smelting product for ancient smelters, as suggested by Rostoker et al. (1989). While some matte fragments exist from the Late Bronze Age onward (Hauptmann, 2020, pp. 228-31), there is a notable absence of matte fragments from earlier periods within the existing literature. Nevertheless, valuable insights can be gleaned from this type of intermediate by-product.

First and foremost, the experimental trials revealed the existence of an intermediate product that is conspicuously absent from the archaeological record, showing a disparity between experimental findings and archaeological evidence, and underscoring the crucial role of the experimental approach in gaining deeper insights into ancient technological processes.

Second, the matte assemblage exhibits consistent characteristics, displaying no discernible differences between phase 1 and phase 2. This reinforces the hypothesis of a one-step smelting process. Additionally, the matte fragments, characterised by their blackish-grey colour (Fig. 9. 11), high porosity, and low density, provide further support for the notion that they represent intermediate products in a very early stage of reduction. In many instances, matte areas were

distinctly identified within the slags. These sections were clearly demarcated from the slag matrix and were predominantly located toward the outer regions of the slags (see Fig. 9. 11). The absence of such distinct separation between the slag matrix and the matte in the archaeological specimens from Orti Bottagone, as well as in the broader contemporary archaeological record, lends further credence to the hypothesis that the slags underwent a systematic process of crushing, collection, and subsequent re-smelting (Bourgarit & Mille, 2005).

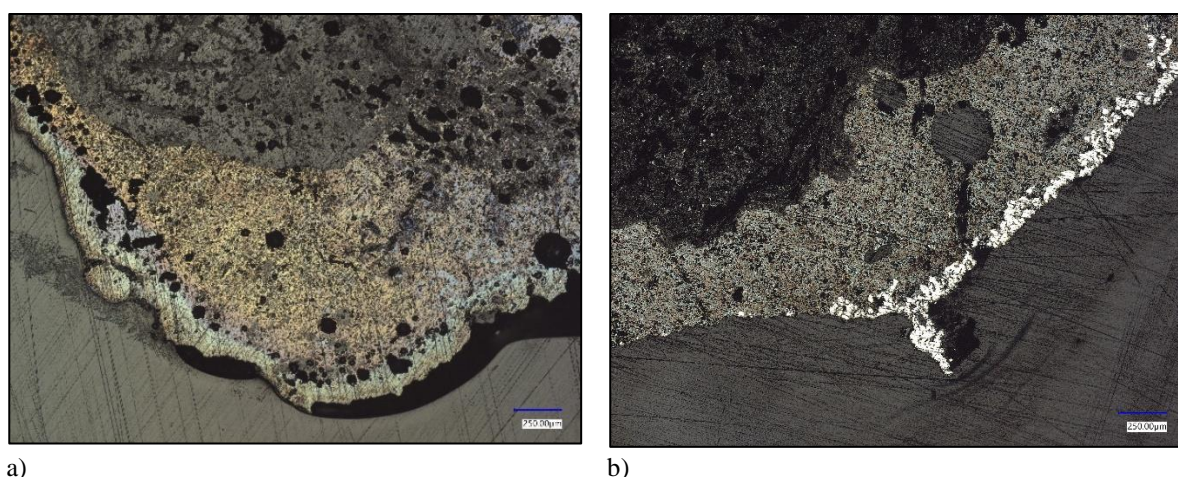


Fig. 9. 11 Optical micrographs showing matte regions, distinctly separated from the slag matrix, predominantly positioned at the outer boundaries of the slag samples; a) sample JH1A_T2_003 (scale bar 250µm), b) sample JH2B_T2_001 (scale bar 250µm).

Further bolstering the argument for matte fragments representing products in an early stage of reduction are the inclusions observed within some of these fragments.

Some of these inclusions, as depicted in figure Fig. 9. 12, may initially seem like remnants of flat slags. However, upon closer examination, they reveal themselves to be elongated structures with a composition resembling fayalitic minerals and quartz. This information holds great value, as it has the potential to significantly influence the interpretation of archaeological findings, rectifying any potential misconceptions that could mislead scientists when analysing similar features in archaeological materials.

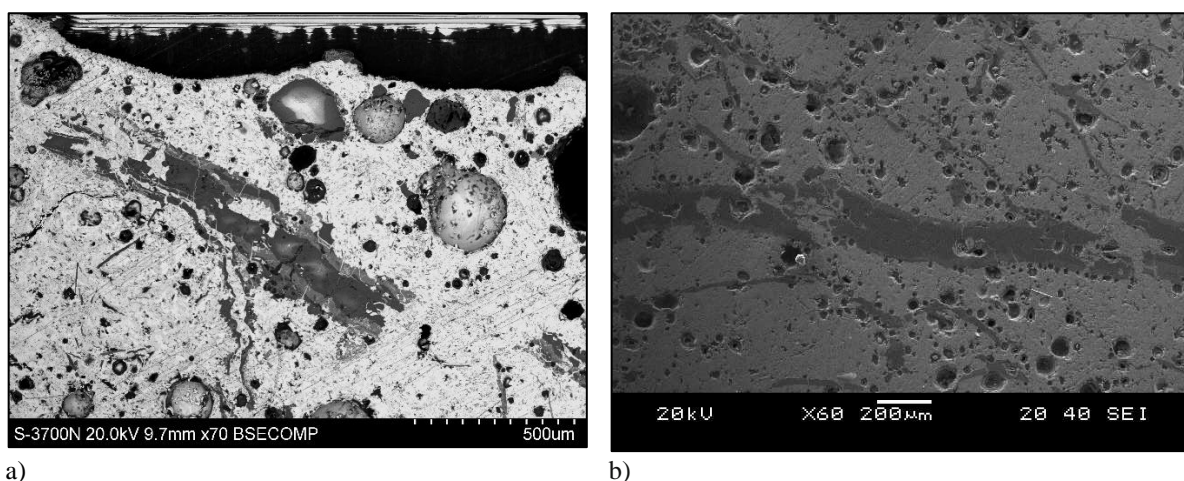


Fig. 9. 12 illustrates a) a BSE and b) a SE micrograph of two samples from trial JH1B_T3 revealing the deceptive morphology, consisting of elongated fayalitic structures that can be misleadingly mistaken for flat slag inclusions.

9.3.3. Crucible reduction technology?

While prior experiments (see Chapter 8) have already established the viability of smelting in open reactors without the use of a crucible, I embarked on a series of experimental trials to smelt local ore without the use of a crucible to contain the initial charge. The origin of this research question can be traced back to the pilot experiments conducted as part of this project. This decision was motivated by several considerations that still require attention. This inquiry was prompted by the conspicuous contrast between the limited number of crucibles discovered in the archaeological record and the abundance of recovered slags and metal objects (Hauptmann, 2020, pp. 462-4).

Scholars have proposed an explanation for this scarcity of crucibles in the archaeological record, suggesting it may be due to the absence of thermal alteration or slag residues lining the crucible walls, making their identification a challenging task. This hypothesis gains support from both archaeological and experimental evidence. For instance, during the excavation conducted at Belovode, Radivojević and Rehren (2021) unearthed a vessel bottom (Feature 35) embedded in the soil. However, neither direct evidence, such as traces of thermal alteration on the crucible, nor indirect evidence from portable XRF analyses indicating metal contamination (p. 122), could definitively establish its connection to metallurgical activities. It was only through the contextual evidence, including traces of ashes and charred surfaces, that the team could confidently identify it as a smelting area. In terms of experimental evidence, a series of smelting experiments conducted in 2013 by the same research team, aimed to replicate the proposed smelting installation (Radivojević & Rehren, 2021). These experiments did not yield any slag adhering to the crucible or traces of copper production inside it, further supporting the

absence of smelting-related traces. Additionally, regarding the initial pilot smelting experiment carried out in this thesis (see Section 6.4.1, Exp.1 – Furnace 1), the observed thermal alteration traces on the rim were the result of misplacing the crucible inside the reactor (see Fig. 6. 6). Otherwise, no other traces would have been detected on it.

However, it is worth noting that all the experiments mentioned above focused on smelting high-grade secondary copper minerals, which typically begin to decompose at approximately 400°C and do not require temperatures exceeding 700-800°C to transform into copper oxides. Within this temperature range, the chemical alteration of the clay minerals in the crucible may have been insufficient to produce visible traces. Therefore, when dealing with such ores, if the crucible is correctly positioned in the reactor and the temperature is carefully controlled, it is possible that very few, if any, traces would be left on the artefact.

In contrast, smelting sulphide ores necessitates much higher temperatures, typically within the range of 1050 to 1250°C, to initiate the required reactions. These elevated temperatures would inevitably lead to thermal alterations or the presence of traces indicating metallurgical activities on the supporting crucible. In accordance with this perspective, the results of the third pilot experiment revealed thermal alteration in the crucible near the rim close to the air flow (Fig. 6. 8a), and predominantly on the bottom, which was covered with molten material. The only viable practical options to retrieve the material adhered to the bottom of the crucible were either breaking the crucible or chiselling the material out. This highlights a crucial point regarding the essential need for a crucible during the initial stages of smelting. The use of crucibles for smelting activities is commonly justified for economic reasons, to prevent the loss of valuable raw material, and for technological purposes, such as minimising heat loss/thermal dissipation and maintaining better control over the reducing environment (Martín-Torres & Rehren, 2014). However, when considering the widely accepted technique for copper recovery, which involves systematic processes of crushing, selection and subsequent re-smelting of intermediate products (Bourgarit & Mille, 2005), it becomes evident that this process requires multiple iterations, each requiring a crucible. This point is further substantiated by a recent experiment conducted by Timberlake (2007), who produced copper sulphide/copper-iron sulphide matte revealing small growths of copper metal. These findings prompted Timberlake to propose that the extraction of copper from the ore was a slow and gradual process, requiring the incremental recovery of copper metal through the processes of crushing and selecting (washing and panning) the semi-smelted ore. As a result, one should either expect to find a higher number of crucibles in the archaeological record, or if the archaeological record accurately reflects ancient smelting practices, an explanation for this shortage of crucibles must be sought. In this vein, a

series of experiments demonstrated that the production of metallic copper could have been carried out without the use of a crucible (Fasnacht, 1999; Hanning *et al.*, 2010b; Timberlake, 2018). As an example, Timberlake (2018) successfully produced a slag cake approximately 10cm in diameter and weighting 250g, containing mm-size metal inclusions in a charcoal bed in a shallow depression in the ground.

The experiments carried out in this research lend support to the idea that the crucibles are not essential for the smelting process. Firstly, the fine-grained charcoal layer covering the bottom of the reactor, a technique derived from the ethnographic report of the “Himalayan model” conducted in the mid-20th century at Sikkim, in Okharbot, western Nepal, (Anfinset, 2001; Blanford, 1861), which was recently compared to Trentino Chalcolithic smelting process (Pearce et al., 2022), proved to be an effective expedient for preventing copper from sinking to the bottom of the reactor. In none of the 12 experiments that I carried out was a single drop spilled or adhered to the reactor walls. Moreover, the “cap” of charcoal placed above the charge may have played a crucial role in maintaining the temperature at the required levels. Secondly, the outcome of the 12 trials consistently involved the melting of the initial charge. This successful result demonstrated efficient heat loss control without the use of crucibles. The required range of temperatures were easily attained within the reactor, and throughout the entire process, heat dissipation remained effectively controlled, as corroborated by the temperatures recorded by the thermocouples in the reactor.

Following the experimental results, the absence of crucibles, without negatively affecting the smelting processes, implies that the archaeological record, which lacks a substantial presence of crucibles, may accurately depict past smelting practices in a less biased manner than commonly assumed. The scarcity of crucible fragments in the archaeological record can be explained by considering that crucibles, including the fragment investigated in this thesis (Chapter 6), may not have been used in the initial smelting stages. During these stages, copper production was limited, and the metal inclusions had to be recovered from the slags through a systematic process of crushing, selecting, and remelting. Instead, these crucibles may have come into play during subsequent stages when larger quantities of copper were produced and needed to be collected as more substantial units. This perspective aligns with the proposition presented by Laschimke & Burger. They suggest that the trough-shaped crucibles discovered at Pfyn Culture sites (dating to the 4th millennium BC) in locations such as Niederwil, Gachnang-Egelsee and Hüttwilen in Kanton Thurgau, Switzerland (Leuzinger, 1997), were probably employed as containers for melting and producing larger copper units (Laschimke & Burger, 2017, 2018).

Chapter 10. Conclusions and avenues of future research

10.1. Introduction

This chapter summarizes the key findings of the research, highlights their significance in the context of early copper metallurgy. It also suggests potential avenues for future research in the study of early metal technology, particularly ore processing and reduction.

10.2. Project results and reflections

In this research endeavour, the central goal was to gain deeper insights into the smelting techniques employed by prehistoric metallurgists during the early 4th millennium BC. The primary emphasis was on their ability to successfully smelt sulphide ores, a rare practice during a period dominated by the use of copper oxides and carbonates. Specifically, the research project examined slag and crucible fragments resulting from early 4th millennium BC (Final Neolithic) smelting activities carried out at Orti Bottagone, an archaeological site in southern Tuscany, Italy. I pursued two primary objectives:

Objective 1: Characterising the copper reduction technology employed at Orti Bottagone.

Objective 2: Investigating early sulphide ore smelting through experimental archaeology.

The research questions for Objective 1 were to:

- Were sulphide ores employed in conjunction with oxides and carbonates, or was the ore usage primarily centred around sulphides?
- What are the types of slags produced? Can they be attributed to specific smelting stages within the overall metallurgical process?
- Is there evidence of intentionally added fluxes, or were self-fluxing ores smelted?
- What parameters (temperatures, reducing /oxidising conditions) were employed?
- Are there any traces of arsenic (As) and/or antimony (Sb) in the slags and in the crucible fragment?

The research questions for Objective 2 were to:

- Is the local ore suitable for smelting without the addition of carbonates/oxides, or the deliberate addition of fluxes, utilising a one-step process (i.e., without roasting)?
- Can we ascertain whether the by-products of the smelting experiments resemble to the archaeological ones, and if such resemblance exists, which experiments and phases yield slag materials that exhibit a greater degree of similarity?
- Which smelting technique proposed in the literature, if any, best fits the experimental residues produced?

Furthermore, while not the central emphasis in this second part of the thesis, prior experiments supporting its viability, I explored smelting using local ore without the use of a crucible.

In pursuit of answers to these research questions, I adopted a multi-analytical methodology combining materials science with experimental archaeology. This holistic approach involved the examination of both archaeological and experimental artefacts. The analytical techniques employed encompassed Optical and Digital Microscopy (OM and DM), X-ray Powder Diffraction (XRD), X-Ray Fluorescence (pXRF), and Scanning Electron Microscopy coupled with Energy Dispersive Spectrometry (SEM-EDX). Recognising the inherent limitations of these techniques in providing a comprehensive understanding of prehistoric smelting processes, I decided to overcome these constraints by integrating the analysis of the archaeological finds with smelting experiments. The primary goal of the experiments was to better understand the technical choices and challenges confronted by ancient metallurgists. This approach shed light on the methods employed by local artisans in smelting sulphide ores. The experimental approach employed in this study served as a heuristic device to partly validate the analytical data and for information collection rather than a mere attempt to replicate the process solely to assess its feasibility.

The findings from Orti Bottagone provide compelling evidence of early 4th millennium BC reduction of sulphur-rich copper ores. This conclusion is substantiated by the examination of both slag samples and an ore fragment from the site. Not only does this discovery validate the feasibility of sulphide smelting during the early 4th millennium BC, but it also establishes a connection with similar smelting processes observed at the neighbouring site of San Carlo, albeit it is slightly later in date (Fedeli & Galiberti, 2016).

The challenge of drawing a definitive conclusion regarding the processing of the charge, arises from the recovery of a single ore fragment at the site, giving rise to two plausible scenarios.

Firstly, the presence of quartz and a high carbonate content suggests the use of a minimally refined charge, potentially indicating a lack of thorough ore processing to remove impurities. Alternatively, it could be suggested that the fragment might have been a discarded piece of country rock with low copper content.

The mineralogical composition of the slags from Orti Bottagone closely aligns with the characteristics of the local ore from the mines of Temperino and Lanzi, located only 12 km away. This suggests that the prehistoric metallurgists at Orti Bottagone were indeed processing local sulphide ores. The slags exhibited a range of characteristics, including high viscosity, compositional heterogeneity with a wide array of mineralogical phases, a significant presence of copper-bearing compounds, and both unreacted and partially reacted inclusions. The presence of polyhedral features in the slag core suggests in-reactor cooling followed by recovery. While determining exact cooling rates proves challenging, the presence of fayalitic olivine structures implies sufficiently high temperatures ranging from 1000°C to 1250°C. Furthermore, their irregular, fragmentary state implies that they were deliberately broken for the recovery of copper prills. Although the use of fluxing agents remains a subject of debate due to the absence of clear evidence, the significant amounts of calcium and silica in the slags may have functioned as self-fluxing agents, potentially aiding the smelting process.

These features collectively point towards an immature slagging process conducted with a charge that deviates from the ideal eutectic “recipe”, under fluctuating reducing/oxidising conditions and variable temperatures within the reactor. These aspects align with the slags identified in the “ephemeral” Chalcolithic smelting model depicted by Bourgarit (2007). However, the identification of two distinct slag types, namely coarse and flat, deviates from Bourgarit’s model and holds significant implications for our understanding of early metallurgical practices in Late Neolithic and Chalcolithic Europe. Notably, the presence of flat slags, characterised by low viscosity, low porosity, and few unreacted inclusions does not align well with Bourgarit’s model. Additionally, the unexpected abundance of slag remnants uncovered challenges the conventional belief in the “slagless” processes of the early periods proposed by Craddock (1995). This hints at a higher degree of technological advancement at this early stage. Traditionally, such slag types have been associated with multi-step copper smelting processes, particularly slagging (coarse slags) and matting (flat slags) stages, observed in more advanced contexts dating from the Middle/Late Bronze Age onwards.

Nevertheless, a re-evaluation of our understanding of early smelting processes becomes imperative, particularly when considering the early chronology of Orti Bottagone. This consideration is coupled with the widely accepted assumption that early metallurgical practices tended to favour simplicity. Adding to the complexity is the assertion by Rostoker et al. (1989)

that processes of co-smelting do not yield both coarse and flat slag types. In response to this complexity, I proposed an alternative interpretation and conducted tests (see below) to explore this hypothesis. According to my alternative interpretation, both types of slags could result from a one-step smelting process, both coexisting within the same open reactor. This challenges the conventional classification of different slag types deriving from distinct smelting stages.

The entire slag assemblage from Orti Bottagone has revealed traces of arsenic. This discovery represents a remarkable breakthrough in our understanding of metal production during the Final Neolithic period in central Italy. It sheds light on potential arsenical copper production, a testament to the high level of expertise achieved by metalworkers during this era. While uncertainties remain about how arsenic found its way into the slag samples and its specific source, several factors lean towards the likelihood of sulphosalts exploitation at the site. This is supported by the absence (or very low quantities) of arsenates in the local geological reports, evidence of sulphosalts exploitation at the nearby site of San Carlo (Artioli et al., 2016), and the presence of sulphur and zinc in the slag samples, linking the slags to the nearby ore deposits. The rarity of slags from sulphosalts deposits in early Europe compared to copper-iron sulphide deposits is noteworthy, and the volatility of arsenic at high temperatures may explain its absence in the slags. In conclusion, the presence of arsenic at Orti Bottagone opens new avenues for research into the complexities of ancient metal production. It has the potential to expand our knowledge of early metallurgy in Europe and highlights the importance of further investigations into the use of arsenical copper during the Final Neolithic period.

This body of evidence provides the first detailed insight into metallurgical practices at an early 4th millennium BC western European site. It not only sheds light on a previously partially unknown technological approach but also underscores its potential significance in the transition from oxide/carbonate to sulphide smelting in prehistoric Europe. While the findings rely on evidence from a single site, they, in conjunction with supporting evidence from San Carlo (Artioli et al., 2016) and preliminary results on Orti Bottagone by Artioli and colleagues (2009), significantly contribute to a broader comprehension of the evolution of metal technology in western Europe in the 4th millennium BC.

The smelting experiments yielded several important insights that complement the analytical data. Firstly, no significant differences were observed between the experiments involving unroasted and partially roasted charges. This suggests that smelting local ore without prior roasting, and without the addition of copper carbonates/oxides or fluxes, may indeed have been the actual process carried out in the past. Roasting, which would have been more time and fuel-consuming, may not have been a necessary step in the process.

Secondly, striking similarities in mineralogical compositions and morphologies were observed between the features found in both experimental and archaeological specimens. Round-shaped Cu-Fe sulphides, wedge-shaped features containing a Cu-Fe sulphide compound, magnetite in prismatic and round morphologies, and elongated pyroxenes within a fayalitic matrix were consistently found in both experimental and archaeological samples. This, coupled with the uniform viscosity and density values of the by-products in both assemblages, strongly suggests that the one-step smelting process in the experiments likely replicated the smelting process adopted in the past. Thirdly, the coexistence of different morphologies and mineralogical compositions, belonging to coarse and flat slag types, within the same reactor during a single process, corroborates the hypothesis that both types of slag could result from a one-step smelting process, as already suggested by Piel *et al.* and Mettel (Piel *et al.*, 1992; Metten, 2003). These variations in slag shape may arise from differences in charge type and reprocessing cycles, influenced by fluctuating temperatures and changing reducing/oxidizing conditions inside the reactor.

While some similarities were noted between the experimental and archaeological assemblages, there were also notable differences. Unlike the archaeological slags, the experimental ones lacked euhedral features, indicating a shorter cooling period inside the reactor. The experimental slags also contained a higher concentration of trapped copper-bearing compounds compared to their archaeological counterparts, suggesting that the smelting process carried out in the past likely extended beyond the 30-minute duration of the experiments.

Matte fragments were consistently observed in the experimental assemblage, yet none were found in the archaeological assemblage. This absence may be attributed to the systematic process of crushing, collecting, and subsequent re-smelting that the slags underwent. This process likely occurred due to the perceived high value of matte, a notion supported by various researchers, such as Rostoker *et al.* (1989), and Bourgarit (2007, 2019).

In summary, the remarkable similarities between experimental and archaeological evidence provide strong support for the idea that the one-step smelting process employed in the experiments may have faithfully recreated the ancient process. The experimental reconstruction of the smelting process, using local sulphide minerals, suggests that sulphide ores might have been directly smelted in a one-step procedure, bypassing the traditional need for roasting the ore before introducing it into the furnace. This aligns with the experimental data presented by Bourgarit *et al.* (2002), demonstrating the effective reduction of sulphide ore in a one-step process without the presence of copper oxide (see Chapter 7). This insight signifies that copper

sulphide smelting could have occurred at the initial stages of metallurgy, under conditions that, although inefficient, successfully transformed the ore into metal.

Lastly, I addressed the scarcity of crucibles found in the archaeological record in comparison to the abundance of recovered slags and metal objects. Scholars have suggested that identifying crucibles in the archaeological record may be challenging due to the absence of thermal alteration or slag residues on crucible walls. I proposed that while this may hold true when dealing with high-grade secondary copper minerals that decompose at lower temperatures, it cannot be the case when smelting sulphide ores, which require significantly higher temperatures, leading to thermal alterations or traces of metallurgical activities on crucibles' walls. Given the early chronology of Orti Bottagone, the limited amount of crucible evidence from that period, and the evidence of sulphide ore exploitation, I explored the possibility of smelting the local sulphide ore without the need for crucibles. The experiments conducted supported ore smelting directly in the reactor, without the use of crucibles. They demonstrate that the absence of crucibles did not negatively impact the smelting processes. This outcome has important implications for the interpretation of the archaeological record, suggesting that crucibles may not have been essential for the initial stages of smelting, and therefore their scarcity in the archaeological record could be attributed to their limited use in primary metallurgical processes. This challenges the conventional view, where the use of crucibles in smelting was assumed to be driven by economic reasons to prevent the loss of valuable raw materials and technological purposes to control heat loss and maintain a relatively reducing environment. It offers a new perspective on the role of crucibles in ancient metallurgical practices. Additionally, it is conceivable that crucibles were reserved for secondary metallurgical processes such as alloying and casting.

Additionally, this thesis addressed a notable research gap by creating a comprehensive catalogue of micrographs that feature both experimental and archaeological by-products from ancient smelting processes. This resource will provide scholars with a valuable reference database, enriching their comprehension of ancient metallurgical by-products and smelting techniques.

In conclusion, this thesis has made significant contributions to the understanding of early metallurgy, particularly the beginnings of sulphide ore reduction in western Europe. This reconstruction not only sheds new light on the smelting technology employed during the nascent stages of metallurgy but also deepens our understanding of this process compared to what is discussed in the literature. This project effectively responds to the calls made by Timberlake (2007) and Dolfini (2014) for more targeted research projects that merge

experimental archaeology and archaeometallurgy. The outcome of the experiments provided valuable insights that shed new light on the nuances of ancient smelting processes. This ultimately emphasizes the importance of experimental research in enhancing and refining knowledge and understanding of ancient technological processes.

The synthesis of archaeological and experimental data, the exploration of sulphide ore smelting, and the development of a reference catalogue collectively advance our knowledge of the technological choices, challenges, and accomplishments of prehistoric metallurgists. The insights thus gained not only enriched our comprehension of the past but also lay the foundation for further investigations and the exploration of new research avenues within the field of archaeometallurgy.

10.3. Avenues for future research

In this section, I explore avenues for future research and outline the paths that should be undertaken to advance our understanding of prehistoric copper metallurgy.

1) Addressing unanswered research questions.

The experiments I have conducted as part of this research have yielded compelling results, providing valuable insights into the smelting techniques used at Orti Bottagone. However, it is important to acknowledge that these experiments, while yielding useful information, have not comprehensively addresses all the research questions. For future research, the following problems should be explored:

- *Smelting of the matte fragments.* The proposal involves conducting experiments focused on smelting matter fragments originating from phases 2 (i.e., the re-smelted products, refer to Section 8.2). The objective is to produce copper from these matte fragments and subsequently compare the results across each phase and with archaeological evidence. The investigation aims to ascertain whether similarities persist between the unroasted and partially roasted charges or if noticeable distinctions in both the quantity and quality of the copper produced can be identified.
- *Testing different initial charges.* Another experiment might focus on the co-smelting of a combination of local sulphide and carbonate/oxide ores. This approach would generate evidence that can be compared with the archaeological specimens. The primary question is whether co-smelting produces different or similar by-products in comparison to the previously tested experiments.

- *Increasing the amount of charge.* To gain a deeper understanding of the reactions involved, experiments can be expanded by using a higher amount of charge. This will allow to investigate whether the reaction behaviour of the charge differs when a greater quantity is employed or if it remains comparable to the charges used in the initial experiments.

The proposed experiments will hold the potential to shed light on the previously inconclusive findings and offer, if not a more comprehensive perspective, at least a more nuanced and critical understanding of the subject matter.

2) **Excavation of the site.**

Future research should prioritise an in-depth excavation of the site of Orti Bottagone to gather additional data that can provide further insights into the archaeological context. The site, which is now a WWF wildlife oasis characterised by alternating patterns of intertidal water streams and patches of shrubs, is submerged under a mixture of water and mud throughout the year, a condition I personally witnessed in July 2022 (see Section 3.7 for details and images). Given the current situation, it is advisable to begin with a geophysical investigation to identify potentially interesting areas for further exploration. The most suitable geophysical technique for approaching this area has already been informally discussed. After consulting the oasis's keeper, the site is not inundated during a brief period at the end of August, following the summer draught. The oasis's keeper has informally expressed their willingness to support and facilitate these preliminary investigations.

3) **Extend the investigation to other sites.**

To enhance our knowledge of metallurgical practices in the region, future research should extend the investigation to the study of metallurgical products and by-products from other chronologically and geographically related sites. These sites are outlined in Chapter 3. This would help determine the existence of regional and super-regional metallurgical *foci* (sensu Chernykh, 1992b, p. 7) and assess similarities in smelting techniques, technological choices, and ore resources.

4) **pXRF investigation of the experimental reactor (ongoing)**

The ongoing research utilises a pXRF device to investigate the reactor I employed in my experiments. The main focus, 18 months post-experiment, is to determine whether there are traces of copper on the reactor's surface and its immediate surroundings, seeking

evidence linking the reactor to smelting activities. If the reactors took the form of firepits dug into the ground, leaving only scant two-dimensional traces challenging to recognise in the field, and if no other evidence, such as fragments of slags, crucibles, tuyeres, connects the reactor to smelting (see Section 2.5), can the pXRF device detect signs of metal contamination through surface analyses? This detection could potentially underscore the value of this analytical technique in identifying areas with only minimal two-dimensional traces remaining, as potential smelting site.

5) Innovative slag analysis using Micro CT.

An innovative approach using X-ray computed tomography (CT) should be developed further for slag analysis. In this thesis, I applied this technique with the specific goal of identifying charcoal samples within in the slags. The primary objective was to explore the inner composition of the slag without the need for physical sectioning, aiming to detect any remaining charcoal fragments and determine the most suitable locations for their extraction. This technique, using simultaneous views from three different planes and heat-maps, enables a thorough investigation of the inner composition and the highlighting of internal features within the slag. It offers a non-invasive means that is invaluable for pinpointing the most informative sections of a sample and potentially identifying charcoal fragments (see Fig. 3. 18 displays a) a simultaneous view of three different planes (XY, YZ, XZ), along with b) the use of a heatmap. This arrangement enables a comprehensive examination of the internal structure of the specimen.). Furthermore, it serves as an ideal means for preserving archaeological artifacts for posterity, ensuring their conservation, and facilitating public data access, enabling researchers to conduct 'digital autopsies' on preserved artifacts. Nevertheless, the full range of potential advantages and implications of this technique in slag analysis requires further investigation.

10.4. Conclusion

In conclusion, this research has significantly contributed to our understanding of early copper sulphide smelting in Western Europe. The thorough exploration of the smelting process has provided key insights into both the technological and socio-economic aspects of this past metallurgical practice. The findings shed light on previously unexplored facets, offering a more nuanced perspective on the challenges and innovations associated with early copper production in the region.

Looking forward, the suggested next steps are designed to address uncertainties and ambiguities within the existing data. The introduction of novel methods and approaches to slag analysis, not only aims to refine out current understanding but also opens avenues for further research. This collective effort is not merely about fine-tuning existing knowledge, but it also serves as a foundation to pave the way for a more solid and comprehensive understanding of the broader context surrounding early copper smelting in western Europe.

References

- Addis, A. (2013). *Late Bronze Age metallurgy in the Italian Eastern Alps: Copper smelting slags and mine exploitation* [PhD Thesis]. Università di Trento.
- Addis, A., Angelini, I., & Artioli, G. (2017). Late Bronze Age copper smelting in the southeastern Alps: How standardized was the smelting process? Evidence from Transacqua and Segonzano, Trentino, Italy. *Archaeological and Anthropological Sciences*, 9(5), 985–999.
- Addis, A., Angelini, I., Nimis, P., & Artioli, G. (2016). Late Bronze Age Copper Smelting Slags from Luserna (Trentino, Italy): Interpretation of the Metallurgical Process: LBA copper smelting slags from Luserna (Trentino, Italy). *Archaeometry*, 58(1), Article 1.
- Almodóvar, G. R., Sáez, R., Pons, J. M., Maestre, A., Toscano, M., & Pascual, E. (1997). Geology and genesis of the Aznalcóllar massive sulphide deposits, Iberian Pyrite Belt, Spain. *Mineralium Deposita*, 33(1–2), 111–136.
- Ambert, P. (1990). Evidence, age, and technical level of prehistoric cupriferous exploitations in Cabrières-Hèrault (south of France). In P. Ambert (Ed.), *Cabrières-Hèrault le plus vieux centre Minier Métallurgique de France. Archéologie en Languedoc, Colloque International, livret-guide de l'excursion du 24 Septembre 1990. Federation Archeologique de l'Herault* (pp. 9–12).
- Ambert, P. (1995). Les mines préhistoriques de Cabrières (Hérault): Quinze ans de recherches. État de la question. *Bulletin de la Société préhistorique française*, 92(4), 499–508. <https://doi.org/10.3406/bspf.1995.10066>
- Ambert, P. (1996). The copper mines of Cabrières (France) and results of the experimental metallurgy. *Archéologie En Languedoc*, 20, 13–19.
- Ambert, P. (2002). Utilisation préhistorique de la technique minière d'abattage au feu dans le district cuprifère de Cabrières (Hérault). *Comptes Rendus Palevol*, 1(8), 711–716.
- Ambert, P., Balestro, F., Laroche, M., Figueroa, V., & Rovira, S. (2013). Technological aspects of the earliest metallurgy in France: 'Furnaces' and slags from La Capitelle du Broum (Pèret, France). *The Origins of Metallurgy in Europe. Historical Metallurgy*, 47(1), 60–74.
- Ambert, P., Barge-Mahieu, H., Bourhis, J.-R., & Espérou, J.-L. (1984). Mines de cuivre préhistoriques de Cabrières (Hérault), premiers résultats. *Bulletin de la Société préhistorique française*, 81(3), Article 3.
- Ambert, P., Bourhis, J.-R., & Happ, J. (1996). Cabrières (France), mines et métallurgie au III^e millénaire BC: Apports de la métallurgie expérimentale. *Archéologie En Languedoc*, 20, 21–26.
- Ambert, P., Figueroa, V., Guendon, J. L., Klemm, V., Laroche, M., Rovira, S., & Strahm, C. (2009). The copper mines of Cabrières (Hérault) in southern France and the Chalcolithic metallurgy. In T. L. Kienlin & B. Roberts (Eds.), *Metals and Societies*. (Verlag Dr Rudolf Habelt GMBH, Bonn, pp. 285–295).
- Andraschko, F. M., & Schmidt, M. (1991). *Experimentelle Archäologie: Masche oder Methode? Anmerkungen zu Geschichte und Methodik einer "neuen" Forschungsrichtung*. Isensee Verlag.
- Anfinset, N. (2001). *Social and technological aspects of mining, smelting and casting copper: An ethnoarchaeological study from Nepal*. Dt. Bergbau-Museum.
- Angelini, I., Artioli, G., Pedrotti, A., & Tecchiati, U. (2013). La metallurgia dell'età del Rame dell'Italia settentrionale con particolare riferimento al Trentino e all'Alto Adige. Le risorse minerarie e i processi di produzione del metallo. *L'età del Rame: La Pianura Padana e Le Alpi al Tempo Di Otzi. Catalogo Della Mostra, Brescia: Compagnia Della Stampa Massetti*, 101–116.
- Anguilano, L., Artioli, G., Angelini, I., Moroni, M., Baumgarten, B., & Oberrauch, H. (2002). Smelting slags from Copper and Bronze Age archaeological sites in Trentino and Alto Adige. *II Congresso Nazionale Di Archeometria*, 627–638.

- Anguilano, L., Oberrauch, H., Hauser, H., Rehren, T., & Artioli, G. (2006). Copper smelting at Fennhals-Kurtatsch (South Tyrol). *Proc. ISA*, 375–382.
- Antonović, D., & Vukadinović, M. (2012). Eneolithic mine Prljuša: Mali Šturac archaeological and geophysical investigations. *Starinar*, 62, 95–106.
- Antonović, D., Vukadinović, M., & Cicović, A. (2014). Praistorijski rudnik na lokalitetu Prljuša, Mali Šturac istraživanje 2012. *Arheologija u Srbiji. Projekti Arheološkog Instituta u, 2012*, 28–31.
- Artioli, G. (2010). *Scientific methods and cultural heritage: An introduction to the application of materials science to archaeometry and conservation science*. Oxford University Press.
- Artioli, G., & Angelini, I. (2010). *Scientific methods and cultural heritage: An introduction to the application of materials science to archaeometry and conservation science*. Oxford University Press.
- Artioli, G., Angelini, I., Addis, A., Canovaro, C., Chiarantini, L., & Benvenuti, M. (2016). Ceramiche tecniche, scorie, minerali e metalli: Interpretazione del processo metallurgico. *Metalli e Metallurghi Della Preistoria. L'insediamento Eneolitico Di San Carlo-Cava Solvay, Pontedera: Tagete Edizioni*, 69–81.
- Artioli, G., Angelini, I., Burger, E., Bourgarit, D., & Colpani, F. (2009). Petrographic and chemical investigations of the earliest copper smelting slags in Italy: Towards a reconstruction of the beginning of copper metallurgy. *Proceedings of the 2nd International Conference Archaeometallurgy in Europe*, 9.
- Artioli, G., Angelini, I., Nimis, P., Addis, A., & Villa, I. M. (2014). Prehistoric copper metallurgy in the Italian Eastern Alps: Recent results. *Historical Metallurgy*, 47(1), 2013.
- Artioli, G., Angelini, I., Tecchiati, U., & Pedrotti, A. (2015). Eneolithic copper smelting slags in the Eastern Alps: Local patterns of metallurgical exploitation in the Copper Age. *Journal of Archaeological Science*, 63, 78–83.
- Artioli, G., Canovaro, C., Nimis, P., & Angelini, I. (2020). LIA of Prehistoric Metals in the Central Mediterranean Area: A Review. *Archaeometry*, 62(S1), Article S1.
- Artioli, G., Colpani, F., Angelini, I., & Anguilano, L. (2005). Attività metallurgiche a Millan (Bressanone, Val d'Isarco, BZ). Analisi mineralogiche delle scorie di fusione. *Convegno Internazionale "Il Sito Fusorio Della Tarda Età Del Rame Di Millan Presso Bressanone Nel Quadro Della Prima Metallurgia Dell'area Alpina", Bolzano–15 Giugno 2005, Abstracts*, 4, 12.
- Ascher, R. (1961). Experimental archeology. *American Anthropologist*, 793–816.
- Bachmann, H. G. (1978). The phase composition of slags from Timna site 39. In B. Rothenberg & R. F. Tylecote (Eds.), *Chalcolithic Copper Smelting* (pp. 21–23). Institute of Archaeo-Metallurgical Studies.
- Bachmann, H. G. (1980). Early copper smelting in Sinai and in the Negev as deduced from slag investigations. In P. T. Craddock (Ed.), *Scientific Studies in Early Mining and Extractive Metallurgy* (pp. 103–135). The British Museum.
- Bachmann, H. G. (1982a). Archäometallurgische Untersuchungen zur antiken Silbergewinnung in Laurion. *Erzmetall*, 35(5), 246–251.
- Bachmann, H. G. (1982b). Copper smelting slags from Cyprus: Review and classification of analytical data. In J. D. Muhly, R. Maddin, & V. Karageorghis (Eds.), *Early metallurgy in Cyprus, 4000-500 B.C.* (pp. 143–151). Pierides Foundation.
- Bachmann, H. G. (1982c). *The Identification of Slags from Archaeological Sites*. Institute of Archaeology, University of London, Occasional Papers 6.
- Bachmann, H. G., & Hauptmann, A. (1984). Zur alten Kupfergewinnung in Fenan und Hirbet en-Nahas im Wadi Arabah in Südjordanien. (L'extraction du cuivre à Fenan et Khirbet en-Nahas dans le Wadi Araba, Jordanie méridionale). *Anschnitt (Der). Zeitschrift Für Kunst Und Kultur Im Bergbau Essen*, 36(4), 110–123.

- Bachmann, H. G., & Rothenberg, B. (1980). Die verhüttungsverfahren von site 30. *Der Anschnitt, Beiheft 1, Veröff. Dtsch. Bergbau-Mus. Bochum, Nr. 20*, 215–236.
- Bachmann, H.-G. (1993). Vom Erz zum Metall (Kupfer, Silber, Eisen)—Die chemischen Prozesse im Schaubild. *Archäologie in Deutschland*, 35–40.
- Barbieri, M., & Cavazzuti, C. (2014). Stone moulds from Terramare (Northern Italy): Analytical approach and experimental reproduction. *Proceedings of the 7th Uk Experimental Archaeology Conference, Cardiff, January 10-11 2013*.
- Barbieri, M., Cavazzuti, C., Pellegrini, L., Scacchetti, F., & Rangone, M. (2015). Experiencing Visible and Invisible Metal Casting Techniques in Bronze Age Italy. *Experimental Archaeology EXARC Journal*, 3.
- Barge, H. (1997). L'installation métallurgique préhistorique de la cabane des Clausis à Saint-Véran (Hautes-Alpes). *Archéologie En Languedoc*, 21, 99–110.
- Bartelheim, M. (2013). Innovation and tradition. The structure of early metal production in the North Alpine region. In S. Burmeister, S. Hansen, M. Kunst, & N. Müller-Scheeßel (Eds.), *Metal matters, Innovative technologies and social change in prehistory and antiquity* (pp. 169–180).
- Bartelheim, M., Eckstein, K., Huijsmans, M., Krauss, R., & Pernicka, E. (2002). Kupferzeitliche metallgewinnung in Brixlegg, Österreich. In M. Bartelheim, R. Krause, & E. Pernicka (Eds.), *Die Anfänge der Metallurgie in der Alten Welt. Freiburger Forschungen zur Archäometrie und Kulturgesch* (Vol. 1, pp. 33-82.).
- Bartelheim, M., Eckstein, K., Huijsmans, M., Krauss, R., & Pernicka, E. (2003). Chalcolithic metal extraction in Brixlegg, Austria. *Archaeometallurgy in Europe, Milan Conference Proceedings, I*, 441-447.
- Baumgartner, D. (1982). *Mineralogische und chemische Untersuchungen jungsteinzeitlicher "Schmelztiegel"*. [Unpublished diploma thesis]. University of Fribourg, Fribourg.
- Blanco-Freijeiro, A., & Rothenberg, B. (1981). *Exploración arqueometalúrgica de Huelva*. Rio Tinto Minera.
- Blanford, H. F. (1861). Description of a native copper mine and smelting works in the Mahanuddi Valley, Sikkim Himalya. *Metallurgy, Part, I*, 388–392.
- Bogosavljević, S. (1995). Drugi svetski rat-žrtve u Jugoslaviji (OGLEDI 2). *Republika*, 7(117), 27–32.
- Böhne, C. (1968). Ueber die Kupferverhüttung der Bronzezeit, Schmelzversuche mit Kupferieserzen. *Archeologica Austriaca*, 44, 49–60.
- Borić, D. (2009). Absolute dating of metallurgical innovations in the Vinča culture of the Balkans. In T. L. Kienlin & B. Roberts (Eds.), *Metals and Societies*. (pp. 191–245). Verlag Dr Rudolf Habelt GMBH.
- Bourgarit, D. (2007). Chalcolithic copper smelting. In S. La Niece, D. Hook, & P. Craddock (Eds.), *Metals and mines. Studies in archaeometallurgy* (pp. 3–14). Archetype Publications.
- Bourgarit, D. (2019). Mineralogy of slags: A key approach for our understanding of ancient copper smelting processes. In G. Artioli (Ed.), *The contribution of mineralogy to cultural heritage* (1st ed., pp. 203–232). Mineralogical Society of Great Britain & Ireland.
- Bourgarit, D., & Mille, B. (1997). La métallurgie chalcolithique de Cabrières: Confrontation des données expérimentales et archéologiques en laboratoire. *Archéologie En Languedoc*, 21, 51–63.
- Bourgarit, D., & Mille, B. (2001). La transformation en métal de minerais de cuivre à base de sulfures: Et pourquoi pas dès le Chalcolithique. *ArchéoSciences, Revue d'Archéométrie*, 25(1), 145–155.
- Bourgarit, D., & Mille, B. (2005). Les nouvelles données de l'atelier métallurgique chalcolithique de La Capitelle du Broum dans le district de Cabrières (Hérault): La transformation des minerais de cuivre à base de sulfures se précise. *Actes du colloque international. Mémoires de la Société préhistorique française*, 37, 97–108.

- Bourgarit, D., Mille, B., Burens, A., & Carozza, L. (2002a). Smelting of chalcopryrite during chalcolithic times: Some have done it in ceramic pots as vase-furnaces. *Proceedings of the 33rd International Symposium on Archaeometry*, 22–26.
- Bourgarit, D., Mille, B., Burens, A., & Carozza, L. (2002b). Smelting of chalcopryrite during chalcolithic times: Some have done it in ceramic pots as vase-furnaces. *Proceedings of the 33rd International Symposium on Archaeometry*, 22–26.
- Bourgarit, D., Mille, B., Prange, M., Ambert, P., & Hauptmann, A. (2003). Chalcolithic fahlore smelting at Cabrières: Reconstruction of smelting processes by archaeometallurgical finds. *Archaeometallurgy in Europe*, 1, 431–440.
- Bourgarit, D., Rostan, P., Burger, E., Carozza, L., Mille, B., & Artioli, G. (2008). The beginning of copper mass production in the western Alps: The Saint-Véran mining area reconsidered. *Historical Metallurgy*, 42(1), 1–11.
- Bowen, N. L., & Schairer, J. F. (1935). The system MgO-FeO-SiO₂. *American Journal of Science*, 5(170), 151–217.
- Boyadziev, Y. D. (1995). Chronology of prehistoric cultures in Bulgaria. *Prehistoric Bulgaria*, 22, 149–191.
- Brandherm, D. (2016). Früher Bergbau und Metallurgie auf der Iberischen Halbinsel 1: Zambujal und die Anfänge der Metallurgie in der Estremadura (Portugal). Technologie der Kupfergewinnung, Herkunft des Metalls und soziokulturelle Bedeutung der Innovation. *Antiquity*, 90(353), 1402.
- Buhrke, V. E., Jenkins, R., Smith, D. K., & Kingsley, D. (1998). *Practical guide for the preparation of specimens for x-ray fluorescence and x-ray diffraction analysis*. Wiley-VCH.
- Bunk, W. G. J., Hauptmann, A., Kölschbach, S., & Woelk, G. (2002). Wind-powered copper smelting technology from the 3rd millennium BC at Feinan/Jordan. In G.-H. Kim, K.-W. Yi, & H.-T. Kang (Eds.), *Messages from the history of metals to the future Metal Age: Proceedings of the 5th International Conference on the Beginnings of the Use of Metals and Alloys (BUMA V)*, 21–24 April 2002 (pp. 331–338).
- Burger, E., Bourgarit, D., Frotté, V., & Pilon, F. (2011). Kinetics of iron–copper sulphides oxidation in relation to protohistoric copper smelting. *Journal of Thermal Analysis and Calorimetry*, 103(1), 249–256.
- Burger, E., Bourgarit, D., Rostan, P., Carozza, L., & Artioli, G. (2007). The mystery of Plattenschlacke in protohistoric copper smelting: Early evidence at the Early Bronze Age site of Saint-Veran, French Alps. *2nd International Conference Archaeometallurgy in Europe Proceedings. Associazione Italiana Di Metalurgia, Milano on CD-ROM*.
- Burger, E., Bourgarit, D., Wattiaux, A., & Fialin, M. (2010). The reconstruction of the first copper-smelting processes in Europe during the 4th and the 3rd millennium BC: Where does the oxygen come from? *Applied Physics A*, 100(3), 713–724.
- Busuttil, C. (2013). Experimental archaeology. *Malta Archaeological Review*, 9, 60–66.
- Cadet, M., Tereygeol, F., Sayavongkhamdy, T., Souksavatdy, V., Luangkoth, T., Chang, N., Dillmann, P., & Pryce, T. O. (2021). Late prehistoric copper smelting in the Lao PDR: Experimental reconstruction based on the Vilabouly Complex evidence. *Journal of Archaeological Science: Reports*, 37, 102932.
- Caley, E. R., & Easby, D. T. (1959). The smelting of sulfide ores of copper in preconquest Peru. *American Antiquity*, 25(1), 59–65.
- Campana, N., Franceschi, E., & Maggi, R. (1997). Analyses of the metal objects. *Arene Candide: A Functional and Environmental Assessment of the Holocene Sequence (Excavations Bernabo Brea-Cardini 1940-50)*, 611–621.
- Campana, N., Maggi, R., Stos-Gale, Z. A., & Houghton, J. (1996). Miniere e metallurgia in Liguria fra IV millennio e IV secolo BC. In *La miniera, l'uomo e l'ambiente. Fonti e metodi a confronto*

- per la storia delle attività minerarie e metallurgiche in Italia*. (pp. 15–52). All'insegna del Giglio.
- Campbell, F. C. (Ed.). (2012). *Phase diagrams: Understanding the basics*. ASM International.
- Campbell, W., & Knight, C. W. (1906). A microscopic examination of lead and silver deposits of Timiskaming. *Economic Geology*, 1(8), 767–776.
- Capitani, G. C., & Mellini, M. (2000). Progressive retrograde crystallization of the Campiglia Marittima skarn. *Neues Jahrbuch Für Mineralogie (Journal of Mineralogy and Geochemistry)*, 97–115.
- Carozza, L., Bourgarit, D., Mille, B., & Burens, A. (1997). L'habitat et l'atelier de métallurgiste chalcolithique d'Al Claus: Analyse et interprétation des témoins d'activité métallurgique. *Archéologie En Languedoc*, 21, 147–164.
- Carozza, L., Georjon, C., & Vignaud, A. (2005). La fin du néolithique et les débuts de la métallurgie en Languedoc central (les habitats de la colline du Puech-Haut à Paulhan, Hérault). *Recherches En Archéologie Préventive*.
- Carozza, L., & Mille, B. (2007). Chalcolithique et complexification sociale: Quelle place pour le métal dans la définition du processus de mutation des sociétés de la fin du Néolithique en France? In J. Guilaine (Ed.), *Chalcolithique et complexification sociale: Séminaires du Collège de France (Paris)* (pp. 195–232).
- Cattoi, E., D'Amico, C., & Fabris, S. (2000). Studio petroarcheometrico di scorie di fusione della fine dell'Età del Bronzo e confronti con scorie dell'Età del Rame/Bronzo Antico in Trentino. *Preistoria Alpina*, 31(1995), 125–145.
- Cattoi, E., D'AMICO, C., Gasparotto, G., & Girani, M. (2001). Petroarcheometry of copper smelting slag in Trentino; provenance and process data. *Preistoria Alpina*, 33 (1997), 151–154.
- Chapman, J. (1981). Vinca Culture of South-East Europe: Studies in Chronology. *Economy and Society. British Archaeological Reports, Oxford*.
- Chapman, R. (2008). Producing Inequalities: Regional Sequences in Later Prehistoric Southern Spain. *Journal of World Prehistory*, 21(3–4), 195–260. <https://doi.org/10.1007/s10963-008-9014-y>
- Chapman, S. G., & Chapman, M. A. (2013). Reconstructing and testing the Pentwyn pit furnaces. *Unpublished Report*.
- Charles, J. A. (1980). The coming of copper and copper-base alloys and iron: A metallurgical sequence. In T. A. Wertheim & J. D. Muhly (Eds.), *The coming of the age of iron* (pp. 151–182). Yale University Press.
- Chen, K., Rehren, T., Mei, J., & Zhao, C. (2009). Special alloys from remote frontiers of the Shang Kingdom: Scientific study of the Hanzhong bronzes from southwest Shaanxi, China. *Journal of Archaeological Science*, 36(10), 2108–2118.
- Chernykh, E. (1978). *Gornoje delo i metalurgija v drevnejšej Bolgarii*. (Bulgarian Academy of Sciences).
- Chernykh, E. (1998). Ancient mining and metallurgy in Eastern Europe: Ecological problems. In B. Hänsel (Ed.), *Mensch und Umwelt in der Bronzezeit Europas* (pp. 129–134). Oetker-Voges Verlag.
- Chernykh, E. N. (1982). Die ältesten Bergleute und Metallurgen Europas. *Das Altertum*, 28(1), 5–15.
- Chernykh, E. N. (1992). *Ancient metallurgy in the USSR: The early metal age*. Cambridge University Press.
- Childs, S. T. (1991). Style, technology, and iron smelting furnaces in Bantu-speaking Africa. *Journal of Anthropological Archaeology*, 10(4), 332–359.
- Childs, S. T., & Killick, D. (1993). Indigenous African metallurgy: Nature and culture. *Annual Review of Anthropology*, 22(1), 317–337.
- Cierny, J. (2008). Prähistorische Kupferproduktion in den südlichen Alpen. *Der Anschnitt, Beiheft*, 22.

- Cierny, J., Marzatico, F., Perini, R., & Weisgerber, G. (1998). Prehistoric copper metallurgy in the southern Alpine region. In C. Mordant, M. Pernot, & V. Rychner (Eds.), *L'Atelier du Bronziera en Europe du XX au VIII siècle avant notre ère.: Vol. II* (pp. 25-34.).
- Cierny, J., Marzatico, F., Perini, R., & Weisgerber, G. (2004). La riduzione del rame in località Acqua Fredda al Passo del Redebus (Trentino) nell'età del Bronzo Recente e Finale. *Alpenkupfer-Rame Delle Alpi. Deutsches Bergbau Museum. Bochum*, 125–154.
- Clarke, D. (1973). Archaeology: The loss of innocence. *Antiquity*, 47(185), 6–18.
- Coghlan, H. H. (1939a). Prehistoric copper and some experiments in smelting. *Transactions of the Newcomen Society*, 20(1), 49–65.
- Coghlan, H. H. (1939b). Some Experiments on the Origin of Early Copper. *Man*, 39, 106–108.
- Coles, J. (1973). *Archaeology by Experiment*.
- Coles, J. (1979). *Experimental archaeology*.
- Colpani, F., Angelini, I., Artioli, G., & Tecchiati, U. (2009). Copper smelting activities at the Millan and Gudon Chalcolithic Sites (Bolzano, Italy): Chemical and mineralogical investigations of the archaeometallurgical finds. *Proc. 36th International Symposium on Archaeometry, Quebec City*, 2–6.
- Constantinou, G. (1982). Geological features and ancient exploitation of the cupriferous sulphide orebodies of Cyprus. *Early Metallurgy in Cyprus*, 400, 13–23.
- Constantinou, G. (2012). Late Bronze Age copper production in Cyprus from a mining geologist's perspective. In *Eastern Mediterranean Metallurgy and Metalwork in the Second Millennium BC*. Oxford and Oakville.
- Cortesogno, L., & Gaggera, L. (2002). Valle Lagorara: Analisi delle conoscenze litologiche nell'Età del Rame. In N. Campana & R. Maggi (Eds.), *Archeologia in Valle Lagorara: Diecimila Anni di Storia Intorno a una Cava do Diaspro*. (pp. 31-52.). Istituto Italiano di Preistoria e Protostoria.
- Cottiaux, R., André, M. F., Ard, V., Augereau, A., Brunet, P., Giovannacci, S., Hamon, T., Ihuel, E., Langry-François, F., & Magne, P. (2006). Projet Collectif de recherches «Du Néolithique récent à l'âge du Bronze ancien dans le Centre Nord de la France: Définitions et interactions des groupes culturels». *Annual Report*.
- Craddock, B., & Craddock, P. (1996). The Beginnings of Metallurgy in South-West Britain: Hypotheses & Evidence. *Mining History*, 13, 52–63.
- Craddock, P. T. (1995). *Early metal mining and metal production*. Edinburgh University Press.
- Craddock, P. T. (2000). From hearth to furnace: Evidences for the earliest metal smelting technologies in the Eastern Mediterranean. *Paléorient*, 26(2), 151–165.
- Craddock, P. T. (2009). Evidences for the earliest smelting processes in western Europe. *Evidences for the Earliest Smelting Processes in Western Europe 2nd International Conference Archaeometallurgy in Europe Proceedings, 17-20 June 2007, Associazione Italiana Di Metalurgia, Milano*, 3–11.
- Craddock, P. T. (2011). The inception and nature of extractive metallurgy in Western Europe. *Povoamento e Exploração Dos Recursos Mineiros Na Europa Atlântica Occidental*, 281–312.
- Craddock, P. T., & Meeks, N. D. (1987). Iron in ancient copper. *Archaeometry*, 29(2), 187–204.
- Cremante, M., & Storti, C. (2005). Attività metallurgiche a Millan: Indagini su campioni di scoria e di rame attraverso analisi chimiche, analisi microstrutturali e analisi metallografiche-Università degli Studi di Milano. *Dipartimento Di Scienze Della Terra, Milano S*, 19–21.
- Cunningham, P., Heeb, J., & Paardekooper, R. (2008). Introduction. In P. Cunningham, J. Heeb, & R. Paardekooper (Eds.), *Proceedings of the Experimental Archaeology Conference. Exeter 2007* (p. V–IX). Oxbow Books, Oxford, UK.
- Cushing, F. H. (1894). Primitive copper working: An experimental study. *American Anthropologist*, 7(1), 93–117.

- Czedik-Eysenberg, F. (1958). Beiträge zur Metallurgie des Kupfers in der Urzeit. *Archaeologia Austriaca*, 3, 1–1.
- Da Mommio, A., Iaccarino, S., Vezzoni, S., Dini, A., Rocchi, S., Brocchini, D., Guideri, S., & Sbrilli, L. (2010). Valorizzazione del geosito «sezione Coquand», Miniera del Temperino (Parco Archeominerario di San Silvestro, Campiglia Marittima). *Atti Della Società Toscana Di Scienze Naturali Residente in Pisa. Memorie. Serie A*, 115, 55–72.
- Dal Ri, L., Rizzi, G., & Tecchiati, U. (2005). Lo scavo di una struttura della tarda età del Rame connessa a processi estrattivi e di riduzione del minerale a Millan presso Bressanone. *Convegno Internazionale “Il Sito Fusorio Della Tarda Età Del Rame Di Millan Presso Bressanone Nel Quadro Della Prima Metallurgia Dell’area Alpina”*, Bolzano–15 Giugno 2005, Abstracts, 4, 12.
- Dal Ri, L., & Tecchiati, U. (2005). Recenti ricerche sull’età del Rame in Val d’Isarco: Bolzano: con un contributo di Lorna Anguilano sulle analisi chimico-petrografiche di scorie di fusione. *Ricerche Paleontologiche Nelle Alpi Occidentali: In Ricordo Di Piero Barocelli e Osvaldo Coisson*. Atti del 2° Congresso Internazionale, Pinerolo, 17-18-19 ottobre 2003.
- D’Amico, C., Gasparotto, G., Pedrotti, A., & Albore Livadie, C. (1998a). Scorie eneolitiche di Gaban e Acquaviva (Trento): Caratteri, provenienza ed estrazione del metallo. *Le Scienze Della Terra e l’Archeometria*, 31–38.
- D’Amico, C., Gasparotto, G., Pedrotti, A., & Albore Livadie, C. (1998b). Scorie eneolitiche di Gaban e Acquaviva (Trento): Caratteri, provenienza ed estrazione del metallo. *Le Scienze Della Terra e l’Archeometria*, 31–38.
- Davenport, W. G., King, M. J., Schlesinger, M. E., & Biswas, A. K. (2002). *Extractive metallurgy of copper*. Elsevier.
- Della Casa, P., Naef, L., & Turck, R. (2016). Prehistoric copper pyrotechnology in the Swiss Alps: Approaches to site detection and chaîne opératoire. *Quaternary International*, 402, 26–34.
- Derikonjić, S., Radivojević, M., Pernicka, E., & Rehren, T. (2011). The Vinča culture mining complex in Jarmovac, southwest Serbia. In A. Hauptmann, D. Modarressi-Tehrani, & M. Prange (Eds.), *Archaeometallurgy in Europe III*. (Vol. 39). Deutsches Bergbau Museum,.
- Dević, S., & Marčeta, L. (2007). Differences in morphological properties between the olivine group minerals formed in natural and industrial processes. *Journal of Mining and Metallurgy, Section B: Metallurgy*, 43(1), 99–105.
- Dimitrov, K. (2002). Die Metallfunde aus den gräberfeldern von Durankulak. In H. Todorova (Ed.), *Durankulak, Die Prähistorischen Gräberfelder* (pp. 127-158.).
- Dini, A., & Boschi, C. (2017). I giacimenti cupriferi delle ofioliti toscane. Geologia e ipotesi genetiche. *Rivista Mineralogica Italiana*, 2(2017), 84–101.
- Dini, A., Guideri, S., & Orlandi, P. (2013). Miniere e minerali del Campigliese. *Milano: Gruppo Mineralogico Lombardo*.
- Dolfini, A. (2013). The Emergence of Metallurgy in the Central Mediterranean Region: A New Model. *European Journal of Archaeology*, 16(1), 21–62.
- Dolfini, A. (2014). *Early metallurgy in the central Mediterranean, Goals for the next decade*. 47, 33–50.
- Dolfini, A. (2023). Metals: Manufacture and Use. In E. Nikita & T. Rehren (Eds.), *Encyclopedia of Archaeology* (2nd Edition). Elsevier.
- Dolfini, A., Angelini, I., & Artioli, G. (2020). Copper to Tuscany – Coals to Newcastle? The dynamics of metalwork exchange in early Italy. *PLOS ONE*, 15(1), 227–259.
- Dolfini, A., & Crellin, R. J. (2016). Metalwork wear analysis: The loss of innocence. *Journal of Archaeological Science*, 66, 78–87.
- Donaldson, C. H. (1976). An experimental investigation of olivine morphology. *Contributions to Mineralogy and Petrology*, 57(2), 187–213.

- Doonan, R. C. (1994). Sweat, fire and brimstone: Pre-treatment of copper ore and the effects on smelting techniques. *J Historical Met Soc*, 28(2), 84–97.
- Doonan, R. C., & Dungworth, D. (2013). Experimental archaeometallurgy in perspective. *Accidental and Experimental Archaeometallurgy*, 1–10.
- Doonan, R., Klemm, S., Ottaway, B. S., Sperl, G., & Weinek, H. (1996). The East Alpine Bronze Age copper smelting process: Evidence from the Ramsau Valley, Eisenerz, Austria. In S. Demirci, A. Özer, & G. Summers (Eds.), *Archaeometry 94: Proceedings of the 29th International Symposium on Archaeometry*. (pp. 17–22).
- Dungworth, D. (2013). Experimental archaeometallurgy: Hypothesis testing, happy accidents and theatrical performances. *Accidental and Experimental Archaeometallurgy, HMS Occasional Publication*, 7, 11–16.
- Dungworth, D., & Doonan, R. C. (2013). *Accidental and experimental archaeometallurgy*. Historical Metallurgy Society.
- Eibner, C. (1982). Kupfererzbergbau in österreichs Alpen. In *Südosteuropa zwischen 1600 und 1000 v Chr.* (Vol. 1, pp. 399–408).
- Ellingham, H. J. T. (1944). Reducibility of oxides and sulphides in metallurgical processes. *J. Soc. Chem. Ind*, 63(5), 125–160.
- Epstein, S. M. (1993). *Cultural choice and technological consequences: Constraint of innovation in the late prehistoric copper smelting industry of Cerro Huaranga, Peru*.
- Ermrich, M., & Oppen, D. (2013). *XRD for the analyst: Getting acquainted with the principles*. PANalytical.
- Espérou, J. L. (1993). La structure métallurgique de Roque-Fenestre (Cabrières, Hérault). *Archéologie En Languedoc*, 17, 32–46.
- Espérou, J.-L. (1981). *La structure minière de Roque Fenestre, Cabrières (Hérault)*. [Mémoire de DEA, Université de Provence].
- Espérou, J.-L., Ambert, P., Bourhis, J.-R., Roques, P., & Gilot, E. (1994). La fosse chalcolithique Pioch-Farrus 448 (Cabrières, Hérault). Datation 14 C et documents métallurgiques. *Bulletin Du Musée d'Anthropologie Préhistorique de Monaco*, 37, 53–62.
- Etiegni, L., & Campbell, A. G. (1991). Physical and chemical characteristics of wood ash. *Bioresource Technology*, 37(2), 173–178.
- Ettler, V., Červinka, R., & Johan, Z. (2009). Mineralogy of medieval slags from lead and silver smelting (Bohutín, Příbram district, Czech Republic): Towards estimation of historical smelting conditions. *Archaeometry*, 51(6), 987–1007.
- Ettler, V., Johan, Z., Touray, J.-C., & Jelínek, E. (2000). Zinc partitioning between glass and silicate phases in historical and modern lead–zinc metallurgical slags from the Příbram district, Czech Republic. *Comptes Rendus de l'Académie Des Sciences-Series IIA-Earth and Planetary Science*, 331(4), 245–250.
- Evans, R. T., & Tylecote, R. F. (1967). Some vitrified products of non-metallurgical significance. *Bulletin of the Historical Metallurgy Group*, 1(9), 22–23.
- Fasani, L. (1990). La sepoltura e il forno di fusione de La Vela di Valbusa (Trento). *Preistoria Alpina*, 24, 165–181.
- Fasnacht, W. (1991). Analyses de scories de l'Age du Bronze en Suisse. *Archéologie Expérimentale. Tome 1. Le Feu: Le Métal, La Céramique*, 156–159.
- Fasnacht, W. (1999). Prähistorischer Kupferbergbau im Oberhalbstein und dessen Spuren in der bronzezeitliche Siedlung Savognin-Padnal. In P. Della Casa (Ed.), *Prehistoric alpine environment, society, and economy. International colloquium PAESE '97 in Zürich* (pp. 267–276).
- Fasnacht, W. (2009). 7000 years of trial and error in copper metallurgy—In one experimental life. *Metals and Societies. Studies in Honour of Barbara S. Ottaway*, 395–399.

- Faure, F., Trolliard, G., Nicollet, C., & Montel, J.-M. (2003). A developmental model of olivine morphology as a function of the cooling rate and the degree of undercooling. *Contributions to Mineralogy and Petrology*, 145(2), 251–263.
- Fedeli, F. (1999). Il sito preistorico degli Orti Bottagone (Piombino, LI). Comunicazione preliminare. *Rassegna Di Archeologia*, 16, 115–127.
- Fedeli, F. (2000). Il sito pluristratificato degli Affitti Gotti (Campiglia Marittima, LI). Primi risultati delle indagini di superficie. *Rassegna Di Archeologia*, 17, 179–192.
- Fedeli, F., & Galiberti, A. (2016). Metalli e metallurghi della preistoria. *L'insediamento Eneolitico Di San Carlo-Cava Solvay. Pontedera: Tagete*.
- Ferguson, C. W., Gimbutas, M., & Suess, H. E. (1976). Historical Dates for Neolithic Sites of Southeast Europe. *Science*, 191(4232), 1170–1172.
- Feyerabend, P. (1975). Against Method: Outline of an Anarchistic Theory of. *Knowledge. NLB*.
- Forbes, R. J. (1971). *et* (1972): *Studies in Ancient Technology, Metallurgy in Antiquity*. VIII et IX, Leyde-New York-Cologne.
- Frahm, E. (2014). Scanning electron microscopy (SEM): Applications in Archaeology. In *Encyclopedia of Global Archaeology* (pp. 6487–6495). Springer New York.
- Freestone, I. C. (1988). Melting points and viscosities of ancient slags: A contribution to the discussion. *Hist. Metall.*, 22(1), 49–51.
- Freestone, I. C., & Tite, M. S. (1986). Refractories in the ancient and preindustrial world. In *High-Technology Ceramics: Past, Present, and Future-The Nature of Innovation and Change in Ceramic Technology* (Vol. 3, pp. 35–63).
- Gale, N., Stos-Gale, S., Raduncheva, A., Panayotov, I., Ivanov, I., Lilov, P., & Todorov, T. (2003). Early metallurgy in Bulgaria. In P. Craddock & J. Lang (Eds.), *Mining and Metal Production through the Ages*. (pp. 122–73.). The British Museum Press,.
- Gattiglia, A., & Rossi, M. (1995). Les céramiques de la mine préhistorique de Saint-Véran (Hautes-Alpes). *Bulletin de La Société Préhistorique Française*, 92(4), 509–518.
- Gauß, R. (2013). The development of metallurgy on the Iberian Peninsula: Technological and social patterns of a long-term innovation process. *Metal Matters. Innovative Technologies and Social Change in Prehistory and Antiquity*, 209–230.
- Gentile, V., & van Gijn, A. (2019). Anatomy of a notch. An in-depth experimental investigation and interpretation of combat traces on Bronze Age swords. *Journal of Archaeological Science*, 105, 130–143.
- Georgakopoulou, M. (2016). *Mobility and Early Bronze Age southern Aegean metal production*. Cambridge University Press.
- Girbal, B. (2013). Experimenting with the bowl furnace. In R. Doonan & D. Dungworth (Eds.), *Accidental and Experimental Archaeometallurgy*. (pp. 83–92).
- Goldenberg, G. (1998). L'exploitation du cuivre dans les Alpes Autrichiennes à l'âge du Bronze. In C. Mordant, M. Pernot, & V. Rychner (Eds.), *L'Atelier du Bronziste en Europe du XX au VIII siècle avant notre ère. Actes du colloque international Bronze '96* (Vol. 2, pp. 9–23.).
- Goldenberg, G. (2004). Ein Verhüttungsplatz der mittleren Bronzezeit bei Jochberg (Nordtirol). In G. Weisgerber & G. Goldenberg (Eds.), *Alpenkupfer—Rame delle Alpi* (pp. 165–176). Deutsches Bergbau Museum.
- Goldenberg, G., Anfinset, N., Silvestri, E., Belgrado, E., Hanning, E., Klauzner, M., Schneider, P., Staudt, M., & Töchterle, U. (2011). Das Nepal-Experiment—Experimentelle Archäometallurgie mit ethnoarchäologischem Ansatz. In K. Oeggl, G. M. Prast, & T. Stöllner (Eds.), *Die Geschichte des Bergbaus in Tirol und seinen angrenzenden Gebieten*. (pp. 83–90).
- Goldenberg, G., Breitenlechner, E., Deschler-Erb, S., Hanke, K., Hiebel, G., Hüster-Plogmann, H., Hye, S., Klauzner, M., Kovács, K., Krismar, M., Lutz, J., Tomedi, G., Maass, A., Moser, M., Nicolussi, K., Oeggl, K., Pernicka, E., Pichler, T., Pöllath, N., Weinold, T. (2011).

- Prähistorischer kupfererzbergbau im Maukental bei Radfeld/ Brixlegg. In G. Goldenberg, U. Töchterle, K. Oegg, & A. Krenn-Leeb (Eds.), *Forschungsprogramm HiMAT: Neues zur Bergbaugeschichte der Ostalpen. Archäologie Österreichs Spezial 4*. (pp. 61-110.).
- Goldstein, J. I., Newbury, D. E., Michael, J. R., Ritchie, N. W. M., Scott, J. H. J., & Joy, D. C. (2018). *Scanning Electron Microscopy and X-Ray Microanalysis*. Springer New York.
- Gowland, W. (1912a). Copper and its alloys in early times. *Journal of the Institute of Metals*, 7, 23–49.
- Gowland, W. (1912b). The metals in antiquity. *The Journal of the Royal Anthropological Institute of Great Britain and Ireland*, 42, 235–287.
- Guilbert, J. M., & Park, C. F. (1986). *The Geology of Ore Deposits*. W. H. H Freeman and Company.
- Hamilton, N. E., & Ferry, M. (2018). ggtern: Ternary diagrams using ggplot2. *Journal of Statistical Software*, 87, 1–17.
- Hanning, E. (2012). Reconstructing Bronze Age Copper Smelting in the Alps: An Ongoing Process. *Experimentelle Archäologie in Europa, Bilanz*, 75-86.
- Hanning, E., Gauß, R., & Goldenberg, G. (2010a). Metal for Zambujal: Experimentally reconstructing a 5000-year-old technology. *Trabajos de Prehistoria*, 67(2), 287–304.
- Hanning, E., Gauß, R., & Goldenberg, G. (2010b). Metal for Zambujal: Experimentally reconstructing a 5000-year-old technology. *Trabajos de Prehistoria*, 67(2), 287–304.
- Hanning, E., & Pils, R. (2011). Experimentelle Untersuchungen zur bronzezeitlichen Kupferverhüttung im ostalpinen Gebiet – Erste Ergebnisse. In: (Eds.). In K. Oegg, G. Goldenberg, T. Stöllner, & T. Prast (Eds.), *Die geschichte des Bergbaus in Tirol und seinen angrenzenden Gebieten.: Vol. Proc 5th milestone meeting SFB-HIMAT, 2010*, (pp. 129–134).
- Hauptmann, A. (1985). *5000 jahre kupfer in Oman: Die entwicklung der kupfermetallurgie vom 3. jahrtausend bis zur neuzeit* (Vol. 1). Die Vereinigung.
- Hauptmann, A. (2000). *Zur frühen Metallurgie des Kupfers in Fenan/Jordanien*. (Der Anschnitt, Beiheft, Vol. 11). Der Anschnitt, Beiheft.
- Hauptmann, A. (2003). Developments in copper metallurgy during the fourth and third millennia BC at Feinan, Jordan. *Mining and Metal Production through the Ages*, 90–100.
- Hauptmann, A. (2014). The investigation of archaeometallurgical slag. In *Archaeometallurgy in Global Perspective* (pp. 91–105). Springer.
- Hauptmann, A. (2020). *Archaeometallurgy-Materials Science Aspects*. Springer.
- Hauptmann, A. (with Deutsches Bergbau-Museum Bochum). (2007). *The archaeometallurgy of copper: Evidence from Faynan, Jordan*. Springer.
- Hauptmann, A., Lutz, J., Pernicka, E., & Yalçın, U. (1993). Zur Technologie der frühesten Kupferverhüttung im östlichen Mittelmeerraum. In M. Frangipane, A. Hauptmann, M. Liverani, P. Matthiae, & M. Mellink (Eds.), *Between the rivers and over the mountains: Archaeologica Anatolica et Mesopotamica Alba Palmieri Dedicata (Rome)*. (pp. 541-563.).
- Heeb, J., & Ottaway, B. S. (2014). Experimental archaeometallurgy. *Archaeometallurgy in Global Perspective*, 161–192.
- Heinrich, K. F. J. (1966). Electron probe microanalysis by specimen current measurement. In R. Castaing (Ed.), *X-ray Optics and Microanalysis* (pp. 159-169.). Hermann.
- Herbert, E. W. (1993). *Iron, Gender, and Power: Rituals of transformation in African societies*. Indiana University Press.
- Herdits, H. (1997). *Ein bronzezeitlicher Kupfererzverhüttungsplatz in Mühlbach/Hochkönig (Salzburg)* [MA Thesis]. Universität Wien.
- Hermann, R., Dolfini, A., Crellin, R. J., Wang, Q., & Uckelmann, M. (2020). Bronze age swordsmanship: New insights from experiments and wear analysis. *Journal of Archaeological Method and Theory*, 27(4), 1040–1083.
- Hodoroaba, V. D. (2020). Energy-dispersive X-ray spectroscopy (EDS). In *Characterization of nanoparticles* (pp. 397–417). Elsevier.

- Hook, D. R., Freestone, I. C., Meeks, N. D., Craddock, P. T., & Moreno Onorato, A. M. (1991). The early production of copper-alloys in south-East Spain. *Archaeometry*, 90, 65–76.
- Höppner, B., Bartelheim, M., Huijsmans, M., Krauss, R., Martinek, K.-P., Pernicka, E., & Schwab, R. (2005). Prehistoric copper production in the Inn valley (Austria), and the earliest copper in Central Europe. *Archaeometry*, 47(2), 293–315.
- Humphris, J., Martinon-Torres, M., Rehren, T., & Reid, A. (2009). Variability in single smelting episodes—a pilot study using iron slag from Uganda. *Journal of Archaeological Science*, 36(2), 359–369.
- Hunt Ortiz, M. A. (2003). *Prehistoric Mining and Metallurgy in South West Iberian Peninsula*. Archeopress, Oxford.
- Iaia, C., & Dolfini, A. (2021). A new seriation and chronology for early Italian metalwork, 4500-2100 BC. *A New Seriation and Chronology for Early Italian Metalwork, 4500-2100 BC.*, 1–43.
- Ineson, P. R. (2014). *Introduction to practical ore microscopy*. Routledge.
- Issel, A. (1879). Sulle tracce di antichissima lavorazione osservate in alcune miniere della Liguria. *Rassegna Settimanale*, 3(70), 348-9.
- Issel, A. (1892). *Liguria Geologica e Preistorica*.
- Ixer, R. A. (1990). *Atlas of opaque and ore minerals in their associations*. Osprey Books.
- Ixer, R. A. (1999). Role of Ore Geology and Ores in the Archaeological Provenancing of Metals. *BAR International Series*, 792, 43–52.
- Ixer, R. A., & Duller, P. R. (1998). *Virtual atlas of opaque and ore minerals in their associations*. Els autors.
- Ixer, R. A., & Patrick, R. A. D. (2003). Copper-arsenic ores and Bronze Age mining and metallurgy with special reference to the British Isles. *Mining and Metal Production through the Ages*, 9, 20.
- Jabalquinto Expósito, I. M. (2022). *La ocupación prehistórica en el Piedemonte y Sierra Morena Central durante el III y II milenio a través de la Cueva del Cañaveralejo en Adamuz (Córdoba, España)* [PhD Thesis, Universidad de Córdoba].
- Janković, S. (1997). The Carpatho-Balkanides and adjacent area: A sector of the Tethyan Eurasian metallogenic belt. *Mineralium Deposita*, 32(5), 426–433.
- Jones, A. (2002). *Archaeological theory and scientific practice* (Vol. 1). Cambridge University Press.
- Jones, A. (2004). Archaeometry and materiality: Materials-based analysis in theory and practice. *Archaeometry*, 46(3), 327–338.
- Jovanović, B. (1971). *Metallurgy of the Eneolithic period in Yugoslavia* (Vol. 9). Archaeological Institute.
- Jovanović, B. (1976). Rudna Glava—Ein Kupferbergwerk des frühen Eneolithikums in Ostserbien. *Der Anschnitt*, 28, 150–157.
- Jovanović, B. (1983). Mali Sturac—Ein neues prähistorisches Kupferbergwerk in Zentralserbien. *Der Anschnitt*, 36, 177-9.
- Jovanović, B., & Ottaway, B. S. (1976). Copper mining and metallurgy in the Vinča group. *Antiquity*, 50(198), 104–113.
- Jurišić, A. (1959). Velika Gradina u Staparima, praistorijsko naselje. *Starinar*, 9(10), 367–368.
- Kearns, T., Martínón-Torres, M., & Rehren, T. (2010). Metal to mould: Alloy identification in experimental casting moulds using XRF. *Historical Metallurgy*, 44(1), 48–58.
- Keesmann, I., & Onorato, A. (1999). Naturwissenschaftliche Untersuchungen zur frühen Technologie von Kupfern und Kupfer-Arsen-Bronze. In A. Hauptmann, E. Pernicka, T. Rehren, & U. Yalçin (Eds.), *The Beginnings of Metallurgy* (pp. 317–332). Deutsches Bergbau-Museum.
- Keller, C. M., & Keller, J. D. (1996). *Cognition and tool use: The blacksmith at work*. Cambridge University Press.

- Kienlin, T. L. (2012). Working copper in the Chalcolithic: A long-term perspective on the development of metallurgical knowledge in central Europe and the Carpathian Basin. *Is There a British Chalcolithic*, 126–143.
- Kienlin, T. L., Roberts, B., & Ottaway, B. S. (2009). *Metals and societies: Studies in honour of Barbara S. Ottaway*. R. Habelt.
- Killick, D. (2014). From ores to metals. In *Archaeometallurgy in global perspective* (pp. 11–45). Springer.
- Killick, D. (2015). The awkward adolescence of archaeological science. *Journal of Archaeological Science*, 56, 242–247.
- Klein, C., & Philpotts, A. R. (2013). *Earth materials: Introduction to mineralogy and petrology*. Cambridge University Press.
- Klemm, S. (1992). In *Fundberichte österreichs* (p. 445).
- Klemm, S. (1993). In *Fundberichte österreichs* (pp. 703–704).
- Klemm, S. (1994). Klemm S., Ausgrabungen in der Eisenerzer Ramsau. *Archäologie Österreichs*, 5(2), 28–29.
- Klemm, S. (1995). Paper given at ‘Prehistoric copper mining and metallurgy in the Alps’. *International Workshop at the University of Innsbruck, Austria. 4th-8th October 1995*.
- Knapp, A. B. (2000). Archaeology, science-based archaeology and the Mediterranean Bronze Age metals trade. *European Journal of Archaeology*, 3(1), 31–56.
- Knight, R. D., Kjarsgaard, B. A., & Russell, H. A. (2021). An analytical protocol for determining the elemental chemistry of Quaternary sediments using a portable X-ray fluorescence spectrometer. *Applied Geochemistry*, 131, 105026.
- Kongoli, F., & Yazawa, A. (2001). Liquidus surface of FeO-Fe₂O₃-SiO₂-CaO slag containing Al₂O₃, MgO, and Cu₂O at intermediate oxygen partial pressures. *Metallurgical and Materials Transactions B*, 32(4), 583–592.
- Koucky, F. L., & Steinberg, A. (1982a). Ancient mining and mineral dressing on Cyprus. In T. A. Wertime & S. F. Wertime (Eds.), *Early Pyrotechnology: The evolution of the first fire-using industries*. (pp. 149–180). Smithsonian Institution Press.
- Koucky, F. L., & Steinberg, A. (1982b). The ancient slags of Cyprus. *Early Metallurgy in Cyprus, 4000(500)*, 117–137.
- Koukouli-Chrysanthaki, H. (2007). Preventive archaeology and major public works in Greece. *European Preventive Archaeology*.
- Kowalski, M., Spencer, P. J., & Neuschütz, D. (1995). Phase Diagrams (Chapter 3) in Slag Atlas, ed. By VDEh. In *Verlag Stahleisen GmbH, Düsseldorf* (Vol. 21).
- Krajnovic, D., & Jankovic, S. (1995). Copper mineralization as potential raw material source of ancient copper metallurgy in Serbia. In B. Jovanovic (Ed.), *Ancient Mining and Metallurgy in Southeast Europe*. Archaeological Institute, Museum of Mining and Metallurgy.
- Krajnović, D., & Janković, S. (1995). Copper mineralization as potential raw material source of ancient copper metallurgy in Serbia. In P. Petrović & S. Djurdjekanović (Eds.), *Ancient Mining and Metallurgy in Southeast Europe*. (Archaeological Institute, Museum of Mining and Metallurgy).
- Kresten, P. (1986). Melting points and viscosities of ancient slags: A discussion. *Historical Metallurgy*, 20(1), 43–45.
- Krismer, M., Töchterle, U., Goldenberg, G., Tropper, P., & Vavtar, F. (2013). Mineralogical and petrological investigations of Early Bronze Age copper-smelting remains from the Kiechlberg (Tyrol, Austria): Early Bronze Age copper-smelting remains from the Kiechlberg (Tyrol, Austria). *Archaeometry*, 55(5), 923–945.
- Kronz, A. (1997). *Phasenbeziehungen und Kristallisationsmechanismen in fayalitischen Schmelzsystemen-Untersuchungen an Eisen- und Buntmetallschlacken*. Fakultät für Geowissenschaften [PhD Thesis]. Dissertation Mainz, Johannes Gutenberg Universität.

- Kucera, M. (2004). Das Experiment in der Archäologie. *Experimentelle Archäologie in Europa, Bilanz*, 3, 7–13.
- La Duc, E., Montero-Ruiz, I., Freestone, I. C., Loras, J. F., Expósito, I. M. J., de la Cruz, J. C. M., Pérez-Lambán, F., Millán, J. V. P., & Martínón-Torres, M. (2022). Diverse strategies for copper production in Chalcolithic Iberia. *Journal of Archaeological Science: Reports*, 46, 103683.
- Lammers-Keijsers, Y. M. . J. (2005). Scientific experiments: A possibility? Presenting a cyclical script for experiments in archaeology. *Journal for (Re) Construction and Experiment in Archaeology*, 2, 18–24.
- Laschimke, R., & Burger, M. (2017). Neolithische Flachbeile aus Kupfer, die ältesten Metallwerkzeuge des menschen–archäometallurgische Experimente zu ihrer Herstellung. *Metall*, 3, 85–88.
- Laschimke, R., & Burger, M. (2018). Die Herstellung von kupferzeitlichen Äxten mit Schaftloch–archäometallurgische Experimente. *Metall*, 6, 239–243.
- Lazzarotto, A., Aldinucci, M., Cirilli, S., Costantini, A., Decandia, F. A., Pandeli, E., Sandrelli, F., & Spina, A. (2003). Stratigraphic correlation of the Upper Palaeozoic-Triassic successions in southern Tuscany, Italy. *Bollettino Della Società Geologica Italiana, Special Volumes*, 2, 25–35.
- Leavis, F. R. (1962). Two cultures? The significance of CP Snow. *Critical Review*, 5, 90.
- Lemonnier, P. (1986). The study of material culture today: Toward an anthropology of technical systems. *Journal of Anthropological Archaeology*, 5(2), Article 2. [https://doi.org/10.1016/0278-4165\(86\)90012-7](https://doi.org/10.1016/0278-4165(86)90012-7)
- Lemonnier, P. (Ed.). (1993a). Introduction. In *Technological choices: Transformation in material cultures since the Neolithic* (pp. 1–35). Routledge.
- Lemonnier, P. (Ed.). (1993b). *Technological choices: Transformation in material cultures since the Neolithic*. Routledge.
- Leng, Y. (2009). *Materials characterization: Introduction to microscopic and spectroscopic methods*. John Wiley & Sons.
- Leroi-Gourhan, A. (1943). *Evolution et techniques: L'homme et la matière* (Vol. 1). A. Michel.
- Leuzinger, U. (1997). Die jungsteinzeitlichen Kupferfunde aus dem Kanton Thurgau. *Arch Switz*, 20, 51–53.
- Lutz, C., Bachmann, H.-G., & Thiemann, U. (1988). Viscosities of slags from non-ferrous metal smelting: Experimental determination and calculation. *Erzmetall*, 41(7), 394–398.
- Maggetti, M. (2010). Neolithic pottery from Switzerland: Raw materials and manufacturing processes. In *From mine to microscope, advances in the study of ancient technology* (pp. 29–42). Oxbow Books, Oxford.
- Maggetti, M., Baumgartner, D., & Galetti, G. (1991). Mineralogical and chemical studies on Swiss Neolithic crucibles. *Archaeometry*, 90, 95–104.
- Maggi, R., Campana, N., & Negrino, F. (1995). Valle Lagorara (I 28): A quarry of radiolarite (jasper) exploited during the Copper and Early Bronze Ages. *Archaeologia Polona*, 33, 187–208.
- Maggi, R., & Del Lucchese, A. (1989). Aspects of the Copper Age in Liguria. *Rassegna Di Archeologia*, 7, 331–338.
- Maggi, R., & Pearce, M. (2005). Mid fourth millennium copper mining in Liguria, north-west Italy: The earliest known copper mines in western Europe. *Antiquity*, 79(303), 66–77.
- Maggi, R., & Pearce, M. (2013). Cronologia mineraria in Liguria. *Cronologia Assoluta e Relativa Dell'Età Del Rame in Italia. Atti Dell'Incontro Di Studi Università Di Verona*, 25, 5–15.
- Manasse, A., & Mellini, M. (2002). Chemical and textural characterisation of medieval slags from the Massa Marittima smelting sites (Tuscany, Italy). *Journal of Cultural Heritage*, 3(3), 187–198.
- Manasse, A., Mellini, M., & Viti, C. (2001). The copper slags of the Capattoli Valley, Campiglia Marittima, Italy. *European Journal of Mineralogy*, 13(5), 949–960.

- Martinek, K. P. (1996). Archäometallurgische Untersuchungen zur frühbronzezeitlichen Kupferproduktion und -verarbeitung auf der Buchberg bei Wiesing, Tirol. *Fundberichte Österreich*, 34, 575–584.
- Martinek, K. P. (2011). Co-smelting, the beginning of early metallurgy—Evidence from the Inn smelting experiments. In A. Hauptmann, D. Modarressi-Tehrani, & M. Prange (Eds.), *Metalla* (Vol. 4, p. 145). Deutsches Bergbau-Museum.
- Martinek, K. P., & Sydow, W. (2004). 'Frühbronzezeitliche Kupfermetallurgie im Unterinntal (Nordtirol)', in G. Goldenberg (eds.), *Alpenkupfer – Rame delle Alpi (Bochum)* (pp. 199–211).
- Martinón-Torres, M. (2018). Ore and Smelting Slag. *The Encyclopedia of Archaeological Sciences*, 1–4.
- Martinón-Torres, M., & Killick, D. (2015). *Archaeological Theories and Archaeological Sciences* (A. Gardner, M. Lake, & U. Sommer, Eds.; Vol. 1). Oxford University Press. <https://doi.org/10.1093/oxfordhb/9780199567942.013.004>
- Martinón-Torres, M., & Rehren, T. (2014). Technical ceramics. In B. W. Roberts & C. P. Thornton (Eds.), *Archaeometallurgy in global perspective: Methods and syntheses* (pp. 107–133). Springer.
- Marzatico, F. (1997). L'industria metallurgica nel Trentino durante l'età del bronzo. In *Le Terramare. La più antica civiltà padana*. (pp. 570–591). Electa.
- Mathieu, J. R. (2002). Experimental archaeology. *BAR International Series*, 1035.
- Matuschik, I. (1998). Kupferfunde und Metallurgie-Belege, zugleich ein Beitrag zur Geschichte der kupferzeitlichen Dolche Mittel-, Ost- und Südosteuropas. In M. Mainberger (Ed.), *Das Moordorf von Reute* (pp. 207–261).
- Mazzei, P., & Dal Santo, N. (2007). Il sito del Neolitico recente di Bottegghino (Parma). *Rivista di Scienze Preistoriche*, LVII, 113–138.
- Meinert, L., Dipple, G. M., & Nicolescu, S. (2005). World Skarn Deposits. *Economic Geology*, 100th Anniversary Volume, 299–336.
- Merkel, J. (1985). Ore beneficiation during the late Bronze/early Iron age at Timna, Israel. *MASCA Journal*, 3(5), 164–169.
- Merkel, J. F. (1990). Experimental reconstruction of Bronze Age copper smelting based on archaeological evidence from Timna. *The Ancient Metallurgy of Copper*, 2, 78–122.
- Metten, B. (2003). Beitrag zur spätbronzezeitlichen Kupfermetallurgie im Trentino (Südalpen) im Vergleich mit anderen prähistorischen Kupferschlacken aus dem Alpenraum. *Metalla*, 10(1/2), 1–122.
- Mille, B., & Carozza, L. (2009). Moving into the metal ages: The social importance of metal at the end of the Neolithic period in France. In T. L. Kienlin & B. W. Roberts (Eds.), *Metals and Society. Studies in honour of Barbara S. Ottaway*. Verlag Dr Rudolf Habelt GMBH. Bonn (pp. 143–171).
- Millson, D. C. (2011). Introduction. In D. C. Millson (Ed.), *Experimentation and interpretation: The use of experimental archaeology in the study of the past* (pp. 1–6). Oxbow Books.
- Milton, C., Dwornik, E. J., Finkelman, R. B., & Toulmin, P. (1976). Slag from an ancient copper smelter at Timna Israel. *Journal of the Historical Metallurgy Society*, 10(1), 24–33.
- Misra, M. K., Ragland, K. W., & Baker, A. J. (1993). Wood ash composition as a function of furnace temperature. *Biomass and Bioenergy*, 4(2), 103–116.
- Moesta, H. (1986). Bronze Age copper smelting. *Interdisciplinary Science Reviews*, 11(1), 73–87.
- Molloy, B. (2011). Use-wear analysis and use-patterns of Bronze Age swords. In M. Uckelmann & M. Mödler (Eds.), *Bronze Age warfare: Manufacture and use of weaponry* (pp. 67–84). Archaeopress.

- Monaco, H. L., Artioli, G., Viterbo, D., Ferraris, G., Gilli, G., Zanotti, G., & Catti, M. (2002). *Fundamentals of crystallography* (Vol. 7). Oxford university press, USA.
- Montero-Ruiz, I. (1993). Bronze Age metallurgy in southeast Spain. *Antiquity*, 67(254), 46–57.
- Montero-Ruiz, I., & Ruiz-Taboada, A. (1996). Enterramiento colectivo y metalurgia en el yacimiento neolítico de Cerro Virtud (Cuevas de Almanzora, Almería). *Trabajos de Prehistoria*, 53(2), 55–75.
- Morton, G. R., & Wingrove, J. (1969a). Constitution of bloomery slags: Part 1: Roman. *Journal of the Iron and Steel Institute*, 207, 1556–1564.
- Morton, G. R., & Wingrove, J. (1969b). Slag, cinder, and bear. *Journal of Historical Metallurgical Society*, 3(2), 55–61.
- Morton, G. R., & Wingrove, J. (1972). Constitution of bloomery slags: Part II: Medieval. *Journal of the Iron and Steel Institute*, 478–487.
- Mottes, E., Bassetti, M., & Silvestri, E. (2012). The Bronze Age Tumuli of Gardolo di Mezzo (Trento, Italy) in the Adige Valley. *Ancestral Landscape. Burial Mounds in the Copper and Bronze Ages (Central and Eastern Europe – Balkans – Adriatic – Aegean, 4th-2nd Millennium B.C.)*, 523–532.
- Mottes, E., Bassetti, M., Silvestri, E., & Stefan, L. (2014). Il sito archeometallurgico dell'età del Rame di Riparo Marchi in Valle dell'Adige (Trento). In *Archeologia delle Alpi* (Vol. 2014, pp. 39–43). Provincia Autonoma di Trento.
- Müller, R., Goldenberg, G., Bartelheim, M., Kunst, M., & Pernicka, E. (2007). Zambujal and the beginnings of metallurgy in southern Portugal. In *Metals and Mines. Studies in Archaeometallurgy* (pp. 15–26). Archetype Publications.
- Müller, R., Rehren, T., & Rovira, S. (2004). Almizaraque and the early copper metallurgy of southeast Spain: New data. *Madrider Mitteilungen*, 45, 33–56.
- Müller, R., Rovira, S., & Rehren, T. (2006). The Question of Early Copper Production at Almizaraque, SE Spain. *34th International Symposium on Archaeometry (Zaragoza 2004)*, 209–219.
- Müller, R., & Soares, A. M. M. (2008). Traces of early copper production at the Chalcolithic fortification of Vila Nova de São Pedro (Azambuja, Portugal). *Madrider Mitteilungen*, 49, 94–114.
- Murdoch, J. (1916). *Microscopical determination of the opaque minerals: An aid to the study of ores*. John Wiley & sons, Incorporated.
- Murillo-Barroso, M., Martín-Torres, M., Massieu, M. D. C., Socas, D. M., & González, F. M. (2017). Early metallurgy in SE Iberia. The workshop of Las Pilas (Mojácar, Almería, Spain). *Archaeological and Anthropological Sciences*, 9(7), 1539–1569.
- Murillo-Barroso, M., & Montero-Ruiz, I. (2012). Copper Ornaments in the Iberian Chalcolithic: Technology versus Social Demand. *Journal of Mediterranean Archaeology*, 25(1), 53–73.
- Murillo-Barroso, M., Montero-Ruiz, I., Martín-Socas, D., Labaune, M., Cattin, F., Nieto, J. M., & Martín-Torres, M. (2020). Captación y selección de materias primas en la primera metalurgia del Sureste de la península ibérica. *Trabajos de Prehistoria*, 77(1), Article 1.
- Needham, S. (2012). Case and place for the British Chalcolithic. *Is There a British Chalcolithic*, 1–26.
- Needham, S. P. (1996). Chronology and periodisation in the British Bronze Age. *Acta Archaeologica*, 67, 121–140.
- Needham, S. P., Leese, M. N., Hook, D. R., & Hughes, M. J. (1989). Developments in the Early Bronze Age metallurgy of southern Britain. *World Archaeology*, 20(3), 383–402.
- Nicholson, P. T. (2007). *Brilliant things for Akhenaten: The production of glass, vitreous materials and pottery at Amarna site O45. I*. Egypt exploration society.
- Nocete, F. (2004). Odiel. Proyecto de investigación arqueológica para el análisis del origen de la desigualdad social en el Suroeste de la Península Ibérica. *Arqueología Monografías*, 19.
- Nocete, F. (2006). The first specialised copper industry in the Iberian peninsula: Cabezo Juré (2900–2200 BC). *Antiquity*, 80(309), 646–657.

- Nocete, F., Escalera, P., Linares, J. A., Lizcano, R., Orihuela, A., Otero, R., Romero, J. C., & Saez, R. (1994). Estudio del material arqueológico del yacimiento de Cabezo Juré (Alosno, Huelva). *Primera Campaña.*, 67–78.
- Nocete, F., Queipo, G., Sáez, R., Nieto, J. M., Inácio, N., Bayona, M. R., Peramo, A., Vargas, J. M., Cruz-Auñón, R., Gil-Ibarguchi, J. I., & Santos, J. F. (2008). The smelting quarter of Valencina de la Concepción (Seville, Spain): The specialised copper industry in a political centre of the Guadalquivir Valley during the Third millennium BC (2750–2500 BC). *Journal of Archaeological Science*, 35(3), 717–732.
- O'Brien. (2004). *Ross Island: Mining, metal and society in early Ireland*. Department of Archaeology, National University of Ireland, Galway.
- O'Brien, W. (2015). *Prehistoric copper mining in Europe, 5500-500 BC* (First Edition). Oxford University Press.
- O'Brien, W., & Comber, M. (2008). Archaeological investigations at Ross Island Cave, Killarney, Co. Kerry. *The Journal of Irish Archaeology*, 19–56.
- Olin, J. S. (1982). Future directions in archaeometry. *Journal of Field Archaeology Boston, Mass*, 9(1), 130–132.
- Ottaway, B. S. (2001). Innovation, production and specialization in early prehistoric copper metallurgy. *European Journal of Archaeology*, 4(1), 87–112.
- Ottaway, B. S., & Wang, Q. (2004). *Casting experiments and microstructure of archaeologically relevant bronzes*. British Archaeological Reports Limited.
- Otto, H., & Witter, W. (1952). *Handbuch der ältesten vorgeschichtlichen Metallurgie in Mitteleuropa*.
- Outram, A. K. (2008). Introduction to experimental archaeology. *World Archaeology*, 40(1), 1–6.
- Paardekooper, R. (2008). Experimental Archaeology. In D. M. Pearsall (Ed.), *Encyclopedia of Archaeology* (pp. 1345–1358).
- Paardekooper, R. (2015). EXARC and Experimental Archaeology. *BAEX: Boletín de Arqueología Experimental*.
- Pearce, M. (2007). *Bright Blades and Red Metal: Essays on north Italian prehistoric metalwork* (Vol. 14). Accordia Research Institute, University of London London.
- Pearce, M. (2015). The spread of early copper mining and metallurgy in Europe: An assessment of the diffusionist model. In A. Hauptmann & D. Modarressi-Tehrani (Eds.), *Archaeometallurgy in Europe III* (pp. 45–54).
- Pearce, M., Merkel, S., Hauptmann, A., & Nicolis, F. (2022). The smelting of copper in the third millennium cal BC Trentino, north-eastern Italy. *Archaeological and Anthropological Sciences*, 14(1), 1–21.
- Pecikoza, V. (2011). Deposits of copper and Vinča sites in the area of Valjevo Mountains. *Kolubara*, 5, 39–46.
- Pedrotti, A. (2002). L'età del Rame. In M. Lanzinger, F. Marzatico, & A. Pedrotti (Eds.), *Storia del Trentino, La preistoria e la protostoria* (Vol. 1, pp. 183–254). Il Mulino.
- Perazzi, P., & Poggesi, G. (2011). *Carta archeologica della Provincia di Prato. Dalla preistoria all'età romana*. All'Insegna del Giglio.
- Perini, R. (1971). I depositi preistorici di Romagnano e Loc (Trento). *Preistoria Alpina*, 7, 7–106.
- Perini, R. (1973). Romagnano–Tof de la Val (Trento). *Preistoria Alpina*, 9, 247–250.
- Perini, R. (1989a). Testimonianze di attività metallurgica dall'eneolitico alle fasi finali dell'età del bronzo nel Trentino». AA. VV., *Per G. Seberta, Biblioteca Comunale Di Trento*, 377.
- Perini, R. (1989b). Testimonianze di attività metallurgica dall'eneolitico alle fasi finali dell'età del bronzo nel Trentino». In *Per G. Sebesta, scritti e nota bibliografica per il settantesimo compleanno* (Biblioteca Comunale di Trento, p. 377).

- Perini, R. (1992). Evidence of metallurgical activity in Trentino from Chalcolithic times to the end of the Bronze Age. In E. A. Sanpaolo (Ed.), *Archeometallurgia Recherche e Prospettive* (pp. 53–76). Clueb.
- Pernicka, E., Adam, K., Böhme, M., Hezarkhani, Z., Nezafati, N., Schreiner, M., Winterholler, B., Momenzadeh, M., & Vatandoust, A. R. (2011). Archaeometallurgical research on the western Central Iranian Plateau. In A. Vatandoust, H. Parzinger, & B. Helwing (Eds.), *Early Mining and Metallurgy on the Western Central Iranian Plateau, Archäologie in Iran und Turan* (Vol. 9, pp. 633–687).
- Pernicka, E., Begemann, F., & Schmitt-Strecke, S. (1993). Eneolithic and Early Bronze Age copper artefacts from the Balkans and their relation to Serbian copper ores. *Prähistorische Zeitschrift*, 68, 1–54.
- Pernicka, E., Begemann, F., Schmitt-Strecke, S., & Todorova, H. (1997). Prehistoric copper in Bulgaria: Its composition and provenance. *Eurasia Antiqua: Zeitschrift Für Archäologie Eurasiens*, 3, 41–180.
- Pfaffenberger, B. (1992). Social anthropology and technology. *Annual Review of Anthropology*, 21, 491–516.
- Phelps. (2013). Scientific examination of materials used in the experiments. In D. Dungworth & R. C. P. Doonan (Eds.), *Accidental and Experimental Archaeometallurgy* (pp. 161–168).
- Piel, M., Hauptmann, A., & Schröder, B. (1992). Naturwissenschaftliche Untersuchungen an bronzezeitlichen Kupferverhüttungsschlacken von Acqua Fredda/Trentino. *Festschrift Zum 50jähigen Bestehen Des Institutes Für Ur-Und Frühgeschichte Der Leopold-Franzens-Universität Innsbruck. Universitätsforschungen Zur Prähistorischen Archäologie*, 8, 463–472.
- Pleiner, R. (2000). *Iron in archaeology: The European bloomery smelters*. Archeologický ústav AVČR.
- Popper, K. R. (1959). *The logic of scientific discovery*. Routledge.
- Pracejus, B. (2015). *The ore minerals under the microscope: An optical guide*. Elsevier.
- Prange, M. (2000). La Roussignole: Geochemische Charakterisierung prähistorischer Abbaue in Cabrières/Hérault. *Metalla*, 7(2), 47–54.
- Prange, M., & Ambert, P. (2005). Caractérisation géochimique et isotopique des minerais et des métaux base cuivre de Cabrières (Hérault). In P. Ambert & J. Vaquer (Eds.), *La première métallurgie en France et dans les pays limitrophes. Mémoires 37 de la Société préhistorique française, Carcassonne* (Mémoires 37 de la Société préhistorique française, pp. 71–81).
- Preuschen, E. (1962). Der urzeitliche Kupfererzbergbau von Vettiole (Trentino). *Der Anschnitt*, 14, 3–7.
- Preuschen, E. (1965). Das urzeitliche Kupfer-Verhüttungsgebiet von Lavarone (Trentino). *Der Anschnitt*, 17(4–5), 8–13.
- Preuschen, E. (1968). Bronzezeitlicher Kupfererzbergbau im Trentino. *Der Anschnitt*, 20(1), 3.
- Preuschen, E. (1973). Estrazione mineraria dell'età del bronzo nel Trentino. *Preistoria Alpina*, 9, 113–150.
- Pryce, T. O. (2009). *Copper production and technological reproduction in the Khao Wong Prachan Valley of Central Thailand* [PhD Thesis]. Unpublished doctoral thesis, UCL Institute of Archaeology, University College London.
- Pryce, T. O., Pigott, V. C., Martín-Torres, M., & Rehren, T. (2010). Prehistoric copper production and technological reproduction in the Khao Wong Prachan Valley of Central Thailand. *Archaeological and Anthropological Sciences*, 2(4), 237–264.
- R Core Team. (2020). *R: A language and environment for statistical computing. R Foundation for Statistical Computing, Vienna, Austria*. URL <https://www.R-project.org/>.
- Rademakers, F. (2015). *Into the crucible. Methodological approaches to reconstructing crucible metallurgy, from New Kingdom Egypt to Late Roman Thrace* [PhD Thesis]. UCL (University College London).

- Rademakers, F. W., Rehren, T., & Voigt, M. M. (2018). Bronze metallurgy in the Late Phrygian settlement of Gordion, Turkey. *Archaeological and Anthropological Sciences*, 10(7), 1645–1672.
- Radi, G., & Danese, E. (2003). Il sito neolitico di Settefonti a Prata d'Ansidonia (L'Aquila). XXXVI Riunione Scientifica Istituto Italiano Preistoria e Protostoria" *Preistoria e Protostoria Dell'Abruzzo*", 163–179.
- Radivojević, M. (2013). Archaeometallurgy of the Vinča culture: A case study of the site of Belovode in eastern Serbia. *Historical Metallurgy*, 47(1), 13–32.
- Radivojević, M. (2015). Inventing Metallurgy in Western Eurasia: A Look Through the Microscope Lens. *Cambridge Archaeological Journal*, 25(01).
- Radivojević, M. (2021). Chapter 5. Introduction to Belovode and results of archaeometallurgical research 1993–2012. In M. Radivojević, B. W. Roberts, M. Marić, J. Kuzmanović-Cvetković, & T. Rehren (Eds.), *The rise of metallurgy in Eurasia: Evolution, organisation and consumption of early metal in the Balkans* (pp. 47–59). Archaeopress Publishing Ltd.
- Radivojević, M., & Kuzmanović-Cvetković, J. (2014). Copper minerals and archaeometallurgical materials from the Vinča culture sites of Belovode and Pločnik: Overview of the evidence and new data. *Starinar*, 64, 7–30.
- Radivojević, M., & Rehren, T. (2016). Paint It Black: The Rise of Metallurgy in the Balkans. *Journal of Archaeological Method and Theory*, 23(1), 200–237.
- Radivojević, M., & Rehren, T. (2021). Chapter 11. Belovode: Technology of metal production. In M. Radivojević, B. W. Roberts, M. Marić, J. Kuzmanović-Cvetković, & T. Rehren (Eds.), *The rise of metallurgy in Eurasia: Evolution, organisation and consumption of early metal in the Balkans* (pp. 123–151). Archaeopress Publishing Ltd.
- Radivojević, M., Rehren, T., Kuzmanović-Cvetković, J., Jovanović, M., & Northover, J. P. (2013). Tainted ores and the rise of tin bronzes in Eurasia, c. 6500 years ago. *Antiquity*, 87(338), 1030–1045.
- Radivojević, M., Rehren, T., Pernicka, E., Šljivar, D., Brauns, M., & Borić, D. (2010). On the origins of extractive metallurgy: New evidence from Europe. *Journal of Archaeological Science*, 37(11), 2775–2787.
- Radivojević, M., Roberts, B., Marić, M., Kuzmanović-Cvetković, J., & Rehren, T. (2021). *The rise of metallurgy in Eurasia: Evolution, organisation and consumption of early metal in the Balkans*. Archaeopress Publishing Ltd.
- Radivojević, M., & Roberts, B. W. (2021). Chapter 3. Balkan metallurgy and society, 6200–3700 BC. In M. Radivojević, B. W. Roberts, M. Marić, J. Kuzmanović-Cvetković, & T. Rehren (Eds.), *The rise of metallurgy in Eurasia: Evolution, organisation and consumption of early metal in the Balkans* (pp. 11–37). Archaeopress Publishing Ltd.
- Ramdohr, P. (2013). *The ore minerals and their intergrowths*. Elsevier.
- Rehder, J. E. (1994). Blowpipes versus Bellows in Ancient Metallurgy. *Journal of Field Archaeology*, 21(3), 345–350.
- Rehren, T. (2009). From mine to microbe – the Neolithic copper melting crucibles from Switzerland. In A. Shortland, I. Freestone, & T. Rehren (Eds.), *From Mine to Microscope. Studies in Honour of Mike Tite*. (pp. 155–162). Oxbow Books: Oxford, United Kingdom.
- Rehren, T., Boscher, L., & Pernicka, E. (2012). Large scale smelting of speiss and arsenical copper at Early Bronze Age Arisman, Iran. *Journal of Archaeological Science*, 39(6), 1717–1727.
- Rehren, T., Leshtakov, P., Penkova, P., Nikolov, V., & Schier, W. (2016). Reconstructing chalcolithic copper smelting at Akladi cheiri, Chernomorets, Bulgaria. *Der Schwarzmeerraum Vom Neolithikum Bis in Die Früheisenzeit (6000-600 v. Chr.). Kulturelle Interferenzen in Der Zirkumpontischen Zone Und Kontakte Mit Ihren Nachbargebieten*, 205–214.
- Rehren, T., Penkova, P., & Pernicka, E. (2020). *The Chalcolithic copper smelting at Akladi Cheiri*.

- Reitmaier-Naef, L., Turck, R., Stöllner, T., & Goldenberg, G. (2019). *Copper smelting slag from the Oberalpbstein (Canton of Grisons, Switzerland). Methodological considerations on typology and morphology.*
- Renzi, M., Georgakopoulou, M., Peege, C., Fasnacht, W., & Rehren, T. (2018). 6. Technology of Copper Smelting at Agia Varvara-Almyras. *Agia Varvara-Almyras: An Iron Age Copper Smelting Site in Cyprus*, 269.
- Reynolds, P. J. (1999). The nature of experiment in archaeology. *Experiment and Design: Archaeological Studies in Honour of John Coles*, 156–162.
- Richter, P. (1992). Experimentelle Archäologie: Ziele, Methoden und Aussagemöglichkeiten. In M. Fansa (Ed.), *Experimentelle Archäologie, Bilanz 1991*. (Staatliches Museum für Naturkunde und Vorgeschichte., pp. 19–49). na.
- Roberts, B. (2008). Creating traditions and shaping technologies: Understanding the earliest metal objects and metal production in Western Europe. *World Archaeology*, 40(3), 354–372.
- Roberts, B. (2009). Production Networks and Consumer Choice in the Earliest Metal of Western Europe. *Journal Of World Prehistory*, 22, 461–481.
- Roberts, B. W., & Thornton, C. P. (Eds.). (2014). *Archaeometallurgy in global perspective: Methods and syntheses*. Springer.
- Roberts, B. W., Thornton, C. P., & Pigott, V. C. (2009). Development of metallurgy in Eurasia. *Antiquity*, 83(322), 1012–1022.
- Rose, T., Hanning, E., & Klein, S. (2019). Verhüttungsexperimente mit Chalkopyrit-Erz nach Vorbildern aus dem bronzezeitlichen Ostalpenraum und Nepal. *Experimentelle Archäologie in Europa*, 18, 47–60.
- Rose, T., Hanning, E., & Klein, S. (2020). Smelting Experiments with chalcopyrite ore based on evidence from the Eastern Alps. *METALLA*, 25.2, 77–100.
- Rossi, M., Gattiglia, A., & Rostan, M. (1997). Una miniera di rame preistorica nelle Alpi Occidentali. *Le Scienze*, 344, 74–80.
- Rostan, P., Gattiglia, A., & Rossi, M. (1994). Ricerche sulle miniere e sulla metallurgia dell'eta del Bronzo nel Briançonnais (Hautes-Alpes, Francia). In F. Zampicininini (Ed.), *De Re Metallica, miniere e materie prime alle soglie del 3° millennio* (pp. 173–181).
- Rostan, P., Gattiglia, A., & Rossi, M. (1997). *Ricerche sulle miniere e sulla metallurgia dell'Età de Bronzo nel Briançonnais (Hautes-Alpes, Francia)*.
- Rostan, P., & Malaterre, J. (1994). Les Clausis-Pinilière: Ensemble minier, Saint-Véran. *Bilan Scientifique. SRA PACA, Marseille*, 34–35.
- Rostan, P., Rossi, P., & Gattiglia, A. (2002). Approche économique et industrielle du complexe minier et métallurgique de Saint-Véran (Hautes-Alpes) dans le contexte de l'Age du Bronze dans les Alpes du sud. *Bulletin d'études Préhistoriques et Archéologiques Alpines*, 13, 77–96.
- Rostoker, W. (1975). Some Experiments in Prehistoric Copper Smelting. *Paléorient*, 3(1), 311–315.
- Rostoker, W., Pigott, V. C., & Dvorak, J. R. (1989). Direct reduction to copper metal by oxide-sulfide mineral interaction. *Archaeomaterials*, 3(1), 69–87.
- Rostoker, W., & Sadowski, M. (1980). The carbon reduction of fully oxidized chalcopyrite (copper) ores. *Journal of the Historical Metallurgy Society*, 14(1), 38–42.
- Rothenberg, B. (1972). Survey im Sinai. *Hadashot Arkheologiot*, 43, 29–31.
- Rothenberg, B. (1973). *Timna* (Thames and Hudson). Lübbe.
- Rothenberg, B. (1990). The Ancient Metallurgy of Copper. Researches in the Arabah 1959e1984, vol. 2. *Institute for Archaeo-Metallurgical Studies. Institute of Archaeology, Univ. College, London*.
- Rothenberg, B., Blanco Freijeiro, A., & Bachmann, H. G. (1981). *Studies in ancient mining and metallurgy in South-we st Spain: Explorations and excavations in the Province of Huelva*.

- Rovira, S. (2007). La producción de bronce en la Prehistoria. In J. Molera, J. Farjas, P. Roura, & T. Pradell (Eds.), *Avances en Arqueometría. Actas Del VI Congreso Ibérico De Arqueometría 2005* (pp. 21–35).
- Rovira, S., & Ambert, P. (2002). Les céramiques à réduire le minerai de cuivre: Une technique métallurgique utilisée en Ibérie, son extension en France méridionale. *Bulletin de La Société Préhistorique Française*, 1. 99(1), 105–126.
- Ruiz-Taboada, A., & Montero-Ruiz, I. (1999). The oldest metallurgy in western Europe. *Antiquity*, 73(282), 897–903.
- Ruttkay, E. (1981). Typologie und Chronologie der Mondsee-Gruppe. In D. Sraub (Ed.), *Das Mondseeland–Geschichte und Kultur. Katalog der Ausstellung des Landes Oberösterreich* (pp. 269–294).
- Ryndina, N., Indenbaum, G., & Kolosova, V. (1999). Copper Production from Polymetallic Sulphide Ores in the Northeastern Balkan Eneolithic Culture. *Journal of Archaeological Science*, 26(8), 1059–1068. <https://doi.org/10.1006/jasc.1999.0410>
- Sáez, R., Almodóvar, G. R., & Pascual, E. (1996). Geological constraints on massive sulphide genesis in the Iberian Pyrite Belt. *Ore Geology Reviews*, 11(6), 429–451.
- Saez, R., Nocete, F., Nieto, J. M., Capitan, M. A., & Rovira, S. (2003). The extractive metallurgy of copper from Cabezo Jurè, Huelva, Spain: Chemical and mineralogical studies of slags dated to the third millennium B.C. *The Canadian Mineralogist*, 41(3), 627–638.
- Sangmeister, E., & Schubart, H. (1981). *Zambujal: Die Grabungen 1964 bis 1973: Vol. 5.1*. Philippe von Zabern.
- Sarti, L., Martini, F., & Poggesi, G. (1999). *Lunga memoria della piana. L'area fiorentina dalla preistoria alla romanizzazione*. <https://usiena-air.unisi.it/handle/11365/31689>
- Sarti, L., Silvestrini, M., & Volante, N. (2005). Il Neolitico recente-finale tra il medio versante adriatico e l'alto versante tirrenico. *Il Neolitico Recente-Finale Tra Il Medio Versante Adriatico e l'alto Versante Tirrenico*, 259–277.
- Sarti, L., & Volante, N. (2002). Neto–Via Verga (Firenze): Il Neolitico tardo e finale e il passaggio all'Eneolitico. In *Atti del Convegno “Il declino del mondo neolitico. Ricerche in Italia centro-settentrionale fra aspetti peninsulari, occidentali e nord-alpin* (Vol. 4, pp. 441–445).
- Schier, W. (1996). The relative and absolute chronology of Vinča: New evidence from the type site. *The Vinča Culture, Its Role and Cultural Connections*, 141–162.
- Schifer, T. (2001). Le minerai de cuivre de Cabrières. *Archéologie En Languedoc (Lattes-Montpellier)*, 24, 71–86.
- Schindler, B. (2018). Experimental Research in Middle Atlantic Archaeology. *Middle Atlantic Prehistory: Foundation and Practice*, 175–189.
- Schlichtherle, H., & Rottländer, R. (1982). Gusstiegel der Pfyner Kultur in Südwestdeutschland. *Fundberichte Aus Baden-Württemberg*, 7, 59–71.
- Schmidt, P. R. (1997). *Iron technology in East Africa: Symbolism, science, and archaeology*. Indiana University Press Bloomington.
- Schöbel, G. (2019). Experimental archaeology. In *The Routledge Handbook of Reenactment Studies* (pp. 67–73). Routledge.
- Scott, D. A. (1991). *Metallography and Microstructure of Ancient and Historic Metals*.
- Šebesta, G. (2000). *La via del rame*. Mueso degli usi e costumi della Gente Trentina.
- Shamsuddin, M. (2020). *Physical chemistry of metallurgical processes*. Springer Nature.
- Shannon, R. D. (1976). Revised effective ionic radii and systematic studies of interatomic distances in halides and chalcogenides. *Acta Crystallographica Section A: Crystal Physics, Diffraction, Theoretical and General Crystallography*, 32(5), 751–767.
- Shimada, I. (2005). Experimental Archaeology. In D. Herbert & G. Maschner (Eds.), *Handbook of Archaeological Methods (Lanham): Vol. I* (pp. 603–642).

- Shugar, A. N. (2000). Archaeometallurgical investigation of the Chalcolithic site of Abu Matar, Israel: A reassessment of technology and its implications for the Ghassulian Culture. *London: University College London*.
- Silvestri, E., Bellintani, P., & Hauptmann, A. (2019). Bronze Age copper ore mining and smelting in Trentino (Italy). *Alpine Copper II–Rame Delle Alpi II–Cuivre Des Alpes II. New Results and Perspectives on Prehistoric Copper Production, Der Anschnitt Beih*, 42, 261–277.
- Silvestri, E., Bellintani, P., Mottes, E., & Nicolis, F. (2014). Evidence of mining without mines: Smelting activity during the Bronze Age in Trentino. In J. Silvertant (Ed.), *Research and preservation of ancient mining areas*, (pp. 89–103). Yearbook of the Institute Europa Subterranea, Trento/Valkenburg aan de Geul.
- Silvestri, E., Hauptmann, A., Bellintani, P., Mottes, E., & Nicolis, F. (2015). Bronzezeitliche Kupferverhüttung in trentino. *Bergauf—Bergab*, 10, 201–208.
- Silvestrini, M., Baglioni, L., Carlini, C., Casciarri, S., Frediani, A., Freguglia, M., Martini, F., Sarti, L., & Volante, N. (2002). Il Neolitico tardo-finale delle Marche. Primi dati su S. Maria in Selva (Treia, Macerata). In *Atti del Convegno Il declino del mondo neolitico. Ricerche in Italia centrosettentrionale fra aspetti peninsulari, occidentali e nord-alpin* (pp. 453–460).
- Skinner, B. J., & Barton, P. B. (1967). Sulfide mineral stabilities in Geochemistry of Hydrothermal Ore Deposits: HL Barnes, Ed. *Geochemistry of Hydrothermal Ore Deposits*, 670, 841–857.
- Šljivar, D. (2006). The earliest copper metallurgy in the Balkans. *Metalurgija—Journal of Metallurgy*, 12, 93–104.
- Šljivar, D., Jacanović, D., & Kuzmanović-Cvetković, J. (2006). New contributions regarding the copper metallurgy in the Vinča culture. In N. Tasić & C. Grozdanov (Eds.), *Homage to Milutin Garašanin* (pp. 251–266).
- Šljivar, D., & Kuzmanović-Cvetković, J. (2009). Pločnik, archaeology and conservation. *Diana (Belgrade)*, 13, 56–61.
- Smith, M. (2017). *Ternary: An R Package for Creating Ternary Plots. Comprehensive R Archive Network*.
- Snow, C. P. (1959). *The two cultures and the scientific revolution*. Cambridge University Press.
- Snyder, D. A., & Carmichael, I. S. (1992). Olivine-liquid equilibria and the chemical activities of FeO, NiO, Fe₂O₃, and MgO in natural basic melts. *Geochimica et Cosmochimica Acta*, 56(1), 303–318.
- Sperl, G. (1980). Metallographic examination of Bronze Age copper. *Metals Technology*, 7(1), 212–217.
- Stanley-Smith, C. (1970). Art, technology, and science: Notes on their historical interaction. *Technology and Culture*, 11(4), Article 4.
- Stanley-Smith, C. (1975). Metallurgy as a human experience. *Metallurgical Transactions A*, 6(4), Article 4.
- Stanley-Smith, C. (1981). *A search for structure. Selected essays on science, art and history*. MA:MIT Press.
- Stanley-Smith, C. (1988). *A History of Metallography*. MA:MIT Press.
- Stanley-Smith, C., & Walruff, B. (1974). Notabilia in essays of oars and mettals—A 17th Century Manuscript. *Journal of the Historical Metallurgy Society*, 8(2), Article 2.
- Stech, T. (1990). Neolithic Copper Metallurgy in Southwest Aisa. *Archaeomaterials*, 4(1), 55–61.
- Stöllner, T., Hanning, E. K., & Hornschuch, A. (2011). Ökonometrie des Kupferproduktionsprozesses am Mitterberger Hauptgang. In K. Oegg, G. Goldenberg, M. Prast, & T. Stöllner (Eds.), *Die Geschichte des Bergbaus in Tirol und seinen angrenzenden Gebieten*. (pp. 115–128).
- Storti, C. (1991). Esame delle scorie del forno di fusione de ‘La Vela’ di Valbusa (Trento). *Sibrium*, 21, 349–361.

- Tanelli, G. (1983). Mineralizzazioni metallifere e minerogenesi della Toscana. *Memorie Della Società Geologica Italiana*, 25, 91–109.
- Tanelli, G., & Benvenuti, M. (1998). Guida ai minerali dell'isola d'Elba e del Campigliese. *Il Libraio*, 164.
- Tanelli, G., & Lattanzi, P. (1986). Metallogeny and mineral exploration in Tuscany: State of the art. *Memorie Della Società Geologica Italiana*, 31, 299–304.
- Tecchiati, U. (2009). Recenti ricerche sull'età del Rame in Val d'Isarco: Bolzano: con un contributo di Lorna Anguilano sulle analisi chimico-petrografiche di scorie di fusione. *Ricerche Paleontologiche Nelle Alpi Occidentali: In Ricordo Di Piero Barocelli e Osvaldo Coisson*.
- Thornton, C. P. (2009). The Emergence of Complex Metallurgy on the Iranian Plateau: Escaping the Levantine Paradigm. *Journal of World Prehistory*, 22(3), 301–327.
- Thornton, C. P., & Rehren, T. (2009). A truly refractory crucible from fourth millennium Tepe Hissar, Northeast Iran. *Journal of Archaeological Science*, 36(12), 2700–2712.
- Thornton, C. P., & Roberts, B. W. (2009). Introduction: The Beginnings of Metallurgy in Global Perspective. *Journal of World Prehistory*, 22(3), 181–184.
- Timberlake, S. (2007). The use of experimental archaeology/ archaeometallurgy for the understanding and reconstruction of Early Bronze Age mining and smelting technologies. In S. La Niece, D. Hook, & P. T. Craddock (Eds.), *Metals and mines. Studies in archaeometallurgy* (pp. 27–36). Archetype Publications.
- Timberlake, S. (2018). Experimental archaeology in bronze age mining and smelting- hard rock, hot metal, new ideas. In P. Eisenach, T. Stöllner, & A. Windler (Eds.), *The RITAK Conf 2013–2014, Der Anschnitt Beih* (Vol. 34, pp. 125–139).
- Töchterle, U., Tropper, P., Trauner, S., & Kaindl, R. (2011). Stilistische und petrographische Untersuchungen prähistorischer Keramik vom Kiechlberg bei Thaur (Nordtirol). *Österreichischer Archäometrikongress Salzburg 2010, Secundus Conventus Austriacus Archaeometriae MMX*, 2, 9–19.
- Trauner, S. (2010). *Petrographische Untersuchung prähistorischer Keramiken vom Kiechlberg bei Thaur (Tirol)*. Unpublished bachelor thesis, University of Innsbruck.
- Tylecote, R. F. (1982). The Late Bronze Age: Copper and bronze metallurgy at Enkomi and Kition. In J. D. Muhly, R. Maddin, & V. Karageorghis (Eds.), *Early Metallurgy in Cyprus, 4000– 500 BC* (pp. 81–100). Pierides Foundation.
- Tylecote, R. F. (1992). *A history of metallurgy* (The Metals Society).
- Tylecote, R. F., & Boydell, P. J. (1978). Experiments on copper smelting based on early furnaces found at Timna. *Archaeo-Metallurgy*, 1, 27–49.
- Tylecote, R. F., Ghaznavi, H. A., & Boydell, P. J. (1977). Partitioning of trace elements between the ores, fluxes, slags and metal during the smelting of copper. *Journal of Archaeological Science*, 4(4), 305–333.
- Tylecote, R. F., & Merkel, J. F. (1985). Experimental Smelting Techniques: Achievements and Future.(Retroactive Coverage). *British Museum Publications Ltd., Furnaces and Smelting Technology in Antiquity*, 3–20.
- Tylecote, R. F., & Tylecote, R. F. (1987). *The early history of metallurgy in Europe*. Longman.
- Valciukas, J. A. (1984). *Kodō Zuroku. A Japanese De Re Metallica. An illustrated book on the smelting of copper*. Burndy Library.
- Vandiver, P. B., Soffer, O., Klima, B., & Svoboda, J. (1989). The origins of ceramic technology at Dolní Věstonice, Czechoslovakia. *Science*, 246(4933), 1002–1008.
- VanPool, T. L., & Leonard, R. D. (2011). *Quantitative analysis in archaeology*. John Wiley & Sons.
- Verly, G. (2017). The smelting furnaces of Ayn Soukhna: The excavations of 2013, 2014 and 2015. *Archaeometallurgy in Europe IV*, 143–158.
- Vidale, M. (1992). *Produzione artigianale protostorica: Etnoarcheologia e archeologia*.

- Volante, N. (2003). La produzione vascolare dell'insediamento di Neto-Via Verga a Sesto Fiorentino tra la fine del Neolitico e la prima Età dei metalli. *Rivista Di Scienze Preistoriche*, 53, 375–504.
- Weber, L., Cerney, I., Ebner, F., Fritz, I., Göd, R., Götzinger, M. A., Gräf, W., Paar, W. H., Prohaska, W., & Sachsenhofer, R. F. (1997). Metallogenetische Karte von Österreich 1: 500.000. *Archiv Für Lagerstättenforschung*, 19.
- Webley, L., Bruck, J., & Adams, S. (2020). Chapter 2. Non-ferrous metalworking: Techniques and materials. In *The Social Context of Technology: Non-ferrous metalworking in later prehistoric Britain and Ireland* (pp. 19–42). Oxbow Books.
- Weisgerber, G. (2004). Schmelzanlagen fruher Kupfergewinnung—Ein Blick u`ber den Alpen. In G. Weisgerber & G. Goldenberg (Eds.), *Alpenkupfer—Rame delle Alpi* (pp. 15–36). Deutsches Bergbau Museum.
- Wenk, H.-R., Yu, R., Tamura, N., Bischoff, D., & Hunkeler, W. (2019). Slags as Evidence for Copper Mining above Casaccia, Val Bregaglia (Central Alps). *Minerals*, 9(5), 292.
- Wertime, T. A. (1968). A metallurgical expedition through the Persian desert. *Science*, 159(3818), 927–935.
- Wertime, T. A. (1973). The Beginnings of Metallurgy: A New Look. *Science, New Series*, 182(4115), 875–887.
- Whittle, A., Bayliss, A., Barclay, A., Gaydarska, B., Bánffy, E., Borić, D., Draşovean, F., Jakucs, J., Marić, M., & Orton, D. C. (2016). A Vinča potscape: Formal chronological models for the use and development of Vinča ceramics in south-east Europe. *Documenta Praehistorica*, 1–60.
- Wickham, H. (2016). *ggplot2: Elegant graphics for data analysis*. springer.
- Williams, R. A. (2014). Linking Bronze age copper smelting slags from Pentwyn on the Great Orme to ore and metal. *Journal of the Historical Metallurgy Society*, 47(1), 94–110.
- Wood, N. (2009). Some implications of the use of wood ash in Chinese stoneware glazes. In A. Shortland, I. C. Freestone, & T. Rehren (Eds.), *From Mine to Microscope. Advances in the Study of Ancient Technology* (pp. 51–60). Oxbow Books.
- Wyss, R. (1977). Motta Vallac, eine bronzzeitliche Hohensiedlung. *Helvetia Archaeologica, Zurich*, 29/30, 35–55.
- Wyss, R. (1982). Die Hohensiedlung Motta Vallac im Oberhalbstein (Salouf, GR). *Archäologie Der Schweiz, Basel.*, 5, 77–82.
- Yahalom-Mack, N., Galili, E., Segal, I., Eliyahu-Behar, A., Boaretto, E., Shilstein, S., & Finkelstein, I. (2014). New insights into Levantine copper trade: Analysis of ingots from the Bronze and Iron Ages in Israel. *Journal of Archaeological Science*, 45, 159–177.

Appendices

Appendix A

Table A. 1 displays the results of the SEM-EDX area analysis (500X) conducted on a certified reference material (SGT11) to assess accuracy and precision. SGT11 is a green soda-lime-silica container glass provided by The Society of Glass Technology. Note: BaO (0.03 wt%) and Cr₂O₃ (0.2 wt%) were not measured. Oxide compositions are presented in wt%.

SGT11	Na₂O	MgO	Al₂O₃	SiO₂	K₂O	CaO	TiO₂	Fe₂O₃	Total
Measure 1	13.4	2.1	2.06	70.5	0.6	10.5	0.1	0.3	99.5
Measure 2	13.7	2.2	1.9	70.8	0.5	10.4	0.1	0.4	100.1
Measure 3	13.5	2.1	1.9	70.6	0.8	10.2	0	0.3	99.3
average measured (1)	13.52	2.12	1.94	70.61	0.65	10.38	0.07	0.31	
certified value (2)	13.60	2.14	1.83	70.70	0.69	10.30	0.07	0.34	
absolute error (3) = (1)-(2)	-0.08	-0.02	0.11	-0.09	-0.04	0.08	0.00	-0.03	
relative error in % (4) = (3/1)*100	-0.57	-0.78	5.51	-0.13	-6.70	0.77	-5.00	-9.15	
correction value (5) = (4)/100	-0.28	-0.13	-0.07	0.04	0.02	0.02	0.13	-0.05	

Appendix B

Table B. 1 displays the SEM-EDX chemical compositional analyses of the archaeological slags from Orti Bottagone. Three random scans, each covering an area of approximately 1 mm², were conducted for each slag. These analyses are graphically depicted in the FeO–Al₂O₃–SiO₂ (wt%) and FeO–CaO–SiO₂ (wt%) ternary systems (see Fig. 5. 12 Ternary plot diagram (FeO–Al₂O₃–SiO₂ (wt%) slag system) of the average composition of the three areas analysed.). It's important to note that for the sake of simplifying the analysis, all elements have been designated as oxides, although it is recognized that certain oxides, such as SO₃, P₂O₅, may not be present in the samples. For a more detailed discussion, please refer to Section 4.2.9. 'b.d.l.' has been used to indicate values that are below the detection limit of the instrument. This notation reflects instances where the concentration of the element was too low to be accurately quantified.

Rep	Type	Square	MgO	Al ₂ O ₃	SiO ₂	SO ₃	Na ₂ O	K ₂ O	P ₂ O ₅	TiO ₂	CaO	MnO	FeO	CuO	ZnO	
ORTB. 3	Ore	B5	1.6	12.6	44.2	b.d.l.	1.4	2.6	17.7	b.d.l.	0.6	9.3	7.5	2.0	b.d.l.	
		G4	b.d.l.	1.1	7.4	4.1	b.d.l.	b.d.l.	b.d.l.	b.d.l.	3.3	0.4	60.5	23.1	b.d.l.	
		M3	1.3	9.0	35.0	b.d.l.	b.d.l.	1.5	b.d.l.	0.6	2.4	33.3	6.1	10.8	b.d.l.	
		Mean	1.5	7.6	28.9	4.1	1.4	2.1	17.7	0.6	2.1	14.3	24.7	12.0	b.d.l.	
		σ	0.2	5.8	19.2	b.d.l.	b.d.l.	0.7	b.d.l.	b.d.l.	1.4	17.0	31.0	10.6	b.d.l.	
ORTB. 5	Coarse	M4	1.1	6.3	22.6	b.d.l.	1.8	0.4	0.8	0.3	0.8	1.8	62.2	0.8	0.6	
		I-H13	0.8	17.4	65.3	0.8	1.9	1.8	b.d.l.	1.0	1.1	b.d.l.	8.0	1.9	b.d.l.	
		G21	0.8	12.0	50.2	b.d.l.	1.1	1.6	b.d.l.	0.7	1.0	0.5	29.9	2.3	b.d.l.	
		Mean	0.9	11.9	46.0	0.8	1.6	1.2	0.8	0.6	1.0	1.1	33.4	1.6	0.6	
		σ	0.2	5.6	21.7	b.d.l.	0.4	0.7	b.d.l.	0.3	0.2	0.9	27.3	0.8	b.d.l.	
ORTB. 6A		P2	3.4	2.6	39.7	2.5	b.d.l.	b.d.l.	b.d.l.	b.d.l.	7.8	b.d.l.	34.0	8.5	1.5	
		F4	5.3	1.8	42.1	b.d.l.	b.d.l.	b.d.l.	b.d.l.	b.d.l.	14.7	b.d.l.	1.4	32.9	2.0	
		N9	4.9	1.6	38.2	2.8	b.d.l.	b.d.l.	b.d.l.	b.d.l.	11.9	1.1	32.3	5.0	2.3	
		Mean	4.5	2.0	40.0	2.6	b.d.l.	b.d.l.	b.d.l.	b.d.l.	11.5	1.1	22.6	15.5	1.9	
		σ	1.0	0.6	2.0	0.3	b.d.l.	b.d.l.	b.d.l.	b.d.l.	3.5		18.4	15.2	0.4	
ORTB. 9		M3	4.6	2.2	46.2	b.d.l.	b.d.l.	b.d.l.	b.d.l.	b.d.l.	13.0	1.2	30.6	0.9	1.3	
		D7	4.0	1.4	33.3	1.5	b.d.l.	b.d.l.	b.d.l.	b.d.l.	5.7	1.1	40.5	11.3	1.3	
		H11	3.4	4.2	43.4	0.9	b.d.l.	b.d.l.	b.d.l.	b.d.l.	9.2	1.2	35.0	2.0	0.8	
		Mean	4.0	2.6	41.0	b.d.l.	b.d.l.	b.d.l.	b.d.l.	b.d.l.	9.3	1.2	35.4	4.7	1.1	
		σ	0.6	1.5	6.8	0.4	b.d.l.	b.d.l.	b.d.l.	b.d.l.	3.7	0.0	5.0	5.7	0.3	
ORTB. 20		M2	0.6	1.3	29.3	2.5	b.d.l.	b.d.l.	b.d.l.	b.d.l.	5.5	1.1	55.7	2.5	1.6	
		F2	0.8	2.1	31.7	0.6	b.d.l.	b.d.l.	b.d.l.	b.d.l.	5.7	1.1	55.8	1.2	1.1	
		B5	0.8	1.2	28.1	1.4	b.d.l.	b.d.l.	b.d.l.	b.d.l.	4.3	1.3	58.0	3.4	1.6	
		Mean	0.7	1.5	29.7	1.5	b.d.l.	b.d.l.	b.d.l.	b.d.l.	5.1	1.2	56.5	2.4	1.4	
		σ	0.1	0.5	1.8	1.0	b.d.l.	b.d.l.	b.d.l.	b.d.l.	0.8	0.1	1.3	1.1	0.3	
ORTB. 8			C7	1.2	6.5	17.5	0.0	b.d.l.	b.d.l.	1.0	b.d.l.	2.8	0.7	65.0	2.4	2.9
			L4	2.4	4.2	29.6	1.1	b.d.l.	b.d.l.	1.2	b.d.l.	8.7	1.3	45.1	1.8	4.7
			P8	0.9	6.5	7.2	b.d.l.	b.d.l.	b.d.l.	1.3	b.d.l.	0.8	0.4	76.5	3.6	2.9
			Mean	1.5	5.7	18.1	0.5	b.d.l.	b.d.l.	1.1	b.d.l.	4.1	0.8	62.2	2.6	3.5
			σ	0.8	1.3	11.2	0.8	b.d.l.	b.d.l.	0.2	b.d.l.	4.1	0.4	15.9	0.9	1.0
ORTB. 12		C5	1.0	1.4	26.8	9.9	b.d.l.	b.d.l.	b.d.l.	b.d.l.	6.0	0.8	48.5	2.3	3.3	

Rep	Type	Square	MgO	Al ₂ O ₃	SiO ₂	SO ₃	Na ₂ O	K ₂ O	P ₂ O ₅	TiO ₂	CaO	MnO	FeO	CuO	ZnO	
	Flat	L5	0.8	1.0	24.7	11.4	b.d.l.	b.d.l.	b.d.l.	b.d.l.	4.7	1.0	48.9	4.2	3.4	
		S5	1.0	1.5	22.7	6.1	b.d.l.	b.d.l.	b.d.l.	b.d.l.	2.2	0.7	59.2	3.7	2.9	
		Mean	1.0	1.3	24.7	9.1	b.d.l.	b.d.l.	b.d.l.	b.d.l.	4.3	0.8	52.2	3.4	3.2	
		σ	0.1	0.3	2.1	2.7	b.d.l.	b.d.l.	b.d.l.	b.d.l.	1.9	0.2	6.1	1.0	0.3	
ORTB. 13		H6	1.6	2.5	32.6	b.d.l.	b.d.l.	b.d.l.	b.d.l.	b.d.l.	6.6	1.4	51.3	2.6	1.5	
		M2	1.3	6.7	23.4	b.d.l.	b.d.l.	0.4	b.d.l.	b.d.l.	26.6	0.6	37.6	2.4	1.0	
		C4	0.9	2.8	20.6	b.d.l.	b.d.l.	b.d.l.	b.d.l.	b.d.l.	2.3	1.2	67.0	4.1	1.2	
		Mean	1.3	4.0	25.5	b.d.l.	b.d.l.	0.4	b.d.l.	b.d.l.	11.9	1.1	52.0	3.0	1.2	
		σ	0.4	2.4	6.3	b.d.l.	b.d.l.	b.d.l.	b.d.l.	b.d.l.	13.0	0.5	14.7	1.0	0.3	
		ORTB. 16	E3	0.9	3.9	27.0	1.7	b.d.l.	0.2	b.d.l.	b.d.l.	4.3	1.5	58.8	0.8	0.9
			D10	0.9	3.6	29.2	1.6	b.d.l.	0.4	b.d.l.	b.d.l.	5.3	1.5	54.3	1.8	1.3
			D17	0.9	3.9	29.2	2.2	b.d.l.	0.7	b.d.l.	b.d.l.	5.8	1.3	53.8	0.9	1.5
Mean			0.9	3.8	28.4	1.9	b.d.l.	0.4	b.d.l.	b.d.l.	5.1	1.4	55.6	1.2	1.3	
		σ	0.0	0.2	1.3	0.3	b.d.l.	0.2	b.d.l.	b.d.l.	0.8	0.2	2.7	0.6	0.3	
		ORTB. 19	D7	0.6	1.6	21.6	3.3	b.d.l.	b.d.l.	b.d.l.	b.d.l.	5.2	0.9	62.5	1.3	3.0
			L12	0.6	1.1	22.3	4.9	b.d.l.	b.d.l.	b.d.l.	b.d.l.	4.5	0.8	60.9	2.4	2.6
			R14	0.7	1.2	21.7	5.2	b.d.l.	b.d.l.	b.d.l.	b.d.l.	4.2	0.9	61.4	2.3	2.5
Mean			0.6	1.3	21.9	4.4	b.d.l.	b.d.l.	b.d.l.	b.d.l.	4.6	0.9	61.6	2.0	2.7	
σ			0.1	0.3	0.4	1.0	b.d.l.	b.d.l.	b.d.l.	b.d.l.	0.6	0.0	0.8	0.6	0.3	

Table B. 2 displays the SEM-EDX chemical compositional analyses of both coarse and flat specimens, which have been graphically represented in the Cu-Fe-S ternary diagram (see Fig. 5. 18). The data are reported in weight percentage ($w_t\%$) rather than oxides ($ox\%$), before being normalized to 100% for representation on the ternary diagram. 'b.d.l.' has been used to indicate values that are below the detection limit of the instrument. This notation reflects instances where the concentration of the element was too low to be accurately quantified.

Rep	Type	Na	Mg	Al	Si	S	P	Cl	K	Ca	Ti	Mn	Fe	Cu	Zn	O	S	Fe	Cu
ORT B. 3	Ore	b.d.l.	b.d.l.	b.d.l.	b.d.l.	28.0	b.d.l.	b.d.l.	b.d.l.	b.d.l.	b.d.l.	b.d.l.	23.3	b.d.l.	b.d.l.	48.6	54.6	45.4	0.0
		b.d.l.	b.d.l.	b.d.l.	1.3	0.4	b.d.l.	b.d.l.	b.d.l.	0.7	b.d.l.	b.d.l.	71.4	2.9	b.d.l.	23.4	0.5	95.6	3.9
		b.d.l.	b.d.l.	1.0	12.2	b.d.l.	b.d.l.	b.d.l.	b.d.l.	0.6	b.d.l.	b.d.l.	49.5	6.0	b.d.l.	30.7	0.0	89.3	10.7
		b.d.l.	b.d.l.	b.d.l.	b.d.l.	20.3	b.d.l.	b.d.l.	b.d.l.	b.d.l.	b.d.l.	b.d.l.	19.4	19.4	b.d.l.	40.9	34.4	32.8	32.8
		b.d.l.	b.d.l.	b.d.l.	b.d.l.	26.7	b.d.l.	b.d.l.	b.d.l.	b.d.l.	b.d.l.	b.d.l.	25.6	0.3	b.d.l.	47.4	50.7	48.6	0.7
		b.d.l.	b.d.l.	b.d.l.	b.d.l.	27.8	b.d.l.	b.d.l.	b.d.l.	b.d.l.	b.d.l.	b.d.l.	23.7	b.d.l.	b.d.l.	48.5	54.0	46.0	0.0
		b.d.l.	b.d.l.	b.d.l.	b.d.l.	20.6	b.d.l.	b.d.l.	b.d.l.	b.d.l.	b.d.l.	b.d.l.	18.7	19.5	b.d.l.	41.1	35.0	31.8	33.2
		b.d.l.	b.d.l.	b.d.l.	3.6	0.6	b.d.l.	b.d.l.	b.d.l.	0.8	b.d.l.	b.d.l.	56.6	13.6	b.d.l.	24.9	0.8	79.9	19.3
		b.d.l.	b.d.l.	b.d.l.	2.2	0.7	b.d.l.	b.d.l.	b.d.l.	0.4	b.d.l.	b.d.l.	49.7	23.1	b.d.l.	23.9	1.0	67.6	31.4
ORT B. 5	Coarse	b.d.l.	b.d.l.	b.d.l.	b.d.l.	20.4	b.d.l.	b.d.l.	b.d.l.	b.d.l.	b.d.l.	b.d.l.	18.8	19.8	b.d.l.	41.0	34.6	31.9	33.5
		1.3	0.7	4.6	21.7	0.3	b.d.l.	b.d.l.	1.2	0.5	0.3	0.9	27.6	1.5	b.d.l.	39.4	1.1	94.0	5.0
		b.d.l.	b.d.l.	b.d.l.	b.d.l.	b.d.l.	b.d.l.	b.d.l.	b.d.l.	b.d.l.	b.d.l.	b.d.l.	0.5	79.4	b.d.l.	20.1	0.0	0.6	99.4
		b.d.l.	b.d.l.	4.1	12.8	b.d.l.	b.d.l.	0.4	2.1	1.3	b.d.l.	0.5	16.7	29.1	b.d.l.	32.3	0.0	36.5	63.6
		b.d.l.	b.d.l.	b.d.l.	b.d.l.	0.3	b.d.l.	b.d.l.	b.d.l.	b.d.l.	b.d.l.	b.d.l.	0.6	78.7	b.d.l.	20.4	0.3	0.8	98.9
		b.d.l.	b.d.l.	0.9	3.2	b.d.l.	b.d.l.	b.d.l.	0.2	b.d.l.	b.d.l.	b.d.l.	3.9	69.0	b.d.l.	22.9	0.0	5.3	94.7
		b.d.l.	b.d.l.	0.5	2.1	2.0	b.d.l.	b.d.l.	b.d.l.	b.d.l.	b.d.l.	b.d.l.	6.2	65.2	b.d.l.	24.0	2.7	8.5	88.9
		b.d.l.	b.d.l.	b.d.l.	b.d.l.	0.3	b.d.l.	b.d.l.	b.d.l.	b.d.l.	b.d.l.	b.d.l.	0.9	78.5	b.d.l.	20.4	0.3	1.1	98.6
		b.d.l.	b.d.l.	b.d.l.	b.d.l.	b.d.l.	b.d.l.	b.d.l.	b.d.l.	b.d.l.	b.d.l.	b.d.l.	1.4	78.5	b.d.l.	20.2	0.0	1.7	98.3
		b.d.l.	b.d.l.	b.d.l.	b.d.l.	b.d.l.	b.d.l.	b.d.l.	b.d.l.	b.d.l.	b.d.l.	b.d.l.	2.5	77.3	b.d.l.	20.2	0.0	3.1	96.9
		b.d.l.	b.d.l.	0.2	0.3	b.d.l.	b.d.l.	b.d.l.	b.d.l.	b.d.l.	b.d.l.	b.d.l.	2.3	76.7	b.d.l.	20.5	0.0	3.0	97.1
		b.d.l.	b.d.l.	0.4	0.8	b.d.l.	b.d.l.	b.d.l.	b.d.l.	b.d.l.	b.d.l.	b.d.l.	3.3	74.7	b.d.l.	20.9	0.0	4.2	95.8
		b.d.l.	b.d.l.	b.d.l.	b.d.l.	b.d.l.	b.d.l.	b.d.l.	b.d.l.	b.d.l.	b.d.l.	b.d.l.	0.4	79.5	b.d.l.	20.1	0.0	0.5	99.5
		b.d.l.	b.d.l.	b.d.l.	b.d.l.	b.d.l.	b.d.l.	b.d.l.	b.d.l.	b.d.l.	b.d.l.	b.d.l.	2.6	77.2	b.d.l.	20.2	0.0	3.3	96.7
		b.d.l.	b.d.l.	b.d.l.	b.d.l.	b.d.l.	b.d.l.	b.d.l.	b.d.l.	b.d.l.	b.d.l.	b.d.l.	0.5	79.3	b.d.l.	20.1	0.0	0.7	99.3
		b.d.l.	b.d.l.	b.d.l.	b.d.l.	11.5	b.d.l.	b.d.l.	b.d.l.	b.d.l.	b.d.l.	b.d.l.	1.6	55.3	b.d.l.	31.6	16.8	2.3	80.8
		0.7	1.0	3.5	21.9	b.d.l.	b.d.l.	b.d.l.	1.0	1.0	b.d.l.	1.6	29.4	0.7	0.5	38.7	0.0	97.8	2.2
		b.d.l.	b.d.l.	0.4	1.3	b.d.l.	b.d.l.	b.d.l.	b.d.l.	b.d.l.	b.d.l.	b.d.l.	3.3	73.7	b.d.l.	21.3	0.0	4.3	95.7
		b.d.l.	b.d.l.	b.d.l.	b.d.l.	b.d.l.	b.d.l.	b.d.l.	b.d.l.	b.d.l.	b.d.l.	b.d.l.	3.1	76.7	b.d.l.	20.2	0.0	3.9	96.1
		b.d.l.	b.d.l.	b.d.l.	b.d.l.	b.d.l.	b.d.l.	b.d.l.	b.d.l.	b.d.l.	b.d.l.	b.d.l.	2.8	77.0	b.d.l.	20.2	0.0	3.5	96.5
		b.d.l.	0.7	2.6	14.5	0.6	b.d.l.	b.d.l.	0.8	0.7	b.d.l.	1.7	39.1	5.6	b.d.l.	33.7	1.3	86.3	12.4
		b.d.l.	b.d.l.	b.d.l.	b.d.l.	b.d.l.	b.d.l.	b.d.l.	b.d.l.	b.d.l.	b.d.l.	b.d.l.	0.7	79.2	b.d.l.	20.1	0.0	0.8	99.2

Rep	Type	Na	Mg	Al	Si	S	P	Cl	K	Ca	Ti	Mn	Fe	Cu	Zn	O	S	Fe	Cu
		1.0	0.8	4.6	20.2	b.d.l.	b.d.l.	b.d.l.	1.2	0.6	0.3	1.0	30.6	1.6	b.d.l.	38.1	0.0	95.1	4.9
		b.d.l.	b.d.l.	b.d.l.	b.d.l.	0.2	b.d.l.	b.d.l.	b.d.l.	b.d.l.	b.d.l.	b.d.l.	0.8	78.7	b.d.l.	20.3	0.2	1.1	98.7
		b.d.l.	b.d.l.	b.d.l.	b.d.l.	b.d.l.	b.d.l.	b.d.l.	b.d.l.	b.d.l.	b.d.l.	b.d.l.	0.5	79.4	b.d.l.	20.1	0.0	0.6	99.4
		0.9	0.8	5.6	21.1	b.d.l.	b.d.l.	b.d.l.	1.2	0.7	0.5	1.0	28.0	0.7	0.4	39.2	0.0	97.7	2.3
		b.d.l.	0.5	2.7	9.1	0.4	b.d.l.	b.d.l.	0.7	0.4	b.d.l.	0.5	10.8	46.1	b.d.l.	28.8	0.7	18.8	80.5
		b.d.l.	b.d.l.	b.d.l.	b.d.l.	b.d.l.	b.d.l.	b.d.l.	b.d.l.	b.d.l.	b.d.l.	b.d.l.	1.3	78.6	b.d.l.	20.2	0.0	1.6	98.4
		b.d.l.	b.d.l.	b.d.l.	b.d.l.	0.2	b.d.l.	b.d.l.	b.d.l.	b.d.l.	b.d.l.	b.d.l.	0.6	78.9	b.d.l.	20.3	0.2	0.7	99.1
		b.d.l.	b.d.l.	b.d.l.	b.d.l.	b.d.l.	b.d.l.	b.d.l.	b.d.l.	b.d.l.	b.d.l.	b.d.l.	0.7	79.2	b.d.l.	20.1	0.0	0.9	99.1
ORT B. 9	Coarse	b.d.l.	b.d.l.	b.d.l.	b.d.l.	18.6	b.d.l.	b.d.l.	b.d.l.	b.d.l.	b.d.l.	b.d.l.	11.4	31.1	b.d.l.	38.9	30.4	18.6	51.0
		b.d.l.	b.d.l.	b.d.l.	b.d.l.	19.5	b.d.l.	b.d.l.	b.d.l.	b.d.l.	b.d.l.	b.d.l.	13.9	26.7	b.d.l.	39.9	32.5	23.1	44.5
		b.d.l.	b.d.l.	b.d.l.	b.d.l.	16.2	b.d.l.	b.d.l.	b.d.l.	b.d.l.	b.d.l.	b.d.l.	5.7	41.7	b.d.l.	36.4	25.5	9.0	65.5
		b.d.l.	b.d.l.	b.d.l.	b.d.l.	13.7	b.d.l.	b.d.l.	b.d.l.	b.d.l.	b.d.l.	b.d.l.	14.4	37.8	b.d.l.	34.2	20.8	21.8	57.4
		b.d.l.	b.d.l.	b.d.l.	b.d.l.	19.6	b.d.l.	b.d.l.	b.d.l.	b.d.l.	b.d.l.	b.d.l.	13.4	20.1	7.0	40.0	37.0	25.3	37.8
		b.d.l.	b.d.l.	0.9	4.3	b.d.l.	b.d.l.	b.d.l.	b.d.l.	0.5	b.d.l.	b.d.l.	25.1	44.8	b.d.l.	24.4	0.0	35.9	64.1
		b.d.l.	b.d.l.	b.d.l.	3.5	b.d.l.	b.d.l.	b.d.l.	b.d.l.	0.5	b.d.l.	b.d.l.	17.3	55.4	b.d.l.	23.2	0.0	23.8	76.2
		b.d.l.	b.d.l.	b.d.l.	4.4	b.d.l.	b.d.l.	b.d.l.	b.d.l.	0.6	b.d.l.	b.d.l.	27.0	44.1	b.d.l.	24.0	0.0	38.0	62.0
		b.d.l.	b.d.l.	b.d.l.	b.d.l.	21.6	b.d.l.	b.d.l.	b.d.l.	b.d.l.	b.d.l.	b.d.l.	32.9	3.0	b.d.l.	42.5	37.6	57.2	5.2
		b.d.l.	b.d.l.	b.d.l.	1.3	13.0	b.d.l.	b.d.l.	b.d.l.	b.d.l.	b.d.l.	b.d.l.	13.5	37.9	b.d.l.	34.3	20.2	21.0	58.8
		b.d.l.	b.d.l.	b.d.l.	4.0	7.1	b.d.l.	b.d.l.	b.d.l.	0.3	b.d.l.	b.d.l.	27.2	30.6	b.d.l.	30.8	10.9	41.9	47.2
		b.d.l.	b.d.l.	0.4	5.0	1.5	b.d.l.	b.d.l.	b.d.l.	0.4	b.d.l.	b.d.l.	49.8	16.1	b.d.l.	26.8	2.2	73.9	23.9
		b.d.l.	b.d.l.	b.d.l.	0.2	22.3	b.d.l.	b.d.l.	b.d.l.	b.d.l.	b.d.l.	b.d.l.	33.5	0.7	b.d.l.	43.4	39.5	59.3	1.2
		b.d.l.	b.d.l.	b.d.l.	b.d.l.	20.4	b.d.l.	b.d.l.	b.d.l.	b.d.l.	b.d.l.	b.d.l.	12.5	26.4	b.d.l.	40.8	34.5	21.0	44.5
		b.d.l.	b.d.l.	b.d.l.	0.2	18.7	b.d.l.	b.d.l.	b.d.l.	b.d.l.	b.d.l.	b.d.l.	9.3	32.7	b.d.l.	39.1	30.8	15.4	53.9
ORT B. 20	Coarse	b.d.l.	b.d.l.	b.d.l.	b.d.l.	18.8	b.d.l.	b.d.l.	b.d.l.	b.d.l.	b.d.l.	b.d.l.	10.1	31.2	0.9	39.0	10.3	58.2	31.6
		b.d.l.	b.d.l.	b.d.l.	b.d.l.	18.1	b.d.l.	b.d.l.	b.d.l.	b.d.l.	b.d.l.	b.d.l.	6.1	37.5	b.d.l.	38.3	31.2	16.9	51.9
		b.d.l.	b.d.l.	b.d.l.	b.d.l.	18.0	b.d.l.	b.d.l.	b.d.l.	b.d.l.	b.d.l.	b.d.l.	11.2	32.5	b.d.l.	38.3	29.3	9.9	60.8
		b.d.l.	b.d.l.	b.d.l.	b.d.l.	17.2	b.d.l.	b.d.l.	b.d.l.	b.d.l.	b.d.l.	b.d.l.	6.0	39.4	b.d.l.	37.4	29.2	18.1	52.7
		b.d.l.	b.d.l.	1.6	6.8	b.d.l.	b.d.l.	b.d.l.	b.d.l.	0.6	b.d.l.	b.d.l.	60.4	1.5	1.5	27.5	27.5	9.6	62.9
		b.d.l.	b.d.l.	b.d.l.	2.2	7.3	b.d.l.	b.d.l.	b.d.l.	0.3	b.d.l.	b.d.l.	27.8	32.6	b.d.l.	29.8	0.0	97.5	2.5
		b.d.l.	b.d.l.	b.d.l.	2.5	7.0	b.d.l.	b.d.l.	b.d.l.	0.2	b.d.l.	b.d.l.	31.9	28.7	b.d.l.	29.7	10.8	41.0	48.2
		b.d.l.	b.d.l.	b.d.l.	b.d.l.	18.4	b.d.l.	b.d.l.	b.d.l.	b.d.l.	b.d.l.	b.d.l.	12.6	30.2	b.d.l.	38.8	10.4	47.2	42.4
		b.d.l.	b.d.l.	b.d.l.	0.3	16.2	b.d.l.	b.d.l.	b.d.l.	0.2	b.d.l.	b.d.l.	5.3	35.2	6.4	36.6	30.1	20.5	49.4
		b.d.l.	b.d.l.	b.d.l.	b.d.l.	18.0	b.d.l.	b.d.l.	b.d.l.	b.d.l.	b.d.l.	b.d.l.	10.3	33.4	b.d.l.	38.3	28.6	9.3	62.1
		b.d.l.	b.d.l.	b.d.l.	b.d.l.	17.2	b.d.l.	b.d.l.	b.d.l.	b.d.l.	b.d.l.	b.d.l.	9.1	36.2	b.d.l.	37.5	29.1	16.8	54.2
		b.d.l.	b.d.l.	b.d.l.	b.d.l.	18.7	b.d.l.	b.d.l.	b.d.l.	b.d.l.	b.d.l.	b.d.l.	4.1	38.4	b.d.l.	38.8	27.6	14.5	58.0
		b.d.l.	b.d.l.	b.d.l.	b.d.l.	19.7	b.d.l.	b.d.l.	b.d.l.	b.d.l.	b.d.l.	b.d.l.	6.0	34.5	b.d.l.	39.9	30.5	6.7	62.8
		b.d.l.	b.d.l.	b.d.l.	b.d.l.	19.5	b.d.l.	b.d.l.	b.d.l.	b.d.l.	b.d.l.	b.d.l.	3.5	37.4	b.d.l.	39.6	32.7	9.9	57.3
																	32.3	5.8	61.9

Rep	Type	Na	Mg	Al	Si	S	P	Cl	K	Ca	Ti	Mn	Fe	Cu	Zn	O	S	Fe	Cu
		b.d.l.	b.d.l.	0.2	1.9	16.7	b.d.l.	b.d.l.	b.d.l.	0.2	b.d.l.	b.d.l.	7.5	35.2	b.d.l.	38.4	28.2	12.6	59.3
		b.d.l.	b.d.l.	b.d.l.	b.d.l.	16.7	b.d.l.	b.d.l.	b.d.l.	b.d.l.	b.d.l.	b.d.l.	6.6	39.8	b.d.l.	36.9	26.5	10.4	63.0
		b.d.l.	b.d.l.	b.d.l.	b.d.l.	18.6	b.d.l.	b.d.l.	b.d.l.	b.d.l.	b.d.l.	b.d.l.	9.6	32.9	b.d.l.	38.9	30.4	15.7	53.9
		b.d.l.	b.d.l.	b.d.l.	b.d.l.	19.7	b.d.l.	b.d.l.	b.d.l.	b.d.l.	b.d.l.	b.d.l.	1.9	38.8	b.d.l.	39.7	32.6	3.1	64.3
		b.d.l.	b.d.l.	2.3	11.0	b.d.l.	b.d.l.	b.d.l.	b.d.l.	0.7	b.d.l.	b.d.l.	45.9	8.8	1.0	30.4	0.0	84.0	16.0
		b.d.l.	b.d.l.	0.3	0.8	15.7	b.d.l.	b.d.l.	b.d.l.	b.d.l.	b.d.l.	b.d.l.	5.8	40.9	b.d.l.	36.6	25.1	9.3	65.6
		b.d.l.	b.d.l.	b.d.l.	b.d.l.	14.2	b.d.l.	b.d.l.	b.d.l.	b.d.l.	b.d.l.	b.d.l.	3.6	48.0	b.d.l.	34.3	21.6	5.4	73.0
		b.d.l.	b.d.l.	b.d.l.	b.d.l.	14.2	b.d.l.	b.d.l.	b.d.l.	b.d.l.	b.d.l.	b.d.l.	1.6	49.9	b.d.l.	34.3	21.6	2.5	75.9
		b.d.l.	b.d.l.	b.d.l.	b.d.l.	14.7	b.d.l.	b.d.l.	b.d.l.	b.d.l.	b.d.l.	b.d.l.	2.3	48.3	b.d.l.	34.8	22.5	3.5	74.0
		b.d.l.	b.d.l.	1.8	7.3	0.5	b.d.l.	b.d.l.	b.d.l.	0.6	b.d.l.	b.d.l.	48.8	12.1	0.8	28.1	0.8	79.5	19.7
		b.d.l.	b.d.l.	b.d.l.	b.d.l.	17.9	b.d.l.	b.d.l.	b.d.l.	b.d.l.	b.d.l.	b.d.l.	11.3	32.7	b.d.l.	38.2	28.9	18.2	52.8
		b.d.l.	b.d.l.	b.d.l.	b.d.l.	18.9	b.d.l.	b.d.l.	b.d.l.	b.d.l.	b.d.l.	b.d.l.	13.4	28.6	b.d.l.	39.2	31.0	22.0	47.0
		b.d.l.	b.d.l.	b.d.l.	0.6	13.7	b.d.l.	b.d.l.	0.2	0.2	b.d.l.	b.d.l.	5.9	45.1	b.d.l.	34.4	21.2	9.1	69.7
		b.d.l.	b.d.l.	b.d.l.	b.d.l.	15.4	b.d.l.	b.d.l.	b.d.l.	b.d.l.	b.d.l.	b.d.l.	0.2	49.0	b.d.l.	35.4	23.8	0.4	75.8
		b.d.l.	b.d.l.	b.d.l.	b.d.l.	17.3	b.d.l.	b.d.l.	b.d.l.	b.d.l.	b.d.l.	b.d.l.	8.6	36.5	b.d.l.	37.6	27.8	13.7	58.5
ORT B. 8	Flat	b.d.l.	b.d.l.	b.d.l.	b.d.l.	14.7	b.d.l.	b.d.l.	b.d.l.	b.d.l.	b.d.l.	b.d.l.	3.1	47.5	b.d.l.	34.8	22.5	4.7	72.8
		b.d.l.	b.d.l.	b.d.l.	b.d.l.	19.1	b.d.l.	b.d.l.	b.d.l.	b.d.l.	b.d.l.	b.d.l.	3.7	38.0	b.d.l.	39.2	31.5	6.1	62.5
		b.d.l.	b.d.l.	0.9	4.3	0.5	b.d.l.	b.d.l.	b.d.l.	0.3	b.d.l.	b.d.l.	30.4	37.6	1.1	25.0	0.8	44.4	54.9
		b.d.l.	b.d.l.	b.d.l.	b.d.l.	b.d.l.	b.d.l.	b.d.l.	b.d.l.	b.d.l.	b.d.l.	b.d.l.	1.0	78.9	b.d.l.	20.1	0.0	1.2	98.8
		b.d.l.	b.d.l.	b.d.l.	0.5	b.d.l.	b.d.l.	b.d.l.	b.d.l.	b.d.l.	b.d.l.	b.d.l.	2.6	76.4	b.d.l.	20.5	0.0	3.3	96.7
		b.d.l.	b.d.l.	b.d.l.	b.d.l.	14.4	b.d.l.	b.d.l.	b.d.l.	b.d.l.	b.d.l.	b.d.l.	2.9	48.2	b.d.l.	34.5	22.0	4.4	73.6
		b.d.l.	b.d.l.	b.d.l.	b.d.l.	15.8	b.d.l.	b.d.l.	b.d.l.	b.d.l.	b.d.l.	b.d.l.	0.7	47.7	b.d.l.	35.8	24.5	1.1	74.3
		b.d.l.	b.d.l.	b.d.l.	0.3	15.6	b.d.l.	b.d.l.	b.d.l.	b.d.l.	b.d.l.	b.d.l.	1.1	47.1	b.d.l.	35.9	24.4	1.8	73.8
		b.d.l.	b.d.l.	1.2	0.8	13.9	b.d.l.	b.d.l.	b.d.l.	0.2	b.d.l.	b.d.l.	13.1	34.4	0.9	35.5	22.6	21.4	56.0
		b.d.l.	b.d.l.	b.d.l.	b.d.l.	14.2	b.d.l.	b.d.l.	b.d.l.	b.d.l.	b.d.l.	b.d.l.	0.8	50.7	b.d.l.	34.2	21.6	1.3	77.2
		b.d.l.	b.d.l.	0.5	2.5	12.4	b.d.l.	b.d.l.	b.d.l.	0.2	b.d.l.	b.d.l.	8.1	41.6	b.d.l.	34.7	19.9	13.0	67.1
		b.d.l.	b.d.l.	b.d.l.	b.d.l.	13.3	b.d.l.	b.d.l.	b.d.l.	b.d.l.	b.d.l.	b.d.l.	1.8	51.4	b.d.l.	33.4	20.0	2.7	77.3
		b.d.l.	b.d.l.	b.d.l.	b.d.l.	b.d.l.	b.d.l.	b.d.l.	b.d.l.	b.d.l.	b.d.l.	b.d.l.	1.8	78.1	b.d.l.	20.2	0.0	2.2	97.8
		b.d.l.	b.d.l.	b.d.l.	6.0	17.7	b.d.l.	b.d.l.	b.d.l.	1.1	b.d.l.	b.d.l.	22.6	15.4	0.8	36.5	31.8	40.6	27.6
		b.d.l.	b.d.l.	b.d.l.	0.3	18.6	b.d.l.	b.d.l.	b.d.l.	b.d.l.	b.d.l.	b.d.l.	1.6	40.8	b.d.l.	38.8	30.5	2.5	66.9
ORT B. 16	Flat	b.d.l.	b.d.l.	b.d.l.	b.d.l.	16.9	b.d.l.	b.d.l.	b.d.l.	b.d.l.	b.d.l.	b.d.l.	8.3	37.7	b.d.l.	37.1	26.9	13.2	59.9
		b.d.l.	b.d.l.	0.8	b.d.l.	b.d.l.	b.d.l.	b.d.l.	b.d.l.	b.d.l.	b.d.l.	b.d.l.	2.2	76.4	b.d.l.	20.6	0.0	2.8	97.2
		b.d.l.	b.d.l.	b.d.l.	b.d.l.	16.1	b.d.l.	b.d.l.	b.d.l.	b.d.l.	b.d.l.	b.d.l.	8.6	39.0	b.d.l.	36.4	25.3	13.5	61.2
		b.d.l.	b.d.l.	4.9	7.7	b.d.l.	b.d.l.	b.d.l.	b.d.l.	0.3	b.d.l.	b.d.l.	52.0	4.7	0.9	29.5	0.0	91.7	8.3
		b.d.l.	b.d.l.	b.d.l.	0.2	17.8	b.d.l.	b.d.l.	b.d.l.	b.d.l.	b.d.l.	b.d.l.	1.0	43.0	b.d.l.	38.0	28.8	1.6	69.7
		b.d.l.	b.d.l.	b.d.l.	b.d.l.	18.9	b.d.l.	b.d.l.	b.d.l.	b.d.l.	b.d.l.	b.d.l.	5.5	36.5	b.d.l.	39.1	31.1	9.0	60.0
		b.d.l.	b.d.l.	b.d.l.	b.d.l.	17.0	b.d.l.	b.d.l.	b.d.l.	b.d.l.	b.d.l.	b.d.l.	8.5	37.3	b.d.l.	37.2	27.0	13.6	59.4
		b.d.l.	b.d.l.	0.7	13.2	b.d.l.	b.d.l.	b.d.l.	0.2	0.4	b.d.l.	b.d.l.	52.0	0.5	1.7	31.3	0.0	99.0	1.0

Rep	Type	Na	Mg	Al	Si	S	P	Cl	K	Ca	Ti	Mn	Fe	Cu	Zn	O	S	Fe	Cu
ORT B. 19	Flat	b.d.l.	b.d.l.	0.8	15.5	b.d.l.	b.d.l.	b.d.l.	0.3	0.3	b.d.l.	b.d.l.	47.2	1.2	2.0	32.8	0.0	97.4	2.6
		b.d.l.	b.d.l.	b.d.l.	b.d.l.	17.3	b.d.l.	b.d.l.	b.d.l.	b.d.l.	b.d.l.	b.d.l.	10.3	34.8	b.d.l.	37.6	27.7	16.5	55.8
		b.d.l.	b.d.l.	b.d.l.	b.d.l.	16.9	b.d.l.	b.d.l.	b.d.l.	b.d.l.	b.d.l.	b.d.l.	10.9	35.0	b.d.l.	37.2	26.9	17.4	55.7
		b.d.l.	b.d.l.	b.d.l.	7.7	b.d.l.	b.d.l.	b.d.l.	b.d.l.	0.3	b.d.l.	b.d.l.	63.3	b.d.l.	1.4	27.4	0.0	100.0	0.0
		b.d.l.	b.d.l.	b.d.l.	b.d.l.	16.8	b.d.l.	b.d.l.	b.d.l.	b.d.l.	b.d.l.	b.d.l.	6.1	40.2	b.d.l.	37.0	26.6	9.7	63.7
		b.d.l.	b.d.l.	b.d.l.	b.d.l.	16.9	b.d.l.	b.d.l.	b.d.l.	b.d.l.	b.d.l.	b.d.l.	8.0	38.1	b.d.l.	37.1	26.8	12.6	60.6
		b.d.l.	b.d.l.	b.d.l.	b.d.l.	16.6	b.d.l.	b.d.l.	b.d.l.	b.d.l.	b.d.l.	b.d.l.	7.2	39.4	b.d.l.	36.8	26.2	11.4	62.4
		b.d.l.	b.d.l.	b.d.l.	b.d.l.	14.9	b.d.l.	b.d.l.	b.d.l.	b.d.l.	b.d.l.	b.d.l.	4.6	45.5	b.d.l.	35.1	23.0	7.0	70.0
		b.d.l.	b.d.l.	b.d.l.	b.d.l.	18.5	b.d.l.	b.d.l.	b.d.l.	b.d.l.	b.d.l.	b.d.l.	6.6	7.6	28.8	38.5	56.5	20.3	23.2
		b.d.l.	b.d.l.	0.8	27.4	b.d.l.	b.d.l.	b.d.l.	0.3	1.4	b.d.l.	b.d.l.	26.9	b.d.l.	2.6	40.8	0.0	100.0	0.0
		b.d.l.	b.d.l.	b.d.l.	b.d.l.	14.2	b.d.l.	b.d.l.	b.d.l.	b.d.l.	b.d.l.	b.d.l.	2.1	49.4	b.d.l.	34.3	21.6	3.2	75.2
		b.d.l.	b.d.l.	2.2	24.0	b.d.l.	b.d.l.	b.d.l.	0.6	1.5	b.d.l.	b.d.l.	29.0	1.0	2.7	39.2	0.0	96.6	3.4
		b.d.l.	b.d.l.	b.d.l.	b.d.l.	17.2	b.d.l.	b.d.l.	b.d.l.	b.d.l.	b.d.l.	b.d.l.	11.3	34.0	b.d.l.	37.5	27.5	18.2	54.4
		b.d.l.	b.d.l.	b.d.l.	b.d.l.	18.3	b.d.l.	b.d.l.	b.d.l.	b.d.l.	b.d.l.	b.d.l.	12.0	31.1	b.d.l.	38.6	29.7	19.6	50.7
		b.d.l.	b.d.l.	b.d.l.	b.d.l.	17.5	b.d.l.	b.d.l.	b.d.l.	b.d.l.	b.d.l.	b.d.l.	10.4	34.3	b.d.l.	37.8	28.1	16.7	55.1
		b.d.l.	b.d.l.	1.4	7.8	0.6	b.d.l.	b.d.l.	b.d.l.	0.3	b.d.l.	b.d.l.	52.9	7.2	1.5	28.4	1.0	87.2	11.8
		b.d.l.	b.d.l.	b.d.l.	b.d.l.	17.2	b.d.l.	b.d.l.	b.d.l.	b.d.l.	b.d.l.	b.d.l.	8.8	36.6	b.d.l.	37.4	27.4	14.1	58.5
		b.d.l.	b.d.l.	1.8	24.4	b.d.l.	b.d.l.	b.d.l.	b.d.l.	0.9	b.d.l.	b.d.l.	29.6	1.0	2.7	39.2	0.0	96.9	3.1
		b.d.l.	b.d.l.	b.d.l.	19.8	b.d.l.	b.d.l.	b.d.l.	b.d.l.	b.d.l.	b.d.l.	b.d.l.	12.6	27.6	b.d.l.	40.1	0.0	31.3	68.7
		b.d.l.	b.d.l.	b.d.l.	b.d.l.	16.6	b.d.l.	b.d.l.	b.d.l.	b.d.l.	b.d.l.	b.d.l.	5.7	40.9	b.d.l.	36.8	26.3	9.1	64.7
		b.d.l.	b.d.l.	1.4	14.5	b.d.l.	b.d.l.	b.d.l.	b.d.l.	0.7	b.d.l.	b.d.l.	48.0	0.8	2.0	32.6	0.0	98.3	1.7
		b.d.l.	b.d.l.	b.d.l.	b.d.l.	17.0	b.d.l.	b.d.l.	b.d.l.	b.d.l.	b.d.l.	b.d.l.	10.3	35.5	b.d.l.	37.3	27.0	16.4	56.6
		b.d.l.	b.d.l.	b.d.l.	b.d.l.	15.6	b.d.l.	b.d.l.	b.d.l.	b.d.l.	b.d.l.	b.d.l.	6.4	42.2	b.d.l.	35.8	24.4	9.9	65.7
		b.d.l.	b.d.l.	b.d.l.	b.d.l.	14.4	b.d.l.	b.d.l.	b.d.l.	b.d.l.	b.d.l.	b.d.l.	6.2	44.7	b.d.l.	34.6	22.0	9.5	68.4
		b.d.l.	b.d.l.	b.d.l.	b.d.l.	17.8	b.d.l.	b.d.l.	b.d.l.	b.d.l.	b.d.l.	b.d.l.	12.0	32.0	b.d.l.	38.2	28.8	19.4	51.8
		b.d.l.	b.d.l.	0.5	10.0	b.d.l.	b.d.l.	0.3	b.d.l.	b.d.l.	b.d.l.	b.d.l.	58.6	b.d.l.	1.7	29.0	0.0	100.0	0.0
		b.d.l.	b.d.l.	b.d.l.	b.d.l.	13.9	b.d.l.	b.d.l.	b.d.l.	b.d.l.	b.d.l.	b.d.l.	2.2	49.9	b.d.l.	34.0	21.1	3.3	75.6
		b.d.l.	b.d.l.	0.4	12.2	b.d.l.	b.d.l.	b.d.l.	b.d.l.	0.2	b.d.l.	b.d.l.	53.9	1.1	b.d.l.	30.5	0.0	97.9	2.1
		b.d.l.	b.d.l.	b.d.l.	b.d.l.	16.0	b.d.l.	b.d.l.	b.d.l.	b.d.l.	b.d.l.	b.d.l.	5.0	42.9	b.d.l.	36.2	25.1	7.8	67.2
		b.d.l.	b.d.l.	b.d.l.	b.d.l.	17.4	b.d.l.	b.d.l.	b.d.l.	b.d.l.	b.d.l.	b.d.l.	11.1	33.8	b.d.l.	37.7	27.9	17.8	54.3
		b.d.l.	b.d.l.	0.6	7.9	b.d.l.	b.d.l.	b.d.l.	b.d.l.	b.d.l.	b.d.l.	b.d.l.	59.2	0.8	3.9	27.6	0.0	98.7	1.3
		b.d.l.	b.d.l.	b.d.l.	0.3	b.d.l.	b.d.l.	b.d.l.	b.d.l.	b.d.l.	b.d.l.	0.4	75.1	0.6	1.3	22.4	0.0	99.3	0.7
		b.d.l.	b.d.l.	b.d.l.	b.d.l.	15.0	b.d.l.	b.d.l.	b.d.l.	b.d.l.	b.d.l.	b.d.l.	1.9	48.0	b.d.l.	35.1	23.1	2.9	74.0
		b.d.l.	b.d.l.	b.d.l.	b.d.l.	15.3	b.d.l.	b.d.l.	b.d.l.	b.d.l.	b.d.l.	b.d.l.	4.5	44.8	b.d.l.	35.4	23.7	6.9	69.4
		b.d.l.	0.3	0.7	2.8	11.2	b.d.l.	b.d.l.	b.d.l.	0.2	b.d.l.	b.d.l.	7.0	44.0	b.d.l.	33.9	18.0	11.2	70.7
		b.d.l.	b.d.l.	0.2	1.4	8.5	b.d.l.	b.d.l.	b.d.l.	0.5	b.d.l.	b.d.l.	34.5	23.9	0.4	30.7	12.8	51.5	35.7
		b.d.l.	b.d.l.	1.0	9.6	0.7	b.d.l.	1.5	b.d.l.	0.3	b.d.l.	b.d.l.	44.7	11.3	1.8	29.1	1.3	78.8	19.9
		b.d.l.	b.d.l.	b.d.l.	b.d.l.	17.2	b.d.l.	b.d.l.	b.d.l.	b.d.l.	b.d.l.	b.d.l.	12.9	32.3	b.d.l.	37.6	27.6	20.7	51.8

Rep	Type	Na	Mg	Al	Si	S	P	Cl	K	Ca	Ti	Mn	Fe	Cu	Zn	O	S	Fe	Cu
ORT B. 12	Flat	b.d.l.	b.d.l.	b.d.l.	0.4	18.6	b.d.l.	b.d.l.	b.d.l.	b.d.l.	b.d.l.	b.d.l.	21.0	15.1	5.5	39.5	34.1	38.4	27.6
		b.d.l.	b.d.l.	b.d.l.	b.d.l.	18.5	b.d.l.	b.d.l.	b.d.l.	b.d.l.	b.d.l.	b.d.l.	15.8	26.7	b.d.l.	39.0	30.4	25.9	43.7
		b.d.l.	b.d.l.	b.d.l.	b.d.l.	17.4	b.d.l.	b.d.l.	b.d.l.	b.d.l.	b.d.l.	b.d.l.	13.8	31.0	b.d.l.	37.8	28.0	22.2	49.9
		b.d.l.	b.d.l.	b.d.l.	b.d.l.	13.6	b.d.l.	b.d.l.	b.d.l.	b.d.l.	b.d.l.	b.d.l.	3.2	49.5	b.d.l.	33.7	20.5	4.9	74.7
		b.d.l.	b.d.l.	b.d.l.	b.d.l.	18.0	b.d.l.	b.d.l.	b.d.l.	b.d.l.	b.d.l.	b.d.l.	12.5	31.2	b.d.l.	38.3	29.1	20.3	50.6
		b.d.l.	b.d.l.	b.d.l.	3.4	0.7	b.d.l.	b.d.l.	b.d.l.	b.d.l.	b.d.l.	b.d.l.	63.2	4.5	3.3	25.0	1.1	92.4	6.5
		b.d.l.	b.d.l.	b.d.l.	0.7	16.7	b.d.l.	b.d.l.	b.d.l.	b.d.l.	b.d.l.	b.d.l.	21.7	20.9	2.3	37.8	28.1	36.6	35.3
		b.d.l.	b.d.l.	b.d.l.	b.d.l.	17.4	b.d.l.	b.d.l.	b.d.l.	b.d.l.	b.d.l.	b.d.l.	13.6	31.3	b.d.l.	37.8	27.9	21.8	50.3
		b.d.l.	b.d.l.	b.d.l.	b.d.l.	17.5	b.d.l.	b.d.l.	b.d.l.	b.d.l.	b.d.l.	b.d.l.	10.3	33.1	1.3	37.8	28.7	17.0	54.4
		b.d.l.	b.d.l.	b.d.l.	b.d.l.	15.6	b.d.l.	b.d.l.	b.d.l.	b.d.l.	b.d.l.	b.d.l.	4.8	43.8	b.d.l.	35.8	24.3	7.5	68.1
		b.d.l.	b.d.l.	b.d.l.	b.d.l.	15.5	b.d.l.	b.d.l.	b.d.l.	b.d.l.	b.d.l.	b.d.l.	5.3	43.4	b.d.l.	35.7	24.2	8.3	67.6
		b.d.l.	b.d.l.	b.d.l.	b.d.l.	18.0	b.d.l.	b.d.l.	b.d.l.	b.d.l.	b.d.l.	b.d.l.	13.1	30.6	b.d.l.	38.4	29.2	21.2	49.6
		b.d.l.	b.d.l.	b.d.l.	6.9	b.d.l.	b.d.l.	0.6	b.d.l.	b.d.l.	b.d.l.	b.d.l.	64.4	b.d.l.	1.4	26.7	0.0	100.0	0.0
		b.d.l.	b.d.l.	b.d.l.	b.d.l.	18.0	b.d.l.	b.d.l.	b.d.l.	b.d.l.	b.d.l.	b.d.l.	12.6	31.1	b.d.l.	38.3	29.1	20.4	50.5
		b.d.l.	b.d.l.	0.5	11.2	b.d.l.	b.d.l.	b.d.l.	b.d.l.	0.3	b.d.l.	b.d.l.	54.7	0.8	2.7	29.8	0.0	98.5	1.5
		b.d.l.	b.d.l.	b.d.l.	0.2	19.3	b.d.l.	b.d.l.	b.d.l.	b.d.l.	b.d.l.	b.d.l.	18.2	22.5	b.d.l.	39.9	32.1	30.3	37.6
		b.d.l.	b.d.l.	0.2	0.4	15.1	b.d.l.	b.d.l.	b.d.l.	b.d.l.	b.d.l.	b.d.l.	38.0	5.1	4.8	36.5	25.9	65.4	8.7
		b.d.l.	b.d.l.	b.d.l.	0.7	17.7	b.d.l.	b.d.l.	b.d.l.	b.d.l.	b.d.l.	b.d.l.	17.1	21.9	4.0	38.6	31.2	30.1	38.7
		b.d.l.	b.d.l.	0.4	1.3	16.6	b.d.l.	b.d.l.	b.d.l.	0.2	b.d.l.	b.d.l.	29.8	7.7	5.5	38.5	30.7	55.1	14.2
		b.d.l.	b.d.l.	b.d.l.	0.4	17.1	b.d.l.	b.d.l.	b.d.l.	b.d.l.	b.d.l.	b.d.l.	19.4	24.3	0.9	37.9	28.1	31.9	40.0
		b.d.l.	b.d.l.	b.d.l.	0.2	15.0	b.d.l.	b.d.l.	b.d.l.	b.d.l.	b.d.l.	b.d.l.	5.3	41.4	2.7	35.3	24.4	8.6	67.0
		b.d.l.	b.d.l.	b.d.l.	b.d.l.	14.0	b.d.l.	b.d.l.	b.d.l.	b.d.l.	b.d.l.	b.d.l.	3.5	48.5	b.d.l.	34.1	21.2	5.3	73.6
		b.d.l.	b.d.l.	b.d.l.	1.6	14.4	b.d.l.	b.d.l.	b.d.l.	0.6	b.d.l.	b.d.l.	24.6	22.6	b.d.l.	36.3	23.4	39.9	36.7

Table B. 3 displays the SEM-EDX chemical compositional analyses of the experimental slags. Three random scans, each covering an area of approximately 1 mm², were conducted for each slag. These analyses are graphically depicted in the FeO–Al₂O₃–SiO₂ (wt%) and FeO–CaO–SiO₂ (wt%) ternary systems (see Fig. 8. 15). It's important to note that for the sake of simplifying the analysis, all elements have been designated as oxides, although it is recognized that certain oxides, such as SO₃, P₂O₅, may not be present in the samples. For a more detailed discussion, please refer to Section 4.2.9. 'b.d.l.' has been used to indicate values that are below the detection limit of the instrument. This notation reflects instances where the concentration of the element was too low to be accurately quantified.

Rep	Trial	Phase	Sq.	Na ₂ O	MgO	Al ₂ O ₃	SiO ₂	SO ₃	K ₂ O	P ₂ O ₅	TiO ₂	CaO	MnO	FeO	CoO	NiO	CuO	ZnO	As	Sb	Pb
JH 2AT3_001	T3	2A	SQ 1	0.4	1.7	16.5	68.7	0.6	2.6	0.2	0.9	2.4	0.0	5.3	b.d.l.	b.d.l.	0.3	0.3	0.0	0.0	b.d.l.
			SQ 2	0.6	1.7	13.9	62.0	0.5	2.8	0.2	0.8	6.6	0.3	8.8	b.d.l.	b.d.l.	0.5	1.2	b.d.l.	b.d.l.	0.2
			SQ 3	0.8	1.5	11.5	59.0	0.2	3.7	0.2	0.7	9.3	0.3	11.5	b.d.l.	b.d.l.	0.4	0.7	b.d.l.	0.2	b.d.l.
			Mean	b.d.l.	1.7	14.0	63.2	0.4	3.0	0.2	0.8	6.1	0.2	8.5	b.d.l.	b.d.l.	0.4	0.7	0.0	0.1	0.2
JH2BT3_001	T3	2B	SQ1	0.5	2.0	3.9	31.8	2.0	1.2	0.4	0.2	25.5	1.3	28.5	0.1	b.d.l.	0.6	1.4	0.0	0.6	0.0
			SQ2	0.5	2.0	4.0	32.3	2.2	1.3	0.6	0.1	25.1	1.3	27.8	0.2	0.1	0.6	1.3	b.d.l.	0.4	0.1
			SQ3	0.3	2.8	3.4	32.4	2.9	0.9	0.5	0.2	27.9	1.2	25.1	0.1	0.1	0.6	1.2	b.d.l.	0.4	0.1
			Mean	b.d.l.	2.3	3.7	32.2	2.4	1.1	0.5	0.2	26.2	1.3	27.1	0.1	0.1	0.6	1.3	0.0	0.5	0.1
JH1BT1_001	T1	1B	SQ1	0.2	0.1	0.2	66.2	3.3	0.1	0.1	0.1	6.2	1.3	21.1	0.2	0.0	0.1	0.5	b.d.l.	0.1	b.d.l.
			SQ2	0.2	0.1	0.3	42.7	5.9	0.1	b.d.l.	0.1	8.7	2.2	38.1	0.3	0.0	0.1	0.8	b.d.l.	0.1	0.2
			SQ3	0.2	0.3	0.3	38.2	5.4	0.1	0.0	0.0	12.3	2.6	39.2	0.3	b.d.l.	0.1	0.6	b.d.l.	0.3	0.0
			Mean	b.d.l.	0.2	0.3	49.0	4.9	0.1	0.0	0.1	9.1	2.0	32.8	0.3	0.0	0.1	0.6	b.d.l.	0.1	0.1
JH2BT1_002	T1	2B	SQ1	0.4	0.5	3.4	24.2	5.5	0.6	0.1	0.1	2.1	0.2	60.5	0.3	0.1	0.9	0.9	b.d.l.	0.1	0.1
			SQ2	0.2	0.1	0.3	35.1	6.0	0.2	b.d.l.	b.d.l.	1.6	0.2	53.4	0.2	b.d.l.	1.4	1.2	b.d.l.	0.0	b.d.l.
			SQ3	0.6	1.8	6.5	34.4	3.5	1.0	0.4	0.3	7.3	0.6	42.2	0.1	b.d.l.	0.5	0.8	b.d.l.	0.1	0.0
			Mean	b.d.l.	0.8	3.4	31.2	5.0	0.6	0.3	0.2	3.7	0.3	52.0	0.2	0.1	0.9	1.0	b.d.l.	0.1	0.1
JH20_PE_Exp.3_F.2_slag(big)		PE	SQ1	0.3	1.9	9.3	60.2	0.1	3.3	0.5	0.6	19.1	0.1	3.8	0.0	0.0	b.d.l.	0.0	b.d.l.	0.8	0.1
			SQ2	0.3	1.2	10.3	78.9	0.2	1.8	0.2	0.9	1.8	0.1	3.9	b.d.l.	b.d.l.	0.1	0.2	b.d.l.	0.0	0.2
			SQ3	0.2	2.1	13.0	59.4	0.0	2.6	0.6	0.9	13.3	0.1	6.3	0.1	b.d.l.	b.d.l.	0.2	b.d.l.	1.1	0.1
			Mean	b.d.l.	1.7	10.9	66.2	0.1	2.6	0.4	0.8	11.4	0.1	4.6	0.1	0.0	0.1	0.1	b.d.l.	0.6	0.1
JH1A_T3_003	T3	1A	SQ1	0.3	1.0	2.2	56.7	1.7	0.2	1.0	0.1	25.2	0.9	7.4	b.d.l.	b.d.l.	0.5	0.5	b.d.l.	2.1	0.2
			SQ2	0.7	0.9	1.9	72.5	2.1	0.3	0.7	0.0	11.9	0.9	6.3	0.0	b.d.l.	0.1	0.7	b.d.l.	0.8	0.2
			SQ3	0.1	0.6	1.1	66.1	0.3	0.5	0.5	0.0	14.6	0.9	11.4	0.1	b.d.l.	0.3	1.9	b.d.l.	1.3	0.3
			Mean	b.d.l.	0.8	1.8	65.1	1.4	0.3	0.7	0.1	17.2	0.9	8.3	0.1	b.d.l.	0.3	1.0	b.d.l.	1.4	0.2
JH2B_T2_001	T2	2B	SQ1	0.4	1.3	1.4	17.7	1.6	2.6	0.6	0.1	22.7	1.7	39.1	0.2	0.1	6.9	2.3	0.1	1.5	0.0

Rep	Trial	Phase	Sq.	Na ₂ O	MgO	Al ₂ O ₃	SiO ₂	SO ₃	K ₂ O	P ₂ O ₅	TiO ₂	CaO	MnO	FeO	CoO	NiO	CuO	ZnO	As	Sb	Pb
			SQ2	0.4	1.9	2.9	25.5	4.3	5.1	0.7	0.2	23.0	1.3	23.9	0.3	0.1	6.9	1.7	b.d.l.	1.8	0.0
			SQ3	0.3	1.5	2.2	20.6	1.5	3.0	0.5	0.1	24.5	1.5	32.7	0.2	0.1	6.9	2.5	b.d.l.	1.7	b.d.l.
			Mean	b.d.l.	1.6	2.2	21.3	2.4	3.6	0.6	0.1	23.4	1.5	31.9	0.2	0.1	6.9	2.2	0.1	1.7	0.0
JH2B_T1_001	T1	2B	SQ1	0.3	1.0	9.0	34.7	15.1	2.5	0.5	0.3	6.7	0.6	20.4	0.2	0.2	6.8	1.3	b.d.l.	0.3	0.2
			SQ2	0.3	1.0	9.6	38.7	11.4	2.9	0.4	0.5	3.4	0.8	21.5	0.0	0.1	7.1	1.3	b.d.l.	0.4	0.6
			SQ3	0.0	1.0	7.3	25.6	19.2	1.6	0.5	0.3	7.6	0.5	24.0	0.1	0.1	10.0	1.1	b.d.l.	0.5	0.7
			Mean	b.d.l.	1.0	8.6	33.0	15.2	2.3	0.5	0.4	5.9	0.6	22.0	0.1	0.1	8.0	1.3	b.d.l.	0.4	0.5
JH21_PE_Exp.3-Furnace 2_Slag (top of the crucible)		PE	SQ1	0.2	8.0	3.3	40.8	0.5	0.8	0.5	0.1	31.1	1.0	10.2	0.1	0.0	0.2	0.1	0.5	2.5	0.1
			SQ2	0.2	12.6	2.7	48.1	0.1	0.2	0.2	0.2	28.1	0.5	4.2	b.d.l.	b.d.l.	0.4	0.2	0.7	1.5	0.2
			SQ3	0.2	10.3	2.8	42.1	0.3	0.2	0.4	0.3	33.9	0.4	6.4	0.0	0.0	0.0	0.1	0.5	2.3	0.0
			Mean	b.d.l.	10.3	2.9	43.7	0.3	0.4	0.3	0.2	31.0	0.6	7.0	0.0	0.0	0.2	0.1	0.6	2.1	0.1
JH2A_T1_002	T1	2A	SQ1	0.3	1.7	3.2	46.0	0.2	1.3	0.7	0.3	22.9	1.1	17.7	0.3	0.0	0.4	1.6	0.1	1.8	0.2
			SQ2	0.4	1.7	3.4	40.5	0.8	1.1	0.4	0.2	24.3	1.1	21.0	0.1	0.0	0.2	2.8	0.0	1.9	0.1
			SQ3	0.3	1.8	1.8	34.4	1.8	0.7	0.4	0.1	28.3	1.2	22.8	b.d.l.	0.2	1.0	2.9	0.0	2.2	0.2
			Mean	b.d.l.	1.7	2.8	40.3	0.9	1.0	0.5	0.2	25.2	1.1	20.5	0.2	0.1	0.5	2.4	0.0	2.0	0.2
JH1A_T2_002	T2	1A	SQ 1	0.4	1.5	1.3	40.6	2.5	0.5	0.5	0.1	20.5	2.6	25.8	0.1	0.1	0.5	1.5	0.1	1.6	0.0
			SQ 2	0.2	1.3	1.1	39.9	5.4	0.3	0.7	0.0	17.1	2.6	27.2	0.2	0.0	2.3	0.8	0.0	0.9	0.0
			SQ 3	0.0	0.2	1.2	91.6	2.4	0.1	0.1	b.d.l.	0.7	0.0	1.8	0.0	0.0	0.3	0.0	0.0	0.2	0.4
			Mean	b.d.l.	1.0	1.2	57.3	3.4	0.3	0.4	0.0	12.8	1.7	18.3	0.1	0.1	1.0	0.8	0.0	0.9	0.2
JH1A_T2_003	T2	1A	SQ 1	0.4	1.2	1.3	37.0	2.8	0.6	0.4	0.0	22.0	2.4	26.0	0.3	0.1	0.7	2.8	0.0	1.9	0.3
			SQ 2	b.d.l.	0.3	0.4	1.4	28.4	9.6	0.2	b.d.l.	1.7	0.6	19.0	0.1	0.5	35.7	1.7	0.0	0.0	0.5
			SQ 3	b.d.l.	0.3	0.2	1.5	21.0	13.0	0.2	0.1	0.9	0.4	15.5	0.1	0.2	45.1	1.1	0.0	0.0	0.2
			Mean	b.d.l.	0.6	0.6	13.3	17.4	7.7	0.3	0.1	8.2	1.1	20.2	0.2	0.3	27.1	1.9	0.0	0.6	0.3
JH1A_T3_001	T3	1A	SQ 1	0.4	1.5	4.6	38.0	0.5	1.0	0.5	0.1	26.1	1.2	19.6	0.2	0.2	0.0	3.0	0.0	2.7	0.4
			SQ 2	0.6	1.8	10.1	47.5	0.5	1.5	0.2	0.6	24.6	0.9	9.3	0.0	0.2	0.1	0.7	0.0	1.5	0.0
			SQ 3	0.5	1.5	13.0	53.8	0.4	1.8	0.5	0.4	19.2	0.3	5.4	0.0	0.0	0.7	0.4	0.0	1.9	0.1
			Mean	b.d.l.	1.6	9.2	46.4	0.5	1.4	0.4	0.4	23.3	0.8	11.4	0.1	0.1	0.3	1.4	0.0	2.0	0.2
JH1A_T3_002	T3	1A	SQ 1	0.4	1.1	1.1	59.3	1.1	0.6	1.2	0.1	17.3	1.1	12.8	b.d.l.	b.d.l.	0.3	2.0	b.d.l.	1.4	0.3
			SQ 2	0.2	0.5	0.8	74.1	1.2	0.2	1.0	0.1	12.3	0.5	6.5	b.d.l.	b.d.l.	0.5	0.6	b.d.l.	0.9	0.5
			SQ 3	0.4	1.4	1.1	61.8	1.6	0.5	0.8	0.1	17.1	0.7	11.5	0.1	b.d.l.	0.5	1.3	b.d.l.	1.2	0.0
			Mean	b.d.l.	1.0	1.0	65.1	1.3	0.4	1.0	0.1	15.5	0.8	10.3	0.1	b.d.l.	0.4	1.3	b.d.l.	1.2	0.3
JH1B_T2_002	T2	1B	SQ 1	0.8	1.5	2.0	39.8	2.7	0.8	0.6	0.0	20.0	3.2	23.3	0.1	0.0	0.8	2.6	0.2	1.6	0.2
			SQ 2	0.9	1.6	1.7	42.2	2.0	1.0	0.5	0.1	17.0	2.6	25.1	0.0	0.0	0.5	3.5	b.d.l.	1.1	0.3

Rep	Trial	Phase	Sq.	Na ₂ O	MgO	Al ₂ O ₃	SiO ₂	SO ₃	K ₂ O	P ₂ O ₅	TiO ₂	CaO	MnO	FeO	CoO	NiO	CuO	ZnO	As	Sb	Pb
			SQ 3	0.9	1.3	1.8	35.4	4.9	1.1	0.3	0.2	19.8	3.0	25.5	0.3	b.d.l.	1.2	2.3	b.d.l.	1.5	0.6
			Mean	b.d.l.	1.5	1.8	39.2	3.2	1.0	0.5	0.1	18.9	3.0	24.6	0.2	0.0	0.8	2.8	0.2	1.4	0.3

Table B. 4 displays the SEM-EDX chemical compositional analyses of the experimental specimens, encompassing both slags and matte fragments. These analyses are graphically depicted in the Cu-Fe-S ternary diagram (see Fig. 8. 19). The data are reported in oxides (ox%) and were subsequently transformed to weight percentage (wt%) before being normalized to 100% for representation on the ternary diagram. 'b.d.l.' has been used to indicate values that are below the detection limit of the instrument. This notation reflects instances where the concentration of the element was too low to be accurately quantified.

Sample	Type	Na ₂ O	MgO	Al ₂ O ₃	SiO ₂	P ₂ O ₅	SO ₃	K ₂ O	CaO	TiO ₂	MnO	FeO	CoO	NiO	CuO	ZnO	AsO	SbO	PbO
1yA_PE	Matte	b.d.l.	0.2	0.0	0.1	0.3	36.2	0.0	0.2	0.1	0.1	16.0	0.1	0.1	43.0	0.5	0.1	b.d.l.	2.5
JH1A_T1_001	Matte	b.d.l.	0.3	0.2	0.1	0.4	36.4	1.4	1.6	0.1	0.4	30.1	0.2	0.4	27.0	0.0	0.1	0.0	1.3
JH1A_T1-T2-T3_009	Reactor	b.d.l.	0.3	0.1	0.3	0.2	15.1	0.5	2.0	0.0	0.3	12.3	0.0	0.1	67.6	1.0	b.d.l.	b.d.l.	0.1
		b.d.l.	0.1	0.1	0.2	0.3	33.5	0.3	0.9	b.d.l.	0.4	19.7	0.1	0.2	42.7	0.6	0.0	0.1	0.7
		b.d.l.	0.3	0.2	0.4	0.0	2.2	0.6	0.2	b.d.l.	0.2	3.9	b.d.l.	0.1	91.0	0.7	0.1	b.d.l.	0.2
		b.d.l.	0.2	0.2	0.4	b.d.l.	0.1	0.2	0.1	b.d.l.	0.0	2.6	b.d.l.	b.d.l.	96.1	0.1	b.d.l.	0.0	0.1
JH1A_T2_002	Slag	b.d.l.	0.7	0.3	0.8	0.5	41.6	0.1	3.1	b.d.l.	0.4	27.0	0.0	b.d.l.	23.6	1.1	b.d.l.	0.3	0.3
		b.d.l.	0.2	0.1	0.1	0.4	38.2	b.d.l.	0.2	0.0	0.6	24.9	0.1	0.2	33.8	0.3	b.d.l.	0.0	1.0
		b.d.l.	0.7	0.2	0.4	0.3	41.3	0.1	2.8	0.2	0.3	24.2	0.3	b.d.l.	27.4	1.0	b.d.l.	0.0	0.8
		b.d.l.	1.4	0.7	3.3	2.7	33.6	0.4	8.5	b.d.l.	0.4	27.7	b.d.l.	0.0	18.9	1.3	0.2	0.4	0.6
		b.d.l.	0.2	0.1	0.2	0.5	43.9	b.d.l.	0.1	0.0	0.4	37.4	0.2	b.d.l.	16.0	0.4	b.d.l.	0.1	0.7
		b.d.l.	1.0	4.1	8.1	0.6	36.4	0.1	8.1	0.1	0.2	20.9	0.1	0.0	18.0	1.3	b.d.l.	0.5	0.8
		b.d.l.	1.0	0.5	1.7	0.5	42.4	0.1	4.1	b.d.l.	0.3	22.8	0.3	0.1	23.6	1.4	0.0	0.3	0.9
JH1A_T2_003	Matte	b.d.l.	0.2	0.2	0.6	0.4	45.5	1.2	3.3	0.0	0.8	25.0	0.2	0.5	17.1	4.2	0.2	0.2	0.5
JH1A_T2_004	Matte	b.d.l.	0.2	0.1	0.1	0.4	39.5	0.0	0.7	b.d.l.	0.8	19.0	0.1	0.0	34.5	3.8	b.d.l.	b.d.l.	0.9
		b.d.l.	0.1	0.1	0.1	0.5	44.6	0.1	0.3	b.d.l.	0.4	39.8	0.2	b.d.l.	13.0	0.1	b.d.l.	b.d.l.	0.7
		b.d.l.	b.d.l.	0.1	0.0	0.5	47.5	0.0	0.1	b.d.l.	0.4	45.2	0.3	b.d.l.	5.0	0.1	0.0	0.0	0.7
		b.d.l.	0.1	0.1	0.1	0.4	38.7	0.1	0.1	0.0	0.2	14.5	0.0	b.d.l.	44.6	0.1	0.1	b.d.l.	0.7
JH1A_T3_001	Slag	b.d.l.	0.4	0.1	0.4	b.d.l.	0.9	b.d.l.	0.3	b.d.l.	0.1	4.6	0.2	0.2	91.9	0.4	0.6	b.d.l.	b.d.l.
		b.d.l.	0.1	0.0	0.6	0.5	40.1	0.1	22.8	b.d.l.	0.0	13.3	0.5	b.d.l.	18.2	1.4	0.0	1.5	b.d.l.
		b.d.l.	0.5	0.3	3.7	3.5	4.4	0.0	11.3	b.d.l.	0.0	4.6	b.d.l.	0.1	70.4	0.3	b.d.l.	0.6	b.d.l.
		b.d.l.	0.2	0.3	0.5	b.d.l.	0.2	b.d.l.	0.1	b.d.l.	b.d.l.	3.6	b.d.l.	0.2	94.2	0.3	0.1	b.d.l.	b.d.l.
		b.d.l.	0.5	0.7	0.8	0.5	40.1	0.2	2.2	b.d.l.	0.6	25.7	0.2	0.1	23.2	3.6	0.1	0.2	1.2
		b.d.l.	b.d.l.	b.d.l.	0.2	0.4	41.0	0.7	0.9	b.d.l.	0.7	24.4	0.2	0.1	25.4	4.6	0.1	b.d.l.	1.1
		0.9	0.1	0.1	0.1	0.3	45.3	0.0	b.d.l.	0.0	1.0	31.3	b.d.l.	0.0	8.3	10.1	0.1	b.d.l.	2.0
		b.d.l.	0.2	0.0	0.1	0.4	41.8	0.0	b.d.l.	b.d.l.	0.6	24.1	0.1	0.2	30.0	0.5	b.d.l.	b.d.l.	1.0
JH1A_T3_002	Slag	b.d.l.	0.2	0.3	0.3	0.4	41.6	0.4	2.0	b.d.l.	0.5	22.7	0.0	0.1	28.6	1.7	b.d.l.	0.0	1.3
		b.d.l.	0.2	0.0	0.4	0.5	43.6	0.2	0.2	b.d.l.	0.5	19.4	0.1	0.1	31.6	1.6	b.d.l.	0.0	1.7
		b.d.l.	0.1	0.0	1.6	0.4	44.8	0.2	0.3	0.0	0.6	21.2	b.d.l.	0.0	26.3	3.1	0.2	0.0	1.0
		b.d.l.	0.1	0.1	0.1	0.3	43.1	0.6	2.3	0.1	0.7	24.8	0.2	0.1	24.1	1.8	0.2	b.d.l.	1.1
JH1A_T3_003	Slag	b.d.l.	0.3	0.0	0.4	0.3	50.1	b.d.l.	0.1	0.0	0.4	23.0	0.1	b.d.l.	20.2	2.9	0.0	0.3	1.7
		b.d.l.	0.2	0.3	0.4	0.4	49.2	b.d.l.	0.1	b.d.l.	0.3	22.2	0.1	b.d.l.	22.1	3.3	0.2	b.d.l.	0.9
		b.d.l.	0.1	0.1	0.2	0.3	44.3	0.0	0.0	b.d.l.	0.3	25.2	0.2	b.d.l.	22.5	5.3	0.1	b.d.l.	0.8
		b.d.l.	0.0	0.1	0.3	0.4	43.3	0.1	0.1	b.d.l.	0.5	25.1	0.2	0.1	28.2	0.5	0.2	b.d.l.	1.0
		b.d.l.	0.1	0.2	0.4	0.6	61.6	0.0	0.0	0.0	0.2	20.8	0.3	0.1	12.7	1.0	0.3	0.1	1.5
		b.d.l.	0.0	b.d.l.	0.4	0.4	44.0	b.d.l.	b.d.l.	b.d.l.	0.4	28.8	0.3	0.0	23.7	0.9	0.2	b.d.l.	0.7
		b.d.l.	b.d.l.	b.d.l.	0.3	0.4	42.5	0.1	0.0	0.1	0.5	22.9	b.d.l.	b.d.l.	27.4	4.7	0.0	0.1	1.0
		b.d.l.	b.d.l.	0.1	0.3	0.5	43.1	0.0	0.1	b.d.l.	0.5	23.8	0.2	b.d.l.	28.6	1.7	b.d.l.	0.1	0.9
		b.d.l.	0.1	0.2	0.6	0.4	44.9	b.d.l.	0.1	0.0	0.8	25.2	0.2	0.1	17.5	9.4	b.d.l.	b.d.l.	0.5

S	Fe	Cu
23.7	20.3	56.1
24.5	39.3	36.2
8.7	13.8	77.6
21.4	24.3	54.3
1.1	3.9	95.0
0.1	2.6	97.4
29.5	37.2	33.3
24.8	31.4	43.7
28.9	32.9	38.2
26.9	43.0	30.2
29.6	48.9	21.5
32.3	35.9	31.8
31.7	33.1	35.2
35.5	37.9	26.6
27.2	25.4	47.4
30.2	52.3	17.6
32.8	60.4	6.8
24.9	18.0	57.1
0.5	4.6	95.0
39.2	25.2	35.6
2.9	5.8	91.3
0.1	3.6	96.3
29.4	36.6	34.0
29.5	34.0	36.5
37.0	49.6	13.5
28.2	31.6	40.3
29.2	30.9	39.9
30.2	26.0	43.7
32.4	29.7	37.9
30.9	34.6	34.5
37.1	33.1	29.8
36.1	31.6	32.3
32.1	35.4	32.5
29.2	32.9	37.9
48.4	31.8	19.8
29.9	38.0	32.2
30.0	31.4	38.6
29.4	31.5	39.0
34.9	38.0	27.1

Sample	Type	Na ₂ O	MgO	Al ₂ O ₃	SiO ₂	P ₂ O ₅	SO ₃	K ₂ O	CaO	TiO ₂	MnO	FeO	CoO	NiO	CuO	ZnO	AsO	SbO	PbO
		b.d.l.	0.1	0.1	0.3	0.4	42.5	0.1	0.1	b.d.l.	0.3	25.6	0.2	b.d.l.	25.8	2.8	b.d.l.	0.0	1.7
		b.d.l.	0.2	0.2	0.2	0.5	44.5	b.d.l.	b.d.l.	0.1	0.3	23.3	0.2	0.1	23.2	5.9	0.1	b.d.l.	0.9
		b.d.l.	0.1	0.2	0.2	0.4	46.0	b.d.l.	0.0	b.d.l.	0.5	25.4	0.3	0.1	21.4	3.3	0.0	b.d.l.	1.5
		b.d.l.	0.1	0.3	0.2	0.4	48.0	0.1	0.1	b.d.l.	0.1	23.8	0.0	b.d.l.	25.9	0.2	b.d.l.	0.1	0.3
		b.d.l.	0.1	0.0	0.3	0.4	41.7	0.1	0.0	b.d.l.	0.3	25.7	0.2	0.1	26.7	2.7	b.d.l.	b.d.l.	1.4
JH1A_T3_004	Matte	b.d.l.	0.1	0.1	0.6	0.4	39.6	0.4	0.2	0.1	0.4	25.0	0.1	0.0	29.5	2.2	0.0	b.d.l.	1.2
		b.d.l.	0.3	b.d.l.	1.1	0.2	38.5	0.2	1.1	0.1	0.3	18.9	0.2	b.d.l.	38.4	0.1	b.d.l.	0.1	0.6
JH1B_T1_001	Slag	b.d.l.	0.3	0.2	0.2	0.4	37.4	0.3	1.9	0.2	0.7	19.4	0.1	b.d.l.	37.0	1.3	b.d.l.	b.d.l.	0.8
		b.d.l.	b.d.l.	b.d.l.	0.2	0.1	44.4	0.0	0.0	0.0	0.1	36.8	0.1	0.3	17.4	0.2	0.0	b.d.l.	0.3
		b.d.l.	b.d.l.	0.1	0.4	0.0	42.1	0.0	0.1	b.d.l.	0.1	53.8	0.1	0.2	2.6	0.2	b.d.l.	b.d.l.	0.3
		0.1	0.1	0.5	1.2	0.0	32.5	0.1	0.5	0.1	0.1	63.1	0.1	0.0	0.7	0.4	b.d.l.	b.d.l.	0.5
		b.d.l.	b.d.l.	b.d.l.	0.1	0.0	50.8	0.0	0.0	0.0	0.1	45.6	0.2	0.6	2.1	b.d.l.	b.d.l.	b.d.l.	0.3
		b.d.l.	0.0	0.1	0.1	b.d.l.	36.5	0.0	b.d.l.	b.d.l.	0.1	20.3	0.2	b.d.l.	42.1	0.1	0.1	b.d.l.	0.4
		b.d.l.	0.1	0.0	0.3	0.0	36.8	0.0	0.1	b.d.l.	0.2	19.2	0.1	0.1	42.2	0.2	b.d.l.	0.1	0.5
		0.1	b.d.l.	0.1	0.2	0.1	50.6	0.0	b.d.l.	b.d.l.	0.2	44.9	0.2	0.6	2.6	0.1	0.1	b.d.l.	0.2
		b.d.l.	0.0	0.0	0.2	0.0	39.3	0.0	0.1	0.0	0.0	15.2	0.0	b.d.l.	44.7	0.1	b.d.l.	0.1	0.3
		b.d.l.	0.0	0.0	0.2	b.d.l.	36.3	0.0	0.0	0.1	0.1	16.1	0.0	0.1	46.7	b.d.l.	b.d.l.	0.1	0.2
		0.1	0.0	0.0	0.3	0.1	36.5	b.d.l.	0.1	b.d.l.	0.0	60.3	0.2	0.1	1.2	0.3	0.1	b.d.l.	0.7
		0.2	0.1	0.0	0.6	0.0	43.4	b.d.l.	0.1	0.1	0.1	52.3	0.2	0.0	0.8	1.8	b.d.l.	b.d.l.	0.3
JH1B_T1_002	Matte	b.d.l.	b.d.l.	0.1	0.2	0.0	50.9	b.d.l.	0.3	b.d.l.	0.3	46.4	0.2	0.2	0.7	0.1	0.0	b.d.l.	0.7
		b.d.l.	b.d.l.	0.0	0.2	0.1	50.9	0.0	0.4	b.d.l.	0.5	46.1	0.2	0.2	0.9	0.0	0.1	0.0	0.4
		0.2	3.0	0.1	0.3	0.0	0.2	b.d.l.	1.5	b.d.l.	5.8	87.8	0.2	b.d.l.	0.2	0.4	b.d.l.	b.d.l.	0.1
		0.1	0.0	b.d.l.	0.2	0.1	51.0	b.d.l.	0.1	b.d.l.	0.6	46.4	0.1	0.1	0.7	0.0	b.d.l.	b.d.l.	0.6
		b.d.l.	b.d.l.	0.0	0.2	b.d.l.	51.0	0.0	0.0	0.0	0.6	46.1	0.2	0.3	0.9	0.2	0.1	0.0	0.5
		0.0	0.1	0.1	0.2	0.1	50.9	0.0	0.0	0.0	0.6	46.4	0.2	0.1	0.8	0.0	b.d.l.	b.d.l.	0.5
		b.d.l.	b.d.l.	0.0	0.2	0.1	39.1	0.1	0.2	0.0	0.3	13.3	0.0	0.0	46.2	b.d.l.	0.0	0.0	0.6
		b.d.l.	b.d.l.	0.1	0.2	0.1	35.9	0.0	0.1	b.d.l.	0.9	17.0	0.1	0.1	45.1	0.1	0.1	b.d.l.	0.3
JH1B_T2_001	Matte	0.8	0.1	0.0	0.5	0.3	28.3	2.5	0.8	b.d.l.	0.5	22.8	0.1	0.1	41.5	0.6	0.1	0.2	0.6
JH1B_T2_002	Slag	b.d.l.	0.1	0.1	0.3	0.4	42.3	0.1	0.0	0.1	0.4	43.5	0.2	0.1	11.5	0.1	0.0	b.d.l.	0.9
		0.5	0.1	0.1	0.3	0.3	41.5	0.5	6.4	0.0	0.9	34.5	b.d.l.	b.d.l.	12.7	0.7	b.d.l.	0.3	1.5
JH1B_T3_001	Matte	0.9	0.1	0.2	2.0	b.d.l.	18.9	2.7	1.4	b.d.l.	1.3	48.7	b.d.l.	b.d.l.	19.6	3.4	b.d.l.	b.d.l.	0.8
		0.9	0.2	0.2	3.0	b.d.l.	15.6	4.0	1.5	0.0	1.4	49.9	b.d.l.	b.d.l.	20.1	2.4	0.0	0.1	0.7
		0.7	0.1	0.3	0.5	0.1	41.6	0.4	0.4	0.0	1.2	28.4	b.d.l.	b.d.l.	18.7	6.8	0.0	0.0	0.8
		b.d.l.	0.0	0.4	0.2	0.1	38.9	0.1	0.1	b.d.l.	0.3	15.1	b.d.l.	b.d.l.	44.1	0.2	b.d.l.	0.0	0.4
		2.3	0.1	0.1	3.8	0.0	25.0	4.4	1.1	0.0	1.0	42.0	b.d.l.	b.d.l.	16.8	2.6	0.0	b.d.l.	0.4
		b.d.l.	0.1	0.1	1.0	0.4	44.0	0.1	0.1	b.d.l.	0.9	27.1	0.2	0.1	20.4	4.6	0.0	0.1	0.8
		b.d.l.	0.3	0.2	2.3	0.5	41.6	0.0	1.8	0.0	1.0	25.6	0.1	0.0	23.8	2.1	0.0	0.1	0.6
JH1B_T3_002	Matte	b.d.l.	0.0	0.2	1.2	0.1	43.8	0.0	0.1	b.d.l.	0.4	27.1	b.d.l.	b.d.l.	24.4	2.0	b.d.l.	b.d.l.	0.7
		0.1	0.1	0.3	2.6	0.0	42.8	0.1	0.3	0.0	0.6	27.9	b.d.l.	b.d.l.	23.1	1.8	0.0	0.1	0.4
		0.1	0.0	0.4	1.4	0.1	43.5	0.1	0.2	b.d.l.	0.7	27.8	b.d.l.	b.d.l.	22.9	2.1	b.d.l.	b.d.l.	0.7
		b.d.l.	0.1	0.2	3.0	0.1	42.8	0.0	0.2	0.0	0.2	25.5	b.d.l.	b.d.l.	25.3	2.1	b.d.l.	0.0	0.5
		0.3	0.1	0.1	0.5	0.4	44.2	0.3	0.1	b.d.l.	1.1	31.4	0.1	0.1	11.7	8.8	0.1	0.0	0.9
JH21_PE_Exp.3-Furnace 2_Slag (top of the crucible)	Slag	b.d.l.	0.2	0.1	0.0	0.4	36.5	0.1	b.d.l.	b.d.l.	0.6	12.8	0.1	0.0	48.5	b.d.l.	0.1	b.d.l.	0.8
		b.d.l.	0.1	0.1	0.1	0.4	36.4	0.1	0.1	0.0	0.3	13.9	0.1	b.d.l.	47.5	b.d.l.	0.1	0.0	0.6
		b.d.l.	1.3	1.5	3.0	0.2	27.3	b.d.l.	1.0	b.d.l.	0.7	19.9	0.1	0.8	41.0	0.5	0.1	b.d.l.	2.7
		b.d.l.	0.2	b.d.l.	0.2	0.5	35.9	0.1	b.d.l.	b.d.l.	0.6	16.3	0.0	0.5	43.1	0.1	0.2	0.0	2.2
		b.d.l.	0.1	0.1	0.3	0.3	37.4	b.d.l.	0.3	b.d.l.	0.2	11.9	0.0	b.d.l.	48.3	b.d.l.	0.2	0.1	0.6

S	Fe	Cu
29.6	34.6	35.9
32.7	33.2	34.0
33.4	35.7	30.9
32.9	31.7	35.4
28.8	34.4	36.8
26.9	33.0	40.0
25.4	24.2	50.5
25.1	25.3	49.6
29.5	47.5	23.0
27.8	68.9	3.4
20.8	78.3	0.9
35.4	61.6	3.0
22.8	24.7	52.5
23.3	23.5	53.2
35.4	61.0	3.6
24.9	18.7	56.5
22.6	19.4	58.0
23.4	75.1	1.5
29.7	69.3	1.1
35.7	63.3	1.0
35.8	62.9	1.3
0.1	99.7	0.2
35.8	63.3	0.9
35.9	62.9	1.2
35.7	63.2	1.2
24.9	16.5	58.6
22.6	20.8	56.6
35.1	62.2	2.8
18.2	28.5	53.3
28.3	56.4	15.3
b.d.l.	b.d.l.	b.d.l.
12.4	62.0	25.7
10.3	63.5	26.3
31.0	41.1	27.9
24.9	18.8	56.3
17.9	58.2	23.9
32.1	38.3	29.7
30.0	35.8	34.3
30.2	36.3	33.6
30.0	37.9	32.2
30.4	37.7	31.9
30.0	34.6	35.4
34.4	47.5	18.1
23.1	15.7	61.2
23.0	17.1	59.9
18.5	26.2	55.4
23.4	20.6	56.1
23.8	14.8	61.4

Sample	Type	Na ₂ O	MgO	Al ₂ O ₃	SiO ₂	P ₂ O ₅	SO ₃	K ₂ O	CaO	TiO ₂	MnO	FeO	CoO	NiO	CuO	ZnO	AsO	SbO	PbO
		b.d.l.	0.2	0.1	0.2	0.3	34.9	0.0	0.1	0.0	0.9	21.0	0.2	0.2	41.0	b.d.l.	0.1	b.d.l.	0.8
		b.d.l.	0.1	0.1	0.2	0.3	35.8	0.1	0.1	b.d.l.	0.6	16.4	0.1	0.1	41.9	0.6	0.2	0.1	3.6
		b.d.l.	0.1	0.0	0.2	0.3	41.3	b.d.l.	0.0	b.d.l.	0.4	33.7	0.2	0.1	21.7	0.1	0.1	0.2	1.3
		b.d.l.	0.1	0.1	0.2	0.3	38.4	0.0	0.1	b.d.l.	0.4	22.7	0.1	0.0	35.4	0.2	0.1	0.1	1.8
		b.d.l.	0.2	0.1	1.2	0.4	36.4	0.1	2.7	b.d.l.	0.3	13.9	0.1	b.d.l.	43.8	0.0	0.1	0.0	0.8
		b.d.l.	0.0	0.2	0.2	b.d.l.	1.5	b.d.l.	0.4	b.d.l.	0.0	95.9	0.4	0.1	1.1	0.1	0.0	0.1	0.2
		b.d.l.	0.1	0.1	0.1	0.0	0.1	b.d.l.	0.4	0.1	0.1	95.9	0.4	0.2	2.0	0.0	0.5	0.0	0.2
		b.d.l.	0.1	0.1	0.2	0.1	0.2	0.1	0.5	b.d.l.	0.1	96.6	0.4	0.1	1.4	0.0	0.0	0.0	0.1
		b.d.l.	0.3	0.3	0.3	b.d.l.	b.d.l.	b.d.l.	0.7	0.0	b.d.l.	1.3	b.d.l.	0.1	60.2	35.9	0.2	b.d.l.	0.6
		b.d.l.	0.5	0.7	2.0	0.1	0.3	0.0	1.9	b.d.l.	0.1	91.4	0.3	0.1	2.3	0.1	b.d.l.	0.1	0.1
		b.d.l.	0.0	0.1	0.2	0.1	0.0	0.0	0.8	0.0	0.0	94.2	0.6	0.1	3.7	b.d.l.	0.1	b.d.l.	0.1
		b.d.l.	0.0	0.1	0.3	0.0	0.1	0.0	0.6	b.d.l.	0.0	94.0	0.8	0.0	3.8	b.d.l.	0.2	b.d.l.	b.d.l.
		b.d.l.	0.1	0.1	0.3	0.1	b.d.l.	0.0	0.9	b.d.l.	0.0	95.2	0.5	0.1	2.4	0.0	0.0	0.1	0.2
		b.d.l.	0.1	0.0	0.1	0.3	35.4	0.0	0.2	0.0	0.1	9.8	b.d.l.	b.d.l.	52.9	0.0	0.2	b.d.l.	0.7
		b.d.l.	0.2	0.1	0.3	0.4	33.2	0.1	0.8	b.d.l.	0.1	4.9	0.0	b.d.l.	59.3	0.1	0.1	0.0	0.4
JH2A_T1_001	Matte	b.d.l.	0.0	0.1	0.1	0.0	0.1	0.0	b.d.l.	b.d.l.	0.0	97.1	b.d.l.	b.d.l.	2.3	0.2	0.1	b.d.l.	b.d.l.
		b.d.l.	b.d.l.	b.d.l.	0.1	0.2	51.1	0.1	0.0	b.d.l.	0.3	42.7	b.d.l.	b.d.l.	2.1	0.0	b.d.l.	0.0	0.5
		b.d.l.	b.d.l.	0.1	0.1	0.1	51.6	0.1	0.1	b.d.l.	0.3	43.1	b.d.l.	b.d.l.	2.0	0.0	0.0	b.d.l.	0.3
		b.d.l.	b.d.l.	0.0	0.1	0.0	52.9	0.0	0.0	b.d.l.	0.3	44.7	b.d.l.	b.d.l.	1.4	0.1	b.d.l.	0.0	0.4
		b.d.l.	0.0	0.0	0.1	b.d.l.	40.5	0.1	0.2	0.0	0.3	11.9	b.d.l.	b.d.l.	46.5	0.0	b.d.l.	0.0	0.3
		0.8	b.d.l.	0.1	0.1	b.d.l.	0.4	1.4	0.1	b.d.l.	0.1	2.9	b.d.l.	b.d.l.	93.5	0.3	b.d.l.	0.1	0.4
		b.d.l.	0.0	0.0	0.1	b.d.l.	36.1	0.3	5.2	b.d.l.	0.5	26.4	b.d.l.	b.d.l.	29.6	0.9	0.0	0.1	0.7
		b.d.l.	0.1	0.1	0.1	0.1	41.6	0.5	3.5	b.d.l.	0.5	21.9	b.d.l.	b.d.l.	29.6	1.3	b.d.l.	0.0	0.7
		1.0	0.0	b.d.l.	0.1	0.1	0.1	0.2	0.0	0.0	0.0	0.8	b.d.l.	b.d.l.	97.2	0.2	b.d.l.	b.d.l.	b.d.l.
		b.d.l.	0.1	0.0	0.2	b.d.l.	0.2	0.0	b.d.l.	0.0	b.d.l.	97.0	b.d.l.	b.d.l.	2.3	b.d.l.	0.1	b.d.l.	b.d.l.
		b.d.l.	b.d.l.	0.1	0.1	0.0	0.1	0.0	0.0	b.d.l.	0.0	97.2	b.d.l.	b.d.l.	2.1	0.1	0.2	0.0	b.d.l.
		1.8	0.0	0.1	0.1	b.d.l.	49.9	b.d.l.	0.0	b.d.l.	1.4	27.9	b.d.l.	b.d.l.	1.1	17.0	0.0	0.0	0.5
		1.8	b.d.l.	0.1	0.1	0.1	49.8	b.d.l.	0.0	b.d.l.	1.7	26.9	b.d.l.	b.d.l.	2.4	16.4	0.1	0.1	0.6
		2.0	b.d.l.	0.1	0.1	0.0	50.0	0.0	0.1	0.0	1.5	27.4	b.d.l.	b.d.l.	1.6	16.5	0.1	0.1	0.7
		b.d.l.	0.1	0.1	0.1	0.1	41.3	0.1	0.2	b.d.l.	0.3	12.6	b.d.l.	b.d.l.	44.8	0.1	0.1	0.1	0.4
		b.d.l.	0.0	0.1	0.0	0.0	41.6	0.1	0.2	b.d.l.	0.3	41.1	b.d.l.	1.4	14.8	0.2	b.d.l.	b.d.l.	0.3
		0.9	0.0	0.1	0.2	0.1	0.1	0.2	0.0	b.d.l.	b.d.l.	0.9	b.d.l.	b.d.l.	97.2	0.2	0.0	0.1	0.0
		0.9	0.0	0.1	0.1	b.d.l.	0.3	0.2	0.1	0.0	0.1	1.1	b.d.l.	b.d.l.	96.9	0.2	b.d.l.	0.0	b.d.l.
		0.8	0.0	0.1	b.d.l.	0.0	0.1	0.2	b.d.l.	0.0	b.d.l.	1.0	b.d.l.	b.d.l.	97.5	0.1	0.0	b.d.l.	0.0
		b.d.l.	0.0	0.0	0.1	b.d.l.	40.6	0.1	0.1	0.0	0.3	12.5	b.d.l.	b.d.l.	45.9	0.1	b.d.l.	b.d.l.	0.3
		1.6	b.d.l.	0.0	0.1	0.0	49.6	0.2	0.0	0.0	1.7	27.9	b.d.l.	b.d.l.	2.3	15.9	b.d.l.	0.1	0.5
		0.5	0.1	b.d.l.	0.1	b.d.l.	0.2	0.2	0.1	b.d.l.	0.1	3.1	b.d.l.	b.d.l.	95.3	0.1	0.1	0.1	0.0
		0.7	b.d.l.	0.0	0.1	0.0	0.2	0.3	0.1	0.0	0.1	2.4	b.d.l.	b.d.l.	94.2	0.2	0.2	b.d.l.	1.4
		b.d.l.	b.d.l.	0.1	b.d.l.	0.1	40.8	0.1	0.1	b.d.l.	0.2	13.1	b.d.l.	b.d.l.	44.5	0.1	b.d.l.	b.d.l.	0.8
		0.1	0.0	b.d.l.	0.1	0.1	51.9	0.1	0.1	0.0	0.5	44.2	b.d.l.	b.d.l.	2.6	0.0	b.d.l.	0.1	0.3
		0.9	b.d.l.	0.2	0.2	0.1	0.2	0.0	0.0	0.0	0.0	1.3	b.d.l.	b.d.l.	96.5	0.1	0.1	b.d.l.	b.d.l.
JH2A_T1_002	Slag	b.d.l.	0.1	0.0	0.1	0.4	35.4	b.d.l.	0.0	b.d.l.	0.1	14.5	0.1	0.2	48.3	0.1	0.1	0.1	0.5
		b.d.l.	0.1	0.1	0.3	0.3	38.3	0.1	0.1	0.0	0.1	15.0	0.1	0.1	44.4	0.1	0.0	b.d.l.	0.8
		b.d.l.	0.6	0.1	0.7	0.3	20.6	1.2	5.4	b.d.l.	0.3	14.9	0.1	0.1	54.2	0.6	0.1	0.3	0.5
		b.d.l.	0.2	0.0	0.3	0.4	37.3	0.4	1.5	b.d.l.	0.4	22.5	0.1	0.1	34.8	0.8	b.d.l.	0.2	1.0
		b.d.l.	0.2	0.1	0.1	0.3	36.4	0.1	0.1	b.d.l.	0.4	14.6	0.0	b.d.l.	46.8	0.2	b.d.l.	b.d.l.	0.7
		b.d.l.	b.d.l.	0.0	0.2	0.1	42.8	0.0	0.0	b.d.l.	0.0	33.1	b.d.l.	b.d.l.	22.3	0.5	0.1	b.d.l.	0.8
		b.d.l.	0.0	0.1	0.3	0.0	40.6	0.1	0.0	0.0	0.0	12.9	b.d.l.	b.d.l.	45.1	0.2	b.d.l.	0.0	0.6

S	Fe	Cu
22.2	25.9	52.0
23.6	21.1	55.3
27.5	43.7	28.8
25.1	28.8	46.2
24.2	17.9	58.0
0.8	98.1	1.2
0.1	97.9	2.1
0.1	98.4	1.5
b.d.l.	2.0	98.0
0.2	97.3	2.5
0.0	96.2	3.8
0.1	95.9	4.0
b.d.l.	97.5	2.5
22.1	11.9	66.0
20.6	5.9	73.5
0.0	97.6	2.4
37.0	60.0	3.0
37.1	60.0	2.9
37.1	60.9	2.0
25.9	14.8	59.3
0.2	2.9	96.9
24.7	35.0	40.3
29.1	29.7	41.3
0.1	0.8	99.1
0.1	97.5	2.4
0.0	97.8	2.2
47.0	50.9	2.1
46.6	48.9	4.5
47.1	50.0	2.9
26.6	15.7	57.6
27.6	52.9	19.5
0.1	0.9	99.0
0.1	1.1	98.8
0.1	1.0	98.9
25.9	15.5	58.6
45.8	50.0	4.2
0.1	3.0	96.9
0.1	2.4	97.5
26.3	16.5	57.2
36.4	60.1	3.6
0.1	1.3	98.6
22.2	17.6	60.3
24.5	18.7	56.8
13.1	18.3	68.6
24.8	29.1	46.1
23.0	17.9	59.1
28.3	42.4	29.3
26.1	16.2	57.8

Sample	Type	Na ₂ O	MgO	Al ₂ O ₃	SiO ₂	P ₂ O ₅	SO ₃	K ₂ O	CaO	TiO ₂	MnO	FeO	CoO	NiO	CuO	ZnO	AsO	SbO	PbO
JH2A_T3_001	Slag	b.d.l.	0.0	0.1	0.3	b.d.l.	47.2	0.0	b.d.l.	b.d.l.	0.2	45.5	b.d.l.	b.d.l.	6.1	0.1	0.0	b.d.l.	0.6
		b.d.l.	b.d.l.	0.1	0.3	0.0	35.3	0.0	0.1	0.0	0.1	11.9	b.d.l.	b.d.l.	51.4	0.1	0.1	0.0	0.5
		b.d.l.	b.d.l.	0.1	0.4	0.0	50.7	b.d.l.	0.0	0.0	0.1	45.3	b.d.l.	b.d.l.	2.5	0.3	0.0	b.d.l.	0.6
		b.d.l.	b.d.l.	0.1	0.5	0.1	39.0	0.1	0.0	b.d.l.	0.1	13.9	b.d.l.	b.d.l.	45.5	0.2	0.0	0.1	0.5
		b.d.l.	b.d.l.	0.1	0.3	0.1	37.5	b.d.l.	0.0	0.1	0.1	12.3	b.d.l.	b.d.l.	48.7	0.2	b.d.l.	0.0	0.6
		b.d.l.	0.0	0.0	0.2	0.1	48.3	0.0	0.1	0.0	0.2	48.1	b.d.l.	b.d.l.	2.1	0.3	0.0	0.1	0.5
		b.d.l.	0.0	0.0	0.4	b.d.l.	50.3	0.1	0.0	b.d.l.	0.0	42.2	b.d.l.	b.d.l.	6.4	0.2	b.d.l.	b.d.l.	0.4
		b.d.l.	0.0	0.0	0.3	b.d.l.	37.5	0.1	b.d.l.	b.d.l.	0.1	11.6	b.d.l.	b.d.l.	49.7	0.1	b.d.l.	b.d.l.	0.6
		b.d.l.	b.d.l.	0.1	0.2	0.1	38.8	0.1	0.1	b.d.l.	0.2	12.7	b.d.l.	b.d.l.	46.7	0.1	0.1	0.0	0.7
		b.d.l.	0.1	0.0	0.1	0.1	49.2	0.1	0.6	b.d.l.	0.2	44.4	b.d.l.	b.d.l.	4.8	0.0	0.0	b.d.l.	0.4
		b.d.l.	0.0	0.1	0.3	0.1	39.9	0.0	0.0	0.1	0.0	12.6	b.d.l.	b.d.l.	46.3	0.1	0.0	b.d.l.	0.6
		b.d.l.	0.1	0.1	0.4	0.0	35.4	b.d.l.	0.1	0.1	0.0	5.8	b.d.l.	b.d.l.	57.1	0.2	0.0	0.1	0.4
		0.3	0.1	0.2	0.7	0.0	34.4	0.1	0.2	0.4	0.0	3.7	b.d.l.	b.d.l.	59.1	0.1	0.1	0.0	0.5
		b.d.l.	0.1	0.0	0.2	b.d.l.	40.3	0.0	0.1	b.d.l.	0.2	13.8	b.d.l.	b.d.l.	44.3	0.5	b.d.l.	b.d.l.	0.5
		0.9	b.d.l.	b.d.l.	0.3	0.1	0.2	0.0	b.d.l.	b.d.l.	0.0	0.9	b.d.l.	b.d.l.	97.3	0.2	b.d.l.	0.0	0.1
		0.9	b.d.l.	0.0	0.3	b.d.l.	0.1	b.d.l.	0.0	0.0	b.d.l.	2.1	b.d.l.	b.d.l.	96.3	0.1	b.d.l.	b.d.l.	0.0
		0.9	0.1	0.0	0.3	0.1	0.2	b.d.l.	b.d.l.	0.0	0.0	1.2	b.d.l.	b.d.l.	96.8	0.1	b.d.l.	b.d.l.	b.d.l.
		b.d.l.	0.0	0.1	0.3	b.d.l.	42.0	b.d.l.	0.0	b.d.l.	0.1	23.8	0.1	0.1	32.0	0.6	0.1	0.1	0.8
		b.d.l.	0.1	0.1	0.3	0.1	42.0	b.d.l.	0.0	b.d.l.	0.2	22.1	0.1	0.1	32.9	1.6	b.d.l.	b.d.l.	0.7
		b.d.l.	0.0	0.0	0.4	0.0	45.4	0.0	0.1	b.d.l.	0.1	38.6	0.2	0.1	13.1	0.9	0.0	b.d.l.	1.0
		b.d.l.	0.1	0.0	0.3	0.0	41.5	0.1	0.1	b.d.l.	0.1	21.4	0.1	0.0	35.1	0.2	b.d.l.	b.d.l.	1.0
		b.d.l.	0.0	0.1	0.4	0.0	38.5	0.0	b.d.l.	b.d.l.	0.2	17.5	0.0	0.0	41.9	0.4	b.d.l.	b.d.l.	1.0
		b.d.l.	0.0	0.1	0.4	0.0	41.5	b.d.l.	0.0	b.d.l.	0.2	27.0	0.2	0.1	27.6	1.8	0.0	b.d.l.	1.2
		b.d.l.	b.d.l.	0.1	0.4	0.0	45.3	0.0	0.1	0.0	0.2	34.5	0.1	b.d.l.	17.8	0.4	b.d.l.	0.0	1.1
		b.d.l.	0.0	0.1	0.5	0.1	46.7	0.0	0.1	b.d.l.	0.1	31.4	0.1	0.2	19.0	1.0	0.0	0.0	0.9
		b.d.l.	0.1	0.0	0.4	0.0	40.7	0.0	0.1	b.d.l.	0.1	18.5	0.0	0.1	38.6	0.8	b.d.l.	0.0	0.5
		b.d.l.	0.0	0.1	0.6	0.0	45.3	b.d.l.	0.0	b.d.l.	0.1	38.8	0.1	0.1	13.1	0.9	0.0	b.d.l.	0.7
		0.1	b.d.l.	0.1	0.4	0.0	43.0	0.0	0.0	b.d.l.	0.2	23.6	0.0	0.1	27.0	4.4	0.1	b.d.l.	0.9
		b.d.l.	b.d.l.	0.1	0.4	0.0	43.0	0.0	0.1	0.0	0.1	15.9	b.d.l.	0.0	39.5	0.2	b.d.l.	0.1	0.7
		b.d.l.	0.1	0.1	0.4	0.1	50.4	0.0	0.1	0.0	0.1	44.4	0.1	0.1	3.3	0.0	b.d.l.	0.0	0.7
		b.d.l.	0.1	0.1	0.4	0.0	42.4	0.1	0.0	b.d.l.	0.1	17.2	b.d.l.	b.d.l.	36.6	2.4	b.d.l.	b.d.l.	0.7
		0.3	0.0	0.1	0.3	0.1	42.5	0.0	0.1	0.0	0.3	15.0	b.d.l.	b.d.l.	35.2	5.0	b.d.l.	b.d.l.	1.1
		b.d.l.	0.0	0.1	0.5	0.0	46.0	0.0	0.1	0.0	0.1	33.2	0.2	b.d.l.	18.2	0.3	0.1	0.0	1.2
JH2A_T3_002	Matte	0.8	0.1	0.0	0.2	0.0	0.2	0.0	0.1	b.d.l.	0.1	1.3	b.d.l.	b.d.l.	96.7	0.1	0.1	0.0	0.2
		0.7	b.d.l.	b.d.l.	0.1	b.d.l.	0.1	0.1	0.1	0.0	b.d.l.	0.6	b.d.l.	b.d.l.	98.0	0.2	b.d.l.	b.d.l.	0.1
		b.d.l.	0.0	0.0	0.1	0.0	38.2	0.1	0.1	0.0	0.3	11.7	b.d.l.	b.d.l.	48.9	0.1	b.d.l.	0.0	0.4
		b.d.l.	0.0	0.0	0.1	0.1	46.1	0.1	2.2	b.d.l.	0.2	39.6	b.d.l.	b.d.l.	10.6	0.3	b.d.l.	0.1	0.6
		0.8	0.1	0.0	0.1	0.1	0.3	0.0	0.1	b.d.l.	0.1	2.8	b.d.l.	b.d.l.	95.3	0.2	b.d.l.	0.1	0.1
		1.0	b.d.l.	0.0	0.1	b.d.l.	0.3	0.0	0.0	b.d.l.	0.1	2.9	b.d.l.	b.d.l.	95.2	0.2	0.1	0.1	0.0
JH2B_T1_001	Slag	0.1	0.1	0.1	0.5	0.1	36.6	0.9	0.1	b.d.l.	0.2	39.5	b.d.l.	b.d.l.	19.1	1.6	b.d.l.	b.d.l.	0.9
		b.d.l.	2.7	0.3	1.0	0.6	41.2	0.1	3.2	0.0	0.6	36.4	b.d.l.	b.d.l.	12.3	0.9	b.d.l.	0.0	0.8
		b.d.l.	0.1	0.2	0.2	0.0	39.6	0.1	0.4	b.d.l.	0.3	16.8	b.d.l.	b.d.l.	41.6	0.1	b.d.l.	b.d.l.	0.5
		0.1	0.0	0.2	0.3	0.1	43.9	0.1	0.3	0.0	0.7	42.3	b.d.l.	b.d.l.	10.9	0.5	b.d.l.	0.0	0.5
		0.1	0.0	0.1	0.7	0.1	43.4	0.2	0.7	b.d.l.	0.7	36.0	b.d.l.	b.d.l.	13.5	3.7	0.0	b.d.l.	0.7
JH2B_T1_002	Slag	0.2	0.0	0.1	0.4	0.0	46.6	0.1	0.3	0.0	0.1	47.3	0.2	0.1	2.1	1.3	0.0	b.d.l.	1.2
		b.d.l.	b.d.l.	0.1	0.4	0.1	46.8	0.1	0.1	0.0	0.0	45.7	0.3	0.1	4.5	1.2	0.1	b.d.l.	0.6
		0.1	0.2	0.2	0.7	0.1	11.8	0.0	0.2	0.0	0.1	81.3	0.2	0.1	3.8	0.5	b.d.l.	0.0	0.4

S	Fe	Cu
31.9	59.8	8.3
21.9	14.3	63.8
35.3	61.2	3.5
24.9	17.2	57.9
23.6	15.1	61.3
33.2	64.0	2.9
34.7	56.5	8.8
23.6	14.1	62.3
24.8	15.7	59.5
34.0	59.5	6.6
25.5	15.6	59.0
22.1	7.0	70.9
21.5	4.6	73.9
25.9	17.3	56.8
0.1	0.9	99.1
0.1	2.0	97.9
0.1	1.2	98.8
27.6	30.4	42.0
27.9	28.5	43.6
31.0	51.2	17.8
27.1	27.2	45.7
24.6	21.8	53.6
27.9	35.2	37.0
30.6	45.4	24.0
32.1	41.9	26.0
26.5	23.4	50.1
30.9	51.3	17.8
30.1	32.1	37.8
28.2	20.2	51.7
35.2	60.2	4.6
28.5	22.4	49.1
29.9	20.6	49.5
31.3	43.9	24.8
0.1	1.3	98.6
0.1	0.6	99.4
24.1	14.3	61.6
32.0	53.4	14.6
0.2	2.8	97.1
0.2	2.9	96.9
24.2	50.7	25.2
30.2	51.8	18.0
25.5	21.0	53.5
29.7	55.6	14.7
30.9	49.9	19.2
32.6	64.4	3.0
32.4	61.4	6.2
6.6	89.1	4.3

Sample	Type	Na ₂ O	MgO	Al ₂ O ₃	SiO ₂	P ₂ O ₅	SO ₃	K ₂ O	CaO	TiO ₂	MnO	FeO	CoO	NiO	CuO	ZnO	AsO	SbO	PbO
		b.d.l.	0.0	0.0	0.2	b.d.l.	49.8	0.0	0.9	0.0	b.d.l.	28.1	0.1	0.0	19.7	0.5	b.d.l.	0.0	0.6
		b.d.l.	0.0	0.1	0.3	0.0	34.9	0.0	0.0	0.0	b.d.l.	23.8	0.1	0.0	39.9	0.1	b.d.l.	0.1	0.6
		b.d.l.	b.d.l.	b.d.l.	0.3	b.d.l.	41.2	0.0	0.0	b.d.l.	0.0	23.3	0.1	b.d.l.	33.5	0.1	0.0	0.0	1.5
		b.d.l.	0.0	0.0	0.3	0.1	49.8	0.0	0.0	0.0	0.1	43.0	0.1	0.1	5.4	0.3	0.0	b.d.l.	0.7
		0.5	b.d.l.	b.d.l.	0.4	0.1	46.0	b.d.l.	0.0	0.0	b.d.l.	31.4	0.2	0.1	13.8	5.5	b.d.l.	b.d.l.	1.9
		b.d.l.	0.0	0.1	0.3	0.0	47.1	b.d.l.	0.0	b.d.l.	b.d.l.	37.2	0.2	0.0	14.0	0.0	0.0	b.d.l.	1.0
		b.d.l.	0.0	0.1	0.2	0.1	45.7	0.0	0.0	0.0	0.0	32.1	0.2	0.0	20.0	0.3	0.0	0.0	1.1
		b.d.l.	0.1	0.1	0.2	0.1	46.2	0.0	0.0	b.d.l.	0.0	36.8	0.1	0.0	15.5	b.d.l.	b.d.l.	0.0	0.8
		b.d.l.	0.0	0.1	0.3	0.0	45.8	0.0	0.0	0.0	b.d.l.	32.1	0.1	0.1	20.2	0.4	b.d.l.	b.d.l.	0.8
		b.d.l.	b.d.l.	0.1	0.3	0.1	46.0	0.0	0.0	b.d.l.	0.0	32.7	0.1	0.1	18.9	0.3	0.0	b.d.l.	1.5
		b.d.l.	0.0	0.1	0.3	0.1	51.8	b.d.l.	0.1	0.0	b.d.l.	39.8	0.2	0.0	7.1	0.1	0.0	0.1	0.4
		b.d.l.	0.0	0.1	0.3	0.0	35.6	0.0	0.0	0.0	0.0	15.1	0.1	0.0	48.0	0.1	0.0	0.1	0.5
		b.d.l.	0.0	0.1	0.2	0.1	47.0	0.0	0.0	b.d.l.	0.0	27.7	0.2	0.1	24.0	0.1	0.0	0.0	0.6
		b.d.l.	0.0	0.1	0.2	0.0	49.0	0.0	0.0	0.0	0.1	46.3	0.2	0.1	3.0	0.0	b.d.l.	b.d.l.	0.8
		b.d.l.	0.1	0.0	0.3	0.0	46.8	0.0	0.0	b.d.l.	b.d.l.	25.3	0.1	0.0	19.5	2.4	b.d.l.	b.d.l.	5.3
		b.d.l.	0.1	0.1	0.3	0.0	46.6	0.0	b.d.l.	b.d.l.	0.1	37.4	0.1	0.1	13.3	0.5	b.d.l.	b.d.l.	1.4
		b.d.l.	b.d.l.	0.0	0.4	0.0	45.4	b.d.l.	0.1	b.d.l.	0.0	33.5	0.0	0.1	18.6	0.9	0.0	0.1	0.9
		b.d.l.	0.0	0.1	0.5	0.1	44.9	0.0	0.0	b.d.l.	0.1	45.5	0.2	0.1	6.9	0.8	b.d.l.	b.d.l.	1.0
		b.d.l.	0.0	0.0	0.3	0.1	47.4	0.0	0.0	0.0	0.1	40.7	0.1	b.d.l.	9.5	0.9	0.0	b.d.l.	0.8
		b.d.l.	0.0	0.1	0.3	0.1	51.5	0.0	0.1	0.0	0.1	44.5	0.2	0.1	2.7	b.d.l.	0.0	b.d.l.	0.5
		b.d.l.	b.d.l.	0.1	0.3	0.0	42.0	0.1	b.d.l.	0.0	0.0	17.2	0.1	0.1	38.2	1.2	0.0	b.d.l.	0.7
		b.d.l.	0.0	0.0	0.3	0.0	35.9	0.0	0.1	b.d.l.	0.0	12.7	0.1	0.1	48.6	0.2	0.1	b.d.l.	1.8
		b.d.l.	0.0	0.1	0.2	0.1	47.1	0.0	0.0	0.0	0.1	34.4	0.1	0.1	16.3	0.9	0.0	b.d.l.	0.6
		b.d.l.	0.1	0.1	0.2	0.1	44.9	b.d.l.	0.0	b.d.l.	0.1	33.4	0.2	0.1	19.8	0.5	b.d.l.	0.0	0.6
		b.d.l.	0.1	0.0	0.3	0.1	44.5	0.0	0.1	b.d.l.	0.0	29.8	0.1	0.1	23.3	0.2	b.d.l.	b.d.l.	1.1
		b.d.l.	b.d.l.	0.1	0.3	b.d.l.	43.3	b.d.l.	0.0	b.d.l.	0.1	31.9	0.1	0.1	22.3	1.4	0.0	b.d.l.	0.4
		b.d.l.	0.1	0.1	0.3	0.1	49.6	0.1	0.0	b.d.l.	0.0	42.4	0.2	0.1	7.0	b.d.l.	b.d.l.	b.d.l.	0.1
		b.d.l.	0.1	0.1	0.3	0.0	48.3	0.0	0.1	0.0	0.1	37.0	0.1	0.1	13.2	0.0	b.d.l.	b.d.l.	0.6
		b.d.l.	0.0	0.1	0.3	0.0	44.1	0.0	0.0	0.0	0.0	24.2	0.1	0.1	30.3	0.1	0.0	0.0	0.5
		b.d.l.	0.0	0.0	0.2	0.0	51.3	b.d.l.	0.0	0.0	0.0	45.5	0.2	0.1	2.1	b.d.l.	b.d.l.	b.d.l.	0.5
		b.d.l.	0.0	0.1	0.3	0.0	39.6	0.0	0.0	b.d.l.	0.0	12.7	0.0	b.d.l.	46.1	0.3	b.d.l.	0.1	0.7
JH2B_T2_001	Slag	b.d.l.	0.1	0.8	0.7	0.1	0.5	0.9	0.9	0.0	0.2	3.0	b.d.l.	b.d.l.	91.6	1.0	b.d.l.	b.d.l.	0.1
		b.d.l.	0.3	0.3	0.6	0.0	17.6	2.1	2.3	0.0	0.5	16.7	b.d.l.	b.d.l.	57.8	0.5	b.d.l.	b.d.l.	1.0
		b.d.l.	0.1	0.1	0.3	b.d.l.	1.1	1.6	0.3	b.d.l.	0.1	4.5	b.d.l.	b.d.l.	91.0	0.6	b.d.l.	b.d.l.	0.2
		b.d.l.	0.1	0.2	0.9	b.d.l.	4.1	2.1	0.1	b.d.l.	0.1	3.4	b.d.l.	b.d.l.	88.4	0.4	0.0	0.1	0.2
		3.5	0.2	0.2	1.7	0.0	3.3	3.2	2.2	b.d.l.	0.3	7.1	b.d.l.	b.d.l.	76.9	1.0	b.d.l.	b.d.l.	0.4
		b.d.l.	0.1	0.1	0.7	0.0	0.7	1.3	1.2	0.0	0.2	8.4	b.d.l.	b.d.l.	85.6	1.4	0.1	b.d.l.	0.1
		b.d.l.	0.2	0.2	0.6	0.1	2.0	1.7	1.0	b.d.l.	0.1	6.0	b.d.l.	b.d.l.	87.0	0.4	b.d.l.	b.d.l.	0.5
		1.6	0.2	0.2	0.8	0.1	29.4	2.8	0.4	0.0	0.6	48.5	b.d.l.	b.d.l.	14.0	0.7	b.d.l.	b.d.l.	0.8
		0.8	0.1	0.2	0.9	0.1	42.7	2.4	0.3	0.0	0.6	35.2	b.d.l.	b.d.l.	15.7	0.5	b.d.l.	b.d.l.	0.5
		b.d.l.	0.1	0.3	0.6	0.1	0.2	1.3	0.7	0.0	0.1	1.9	b.d.l.	b.d.l.	93.6	0.7	b.d.l.	0.0	0.2
JH2B_T3_001	Matte	b.d.l.	0.1	0.4	0.2	0.1	42.6	0.8	0.3	b.d.l.	0.3	13.2	0.1	0.1	41.5	0.2	b.d.l.	0.0	0.4
		0.8	0.0	0.4	0.2	0.1	46.3	0.5	2.3	b.d.l.	0.6	22.1	0.1	0.0	18.1	8.1	b.d.l.	b.d.l.	0.5
		0.1	0.0	0.1	0.2	0.0	35.1	0.2	23.9	0.0	0.2	37.3	0.1	b.d.l.	1.4	b.d.l.	0.3	0.2	0.8
		0.1	0.0	0.1	0.2	0.1	50.1	0.1	0.4	0.0	0.6	29.2	0.1	b.d.l.	14.8	b.d.l.	3.5	0.1	0.8
		b.d.l.	0.0	0.1	0.2	b.d.l.	35.5	0.4	23.9	0.1	0.2	37.1	0.1	0.0	1.9	b.d.l.	0.2	b.d.l.	0.3

S	Fe	Cu
34.7	38.0	27.3
21.7	28.8	49.5
26.9	29.5	43.6
34.6	57.9	7.5
34.2	45.4	20.5
32.0	49.1	18.9
30.9	42.1	27.0
31.1	48.1	20.9
30.9	42.0	27.2
31.3	43.1	25.7
36.2	54.0	9.8
22.1	18.3	59.6
31.6	36.2	32.2
33.8	62.0	4.2
34.7	36.4	28.9
32.0	49.8	18.2
30.8	44.1	25.1
30.6	60.1	9.3
32.6	54.3	13.1
35.9	60.3	3.8
27.7	22.0	50.3
22.8	15.7	61.5
32.1	45.7	22.2
30.1	43.4	26.5
29.9	38.8	31.3
28.9	41.3	29.7
34.0	56.4	9.6
33.0	49.0	17.9
29.1	31.0	39.9
35.7	61.4	2.9
25.3	15.8	58.9
0.3	3.1	96.7
10.6	19.6	69.8
0.6	4.6	94.9
2.2	3.5	94.3
1.9	8.1	90.0
0.4	8.7	91.0
1.1	6.3	92.7
19.4	62.2	18.4
30.0	48.0	22.0
0.1	2.0	97.9
28.2	16.9	54.9
37.0	34.2	28.8
31.8	65.7	2.5
36.7	41.6	21.7
31.8	64.7	3.5

Sample	Type	Na ₂ O	MgO	Al ₂ O ₃	SiO ₂	P ₂ O ₅	SO ₃	K ₂ O	CaO	TiO ₂	MnO	FeO	CoO	NiO	CuO	ZnO	AsO	SbO	PbO
		0.1	0.1	0.1	0.1	b.d.l.	38.5	0.1	25.9	b.d.l.	0.2	31.1	0.0	0.1	1.8	b.d.l.	1.4	b.d.l.	0.6
		b.d.l.	b.d.l.	0.0	0.2	0.0	40.4	0.3	13.7	b.d.l.	0.2	28.4	b.d.l.	b.d.l.	15.3	0.6	b.d.l.	b.d.l.	0.9
		b.d.l.	0.1	0.1	0.4	0.0	49.2	0.1	0.4	b.d.l.	0.2	27.4	0.1	0.0	19.1	2.2	b.d.l.	0.0	0.7

S	Fe	Cu
37.6	58.9	3.5
32.0	43.8	24.2
35.0	37.9	27.2

Appendix C

This Appendix presents an extensive collection of detailed high-resolution images (OM and SEM) and information regarding the mineralogical phases and inclusions observed in both archaeological and experimental slagse. The primary aim is to create a reference catalogue that researchers can consult to enhance their knowledge and analysis in this field. Section B.1 is for the archaeological materials, whereas Section B.2 is for the experimental specimens.

- Archaeological materials –

- Fe-bearing compounds

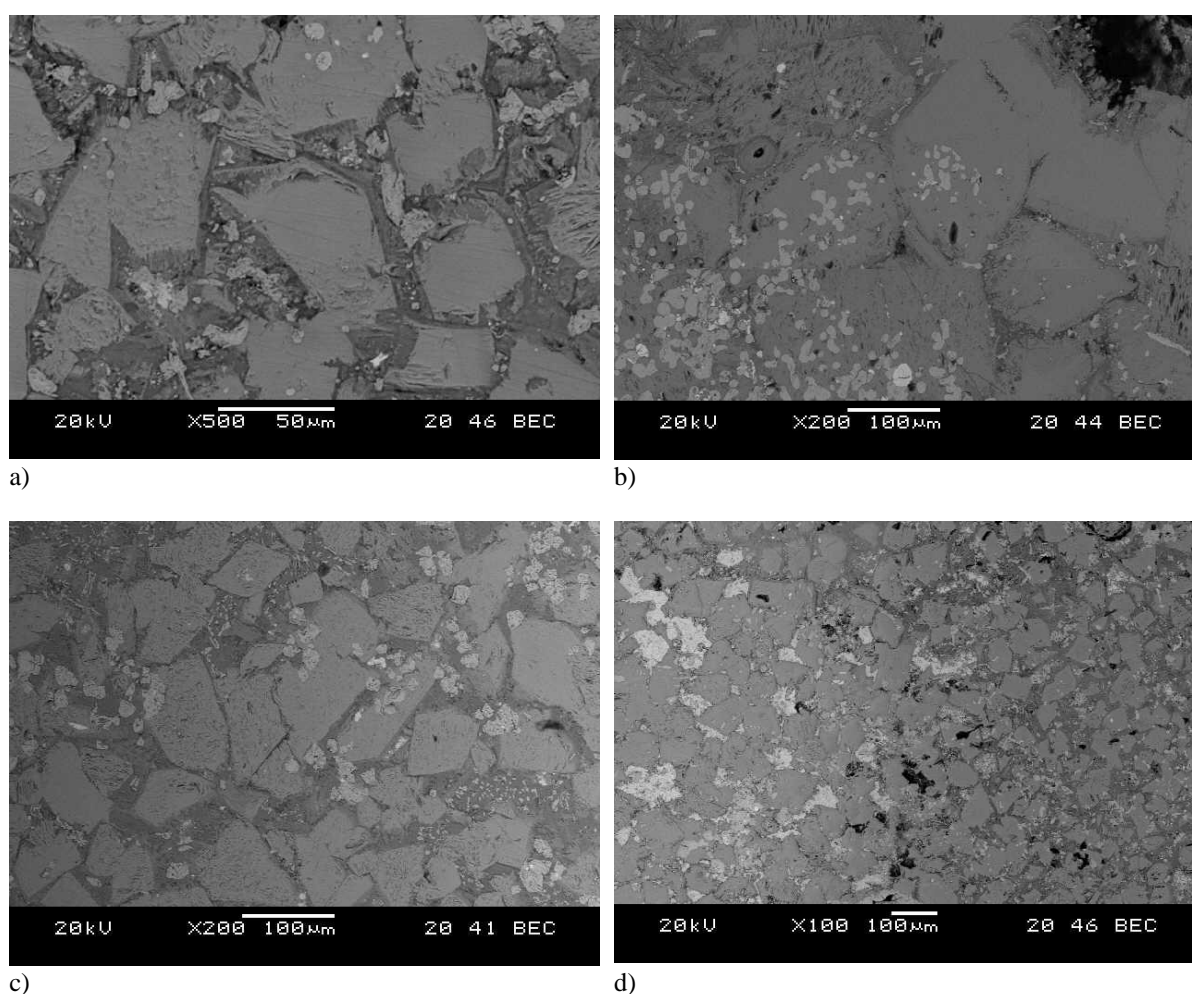


Fig. C. 1 depicts fayalitic crystallized polyhedral grains, featuring cubic to prismatic crystals. Notably, the grains exhibit larger dimensions in the core (d left) and smaller dimensions toward the surface (d right), suggesting variations in cooling rates. Samples: a) ORTB 12, b) ORTB 19, c-d) ORTB 20.

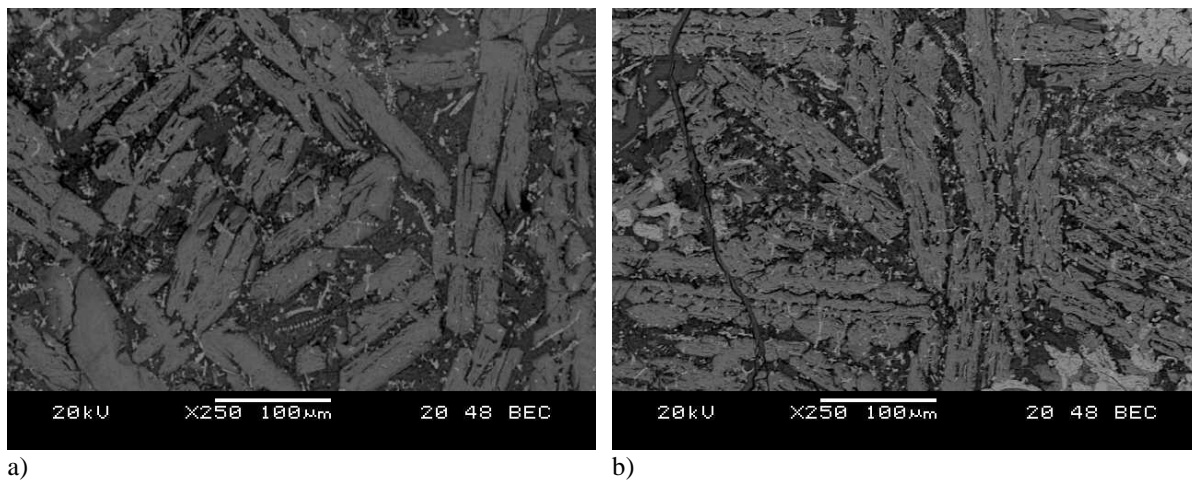


Fig. C. 2 illustrates distinctive fayalitic crystallized structures featuring hoppers-like morphologies. Sample: ORTB 16.

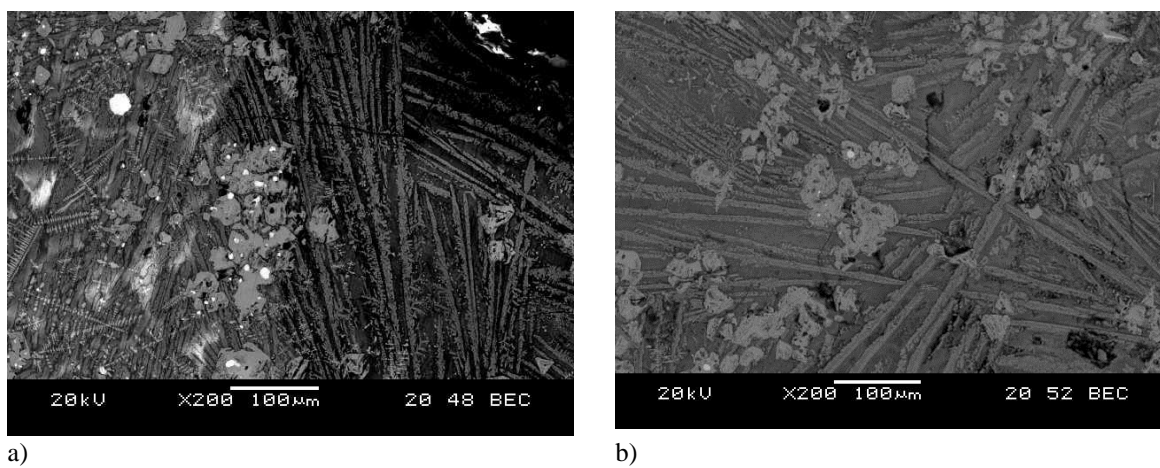


Fig. C. 3 illustrates distinctive fayalitic crystallized features, showcasing small elongated dendritic needles in a fayalitic matrix. Sample: ORTB 8.

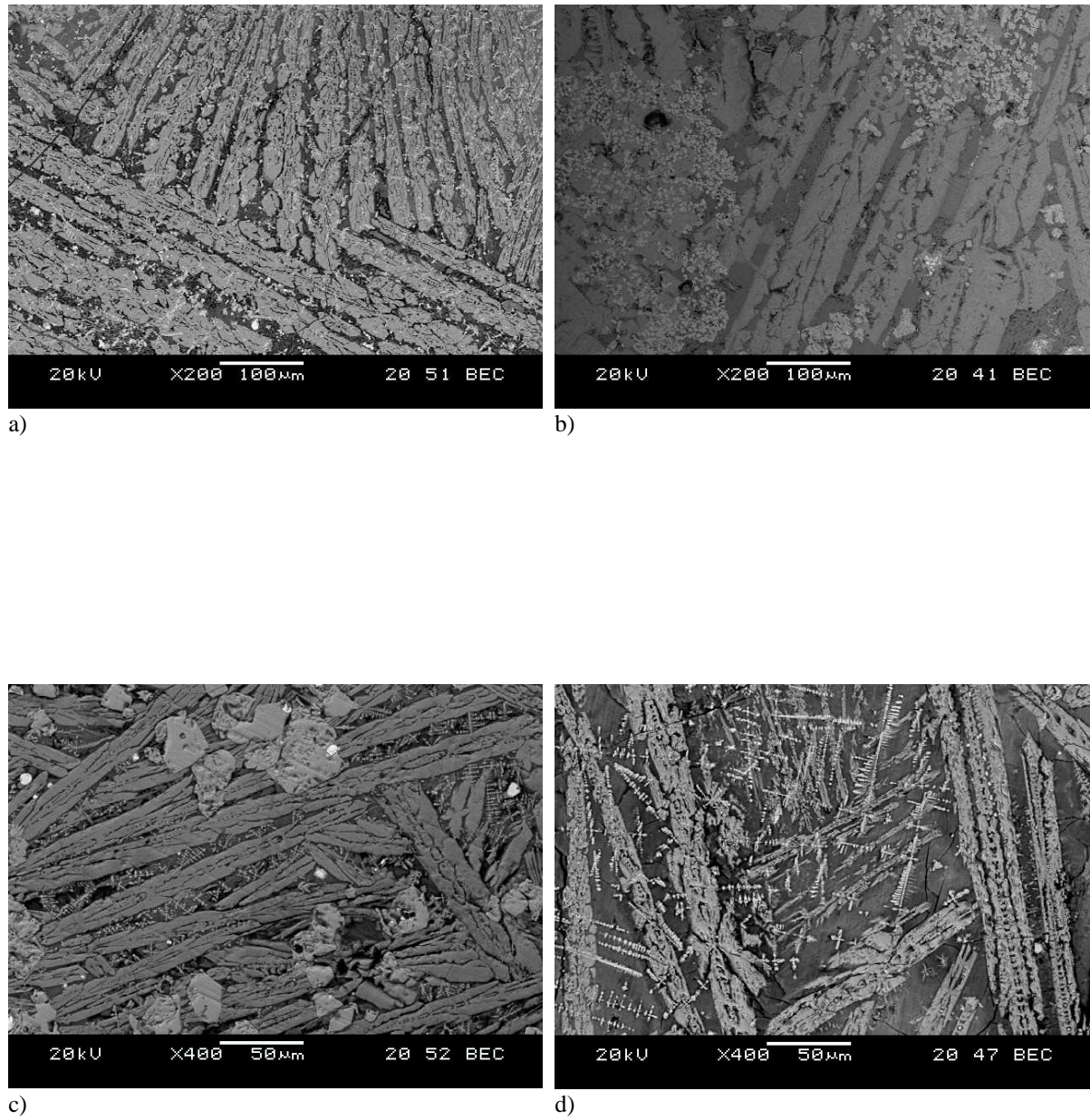


Fig. C. 4 highlights distinctive fayalitic crystallized features, presenting large chain structures. Samples: a) ORTB 16, b) ORTB 20, c) ORTB 5, d) ORTB 8.

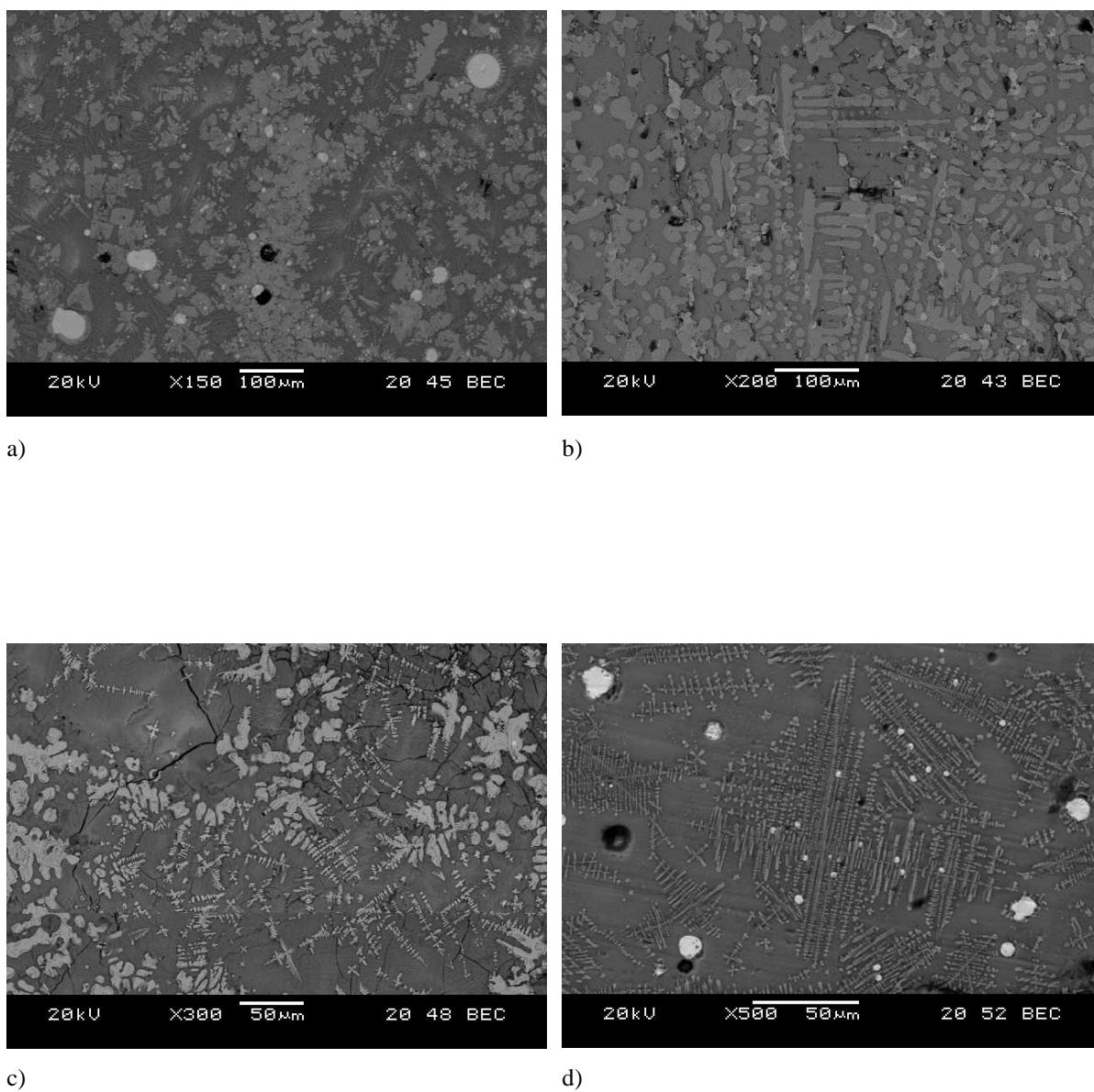


Fig. C. 5 showcases a series of BSE micrographs revealing diverse iron-rich spinel morphologies/phases identified in the slags. This includes euhedral crystals, ranging from cubic to prismatic (a), dendritic growths (c, d), and round features (b, d), all embedded in a fayalitic matrix. Samples: a) ORTB 8, b) ORTB 19, c) ORTB 8, d) ORTB 5.

- Cu- bearing compounds

Ore

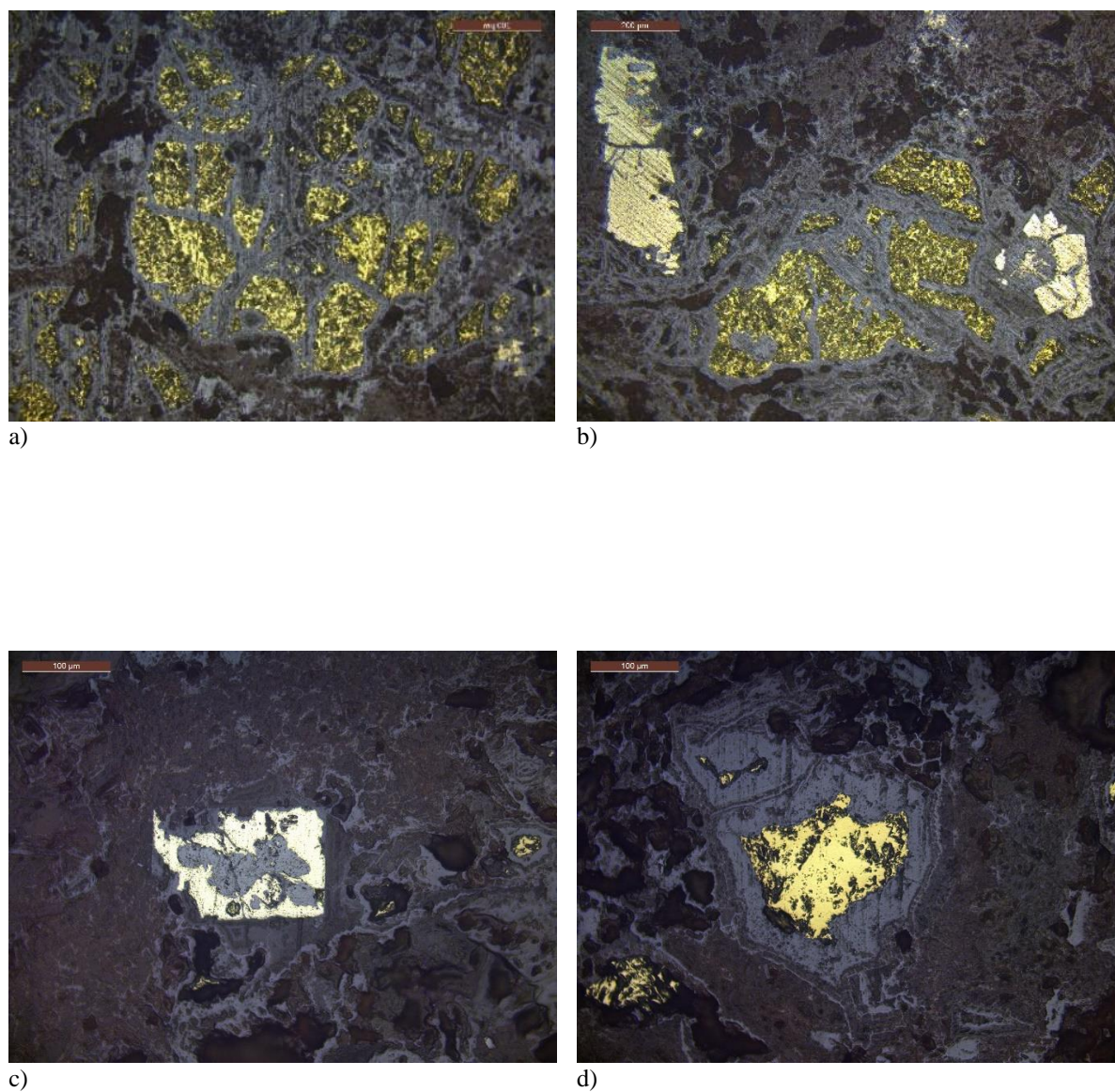


Fig. C. 6 Optical micrographs showing a range of compositions and morphologies found in the brown ore sample: semi reacted pyrrhotite (bright yellow) and chalcopyrite (gold yellow) in a matrix of iron hydroxides (mid-grey) and quartz (dark grey). Sample: ORTB 3.

Slags

Copper-bearing compounds in the slags are predominantly present as copper-iron sulphides and prills. Below is a selection of optical micrographs highlighting various compositions and morphologies of copper-bearing compounds identified in the slags.

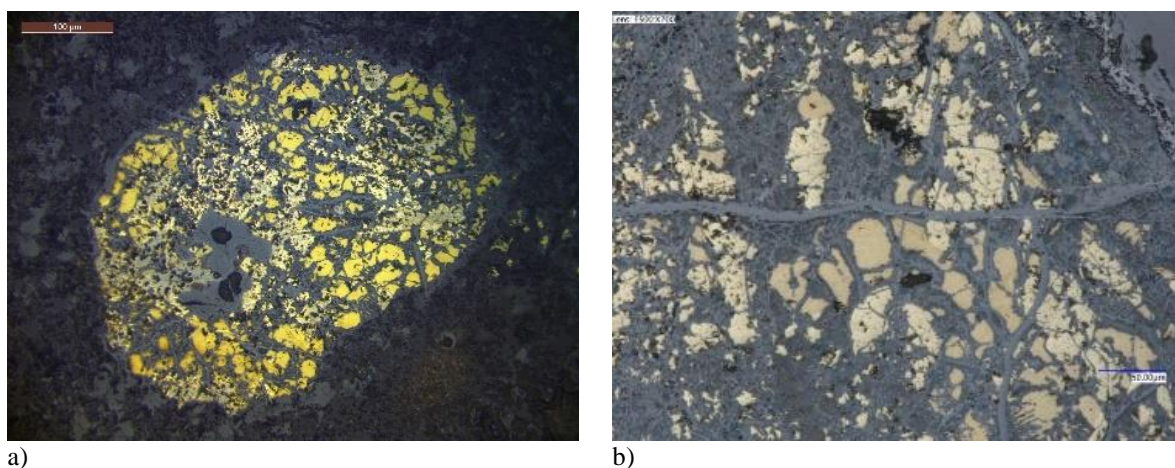


Fig. C. 7 Variations in copper-iron sulphide reactions depicted at different stages: remnants of chalcopyrite (yellow) displaying minimal bornite exsolutions (orange), intricately captured within a fayalitic matrix. Magnetite is also present as squared inclusions (a) and a continuous rim (b). Sample: ORTB 6.

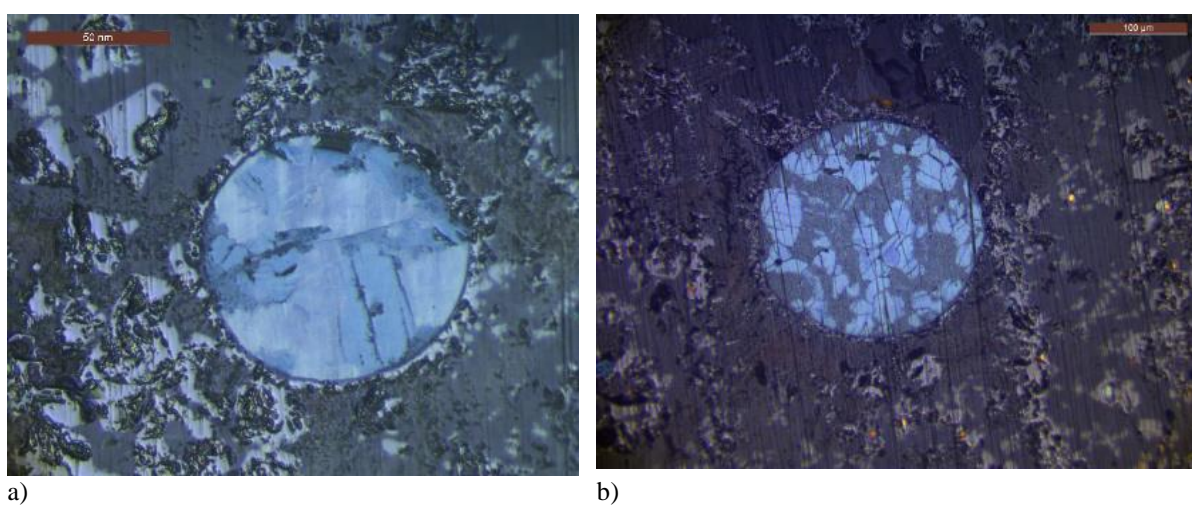


Fig. C. 8 round-shaped recrystallized compounds characterised by covellite-like (blue) and chalcocite-like (greyish) compositions. Sample: ORTB 8.

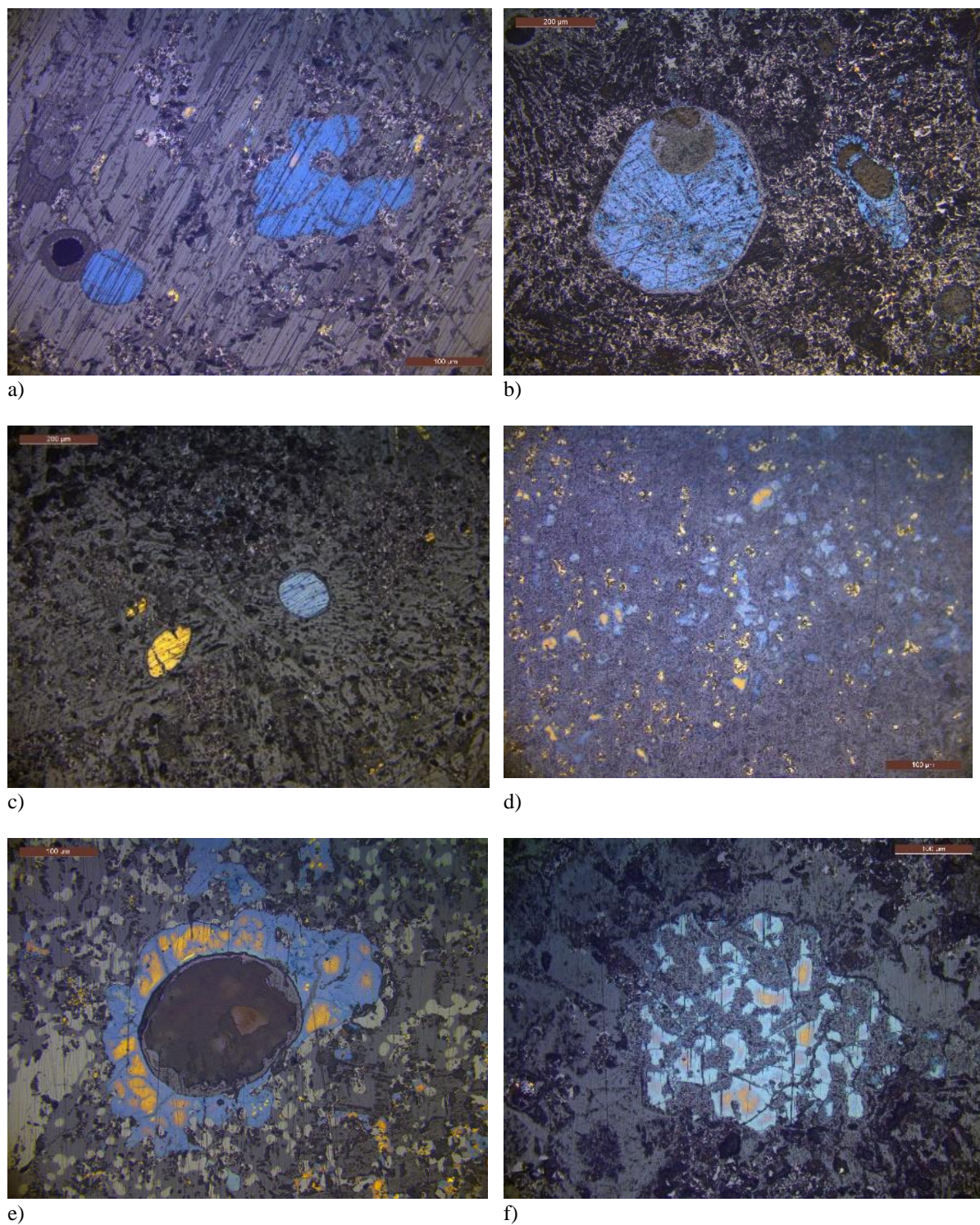


Fig. C. 9 illustrates recrystallized compounds with covellite-like (blue) and chalcocite-like (greyish) compositions. Yellow compounds denote partially reacted chalcopyrite. Covellite, characterized by its deep blue to indigo colour, derives its hue from copper ions in its crystal structure. The colour may exhibit variations within the blue spectrum, influenced by factors such as specific mineral samples and impurities. Samples: a) ORTB 13, b) ORTB 16, c) ORTB 13, d) ORTB 20, e) ORTB 19, f) ORTB 13.

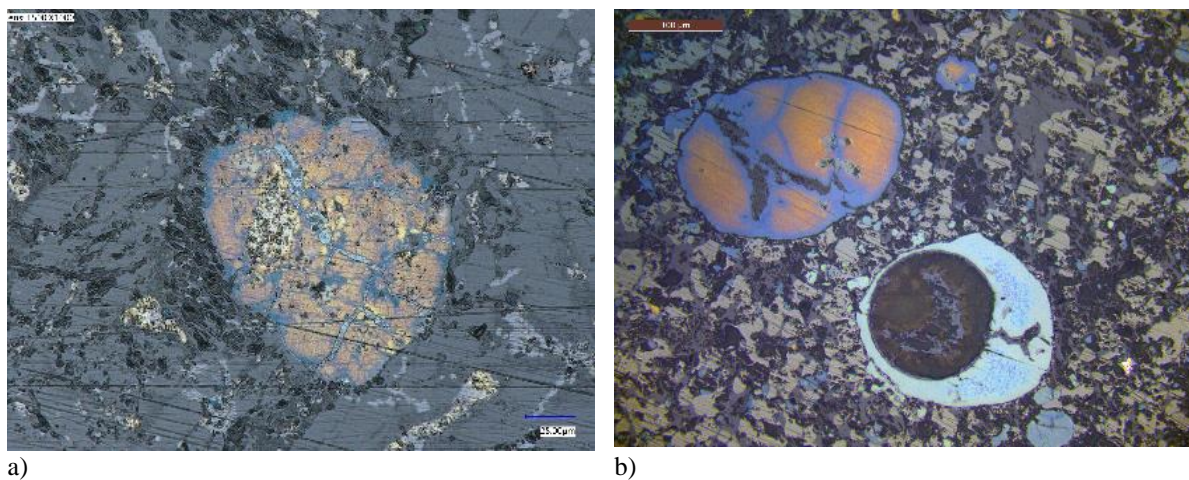


Fig. C. 10 showcases unreacted chalcopyrite-pyrrhotite (yellow), partially reacted chalcopyrite (yellow orange), and distinct stripes of secondary sulphide exhibiting bornite-covellite composition (blue). Notably, a ring-shaped formation with a covellite-like composition (light blue) is highlighted in Fig. b). Samples: a) ORTB 19, b) ORTB 12.

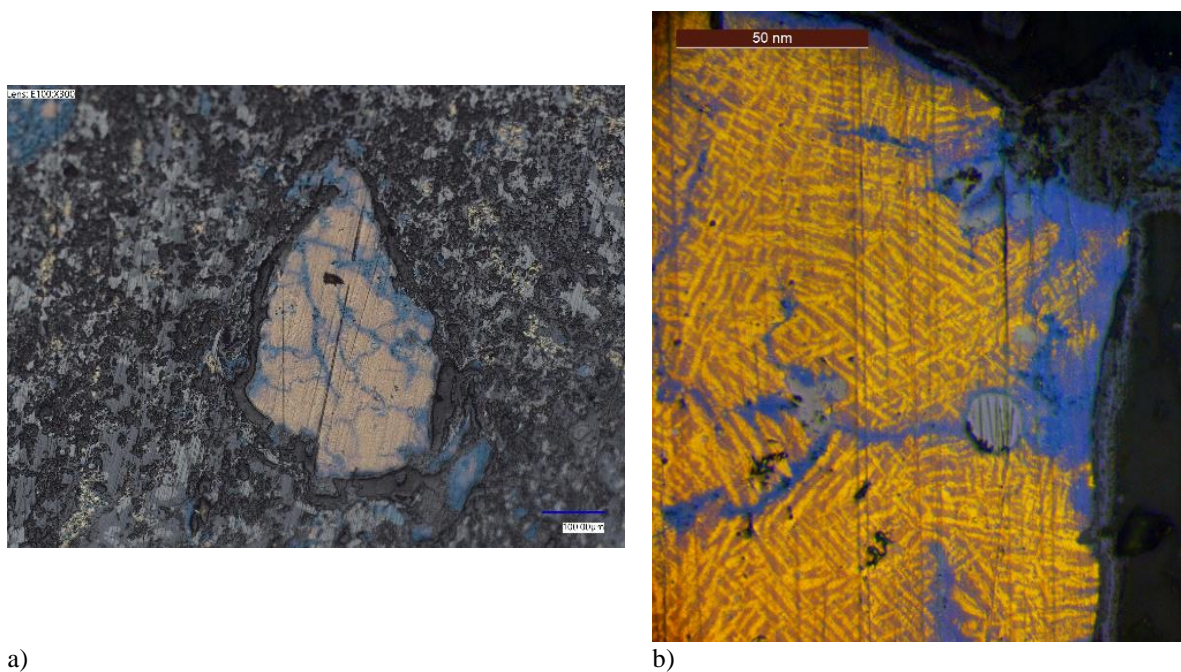


Fig. C. 11 presents a) a chalcopyrite-dominant area featuring b) the exsolution of bornite (pinkish brown) and partially oxidized bornite (sky blue), accompanied by a covellite prill (light blue). Sample: ORTB 19.

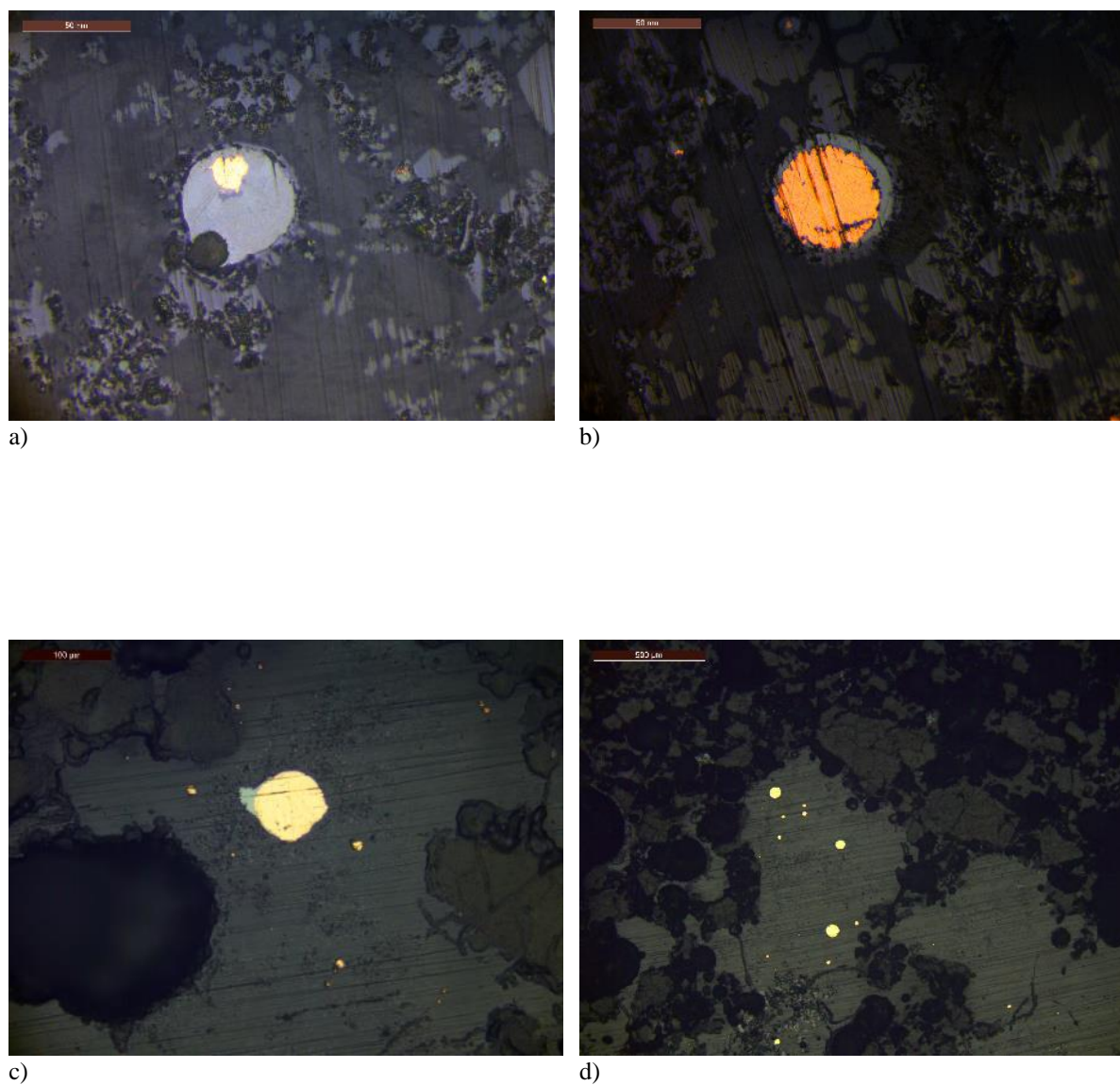


Fig. C. 12 displays four optical micrographs illustrating four distinct stages of copper formation: a) a round-shaped prill with a small pure copper core (orange) surrounded by recrystallized digenite (bluish grey), b) a round-shaped prill with a larger pure copper core (orange) encircled by a ring of recrystallized digenite (bluish grey), c) a pure copper prill with recrystallized digenite or chalcocite extrusion, and d) pure copper prills. Samples: a-b) ORTB 8, c- d) ORTB 5.

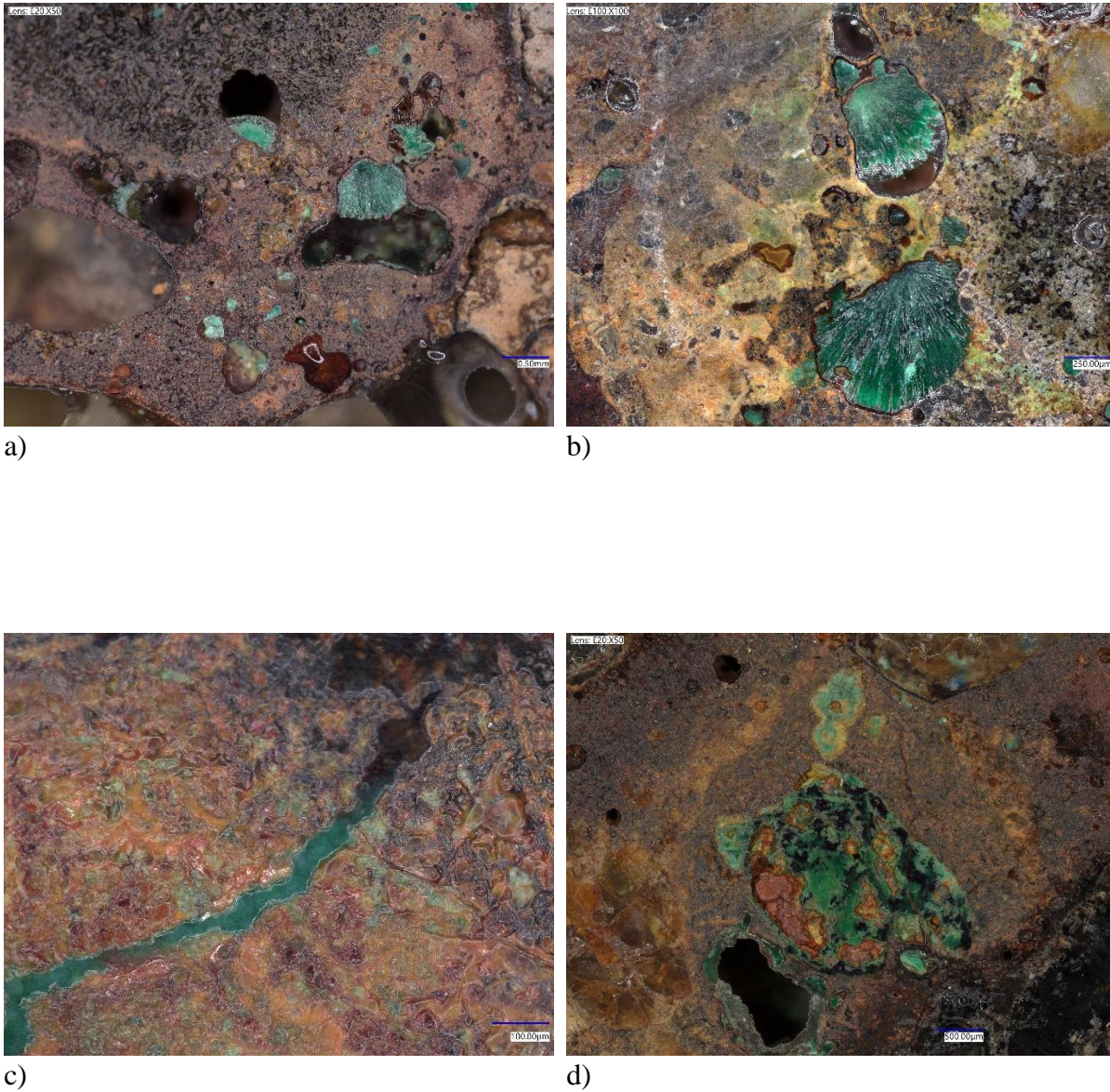
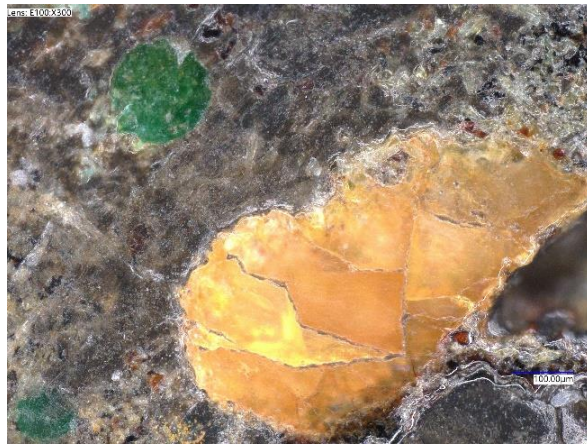
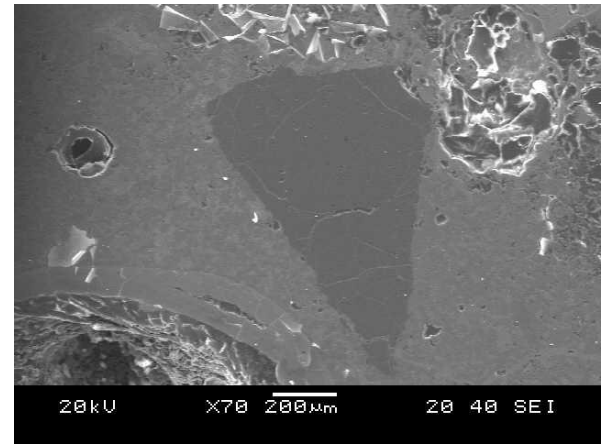


Fig. C. 13 presents optical micrographs capturing the evolution of copper phases through post-depositional growth. Newly developed phases of copper hydroxides (e.g., $\text{Cu}(\text{OH})_2$, and $\text{CuCl}_2 \cdot 2\text{H}_2\text{O}$) are observed filling the empty spaces left in the slag matrix.. Samples: a) ORTB 20, b) ORTB 6, c-d) ORTB 26.

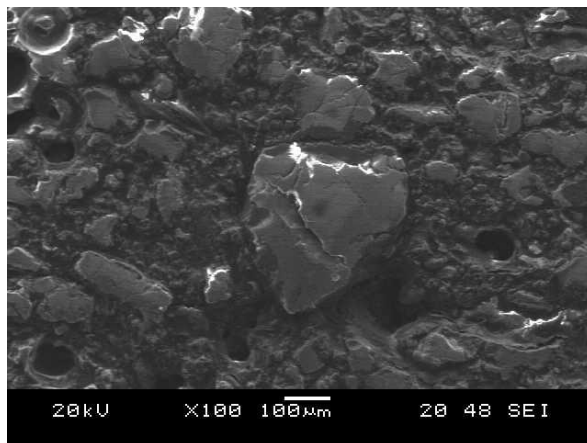
- Inclusions



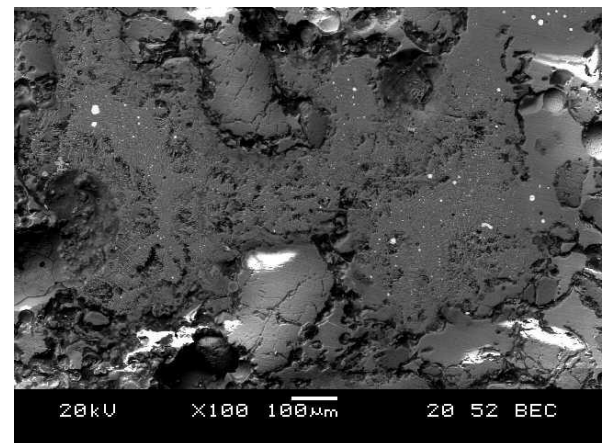
a)



b)

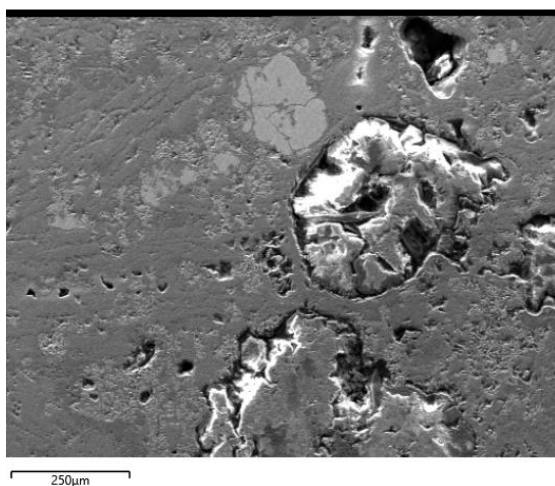


c)

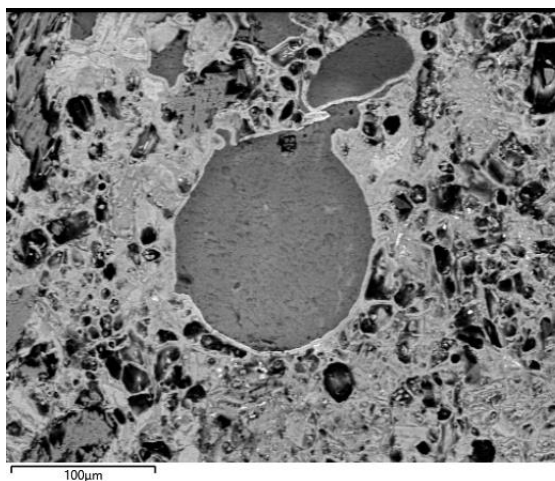


d)

Fig. C. 14 displays a series of Optical (a) and BSE (b-d) micrographs of quartz inclusions identified. Samples: a-b) ORTB 6, c-d) ORTB 5.



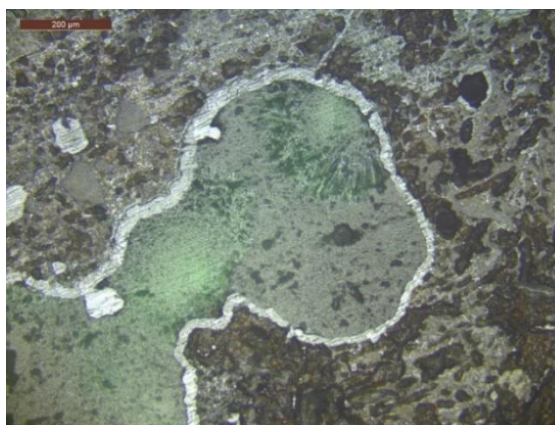
a)



b)



c)



d)

Fig. C. 15 displays a series of SEM (a-c) and optical (d) micrographs showing a) relics of calcium carbonate as inclusions in a fayalitic glassy matrix; b) relics of calcium carbonates found as inclusions in a fayalitic glassy matrix; c) quartz and Ca inclusions; d) semi-reacted inclusion of a possible Ca carbonate. CaO is the main compound in the grey rim. Samples: a) ORTB 13, b-c) ORTB 20, d) ORTB 9.

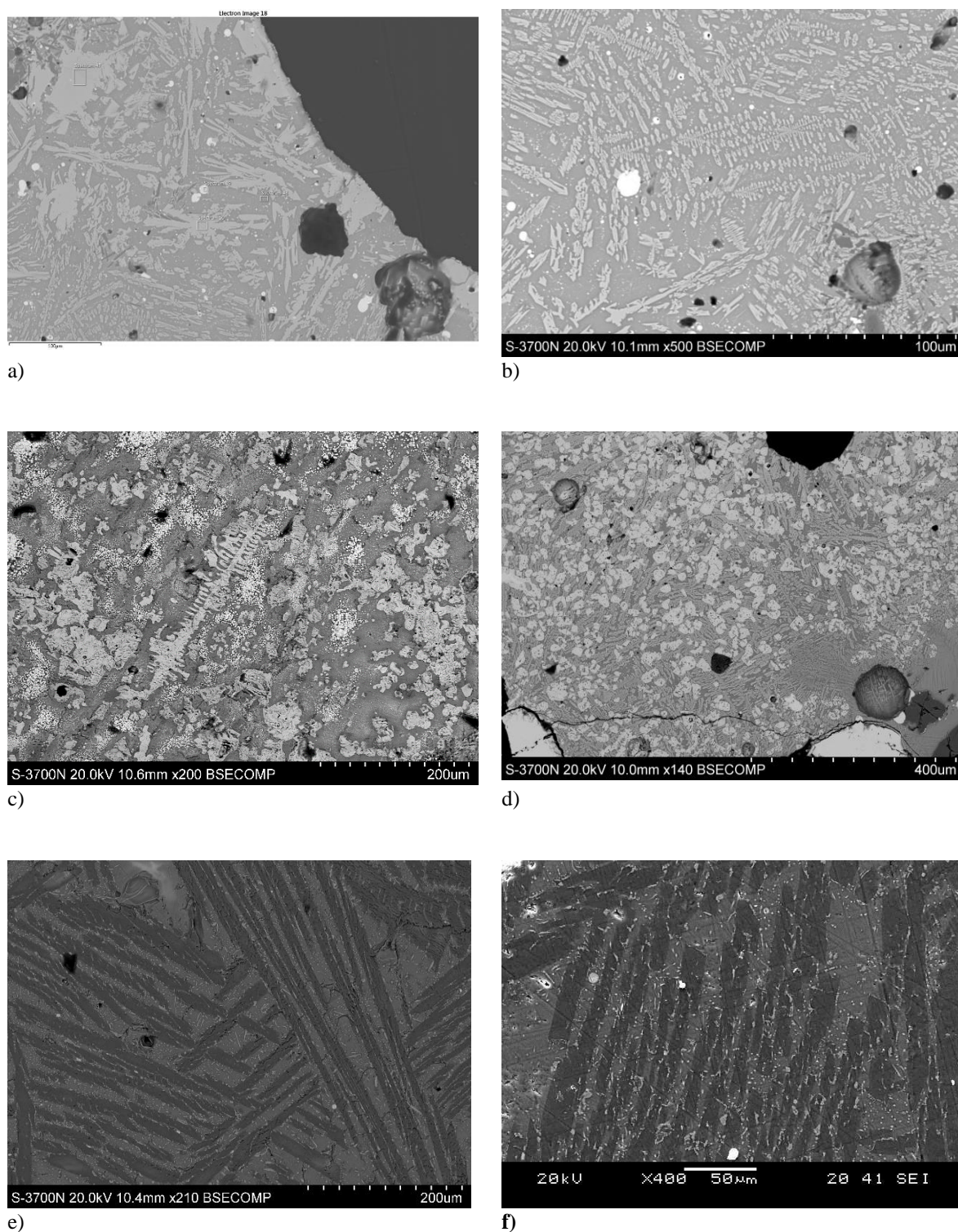
-Experimental materials-**- Fe-bearing compounds**

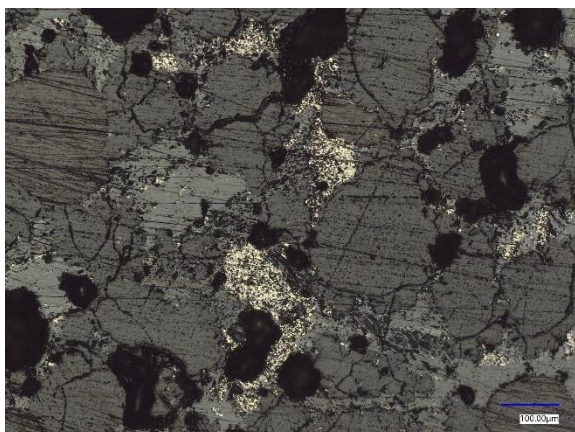
Fig. C. 16 presents a series of BSE micrographs depicting diverse morphologies observed in the experimental slags: a) elongated hoppers and b) primary dendritic olivine (light grey) in a fayalite matrix (grey); c-d) Ca-rich

dendritic structure with magnetite euhedral crystals (light grey) in a fayalite matrix (grey). Copper at an intermediate stage of transformation is also shown (white); e-f) chain olivines and dendrites (dark grey) with a lot of tiny iron oxide phases (white) in a fayalitic matrix (grey). Samples: a-b) JH2B_T1_002, c-d) JH2B_T2_001, e) JH2B_T1_002, e-f) JH2A_T1_001.

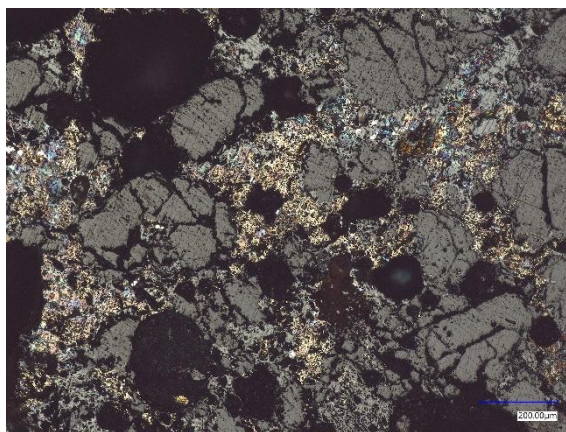
Cu-bearing compounds

Copper-bearing compounds in the experimental slags are predominantly present as copper-iron sulphides and matte. Below is a selection of optical micrographs highlighting various compositions and morphologies of copper-bearing compounds identified in the experimental slags.

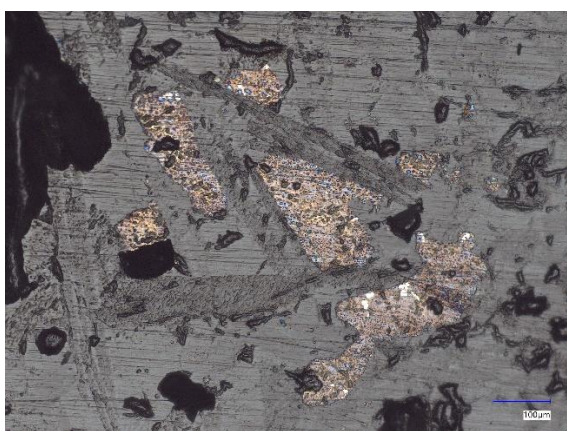
Slags



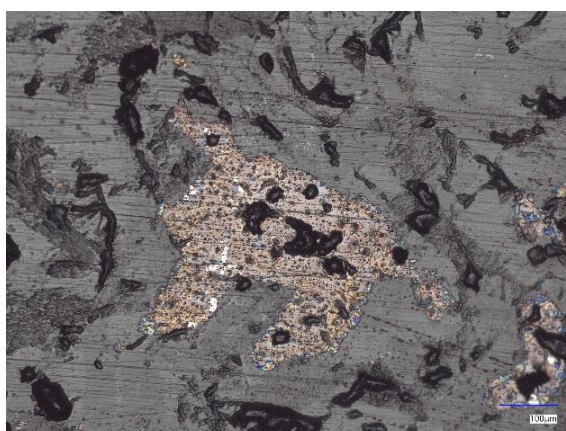
a)



b)



c)



d)

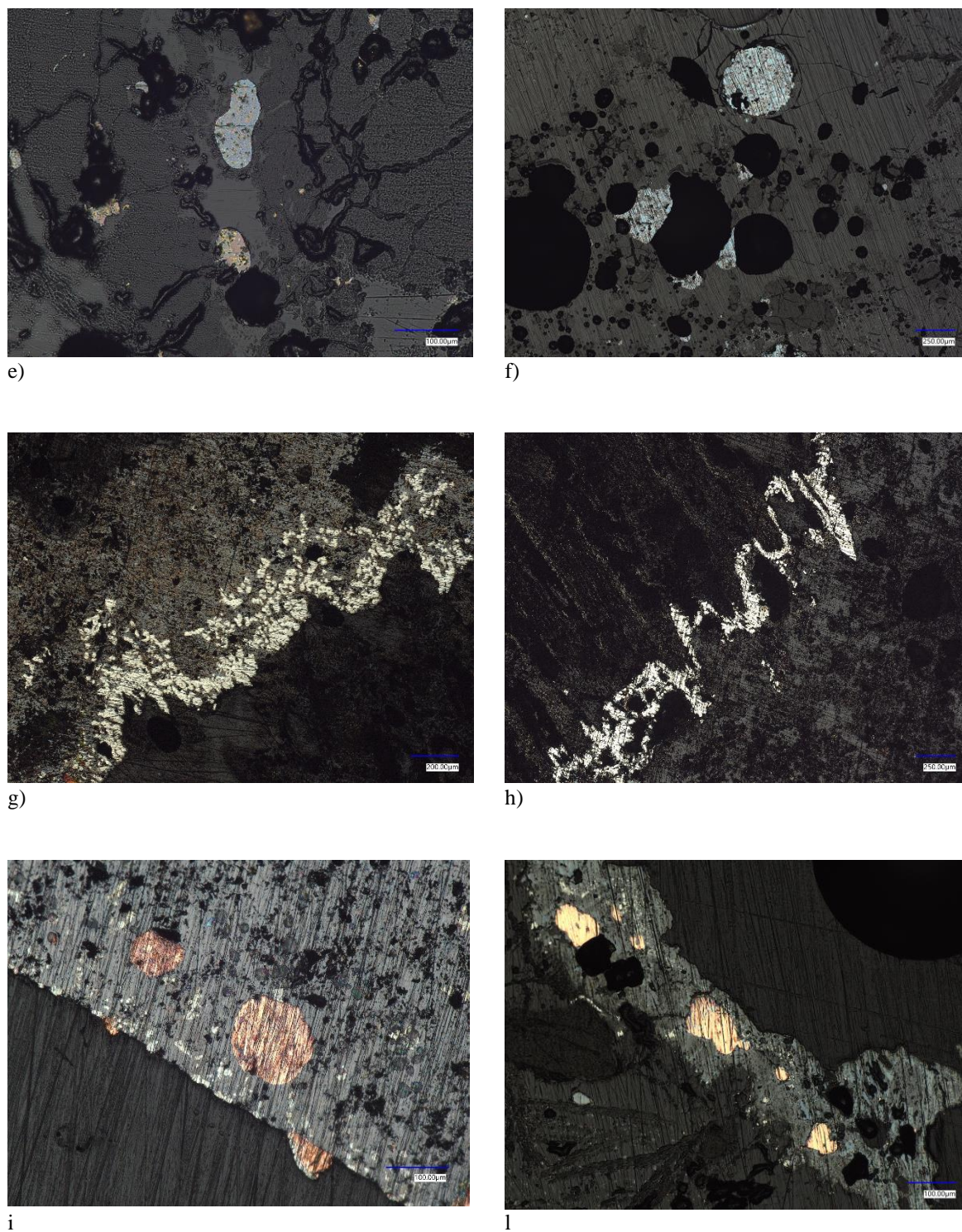


Fig. C. 17 showcases a collection of optical micrographs highlighting diverse compositions and morphologies of copper-iron sulphides within the experimental samples. A spectrum of colors, shapes, and chemical compositions is evident: a-b) Partially reacted chalcopyrite (gold yellow) within a matrix of iron oxides (mid-grey) and quartz (dark grey). c) Wedge-shaped partially reacted Cu-Fe sulphide situated between two converging pyroxene dendritic structures, indicating an incomplete process that prevented Cu-Fe sulphides from migrating out of the slag. d) Irregularly shaped partially reacted Cu-Fe sulphide within a matrix of iron oxides. e-f) Elongated and round-shaped partially reacted Cu-Fe sulphide and recrystallized compounds with covellite-like (blueish) and chalcocite-like (greyish) compositions. g-h) Partially reacted copper sulphide, possibly carrollite, in a matte (g) and fayalitic matrix (h). i-l) Round and elongated pure copper prills. Samples: a-b) JH1B_T1_001, c-d) JH1B_T2_002, e-f) JH1A_T3_003, g-h) JH2B_T2_001, i) JH2A_T3_002, l) JH1A_T3_001.

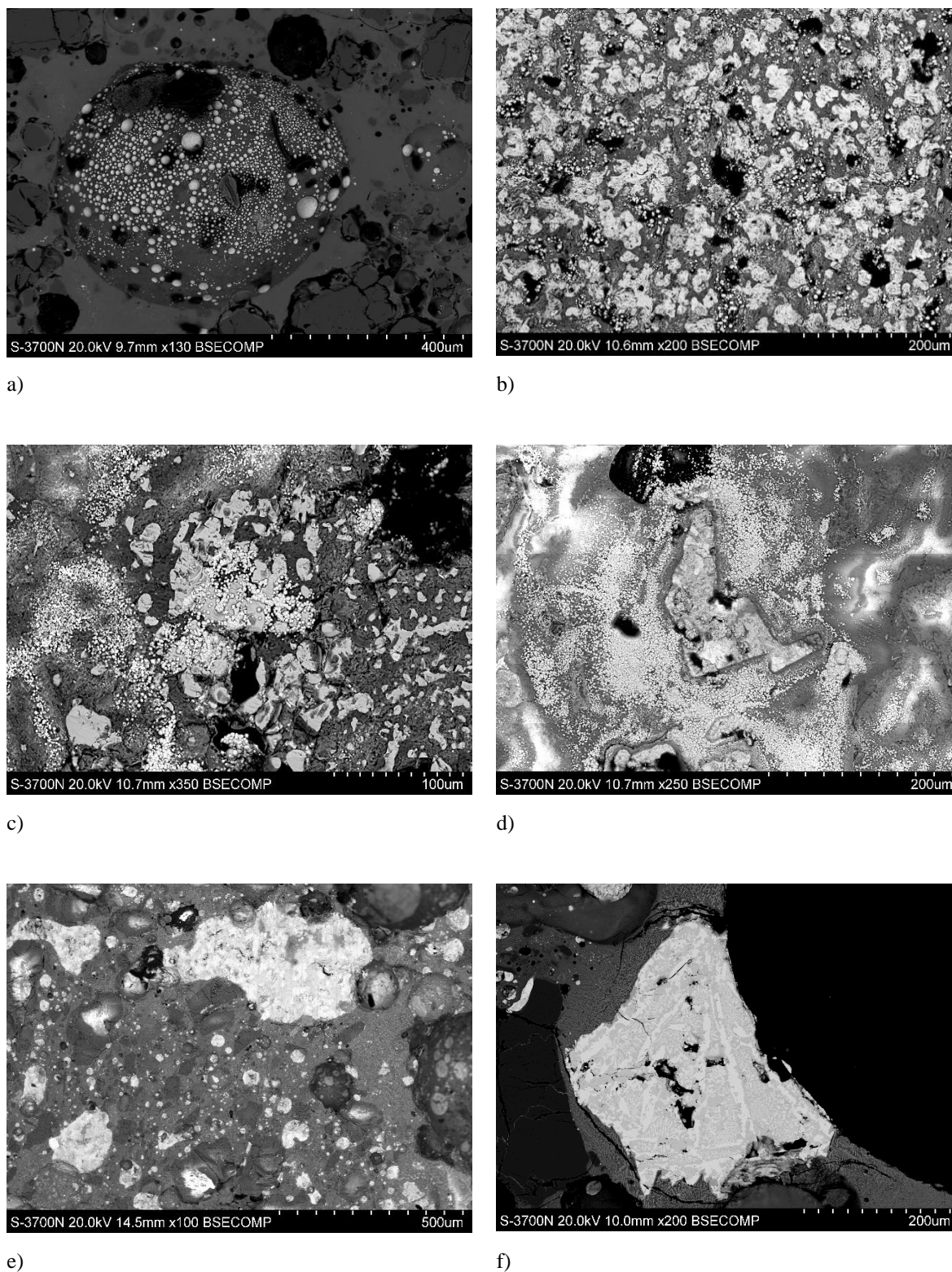


Fig. C. 18 presents a sequence of BSE micrographs illustrating the step-by-step accumulation of copper throughout the experimental 30-minute smelting process. The images depict the diverse features that copper assumes at various stages of transformation, highlighting the continuous increase in copper accumulation (light grey and white). Samples: a) JH2A_T3_001, b) JH2B_T2_001, c-d) JH2B_T2_001, e) JH2B_T1_001, f) JH2B_T1_002.

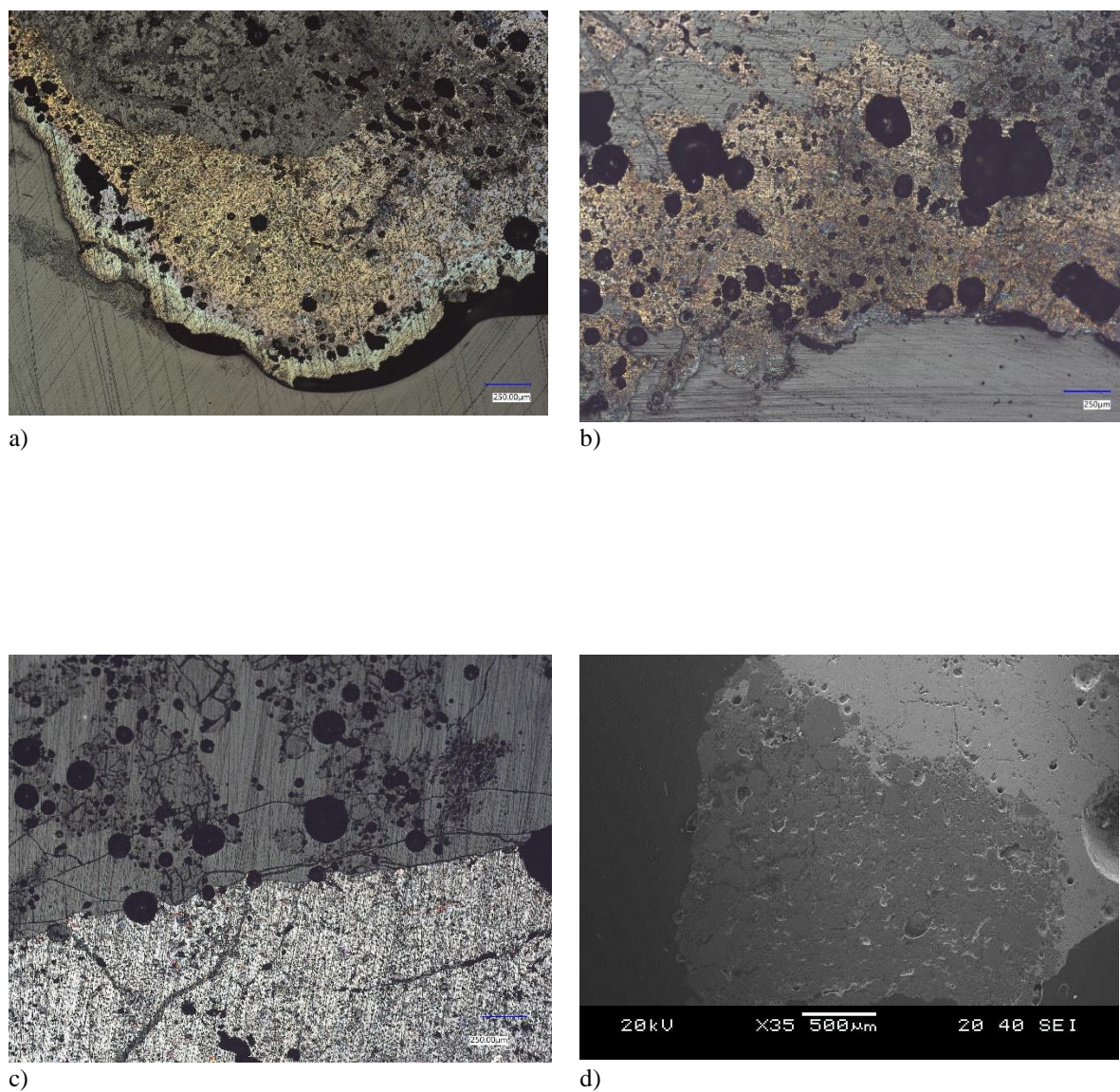
Matte

Fig. C. 19 presents optical micrographs (a-c) and a BSE micrograph (d), illustrating the distinct separation of the matte area from the slag matrix, predominantly observed toward the outer edges of the slag. Samples: a) JH1A_T2_003, b) JH1B_T2_002; c) JH2A_T3_001, d) JH1B_T3_001.

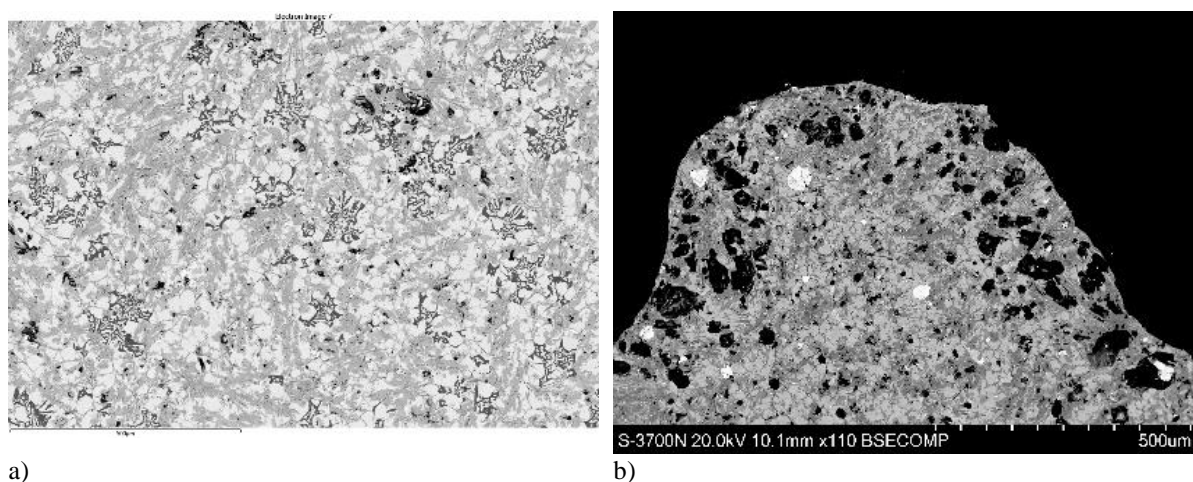


Fig. C. 20 presents a series of BSE micrographs showing a) the two main chemical compositions detected in the matte fragments: 1) Cu-Fe sulphide high in copper and iron (white) and 2) Cu-Fe sulphide high in sulphur; b) the copper prills (bright white) and cavities circular/elliptical vesicles entrapped in the matte. Samples: a) JH2A_T1_001, b) JH2A_T3_002.

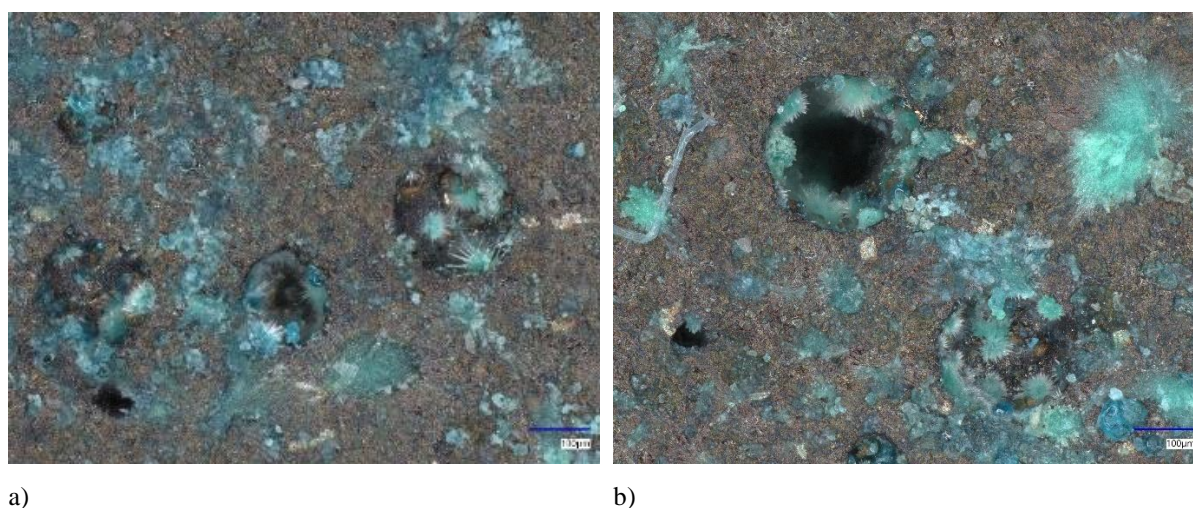


Fig. C. 21 presents optical micrographs capturing the emergence of newly developed phases, including copper hydroxides (e.g., $\text{Cu}(\text{OH})_2$) and $\text{CuCl}_2 \cdot 2\text{H}_2\text{O}$. Stalagmitic masses featuring copper carbonate radiating crystals are observed, having found space to grow within the cavities/voids of the matte fragment. The presence of water, whether due to humidity in storage or residual water from the sample preparation, facilitated chemical precipitation. Sample: a-b) JH1A_T1_001.

Inclusions

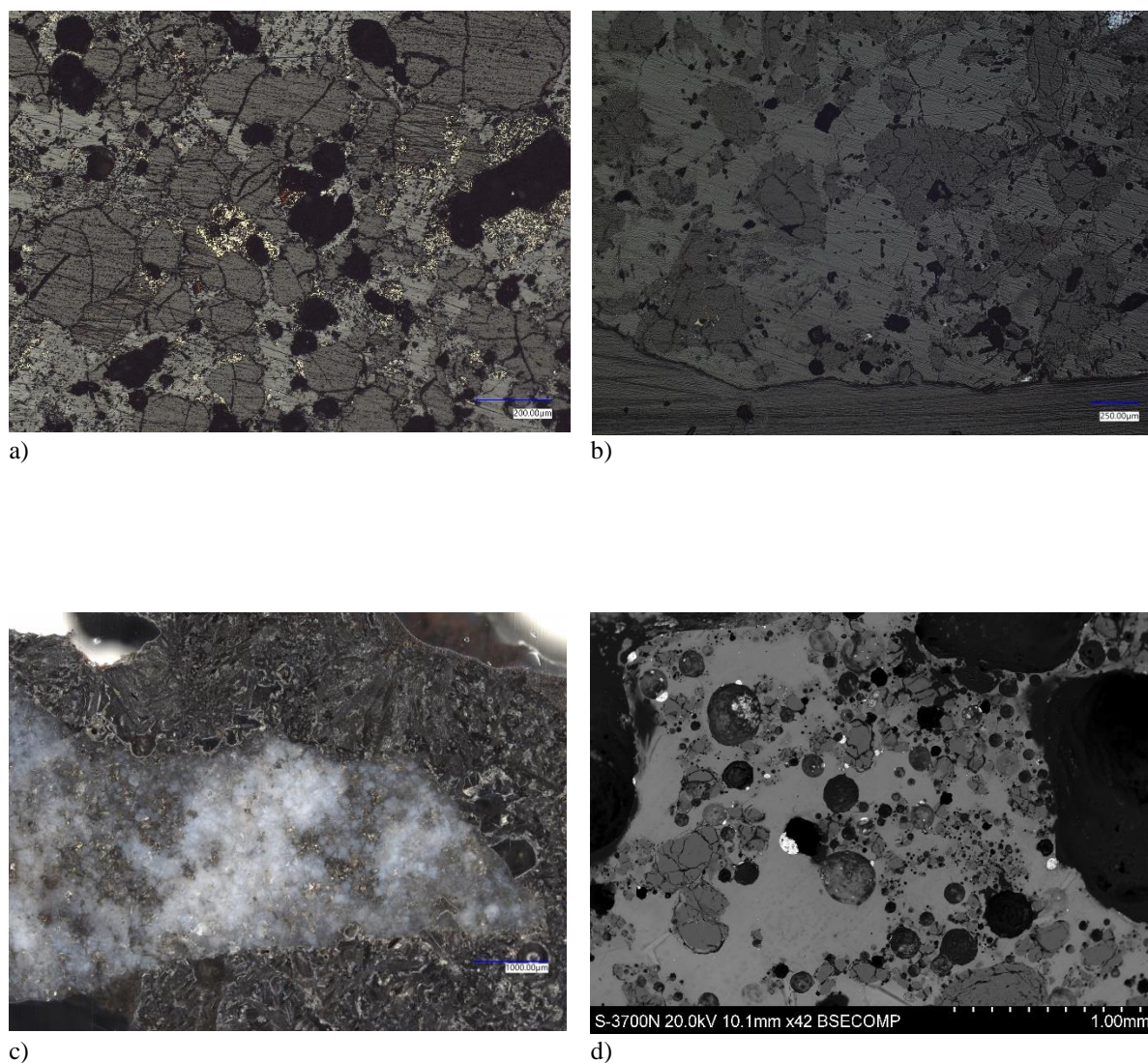


Fig. C. 22 illustrates a series of optical micrographs (a-c) and a BSE micrograph (d) displaying quartz inclusions in various phases of the experimental slags. Samples: a) JH1B_T1_001, b) JH1A_T3_003, c) JH1A_T2_001, d) JH2A_T3_001.

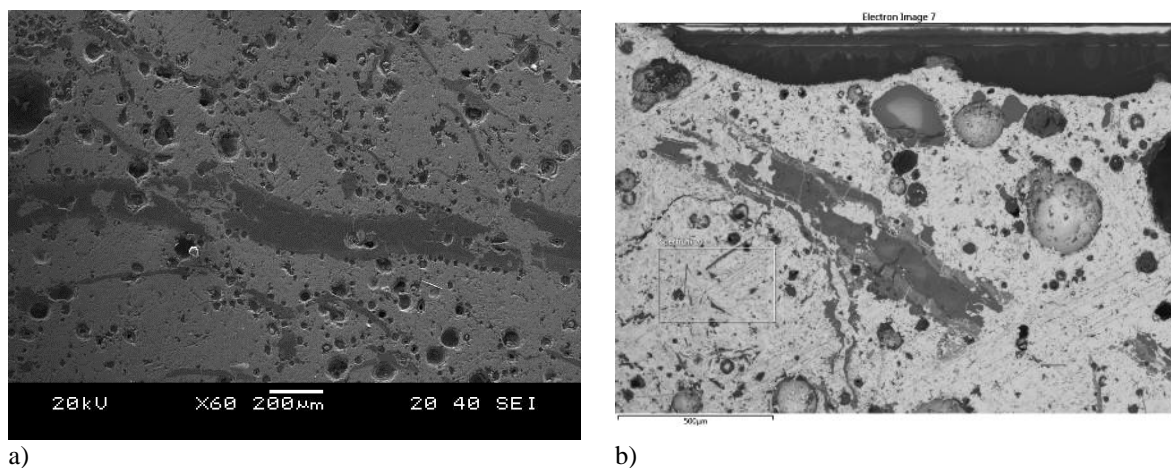


Fig. C. 23 illustrates a) a BSE and b) a SE micrograph of two samples from trial JH1B_T3, revealing elongated fayalitic structures that might be mistakenly interpreted as flat slag inclusions. Some of these inclusions may initially appear as remnants of flat slags. However, upon closer examination, they reveal themselves to be elongated structures with a composition resembling fayalitic minerals and quartz. This information holds significant value, potentially influencing the interpretation of archaeological findings and rectifying any potential misconceptions that could mislead scientists when analysing similar features in archaeological materials. Samples: a) JH1B_T3_001, b) JH1B_T3_002.

Charcoal

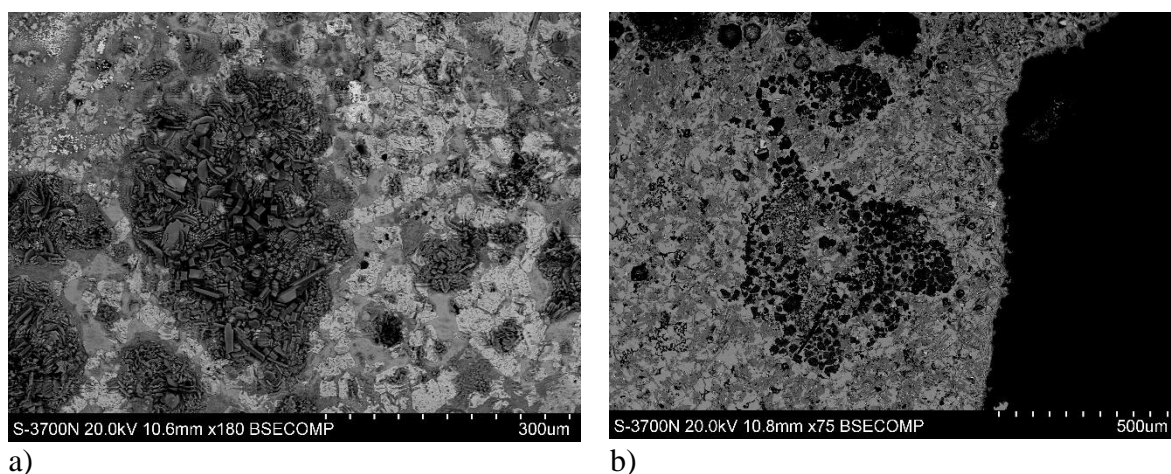


Fig. C. 24 illustrates two distinct occurrences of charcoal in the experimental fragments: a) depicts the typical structure of a charcoal fragment that remained entrapped on a matte fragment, while b) reveals negative traces in the form of voids left from the deterioration or burn of a charcoal fragment. Samples: a) JH2B_T2_001, b) JH2A_T1_001

Appendix D

Table D. 1 In the following table a comprehensive and up-to-date overview of the techniques of slags investigation (both archaeological and experimental) employed over the past two decades. This includes both the well-established methods and those still in the nascent stages of development for this type of investigation. For description of the techniques refer to the references in the last three rows of the table. See the end of the table for explanations of techniques acronyms.

Year	Site/Area	Density	OM	XRD	pXRF	XRF (lab-based)	SEM-EDX	WDXS	ICP-OES	LA-ICP-MS	MC-ICP-MS	PIXE	EPMA	AES or OES	AAS	MS	MoS	Raman	XANES	LIA	Reference
1995	Luserna, Romagnano, Acquafredda, Trentino, Italy		X	X		X									X						Cattoi et al. 1995
1997	Gaban, Acquaviva, Romagnano, Trentino, Italy						X														Cattoi et al. 1997
1999	Mina Guadalupe, Cerro Virtud, Spain					X	X														Ruiz Taboada & Montero Ruiz 1999
2001	Capattoli, Tuscany, Italy		X	X		X	X														Manasse et al. 2001
2002	Experimental samples		X	X			X					X									Bourgarit et al. 2002
2002	Massa Marittima, Tuscany, Italy		X	X		X	X														Manasse et al. 2002
2003	La Capitelte du Broum, France	X	X + Binocular lenses	X			X					X									Bourgarit et al. 2003
2003	La Capitelte du Broum, France		X																	X	Prange et al. 2003
2003	Cabezo Jure', Spain		X (RL, TL)	X		X	X														Saez et al. 2003
2003	Shahr-i Sokhta, Iran		X	X		X	X						X		X					X (TIMS)	Hauptmann et al. 2003

2004	Almizaraque, Spain		X (PPL, XPL)			X	X						X							Muller et al. 2004
2005	Mariahilfbergl, Inn valley, Austria		X				X													Hoppner et al. 2005
2005	Brixlegg, Inn Valley, Austria					X					X									Hoppner et al. 2005
2005	Millan, Alto Adige, Italy	X		X		X								X	X					Cremante & Storti 2005
2005	Millan, Bressanone		X	X			X													Artioli et al. 2005
2006	Fennhals-Kurtatsch, South Tyrol, Italy		X			X	X													Anguilano et al. 2006
2007	Slags in Italy		X	X			X					X								Artioli et al. 2007
2007	Faynan, Jordan																			Hauptmann 2007
2007	San Blas, Spain					X	X													Hunt Ortiz et al., 2007
2007	Spain		X				X													Rovira 2007
2007	Copper smelting slags, Northern Italy		X (RL)	X			X					X								Artioli et al. 2007
2008	Saint-Véran, France		X	X			X					X					X	X		Bourgarit et al. 2008
2008	Valencina de la Concepcion, Spain						X													Nocete et al. 2008
2009	Copper smelting slags, Alto Adige, Italy		X (RL)		X	X	X													Del Ri & Tecchiati 2009
2009	Millan, Gudon, Trentino, Italy		X (RL, TL)	X			X						X							Colpani et al. 2009
2010	Experimental samples			X				X				X					X		X	Burger et al. 2010
2010	Belovode, Serbia		X			X (PED)	X				X		X						X	Radivojevic et al. 2010
2012	Pyrgos-Mavroraki, Cyprus		X	X		X	X								X					Belgiorno et al. 2012
2013	Northern Italy	X	X	X		X	X												X	Addis 2013
2013	La Capitelte du Broum, France		X			X	X													Ambert et al 2013
2013			X	X			X													Phelps 2013
2013	Slags from Pentrwyn, Great Orme, UK		X (RL)	X						X	X									Williams 2013

2013	Kiechlberg, Tyrol, Austria		X (TL)	X		X							X							Krismer et al. 2013
2013	Belovode, Serbia		X				X						X							Radivojevic 2013
2014	Riparo Marchi, Trentino, Italy		X				X													Mottes et al. 2014
2015	S1, Styria, Austria		X (RL, TL)			X	X										X			Kraus et al. 2015
2015	Eneolithic copper smelting slags in the Eastern Alps		X	X			X													Artioli et al. 2015
2016	Belovode, Pločnik, Vinča and Gornja Tuzla, Serbia		X				X						X							Radivojevic & Rehren 2016
2016	Luserna, Trentino, Italy		X	X		X	X													Addis et al. 2016
2016	Sagalassos, Turkey				X															Scott et al. 2016
2017	CatalHoyuk, Turkey		X				X			X	X									Radivojevic et al. 2017
2017	Transaqua, Segonzano, Trentino, Italy		X	X		X	X													Addis et al. 2017
2017	Prein, Lower Austria					X	X													Haubner et al. 2017
2019	Mota Farun, Switzerland.			X			X													Wenk et al. 2019
2020	Experimental samples			X																Rose et al. 2020
2022	La Vela di Valbusa, Riparo di Monte Terlago, Trentino, Italy		X (Thin sections)	X			X			X										Pearce et al. 2022
2022	Chalcolithic Iberia		X (PPL, XPL)				X													Le Duc et al. 2022
2010	Overview (from Handbook)		X	X		X	X		X			X			X	X			X	Artioli et al. 2010
2014	Overview (from Handbook)		X	X	X	X	X		X				X						X	Hauptmann 2014

2019	Overview (from Handbook)		X				X	X									X		X		Bourgarit 2019
------	--------------------------	--	---	--	--	--	---	---	--	--	--	--	--	--	--	--	---	--	---	--	----------------

Acronyms:

OM, DM - Optical and Digital microscopy (RL – Reflected Light; TL – Transmitted Light; PPL - Plane-Polarized Light; XPL - Cross-Polarized Light)

XRD - X-ray diffractometry

pXRF - X-ray Fluorescence spectroscopy with a portable device

XRF - X-ray Fluorescence spectroscopy with a lab-based device (PED – Polarised Energy Dispersive)

LIA - Lead Isotope analysis

SEM-EDX - Scanning electron microscopy with energy dispersive X-ray spectroscopy

WDXS - Wavelength-Dispersive X-ray Spectroscopy

ICP-OES - Optical Emission Spectroscopy Coupled with a Plasma Source

LA-ICP-MS - Laser Ablation – Inductively Coupled Plasma-Mass Spectrometry

MC-ICP-MS - Multi Collector – Inductively Coupled Plasma-Mass Spectrometry

PIXE - Proton Induced X-ray Emission Spectroscopy

EPMA - Electron Probe Micro Analysis

AES or OES - Atomic or Optical Emission Spectroscopy

AAS - Atomic absorption spectroscopy

MS - Mass Spectrometry

MöS - Mossbauer spectrometry

Raman - Micro-Raman Spectrometry

XANES - X-ray Absorption Near Edge Spectroscopy

TIMS - Thermal Ionisation solid-source Mass Spectrometry

Appendix E

Instruments and Software used.

Archaeometallurgical analysis:

- Optical and digital devices
 - Stereoscope (Sz-Pt Olympus) with the related camera and software (LissView7)
 - Inverted reflected light microscope (Leica DFC295) equipped with a Leica DFC295 digital microscope color camera. Images acquired with the related LAS V4.7 software.
 - Digital microscope (Keyence VHX7000)
- SEM-EDX
 - Jeol JSM-5600LV equipped with an Oxford INCAx-act EDX (Software: Inca, Aztec 3).
 - Hitachi S-3700 equipped with (Software: Aztec 5.1).
- pXRF
 - Bruker Tracer III-SD Handheld X-Ray Fluorescence Spectrometer (Software: S1PXRF®, ARTAX, CloudCal).
- XRD
 - AXS-Bruker D-8 powder X-ray diffractometer (Software: DiffracPlus EVA)

Data analysis:

- Microsoft Office Package (Excel)
- R Studio (R-4.3.1). Packages: *dplyr*, *ggplot2*, *ggtern* (basic statistics and data graphic visualization).

Writing and editing:

- Microsoft Office Package (Word, Excel, PowerPoint)
- Adobe Creative Suite (PhotoshopCS6, IllustratorCS6, InDesignCS6).
- Zotero (references)